DUAL ROLE OF MICROGLIA IN HEALTH AND DISEASE: PUSHING THE BALANCE TOWARDS REPAIR

EDITED BY: Raquel Ferreira, Liliana Bernardino, Maria Beatrice Passan and Cinzia Volonté

PUBLISHED IN: Frontiers in Cellular Neuroscience and Frontiers in Molecular Neuroscience

frontiers Research Topics

ISSN 1664-8714
ISBN 978-2-88966-106-0
DOI 10.3389/978-2-88966-106-0

About Frontiers

Frontiers is more than just an open-access publisher of scholarly articles: it is a pioneering approach to the world of academia, radically improving the way scholarly research is managed. The grand vision of Frontiers is a world where all people have an equal opportunity to seek, share and generate knowledge. Frontiers provides immediate and permanent online open access to all its publications, but this alone is not enough to realize our grand goals.

Frontiers Journal Series

The Frontiers Journal Series is a multi-tier and interdisciplinary set of open-access, online journals, promising a paradigm shift from the current review, selection and dissemination processes in academic publishing. All Frontiers journals are driven by researchers for researchers; therefore, they constitute a service to the scholarly community. At the same time, the Frontiers Journal Series operates on a revolutionary invention, the tiered publishing system, initially addressing specific communities of scholars, and gradually climbing up to broader public understanding, thus serving the interests of the lay society, too.

Dedication to Quality

Each Frontiers article is a landmark of the highest quality, thanks to genuinely collaborative interactions between authors and review editors, who include some of the world's best academicians. Research must be certified by peers before entering a stream of knowledge that may eventually reach the public - and shape society; therefore, Frontiers only applies the most rigorous and unbiased reviews.
Frontiers revolutionizes research publishing by freely delivering the most outstanding research, evaluated with no bias from both the academic and social point of view. By applying the most advanced information technologies, Frontiers is catapulting scholarly publishing into a new generation.

What are Frontiers Research Topics?

Frontiers Research Topics are very popular trademarks of the Frontiers Journals Series: they are collections of at least ten articles, all centered on a particular subject. With their unique mix of varied contributions from Original Research to Review Articles, Frontiers Research Topics unify the most influential researchers, the latest key findings and historical advances in a hot research area! Find out more on how to host your own Frontiers Research Topic or contribute to one as an author by contacting the Frontiers Editorial Office: researchtopics@frontiersin.org

DUAL ROLE OF MICROGLIA IN HEALTH AND DISEASE: PUSHING THE BALANCE TOWARDS REPAIR

Topic Editors:
Raquel Ferreira, University of Beira Interior, Portugal
Liliana Bernardino, University of Beira Interior, Portugal
Maria Beatrice Passani, University of Florence, Italy
Cinzia Volonté, National Research Council (CNR), Italy

Citation: Ferreira, R., Bernardino, L., Passani, M. B., Volonté, C., eds. (2020). Dual Role of Microglia in Health and Disease: Pushing the Balance Towards Repair. Lausanne: Frontiers Media SA. doi: 10.3389/978-2-88966-106-0

Table of Contents

frontiers in Cellular Neuroscience

EDITORIAL
published: 28 August 2020
doi: 10.3389/fncel.2020.00259

Editorial: Dual Role of Microglia in Health and Disease: Pushing the Balance Towards Repair

Liliana Bernardino [1†], Cinzia Volonté [2,3*†], Maria Beatrice Passani [4*†] and Raquel Ferreira [1*†]*

[1] Faculty of Health Sciences, Health Sciences Research Centre (CICS-UBI), University of Beira Interior, Covilhã, Portugal, [2] CNR, Antonio Ruberti Institute for Systems Analysis and Computer Science (IASI), Rome, Italy, [3] Fondazione Santa Lucia IRCCS, Rome, Italy, [4] Section of Clinical Pharmacology and Oncology, Department of Health Sciences, University of Florence, Florence, Italy

Keywords: microglia, neuroinflammation, intercellular communication, neurodegenerative diseases, cytokines, phagocytosis

Editorial on the Research Topic

Dual Role of Microglia in Health and Disease: Pushing the Balance Towards Repair

Microglial cells are innate immune cells in the Central Nervous System (CNS) that provide support and facilitate tissue repair through the avid production of several inflammatory mediators (e.g., chemokines and cytokines) and growth factors (e.g., BDNF). They also remove menacing foreign or pathogenic elements and ensure the establishment and maintenance of proper synaptic connections. These diverse functions are addressed by the contributors of the present Research Topic.

He et al. explored the relationship between microglia activation and chemokine expression in a context of neuropathic hypersensitivity. In their study, the tetracycline antibiotic minocycline was administered in the hippocampus after nerve injury and clearly inhibited allodynia (i.e., a condition in which pain is caused by an innocuous stimulus). This analgesic effect was produced at the molecular level via downregulation of toll-like receptors and suppression of chemokine expression, which further emphasizes the role of minocycline on microglia activity. Burmeister and Marriott reviewed the role of the glial-derived interleukin (IL)-10 family of cytokines, which includes IL-19, IL-20, IL-22, and IL-24, in neuroinflammation. While IL-10 is generally accepted as a classical anti-inflammatory cytokine, IL-20 appears to have a pro-inflammatory effect and IL-22 can act either way. This reinforces the notion that our knowledge on these cytokines remains limited and warrants further attention to explore their potential in inflammatory brain disorders.

Blood coagulation factor fibrinogen has been associated to the development of depressive symptoms in Alzheimer's disease. In the context of brain dementia, Piers et al. showed how fibrinogen triggers an inflammatory microglial phenotype, assessed by genetic microarray analysis (microglial cell line) and proteome cytokine profiling (primary microglia). The consequent endoplasmic reticulum stress was blocked by inhibiting tumor necrosis factor (TNF)-α transcription or neuronal caspase activity, paving the way for the use of TNF inhibitors in inflammatory-mediated dementias. On a broader subject, Lee and Suk reviewed evidence on the role of protein kinases in neurodegenerative diseases such as Alzheimer's disease, Parkinson's disease, and amyotrophic lateral sclerosis. Specifically, authors review microglial activity via protein kinase modulation in inflammatory contexts to treat or alleviate symptoms manifested in neurodegenerative conditions. In amyotrophic lateral sclerosis, Vaz et al. evaluated the effects of wild-type and mutant superoxide dismutase 1 (SOD1) expression in microglia upon overexpression of wild-type (hSOD1WT) and mutated G93A (hSOD1G93A) protein, to uncover possible therapeutic targets. Both transduced cells displayed lower expression of anti-inflammatory

OPEN ACCESS

Approved by:
Dirk M. Hermann, University of Duisburg-Essen, Germany

***Correspondence:**
Liliana Bernardino
libernardinho@fcsaude.ubi.pt
Cinzia Volonté
c.volonte@hsantalucia.it
Maria Beatrice Passani
beatrice.passani@unifi.it
Raquel Ferreira
raquelmargarida@gmail.com

† These authors have contributed equally to this work

Specialty section:
This article was submitted to Cellular Neuropathology, a section of the journal Frontiers in Cellular Neuroscience

Received: *22 July 2020*
Accepted: *24 July 2020*
Published: *28 August 2020*

Citation:
Bernardino L, Volonté C, Passani MB and Ferreira R (2020) Editorial: Dual Role of Microglia in Health and Disease: Pushing the Balance Towards Repair. Front. Cell. Neurosci. 14:259. doi: 10.3389/fncel.2020.00259

targets but only microglia transduced with hSOD1G93A had higher expression of pro-inflammatory markers. Moreover, their exosomes were enriched with SOD1 and HMGB1. While overexpressed hSOD1WT attenuated activation, hSOD1G93A produced a reactive phenotype albeit with low responsiveness. To extend their previous works, two molecules known to elicit neuroregeneration, glycoursodeoxycholic acid and dipeptidyl vinyl sulfone, were successfully tested. Both exerted immunomodulatory properties over the hSOD1G93A microglia, but through specific molecular pathways.

In addition to exosomes, there are other types of vesicles that mediate extracellular communication. Grimaldi et al. investigated the therapeutic potential of microvesicles derived from microglial cells in a glioma context. Vesicles were first obtained from microglial cells stimulated with lipopolysaccharide and interferon-γ, and then infused into mice injected with glioma cells in their striatal brain region. The group observed the induction of a protective phenotype and reduced tumor size, which was attributed to the microvesicle cargo enriched in transcripts for several inflammation-related genes.

Regarding microglia-secreted hormones, the potential of insulin-like growth factor-1 (IGF-1) was evidenced by several articles. Myhre et al. researched and compared IGF-1 and TNF expression, and the amyloid-β (Aβ) plaque load in adult and old APPswe/PS1dE9 transgenic vs. wild-type mice. In the wild-type animals, IGF-1 remained constant whereas TNF expression increased with aging. IGF-1 and TNF levels were found elevated in the aged transgenic group; Aβ plaque load increased and plateaued in this group. The main contributor of IGF-1 was microglial cells and the ability to retain expression alludes to the therapeutic potential of modulating this cell population in Alzheimer's disease. IGF-1 is also pivotal for neurotransmission, particularly in the developing and mature auditory system. Fuentes-Santamaría et al. used knockout-out mice to study the mechanisms involved in excitatory synaptic plasticity occurring in the cochlear nuclei. The *Igf1*$^{-/-}$ mice exhibited lower levels in markers related to microglial and astrocyte activation, higher glutamate transporter 1 expression and reduced metabotropic glutamate receptor expression. Therefore, the imbalances in neurotransmission observed in cochlear nuclei may be a consequence of microglia and astrocyte impairment. Wlodarczyk et al. showed that the stimulation of the colony stimulating factor-1 receptor (CSF1R) promoted the expansion of CD11c-positive microglia. This cell subpopulation provided primary myelination and constituted a major source of IGF-1, which is critical for neuronal survival. Using a model of experimental autoimmune encephalomyelitis, which mimics human inflammatory demyelinating disease, the CSF1R stimulation caused CCL2 overexpression and an increase of CD11c-positive microglia, later reflecting the amelioration of symptoms and reduced demyelination.

Phagocytosis of cell debris and invading pathogens is also a hallmark of microglia activity. In this sense, Reichert and Rotshenker demonstrated how galectin-3 could trigger complement receptor 3-mediated phagocytosis of myelin debris. Galectin-3 knockdown reduced phagocytosis and changed cell morphology from "amoeboid-like" to "branched-like" microglia. This effect was produced by reorganization of actin filaments and cofilin inactivation. Galactin-3 acts by activating cofilin and then K-Ras signaling, thus controlling microglia cytoskeleton and phagocytic activity. In addition, Akhmetzyanova et al. assessed if microglia phagocytic activity in the acute period of spinal cord injury could influence post-traumatic processes by transplanting genetically modified microglial cells (Ad5-GDNF or Ad5-EGFP) into the spinal injured area. While Ad5-GDNF microglial have decreased phagocytic activity, Ad5-EGFP microglia are amoeboid active phagocytic cells. The area of intact nervous tissue was lower in the first group but differences in functional recovery were not observed. Hence, further studies are warranted to determine how enhanced tissue sparing can positively correlate with a functional outcome.

Finally, Lively et al. evaluated the importance of sex differences and age in microglial responses. Most animal studies favor the use of male adult rodents. Hence, microglia from sex-segregated postnatal day 1 and postnatal day 21 rats were analyzed regarding their response to pro- or anti-inflammatory stimulation. The extensive evaluation of migration ability, expression of inflammatory mediators and phagocytosis-related molecules, revealed several alterations at the transcriptional and functional level associated to age but not to sexual dimorphism.

Altogether, we expect the work presented in this topic will shed light on the role of microglia on intercellular communication in the brain parenchyma, thus stimulating a further scientific debate and encouraging novel therapeutic approaches to efficiently repair the injured CNS.

AUTHOR CONTRIBUTIONS

All authors listed have made a substantial, direct and intellectual contribution to the work, and approved it for publication.

Conflict of Interest: The authors declare that the research was conducted in the absence of any commercial or financial relationships that could be construed as a potential conflict of interest.

frontiers in Cellular Neuroscience

ORIGINAL RESEARCH
published: 19 November 2018
doi: 10.3389/fncel.2018.00404

Soluble Fibrinogen Triggers Non-cell Autonomous ER Stress-Mediated Microglial-Induced Neurotoxicity

*Thomas M. Piers[1], Emma East[1], Claudio Villegas-Llerena[1,2], Ioanna G. Sevastou[1], Mar Matarin[2,3], John Hardy[2] and Jennifer M. Pocock[1]**

[1] Cell Signalling Laboratory, Department of Neuroinflammation, Institute of Neurology, University College London, London, United Kingdom, [2] Department of Molecular Neuroscience, Institute of Neurology, University College London, London, United Kingdom, [3] Department of Neuropsychology, National Hospital for Neurology and Neurosurgery, University College London Hospitals, London, United Kingdom

Aberrant or chronic microglial activation is strongly implicated in neurodegeneration, where prolonged induction of classical inflammatory pathways may lead to a compromised blood-brain barrier (BBB) or vasculature, features of many neurodegenerative disorders and implicated in the observed cognitive decline. BBB disruption or vascular disease may expose the brain parenchyma to "foreign" plasma proteins which subsequently impact on neuronal network integrity through neurotoxicity, synaptic loss and the potentiation of microglial inflammation. Here we show that the blood coagulation factor fibrinogen (FG), implicated in the pathogenesis of dementias such as Alzheimer's disease (AD), induces an inflammatory microglial phenotype as identified through genetic microarray analysis of a microglial cell line, and proteome cytokine profiling of primary microglia. We also identify a FG-mediated induction of non-cell autonomous ER stress-associated neurotoxicity via a signaling pathway that can be blocked by pharmacological inhibition of microglial TNFα transcription or neuronal caspase-12 activity, supporting a disease relevant role for plasma components in neuronal dysfunction.

Keywords: microglia, neurodegeneration, Alzheimer's disease, ER stress, fibrinogen

OPEN ACCESS

Edited by:
Liliana Bernardino, Universidade da Beira Interior, Portugal

Reviewed by:
Gordon Meares, West Virginia University, United States
Marta Fumagalli, Università degli Studi di Milano, Italy

****Correspondence:***
Jennifer M. Pocock
j.pocock@ucl.ac.uk

Received: *03 September 2018*
Accepted: *19 October 2018*
Published: *19 November 2018*

Citation:
Piers TM, East E, Villegas-Llerena C, Sevastou IG, Matarin M, Hardy J and Pocock JM (2018) Soluble Fibrinogen Triggers Non-cell Autonomous ER Stress-Mediated Microglial-Induced Neurotoxicity. Front. Cell. Neurosci. 12:404. doi: 10.3389/fncel.2018.00404

INTRODUCTION

Midlife elevated plasma levels of systemic inflammatory markers such as fibrinogen and albumin are correlated with reduced brain volumes in brain areas associated with dementia such as Alzheimer's disease (AD) in later life (Walker et al., 2017). Blood brain barrier (BBB) and cerebral vascular integrity can weaken in normal aging and in neurodegenerative diseases, and may contribute to cognitive decline (Hainsworth et al., 2017; Sweeney et al., 2018). Deposition of blood-borne proteins in the CNS parenchyma may occur in neurodegenerative diseases such as AD (Lipinski and Sajdel-Sulkowska, 2006; Ryu and McLarnon, 2009; Miners et al., 2018) and depletion of blood-borne factors, specifically fibrinogen (FG) are protective in animal models of neurodegeneration (Cortes-Canteli et al., 2012).

Fibrinogen may enter the brain via small cerebral microbleeds or microhaemorrhages (Werring et al., 2010), which are associated with the development of depressive symptoms in AD (Leeuwis et al., 2017), an often early event in AD (Cortés et al., 2018), and the inflammatory activation of microglia (Ahn et al., 2018). In line with this, infiltration of plasma proteins into the CNS precipitates neurotoxic signaling cascades through the activation of microglia (Huang et al., 2008; Hooper et al., 2009; Ryu and McLarnon, 2009; Weinstein et al., 2009). Furthermore, systemic inflammation is correlated with future cognitive decline in AD (Holmes et al., 2009). Moreover FG can induce pro-inflammatory cytokine secretion from peripheral blood cells (Jensen et al., 2007). In addition, elevated plasma FG levels are a risk factor for AD and vascular dementia, (van Oijen et al., 2005; Xu et al., 2008), a proposed CFS biomarker for AD (Lee et al., 2007) and the development of cognitive impairment after stroke (Gillett et al., 2018).

Fibrinogen signals through an integrin class of receptor, Mac-1 (or αMβ2, CD11b/CD18), expressed by microglia and macrophages (Adams et al., 2007) which is upregulated in AD brain (Akiyama and McGeer, 1990). This signaling stimulates the secretion of pro-inflammatory cytokines and chemokines (Smiley et al., 2001; Piers et al., 2011). Thus, it seems plausible that FG-induced deficits in neuronal viability are due to aberrant inflammatory signaling. Historically, investigations into chronic, aberrant neuronal loss have focussed on classic apoptotic pathways centered on mitochondrial signaling. However, an endoplasmic reticulum (ER) centered hypothesis for the neuronal death occurring in neurodegenerative diseases has also been proposed (Lindholm et al., 2006). ER stress is a well-characterized cellular phenomenon, whereby an accumulation of misfolded proteins and calcium dys-homeostasis lead to disturbances in the structure and function of the ER (Gerakis and Hetz, 2018). Under normal circumstances, highly conserved unfolded protein response (UPR) adaptive mechanisms rebalance cellular homeostasis. However, if the accumulation of misfolded proteins is prolonged, as observed in AD models (Nakagawa et al., 2000), apoptotic cell signaling cascades are induced, leading to significant cytotoxicity (Nakagawa et al., 2000; Gerakis and Hetz, 2018; Morris et al., 2018). Interestingly, increased pro-inflammatory cytokine release, specifically tumor necrosis factor-α (TNFα) and interleukin-6 (IL-6), can induce ER stress signaling in fibroblast cell lines and *in vivo* (Xue et al., 2005; Denis et al., 2010; O'Neill et al., 2013). Conversely, ER stress can also mediate upregulation of pro-inflammatory cytokines (Chen et al., 2013), suggesting the possibility of a self-perpetuating mechanism of detrimental signaling in neurodegenerative diseases centered on ER stress and aberrant, or chronic, inflammatory signaling. With this in mind, we aimed to identify if exposure to FG modulated inflammatory signaling and subsequent neuronal toxicity in a well-characterized *in vitro* neuronal cell culture model, which can be pharmacologically manipulated to eliminate the presence of microglia (Piers et al., 2011; Jebelli et al., 2015). Here, we identify for the first time, a FG-induced increase in neurotoxicity via a non-cell autonomous mechanism involving a microglial TNFα-mediated induction of neuronal ER stress signaling.

MATERIALS AND METHODS

Materials

Fibrinogen, lipopolysaccharide from *Escherichia coli* (055:B5; LPS), tunicamycin, thapsigargin, leucine-methyl-ester (LME), staurosporine, hirudin, and Isolectin B_4 from *Griffonia simplicifolia*-FITC conjugated were from Sigma (Dorset, United Kingdom) and thalidomide was from Tocris Bioscience (Bristol, United Kingdom). Quantikine M TNFα. TGF-β and IL-6 ELISA kits, z-VAD-FMK and z-ATAD-FMK were from R&D Systems (Abingdon, United Kingdom). Caspase 12 (FITC-ATAD-FMK) activity kits were from Promokine (Heidelberg, Germany) and caspase 3/7 (FAM-DEVD-FMK) activity kits were from Millipore (Watford, United Kingdom). Anti-ED1, anti-CD11b and rat IgG isotype controls were from AbD Serotec (Kidlington, United Kingdom), anti-caspase 12 and goat anti-rat-FITC were from Abcam (Cambridge, United Kingdom). Goat anti-rabbit IgG horseradish peroxidase (HRP) and goat anti-mouse IgG HRP were from Autogen Bioclear (Calne, United Kingdom).

Methods

BV2 Microglial Cell Line Culture

BV2 microglia were maintained in DMEM with 10% foetal bovine serum (FBS), supplemented with 2 mM L-glutamine, 100 U/ml penicillin and 100 mg/ml streptomycin at 37°C in a humidified atmosphere with 5% CO_2. Prior to experimentation, BV2 microglia were harvested and plated in serum-free DMEM.

Preparation of Enriched Neuronal-Glial Cultures (ENGC)

Primary cultures of enriched neuronal-glial cerebellar cultures were isolated from 3 to 6 day-old Sprague Dawley rat pups and prepared as described previously (Piers et al., 2011) in accordance with the United Kingdom Animals (Scientific Procedures) Act, 1986. Cells were plated on 13 mm poly-D-lysine (PDL) coated glass coverslips at a density of 8×10^5 per coverslip and maintained in ENGC medium (Neurobasal medium with 2% B27 neuronal supplement, 20 mM KCl, 6 g/l D-Glucose, 2 mM L-Glutamine, 50 U/ml penicillin, and 50 μg/ml streptomycin). After 36 h *in vitro*, cytosine furanoarabinoside (10 μM) was added to prevent proliferation of non-neuronal cells. The cultures were maintained at 37°C in 5% CO_2 and used at 7 DIV.

Microglial Ablation From ENGCs

Microglia present in the ENGCs were depleted with 25 mM leucine-methyl-ester (LME), as previously described (Jebelli et al., 2015).

Preparation of Primary Cultured Microglia

Microglia were isolated from 5-day-old Sprague Dawley rat pups, as previously described (Piers et al., 2011) in accordance with the United Kingdom Animals (Scientific Procedures) Act, 1986. Cells were plated at a density of 5×10^4/well on 13 mm coverslips or 1×10^6/well in 60 mm culture dishes. After 24 h *in vitro*, the

medium was replaced with serum-free ENGC medium and the cultures were left to rest for at least 3 h prior to stimulation.

Fibrinogen Preparation

Fibrinogen was prepared in ultrapure, endotoxin-free water at 1000 × final concentration and sonicated prior to addition to cell cultures. The final concentrations used are in line with those previously used *in vitro* (Schachtrup et al., 2010).

Microarray Analyses

Extracted RNA from control and FG-treated BV2 cultures (miRNeasy; Qiagen) was sent to AROS Applied Biotechnology (Denmark) for microarray analysis using a MouseRef-8 v2.0 Expression Array (Illumina). Experimental procedures (cDNA labeling and hybridization) were performed according to manufacturer's instructions. Bead Arrays were scanned using the Illumina Bead Station 500X, and raw intensity values were saved in Illumina's Bead Studio program manager. For array hybridization, all samples were distributed among different arrays to minimize batch effect. Analysis was performed using Partek Genomics Suite 6.6 (Partek, Inc., St. Louis, MO, United States) and Lumi R package (Bioconductor, Du et al., 2008). Raw expression data were log2 transformed, and all samples were quantile normalized. QC plots before and after normalization were generated for data quality analysis. Individual probes were excluded from analysis if the detection *p*-value was >0.05 in more than 2 out of the 3 repeats for any condition. Samples were also excluded if <95% of the probes were detected (all samples met this quality control criterion). A conservative statistical threshold of FDR <0.05 and minimum fold difference ≥ 1.5 between sample groups was used in all comparisons and to generate gene lists.

Assessment of Cell Death

Live ENGCs were incubated with propidium iodide (PI; 5 μg/ml) and Hoechst 33342 (5 μg/ml). Using Image J analysis software (NIH, United States), dead cells (PI^+) were quantified as a percentage of total cell number, the latter obtained by Hoechst 33342 staining. A minimum of 3 fields per coverslip were counted, and at least 3 coverslips were assessed for each variable per experiment in at least 3 separate experiments as previously described (Piers et al., 2011).

Immunocytochemistry

Cultures were fixed in 4% paraformaldehyde (PFA) in phosphate buffered saline (PBS) then permeabilised in 100% methanol. Cells were blocked with PBS containing 4% normal goat serum and then incubated with primary antibodies overnight at 4°C (1:100 anti-ED1, 1:100 anti-CD11b, or anti-rat IgG isotype control). After washing, cells were incubated with goat anti-rat FITC (1:100) in PBS. For microglia identification, FITC conjugated lectin (IB_4) (Streit, 1990) was administered at the same time as the secondary antibodies. Cultures were washed and incubated with DAPI solution prior to mounting with Vectashield (Vector Labs Inc, Burlingame, CA, United States).

Assessment of Caspase 12 or Caspase 3/7 Induction

ENGCs were assessed for the induction of caspase-12 and caspase-3/7 after treatment as per the manufacturer's instructions. After treatment, coverslips were removed and mounted into a basic medium consisting of 153 mM NaCl, 3.5 mM KCl, 0.4 mM KH_2PO_4, 20 mM N-Tris (hydroxymethyl)methyl-2-aminoethanesulphonic acid (TES), 5 mM $NaHCO_3$, 1.2 mM Na_2SO_4, 1.2 mM $MgCl_2$, 1.3 mM $CaCl_2$, 5 mM glucose, warmed to 37°C and observed immediately using fluorescence microscopy (Zeiss, Oberkochen, Germany). Cultures were counterstained with Hoechst for total cell number and PI for total cell death using automatic exposure settings. A minimum of 3 fields per coverslip was counted, and at least 4 coverslips were assessed for each treatment per experiment. Manual exposure settings were optimized against a positive control then fixed for entire experiments. Analysis was performed using Image J software (NIH, United States).

Western Blotting

Soluble protein lysates were resolved by SDS-PAGE electrophoresis and transferred to PVDF membranes using standard techniques. The following antibodies were used: anti-caspase 12 (Abcam; 1:1000), anti-β-actin (Sigma; 1:10,000). Immunoreactive bands were imaged and optical densities were quantified using ImageJ software (NIH, United States) and normalized to β-actin protein levels.

ELISA Determination of TNFα, TGF-β1 and IL-6

Quantification of secreted inflammatory cytokines TNFα, IL-6 and TGF-β1 in microglial and ENGC culture supernatants was determined with Quantikine M Rat Immunoassay kits according to the manufacturer's instructions. Briefly, microglial-conditioned medium or ENGC-conditioned medium (MGCM or ENGC-CM, respectively) was centrifuged at 4500 × *g* for 1 min to remove any floating cells and assayed essentially as previously described (Taylor et al., 2005). Cytokine concentrations were determined against a standard concentration curve.

Cytokine Arrays and Pro-inflammatory Cytokine Panel

MGCM was collected as above for cytokine analysis, supernatants pooled from 3 independent experiments and incubated with Proteome ProfilerTM Rat Cytokine array membranes (R&D systems Panel A) as per the manufacturer's instructions. Data were analyzed using the Protein Array Analyser Palette plugin (ImageJ), and plotted, as a mean ± SEM after normalizing to membrane reference positive controls and intracellular protein concentrations.

Statistical Analysis

All Western blots and PCR analyses were carried out at least three times and those shown are representative. All experiments were performed from at least three separate cell preparations with internal replicates of at least 3 per experiment. Significant differences were estimated using Welch's two-sided *t*-test or Student's un-paired *t*-test with levels of significance at

$^{***}p < 0.001$, $^{**}p < 0.01$, and $^{*}p < 0.05$; $p > 0.05$ was not significant.

RESULTS

FG Exposure Enhances Inflammatory Gene Expression and Release of Pro-inflammatory Cytokines

To extend previous findings that FG can induce an inflammatory microglial phenotype, we performed, in parallel, genetic microarray analysis of the well-characterized BV2 mouse microglia cell line, and pro-inflammatory cytokine release from primary rat microglia cultures and enriched neuronal glial cultures (ENGCs). Microarray analysis of BV2 cultures after 6 h of FG exposure identified a significant over-representation, amongst others, of immune system and inflammatory gene upregulation, including *tnf*, which encodes TNFα (**Figure 1A** and **Table 1**). These findings were supported by cytokine release data from rat microglia cultures where primary microglia exposed to FG or lipopolysaccharide (LPS; as a positive control) for 24 h showed significant TNFα secretion (**Figure 1B**). A number of cytokines and chemokines, many of which are regarded as inflammatory (Owen et al., 2011), were secreted to significance by FG (**Figure 1B**) including TNFα, MMP-2, IL-6, CXCL2, and CCL2. Whilst many mirrored the release evoked with LPS, Fibulin-3 was secreted by FG stimulation only, whereas IL-1β or IL-1α secretion was observed after LPS treatment, but was absent in FG-treated cultures indicating that FG stimulation of microglia is nuanced compared with LPS stimulation.

In support of previously published data identifying microglial CD11b as a putative receptor for FG (Adams et al., 2007), pre-incubation of primary microglial cultures with a CD11b blocking antibody significantly attenuated the FG-induced TNFα release, but had no effect on LPS-induced secretion (**Figure 1C**). Given the perceived importance of microglia in mediating the inflammatory effects of FG, and the potential for this inflammation to impact on neuronal integrity, we determined if the microglia present in ENGCs responded in a similar way to isolated primary microglia. The ability to specifically ablate microglia from the ENGCs (Jebelli et al., 2015) allows us to determine any particular dependencies on these cells. In accord with the data for proteome analysis for release of cytokines from primary cultured microglia, exposure of ENGCs to either FG or LPS significantly enhanced the release of TNFα (**Figure 1D**) and another pro-inflammatory cytokine, interleukin-6 (IL-6; **Figure 1E**), in a manner similar to that observed in primary microglia cultures. Critically, when microglia were ablated from ENGCs, the LPS- or FG-induced TNFα release (**Figure 1C**) and IL-6 release (**Figure 1D**) were significantly attenuated. Further characterization of cytokine release in the ENGCs revealed that transforming growth factor-β1 (TGF-β1) secretion, a cytokine known to have opposing cellular effects to TNFα (Bitzer et al., 2000), was not significantly modulated by either LPS or FG exposure, irrespective of the presence of microglia (**Figure 1E**), this is possibly due to the dominating expression of this cytokine by the astrocyte population present in the ENGCs (De Groot et al., 1999). Taken together, these data suggest that FG exposure skews microglia toward a pro-inflammatory phenotype.

FG Induced a Reactive Microglial Phenotype

Confirmation of a FG-mediated induction of a reactive microglial phenotype, as previously indicated (Adams et al., 2007; Piers et al., 2011) was performed by immunocytochemical analysis of characterized activated microglial markers. Control, unstimulated, primary microglial cultures expressed low levels of the activated microglial marker ED-1 (**Figure 2Ai**), and > 95% of cells stained positive for IB_4 (**Supplementary Figure S1**), suggesting highly purified cultures, in a down-regulated state. In support of FG-mediated activation, ED1 protein expression was significantly enhanced when compared with non-treated control cultures (**Figure 2Aii**). Furthermore, FG treatment significantly increased the surface expression of its putative receptor, CD11b (**Figures 2Bi,ii**), induction of which has previously been associated with a phagocytic microglial phenotype (Adams et al., 2007). These findings provide further support for a shift in microglial activation when the cells are exposed to FG, although interestingly whilst LPS evoked inducible nitric oxide synthase (iNOS) expression in the microglia, FG did not, suggesting a further divergence in activation profiles (**Figure 2Aiii**).

FG-Mediated Neurotoxicity Is Dependent on Secreted Microglial Factors

Whilst it is clear that FG exposure can induce a pro-inflammatory microglial phenotype, it is unclear whether this induced phenotype would have an effect on neuronal viability. To study this, we exposed ENGCs to FG and performed live cell staining with Hoescht/propidium iodide (PI) for total/dead cell analysis, respectively. After 24 h of exposure to FG, the number of PI-positive cells increased significantly when compared with non-treated controls (**Figures 3Ai,Aii**), which did not increase further after 48 h of exposure (**Figure 3Aii**). The cleavage of fibrinogen to fibrin by thrombin is a well-defined mechanism in the coagulation cascade (Binnie and Lord, 1993), and thrombin transcripts are present in these cultures when exposed to FG for 48 h (**Supplementary Figure S2**). Therefore, it was possible that the observed toxicity was due to cleavage of soluble fibrinogen to insoluble fibrin deposits. To clarify this, cultures were co-treated with FG and the thrombin inhibitor hirudin for 24 h. The percentage of PI-positive cells in the FG + hirudin-treated cultures was not significantly different from cultures treated with FG alone (**Figure 3B**) suggesting soluble FG rather than cleaved fibrin is the cause of the observed reduced neuronal viability. Death was not due to endotoxin contamination of FG since polymyxin B (PMX) treatment to remove endotoxin did not ablate FG-induced death but did ablate LPS induced death (**Supplementary Figure S3**).

To further characterize the death-signaling pathways induced in the ENGCs by FG exposure, live cell staining for the apoptotic executioner caspase-3/7 was performed, using the

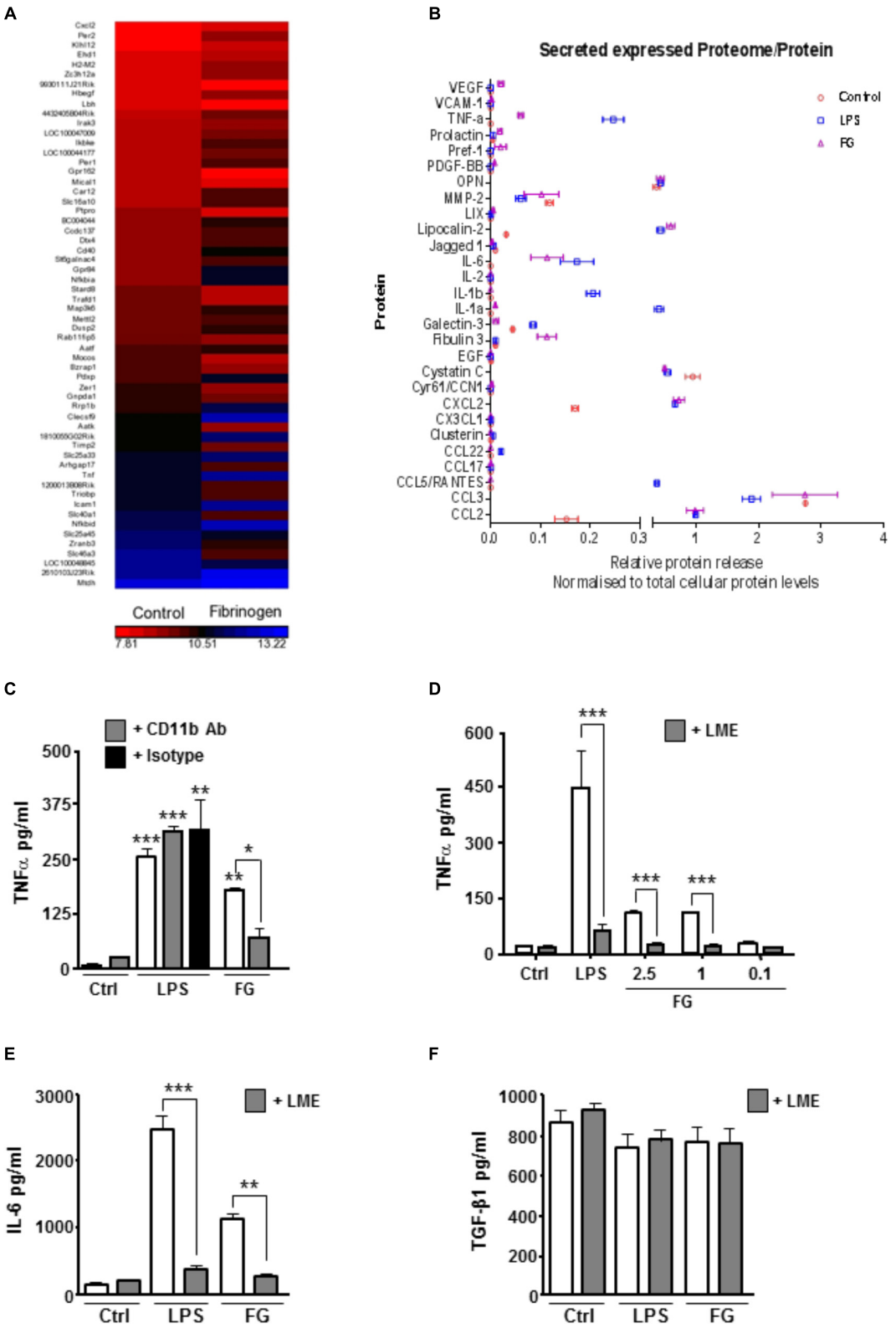

FIGURE 1 | FG induces early upregulation of inflammatory related genes and release of inflammatory cytokines. **(A)** Gene microarray performed on the BV2 microglial cell line after Fibrinogen (2.5 mg/ml) exposure for 6 h compared with non-stimulated (Control) BV2 cells at 6 h. **(B)** Proteome array performed on primary microglia following 24 h of stimulation with lipopolysaccharide (LPS, 1 μg/ml), Fibrinogen (FG, 2.5 mg/ml) or non-stimulated cells (Control). **(C)** TNFα secretion in cell

(Continued)

FIGURE 1 | Continued
culture medium by ELISA following treatment of primary microglia for 24 h with LPS (1 μg/ml), FG (2.5 mg/ml) or non-stimulated (Ctrl) ± MAC-1 receptor blocking antibody (+ CD11b, 10 μg/ml) or rat IgG as isotype control (+ IgG, 10 μg/ml). **(D)** ENGCs treated for 24 h with LPS (1 μg/ml), FG (0.1–2.5 mg/ml) or non-stimulated (Ctrl), and where indicated, pre-treated with 25 mM leucine-methyl-ester (+ LME) for microglia ablation, followed by ELISA analysis of TNFα secretion in culture medium. **(E)** ENGCs treated as **(D)** followed by ELISA analysis of IL-6 secretion in culture medium. **(F)** ENGCs treated as **(D)** followed by ELISA analysis of TGFβ secretion in culture medium. In all graphs, data are the mean ± SEM from 3 independent experiments with internal replicates of at least 3. Significance levels compared with control condition unless otherwise indicated, $*p < 0.05$, $**p < 0.01$, $***p < 0.001$.

fluorescent substrate FAM-DEVD-FMK (Darzynkiewicz et al., 2002). Following 24 h exposure to FG, a significant increase in caspase-3/7 activity was observed, when compared with non-treated control cultures (**Figures 3Ci,Cii**). Interestingly the most pronounced staining seemed to correlate with cells with large, rounded cytoplasmic morphology, uncharacteristic of neuronal anatomy (white arrow heads, **Figure 3Ci**), and unlike the prominent staining observed after staurosporine (STS; positive control for the induction of apoptosis) exposure (**Figures 3Ci,Cii**). These cells fit the description of microglia that we know are present in the ENGCs as confirmed with IB_4 staining and previously published literature (**Figure 3Ciii**; Piers et al., 2011; Jebelli et al., 2015). Furthermore, previous studies have suggested that microglial activation is dependent on non-apoptotic caspase-3 activity (Shen et al., 2017). Therefore, we wanted to identify whether microglial caspase-3 activity was important in the observed reduction in neuronal viability. Initially, we performed microglial ablation on ENGCs and found that removal of microglia from the cultures significantly attenuated the observed FG-mediated neuronal death (**Figure 3D**). Interestingly, LPS mediated neuronal death was not significantly different from control levels, suggesting that whilst the ability of FG and LPS to modulate microglial reactivity is similar in terms of cytokine release, the underlying mechanisms of any subsequent neuronal insults differ (**Figure 3D**).

TABLE 1 | PANTHER over-representation analysis of fibrinogen regulated genes.

PANTHER GO-Slim Biological Process	Mus musculus – REFLIST (22320)	FG regulated genes (98)	FG regulated genes (expected)	FG regulated genes (over/under)	FG regulated genes (fold enrichment)	(*P*-value)
Phosphate-containing compound metabolic process (GO:0006796)	931	36	4.09	+	>5	2.92E-22
Catabolic process (GO:0009056)	405	27	1.78	+	>5	6.23E-22
Nitrogen compound metabolic process (GO:0006807)	1064	29	4.67	+	>5	2.50E-13
Localization (GO:0051179)	2788	42	12.24	+	3.43	1.66E-11
Transport (GO:0006810)	2658	41	11.67	+	3.51	1.76E-11
Coenzyme metabolic process (GO:0006732)	97	9	0.43	+	>5	1.36E-07
Metabolic process (GO:0008152)	8467	67	37.18	+	1.8	2.26E-07
Immune system process (GO:0002376)	**1480**	**25**	**6.5**	**+**	**3.85**	**8.65E-07**
Cellular process (GO:0009987)	7033	59	30.88	+	1.91	1.04E-06
acyl-CoA metabolic process (GO:0006637)	31	6	0.14	+	>5	1.50E-06
Fatty acid beta-oxidation (GO:0006635)	32	6	0.14	+	>5	1.80E-06
Primary metabolic process (GO:0044238)	6997	57	30.72	+	1.86	8.69E-06
Response to toxic substance (GO:0009636)	55	6	0.24	+	>5	4.29E-05
Nucleobase-containing compound metabolic process (GO:0006139)	3425	35	15.04	+	2.33	1.32E-04
Antigen processing and presentation (GO:0019882)	77	6	0.34	+	>5	2.99E-04
Generation of precursor metabolites and energy (GO:0006091)	290	9	1.27	+	>5	1.30E-03
Fatty acid metabolic process (GO:0006631)	252	8	1.11	+	>5	3.72E-03
Extracellular transport (GO:0006858)	121	6	0.53	+	>5	3.85E-03
Lipid metabolic process (GO:0006629)	966	15	4.24	+	3.54	4.67E-03
Tricarboxylic acid cycle (GO:0006099)	21	3	0.09	+	>5	2.62E-02

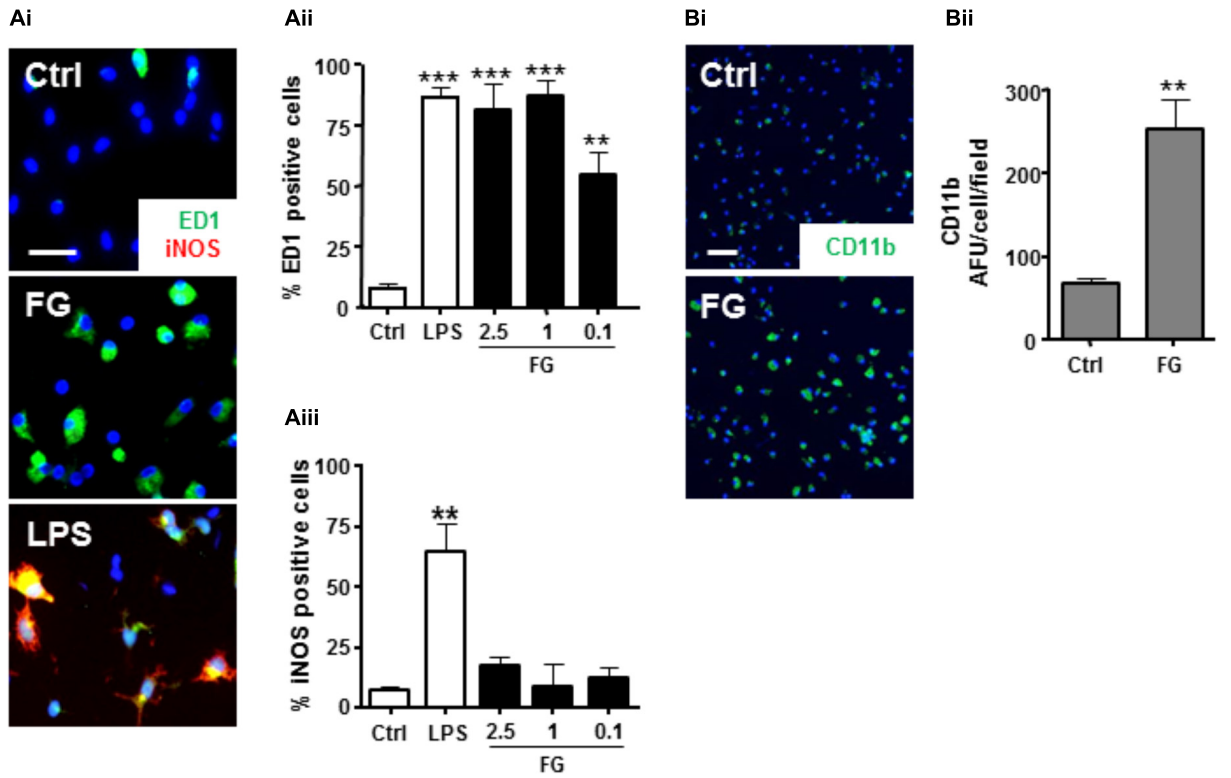

FIGURE 2 | FG induces microglial reactivity. (A) Control primary rat microglia (Ctrl) or microglia exposed to FG (2.5 mg/ml) or LPS (1 μg/ml) for 24 h followed by immunocytochemistry for ED1 and iNOS (Scale bar: 30 μm; **Ai**), and nuclear co-staining with DAPI (blue), quantified as a % percentage of cells expressing ED1 **(Aii)**, or iNOS **(Aiii)**. **(B)** Immunofluorescence of surface CD11b staining in primary microglial cultures following 24 h of FG treatment (Scale bar: 60 μm; **Bi**) and nuclear co-staining with DAPI (blue), quantified as a % percentage of $CD11b^+$ cells, compared with control **(Bii)**. Data represent the mean ± SEM of 5 defined fields from at least three independent experiments. Significance levels are $^{***}p < 0.001$, $^{**}p < 0.01$ compared with relevant control.

Further support for the involvement of microglia in FG-mediated neuronal death, specifically, the secreted factors from microglia, was identified by exposing microglia-depleted ENGCs to conditioned medium from primary microglia cultures (MGCM) exposed to FG (**Figure 3E**). We observed a significant increase in neuronal death when ENGCs were exposed to MGCM from FG-treated microglial cultures when compared to the addition of control MGCM, which could be attenuated by boiling the MGCM prior to its addition to the ENGCs (**Figure 3E**). Carry-over of FG in MGCM to exert a direct effect is also unlikely since negligible FG was detected in FG-MGCM (**Supplementary Figure S4**). Finally, we found it was possible to attenuate the effect of MGCM from FG-treated microglia cultures on ENGCs by pre-incubating the microglia cultures with the caspase-3/7 inhibitor z-VAD-FMK (**Figure 3F**). MG exposed to FG, or LPS, showed caspase-3 activation but no pyknotic nuclei suggesting non-apoptotic activation of caspase-3 (**Supplementary Figure S6**). Taken together, these data strongly support a microglial-mediated mechanism for the observed increase in FG-induced neurotoxicity, centered on the release of soluble factors, and suggests a possible role for non-apoptotic activation of caspase-3 in microglia within this mechanism, as our previous investigations found no significant increase in PI-positive (i.e., dead cells) nuclei in primary microglial cultures exposed to FG (Piers et al., 2011).

FG Induces ER Stress-Associated Neuronal Death via Microglial TNFα Release

Based on our microarray and cytokine release data, one candidate for a soluble released factor from microglia that may enhance neurotoxicity is TNFα. Studies suggest inflammatory cytokines including TNFα can induce ER stress signaling (Xue et al., 2005; Denis et al., 2010; O'Neill et al., 2013; Dandekar et al., 2015). Cleavage of the ER-located caspase-12 during ER stress triggers downstream apoptotic pathways and is implicated in neurodegenerative disease models associated with BBB dysfunction (Nakagawa et al., 2000). Therefore, we investigated a possible role for TNFα in an ER stress associated mechanism of neurotoxicity. Initially, we found that exposure of ENGCs to FG induced an increase in activated caspase-12 expression as measured by western blotting for the cleaved form of the protein (**Figures 4Ai,Aii,Aiii**), to levels comparable with the known ER stress inducers, thapsigargin (a specific inhibitor of the sarco-ER calcium-ATPase, SERCA), or tunicamycin (a blocker of protein glycosylation; Nair et al., 2007; Tu). In

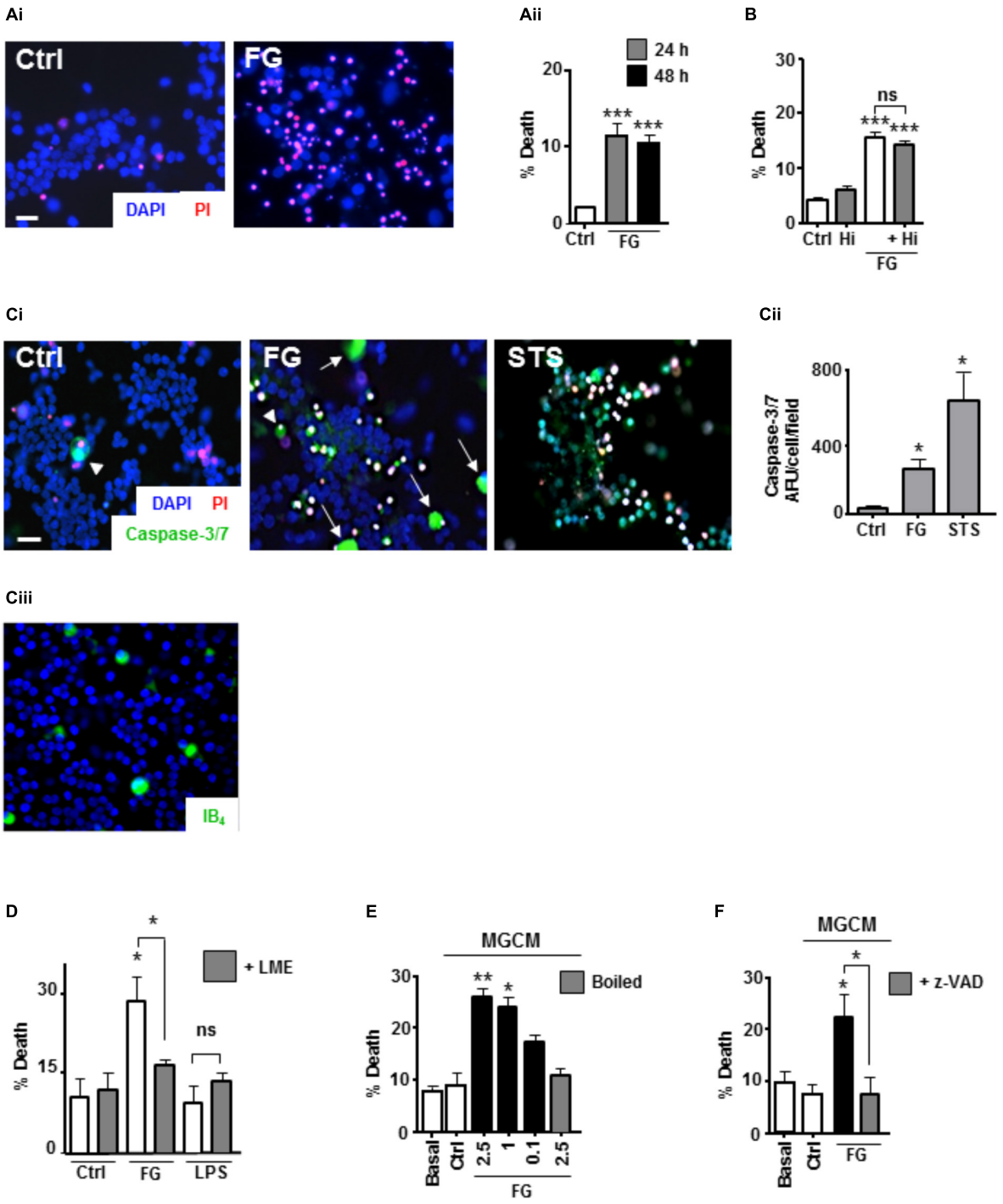

FIGURE 3 | FG-mediated neurotoxicity is dependent on secreted microglial factors. **(A)** Live cell staining with propidium iodide (PI) of ENGCs for analysis of cellular death after FG treatment for 24–48 h (Scale bar: 15 μm; **Ai**), quantified as a percentage of PI^+ cells in the population (**Aii**). **(B)** Quantification of cell death in ENGCs after treatment with 2.5 mg/ml FG for 24 h + /– hirudin (40 U/ml). **(C)** Analysis of caspase 3/7 activity by FAM-DEVD-FMK live cell staining in ENGCs following exposure to FG (2.5 mg/ml) or staurosporine (STS, 0.5 μM; Scale bar: 20 μm) for 24 h, **Ci**. Data were quantified and presented as arbitrary fluorescence units (AFU)/cell/field of view; **Cii**). Confirmation of the presence of microglia in ENGCs with IB_4 cell staining (**Ciii**). All cellular populations were counterstained with Hoechst 33342 (blue). **(D)** Assessment of ENGC death by PI live cell staining after treatment with FG (2.5 mg/ml) or LPS (1 μg/ml) for 24 h before and after microglial ablation (+ LME). **(E)** Analysis of ENGC death by PI live cell staining after exposure to microglial conditioned medium (MGCM) collected from cultures treated for 24 h with FG (0.1–2.5 mg/ml) or untreated (Ctrl). Some MGCM samples from FG treated cultures were boiled to inactivate prior to addition. **(F)** Analysis of ENGC death by PI live cell staining after exposure to MGCM collected from cultures treated for 24 h with FG (2.5 mg/ml) + /– z-VAD-FMK, or untreated (Ctrl). In all graphs, data are the mean ± SEM from at least three independent experiments with internal replicates of at least 3. Significance levels are compared with control condition in each graph unless otherwise indicated, $*p < 0.05$, $**p < 0.01$, $***p < 0.001$.

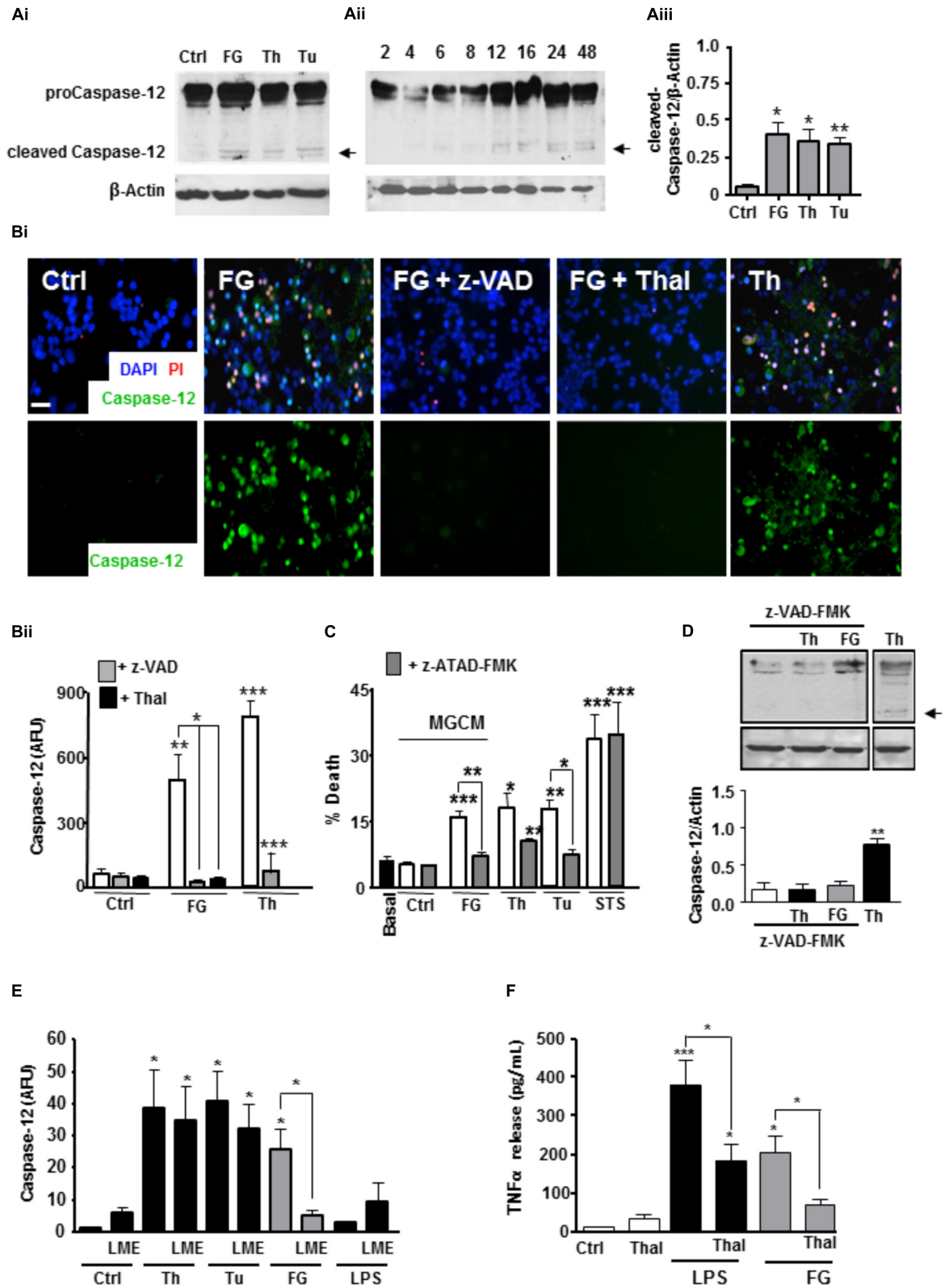

FIGURE 4 | FG inducesneuronal ER stress signaling via microglial TNFα release. **(A)** Expression of pro-caspase 12 (55 kDa) and cleaved active caspase 12 (36 kDa) in ENGCs from control cultures (Ctrl), or cultures treated with FG (2.5 mg/ml), thapsigargin (Th, 2 μM), or tunicamycin (Tu, 1 μg/ml) for 24 h as shown in the

(Continued)

FIGURE 4 | Continued
representative blot **(Ai)**, and quantified by densitometry of cleaved caspase-12 relative to β-Actin levels **(Aiii)**. **Aii** represents a blot showing time course of expression of cleaved caspase-12 in ENGCs treated with FG (2.5 mg/ml) over time (h). **(B)** Analysis of caspase-12 activity by FITC-ATAD-FMK live cell staining in ENGCs following exposure to FG + /− thalidomide (Thal; 40 μM) or z-VAD-FMK (z-VAD; 1 μg/ml), or thapsigargin (Th, 2 μM) for 24 h. **(Bi)**, Scale bar: 20 μm. Data were quantified and presented as arbitrary fluorescence units (AFU)/cell/field of view; **Bii**). **(C)** Analysis of death in ENGCs by PI live cell staining after exposure to microglial conditioned medium (MGCM) collected from cultures treated FG (2.5 mg/ml) or untreated (Ctrl) + /− direct administration of the caspase-12 specific inhibitor z-ATAD-FMK. Th, thapsigargin, 2 μM, Tu, Tunicamycin, 1 μg/ml Staurosporine (STS; 0.5 μM) was used as a positive control for neuronal death. **(D)** Western blot of cleaved caspase-12 in ENGCs following expose to Thapsigargin (Th, 2 μM) or FG (2.5 mg/ml) in the presence of z-VAD-FMK (1μg/ml) showing inhibition of caspase-12 cleavage (arrow). **(E)** Quantification of the relative active caspase-12 fluorescence intensity/cell in ENGC cultures after treatment with Th (2 μM), Tu (1 μg/ml), FG (2.5 mg/ml), or LPS (1 μg/ml) for 24 h, + /− LME pre-treatment for the depletion of microglia (LME). Data are presented in arbitrary fluorescent units (AFU)/cell/field of view). **(F)** ELISA of TNFα secretion from primary microglial cultures following treatment for 24 h with FG (2.5 mg/ml, or LPS (1 μg/ml), co-treated with thalidomide (Thal; 10 μg/ml). In all graphs, data are the mean ± SEM from at least three independent experiments encompassing 5 separate fields of view or from samples from at least three independent experiments. Significance levels are compared with control condition in each graph unless otherwise indicated, $^{*}p < 0.05$, $^{**}p < 0.01$, $^{***}p < 0.001$.

support of these findings, live cell staining experiments of ENGCs after FG treatment identified significant increases in caspase-12 activity, comparable with levels observed after thapsigargin treatment (**Figures 4Bi,Bii**). Furthermore, inhibition of caspase-3/7 with z-VAD-FMK, or specific inhibition of TNFα synthesis by thalidomide treatment, was sufficient to attenuate the increased levels of caspase-12 expression (**Figures 4Bi,Bii**), supporting the hypothesis that a released factor involved in the induction of neurotoxic ER stress signaling was TNFα. In confirmation of ER stress activation, we found CHOP transcripts were also significantly enhanced in microglia exposed to FG (2.5 mg/ml) or LPS (1 μg/ml) for 24 h or Thapsigargin (2μM, as a positive activator of ER stress) (**Supplementary Figure S5**).

In support of the critical induction of these signaling cascades in the observed FG-mediated neurotoxicity, MGCM from cultures exposed to FG were unable to induce significant neuronal toxicity in ENGCs pre-treated with the caspase-12 specific inhibitor z-ATAD-FMK (**Figure 4C**). Inhibition of caspase-3/7 also reduced caspase-12 cleavage in ENGCs, suggestive of an upstream mechanism involving microglial activation (**Figure 4D**). Concomitantly, removal of microglia from ENGCs prevent FG-mediated induction of caspase-12, further supporting a non-cell autonomous mechanism (**Figure 4E**). Moreover, thalidomide significantly reduced TNFα secretion from microglia treated with FG (**Figure 4F**). Together, these findings suggest a signaling cascade initiated by FG-mediated microglial activation leading to a non-cell autonomous neurotoxicity via released TNFα and subsequent induction of neuronal ER stress signaling.

DISCUSSION

After confirming an immune/inflammatory consequence in microglia after exposure to FG, both through microarray analysis of a microglial cell line and proteome analysis of secreted cytokines in primary cultures, we identified a non-cell autonomous signaling cascade capable of inducing neurotoxicity through a mechanism that depended on microglial-released TNFα and neuronal ER stress. Importantly we were able to pharmacologically inhibit the FG-induced neurotoxicity either by targeting TNFα transcription with the putative inhibitor, thalidomide, or by blocking neuronal caspase-12 activity with the specific inhibitory peptide z-ATAD-FMK. It cannot be discounted that thalidomide may also block transcription of other inflammatory mediators such as IL-6 or that other factors play a role in death cascades induced by FG. For example we show also that IL-6 is secreted by microglia in response to FG. However, thalidomide has been shown to selectively inhibit TNFα secretion from immune cells (Sampaio et al., 1991) strongly suggesting TNFα plays a pivotal role in the inflammatory-linked neurotoxicity observed here. Linkage between increased pro-inflammatory cytokine release, particularly TNFα and IL-6, and the induction of ER stress signaling is supported by others (Xue et al., 2005; Denis et al., 2010; Lourenco et al., 2013; O'Neill et al., 2013). Interestingly elevated systemic fibrinogen, TNFα and IL-6 in mid-life have also been linked with brain shrinkage, cognitive decline, and AD in later life (Marsland et al., 2008; Holmes et al., 2009). Furthermore, ER stress can mediate upregulation of pro-inflammatory cytokines (Chen et al., 2013; Morris et al., 2018) and neuronal ER stress has been linked to inflammation and AD pathology (Salminen et al., 2009). Whilst in rodents, activation of caspase 12 leads to ER stress, in humans, the gene may produce a truncated non-functional protein; caspase 4 in humans is regarded as the homolog for caspase 12 in rodents (Gao and Wells, 2013). Human cell lines have been shown to respond to AD-linked amyloid beta peptides, with ER stress induced caspase-4 activation similarly to the activation of ER stress and subsequent caspase-12 by AD-linked amyloid beta peptides in rodents (Nakagawa et al., 2000). Thus future work on human microglia should take into consideration the role of both caspase 4 (Hitomi et al., 2004) and caspase 12 in fibrinogen-induced activation of microglia.

Taken together our present findings are the first to directly link FG induced release of TNFα to an induction of neuronal ER stress. The current neurotoxicity results are unlikely to be due to a direct FG crossover in the MGCM because blotting of the conditioned medium for FG revealed extremely low levels of the protein, below the effective concentration.

It is of course highly likely that other unidentified factors contribute to the mechanism. Previously we identified that TNFα-induced neuronal death cascades required a cofactor (Taylor et al., 2005), and indeed, Denis et al. (2010) found TNFα alone was unable to induce a full ER stress response. Interestingly, however,

TNF inhibitors have been recently proposed as a repurposed therapy for dementias such as AD (Mason et al., 2018). Furthermore, as mentioned above, IL-6 was also secreted in response to FG and elevation of this cytokine has been implicated in a number of neurodegenerative diseases including AD (Rothaug et al., 2016). Increasing evidence links changes in brain parenchymal and plasma levels of fibrinogen with microglial and inflammatory responses in a number of neurodegenerative diseases including multiple sclerosis (Adams et al., 2007; Ryu and McLarnon, 2009; Acuña et al., 2017) and Alzheimer's disease (Cortes-Canteli et al., 2012) and following stroke (Luan et al., 2017). Here we present new evidence of a pathway activated in microglia by fibrinogen which has ramifications for neuronal survival and which has not yet been observed in these conditions.

CONCLUSION

Our findings suggest a FG-induced TNFα-non-cell autonomous microglial-neuronal ER stress mediated pathway with implications for early signaling cascades activated in inflammatory-mediated dementias such as AD.

AUTHOR CONTRIBUTIONS

JP and EE conceived the project. JP, EE, and TP designed the experiments. TP, EE, CV-L, and IS carried out the experiments. TP, EE, CV-L, and MM carried out the data analysis. JH facilitated genome data analysis. JP and JH obtained the funding. TP, EE, and JP wrote the paper.

FUNDING

This work was supported by funding from Aims2Cure, United Kingdom, the Brain Research Trust, United Kingdom, the Medical Research Council, United Kingdom, and Ministerio de Educación del Perú - PRONABEC (Programa Nacional de Becas y Crédito Educativo).

SUPPLEMENTARY MATERIAL

The Supplementary Material for this article can be found online at: https://www.frontiersin.org/articles/10.3389/fncel.2018.00404/full#supplementary-material

REFERENCES

Acuña, J. M., Hidalgo de la Cruz, M., Lozano Ros, A., Prasc Tapia, S., Martinez Gines, M. L., and de Andres Frutos, C. D. (2017). Elevated plasma fibrinogen levels in multiple sclerosis patients during relapse. *Mult. Scler. Relat. Disord.* 18, 157–160. doi: 10.1016/j.msard.2017.09.033

Adams, R. A., Schachtrup, C., Davalos, D., Tsigelny, I., and Akassoglou, K. (2007). Fibrinogen signal transduction as a mediator and therapeutic target in inflammation: lessons from multiple sclerosis. *Curr. Med. Chem.* 14, 2925–2936. doi: 10.2174/092986707782360015

Ahn, S. J., Anrather, J., Nishimura, N., and Schaffer, C. B. (2018). Diverse inflammatory response after cerebral microbleeds includes coordinated microglial migration and proliferation. *Stroke* 49, 1719–1726. doi: 10.1161/STROKEAHA.117.020461

Akiyama, H., and McGeer, P. L. (1990). Brain microglia constitutively express beta-2 integrins. *J. Neuroimmunol.* 30, 81–93. doi: 10.1016/0165-5728(90)90055-R

Binnie, C. G., and Lord, S. T. (1993). The fibrinogen sequences that interact with thrombin. *Blood* 15, 3186–3192.

Bitzer, M., von Gersdorff, G., Liang, D., Dominguez-Rosales, A., Beg, A. A., Rojkind, M., et al. (2000). A mechanism of suppression of TGF-beta/SMAD signaling by NF-kappa B/RelA. *Genes Dev.* 14, 187–197.

Chen, Y., Chen, M., Wu, Z., and Zhao, S. (2013). Ox-LDL induces ER stress and promotes the adipokines secretion in 3T3-L1 adipocytes. *PLoS One* 22:e81379. doi: 10.1371/journal.pone.0081379

Cortés, N., Andrade, V., and Maccioni, R. B. (2018). Behavioral and neuropsychiatric disorders in Alzheimer's disease. *J. Alzheimers Dis.* 63, 899–910. doi: 10.3233/JAD-180005

Cortes-Canteli, M., Zamolodchikov, D., Ahn, H. J., Strickland, S., and Norris, E. H. (2012). Fibrinogen and altered hemostasis in Alzheimer's brain. *J. Alzheimers Dis.* 32, 599–608. doi: 10.3233/JAD-2012-120820

Dandekar, A., Mendez, R., and Zhang, K. (2015). Cross talk between ER stress, oxidative stress, and inflammation in health and disease. *Methods Mol. Biol.* 1292, 205–214. doi: 10.1007/978-1-4939-2522-3_15

Darzynkiewicz, Z., Bedner, E., Smolewski, P., Lee, B. W., and Johnson, G. L. (2002). Detection of caspases activation in situ by fluorochrome-labeled inhibitors of caspases (FLICA). *Methods Mol. Biol.* 203, 289–299. doi: 10.1385/1-59259-179-5:289

De Groot, C. J., Montagne, L., Barten, A. D., Sminia, P., and Van Der Valk, P. (1999). Expression of transforming growth factor (TGF)-beta1, -beta2, and -beta3 isoforms and TGF-beta type I and type II receptors in multiple sclerosis lesions and human adult astrocyte cultures. *J. Neuropathol. Exp. Neurol.* 58, 174–187. doi: 10.1097/00005072-199902000-00007

Denis, R. G., Arruda, A. P., Romanatto, T., Milanski, M., Coope, A., Solon, C., et al. (2010). TNF-α transiently induces endoplasmic reticulum stress and an incomplete unfolded protein response in the hypothalamus. *J. Neurosci.* 170, 1035–1044. doi: 10.1016/j.neuroscience.2010.08.013

Du, P., Kibbe, W. A., and Lin, S. M. (2008). lumi: a pipeline for processing Illumina microarray. *Bioinformatics* 24, 1547–1548. doi: 10.1093/bioinformatics/btn224

Gao, J., and Wells, J. A. (2013). "Chapter 510 – caspase-4 and caspase-5," in *Handbook of Proteolytic Enzymes*, eds A. J. Barrett, N. D. Rawlings, and J. F. Woessner (Cambridge, MA: Academic Press), 2265–2269.

Gerakis, Y., and Hetz, C. (2018). Emerging roles of ER stress in the etiology and pathogenesis of Alzheimer's disease. *FEBS J.* 285, 995–1011. doi: 10.1111/febs.14332

Gillett, S. R., McClure, L. A., Callas, P. W., Thacker, E. L., Unverzagt, F. W., Wadley, V. G., et al. (2018). Haemostasis biomarkers and incident cognitive impairment: the REGARDS study. *J. Thromb. Haemost.* doi: 10.1111/jth.14138 [Epub ahead of print].

Hainsworth, A. H., Minett, T., Andoh, J., Forster, G., Bhide, I., Barrick, T. R., et al. (2017). Neuropathology of white matter lesions, blood-brain barrier dysfunction and dementia. *Stroke* 48, 2799–2804. doi: 10.1161/STROKEAHA.117.018101

Hitomi, J., Katayama, T., Eguchi, Y., Kudo, T., Taniguchi, M., Koyama, Y., et al. (2004). Involvement of caspase-4 in endoplasmic reticulum stress-induced apoptosis and Aβ-induced cell death. *J. Biol. Chem.* 165, 347–356. doi: 10.1083/jcb.200310015

Holmes, C., Cunningham, C., Zotova, E., Woolford, J., Dean, C., Kerr, S., et al. (2009). Systemic inflammation and disease progression in Alzheimer disease. *Neurology* 73, 768–774. doi: 10.1212/WNL.0b013e3181b6bb95

Hooper, C., Pinteaux-Jones, F., Fry, V. A., Sevastou, I. G., Baker, D., Heales, S. J., et al. (2009). Differential effects of albumin on microglia and macrophages; implications for neurodegeneration following blood-brain barrier damage. *J. Neurochem.* 109, 694–705. doi: 10.1111/j.1471-4159.2009.05953.x

Huang, C. F., Li, G., Ma, R., Sun, S. G., and Chen, J. G. (2008). Thrombin-induced microglial activation contributes to the degeneration of nigral dopaminergic neurons in vivo. *Neurosci. Bull.* 24, 66–72. doi: 10.1007/s12264-008-0066-x

Jebelli, J., Piers, T. M., and Pocock, J. M. (2015). Selective depletion of microglia from cerebellar granule cells using leucine methyl ester. *J. Vis. Exp.* 101:e52983. doi: 10.3791/52983

Jensen, T., Kierulf, P., Sandset, P. M., Klingenberg, O., Joø, G. B., Godal, H. C., et al. (2007). Fibrinogen and fibrin induce synthesis of proinflammatory cytokines from isolated peripheral blood mononuclear cells. *Thromb. Haemost.* 97, 822–829. doi: 10.1160/TH07-01-0039

Lee, J. W., Namkoong, K. W., Kim, H. K., Hwang, D. W., Na, H. R., Ha, S. A., et al. (2007). Fibrinogen gamma-A chain precursor in CSF: a candidate biomarker for Alzheimer's disease. *BMC Neurol.* 7:14. doi: 10.1186/1471-2377-7-14

Leeuwis, A. E., Prins, N. D., Hooghiemstra, A. M., Benedictus, M. R., Scheltens, P., Barkhof, F., et al. (2017). Microbleeds are associated with depressive symptoms in Alzheimer's disease. *Alzheimers Dement.* 10, 112–120. doi: 10.1016/j.dadm.2017.11.006

Lindholm, D., Wootz, H., and Korhonen, L. (2006). ER stress and neurodegenerative diseases. *Cell Death Differ.* 13, 385–392. doi: 10.1038/sj.cdd.4401778

Lipinski, B., and Sajdel-Sulkowska, E. M. (2006). New insights into Alzheimer's disease: demonstration of fibrin(ogen)-serum albumin insoluble deposits in brain tissue. *Alzheimers Dis. Assoc. Disord.* 20, 323–326. doi: 10.1097/01.wad.0000213844.21001.a2

Lourenco, M. V., Clarke, J. R., Frozza, R. L., Bomfim, T. R., Forny-Germano, L., Batista, A. F., et al. (2013). TNF-α mediates PKR-dependent memory impairment and brain IRS-1 inhibition induced by Alzheimer's β-amyloid oligomers in mice and monkeys. *Cell Metab.* 18, 831–843. doi: 10.1016/j.cmet.2013.11.002

Luan, X., Shen, H., Zhao, K., Qiu, H., Chen, H., and He, J. (2017). Plasma fibrinogen: an independent risk factor for post-stroke depression. *Neuropsychiatry* 7, 832–838. doi: 10.4172/Neuropsychiatry.1000288

Marsland, A. L., Gianaros, P. J., Abramowitch, S. M., Manuck, S. B., and Hariri, A. R. (2008). Interleukin-6 covaries inversely with hippocampal grey matter volume in middle-aged adults. *Biol. Psychiatry* 64, 84–90. doi: 10.1016/j.biopsych.2008.04.016

Mason, A., Holmes, C., and Edwards, C. J. (2018). Inflammation and dementia: using rheumatoid arthritis as a model to develop treatments? *Autoimmun. Rev.* doi: 10.1016/j.autrev.2018.04.001 [Epub ahead of print].

Miners, J. S., Schulz, I., and Love, S. (2018). Differing associations between Aβ accumulation, hypoperfusion, blood-brain barrier dysfunction and loss of PDGFRB pericyte marker in the precuneus and parietal white matter in Alzheimer's disease. *J. Cereb. Blood Flow Metab.* 38, 103–115. doi: 10.1177/0271678X17690761

Morris, G., Puri, B. K., Walder, K., Berk, M., Stubbs, B., Maes, M., et al. (2018). The endoplasmic reticulum stress response in neuroprogressive diseases: emerging pathophysiological role and translational implications. *Mol. Neurobiol.* doi: 10.1007/s12035-018-1028-6 [Epub ahead of print].

Nair, S., Xu, S., Shen, G., Hebbar, V., Gopalakrishnan, A., Hu, R., et al. (2007). Toxicogenomics of endoplasmic reticulum stress inducer tunicamycin in the small intestine and liver of Nrf2 knockout and C57BL/6J mice. *Toxicol. Lett.* 168, 21–39. doi: 10.1016/j.toxlet.2006.10.012

Nakagawa, T., Zhu, H., Morishima, N., Li, E., Xu, J., Yankner, B. A., et al. (2000). Caspase-12 mediates endoplasmic-reticulum-specific apoptosis and cytotoxicity by amyloid-beta. *Nature* 403, 98–103. doi: 10.1038/47513

O'Neill, C. M., Lu, C., Corbin, K. L., Sharma, P. R., Dula, S. B., Carter, J. D., et al. (2013). Circulating levels of IL-1B + IL-6 cause ER stress and dysfunction in islets from prediabetic male mice. *Endocrinology* 154, 3077–3088. doi: 10.1210/en.2012-2138

Owen, J. L., Criscitiello, M. F., Libreros, S., Garcia-Areas, R., Guthrie, K., Torroella-Kouri, M., et al. (2011). Expression of the inflammatory chemokines CCL2, CCL5 and CXCL2 and the receptors CCR1-3 and CXCR2 in T lymphocytes from mammary tumour-bearing mice. *Cell Immunol.* 270, 172–182. doi: 10.1016/j.cellimm.2011.05.004

Piers, T. M., Heales, S. J., and Pocock, J. M. (2011). Positive allosteric modulation of metabotropic glutamate receptor 5 down-regulates fibrinogen-activated microglia providing neuronal protection. *Neurosci. Lett.* 505, 140–145. doi: 10.1016/j.neulet.2011.10.007

Rothaug, M., Becker-Pauly, C., and Rose-John, S. (2016). The role of interleukin-6 signaling in nervous tissue. *Biochim. Biophys. Acta* 1863, 1218–1227. doi: 10.1016/j.bbamcr.2016.03.018

Ryu, J. K., and McLarnon, J. G. (2009). A leaky blood-brain barrier, fibrinogen infiltration and microglial reactivity in inflamed Alzheimer's disease brain. *J. Cell. Mol. Med.* 13, 2911–2925. doi: 10.1111/j.1582-4934.2008.00434.x

Salminen, A., Kauppinen, A., Suuronen, T., Kaarniranta, K., and Ojala, J. (2009). ER stress in Alzheimer's disease: a novel neuronal trigger for inflammation and Alzheimer's pathology. *J. Neuroinflammation* 6, 41–45. doi: 10.1186/1742-2094-6-41

Sampaio, E. P., Sarno, E. N., Galilly, R., Cohn, Z. A., and Kaplan, G. (1991). Thalidomide selectively inhibits tumor necrosis factor α production by stimulated human monocytes. *J. Exp. Med.* 173, 699–703. doi: 10.1084/jem.173.3.699

Schachtrup, C., Ryu, J. K., Helmrick, M. J., Vagena, E., Galanakis, D. K., Degen, J. L., et al. (2010). Fibrinogen triggers astrocyte scar formation by promoting the availability of active TGF-(after vascular damage. *J. Neurosci.* 30, 5843–5854. doi: 10.1523/JNEUROSCI.0137-10.2010

Shen, X., Burguillos, M. A., and Joseph, B. (2017). Guilt by association, caspase-3 regulates microglia polarisation. *Cell Cycle* 16, 306–307. doi: 10.1080/15384101.2016.1254979

Smiley, S. T., King, J. A., and Hancock, W. W. (2001). Fibrinogen stimulates macrophage chemokine secretion through toll-like receptor 4. *J. Immunol.* 167, 2887–2894. doi: 10.4049/jimmunol.167.5.2887

Streit, W. J. (1990). An improved staining method for rat microglial cells using the lectin from *Griffonia simplicifolia* (GSA I-B4). *J. Histochem. Cytochem.* 38, 1683–1686. doi: 10.1177/38.11.2212623

Sweeney, M. D., Sagare, A. P., and Zlokovic, B. V. (2018). Blood-brain barrier breakdown in Alzheimer disease and other neurodegenerative disorders. *Nat. Rev. Neurol.* 14, 133–150. doi: 10.1038/nrneurol.2017.188

Taylor, D. L., Jones, F., Kubota, E. S., and Pocock, J. M. (2005). Stimulation of microglial metabotropic glutamate receptor mGlu2 triggers tumor necrosis factor alpha-induced neurotoxicity in concert with microglial-derived Fas ligand. *J. Neurosci.* 25, 2952–2964. doi: 10.1523/JNEUROSCI.4456-04.2005

van Oijen, M., Witteman, J. C., Hofman, A., Koudstaal, P. J., and Breteler, M. M. (2005). Fibrinogen is associated with an increased risk of Alzheimer's disease and vascular dementia. *Stroke* 36, 2637–2641. doi: 10.1161/01.STR.0000189721.31432.26

Walker, K. A., Hoogeveen, R. C., Folsom, A. R., Ballantyne, C. M., Knopman, D. S., Windham, B. G., et al. (2017). Midlife systemic inflammatory markers are associated with late-life brain volume. The ARIC study. *Neurology* 89, 2262–2270. doi: 10.1212/WNL.0000000000004688

Weinstein, J. R., Zhang, M., Kutlubaev, M., Lee, R., Bishop, C., Andersen, H., et al. (2009). Thrombin-induced regulation of CD95(Fas) expression in the N9 microglial cell line: evidence for involvement of proteinase-activated receptor(1) and extracellular signal-regulated kinase 1/2. *Neurochem. Res.* 34, 445–452. doi: 10.1007/s11064-008-9803-9

Werring, D. J., Gregoire, S. M., and Cipolotti, L. (2010). Cerebral microbleeds and vascular cognitive impairment. *J. Neurol. Sci.* 299, 131–135. doi: 10.1016/j.jns.2010.08.034

Xu, G., Zhang, S., Fan, X., and Liu, X. (2008). Plasma fibrinogen is associated with cognitive decline and risk for dementia in patients with mild cognitive impairment. *Int. J. Clin. Pract.* 62, 1070–1075. doi: 10.1111/j.1742-1241.2007.01268.x

Xue, X., Piao, J. H., Nakajima, A., Sakon-Komazawa, S., Kojima, Y., Mori, K., et al. (2005). Tumour necrosis factor alpha (TNFα) induces the unfolded protein response (UPR) in a reactive oxygen species (ROS)-dependent fashion, and the UPR counteracts ROS accumulation by TNFalpha. *J. Biol. Chem.* 280, 33917–33925. doi: 10.1074/jbc.M505818200

Conflict of Interest Statement: The authors declare that the research was conducted in the absence of any commercial or financial relationships that could be construed as a potential conflict of interest.

frontiers in Cellular Neuroscience

ORIGINAL RESEARCH
published: 20 November 2018
doi: 10.3389/fncel.2018.00433

Sex- and Development-Dependent Responses of Rat Microglia to Pro- and Anti-inflammatory Stimulation

Starlee Lively[1], Raymond Wong[1,2], Doris Lam[1,2†] and Lyanne C. Schlichter[1,2]**

[1] Division of Genetics & Development, Krembil Research Institute, University Health Network, Toronto, ON, Canada,
[2] Department of Physiology, University of Toronto, Toronto, ON, Canada

OPEN ACCESS

Edited by:
Liliana Bernardino, Universidade da Beira Interior, Portugal

Reviewed by:
Dora Brites, Universidade de Lisboa, Portugal
Christiane Charriaut-Marlangue, Institut National de la Santé et de la Recherche Médicale (INSERM), France

***Correspondence:**
Starlee Lively
Starlee.Lively@uhnresearch.ca
Lyanne C. Schlichter
Lyanne.Schlichter@uhnresearch.ca

†Present address:
Doris Lam, Physical and Life Sciences Directorate, Lawrence Livermore National Laboratory, Livermore, CA, United States

Received: *27 July 2018*
Accepted: *31 October 2018*
Published: *20 November 2018*

Citation:
Lively S, Wong R, Lam D and Schlichter LC (2018) Sex- and Development-Dependent Responses of Rat Microglia to Pro- and Anti-inflammatory Stimulation. Front. Cell. Neurosci. 12:433. doi: 10.3389/fncel.2018.00433

Addressing potential sex differences in pre-clinical studies is crucial for developing therapeutic interventions. Although sex differences have been reported in epidemiological studies and from clinical experience, most pre-clinical studies of neuroinflammation use male rodents; however, sexual dimorphisms in microglia might affect the CNS inflammatory response. Developmental changes are also important and, in rodents, there is a critical period of sexual brain differentiation in the first 3 weeks after birth. We compared rat microglia from sex-segregated neonates (P1) and at about the time of weaning (P21). To study transitions from a basal homeostatic state (untreated), microglia were subjected to a pro-inflammatory (IFNγ + TNFα) or anti-inflammatory (IL-4) stimulus. Responses were compared by quantifying changes in nitric oxide production, migration, and expression of nearly 70 genes, including inflammatory mediators and receptors, inflammasome molecules, immune modulators, and genes that regulate microglial physiological functions. No sex differences were seen in transcriptional responses in either age group but the IL-4-evoked migration increase was larger in male cells at both ages. Protein changes for the hallmark molecules, NOS2, COX-2, PYK2 and CD206 correlated with mRNA changes. P1 and P21 microglia showed substantial differences, including expression of genes related to developmental roles. That is, P21 microglia had a more mature phenotype, with higher basal and stimulated levels of many inflammatory genes, while P1 cells had higher expression of phagocytosis-related molecules. Nevertheless, cells of both ages responded to IL-4 and IFNγ + TNFα. We examined the Kv1.3 potassium channel (a potential target for modulating neuroinflammation) and the Kir2.1 channel, which regulate several microglia functions. Kv1.3 mRNA (*Kcna3*) was higher at P21 under all conditions and male P21 cells had higher mRNA and Kv currents in response to IFNγ + TNFα. Overall, numerous transcriptional and functional responses of microglia changed during the first 3 weeks after birth but few sex-dependent changes were seen.

Keywords: microglial activation, brain development, IFNγ plus TNFα, transcription profiling, IL-4, sex, female, ion channels

INTRODUCTION

Increasingly, it is recognized that sex can profoundly influence both the susceptibility and response to disease (Ober et al., 2008; Regitz-Zagrosek, 2012). Consequently, funding and government agencies have begun to mandate that both females and males be used in pre-clinical and clinical studies. Concerns about sexual dimorphisms extend to the central nervous system (CNS), where disparities are seen in the prevalence, severity, and outcomes of several diseases and disorders (Bilbo, 2018). Innate and adaptive immune responses contribute to the pathogenesis and severity of many CNS disorders (Shabab et al., 2017; Skaper et al., 2018) and there is growing evidence for sex differences in inflammatory responses both peripherally and in the CNS (Hanamsagar and Bilbo, 2016; Klein and Flanagan, 2016).

Sex differences arise from both chromosomal and hormonal influences. Genes on the sex chromosomes play essential roles in sex differentiation of the CNS, especially the male-inducing SRY gene (Manoli and Tollkuhn, 2018). Also, the X chromosome has a disproportionately high number of immune-related genes (Bianchi et al., 2012). In females, Barr body formation silences alleles on the extra X chromosome to prevent gene over-expression (Berletch et al., 2011) but genes escaping this inactivation might also confer sex-dependent differences. Early developmental and hormonal changes can also contribute to sex differences in the brain. Male rodents experience a surge in testosterone shortly before birth, which dissipates within a few hours and then sex differences begin to emerge. The testosterone surge influences development of neural cells and plays important organizational roles in establishing sexual dimorphisms in neural circuitry, notably in areas responsible for sexually divergent behaviors (Clarkson and Herbison, 2016). CNS changes include a transient enlargement of the parietal cortex, hippocampus and amygdala in males, and a transient increase in the number of microglia in these regions (Schwarz et al., 2012). Not enough is known about whether there are sex differences in responses of individual CNS cell types. For instance, both genetic differences and early exposure to sex hormones have the potential to alter microglial responses to inflammatory stimuli, and it is possible that such changes are sustained after they are removed from the brain.

Microglia react to CNS damage by acquiring characteristics conducive to dealing with altered homeostasis (Colonna and Butovsky, 2017; Li and Barres, 2018). Responses include receptor-mediated signaling that can change their morphology, migratory and phagocytic capacities, proliferation, expression of intracellular enzymes and antigen-presenting surface receptors, and release of pro- and anti-inflammatory molecules into the extracellular environment (Kabba et al., 2018; Li and Barres, 2018). A pro-inflammatory phenotype can be induced in neonatal microglia using a combination of interferon-γ (IFNg) and tumor necrosis factor-α (TNFα) (IFNγ + TNFα; 'I+T') *in vitro* (Spanaus et al., 1998; Lam et al., 2017). As recently summarized (Lively and Schlichter, 2018), both cytokines are rapidly up-regulated after acute CNS damage and are especially relevant in the absence of pathogenic organisms. Isolated microglia can also be skewed to various anti-inflammatory states by interleukin (IL)-4, IL-10, transforming growth factor β1 (TGFβ1) or glucocorticoids, and then they release immune mediators that promote scavenging, inflammation resolution, and repair (Kabba et al., 2018).

Microglial responses are routinely studied *in vitro* but most often using cells isolated from neonatal pups. Based on intrinsic differences at the chromosome level and early developmental and hormonal changes, we compared neonatal (P1) and prepubertal (P21) rat microglia and asked whether they show sexually dimorphic responses to I+T and IL-4. These ages were chosen for several reasons. First, microglia have very different morphologies and functions at these times. At birth, microglia are amoeboid, with or without short processes; and they are highly migratory and phagocytic, actively engulfing apoptotic neurons (Colonna and Butovsky, 2017; Li and Barres, 2018). Second, by P20 (just before weaning), the rat cortex has reached 90% of its final weight, neurons have migrated to their appropriate positions, synaptogenesis and myelination are well underway, and intriguingly, the regenerative resiliency observed in younger animals is lost (Semple et al., 2013). Third, by P20, rodent microglia are more ramified, and the main homeostatic functions are surveillance, synaptic pruning, and promoting oligodendrocyte progenitor cell survival and differentiation (Colonna and Butovsky, 2017; Li and Barres, 2018).

To assess the initial state and stimulus-evoked responses, we quantified transcript expression of a wide range of inflammatory mediators, immune receptors and modulators; and molecules related to microglia physiological functions, including phagocytosis and production of reactive oxygen species. Although microglia of both sexes and ages showed many transcriptional changes in response to I+T and IL-4; no sex differences were apparent before or after stimulation. In the age comparison (P1 versus P21), we found substantial differences in gene expression, with or without inflammatory stimuli. Last, we examined expression of two K^+ channels (Kv1.3/*Kcna3*, Kir2.1/*Kcnj2*) and the Kv and Kir currents (at P21), which are known to regulate some microglial functions that are important during the first 3 weeks after birth. The only sex difference was that the I+T-induced increase in Kv current in P21 microglia was higher in males. The only age difference was that *Kcna3* expression was higher at P21 under all conditions. Overall, the results suggest that there are early developmental changes in microglia and their inflammatory responses that persist *in vitro*. However, if there are sex differences at these times, most were not manifest in isolated rat microglia.

MATERIALS AND METHODS

All procedures were performed in accordance with guidelines established by the Canadian Council on Animal Care; and were approved by the University Health Network Animal Care Committee (animal protocol #914).

Microglia Cultures and Treatments

Sprague-Dawley rats (Charles River; St Constant, QC, Canada) were disaggregated by sex on the basis of the presence of gonads (P21) or anogenital distance (P1; (Jackson, 1912). For P1 animals, tail snips were sent to Transnetyx, Inc. (Cordova, TN, United States)[1] where they confirmed the sex using real-time PCR with rat-specific primers for the *Sry* gene: GGGACAACAACCTACACACTATCAT (forward primer), TGTCCACAGGCTGTAAATAAATGCT (reverse primer).

Cell Cultures

Neonatal microglia (P1) were isolated using the same procedures as in our recent papers (Lam et al., 2017; Lively and Schlichter, 2018). In our hands, these methods yield 98–100% microglial purity, as determined by labeling with tomato lectin or antibodies against Iba1 or CD11b (e.g., Siddiqui et al., 2012, 2016; Lively et al., 2018). For instance, we very recently stained for CD11b and DAPI, and showed essentially pure microglia in these cultures (Lively and Schlichter, 2018).

Prepubertal (P21) microglia were isolated after rats were deeply anesthetized using isoflurane and killed by decapitation. About 400 mg of brain tissue from one cortical hemisphere was dissociated using a Neural Tissue Dissociation Kit (Miltenyi #130-092-628). Myelin was removed with myelin-specific magnetic beads (Miltenyi #130-105-634), and the cell suspension was incubated with CD11b magnetic microbeads (Miltenyi #130-105-634) to capture microglia. Microglia were seeded in MEM with 10% FBS and incubated for 2–3 days, at which time most were unipolar.

Stimulation

We chose the cytokines, their concentrations and duration of treatment based on numerous studies from our laboratory (e.g., Lam et al., 2017; Lively and Schlichter, 2018) and others (Spanaus et al., 1998). The rationale for using I+T is detailed in our recent paper (Lively and Schlichter, 2018). In brief, both cytokines are rapidly elevated in numerous *in vivo* rodent models of CNS damage and disease (Benveniste and Benos, 1995; Barcia et al., 2011; Woodcock and Morganti-Kossmann, 2013). Moreover, our recent *in vitro* studies show that I+T evokes numerous transcriptional and functional changes that could have important consequences for microglial roles after CNS damage (Siddiqui et al., 2016). IL-4 is well known to exert anti-inflammatory actions on rodent microglia (Colton, 2009) and there is considerable information about the molecular and functional changes it evokes. For instance, the dose of IL-4 used here increases migration, invasion (Lively and Schlichter, 2013), and Kv1.3 channel expression and current (Lam et al., 2017).

In the present study, microglia were left untreated (control, CTL) or incubated with 20 ng/mL IFNγ plus 50 ng/mL TNFα (I+T) or with 20 ng/mL IL-4. Treatments were 24 h for mRNA, protein and functional analyses (nitric oxide [NO] production, migration), as before (Lam et al., 2017; Lively and Schlichter, 2018). A longer time (30 h) was used for patch-clamp analysis to allow for channel trafficking and potential post-translational modifications, as before (Lam et al., 2017; Lively et al., 2018).

Staining

Procedures were the same as in our recent papers (Lam et al., 2017; Lively and Schlichter, 2018). In brief, microglia on coverslips (8×10^4 cells/coverslip; 5–6 independent cultures used for each sex and age) were quickly washed in PBS, fixed in 4% paraformaldehyde (PFA; Electron Microscopy Sciences, Hatfield, PA, United States; Cat# 15710), washed again in PBS, and then permeabilized with 0.2% Triton X-100. The F-actin label, Acti-stain 488 phalloidin (1:100 in PBS; Cytoskeleton Inc., RRID:SCR_013532; Cat# PHDG1-A) was added for 1 h, and then the nuclear dye, 4′,6-diamidino-2-phenylindole (DAPI; 1:3000 in PBS; Sigma-Aldrich; Cat# D9542) was added for 5 min. Coverslips were mounted on glass slides with DAKO mounting medium (Agilent-Dako, RRID:SCR_013530; Cat# S302380-2) and stored in the dark at 4°C. Images were acquired with a Zeiss 880 confocal microscope (model LSM880; Zeiss, Oberkochen, Germany) and Zen software (version 2.3 SPI; Zeiss, Toronto, ON, Canada).

Functional Assessment

Nitric Oxide Production

The colorimetric Griess assay was used to measure nitrite (Lam et al., 2017; Lively and Schlichter, 2018). Briefly, microglia (8×10^4 cells/coverslip; 17–19 independent cultures for each sex at P1; 9–13 independent cultures for each sex at P21) were incubated for 24 h with I+T or IL-4 (as above) and then aliquots of the supernatants were added to 96-well plates containing 1% sulfanilic acid (Sigma-Aldrich; Cat#86090). After adding 0.1% *N*-(1-naphthyl)ethylene diamine dihydrochloride (Sigma-Aldrich; Cat#222488), the plates were incubated for 30 min in the dark. The resulting color change (absorbance at 570 nm) was quantified using a plate counter (Victor^3 1420, Perkin Elmer, Woodbridge, ON, Canada), and the nitrite concentration calculated by interpolation from a standard curve.

Migration

Microglia were seeded at 3×10^4 cells/filter in 500 μL MEM with 2% FBS onto Transwell inserts bearing 8 μm-diameter holes (VWR; Cat# CA 62406-198), as before (Lively and Schlichter, 2013; Lam et al., 2017; Lively and Schlichter, 2018). Independent cultures for each sex numbered 24 at P1 and 7–11 at P21. After the cells were incubated for 30 min (37°C, 5% CO_2), 500 μL solution (MEM with 2% FBS) was added to the lower wells, and a stimulating cytokine was added (I+T or IL-4, as above). 24 h later, the cells were fixed in 4% PFA (10 min) and rinsed 3× with PBS. Cells that had not migrated were removed by swirling the upper face of the insert with a Q-tip. The migrated cells were stained with 0.3% crystal violet (1 min), viewed at 20× magnification with an Olympus CK2 inverted microscope (Olympus, Tokyo, Japan) and summed from 5 random fields/filter. Then, the counts were normalized to the unstimulated (control) group.

[1] http://www.transnetyx.com/

Transcription Analysis

Microglia (0.5–1 × 10^6cells/coverslip; 5–7 independent cell cultures for each sex and age) were plated in 12-well culture plates and left untreated or stimulated for 24 h with 20 ng/mL IFNγ + 50 ng/mL TNFα or 20 ng/mL IL-4, as above. The remaining methods were as before (Lam et al., 2017). In brief, total RNA was extracted (TRIzol reagent; ThermoFisher Scientific; Cat# 15596018) and RNeasy Mini Kits (QIAGEN, Mississauga, ON, Canada; Cat# 74104). The gene expression assay (NanoString nCounter™ technologies) was conducted at the Princess Margaret Genomics Centre (Toronto, ON, Canada)[2] using 100 ng of extracted RNA from each sample. The code set, which was designed by NanoString, consists of capture and reporter probes (**Supplementary Table 1**). Raw data were analyzed (nSolver™ Analysis Software ver3.0; RRID:SCR_00342), the background was subtracted using negative reporter probes, and irrelevant control genes were added to assess hybridization efficiency, detection range, and to calculate a scaling factor that was applied to all mRNA counts in each sample. A reference gene scaling factor was calculated using 5 housekeeping genes: Gapdh (glyceraldehyde 3-phosphate dehydrogenase), Gusb (glucuronidase beta), Hprt1 (hypoxanthine phosphoribosyltransferase 1), Rpl32 (ribosomal protein L32), and Sdha (succinate dehydrogenase complex flavoprotein subunit A. For statistical analysis, the normalized data were log2-transformed. In the Figures, transcript expression data are shown as normalized mRNA counts/100 ng of total RNA. In **Supplementary Tables**, control data are also shown as normalized mRNA counts, and then treatment effects (I+T; IL-4) are highlighted by showing fold changes.

Western Blots

The methods for conducting and analyzing Western blots were essentially as before (Lam et al., 2017). Microglia were seeded (1–3 × 10^6 cells/well; 5–12 independent cell cultures for each sex and age), and then treated with I+T or IL-4, as above. Cells were harvested, lysed in ice-cold RIPA and a mammalian protease inhibitor cocktail (Sigma-Aldrich; Cat# P3840), and centrifuged to remove insoluble material. Protein concentrations were determined with a Pierce™ BCA protein assay (ThermoFisher Scientific; Cat# 23225), and then proteins were denatured (100°C for 5 min in a dry-bath incubator) in NuPage LDS sample buffer (ThermoFisher Scientific; Cat# NP0007) containing 5% 2-β-mercaptoethanol. 8% acrylamide gels were loaded with 10 μg protein/lane, which were separated by SDS-PAGE and transferred to a PVDF membrane, and then blocked for 2–3 h in 5% non-fat dry milk in Tris-Tween buffered saline (TTBS).

Protein levels were measured for exemplary pro- (iNOS, PYK2, COX-2) and anti-inflammatory (CD206) markers, as before (Lively and Schlichter, 2018). Primary antibodies were diluted in TTBS with 1% BSA and applied overnight at 4°C. They were: mouse anti-iNOS (1:250; Abcam Cat# ab49999, RRID:AB_881438), rabbit anti-PYK2 (1:500; Abcam Cat# ab32571, RRID:AB_777566), rabbit anti-COX-2 (1:1000; Abcam Cat# ab15191, RRID:AB_2085144), and rabbit anti-CD206 (1:2000; Abcam, Cat# ab64693, RRID:AB_1523910). Horseradish peroxidase-labeled secondary antibodies in 1% BSA-TTBS were applied for 1 h (1:3000; Cedarlane, Burlington, ON, Canada, RRID:SCR_004462; anti-rabbit IgG: Cat# CLCC42007; anti-mouse IgG: Cat # CLCC30207), and after repeated washing, the membranes were treated with GE Healthcare ECL Start Western Blotting Detection Reagent (Sigma-Aldrich; Cat# GERPN3243). Protein band intensities were determined with a ChemiDoc XRS System (Bio-Rad).

Total protein normalization was used to compare changes using the Coomassie blue staining method (Welinder and Ekblad, 2011). We previously found that this method was preferable to a single reference protein (e.g., β actin) because such 'housekeeping' proteins can change with microglial activation states (Lam et al., 2017). A 0.1% solution of Coomassie Brilliant Blue G (Sigma-Aldrich; Cat# B8522) was applied (1 min), and then slides were de-stained (2 min) in acetic acid/methanol/water (1:5:4) and air-dried. Blots were imaged with a ChemiDocTM XRS System, and then analyzed using Image Lab (ver.5.2.1; RRID:SCR_014210) to identify gel lanes and bands of interest, and to subtract the background and determine signal intensities of identified bands. For each blot, the band of interest was normalized to total Coomassie-blue stained protein in that lane (as a loading control), and then fold-changes were calculated with respect to unstimulated (control) microglia. Uncropped images of representative blots are shown in **Supplementary Figure 1**.

Patch-Clamp Electrophysiology

Experiments were conducted on prepubertal microglia isolated at P21. Immediately after isolation, microglia were plated on glass coverslips (∼7 × 10^4 cells/coverslip) and then incubated in tissue culture medium, as above. Recording methods were as before (Lam et al., 2017; Lively et al., 2018). Coverslips were placed in a 300 μL perfusion chamber (Model RC-25, Warner Instruments, Hamden, CT, United States) containing bath solution (in mM): 125 NaCl, 5 KCl, 1 $CaCl_2$, 1 $MgCl_2$, 10 HEPES, 5 D-glucose, adjusted to pH 7.4 and 290–300 mOsm. Whole-cell K^+ currents were recorded at room temperature using fire-polished patch pipettes (4–8 MΩ resistance) and a pipette solution consisting of (in mM): 40 Cl, 100 KAsp, 1 $MgCl_2$,10 HEPES, 2 MgATP; pH 7.2, 290–300 mOsm. Data were acquired with an Axopatch 200A amplifier and DigiDATA 1322A board (Molecular Devices, Sunnyvale, CA, United States); filtered at 5 Hz and analyzed using pCLAMP (ver10; RRID:SCR_011323). Series resistance and capacitance transients were compensated on-line, junction potentials were calculated with a utility in pCLAMP (and corrected in the figures), and the data were analyzed using Origin (ver 9.0; RRID:SCR_014212; Microcal, Northampton, MA, United States) and GraphPad Prism (ver6.0; RRID:SCR_002798; La Jolla, CA, United States).

Statistics

Data are expressed as mean ± SEM in bar graphs and mean ± SD in scatterplots and tables for the number of biological replicates indicated. Statistical analyses were conducted in GraphPad Prism. To identify expression changes induced by stimulation in

[2]https://www.pmgenomics.ca/pmgenomics

either a sex- or age-dependent manner, log2-transformed counts obtained from NanoString (described above) were analyzed by two-way ANOVA with Fisher's LSD test. The resulting *p*-value for each gene was then corrected for multiple comparisons using a 5% false discovery rate (FDR; Benjamini and Yekutieli, 2001) in the program R (version 3.3.1; RRID:SCR_001905). For all other data (i.e., NO production, migration, Western blotting and patch-clamp electrophysiology), data were analyzed by a two-way ANOVA followed by Tukey's *post hoc* test. Differences were considered significant if $p < 0.05$.

RESULTS

Neonatal and Prepubertal Female and Male Microglia Respond to IFNγ + TNFα and IL-4

Microglia morphology was examined as an indicator of their general health and responsiveness to cytokines (**Figure 1A**). While staining fixed cells only shows a snapshot in time, unstimulated cells were predominantly unipolar with an F-actin-rich lamellum and a uropod, and occasionally more rounded with spiky processes. This is similar to our studies showing that unipolar microglia were highly migratory (e.g., Siddiqui et al., 2012; Lively and Schlichter, 2013, 2018; Siddiqui et al., 2014; Lam et al., 2017). Importantly, cells did not display apoptotic blebs, and the nuclear morphology was not pyknotic under any condition (age, sex, treatments). We did not conduct a detailed morphological analysis because they are highly malleable (live imaging); and we already know that their shape need not correlate with gene expression patterns. For instance, unstimulated, IL-4- and IL-10-treated rat microglia are morphologically similar but differ greatly in gene expression (Siddiqui et al., 2016; Lam et al., 2017). We then noted I+T-evoked shape changes simply as a means of verifying that microglia from both sexes and ages had responded, and observed that most rounded up and formed chain-like groupings. IL-4 did not greatly affect their shape. While the cell bodies might appear larger, visual inspection is not a reliable measure of surface area because retraction of processes, membrane ruffling and changes in cell height can occur without changing membrane area. As described in the section on K^+ currents (below), cell capacitance is a better indicator of size changes; capacitance did not change after IL-4 (Lam et al., 2017). Prepubertal (P21) microglia had variable shapes, ranging from unipolar to flat and angular, and they responded to the cytokines in a similar manner to neonatal cells. Thus, instead of relying on morphology, we quantified two known correlates of their activation state, nitric oxide (NO) production and migratory capacity.

Increased NO production (due to up-regulation of *Nos2* mRNA and iNOS protein) is commonly used to indicate a pro-inflammatory microglial activation state. Initial evidence that unstimulated microglia were not 'activated' is that NO production (monitored as nitrite accumulation in the culture medium) was low and similar regardless of sex or age. Nitrite concentrations in the medium were 2.00 μM ± 0.41 (SD; $n = 19$) for P1 males; 2.15 ± 0.42 ($n = 17$) for P1 females; 2.31 ± 0.43 ($n = 10$) for P21 males; and 2.33 ± 0.49 ($n = 13$) for P21 females. There were no statistical differences (two-way ANOVA with Tukey's test). These data are also consistent with our earlier studies showing low NO production by combined-sex neonatal microglia (e.g., Sivagnanam et al., 2010; Lam et al., 2017; Lively and Schlichter, 2018). Further evidence that unstimulated microglia were not activated is presented in the sections on transcriptional responses, below.

A 24-h treatment with I+T increased NO production in both sexes and at both ages. For P1 cells, I+T evoked about a 4-fold increase in NO production: 3.8 ± 1.2 fold in males ($n = 19$ individual cultures) and 4.1 ± 2.2 fold in females ($n = 17$) (**Figure 1B**). At P21, the increase was somewhat smaller: 2.4 ± 1.0 fold in both sexes ($n = 10$–13). As expected, IL-4 had no effect on NO production. These results extend our recent studies using neonatal rat microglia of combined sexes (Lam et al., 2017; Lively and Schlichter, 2018). For unstimulated P1 microglia, migration was 50% higher in males (30 ± 23 cells/5 fields of view; mean ± SD, $n = 19$) than in females (20 ± 9, $n = 17$) but the variability was too large in males to confirm a statistically significant difference. There were some sex and age differences. At P1, migration was decreased by I+T and increased by IL-4 in both sexes but male IL-4-treated cells migrated 44% more than female cells (**Figure 1C**). For unstimulated P21 cells, migration was comparable in males (41 ± 27 cells/5-fields of view, $n = 7$) and females (47 ± 21, $n = 10$) but I+T did not reduce migration. At P21, the sex dimorphism was preserved, with IL-4 increasing migration of male cells 29% more than females.

Sex Comparison of Transcriptional Responses

We routinely use targeted analysis of >50 genes to assess responses of neonatal microglia from rats and mice to pro-inflammatory (lipopolysaccharide [LPS], I+T) and anti-inflammatory stimuli (IL-4, IL-10, TGFβ1) (e.g., Lam et al., 2017; Lively and Schlichter, 2018; Lively et al., 2018). Our previous studies always combined microglia from both sexes. Here, we separated males and females to examine responses of 69 genes to I+T and IL-4. The starting state will affect the ability of microglia to respond to stimuli. Gene expression data are useful to define the initial state before inducing various perturbed or 'activated' states. As in our previous studies of mixed sex microglia (some cited above), unstimulated P1 rat microglia were in a relatively non-inflammatory state (which some would call 'resting'), as judged by low expression of many inflammatory molecules in both sexes. For instance, they had low expression (arbitrary cutoff, <250 mRNA counts/100 ng RNA) of pro-inflammatory (*Casp1*, *Cd274*, *Cxcl10*, *Ifnb1*, *Ifng*, *Il1a*, *Il1b*, *Il6*, *Nos2*, *Ptgs2*, *Tnf*) and anti-inflammatory genes (*Arg1*, *Ccl22*, *Cd163*, *Il4*, *Il10*, *Pparg*, *Retnla*).

Next, sex-segregated microglia were stimulated for 24 h with I+T or IL-4 to ask whether their transcriptional responses differed. Many gene expression studies examine a single time point and we chose 24 h because it is commonly used to investigate changes in microglial gene expression

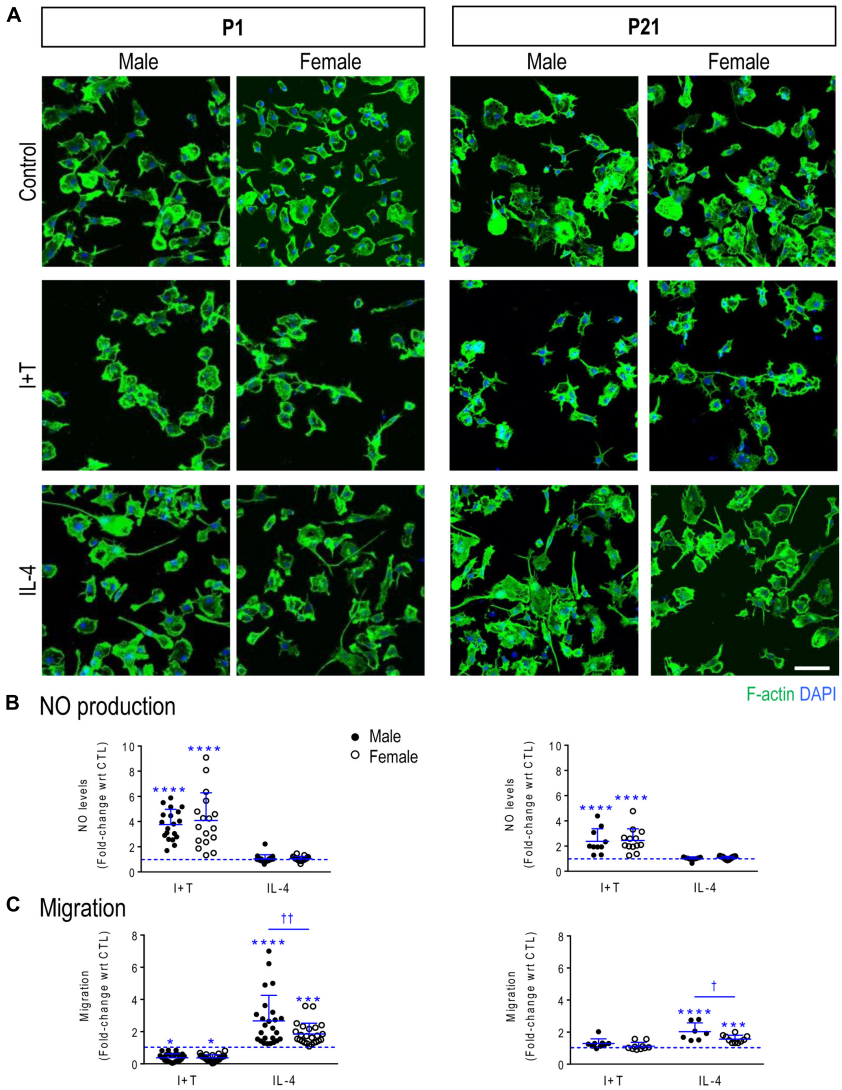

FIGURE 1 | Verifying that primary rat microglia responded to IFNγ + TNFα and to IL-4 at P1 and P21. Male and female neonatal (P1) and prepubertal (P21) microglia were sex-segregated (see Materials and Methods). **(A)** Representative fluorescence images of primary rat microglia (unstimulated, CTL) and 24 h after treatment with I+T or IL-4. Microglia were fixed and stained for F actin (phalloidin; green) and nuclei (DAPI; blue). Scale bar, 50 μm. **(B)** Cumulative NO production for the 24 h period after stimulation. Each circle represents an individual culture (closed, male; open, female). **(C)** The activation state differently affects migration of microglia at P1 and P21. All graphical results are expressed as fold changes normalized to unstimulated cells, which are indicated by dashed lines. Individual values are plotted, mean ± SD indicated, and differences shown are with respect to control microglia (*) and between sexes (†). One symbol of either type indicates $p < 0.05$; two symbols, $p < 0.01$; three symbols, $p < 0.001$; four symbols, $p < 0.0001$.

(Kobayashi et al., 2013; Zhang et al., 2015) and it facilitates comparison with our recent studies of I+T and IL-4 at 24 h that also included pilot studies showing similar responses at 6 h (Lam et al., 2017; Lively and Schlichter, 2018). [Note: Because we saw no sex differences, the segregated gene expression data and statistical outcomes are in **Supplementary Tables 2–5** for P1 and 6–9 for P21.] For P1 microglia, none of the genes showed sex differences in their responses to I+T or IL-4, and their responses were similar to our earlier combined-sex neonatal cultures. For instance, I+T increased genes associated with pro-inflammatory responses (*Casp1*, *Cybb*, *Kcna3*, *Kcnj2*, *Ncf1*, *Nos2*, *Ptgs2*, *Ptk2b*, *Tnf*) and decreased homeostatic molecules (*P2ry12*, *Cx3cr1*). IL-4 increased *Arg1*, *Ccl22* and *Mrc1*. Next, we examined changes at the protein level for four of these molecules (**Figure 2**). Consistent with the transcript changes, I+T increased NOS2, PYK2 and COX-2 (p value for female cells was 0.07), and IL-4 increased CD206. IL-4 also increased COX-2 protein, consistent with the increases in mRNA (8.4-fold in males, 11.3-fold in females), but protein changes did not reach statistical significance. No sex differences were evident.

The present study included sex-comparisons of 19 genes we had not previously examined; i.e., pro-inflammatory (*Cd274*/PD-L1, *Cxcl10*, *Ifnb1*, *Il1a*) and anti-inflammatory molecules (*Il13*, *Il13ra1*, *Pprc1*/PRC), members of the inflammasome

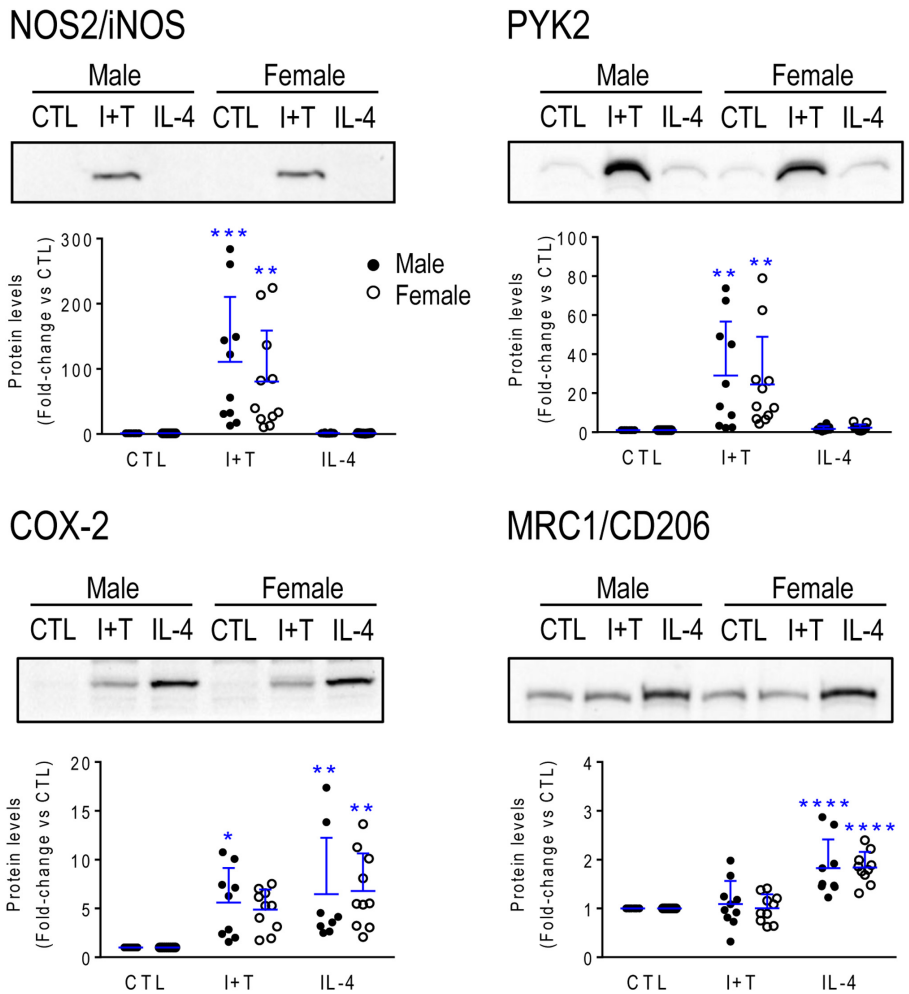

FIGURE 2 | Neonatal (P1) microglia: Exemplary pro- and anti-inflammatory proteins. Rat microglia were harvested 24 h after treatment with IFNγ + TNFα (I+T) or IL-4. **(Upper)** Representative Western blots for the pro-inflammatory markers, iNOS, COX-2 and PYK2, and the anti-inflammatory marker, MRC1/CD206. **(Lower)** Individual values show fold-changes with respect to unstimulated (control) microglia and the mean ± SD is indicated. Differences from control microglia are shown as: *$p < 0.05$; **$p < 0.01$; ***$p < 0.001$, and ****$p < 0.0001$.

(*Nlrp3*, *Pycard*), immune modulators and genes related to microglial physiology (*Cd200r1*, *Csf1*, *F2r*/PAR-1, *Hmox1*/Heme oxygenase 1, *Lcn2*/NGAL, *Mmp9*, *Nfe2l2*/NRF2, *P2rx4*, *Pdcd1*/PD-1, *Tfrc)*. There were numerous responses to cytokines; e.g., at P1, I+T increased *Cd274*, *Cxcl10*, *Il1a*, *Il4r*, *Il13ra1*, *Nlrp3*, *Hmox1*, *Nfe2l2,* and *P2rx4*; and decreased *Cd200r1* and *Csf1*. IL-4 increased *Csf1* and *F2r*, decreased *Il13ra1* and *P2rx4*; and surprisingly, it also increased the pro-inflammatory genes, *Cd274* and *Il1a*. Again, there were no sex differences at either age; hence, the data are shown in **Supplementary Tables 2–9**.

Age-Related Differences in Gene Expression and Responses

As there were no sex differences, to assess potential age-related differences (P1 *versus* P21), we then combined data from male and female microglia. Numerical data and statistics are shown in **Figures 3–6**, and organized into the same four categories: pro-inflammatory (**Figure 3**), anti-inflammatory (**Figure 4**), microglial markers and immune modulators (**Figure 5**), and genes related to microglia physiological functions (**Figure 6**). Then, to highlight similarities and differences, responses to I+T and IL-4 are pictorially summarized according to the age (**Figure 7**). For completeness, age comparisons of the sex-segregated data and accompanying statistics are shown in **Supplementary Tables 10–17**.

Baseline Levels in Unstimulated Microglia

Because microglia were isolated by different methods at the two ages, it is important to compare their starting state as well as responses to I+T and IL-4. P1 and P21 microglia had comparable baseline levels for many genes from all four categories: pro-inflammatory (*Cd274, Cxcl10*, *Ifnb1*, *Ifng*, *Il1r1*, *Ptk2b*, *Tnf*, *Tnfrsf1a*, *Tnfrsf1b*), anti-inflammatory (*Arg1*, *Il1rn*, *Il4*, *Il4r*, *Il10rb*, *Il13*, *Il13ra1*, *Retnla*, *Tgfb1*, *Tgfbr1*, *Tgfbr2*), markers and immune modulators (*Aif1*, *Cd200r1*, *Csf1*, *F2r*, *Hmox1*, *Nfe2l2*,

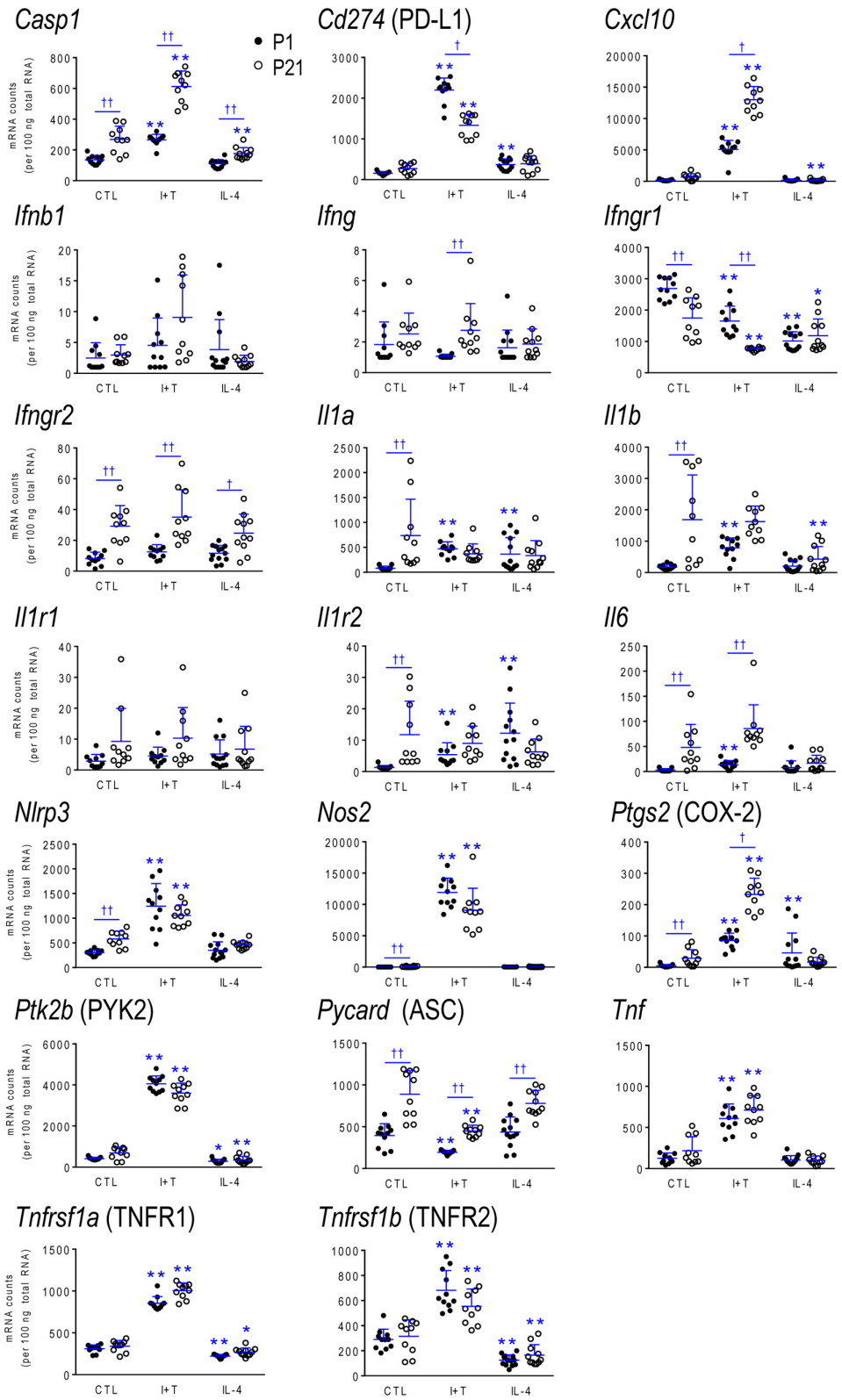

FIGURE 3 | Age-dependent transcriptional responses: Pro-inflammatory mediators. Rat microglia were unstimulated (CTL) or stimulated for 24 h with IFNγ and TNFα (I+T) or IL-4. Transcript expression of each gene is shown as mRNA counts normalized to two housekeeping genes (see Materials and Methods). For clarity, protein names are included for some genes. The scatterplots show individual values and the mean ± SD. Differences shown are with respect to control microglia (*) and between P1 and P21 cells (†). One symbol of either type indicates $p < 0.05$; two symbols, $p < 0.01$.

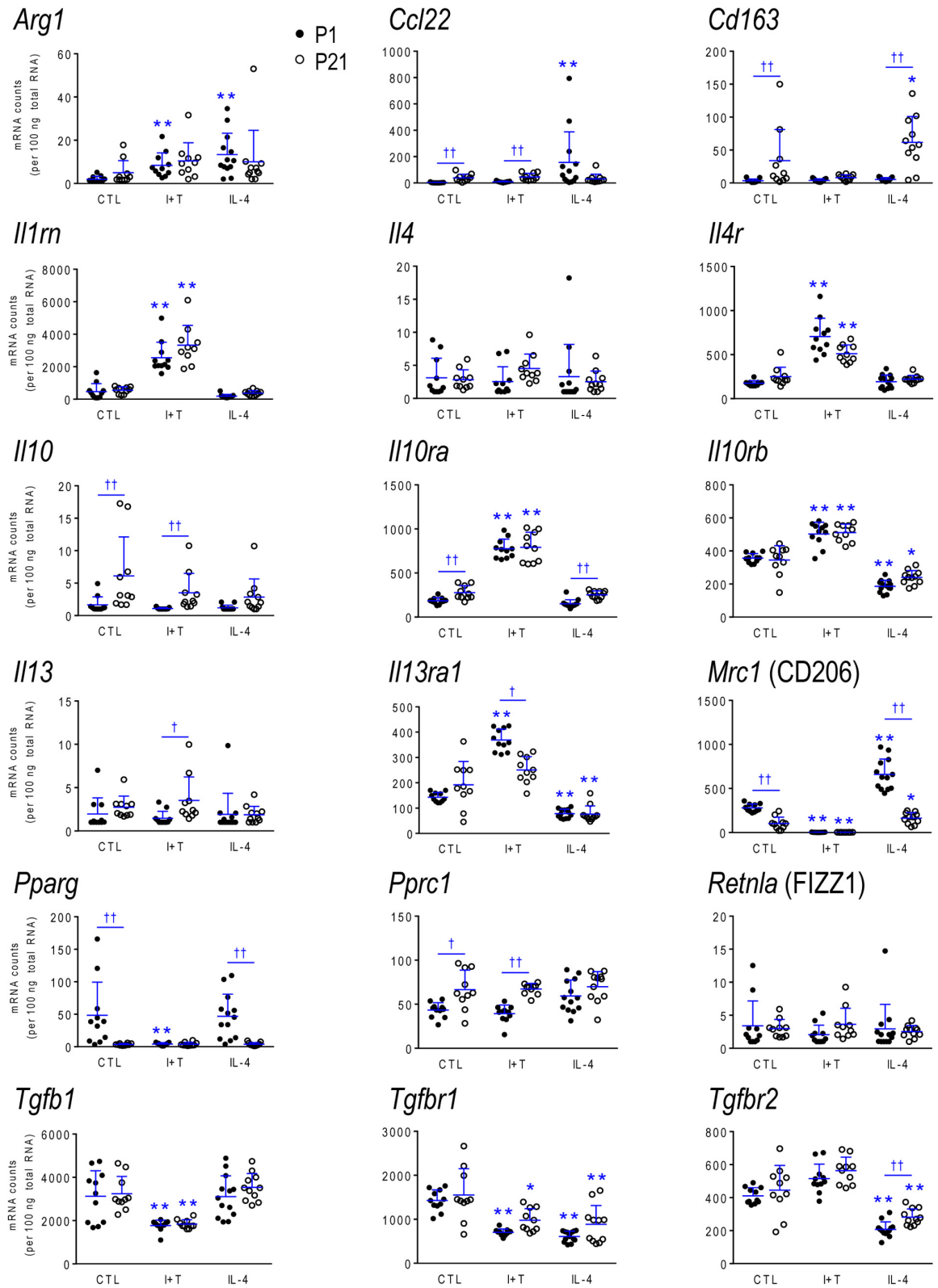

FIGURE 4 | Age-dependent transcriptional responses: Anti-inflammatory mediators. As in **Figure 2**, microglia were stimulated for 24 h with IFNγ and TNFα (I+T) or IL-4. The scatterplots show individual mRNA values (normalized; see Materials and Methods) and the mean ± SD. Differences shown are with respect to control microglia (*) and between P1 and P21 cells (†). One symbol of either type indicates $p < 0.05$; two symbols, $p < 0.01$.

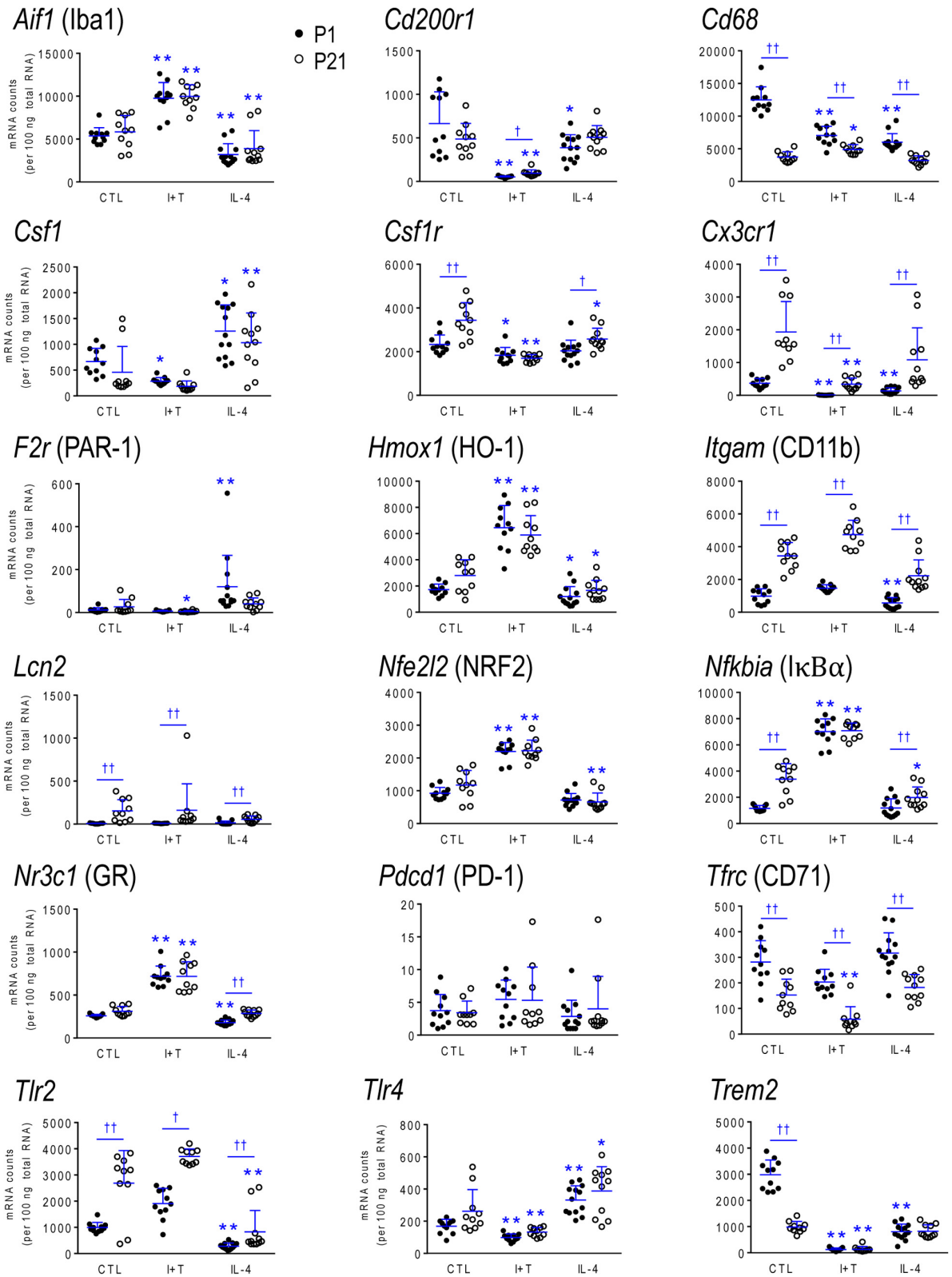

FIGURE 5 | Age-dependent transcriptional responses: Microglia markers and modulators. As in **Figure 2**, microglia were stimulated for 24 h with IFNγ and TNFα (I+T) or IL-4. The scatterplots show individual mRNA values (normalized; see Materials and Methods) and the mean ± SD. Differences shown are with respect to control microglia (*) and between P1 and P21 cells (†). One symbol of either type indicates $p < 0.05$; two symbols, $p < 0.01$.

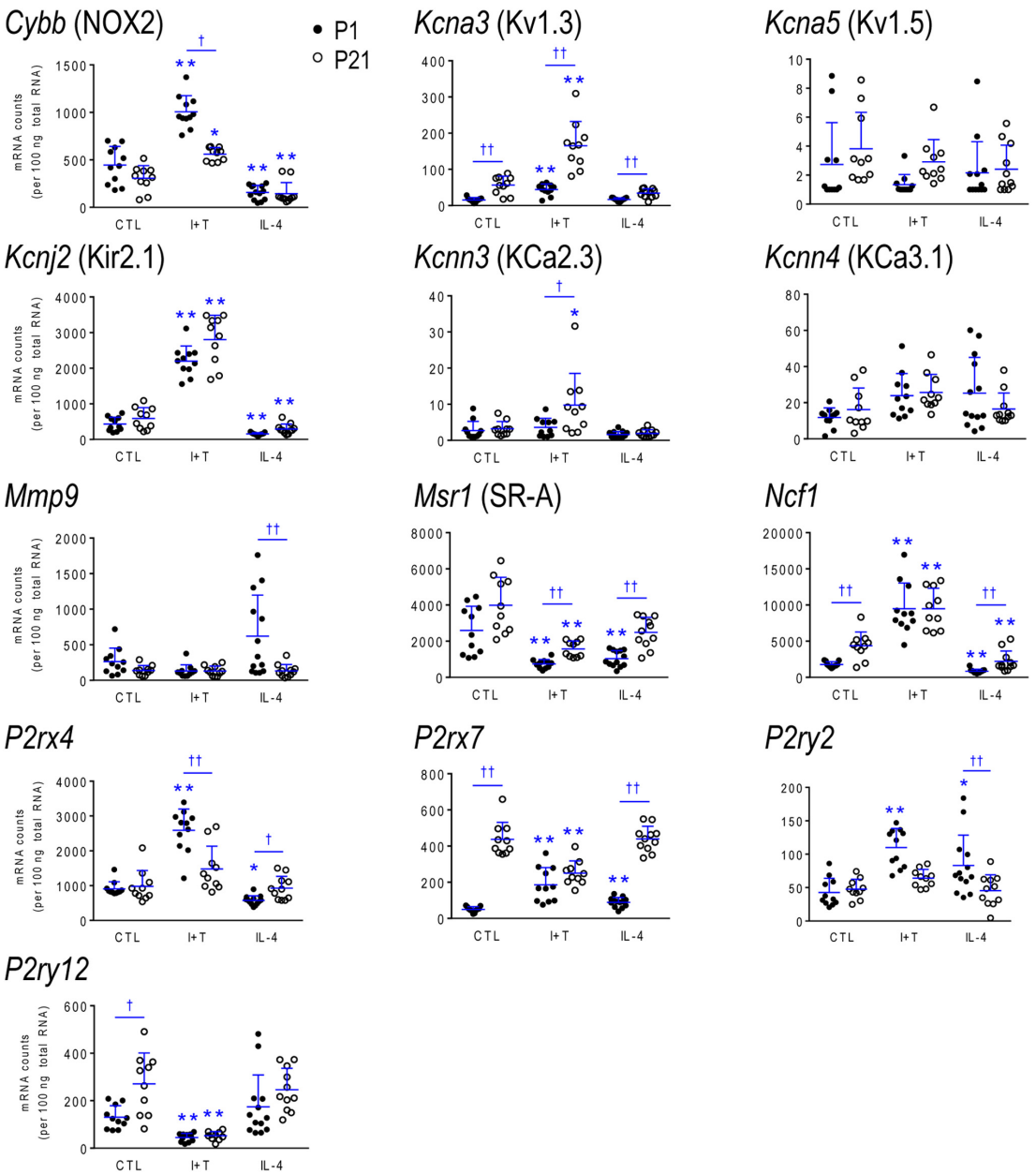

FIGURE 6 | Age-dependent transcriptional responses: Molecules related to selected physiological functions. As in **Figure 2**, microglia were stimulated for 24 h with IFNγ and TNFα (I+T) or IL-4. The scatterplots show individual mRNA values (normalized; see Materials and Methods) and the mean ± SD. Differences shown are with respect to control microglia (*) and between P1 and P21 cells (†). One symbol of either type indicates $p < 0.05$; two symbols, $p < 0.01$.

Nr3c1, *Pdcd1*, *Tlr4*), and genes related to microglial physiology (*Cybb*, *Kcna5*, *Kcnj2*, *Kcnn3*, *Kcnn4*, *Mmp9*, *Msr1, P2rx4*, *P2ry2*). However, other genes differed and had higher basal expression at P21: pro-inflammatory (*Casp1*, *Ifngr2*, *Il1a*, *Il1b*, *Il1r2*, *Il6*, *Nlrp3*, *Nos2*, *Ptgs2*, *Pycard*), anti-inflammatory (*Ccl22*, *Cd163*, *Il10*, *Il10ra*, *Pprc1*), markers and modulators (*Csf1r*, *Cx3cr1*, *Itgam*, *Lcn2*, *Nfkbia*, *Tlr2*), and genes related to microglial physiology (*Kcna3*, *Ncf1*, *P2rx7*, *P2ry12*). A few genes had lower baseline expression at P21 (*Ifngr1*, *Tfrc*, *Mrc1*, *Pparg*, *Cd68*, *Trem2*). When all genes are considered, it is evident that P21 cells are not simply more or less 'activated' [Eleven genes were expressed at low levels (< 50 mRNA counts/100 ng RNA) at both ages and were not altered by I+T or IL-4 (*Ifnb1*, *Ifng*, *Ifngr2*, *Il1r1*, *Il4*, *Il10*, *Il13*, *Kcna5*, *Kcnn4*, *Retnla*, and *Pdcd1*) and will not be discussed further].

I+T Treated Microglia

Many genes showed similar general responses, or lack thereof, at P1 and P21, with similarities in 12/16 pro-inflammatory genes (**Figures 3**, **7**), 7/13 anti-inflammatory genes (**Figures 4**, **7**), 11/16

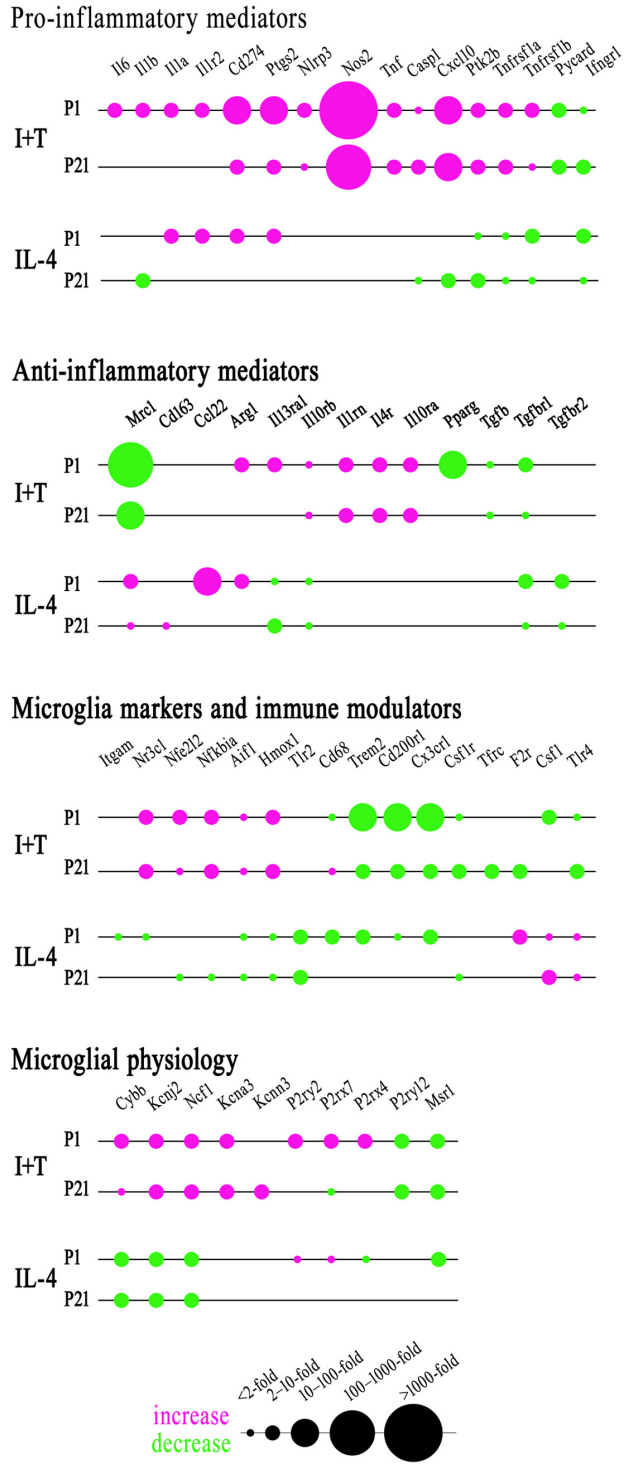

FIGURE 7 | Summary of the magnitude and direction of gene expression changes in neonatal (P1) and prepubertal (P21) microglia. Sexes were combined because no sex differences were identified at either age. To create the bubble chart, fold changes were sorted into bins according to the ranges stated on the figure. Only genes showing changes in expression were included. See **Figures 3**–**6** for full data and significance levels. The chart shows fold changes evoked by I+T or IL-4 relative to control values (magenta = increases; green = decreases).

microglial markers and modulators (**Figures 5**, **7**), and 6/10 genes related to microglial physiology (**Figures 6**, **7**). After omitting the non-responding genes, 30% of the I+T-affected genes showed nearly identical transcript levels at P1 and P21 both before and after stimulation. Transcripts that increased were *Aif1*, *Hmox1*, *Il1rn*, *Il4r*, *Il10rb*, *Kcnj2*, *Nfe2l2*, *Nr3c1*, *Ptk2b*, *Tnf*, *Tnfrsf1a*, *Tnfrs1b*. Decreases were seen in *Tgfb1*, *Tgfbr1* and *Tlr4*.

Some age-dependent differences in responses to I+T also emerged, with four patterns seen. (i) Those in which baseline levels differed with age but became similar after I+T treatment. Transcript levels increased for *Il10ra*, *Ncf1*, *Nfkbia*, *Nlrp3* and *Nos2*; and decreased for *Csf1r*, *Mrc1*, *P2ry12,* and *Trem2*. Note that baseline levels of most of these molecules were higher at P21 (except *Mrc1* and *Trem2* were higher at P1). (ii) Some genes showed the same direction of response to I+T but age-related differences in the basal levels resulted in differences after I+T. Again, expression was often higher at P21. Expression increased for *Casp1*, *Kcna3* and *Ptgs2*; decreased for *Cx3cr1*, *Ifngr1* and *Pycard*; and was unchanged for *Ccl22*, *Cd11b*, *Lcn2*, *Pprc1* and *Tlr2*. (iii) For a few genes, unstimulated levels were comparable at P1 and P21, but responses to I+T were greater at one age. Greater P1 responses were the increases in *Cd274* and *Cybb* and decreases in *Cd200r1* and *Msr1*. The only larger P21 response was the increase in *Cxcl10*. (iv) Some responses were specific to one age. Only at P1 did I+T increase *Arg1*, *Il13ra1*, *P2rx4* and *P2ry2*, and decrease *Csf1*. Only at P21 did I+T increase *Kcnn3* and decrease *F2r* and *Tfrc*. At P1, *Il1a*, *Il1b*, *Il1r2* and *Il6* were selectively increased; but interestingly, P21 microglia already had higher baseline levels and were not increased by I+T. At P1, I+T decreased *Pparg* but baseline levels at P21 were already lower. Two opposite I+T-mediated responses were seen between the two ages. *Cd68*, a lysosomal marker often used as an indicator of phagocytosis *in vivo* (Damoiseaux et al., 1994), was reduced by I+T at P1 (from a much higher baseline level) but increased at P21. The *P2rx7* transcript level increased at P1, but decreased at P21 (from a much higher baseline level).

IL-4 Treated Microglia

Some responses were similar at both ages; 4/16 pro-inflammatory genes (**Figures 3**, **7**), 5/13 anti-inflammatory genes (**Figures 4**, **7**), 5/16 microglia markers and immune modulators (**Figures 5**, **7**) and 3/10 genes related to microglial physiology (**Figures 6**, **7**). However, numerous similarities (14 genes) were simply a lack of response to IL-4.

For the IL-4-responding genes, several patterns were seen. (i) 29% (12/41) of genes showed comparable transcript levels at both ages before and after stimulation with IL-4. Unlike I+T, the IL-4-induced changes were mainly decreases; i.e., in *Aif1*, *Cybb*, *Hmox1*, *Il10rb*, *Il13ra1*, *Kcnj2*, *Ptk2b*, *Tgfbr1*, *Tnfrsf1a* and *Tnfrsf1b*, although *Csf1,* and *Tlr4* increased. (ii) There were some age-related differences that suggest developmental gene regulation. While the direction of the IL-4 response was the same, some transcript levels differed before and/or after adding IL-4; i.e., the amount of increase in *Mrc1* and decreases in *Ifngr1*, *Ncf1*, *Tgfbr2,* and *Tlr2*. (iii) Responses at P1 only. IL-4 increased some anti-inflammatory markers (*Arg1*, *Ccl22*) and purinergic receptors (*P2rx7*, *P2ry2*) but surprisingly, it also increased several

pro-inflammatory molecules (*Cd274*, *F2r*, *Il1a*, *Il1r2*, *Ptgs2*). Also surprising was that IL-4 decreased molecules related to microglial quiescence (*Cd200r1*, *Cx3cr1*) and phagocytosis (*Cd11b*, *Cd68*, *Msr1*, *Nr3c1*, *P2rx4*, *Trem2*). [*Cd68* and *Trem2* were reduced from higher baseline levels at P1.] (iv) Responses at P21 only. IL-4 decreased expression of some pro-inflammatory genes (*Casp1*, *Cxcl10*, *Il1b*) and immune modulators (*Csf1r*, *Nfe2l2*, *Nfkbia*), of which four (*Casp1*, *Csf1r*, *Il1b*, *Nfkbia*) had higher baseline levels at P21. *Cd163* was the only IL-4-mediated increase specific to prepubertal microglia. Overall, at both ages, IL-4 decreased expression of several genes involved in general activation (*Aif1*), pro-inflammatory responses (*Kcnj2, Ptk2b*) and oxidative stress (*Cybb*, *Hmox1*). IL-4 also decreased both pro- and anti-inflammatory receptors (*Il10rb*, *Il13ra1*, *Tgfbr1*, *Tnfrsf1a*, *Tnfrsf1b*) suggesting that it skews microglia toward a refractory state.

Again, age-related responses of a few hallmark proteins were compared (**Figure 8**). As expected from the higher *Nos2* mRNA and NO production in P1 microglia after I+T stimulation, P1 microglia had higher levels of NOS2 protein. Also expected in P1 microglia, were the larger I+T-mediated increase in PYK2 protein, and larger IL-4-mediated increase in MRC1.

Kv and Kir Currents in Prepubertal (P21) Microglia

Rat microglia express outward-rectifying Kv and inward-rectifying Kir currents, which have been extensively characterized in combined-sex neonatal microglia (see Discussion). Before undertaking the present study on prepubertal (P21) microglia, we conducted a pilot study on unstimulated P1 rat cells. There was no sex difference in the total Kv current amplitude: at +40 mV it was 15.1 ± 5.0 pA/pF (mean ± SEM; n = 6) in females and 12.7 ± 1.7 pA/pF (n = 15) in males.

This was not surprising because, in our many studies on ion currents in neonatal rat microglia, we have observed relatively small amplitude variations without evidence of a bimodal distribution that would suggest sex differences. Those studies include Kv and Kir currents after I+T or IL-4 treatment of mixed-sex microglia (Lam and Schlichter, 2015; Lam et al., 2017; Lively et al., 2018). Furthermore, the only age difference in mRNA expression for Kv and Kir channels was that *Kcna3* (Kv1.3) expression was higher at P21. Therefore, we next addressed potential sex differences in Kv and Kir currents, with and without stimulation by I+T or IL-4.

Kv Current

Figure 9A shows representative Kv current traces from untreated (control) P21 male and female microglia in response to a voltage ramp, which gives a direct read-out of the current-versus-voltage (I–V) relationship. Control I–V curves were similar to our previous papers on unsexed rat microglia from neonates (see references above) and adults (Lively et al., 2018), and I+T increased the current in the male cell. IL-4 appeared to increase the current in microglia of both sexes. In choosing to assess the total Kv current, we recognize that more than one Kv channel type is likely involved (see Discussion). That is, only about half

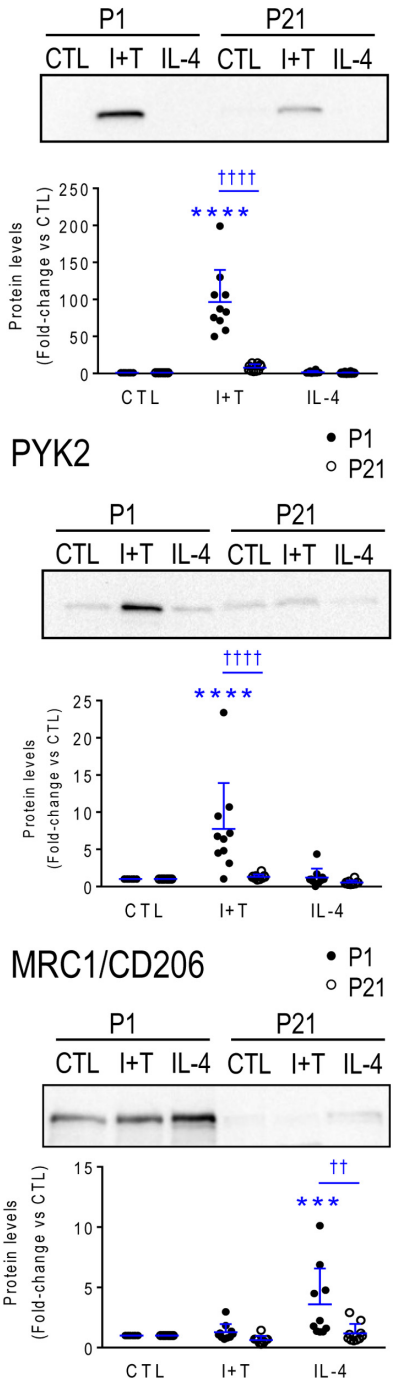

FIGURE 8 | Neonatal (P1) versus prepubertal (P21) microglia: Exemplary pro- and anti-inflammatory proteins. Rat microglia were harvested 24 h after treatment with IFNγ + TNFα (I+T) or IL-4. **(Upper)** Representative Western blots for the pro-inflammatory markers, iNOS and PYK2, and the anti-inflammatory marker, MRC1/CD206. **(Lower)** Individual values of fold-changes with respect to unstimulated (control) microglia and the mean ± SD are shown. Significant differences are shown between control and treated cells (*) and between P1 and P21 microglia (†). Two symbols of either type indicate $p < 0.01$; 3 indicates $p < 0.001$ and 4 indicates $p < 0.0001$.

the current was blocked by the potent Kv1.3 blocker, agitoxin-2 (pilot study, not shown). While the remaining Kv current was not identified, we previously observed an additional Kv current (Lam et al., 2017) and also showed that Kv1.5 contributes to the microglia current in *ex vivo* tissue prints made from rat brain slices (Kotecha and Schlichter, 1999). **Figure 9B** shows a statistical comparison of male and female P21 microglia. The Kv current amplitude at +40 mV (in pA) was normalized to the cell size (membrane capacitance; in pF), as before (Lam et al., 2017; Lively et al., 2018). Capacitance is a useful way of accounting for cell size because it is independent of shape changes, such as retraction of cell processes, membrane ruffling, and loss of the lamellum that occurs after I+T treatment. In unstimulated (control) microglia, the Kv amplitude was the same in females and males. While there were apparent increases in Kv current in response to I+T and IL-4, the only statistically significant sex difference was that males had a nearly 2-fold higher response to I+T.

Kir Current

Figure 9C shows typical Kir currents in female and male P21 microglia. They are very similar to isolated Kir2.1 currents in neonatal (Lam and Schlichter, 2015; Lam et al., 2017) and adult rat microglia (Lam et al., 2017). For the analysis in **Figure 9D**, the Kir current was measured at −140 mV and normalized to cell size (capacitance, as above). While there were no statistically significant sex differences, there was a clear trend toward a larger response of female cells to IL-4.

TGFβ1 Response

Finally, although not part of this overall study, but for comparison with our recent paper on TGFβ1-treated rat and mouse microglia (Lively et al., 2018), we report effects of TGFβ1 treatment on the K+ currents in P21 rat microglia. Although the total Kv current at +40 mV was the same (888 ± 196 pA in males; 887 ± 171 in females), the cell size (capacitance) differed (32.9 ± 2.3 pF in males; 19.4 ± 1.5 pF in females) and, consequently, the size-adjusted current (pA/pF) was larger in females (46.4 ± 8.7 pA/pF; $n = 14$) than in males (29.5 ± 8.2 pA/pF; $n = 9$). For the Kir current, there was no sex difference after TGFβ1 treatment: it was 15.3 ± 3.7 pA/pF ($n = 14$) in females, and 11.8 ± 2.9 pA/pF ($n = 9$) in males.

DISCUSSION

Sex Differences in Brain Development and Pathology

Sex differences are now recognized in brain development, adult brain structure and chemistry (Cosgrove et al., 2007); however, little is known about sex differences in specific brain cells. Recent studies have focused on how developmental disruptions might interfere with sex differentiation in the brain and lead to sex differences in later disease prevalence (Manoli and Tollkuhn, 2018). For instance, infant males are more prone to perinatal stroke, cerebral palsy, and to later development of autism spectrum disorders, attention deficit hyperactivity disorder, Tourette's syndrome, early onset schizophrenia, amyotrophic lateral sclerosis, and Parkinson's disease (Yanguas-Casas, 2017; Mallard et al., 2018). In many species, females have stronger immune systems and reduced susceptibility to infection and disease (Hanamsagar and Bilbo, 2016) but they are at risk of developing hyperactive immune systems and are more prone to developing multiple sclerosis, mood-related disorders, and Alzheimer's disease (Yanguas-Casas, 2017). Early sex differences in the prevalence of CNS disorders are established before sexual maturation and adult circulating levels of sex hormones are attained. For this reason, we compared neonatal and prepubertal microglia.

The classical 'organization-activation' hypothesis posits that perinatal exposure to sex hormones organizes tissues (including sex-specific brain circuitry) such that a secondary exposure at maturation activates sexual dimorphisms (Arnold, 2009). In the perinatal male brain, there is a surge of testosterone, which is aromatized to estradiol (McCarthy, 2008). Sex-related behavioral differences can emerge at a very young age. For instance, in human infants, males have better object tracking abilities, while females react more intensely to painful stimuli (Manoli and Tollkuhn, 2018). Abnormal exposure to sex hormones early in development can have a profound effect on subsequent behavior. Female mice treated with estradiol at birth later exhibit male levels of territorial aggression (Wu et al., 2009). At the cellular level, the perinatal testosterone surge results in elevated numbers of neural progenitor cells in the hippocampus of male rats at birth; however, this difference is abolished if males are treated with an estrogen receptor antagonist (or aromatase inhibitor) or if females are treated with estradiol (Bowers et al., 2010). Most research has focused on organizational roles of sex hormones during development but differences also arise from sex chromosomes and gene expression (Hanamsagar and Bilbo, 2016; Nelson and Lenz, 2017).

Sex Differences in Developing Microglia

There is increasing interest in potential sex differences in microglia, owing to their well-established roles in the CNS immune response and recent evidence for non-immunological roles in fine-tuning and maintaining neural circuitry (Nelson et al., 2017; Sominsky et al., 2018). Many studies investigate *in vitro* properties of neonatal microglia and there is increasing interest in possible sex differences in microglia during development and after CNS injury (Colonna and Butovsky, 2017; Dotson and Offner, 2017). The motivation for the present study was that early developmental differences between the sexes (testosterone surge, chromosomal differences) might influence their transcriptional and functional responses to well-known activating stimuli. To this end, we compared neonatal (P1) and prepubertal (P21) microglia of both sexes, with or without exposure to the pro-inflammatory cytokines, IFNγ + TNFα (I+T) or the anti-inflammatory cytokine, IL-4.

One functional sex difference we observed was in migration and its modulation by IL-4. IL-4 increases the migratory capacity of neonatal rat (Lively and Schlichter, 2013) and mouse microglia (Lam et al., 2017) in mixed-sex cultures. Here, IL-4 increased migration to a greater extent in male microglia, especially

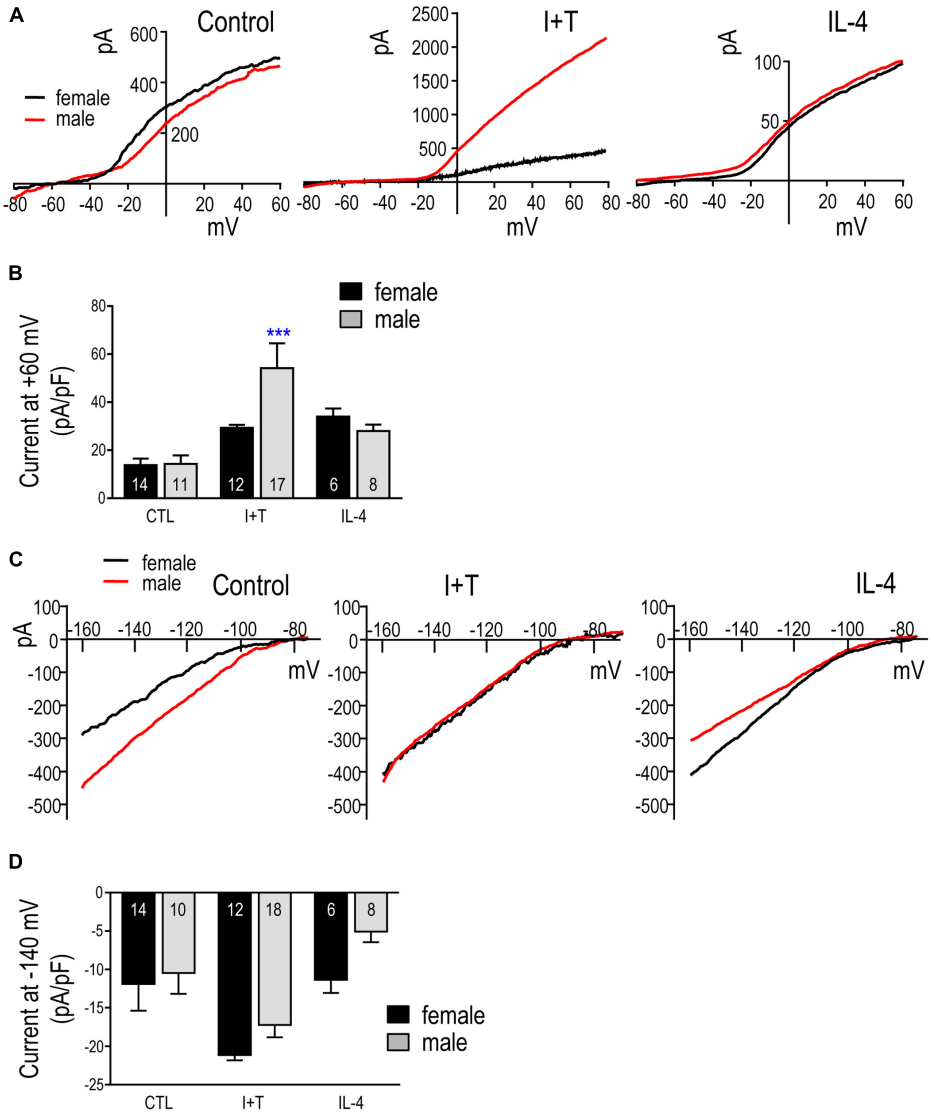

FIGURE 9 | Kv and Kir currents in prepubertal (P21) microglia. **(A)** Representative whole-cell outward-rectifying Kv currents from male and female P21 microglia at 24 h in untreated cells (control) or after treatment with I+T or IL-4. For each recording, the voltage was ramped to +40 mV from a holding potential of –110 mV. **(B)** Summary of Kv current density (pA/pF) measured at +40 mV. Graphical summaries in **(B,D)** show mean ± SEM for the number of replicates indicated on each bar; and were analyzed by two-way ANOVA and Bonferroni *post hoc* test. ***$p < 0.001$ indicates a difference from the control current. **(C)** Representative inward-rectifier (Kir) currents at 24 h in untreated microglia (control) or after treatment with I+T or IL-4. From a holding potential of –110 mV, the voltage was ramped from –160 to –60 mV. **(D)** Summary of peak Kir inward current density (pA/pF) measured at –140 mV.

at P1. Greater migration of unstimulated neonatal male rat microglia was recently observed (Yanguas-Casas et al., 2018). These findings might help explain several *in vivo* observations. In male mice, microglia/macrophages began to surround the lesion earlier after traumatic brain injury (Villapol et al., 2017) and after a stab wound, which correlated with better preservation of neuron density (Acaz-Fonseca et al., 2015). Male mice also had more infiltrating immune cells after transient ischemia, and this difference was lost in IL-4 knockout mice (Xiong et al., 2015). Thus, IL-4 appears to play an important role in microglial migration and accumulation of inflammatory cells at sites of injury; responses that are greater in males. Many species, from insects to humans, display sexually divergent immune responses (Klein and Flanagan, 2016). Thus, we were surprised to find no sex-related differences in expression or responses of the >50 inflammation-related genes examined. Here, we will address several possible explanations.

(1) It is possible that the genes we examined are not regulated in a sex-dependent manner, under the activation conditions used, or at the ages examined. Consistent with our results, a recent study of embryonic, postnatal and adult male and female mouse hippocampal microglia found that basal gene expression was similar during development, and that sex differences only emerged at maturity (Hanamsagar et al., 2017). In adult mouse

microglia, sex differences were seen in basal gene expression, and 37% of such genes were related to inflammation (Villa et al., 2018). Adult female mouse microglia had higher expression of inflammatory genes, especially those regulated by IFNγ (Thion et al., 2018); while male mouse microglia had higher NF-κB activity and expression of genes involved in cytokine secretion and migration (Villa et al., 2018). After CNS damage, some studies have reported a lack of sex differences in inflammatory responses; e.g., at 1 week after partial sciatic nerve ligation or traumatic brain injury in mice (Bruce-Keller et al., 2007; Lopes et al., 2017). However, others have noted sexual dimorphisms; e.g., at P3, female mouse microglia had higher basal expression of *Il1b*, *Il6*, *Il10*, *Tnf* (Crain et al., 2013) and the purinergic receptors, *P2rx5* and *P2ry4* (Crain et al., 2009). The potential for species differences needs to be addressed in future. We found that rat and mouse microglia differ in gene-expression profiles, both under baseline conditions and in response to pro- (I+T) and anti-inflammatory (IL-4, IL-10, TGFβ1) stimuli (Lam et al., 2017; Lively et al., 2018). Responses will also depend on the stimulus used. IL-4, IL-10 and TGFβ1 evoke different gene expression changes within a rodent species (Lam et al., 2017; Lively et al., 2018), and I+T evokes different responses from LPS (Lively and Schlichter, 2018). Not all results are consistent in the literature. In neonatal rat microglia, LPS evoked a higher increase in *Il1b* in males in one study (Loram et al., 2012) but not in another (Turano et al., 2017). However, in those two studies, the decrease in *Tlr4* was equal in both sexes (Loram et al., 2012; Turano et al., 2017), as it was after I+T in the present study. At puberty, a second surge of sex hormones activates many sexual dimorphisms throughout the body (Arnold, 2009), and it is possible that sex differences in microglial responses will emerge in microglia from older animals.

(2) Microglial gene expression might be regulated in a region-specific manner (we isolated microglia from whole brains, except the cerebellum) or depend on cell-cell interactions and the chemical milieu of the brain, which are lost after cell isolation. Most sex studies have focused on the intact brain, assessing cell numbers, morphology and basal gene expression (Nelson and Lenz, 2017). Before birth, microglial numbers and morphology were comparable between the sexes in the rat cortex, hippocampus and amygdala (Schwarz and Bilbo, 2012). However, at birth, females had a transient increase in amoeboid microglia in the amygdala, paraventricular nucleus and hippocampal CA3 region, which might be the result of increased volume in those regions in females. At P4, males had more amoeboid microglia in the amygdala, hippocampus and parietal cortex. Another study found that, at P3, male rats had more microglia overall, and more amoeboid cells in the preoptic area of the hypothalamus; treating females with estradiol at birth increased microglial number to male levels (Lenz et al., 2013). Not all results are consistent, as sex-related differences in these parameters were not seen at P3 in the rat hippocampus (Nelson et al., 2017). Instead, females had more microglia bearing phagocytic cups, and this was abrogated by estradiol treatment. Regional differences in gene expression have also been reported. At birth, male rat hippocampal and cortical tissue had higher expression of *Ccl4* and *Ccl20*, while females had higher *Il10*, *Il10ra* and *Il1r1* (Schwarz and Bilbo, 2012) but the cellular source of these immune mediators was not determined. Human microglia and whole cortical tissue show strikingly different gene expression profiles (Galatro et al., 2017), which might be due, at least in part, to astrocytes, which are also immunocompetent cells (Dong and Benveniste, 2001).

(3) Sex differences were not seen in baseline (control) gene expression or after I+T or IL-4 treatment. However, we examined only a single, 24 h time point. It is possible that sex differences in these responses occur at other times, whether later or transiently at earlier times.

Age Differences in Microglia

As noted above, the rodent brain undergoes substantial developmental changes in the first 3 weeks after birth. Between P1 and P21, we observed many differences in baseline gene expression in rat microglia; and some are consistent with their known developmental roles. Neonatal (P1) microglia had higher levels of phagocytosis- (*Mrc1*, *Cd68*, *Pparg*, *Trem2*) and endocytosis- (*Tfrc*) related genes, as expected for their greater phagocytic activity (Li and Barres, 2018). Consistent with these results, neonatal mouse microglia have prominent phagocytic cups and enrichment of phagocytosis-related genes (Attaai et al., 2018). Prepubertal (P21) microglia had higher expression of some genes that are characteristic of mature microglia, including sensome-related molecules (*Csf1r*, *Cx3cr1*, *Itgam*, *Kcna3*, *P2ry12*), pro-inflammatory (*Casp1*, *Ifngr2*, *Il6*, *Ptgs2*, *Pycard*) and anti-inflammatory genes (*Ccl22*, *Cd163*, *Il10*, *Il10ra*), and immune modulators (*Nfkbia*, *Tlr2*). Similarly, in mouse microglia, expression of molecules related to pro-inflammatory responses becomes more prominent the third week of postnatal development (Attaai et al., 2018). Previous studies comparing microglia from embryonic, early postnatal and adult mice have also reported increased expression of many sensome-related genes at maturity in both sexes (Hanamsagar et al., 2017; Thion et al., 2018). The increases in sensome molecules we observed at P21 suggest that they are better primed to respond to disturbances. Pronounced apoptosis of microglia starts in the third postnatal week and is needed to achieve their adult numbers (Nikodemova et al., 2015); thus, the higher expression of immune-related molecules might be a response to microglial apoptosis. Importantly, over half the genes we examined (including all four categories) had comparable baseline levels at both ages; thus, P21 microglia are not simply more 'activated.' In future studies, it will be important to consider consequences of differences in specific genes. It is worth noting that there might also be species differences; e.g., *Nos2* and *Arg1* expression were very low at P1 in rat microglia (Lam et al., 2017; Lively et al., 2018); present study) but they peaked at P3 in mouse (Crain et al., 2013).

Age-dependent differences in gene expression can influence microglial responses to CNS insults and, conversely, brain insults can affect microglia development and their subsequent responses (Hanamsagar and Bilbo, 2017). Here, we will focus on a few molecules for comparison with the literature. Some responses were similar at P1 and P21. I+T increased expression and IL-4 decreased expression of *Aif1* and some pro-inflammatory mediators (*Hmox1*, *Pyk2*), but also several

receptors (*Il10rb*, *Tgfbr1*, *Tnfrsf1a*, *Tnfrsf1b*) that suggest a priming toward subsequent resolution of pro-inflammatory responses. IL-4 increased the pattern recognition receptor, *Tlr4*, while I+T decreased it, consistent with IL-4 priming for subsequent innate immune responses. Many age-dependent differences were seen in response to the pro- and anti-inflammatory stimuli. I+T-mediated changes seen only at P1 include decreases in *Cd68*, *Pparg* and *Csf1*, and increases in several genes; i.e., some pro-inflammatory interleukins (*Il1a*, *Il1b*, *Il1r2, Il6*), anti-inflammatory molecules (*Arg1*, *Ccl22*, *Il13ra1*), and purinergic receptors (*P2rx4*, *P2rx7*, *P2ry2*). Only at P1 did IL-4 increase the protease activated receptor 1 (PAR-1/*F2r*), which is interesting because it is up-regulated in mouse microglia after intracerebral hemorrhage and contributes to edema, pro-inflammatory cytokine production and neuron death (Wan et al., 2016). A few changes were only seen at P21; e.g., I+T-mediated increases in *Cd68* and *Kcnn3* and decreases in *P2rx7* and *F2r*; and the IL-4-mediated increase in *Cd163* and decreases in *Csf1r*, *Cxcl10*, *Il1b* and *Nfkbia*. In addition, I+T evoked greater increases in *Cd274*/PD-L1 and *Cybb* at P1 but higher *Cxcl10* at P21. PD-L1 is interesting because LPS and IFNγ greatly increase it in mouse peritoneal macrophages (Loke and Allison, 2003), while CXCL10 propagates pro-inflammatory responses and promotes peripheral cell recruitment into the CNS (Scolletta et al., 2013). Overall, P21 microglia had higher basal and stimulated levels of many inflammatory genes, while P1 cells had higher expression of phagocytosis-related molecules.

Kv and Kir Currents

Microglia express several K^+ channels and, based on both *in vitro* and *in vivo* studies, Kv1.3 and is being considered as therapeutic targets to control CNS inflammation (recently reviewed in Peng et al., 2014; Feske et al., 2015). Most work that is relevant to the present study on Kv and Kir has used neonatal rodent cells *in vitro* to measure the currents and delineate roles for the channels. There appears to be no previous information on these channels in sex-segregated microglia. The only sex-relevant study we found was a report that estrogen inhibited the Kir2.1 current in the BV2 microglial cell line (Wu et al., 2016). For neonatal rats, we previously used combined-sex microglia, both unstimulated and cytokine-treated; and characterized Kv1.3 (e.g., Kotecha and Schlichter, 1999; Lam et al., 2017; Lively et al., 2018) and Kir2.1 currents (Lam and Schlichter, 2015; Lam et al., 2017; Lively et al., 2018). Most of those studies used selective blockers to isolate Kv1.3 and Kir2.1 currents from other potential K^+ currents. Studies have begun to assess whether microglial K^+ currents and their roles are activation-state dependent. Functionally, Kir2.1 regulates Ca^{2+} entry (Franchini et al., 2004; Lam and Schlichter, 2015), which is important for many cell functions, and blocking Kir2.1 reduced migration with or without microglial stimulation by IL-4, IL-10 or I+T (Franchini et al., 2004; Lam and Schlichter, 2015). Kv1.3 blockers decreased Ca^{2+} entry (Feske et al., 2015), NFκB activation, production of pro-inflammatory mediators, and microglia-mediated neuron killing (Khanna et al., 2001; Fordyce et al., 2005) but increased migration, regardless of the activation state (Lam et al., 2017). While Kv1.3 block did not affect phagocytosis of myelin in rat microglia (Siddiqui et al., 2016), it reduced phagocytosis of fluorescent beads in mouse microglia (Grimaldi et al., 2018). Neuroprotective effects of Kv1.3 blockers have been extended to *in vivo* injury models. For instance, Kv1.3 blockers reduced the infarct size after ischemia (Chen et al., 2018), radiation-induced brain injury (Peng et al., 2014), Alzheimer's symptoms in mouse models (Maezawa et al., 2018), and microglia infiltration into glioblastoma tumors (Grimaldi et al., 2018).

There is still uncertainty about potential developmental regulation of Kv and Kir currents in microglia, and there appear to be species differences (Lam et al., 2017; Nguyen et al., 2017; Lively et al., 2018). Here, we were interested in the total Kv current that can contribute to cell function; rather than separating the specific Kv1.3 component, which is more relevant to drug targeting. No separation was needed for Kir because the total inward current in rat microglia is almost entirely Kir2.1 (Lam and Schlichter, 2015; Lam et al., 2017; Lively et al., 2018). In fact, most studies report Kv and Kir currents in neonatal rodent microglia. However, we did not find any patch-clamp studies on P21 or similar-aged prepubertal microglia, so comparisons will mainly concern neonatal rodent microglia. [It is worth noting that Kv and Kir currents have been reported in adult rodent microglia following acute CNS injury *in situ* (e.g., Lyons et al., 2000; Menteyne et al., 2009) but some studies have not observed them (e.g, Schilling and Eder, 2007; Arnoux et al., 2013; Chen et al., 2016). In neonatal rat microglia, K^+ current amplitudes can change with cell activation states. Kv1.3 current was increased by I+T and IL-4 in rat and mouse microglia; whereas, Kir2.1 was decreased by IL-4 in rat and by I+T and IL-10 in mouse (Lam et al., 2017). TGFβ1 increased the Kv1.3 current in both species but did not affect Kir2.1 (Lively et al., 2018). Here, we addressed potential sex differences in Kv and Kir currents in P21 microglia, with and without stimulation by I+T or IL-4. Minor sex differences were seen. In response to IL-4, the Kir current appeared to increase slightly more in females but did not reach statistical significance for the sample size used. Although I+T increased Kv1.3 and Kir2.1 transcript expression in both sexes, the Kv current was increased much more in males. It remains to be determined whether Kv current sex differences under pro-inflammatory conditions occur *in vivo* and affect the ability of Kv1.3 blockers to ameliorate disease outcomes.

CONCLUSION AND FUTURE DIRECTIONS

It is increasingly recognized that microglia are malleable in their responses to insults *in vitro* and *in vivo*. If transcript expression and cytokine-evoked changes in the genes and functions we examined were 'hard-wired' during development or by the sex chromosomes, we would expect they would be maintained *in vitro*. However, epigenetic responses to the brain's chemical milieu are expected to be more malleable and might revert after isolating the cells, which would be a specific limitation of *in vitro* studies. Even microglia development *in situ* can be altered by systemic (e.g., peripheral infection, gut microbiome) and environmental factors (e.g., pollution) (Hanamsagar and Bilbo, 2017). The present study assessed a

targeted panel of genes to create a fingerprint of their initial state as well as responses to pro- and anti-inflammatory stimuli. Despite culturing the cells, we observed numerous age-dependent differences in basal and stimulated gene expression that are consistent with stable programming. Overall, both P1 and P21 cells were quite responsive to IL-4 and I+T. The minor sex differences observed — male microglia had greater migration after IL-4 and greater increases in Kv1.3 mRNA (*Kcna3*) and Kv current after I+T — raise the possibility that the testosterone surge had selective and enduring effects on the male brain. The surprising lack of sex differences in the genes we examined suggests they were either absent or that innate differences were not sustained during culture. The present results provide a framework for further investigating pro- and anti-inflammatory responses and it will be important to extend the study to *in vivo* damage models.

DATA AVAILABILITY

The raw data supporting the conclusions of this manuscript will be made available by the authors, without undue reservation, to any qualified researcher.

AUTHOR CONTRIBUTIONS

SL and LS were conceived the project and wrote the manuscript. SL performed the NanoString sample collection, Western Blotting, staining, migration and Griess assays, and associated data analysis. RW and DL performed the patch-clamping and analysis.

FUNDING

This work was supported by operating grants to LS from the Canadian Institutes of Health Research (CIHR; MOP 119578) and by the Toronto General/Toronto Western Hospital Foundation.

ACKNOWLEDGMENTS

We thank Dr. Elise Stanley for supporting the NanoString studies and for helpful discussions and comments on the manuscript; Samireh Ghafouri for preliminary P1 patch-clamp Kv data and help with isolating microglia; Chunxiang Fan for help with microglial culturing; and Govind Peringod for help with mining the literature.

SUPPLEMENTARY MATERIAL

The Supplementary Material for this article can be found online at: https://www.frontiersin.org/articles/10.3389/fncel.2018.00433/full#supplementary-material

REFERENCES

Acaz-Fonseca, E., Duran, J. C., Carrero, P., Garcia-Segura, L. M., and Arevalo, M. A. (2015). Sex differences in glia reactivity after cortical brain injury. *Glia* 63, 1966–1981. doi: 10.1002/glia.22867

Arnold, A. P. (2009). The organizational-activational hypothesis as the foundation for a unified theory of sexual differentiation of all mammalian tissues. *Horm. Behav.* 55, 570–578. doi: 10.1016/j.yhbeh.2009.03.011

Arnoux, I., Hoshiko, M., Mandavy, L., Avignone, E., Yamamoto, N., and Audinat, E. (2013). Adaptive phenotype of microglial cells during the normal postnatal development of the somatosensory "Barrel" cortex. *Glia* 61, 1582–1594. doi: 10.1002/glia.22503

Attaai, A., Neidert, N., von Ehr, A., Potru, P. S., Zoller, T., and Spittau, B. (2018). Postnatal maturation of microglia is associated with alternative activation and activated TGFbeta signaling. *Glia* doi: 10.1002/glia.23332 [Epub ahead of print].

Barcia, C., Ros, C. M., Annese, V., Gomez, A., Ros-Bernal, F., Aguado-Yera, D., et al. (2011). IFN-gamma signaling, with the synergistic contribution of TNF-alpha, mediates cell specific microglial and astroglial activation in experimental models of Parkinson's disease. *Cell Death Dis.* 2:e142. doi: 10.1038/cddis.2011.17

Benjamini, Y., and Yekutieli, D. (2001). The control of the false discovery rate in multiple testing under dependency. *Ann. Stat.* 29, 1165–1188. doi: 10.1214/aos/1013699998

Benveniste, E. N., and Benos, D. J. (1995). TNF-alpha- and IFN-gamma-mediated signal transduction pathways: effects on glial cell gene expression and function. *FASEB J.* 9, 1577–1584. doi: 10.1096/fasebj.9.15.8529837

Berletch, J. B., Yang, F., Xu, J., Carrel, L., and Disteche, C. M. (2011). Genes that escape from X inactivation. *Hum. Genet.* 130, 237–245. doi: 10.1007/s00439-011-1011-z

Bianchi, I., Lleo, A., Gershwin, M. E., and Invernizzi, P. (2012). The X chromosome and immune associated genes. *J. Autoimmun.* 38, J187–J192. doi: 10.1016/j.jaut.2011.11.012

Bilbo, S. D. (2018). Sex differences shape brain development and function, in health and disease: policy implications. *Policy Insights Behav. Brain Sci.* 5, 104–109. doi: 10.1177/2372732217742673

Bowers, J. M., Waddell, J., and McCarthy, M. M. (2010). A developmental sex difference in hippocampal neurogenesis is mediated by endogenous oestradiol. *Biol. Sex. Differ.* 1:8. doi: 10.1186/2042-6410-1-8

Bruce-Keller, A. J., Dimayuga, F. O., Reed, J. L., Wang, C., Angers, R., Wilson, M. E., et al. (2007). Gender and estrogen manipulation do not affect traumatic brain injury in mice. *J. Neurotrauma* 24, 203–215. doi: 10.1089/neu.2006.0163

Chen, Y. J., Nguyen, H. M., Maezawa, I., Grossinger, E. M., Garing, A. L., Kohler, R., et al. (2016). The potassium channel KCa3.1 constitutes a pharmacological target for neuroinflammation associated with ischemia/reperfusion stroke. *J. Cereb. Blood Flow Metab.* 36, 2146–2161. doi: 10.1177/0271678X15611434

Chen, Y. J., Nguyen, H. M., Maezawa, I., Jin, L. W., and Wulff, H. (2018). Inhibition of the potassium channel Kv1.3 reduces infarction and inflammation in ischemic stroke. *Ann. Clin. Transl. Neurol.* 5, 147–161. doi: 10.1002/acn3.513

Clarkson, J., and Herbison, A. E. (2016). Hypothalamic control of the male neonatal testosterone surge. *Philos. Trans. R. Soc. Lond. B Biol. Sci.* 371:20150115. doi: 10.1098/rstb.2015.0115

Colonna, M., and Butovsky, O. (2017). Microglia function in the central nervous system during health and neurodegeneration. *Annu. Rev. Immunol.* 35, 441–468. doi: 10.1146/annurev-immunol-051116-052358

Colton, C. A. (2009). Heterogeneity of microglial activation in the innate immune response in the brain. *J. Neuroimmune Pharmacol.* 4, 399–418. doi: 10.1007/s11481-009-9164-4

Cosgrove, K. P., Mazure, C. M., and Staley, J. K. (2007). Evolving knowledge of sex differences in brain structure, function, and chemistry. *Biol. Psychiatry* 62, 847–855. doi: 10.1016/j.biopsych.2007.03.001

Crain, J. M., Nikodemova, M., and Watters, J. J. (2009). Expression of P2 nucleotide receptors varies with age and sex in murine brain microglia. *J. Neuroinflammation* 6:24. doi: 10.1186/1742-2094-6-24

Crain, J. M., Nikodemova, M., and Watters, J. J. (2013). Microglia express distinct M1 and M2 phenotypic markers in the postnatal and adult central nervous system in male and female mice. *J. Neurosci. Res.* 91, 1143–1151. doi: 10.1002/jnr.23242

Damoiseaux, J. G., Dopp, E. A., Calame, W., Chao, D., MacPherson, G. G., and Dijkstra, C. D. (1994). Rat macrophage lysosomal membrane antigen recognized by monoclonal antibody ED1. *Immunology* 83, 140–147.

Dong, Y., and Benveniste, E. N. (2001). Immune function of astrocytes. *Glia* 36, 180–190. doi: 10.1002/glia.1107

Dotson, A. L., and Offner, H. (2017). Sex differences in the immune response to experimental stroke: implications for translational research. *J. Neurosci. Res.* 95, 437–446. doi: 10.1002/jnr.23784

Feske, S., Wulff, H., and Skolnik, E. Y. (2015). Ion channels in innate and adaptive immunity. *Annu. Rev. Immunol.* 33, 291–353. doi: 10.1146/annurev-immunol-032414-112212

Fordyce, C. B., Jagasia, R., Zhu, X., and Schlichter, L. C. (2005). Microglia Kv1.3 channels contribute to their ability to kill neurons. *J. Neurosci.* 25, 7139–7149. doi: 10.1523/JNEUROSCI.1251-05.2005

Franchini, L., Levi, G., and Visentin, S. (2004). Inwardly rectifying K+ channels influence Ca^{2+} entry due to nucleotide receptor activation in microglia. *Cell Calcium* 35, 449–459. doi: 10.1016/j.ceca.2003.11.001

Galatro, T. F., Holtman, I. R., Lerario, A. M., Vainchtein, I. D., Brouwer, N., Sola, P. R., et al. (2017). Transcriptomic analysis of purified human cortical microglia reveals age-associated changes. *Nat. Neurosci.* 20, 1162–1171. doi: 10.1038/nn.4597

Grimaldi, A., D'Alessandro, G., Di Castro, M. A., Lauro, C., Singh, V., Pagani, F., et al. (2018). Kv1.3 activity perturbs the homeostatic properties of astrocytes in glioma. *Sci. Rep.* 8:7654. doi: 10.1038/s41598-018-25940-5

Hanamsagar, R., Alter, M. D., Block, C. S., Sullivan, H., Bolton, J. L., and Bilbo, S. D. (2017). Generation of a microglial developmental index in mice and in humans reveals a sex difference in maturation and immune reactivity. *Glia* 65, 1504–1520. doi: 10.1002/glia.23176

Hanamsagar, R., and Bilbo, S. D. (2016). Sex differences in neurodevelopmental and neurodegenerative disorders: focus on microglial function and neuroinflammation during development. *J. Steroid Biochem. Mol. Biol.* 160, 127–133. doi: 10.1016/j.jsbmb.2015.09.039

Hanamsagar, R., and Bilbo, S. D. (2017). Environment matters: microglia function and dysfunction in a changing world. *Curr. Opin. Neurobiol.* 47, 146–155. doi: 10.1016/j.conb.2017.10.007

Jackson, C. M. (1912). On the recognition of sex through external characters in the young rat. *Biol. Bull.* 23, 171–173. doi: 10.2307/1535914

Kabba, J. A., Xu, Y., Christian, H., Ruan, W., Chenai, K., Xiang, Y., et al. (2018). Microglia: housekeeper of the central nervous system. *Cell Mol. Neurobiol.* 38, 53–71. doi: 10.1007/s10571-017-0504-2

Khanna, R., Roy, L., Zhu, X., and Schlichter, L. C. (2001). K+ channels and the microglial respiratory burst. *Am. J. Physiol. Cell Physiol.* 280, C796–C806. doi: 10.1152/ajpcell.2001.280.4.C796

Klein, S. L., and Flanagan, K. L. (2016). Sex differences in immune responses. *Nat. Rev. Immunol.* 16, 626–638. doi: 10.1038/nri.2016.90

Kobayashi, K., Imagama, S., Ohgomori, T., Hirano, K., Uchimura, K., Sakamoto, K., et al. (2013). Minocycline selectively inhibits M1 polarization of microglia. *Cell Death Dis.* 4:e525. doi: 10.1038/cddis.2013.54

Kotecha, S. A., and Schlichter, L. C. (1999). A Kv1.5 to Kv1.3 switch in endogenous hippocampal microglia and a role in proliferation. *J. Neurosci.* 19, 10680–10693. doi: 10.1523/JNEUROSCI.19-24-10680.1999

Lam, D., Lively, S., and Schlichter, L. C. (2017). Responses of rat and mouse primary microglia to pro- and anti-inflammatory stimuli: molecular profiles. K+ channels and migration. *J. Neuroinflammation* 14:166. doi: 10.1186/s12974-017-0941-3

Lam, D., and Schlichter, L. C. (2015). Expression and contributions of the Kir2.1 inward-rectifier K+ channel to proliferation, migration and chemotaxis of microglia in unstimulated and anti-inflammatory states. *Front. Cell. Neurosci.* 9:185. doi: 10.3389/fncel.2015.00185

Lenz, K. M., Nugent, B. M., Haliyur, R., and McCarthy, M. M. (2013). Microglia are essential to masculinization of brain and behavior. *J. Neurosci.* 33, 2761–2772. doi: 10.1523/JNEUROSCI.1268-12.2013

Li, Q., and Barres, B. A. (2018). Microglia and macrophages in brain homeostasis and disease. *Nat. Rev. Immunol.* 18, 225–242. doi: 10.1038/nri.2017.125

Lively, S., Lam, D., Wong, R., and Schlichter, L. C. (2018). Comparing effects of transforming growth factor beta1 on microglia from rat and mouse: transcriptional profiles and potassium channels. *Front. Cell. Neurosci.* 12:115. doi: 10.3389/fncel.2018.00115

Lively, S., and Schlichter, L. C. (2013). The microglial activation state regulates migration and roles of matrix-dissolving enzymes for invasion. *J. Neuroinflammation* 10:75. doi: 10.1186/1742-2094-10-75

Lively, S., and Schlichter, L. C. (2018). Microglia responses to pro-inflammatory stimuli (LPS, IFNγ + TNFα) and reprogramming by resolving cytokines (IL-4, IL-10). *Front. Cell. Neurosci.* 12:215. doi: 10.3389/fncel.2018.00215

Loke, P., and Allison, J. P. (2003). PD-L1 and PD-L2 are differentially regulated by Th1 and Th2 cells. *Proc. Natl. Acad. Sci. U.S.A.* 100, 5336–5341. doi: 10.1073/pnas.0931259100

Lopes, D. M., Malek, N., Edye, M., Jager, S. B., McMurray, S., McMahon, S. B., et al. (2017). Sex differences in peripheral not central immune responses to pain-inducing injury. *Sci. Rep.* 7:16460. doi: 10.1038/s41598-017-16664-z

Loram, L. C., Sholar, P. W., Taylor, F. R., Wiesler, J. L., Babb, J. A., Strand, K. A., et al. (2012). Sex and estradiol influence glial pro-inflammatory responses to lipopolysaccharide in rats. *Psychoneuroendocrinology* 37, 1688–1699. doi: 10.1016/j.psyneuen.2012.02.018

Lyons, S. A., Pastor, A., Ohlemeyer, C., Kann, O., Wiegand, F., Prass, K., et al. (2000). Distinct physiologic properties of microglia and blood-borne cells in rat brain slices after permanent middle cerebral artery occlusion. *J. Cereb. Blood Flow Metab.* 20, 1537–1549. doi: 10.1097/00004647-200011000-00003

Maezawa, I., Nguyen, H. M., Di Lucente, J., Jenkins, D. P., Singh, V., Hilt, S., et al. (2018). Kv1.3 inhibition as a potential microglia-targeted therapy for Alzheimer's disease: preclinical proof of concept. *Brain* 141, 596–612. doi: 10.1093/brain/awx346

Mallard, C., Tremblay, M. E., and Vexler, Z. S. (2018). Microglia and neonatal brain injury. *Neuroscience* doi: 10.1016/j.neuroscience.2018.01.023 [Epub ahead of print].

Manoli, D. S., and Tollkuhn, J. (2018). Gene regulatory mechanisms underlying sex differences in brain development and psychiatric disease. *Ann. N. Y. Acad. Sci.* 1420, 26–45. doi: 10.1111/nyas.13564

McCarthy, M. M. (2008). Estradiol and the developing brain. *Physiol. Rev.* 88, 91–124. doi: 10.1152/physrev.00010.2007

Menteyne, A., Levavasseur, F., Audinat, E., and Avignone, E. (2009). Predominant functional expression of Kv1.3 by activated microglia of the hippocampus after Status epilepticus. *PLoS One* 4:e6770. doi: 10.1371/journal.pone.0006770

Nelson, L. H., and Lenz, K. M. (2017). The immune system as a novel regulator of sex differences in brain and behavioral development. *J. Neurosci. Res.* 95, 447–461. doi: 10.1002/jnr.23821

Nelson, L. H., Warden, S., and Lenz, K. M. (2017). Sex differences in microglial phagocytosis in the neonatal hippocampus. *Brain Behav. Immun.* 64, 11–22. doi: 10.1016/j.bbi.2017.03.010

Nguyen, H. M., Blomster, L. V., Christophersen, P., and Wulff, H. (2017). Potassium channel expression and function in microglia: plasticity and possible species variations. *Channels* 11, 305–315. doi: 10.1080/19336950.2017.1300738

Nikodemova, M., Kimyon, R. S., De, I., Small, A. L., Collier, L. S., and Watters, J. J. (2015). Microglial numbers attain adult levels after undergoing a rapid decrease in cell number in the third postnatal week. *J. Neuroimmunol.* 278, 280–288. doi: 10.1016/j.jneuroim.2014.11.018

Ober, C., Loisel, D. A., and Gilad, Y. (2008). Sex-specific genetic architecture of human disease. *Nat. Rev. Genet.* 9, 911–922. doi: 10.1038/nrg2415

Peng, Y., Lu, K., Li, Z., Zhao, Y., Wang, Y., Hu, B., et al. (2014). Blockade of Kv1.3 channels ameliorates radiation-induced brain injury. *Neuro Oncol.* 16, 528–539. doi: 10.1093/neuonc/not221

Regitz-Zagrosek, V. (2012). Sex and gender differences in health. *EMBO Rep.* 13, 596–603. doi: 10.1038/embor.2012.87

Schilling, T., and Eder, C. (2007). Ion channel expression in resting and activated microglia of hippocampal slices from juvenile mice. *Brain Res.* 1186, 21–28. doi: 10.1016/j.brainres.2007.10.027

Schwarz, J. M., and Bilbo, S. D. (2012). Sex, glia, and development: interactions in health and disease. *Horm. Behav.* 62, 243–253. doi: 10.1016/j.yhbeh.2012.02.018

Schwarz, J. M., Sholar, P. W., and Bilbo, S. D. (2012). Sex differences in microglial colonization of the developing rat brain. *J. Neurochem.* 120, 948–963. doi: 10.1111/j.1471-4159.2011.07630.x

Scolletta, S., Colletti, M., Di Luigi, L., and Crescioli, C. (2013). Vitamin D receptor agonists target CXCL10: new therapeutic tools for resolution of inflammation. *Mediators Inflamm.* 2013:876319. doi: 10.1155/2013/876319

Semple, B. D., Blomgren, K., Gimlin, K., Ferriero, D. M., and Noble-Haeusslein, L. J. (2013). Brain development in rodents and humans: identifying benchmarks of maturation and vulnerability to injury across species. *Prog. Neurobiol.* 10, 1–16. doi: 10.1016/j.pneurobio.2013.04.001

Shabab, T., Khanabdali, R., Moghadamtousi, S. Z., Kadir, H. A., and Mohan, G. (2017). Neuroinflammation pathways: a general review. *Int. J. Neurosci.* 127, 624–633. doi: 10.1080/00207454.2016.1212854

Siddiqui, T., Lively, S., Ferreira, R., Wong, R., and Schlichter, L. C. (2014). Expression and contributions of TRPM7 and KCa2.3/SK3 channels to the increased migration and invasion of microglia in anti-inflammatory activation states. *PLoS One* 9:e106087. doi: 10.1371/journal.pone.0106087

Siddiqui, T. A., Lively, S., and Schlichter, L. C. (2016). Complex molecular and functional outcomes of single versus sequential cytokine stimulation of rat microglia. *J. Neuroinflammation* 13:66. doi: 10.1186/s12974-016-0531-9

Siddiqui, T. A., Lively, S., Vincent, C., and Schlichter, L. C. (2012). Regulation of podosome formation, microglial migration and invasion by Ca^{2+}-signaling molecules expressed in podosomes. *J. Neuroinflammation* 9:250. doi: 10.1186/1742-2094-9-250

Sivagnanam, V., Zhu, X., and Schlichter, L. C. (2010). Dominance of *E. coli* phagocytosis over LPS in the inflammatory response of microglia. *J. Neuroimmunol.* 227, 111–119. doi: 10.1016/j.jneuroim.2010.06.021

Skaper, S. D., Facci, L., Zusso, M., and Giusti, P. (2018). An inflammation-centric view of neurological disease: beyond the neuron. *Front. Cell. Neurosci.* 12:72. doi: 10.3389/fncel.2018.00072

Sominsky, L., De Luca, S., and Spencer, S. J. (2018). Microglia: key players in neurodevelopment and neuronal plasticity. *Int. J. Biochem. Cell Biol.* 94, 56–60. doi: 10.1016/j.biocel.2017.11.012

Spanaus, K. S., Schlapbach, R., and Fontana, A. (1998). TNF-alpha and IFN-gamma render microglia sensitive to Fas ligand-induced apoptosis by induction of Fas expression and down-regulation of Bcl-2 and Bcl-xL. *Eur. J. Immunol.* 28, 4398–4408. doi: 10.1002/(SICI)1521-4141(199812)28:12<4398::AID-IMMU4398>3.0.CO;2-Y

Thion, M. S., Low, D., Silvin, A., Chen, J., Grisel, P., Schulte-Schrepping, J., et al. (2018). Microbiome influences prenatal and adult microglia in a sex-specific manner. *Cell* 172, 500.e16–516.e16. doi: 10.1016/j.cell.2017.11.042

Turano, A., Lawrence, J. H., and Schwarz, J. M. (2017). Activation of neonatal microglia can be influenced by other neural cells. *Neurosci. Lett.* 657, 32–37. doi: 10.1016/j.neulet.2017.07.052

Villa, A., Gelosa, P., Castiglioni, L., Cimino, M., Rizzi, N., Pepe, G., et al. (2018). Sex-specific features of microglia from adult mice. *Cell Rep.* 23, 3501–3511. doi: 10.1016/j.celrep.2018-05.048

Villapol, S., Loane, D. J., and Burns, M. P. (2017). Sexual dimorphism in the inflammatory response to traumatic brain injury. *Glia* 65, 1423–1438. doi: 10.1002/glia.23171

Wan, S., Cheng, Y., Jin, H., Guo, D., Hua, Y., Keep, R. F., et al. (2016). Microglia activation and polarization after intracerebral hemorrhage in mice: the role of protease-activated receptor-1. *Transl. Stroke Res.* 7, 478–487. doi: 10.1007/s12975-016-0472-8

Welinder, C., and Ekblad, L. (2011). Coomassie staining as loading control in Western blot analysis. *J. Proteome Res.* 10, 1416–1419. doi: 10.1021/pr1011476

Woodcock, T., and Morganti-Kossmann, M. C. (2013). The role of markers of inflammation in traumatic brain injury. *Front. Neurol.* 4:18. doi: 10.3389/fneur.2013.00018

Wu, M. V., Manoli, D. S., Fraser, E. J., Coats, J. K., Tollkuhn, J., Honda, S., et al. (2009). Estrogen masculinizes neural pathways and sex-specific behaviors. *Cell* 139, 61–72. doi: 10.1016/j.cell.2009.07.036

Wu, S. Y., Chen, Y. W., Tsai, S. F., Wu, S. N., Shih, Y. H., Jiang-Shieh, Y. F., et al. (2016). Estrogen ameliorates microglial activation by inhibiting the Kir2.1 inward-rectifier K^+ channel. *Sci. Rep.* 6:22864. doi: 10.1038/srep22864

Xiong, X., Xu, L., Wei, L., White, R. E., Ouyang, Y. B., and Giffard, R. G. (2015). IL-4 is required for sex differences in vulnerability to focal ischemia in mice. *Stroke* 46, 2271–2276. doi: 10.1161/STROKEAHA.115.008897

Yanguas-Casas, N. (2017). Sex differences in neurodegenerative diseases. *SM J. Neurol. Disord. Stroke* 3:1014.

Yanguas-Casas, N., Crespo-Castrillo, A., de Ceballos, M. L., Chowen, J. A., Azcoitia, I., Arevalo, M. A., et al. (2018). Sex differences in the phagocytic and migratory activity of microglia and their impairment by palmitic acid. *Glia* 66, 522–537. doi: 10.1002/glia.23263

Zhang, X., Dong, H., Zhang, S., Lu, S., Sun, J., and Qian, Y. (2015). Enhancement of LPS-induced microglial inflammation response via TLR4 under high glucose conditions. *Cell Physiol. Biochem.* 35, 1571–1581. doi: 10.1159/000373972

Conflict of Interest Statement: The authors declare that the research was conducted in the absence of any commercial or financial relationships that could be construed as a potential conflict of interest.

frontiers in Cellular Neuroscience

REVIEW
published: 27 November 2018
doi: 10.3389/fncel.2018.00458

The Interleukin-10 Family of Cytokines and Their Role in the CNS

*Amanda R. Burmeister and Ian Marriott**

Department of Biological Sciences, The University of North Carolina at Charlotte, Charlotte, NC, United States

Resident cells of the central nervous system (CNS) play an important role in detecting insults and initiating protective or sometimes detrimental host immunity. At peripheral sites, immune responses follow a biphasic course with the rapid, but transient, production of inflammatory mediators giving way to the delayed release of factors that promote resolution and repair. Within the CNS, it is well known that glial cells contribute to the onset and progression of neuroinflammation, but it is only now becoming apparent that microglia and astrocytes also play an important role in producing and responding to immunosuppressive factors that serve to limit the detrimental effects of such responses. Interleukin-10 (IL-10) is generally considered to be the quintessential immunosuppressive cytokine, and its ability to resolve inflammation and promote wound repair at peripheral sites is well documented. In the present review article, we discuss the evidence for the production of IL-10 by glia, and describe the ability of CNS cells, including microglia and astrocytes, to respond to this suppressive factor. Furthermore, we review the literature for the expression of other members of the IL-10 cytokine family, IL-19, IL-20, IL-22 and IL-24, within the brain, and discuss the evidence of a role for these poorly understood cytokines in the regulation of infectious and sterile neuroinflammation. In concert, the available data indicate that glia can produce IL-10 and the related cytokines IL-19 and IL-24 in a delayed manner, and these cytokines can limit glial inflammatory responses and/or provide protection against CNS insult. However, the roles of other IL-10 family members within the CNS remain unclear, with IL-20 appearing to act as a pro-inflammatory factor, while IL-22 may play a protective role in some instances and a detrimental role in others, perhaps reflecting the pleiotropic nature of this cytokine family. What is clear is that our current understanding of the role of IL-10 and related cytokines within the CNS is limited at best, and further research is required to define the actions of this understudied family in inflammatory brain disorders.

Keywords: interleukin-10, IL-19, IL-20, IL-22, IL-24, microglia, astrocytes, neuroinflammation

OPEN ACCESS

Edited by:
Raquel Ferreira,
Universidade da Beira Interior, Portugal

Reviewed by:
Marcella Reale,
Università degli Studi G. d'Annunzio Chieti e Pescara, Italy
Takumi Takizawa,
Gunma University, Japan

****Correspondence:***
Ian Marriott
imarriot@uncc.edu

Received: *14 September 2018*
Accepted: *12 November 2018*
Published: *27 November 2018*

Citation:
Burmeister AR and Marriott I (2018) The Interleukin-10 Family of Cytokines and Their Role in the CNS. Front. Cell. Neurosci. 12:458. doi: 10.3389/fncel.2018.00458

INTRODUCTION

Inflammation within the central nervous system (CNS) has devastating consequences. While it was once thought that the brain is a victim organ of infiltrating leukocytes, it is now appreciated that resident brain cells play a critical role in the initiation and/or progression of inflammatory responses within the CNS that contribute to disease states. Resident CNS cells, such as microglia and astrocytes, are able to recognize and respond to either pathogen associated molecular patterns (PAMPs) or damage associated molecular patterns (DAMPs) via their expression of innate

immune pattern recognition receptors (PRRs; Bowman et al., 2003; Tsung et al., 2014; Crill et al., 2015; Serramía et al., 2015). Similar to other myeloid immune cells such as macrophages, microglia express an array of cell surface, endosomal and cytoplasmic PRRs, allowing them to rapidly respond to the presence of PAMPs and DAMPs in the extracellular milieu and within the cytosol. In addition to the well-studied Toll-like and nucleotide-binding oligomerization domain (NOD)-like families of receptors (TLR and NLR, respectively), more recent work has demonstrated the ability of these sentinel cells to functionally express molecules that serve as cytosolic sensors for foreign and/or damaged nucleic acid motifs that include DNA-dependent activator of interferon-regulatory factors (DAI), retinoic acid-inducible gene (RIG)-like receptors (RLR) and cyclic guanosine monophosphate-adenosine monophosphate synthase (cGAS; Bowman et al., 2003; Liu et al., 2010; Furr et al., 2011; Crill et al., 2015; Jeffries and Marriott, 2017). Interestingly, non-leukocytic CNS cells, including astrocytes, can also express such innate immune sensing molecules although, in contrast to microglia, such cells appear to constitutively express fewer PRR types and expression levels (Bsibsi et al., 2002, 2006). However, following activation or infection, astrocytes show rapid elevations in the repertoire and levels of expression of PRRs, suggesting that these cells may become sensitized to the presence of danger signals (Bsibsi et al., 2002; Bowman et al., 2003; McKimmie and Fazakerley, 2005).

Acute inflammatory responses play an important role in pathogen clearance in peripheral tissues and organs, as discussed elsewhere (Ma et al., 2015; Gyurkovska and Ivanovska, 2016; Newton et al., 2016). While inflammation can similarly be protective within the CNS, such responses can have severe detrimental consequences if they are too extreme or sustained. Following activation, glial cells are capable of the rapid production of chemokines and cytokines that can alter the integrity of the blood brain barrier (BBB), recruit and activate circulating leukocytes to the site of the insult, and cause cerebral edema that increases cranial pressure which, in severe cases, can result in death due to herniation, blood clots, and subsequent ischemic stroke (Bowman et al., 2003; Liu et al., 2010; Furr et al., 2011; Barichello et al., 2012; Fayeye et al., 2013; Minkiewicz et al., 2013; Pelegrín et al., 2014; Tibussek et al., 2015; Papandreou et al., 2016; Sun et al., 2016; Shah, 2018). Microglia and astrocytes respond to PAMPs (Furr et al., 2010; Liu et al., 2010; Serramía et al., 2015; Sun et al., 2016) and DAMPs (Minkiewicz et al., 2013; Tsung et al., 2014) by releasing the signature inflammatory cytokines, interleukin-6 (IL-6) and tumor necrosis factor-α (TNF-α), and the chemokine IL-8. While these mediators can assist in the recruitment of leukocytes that include those responsible for protective adaptive immune responses, long-term exposure to these cytokines results in local tissue damage. As such, it is essential that this acute inflammatory phase is regulated and limited to prevent neurological damage. In this review article, we will discuss the ability of glial cells to produce mediators that can limit or resolve sterile or pathogen-induced neuroinflammation, with a particular emphasis on the IL-10 family of cytokines.

CNS CELLS CAN CONTRIBUTE TO THE RESOLUTION PHASE OF IMMUNE RESPONSES WITHIN THE BRAIN

Inflammation is typically biphasic and features the rapid production of pro-inflammatory mediators, followed by a decrease in their release and the subsequent delayed expression of immunosuppressive factors that limit their production and/or effect (Mino and Takeuchi, 2013; Shen et al., 2013; Headland and Norling, 2015). Such a change in the cytokine expression profile during this resolution phase serves to prevent prolonged exposure to inflammatory mediators and limits associated tissue damage. The transient nature of pro-inflammatory cytokine and chemokine production by glia and leukocytes (Conti et al., 2004; Barichello et al., 2011) results, at least in part, by a modification in cytokine mRNA stability by RNA binding proteins, which bind to the adenylate-uridylate (AU)-rich elements (ARE) in the 3′ untranslated region (UTR) of the mRNA. For example, the RNA binding protein tristetraprolin (TTP) has been demonstrated to have an anti-inflammatory role as it binds to the UTR of mRNA encoding the key pro-inflammatory cytokine TNF-α, thereby destabilizing it (Liu et al., 2013; Patial et al., 2016; Astakhova et al., 2018).

In addition to factors that can limit the production of inflammatory mediators in the continued presence of activating stimuli, other components can be upregulated in glial cells or their neighbors that attenuate their effects. Anti-inflammatory response (AIR) gene products include suppressor of cytokine signaling (SOCS) molecules, and these proteins are potent inhibitors of inflammatory mediator signaling cascades (Croker et al., 2003; Hutchins et al., 2012). For example, SOCS3 functions by binding to the IL-6 family receptor subunit, gp130, and inhibiting the signal cascade for this cytokine family (Babon et al., 2014; Wilbers et al., 2017). Importantly, cytokines that are recognized to have immunosuppressive effects, including IL-4 and IL-13, can induce the expression of SOCS molecules in both peripheral immune cells and non-leukocytic cell types, thereby contributing to their anti-inflammatory effects (Hebenstreit et al., 2003; Jackson et al., 2004; Albanesi et al., 2007; Dickensheets et al., 2007). Within the CNS, activated glial cells have been shown to express members of the SOCS family of molecules and their importance has been discussed in detail in other literature reviews (Campbell, 2005; Baker et al., 2009). Additionally, soluble cytokine decoy receptors, such as decoy receptor 3 and IL-2 receptor 2 (IL-1R2), that can bind inflammatory factors and prevent their interaction with target cell receptors, can be produced during this anti-inflammatory period (Francis et al., 2001; Ichiyama et al., 2008; Liu et al., 2015; Bonecchi et al., 2016).

However, a major component in the transition of immune responses from an inflammatory to a resolution phase is the delayed secondary production of mediators that are immunosuppressive and/or neuroprotective. For example, pathogen recognition via PRRs generates a complex response that includes the production of both inflammatory mediators and factors that can restore an immunoquiescent environment,

such as microRNAs (miRNAs). Once thought of as "junk" RNA that is generated during gene transcription, miRNAs have been identified to play a major role in switching off acute inflammatory responses, and several have been shown to have such functions within the CNS (Ponomarev et al., 2011; Iyer et al., 2012; Cho et al., 2015). miRNAs appear to contribute to the maintenance of an immunoquiescent environment in the CNS by reducing the production of inflammatory mediators by microglia, perivascular macrophages, and astrocytes, and by downregulating the expression of molecules involved in innate immune sensing pathways that render these cells less responsive to insult (Ponomarev et al., 2011; Iyer et al., 2012; Lai et al., 2013; Zhao et al., 2013; Cho et al., 2015; Sun et al., 2015; Qin et al., 2016).

In addition, microglia and astrocytes play a critical role in providing neurons with a protective homeostatic environment within the brain by expressing excitatory amino acid transporters (EAAT), such as glutamate transporter 1 (GLT-1; Almeida et al., 2005; Persson et al., 2005, 2007). During inflammation, extracellular glutamate levels show increases that could potentially be neurotoxic (Zou and Crews, 2005), but EAAT expression and glutamate uptake by glia are elevated, thereby protecting neurons from excitotoxicity (Moidunny et al., 2016).

Furthermore, and in contrast to the rapid production of pro-inflammatory mediators, immunosuppressive cytokines are typically produced at peripheral sites in a delayed manner to promote tissue repair. These suppressive cytokines include IL-4, IL-10, IL-13 and transforming growth factor-β (TGF-β), which can significantly reduce the level of pro-inflammatory cytokine production by activated CNS cells (Moore et al., 2001; Qian et al., 2008). In addition, these soluble mediators can alter microglial phenotype polarization from the predominantly inflammatory "M1" phenotype to a more immunoregulatory "M2" phenotype that expresses protective and/or repairing factors (Qian et al., 2008; Guglielmetti et al., 2016; Rossi et al., 2018). Of these anti-inflammatory factors, IL-10 is generally considered to be the quintessential immunosuppressive cytokine produced within the CNS.

IL-10 IS EXPRESSED WITHIN THE CNS AND LIMITS GLIAL INFLAMMATORY RESPONSES

It is known that IL-10 plays a critical role in the resolution of peripheral inflammation and this molecule has been the most widely studied anti-inflammatory cytokine, as discussed in numerous reviews (Hutchins et al., 2013; Headland and Norling, 2015; Mingomataj and Bakiri, 2016). Since its initial discovery, IL-10 has been found to be produced by an array of leukocytic cell types, including monocytes and granulocytes, as well as non-immune cells such as epithelial cells and keratinocytes (Moore et al., 2001; Moser and Zhang, 2008). Importantly, isolated microglia and astrocytes produce IL-10 in a delayed manner, with increased IL-10 mRNA expression seen at 8 h after activation with TLR ligands or microbial pathogens, and detectible protein release at 24 h following stimulation (Jack et al., 2005; Bsibsi et al., 2006; Rasley et al., 2006; Park et al., 2007; Gautam et al., 2011; Werry et al., 2011; Gutierrez-Murgas et al., 2016). In addition, these resident CNS cells have been demonstrated to express IL-10 *in situ* following *in vivo* LPS challenge (Park et al., 2007).

Interestingly, such delayed IL-10 production by glia appears to occur secondary to the release of inflammatory mediators, as we have shown the rapid induction of this cytokine following exposure to conditioned media from bacterially challenged cells (Rasley et al., 2006). Furthermore, the inflammatory cytokines IL-6 and TNF-α have been demonstrated to induce IL-10 production by microglia in a dose dependent manner (Sheng et al., 1995). IL-10 production by cytokine-challenged microglia can be further augmented by neurotransmitters including glutamate (Werry et al., 2011), and damage-associated molecules such as adenosine (Koscsó et al., 2012). In contrast, the neuropeptide, substance P (SP), appears to play a role in the reduction of IL-10 levels within the CNS that occurs following bacterial infection, as this effect was not seen following prophylactic administration of an antagonist for its high affinity receptor (Chauhan et al., 2008, 2011). Such an effect suggests that SP can promote neuroinflammation in two ways, first by exacerbating pro-inflammatory glial and infiltrating leukocyte responses, as discussed in our recent review on this topic (Johnson et al., 2017), and second by limiting the expression of immunosuppressive mediator production within the brain.

IL-10 exerts local effects on cells that express a receptor that are composed of two subunits, IL-10 receptor (IL-10R)1 and IL-10R2 (Moore et al., 2001) as shown in **Figure 1**. While most cell types are known to express IL-10R2 constitutively, IL-10R1 expression tends to be restricted to cells of hematopoietic lineage (Moore et al., 2001; Wolk et al., 2002; Moser and Zhang, 2008). As might be expected given their myeloid lineage, microglia constitutively express both IL-10R1 and IL-10R2 (Hulshof et al., 2002). More surprisingly, resting astrocytes also express both IL-10 receptor subunits (Molina-Holgado et al., 2001; Ledeboer et al., 2002; Xin et al., 2011; Perriard et al., 2015; **Table 1**). However, such expression by other glial cell types remains controversial with reports of IL-10R1 expression by rat oligodendrocytes (OD) but not human cells (Molina-Holgado et al., 2001; Hulshof et al., 2002), and may also be expressed by neurons (Sharma et al., 2011).

Following IL-10 binding to its receptor, this cytokine initiates its cellular effects via a canonical Janus kinase (JAK)/signal transducer and activator of transcription (STAT) pathway that features JAK1 and STAT3, which subsequently induces the expression of genes associated with immunosuppression (Moore et al., 2001; Hutchins et al., 2013). As we have demonstrated, STAT3 is phosphorylated in murine microglia following exposure to IL-10 (Rasley et al., 2006). Similarly, STAT3 phosphorylation has been observed in cortical neurons and retinal ganglion cells (RGCs) in response to IL-10, although this cytokine has also been shown to activate other signaling components including Akt in these cells (Boyd et al., 2003; Sharma et al., 2011).

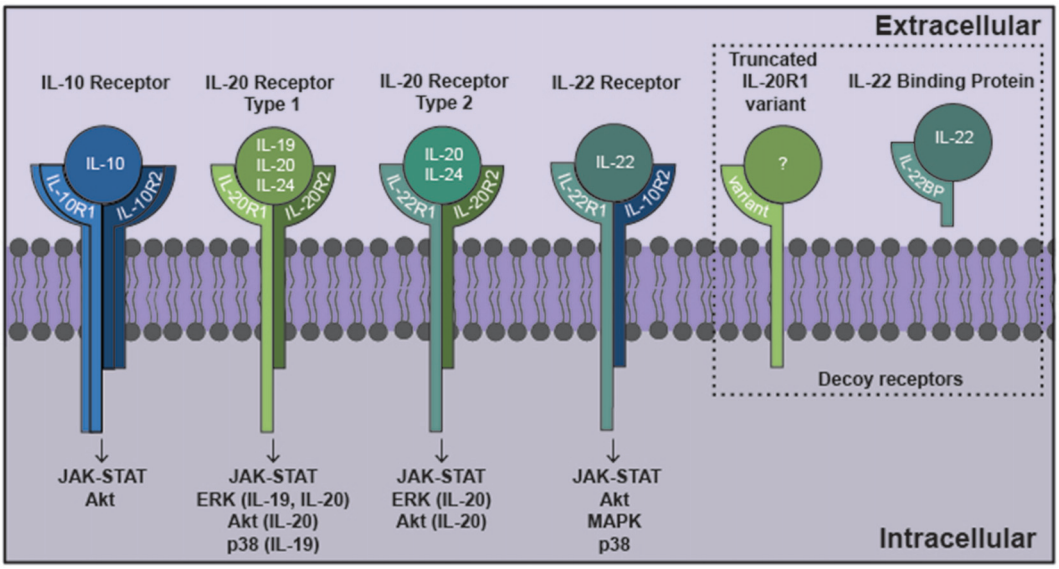

FIGURE 1 | The interleukin-10 (IL-10) family of cytokines exert their effects via heterodimeric receptor subunits. IL-10 signals through a complex of two IL-10R1 and two IL-10R2 subunits. IL-22 signals via an IL-22R1 subunit in combination with an IL-10R2 subunit. IL-19 signals through the type 1 IL-20R consisting of IL-20R1 and IL-20R2 subunits. IL-20 and IL-24 can signal via either type 1 IL-20R or the type 2 IL-20R consisting of IL-22R1 and IL-20R2 subunits. Signaling through these cognate cell surface receptors initiates the activation of canonical Janus kinase (JAK)-signal transducer and activator of transcription (STAT) signaling pathways. Additionally, other signaling cascades have been identified for this family that includes ERK, Akt, mitogen activated protein kinase (MAPK) and p38. Potential decoy receptors for these cytokines include IL-22 binding protein (IL-22BP) and a truncated IL-20R1 variant that bind IL-22 and an undetermined ligand, respectively.

The ability of IL-10 to regulate inflammatory TH1 responses has been well characterized (Couper et al., 2008; Moser and Zhang, 2008), and it exerts its immunosuppressive effects by decreasing pro-inflammatory mediator and co-stimulatory molecule expression by leukocytes (Fiorentino et al., 1991; Ding et al., 1993). Furthermore, IL-10 has been shown to induce the expression of anti-inflammatory miRNAs that have been shown to negatively regulate signaling via TLRs and alter the stability of inflammatory cytokine mRNA (Couper et al., 2008; Moser and Zhang, 2008; Curtale et al., 2013; Wilbers et al., 2017). Consistent with this role in the periphery, IL-10 plays an important role in maintaining homeostasis within the CNS (Gutierrez-Murgas et al., 2016). It contributes to the regulation of synaptic pruning by glial cells (Lim et al., 2013; Schwartz et al., 2013; Ellwardt et al., 2016) and limits the damaging effects of neuroinflammation. Specifically, IL-10 reduces glial pro-inflammatory mediator production and reactive astrogliosis in response to the presence of pathogenic microbes or their components (Balasingam and Yong, 1996; Ledeboer et al., 2000; Rasley et al., 2006; Chang et al., 2009; Curtale et al., 2013; Hutchins et al., 2013). Furthermore, this cytokine can alter microglial and astrocyte phenotypes to those that can limit inflammation, promote the production of another immunosuppressive mediator, TGF-β by astrocytes, and induce the expression of mRNA encoding the negative regulator of cytokine signaling SOCS3 (Balasingam and Yong, 1996; Rasley et al., 2006; Norden et al., 2014).

Consistent with these *in vitro* findings, the importance of IL-10 in the regulation of neuroinflammatory damage has been demonstrated *in vivo* in animal models of CNS disorders. IL-10 deficient mice show uncontrolled inflammation and increased susceptibility to bacterial, parasitic and viral infections of the CNS (Gazzinelli et al., 1996; Gutierrez-Murgas et al., 2016; Martin and Griffin, 2017). In these studies, increased mortality was associated with elevated levels of inflammatory mediators in the absence of endogenous IL-10 expression (Gazzinelli et al., 1996). In addition to infectious CNS disorders, a role for IL-10 in limiting detrimental neuroinflammation in "sterile" autoimmune diseases, including multiple sclerosis (MS), has been suggested. Genetic polymorphisms of the IL-10 gene that result in reduced expression of this cytokine have been associated with the incidence of MS in human subjects (Martinez Doncel et al., 2002; Myhr et al., 2002; Talaat et al., 2016). Similarly, increased levels of IL-10 in the CNS have been shown to reduce disease severity in mouse models of experimental autoimmune encephalomyelitis (EAE; O'Neill et al., 2006; Klose et al., 2013).

Taken together, the available data indicates that IL-10 plays a critical role in limiting CNS inflammation in a similar manner to that seen at peripheral sites by altering the ability of resident glia and infiltrating leukocytes to respond to activating stimuli, and by reducing the production of inflammatory mediators by these cells. However, IL-10 is only one member of a family of cytokines that are grouped together based upon their similar structures and their sharing of common receptor subunits (Ouyang et al., 2011; Rutz et al., 2014). This family includes IL-19, IL-20, IL-22, and IL-24 (Ouyang et al., 2011; Rutz et al., 2014), and these IL-10 relatives are only now being recognized to exert a regulatory role within the CNS.

TABLE 1 | Glial sources and targets of the interleukin-10 (IL-10) family within the brain.

IL-10 family member	CNS cellular source	Inducers of expression	CNS cellular target	Receptor subunits	Decoy receptor
IL-10	Microglia Astrocytes	*Neisseria meningitidis* *Borrelia burgdorferi* LPS TLR3 ligand IL-6 TNF-α Adenosine Glutamate	Microglia	IL-10R1/IL-10R2	
			Astrocytes	IL-10R1/IL-10R2	
			Oligodendrocytes	IL-10R1	
IL-19	Microglia Astrocytes	*Staphylococcus aureus* *Neisseria meningitidis* *Streptococcus pneumoniae* Parasitic nematode Gamma radiation LPS TLR5 ligand	Microglia	IL-20R2 Perhaps IL-20R1	Truncated IL-20R1 variant
			Astrocytes	IL-20R1-/IL-20R2	
IL-20	Glioblastoma cells Mixed glial cells	Ischemia-hypoxia LPS	Microglia	IL-22R1/IL-20R2	Truncated IL-20R1 variant
			Astrocytes	IL-20R1/IL-20R2 IL-22R1/IL-20R2	
IL-22	Unknown	West Nile virus TMEV IL-23 IL-6	Microglia	IL-22R1/IL-10R2	IL-22BP
			Astrocytes	IL-22R1/IL-10R2	
			BBB endothelial cells	IL-22R1/IL-10R2	
			Glioblastoma	IL-22R1/IL-10R2	
IL-24	Astrocytes	Chikungunya virus *Neisseria meningitidis* LPS	Microglia	IL-22R1/IL-20R2	Truncated IL-20R1 variant
			Astrocytes	IL-20R1/IL-20R2 IL-22R1/IL-20R2	

LPS, Lipopolysaccharide; TLR, Toll-like receptor; TMEV, Theiler's murine encephalomyelitis virus.

IL-19 MAY FUNCTION IN A SIMILAR IMMUNOSUPPRESSIVE MANNER TO IL-10 IN THE CNS

Around the time that IL-10 was discovered, a number of proteins showing a high degree of homology to this cytokine were identified that were subsequently categorized as the IL-10 family. Gallagher et al. (2000) described a list of potential IL-10 family members based upon homologous gene sequences. This work led to the identification of IL-19, a IL-10 homolog expressed by bacterial LPS challenged immune cells, including monocytes and T and B lymphocytes, which can be detected at sites such as the skin following *Staphylococcus aureus* infection (Gallagher et al., 2000, 2004; Wolk et al., 2002; Reiss-Mandel et al., 2018).

Interestingly, elevated levels of mRNA encoding IL-19 have been observed in mouse brain parenchyma after gamma radiation treatment (Baluchamy et al., 2010), and three studies have shown that isolated murine astrocytes express IL-19 mRNA and protein following challenge with bacteria or their components (Cooley et al., 2014; Nikfarjam et al., 2014; Horiuchi et al., 2015; **Table 1**). However, the question of whether microglia are a significant source of IL-19 remains contentious, with one study reporting the ability of neonatal murine microglia to release high levels of IL-19 in response to LPS (Horiuchi et al., 2015), while our own work indicates that these cells and a murine microglial cell line express little or no mRNA encoding IL-19 following challenge with either LPS or *N. meningitidis* (Cooley et al., 2014). Importantly, IL-19 expression within the CNS and by isolated glia following challenge demonstrates delayed kinetics of induction, which is consistent with a secondary, and perhaps protective, response (Cooley et al., 2014; Nikfarjam et al., 2014). Similarly, IL-19 is produced in a delayed manner within the brain cortex of mice infected with a parasitic nematode (Yu et al., 2015), although the precise function of this cytokine in this model has not been determined.

As shown in **Figure 1**, IL-19 exerts its effects on cells expressing a heterodimeric receptor that consists of the subunits IL-20 receptor (IL-20R)1 and IL-20R2 (Rutz et al., 2014). While this dimeric receptor is commonly referred to as IL-20R, it has been demonstrated that IL-19 binds to the IL-20R2 subunit with a higher affinity than IL-20 (Dumoutier et al., 2001; Logsdon et al., 2012). This cognate receptor is constitutively expressed in human tissues including the pancreas, liver and skin (Wolk et al., 2002). In contrast, immune cells express the IL-20R2 subunit but fail to express IL-20R1 either at rest or following exposure to LPS (Wolk et al., 2002; Kunz et al., 2006; Ouyang et al., 2011). Consistent with this, we have demonstrated that astrocytes constitutively express both IL-20R1 and IL-20R2, while microglia exclusively

possess the IL-20R2 subunit (Cooley et al., 2014; **Table 1**). However, it should be noted that one study has reported the contradictory finding that microglia express the cognate receptor while astrocytes express just the IL-20R2 subunit (Horiuchi et al., 2015). To date, the reason for the apparent discrepancy in these findings remains unclear. Finally, we have also detected a novel truncated IL-20R1 subunit (IL-20R1 variant) in the mouse cortical brain (**Table 1**) that lacks the cytoplasmic signaling tail (Cooley et al., 2014). As such, it is possible that this truncated protein serves as a decoy receptor for IL-19, and we have reported the intriguing finding that the expression of this receptor is downregulated following infection (Cooley et al., 2014), an effect that could render CNS cells more susceptible to the effects of IL-19.

Following complexing of IL-19 with IL-20R1/IL-20R2, JAK associates with the cytoplasmic tail of IL-20R1 and phosphorylates the transcription factor STAT3 (Gallagher, 2010; Wegenka, 2010; Rutz et al., 2014). Within the CNS, IL-19 has been demonstrated to activate JAK/STAT signaling in microglia, as evidenced by STAT3 phosphorylation in these cells following IL-19 exposure (Horiuchi et al., 2015). However, defining the role of IL-19 in inflammatory responses in the periphery and the CNS has been hampered by inconsistent reports. Despite these issues, and evidence that IL-19 can exert pleiotropic effects that are dependent on the target cell type and stage of the insult, the preponderance of available evidence indicates that IL-19 is immunosuppressive. Similarly, while the reported effects of IL-19 on glial immune responses have shown variability, they are generally consistent with an immunosuppressive role for this cytokine. For example, our laboratory showed that IL-19 administration increases the expression of mRNA encoding the negative regulator of inflammatory cytokine signaling, SOCS3, in primary murine astrocytes, and decreases the production of IL-6 and TNF-α by these cells following stimulation (Cooley et al., 2014). Furthermore, other investigators demonstrated that LPS challenged microglia isolated from IL-19 deficient mice produce significantly higher levels of IL-6 and TNF-α, consistent with the removal of an inhibitory effect on these cells, that was reversible with recombinant IL-19 addition (Horiuchi et al., 2015). However, it should be noted that IL-19 treatment did not exert a demonstrable effect on the production of inflammatory mediators by LPS-challenged astrocytes in this study (Horiuchi et al., 2015).

Additionally, some evidence suggests that IL-19 may serve to limit CNS damage in cases of "sterile" neuroinflammation. For example, elevations in the expression of mRNA encoding IL-19 have been noted in peripheral blood mononuclear cells in an animal model of stroke (Rodriguez-Mercado et al., 2012), and IL-19 administration prior to ischemia-reperfusion injury has been associated with decreased leukocyte activation/infiltration and lessened neurological damage (Xie et al., 2016). Finally, genetic polymorphisms in the IL-19 locus have been associated with the risk of MS development (Khodakheir et al., 2017), similar to that seen for IL-10, although mechanistic links between these and MS neuropathology have not been defined.

IL-22 CAN EXERT BOTH PROTECTIVE AND DETRIMENTAL EFFECTS WITHIN THE CNS

IL-22 was first identified as a product of cytokine-activated lymphoma cells (Dumoutier et al., 2000) and subsequent studies demonstrated that IL-22 is a major product of the TH17 subpopulation of $CD4^+$ lymphocytes (Liang et al., 2006). However, IL-22 expression does not appear to be limited to T-cells as other leukocytes, including macrophages, can also express this cytokine (as reviewed in Dudakov et al., 2015). Importantly, constitutive expression of IL-22 has been described in the CNS (Zenewicz and Flavell, 2008; Dudakov et al., 2015) and immunohistochemical staining of human brain tissue has shown that IL-22 is present in both gray and white matter in healthy individuals (Perriard et al., 2015). Furthermore, IL-22 expression within the CNS has been demonstrated to increase following viral infection (Levillayer et al., 2007; Wang et al., 2012), and it is tempting to speculate that such increases result from local production of inflammatory cytokines. However, such a mechanism of induction has not been investigated, and the specific CNS cell type(s) responsible for constitutive and/or inducible IL-22 production have yet to be determined.

The functional receptor for IL-22 is a heterodimer composed of IL-22R1 and IL-10R2 (Zenewicz and Flavell, 2008; Dudakov et al., 2015; **Figure 1**), and binding of IL-22 to the IL-22R1 subunit allows for IL-10R2 to form a complex that initiates a signaling cascade (Dudakov et al., 2015). The IL-22 receptor is highly expressed in the pancreas, kidney, skin and liver, and expression can be further upregulated following stimuli such as *S. aureus* infection (Myles et al., 2013; Rutz et al., 2014; Dudakov et al., 2015). While early work failed to detect the presence of IL-22R1 in immune cells, subsequent studies have reported the induction of receptor subunit expression in myeloid cells following bacterial challenge and the ability of these cells to respond to IL-22 (Dhiman et al., 2009, 2014; Zeng et al., 2011). In the brain, BBB endothelial cells, astrocytes and glioblastoma cells have all been shown to constitutively express both the IL-22R1 and IL-10R2 subunits (Kebir et al., 2007; Akil et al., 2015; Perriard et al., 2015; **Table 1**). Interestingly, and in contrast to other myeloid cells, we have recently demonstrated that microglia constitutively express robust levels of the IL-22R1 protein (Burmeister et al., unpublished observations).

Decoy receptors are known to play an important role in regulating the effects of their associated cytokines, and IL-22 binding protein (IL-22BP) serves as a soluble decoy receptor for IL-22 by binding this cytokine with higher affinity than cell associated IL-22R1 (Martin et al., 2017). Leukocytes such as dendritic cells can release IL-22BP but the effects of higher decoy receptor expression, and hence lower levels of available IL-22, appear to vary according to the disease condition, with decreased disease severity in an animal model of psoriasis (Martin et al., 2017) and greater hepatic fibrosis in human schistosomiasis patients (Sertorio et al., 2015). These data therefore indicate that IL-22 can serve both detrimental and protective roles. In the CNS, IL-22BP expression is upregulated in the cerebral spinal fluid (CSF) of patients with active MS (Perriard et al., 2015) and mice deficient in the expression of IL-22BP show

less severe disease in a mouse model of EAE (Laaksonen et al., 2014), while increased IL-22BP expression correlates with greater macrophage infiltration and more severe neuroinflammation in a rat EAE model. Together, these findings support the notion that IL-22 limits the damaging effects of CNS inflammation (Beyeen et al., 2010).

Like other IL-10 family members, binding of IL-22 to its transmembrane receptor initiates a JAK/STAT signaling cascade in target cells (Dudakov et al., 2015). Typically, tyrosine kinase 2 (Tyk2) and/or JAK1 activation is associated with IL-22 signaling, with subsequent promiscuous STAT phosphorylation (Lejeune et al., 2002). STAT1, STAT3 and STAT5 activation have all been reported following exposure to IL-22 (Lejeune et al., 2002; Dudakov et al., 2015). However, IL-22 has also been demonstrated to activate mitogen activated protein kinase (MAPK) and p38 pathways in keratinocytes and synovial fibroblasts (Ikeuchi et al., 2005; Andoh et al., 2009). Consistent with this, human glioblastoma cell lines exposed to IL-22 show increases in both STAT3 and Akt phosphorylation (Akil et al., 2015).

As reviewed elsewhere, IL-22 appears to contribute to host defense at peripheral sites (Zenewicz and Flavell, 2008; Ouyang et al., 2011; Rutz et al., 2014), while in the brain IL-22 can function as a cell survival factor as it protects glioblastoma cells from the apoptosis-inducing effects of serum starvation and Fas ligand exposure (Akil et al., 2015). Similarly, primary human astrocytes treated with IL-22 demonstrate increased survival rates following challenge with TNF-α (Perriard et al., 2015). However, IL-22 may also disrupt the integrity of BBB tight junctions by reducing the level of expression of occludin by endothelial cells, and promote the recruitment of $CD4^+$ lymphocytes by elevating the production of CCL2 (MCP-1) by these BBB cells (Kebir et al., 2007). As such, IL-22 may either act in a protective manner or may exacerbate detrimental host immune responses.

Elevated IL-22 levels have been detected in the blood plasma of patients with peripheral inflammatory diseases such as psoriasis and Crohn's disease (Wilson et al., 2010), and the severity of Guillain-Barré Syndrome (GBS) appears to correlate with CSF and plasma concentrations of this cytokine (Wilson et al., 2010). However, it is not known whether such elevations underlie these disorders or, rather, represent a compensatory response of the host to limit inflammatory damage. Within the CNS, it is similarly unclear whether IL-22 provides protection during MS/EAE (Beyeen et al., 2010; Laaksonen et al., 2014; Perriard et al., 2015). Increased levels of IL-22 protein have been reported in the serum, but not the CSF, of patients with active MS (Perriard et al., 2015), while IL-22 has been found to be expressed in the CNS early in the development of EAE in the rat (Almolda et al., 2011). The finding that IL-22 expression diminishes during resolution in this rodent model has been taken as an indication that it contributes to the inflammatory phase of this MS-like disease (Almolda et al., 2011). However, it is important to note that mice lacking IL-22 show no significant difference in the level of EAE-associated neuroinflammation, suggesting that this cytokine is not a major driving force for disease development (Kreymborg et al., 2007).

In an animal model of West Nile virus associated encephalitis, mice lacking IL-22 fail to show significant differences in protective IFN-β expression, but do exhibit elevated levels of the key inflammatory cytokines, TNF-α and IL-6, and have higher viral loads following intra-cranial administration (Wang et al., 2012). However, when such mice were infected through the foot pad, they demonstrated less viral dissemination to the brain, decreased inflammatory mediator production, reduced leukocytes recruitment to the CNS, and lower mortality, compared to that seen in wild type animals (Wang et al., 2012). As such, these seemingly contradictory findings may indicate a double-edged role for IL-22 in viral infections, where this cytokine promotes pathogen spread to the CNS, but also limits inflammatory damage within the brain once the BBB has been breached.

THE ROLE OF IL-20 AND IL-24 IN THE CNS REMAINS UNCLEAR

While a considerable amount of evidence supports the protective immunosuppressive effects of IL-10 and IL-19 within the CNS, and at least some evidence supports a similar function for IL-22 in the brain, the role of IL-20 and IL-24 at this site remain largely unknown. Whereas IL-20 was first identified based upon a gene sequence predicted to yield a helical protein structure similar to IL-10 (Blumberg et al., 2001), the discovery of IL-24 was based upon its ability to induce apoptosis in cancer cells (Wang and Liang, 2005; Persaud et al., 2016) and this protein remains the subject of extensive research as an oncolytic therapy (Fisher et al., 2003; Sauane et al., 2003; Fisher, 2005; Buzas et al., 2011; Persaud et al., 2016; Ma et al., 2018). These studies have extended to brain cancers, including neuroblastomas and IL-24 was found to induce apoptosis in these cells when overexpressed following gene delivery using viral vectors (Bhoopathi et al., 2017).

Both IL-20 and IL-24 are expressed in myeloid cells following stimulation with TLR ligands, activated TH2 lymphocytes (Wolk et al., 2002; Rutz et al., 2014), and non-leukocytic cells such as keratinocytes (Wolk et al., 2009; Martin et al., 2017). Interestingly, the expression of IL-20 and IL-24 by keratinocytes has been reported to be induced by IL-22 suggesting an ability of IL-10 family members to function in a cooperative manner (Wolk et al., 2009; Martin et al., 2017). However, there are few reports of the expression of these cytokines within the CNS. Hypoxia has been shown to induce the expression of IL-20 mRNA and protein by glioblastoma cells (Chen and Chang, 2009), while mixed primary glia show a rapid (within 2 h) and transient expression of mRNA encoding IL-20 following challenge with bacterial LPS (Hosoi et al., 2004). Similarly, we have reported the expression of IL-20 mRNA by murine astrocytes exposed to *Neisseria meningitidis* (Cooley et al., 2014; **Table 1**). While IL-24 mRNA expression has also been demonstrated in murine astrocytes following alphavirus infection (Das et al., 2015) or bacterial challenge (Cooley et al., 2014), our recent observations indicate that such expression is delayed

with kinetics of induction that resemble IL-10 and IL-19 (Burmeister et al., unpublished observations). Additionally, pulsed electromagnetic field treatment following cerebral ischemia has been associated with upregulated mRNA encoding IL-24 within brain tissue at 7 days post-treatment (Pena-Philippides et al., 2014).

Neither IL-20 nor IL-24 signal via either of the IL-10R subunits (Zhang et al., 2000), but unlike the other members of the IL-10 cytokine family that have been discussed thus far, IL-20 and IL-24 can both signal through two different heterodimeric receptors, IL-20 receptor types 1 and 2, which are composed of IL-20R1 and IL-20R2, and IL-22R1 and IL-20R2 subunits, respectively (Ouyang et al., 2011; Rutz et al., 2014; **Figure 1**). As mentioned earlier, these receptor subunits are primarily expressed by non-hematopoietic cells, and have been reported to be present in microglia, astrocytes and an astrocytic glioblastoma (Dumoutier et al., 2001; Wolk et al., 2002; Cooley et al., 2014; Horiuchi et al., 2015; Perriard et al., 2015). Following cytokine binding, these receptors initiate JAK/STAT signaling pathways in the target cell. IL-20 and IL-24 utilizes JAK1 and STAT1 or, more predominantly, STAT3, in embryonic kidney cells and colonic epithelial cells (Dumoutier et al., 2001; Parrish-Novak et al., 2002; Andoh et al., 2009), and can also initiate the phosphorylation of ERK1/2 and p38 in keratinocytes (Andoh et al., 2009; Lee et al., 2013; Hsu et al., 2015). Similarly, glioblastoma cells exposed to IL-20 demonstrate phosphorylation of STAT3, ERK and Akt (Chen and Chang, 2009). To date, however, the signaling pathways activated in glial cells by IL-24 have not been defined.

Despite the reported expression of IL-20, IL-24 and their receptors by glial cells, little is known about the function of these cytokines within the CNS. In the periphery, elevated IL-20 and IL-24 levels have been detected in the serum of patients with chronic inflammatory disorders, such as Crohn's disease, psoriasis and rheumatoid arthritis (He and Liang, 2010; Rutz et al., 2014), and genetic polymorphisms for these cytokines have been identified as risk factors for some of these chronic inflammatory diseases (Kumari et al., 2013; Khodakheir et al., 2017). Within the CNS, inhibition of IL-20 using a neutralizing antibody has been shown to limit the inflammatory damage associated with acute ischemic brain injury (Chen and Chang, 2009), and IL-20 exposure has been demonstrated to promote the release of the potent chemoattractants MCP-1 and IL-8 by a glioblastoma cell line (Chen and Chang, 2009). In contrast, we have recently shown that IL-24 can induce the expression of SOCS3, a signaling component that inhibits the effects of IL-6, in murine astrocytes and can attenuate inflammatory mediator production by these cells following bacterial challenge (Burmeister et al., unpublished observations). Furthermore, we have determined

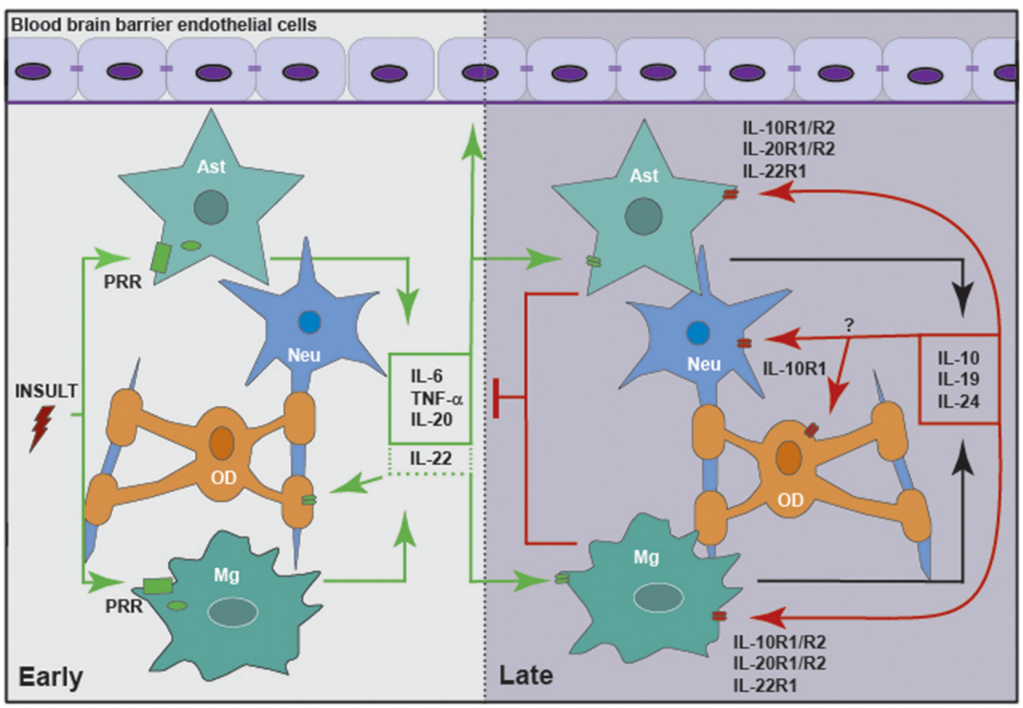

FIGURE 2 | Members of the IL-10 family of cytokines are produced by glia in response to central nervous system (CNS) insult, either directly or in a delayed indirect manner, to exacerbate or limit neuroinflammation. Glial cells, including microglia (Mg) and astrocytes (Ast), respond to insult via pattern recognition receptors (PRRs), including cell surface and cytosolic receptors. Following activation, glia release pro-inflammatory cytokines, including IL-6, tumor necrosis factor-α (TNF-α), IL-20 and perhaps IL-22. These mediators act to promote the clearance of the initial insult by altering the integrity of the blood brain barrier (BBB) and recruiting leukocytes from the circulation. In addition, inflammatory mediators act in an autocrine and/or paracrine manner to promote the delayed expression of IL-10, IL-19 and IL-24 by glia. These cytokines act via their cognate receptors expressed by astrocytes and microglia, and perhaps oligodendrocytes (OD) and neurons (Neu), to curtail the inflammatory responses of these cells and/or recruited leukocytes.

that IL-24 can also augment the expression of IL-10 by astrocytes following activation, providing another potential means by which this cytokine could limit neuroinflammation. Clearly, much further work is needed to define the apparently opposing actions of IL-20 and IL-24 on glial immune functions.

CONCLUDING REMARKS

Within the brain, it has become increasing apparent that glial cells contribute both to the maintenance of an immunoquiescent environment within the CNS, and to the initiation and progression of potentially damaging neuroinflammation. It is clear that both microglia and astrocytes can be a source of IL-10, and that they are responsive to the immunosuppressive actions of this cytokine (Jack et al., 2005; Bsibsi et al., 2006; Rasley et al., 2006; Park et al., 2007; Gautam et al., 2011; Gutierrez-Murgas et al., 2016). The kinetics of induction of IL-10 are consistent with a role in the resolution of glial inflammatory responses, and the association of human patient IL-10 gene polymorphisms with neuroinflammatory disorders support such a role (Martinez Doncel et al., 2002; Myhr et al., 2002; Talaat et al., 2016). Likewise, the preponderance of available evidence supports a similar function for IL-19, which demonstrates similar delayed kinetics of induction and can also limit inflammatory mediator production by glial cells (Cooley et al., 2014; Nikfarjam et al., 2014). However, the purpose of other IL-10 family members within the CNS is far less defined, with IL-22 being suggested to play a protective immunosuppressive role in some instances, and a detrimental pro-inflammatory function in others, perhaps reflecting the pleiotropic nature of these cytokines (Kebir et al., 2007; Beyeen et al., 2010; Laaksonen et al., 2014; Akil et al., 2015; Perriard et al., 2015). The limited information available for IL-24 suggests that it may act like IL-10 and IL-19, providing delayed protection during CNS inflammation, while IL-20 seems to contribute primarily to the inflammatory phase, demonstrating rapid induction kinetics (Hosoi et al., 2004).

However, it is evident that our current understanding of the role of IL-10 and the other members of this cytokine family within the CNS is limited at best. While it is clear that glia can be a significant source of IL-10, IL-19 and perhaps IL-20 and IL-24, and these resident CNS cells are responsive to their actions (as summarized in **Figure 2**), the functions of the IL-10 cytokine family in health and brain disorders have been understudied. Given the available evidence that IL-10 and its relatives are present in inflammatory diseases of peripheral organs and tissues, and that they exert a significant effect on the incidence and severity of such conditions, it is not unreasonable to assume that these cytokines are similarly important within the CNS during infection or other inflammatory brain disorders. Clearly, more research is warranted to define the actions of the IL-10 family within the CNS and their role in the regulation of neuroinflammation.

AUTHOR CONTRIBUTIONS

AB and IM wrote and edited this review article.

FUNDING

This work was supported by the National Institute of Neurological Disorders and Stroke (NINDS) research grants R01 NS050325 and R03 NS097840 awarded to IM.

REFERENCES

Akil, H., Abbaci, A., Lalloué, F., Bessette, B., Costes, L. M. M., Domballe, L., et al. (2015). IL22/IL-22R pathway induces cell survival in human glioblastoma cells. *PLoS One* 10:e0119872. doi: 10.1371/journal.pone.0119872

Albanesi, C., Fairchild, H. R., Madonna, S., Scarponi, C., De Pità, O., Leung, D. Y. M., et al. (2007). IL-4 and IL-13 negatively regulate TNF-α- and IFN-γ-induced β-defensin expression through stat-6, suppressor of cytokine signaling (SOCS)-1, and SOCS-3. *J. Immunol.* 179, 984–992. doi: 10.4049/jimmunol.179.2.984

Almeida, R. D., Manadas, B. J., Melo, C. V., Gomes, J. R., Mendes, C. S., Grãos, M. M., et al. (2005). Neuroprotection by BDNF against glutamate-induced apoptotic cell death is mediated by ERK and PI3-kinase pathways. *Cell Death Differ.* 12, 1329–1343. doi: 10.1038/sj.cdd.4401662

Almolda, B., Costa, M., Montoya, M., González, B., and Castellano, B. (2011). Increase in th17 and t-reg lymphocytes and decrease of il22 correlate with the recovery phase of acute EAE in rat. *PLoS One* 6:e27473. doi: 10.1371/journal.pone.0027473

Andoh, A., Shioya, M., Nishida, A., Bamba, S., Tsujikawa, T., Kim-Mitsuyama, S., et al. (2009). Expression of IL-24, an activator of the JAK1/STAT3/SOCS3 cascade, is enhanced in inflammatory bowel disease. *J. Immunol.* 183, 687–695. doi: 10.4049/jimmunol.0804169

Astakhova, A. A., Chistyakov, D. V., Sergeeva, M. G., and Reiser, G. (2018). Regulation of the ARE-binding proteins, TTP (tristetraprolin) and HuR (human antigen R), in inflammatory response in astrocytes. *Neurochem. Int.* 118, 82–90. doi: 10.1016/j.neuint.2018.04.014

Babon, J. J., Varghese, L. N., and Nicola, N. A. (2014). Inhibition of IL-6 family cytokines by SOCS3. *Semin. Immunol.* 26, 13–19. doi: 10.1016/j.smim.2013.12.004

Baker, B. J., Akhtar, L. N., and Benveniste, E. N. (2009). SOCS1 and SOCS3 in the control of CNS immunity. *Trends Immunol.* 30, 392–400. doi: 10.1016/j.it.2009.07.001

Balasingam, V., and Yong, V. W. (1996). Attenuation of astroglial reactivity by interleukin-10. *J. Neurosci.* 16, 2945–2955. doi: 10.1523/JNEUROSCI.16-09-02945.1996

Baluchamy, S., Zhang, Y., Ravichandran, P., Ramesh, V., Sodipe, A., Hall, J. C., et al. (2010). Differential oxidative stress gene expression profile in mouse brain after proton exposure. *In Vitro Cell. Dev. Biol. Anim.* 46, 718–725. doi: 10.1007/s11626-010-9330-2

Barichello, T., Fagundes, G. D., Generoso, J. S., Paula Moreira, A., Costa, C. S., Zanatta, J. R., et al. (2012). Brain-blood barrier breakdown and pro-inflammatory mediators in neonate rats submitted meningitis by *Streptococcus pneumoniae*. *Brain Res.* 1471, 162–168. doi: 10.1016/j.brainres.2012.06.054

Barichello, T., Pereira, J. S., Savi, G. D., Generoso, J. S., Cipriano, A. L., Silvestre, C., et al. (2011). A kinetic study of the cytokine/chemokines levels and disruption of blood-brain barrier in infant rats after pneumococcal meningitis. *J. Neuroimmunol.* 233, 12–17. doi: 10.1016/j.jneuroim.2010.10.035

Beyeen, A. D., Adzemovic, M. Z., Ockinger, J., Stridh, P., Becanovic, K., Laaksonen, H., et al. (2010). IL-22RA2 associates with multiple sclerosis and macrophage effector mechanisms in experimental neuroinflammation. *J. Immunol.* 185, 6883–6890. doi: 10.4049/jimmunol.1001392

Bhoopathi, P., Lee, N., Pradhan, A. K., Shen, X.-N., Das, S. K., Sarkar, D., et al. (2017). *mda-7/IL-24* induces cell death in neuroblastoma through

a novel mechanism involving AIF and ATM. *Cancer Res.* 76, 3572–3582. doi: 10.1158/0008-5472.can-15-2959

Blumberg, H., Conklin, D., Xu, W., Grossmann, A., Brender, T., Carollo, S., et al. (2001). Interleukin 20: discovery, receptor identification, and role in epidermal function. *Cell* 104, 9–19. doi: 10.1016/S0092-8674(01)00187-8

Bonecchi, R., Garlanda, C., Mantovani, A., and Riva, F. (2016). Cytokine decoy and scavenger receptors as key regulators of immunity and inflammation. *Cytokine* 87, 37–45. doi: 10.1016/j.cyto.2016.06.023

Bowman, C. C., Rasley, A., Tranguch, S. L., and Marriott, I. (2003). Cultured astrocytes express toll-like receptors for bacterial products. *Glia* 43, 281–291. doi: 10.1002/glia.10256

Boyd, Z. S., Kriatchko, A., Yang, J., Agarwal, N., Wax, M. B., and Patil, R. V. (2003). Interleukin-10 receptor signaling through STAT-3 regulates the apoptosis of retinal ganglion cells in response to stress. *Invest. Ophthalmol. Vis. Sci.* 44, 5206–5211. doi: 10.1167/iovs.03-0534

Bsibsi, M., Persoon-Deen, C., Verwer, R. W. H., Meeuwsen, S., Ravid, R., Van Noort, J. M., et al. (2006). Toll-like receptor 3 on adult human astrocytes triggers production of neuroprotective mediators. *Glia* 53, 688–695. doi: 10.1002/glia.20328

Bsibsi, M., Ravid, R., Gveric, D., and van Noort, J. M. (2002). Broad expression of toll-like receptors in the human central nervous system. *J. Neuropathol. Exp. Neurol.* 61, 1013–1021. doi: 10.1093/jnen/61.11.1013

Buzas, K., Oppenheim, J. J., and Zack Howard, O. M. (2011). Myeloid cells migrate in response to IL-24. *Cytokine* 55, 429–434. doi: 10.1016/j.cyto.2011.05.018

Campbell, I. L. (2005). Cytokine-mediated inflammation, tumorigenesis, and disease-associated JAK/STAT/SOCS signaling circuits in the CNS. *Brain Res. Rev.* 48, 166–177. doi: 10.1016/j.brainresrev.2004.12.006

Chang, J., Kunkel, S. L., and Chang, C.-H. (2009). Negative regulation of MyD88-dependent signaling by IL-10 in dendritic cells. *Proc. Natl. Acad. Sci. U S A* 106, 18327–18332. doi: 10.1073/pnas.0905815106

Chauhan, V. S., Kluttz, J. M., Bost, K. L., and Marriott, I. (2011). Prophylactic and therapeutic targeting of the neurokinin-1 receptor limits neuroinflammation in a murine model of pneumococcal meningitis. *J. Immunol.* 186, 7255–7263. doi: 10.4049/jimmunol.1100721

Chauhan, V. S., Sterka, D. G. Jr., Gray, D. L., Bost, K. L., and Marriott, I. (2008). Neurogenic exacerbation of microglial and astrocyte responses to *Neisseria meningitidis* and *Borrelia burgdorferi*. *J. Immunol.* 180, 8241–8249. doi: 10.4049/jimmunol.180.12.8241

Chen, W.-Y., and Chang, M.-S. (2009). IL-20 is regulated by hypoxia-inducible factor and up-regulated after experimental ischemic stroke. *J. Immunol.* 182, 5003–5012. doi: 10.4049/jimmunol.0803653

Cho, K. J., Song, J., Oh, Y., and Lee, J. E. (2015). MicroRNA-Let-7a regulates the function of microglia in inflammation. *Mol. Cell. Neurosci.* 68, 167–176. doi: 10.1016/j.mcn.2015.07.004

Conti, B., Tabarean, I., Andrei, C., and Bartfai, T. (2004). Cytokines and fever. *Front. Biosci.* 9, 1433–1449. doi: 10.2741/1341

Cooley, I. D., Chauhan, V. S., Donneyz, M. A., and Marriott, I. (2014). Astrocytes produce IL-19 in response to bacterial challenge and are sensitive to the immunosuppressive effects of this IL-10 family member. *Glia* 62, 818–828. doi: 10.1002/glia.22644

Couper, K. N., Blount, D. G., and Riley, E. M. (2008). IL-10: the master regulator of immunity to infection. *J. Immunol.* 180, 5771–5777. doi: 10.4049/jimmunol.180.9.5771

Crill, E. K., Furr-Rogers, S. R., and Marriott, I. (2015). RIG-I is required for VSV-induced cytokine production by murine glia and acts in combination with DAI to initiate responses to HSV-1. *Glia* 63, 2168–2180. doi: 10.1002/glia.22883

Croker, B. A., Krebs, D. L., Zhang, J. G., Wormald, S., Willson, T. A., Stanley, E. G., et al. (2003). SOCS3 negatively regulates IL-6 signaling *in vivo*. *Nat. Immunol.* 4, 540–545. doi: 10.1038/ni931

Curtale, G., Mirolo, M., Renzi, T. A., Rossato, M., Bazzoni, F., and Locati, M. (2013). Negative regulation of Toll-like receptor 4 signaling by IL-10-dependent microRNA-146b. *Proc. Natl. Acad. Sci. U S A* 110, 11499–11504. doi: 10.1073/pnas.1219852110

Das, T., Hoarau, J. J., Bandjee, M. C. J., Marianne, M., and Gasque, P. (2015). Multifaceted innate immune responses engaged by astrocytes, microglia, and resident dendritic cells against Chikungunya neuroinfection. *J. Gen. Virol.* 96, 294–310. doi: 10.1099/vir.0.071175-0

Dhiman, R., Indramohan, M., Barnes, P. F., Nayak, R. C., Paidipally, P., Rao, L. V. M., et al. (2009). IL-22 produced by human NK cells inhibits growth of *Mycobacterium tuberculosis* by enhancing phagolysosomal fusion. *J. Immunol.* 183, 6639–6645. doi: 10.4049/jimmunol.0902587

Dhiman, R., Venkatasubramanian, S., Paidipally, P., Barnes, P. F., Tvinnereim, A., and Vankayalapati, R. (2014). Interleukin 22 inhibits intracellular growth of *Mycobacterium tuberculosis* by enhancing calgranulin a expression. *J. Infect. Dis.* 209, 578–587. doi: 10.1093/infdis/jit495

Dickensheets, H., Vazquez, N., Sheikh, F., Gingras, S., Murray, P. J., Ryan, J. J., et al. (2007). Suppressor of cytokine signaling-1 is an IL-4-inducible gene in macrophages and feedback inhibits IL-4 signaling. *Genes Immun.* 8, 21–27. doi: 10.1038/sj.gene.6364352

Ding, L., Linsley, P. S., Huang, L. Y., Germain, R. N., and Shevach, E. M. (1993). IL-10 inhibits macrophage costimulatory activity by selectively inhibiting the up-regulation of B7 expression. *J. Immunol.* 151, 1224–1234.

Dudakov, J. A., Hanash, A. M., and van den Brink, M. R. M. (2015). Interleukin-22: immunobiology and pathology. *Annu. Rev. Immunol.* 33, 747–785. doi: 10.1146/annurev-immunol-032414-112123

Dumoutier, L., Leemans, C., Lejeune, D., Kotenko, S. V., and Renauld, J.-C. (2001). Cutting edge: STAT activation by il-19, IL-20 and mda-7 through il-20 receptor complexes of two types. *J. Immunol.* 167, 3545–3549. doi: 10.4049/jimmunol.167.7.3545

Dumoutier, L., Louahed, J., and Renauld, J.-C. (2000). Cloning and characterization of il-10-related T cell-derived inducible factor (IL-TIF), a novel cytokine structurally related to IL-10 and inducible by IL-9. *J. Immunol.* 164, 1814–1819. doi: 10.4049/jimmunol.164.4.1814

Ellwardt, E., Walsh, J. T., Kipnis, J., and Zipp, F. (2016). Understanding the role of T cells in CNS homeostasis. *Trends Immunol.* 37, 154–165. doi: 10.1016/j.it.2015.12.008

Fayeye, O., Pettorini, B. L., Smith, M., Williams, H., Rodrigues, D., and Kay, A. (2013). *Meningococcal encephalitis* associated with cerebellar tonsillar herniation and acute cervicomedullary injury Case report. *Br. J. Neurosurg.* 27, 513–515. doi: 10.3109/02688697.2013.764967

Fiorentino, D. F., Zlotnik, A., Vierira, P., Mosmann, T. R., Howard, M., Moore, K. W., et al. (1991). IL-10 acts on the antigen-presenting cell to inhibit cytokine production by Th1 cells. *J. Immunol.* 146, 3444–3451.

Fisher, P. B. (2005). Is *mda-7/IL-24* a "magic bullet" for cancer? *Cancer Res.* 65, 10128–10138. doi: 10.1158/0008-5472.CAN-05-3127

Fisher, P. B., Gopalkrishnan, R. V., Chada, S., Ramesh, R., Grimm, E. A., Rosengeld, M. R., et al. (2003). *mda-7/IL-24*, a novel cancer selective apoptosis inducing cytokine gene: from the laboratory into the clinic. *Cancer Biol. Ther.* 2, 23–37. doi: 10.4161/cbt.458

Francis, J., MohanKumar, P. S., and MohanKumar, S. M. J. (2001). Lipopolysaccharide stimulates norepinephrine efflux from the rat hypothalamus *in vitro*: blockade by soluble il-1 receptor. *Neurosci. Lett.* 308, 71–74. doi: 10.1016/s0304-3940(01)01903-6

Furr, S. R., Chauhan, V. S., Moerdyk-Schauwecker, M. J., and Marriott, I. (2011). A role for DNA-dependent activator of interferon regulatory factor in the recognition of herpes simplex virus type 1 by glial cells. *J. Neuroinflammation* 8:99. doi: 10.1186/1742-2094-8-99

Furr, S. R., Moerdyk-Schauwecker, M., Grdzelishvili, V. Z., and Marriott, I. (2010). RIG-I mediates non-segmented negative-sense RNA virus-induced inflammatory immune responses of primary human astrocytes. *Glia* 58, 1620–1629. doi: 10.1002/glia.21034

Gallagher, G. (2010). Interleukin-19: multiple roles in immune regulation and disease. *Cytokine Growth Factor Rev.* 21, 345–352. doi: 10.1016/j.cytogfr.2010.08.005

Gallagher, G., Dickensheets, H., Eskdale, J., Izotova, L. S., Mirochnitchenko, O. V., Peat, J. D., et al. (2000). Cloning, expression and initial characterisation of interleukin-19 (IL-19), a novel homologue of human interleukin-10 (IL-10). *Genes Immun.* 1, 442–450. doi: 10.1038/sj.gene.6363714

Gallagher, G., Eskdale, J., Jordan, W., Peat, J., Campbell, J., Boniotto, M., et al. (2004). Human interleukin-19 and its receptor: a potential role in the induction of Th2 responses. *Int. Immunopharmacol.* 4, 615–626. doi: 10.1016/j.intimp.2004.01.005

Gautam, A., Dixit, S., Philipp, M. T., Singh, S. R., Morici, L. A., Kaushal, D., et al. (2011). Interleukin-10 alters effector functions of multiple genes induced by *Borrelia burgdorferi* in macrophages to regulate lyme

disease inflammation. *Infect. Immun.* 79, 4876–4892. doi: 10.1128/iai.05451-11

Gazzinelli, R. T., Wysocka, M., Hieny, S., Scharton-kersten, T., Cheever, A., Kuhn, R., et al. (1996). In the absence of endogenous IL-10, mice acutely infected with Toxoplasma gondii succumb to a lethal immune response dependent on $CD4^+$ T cells and accompanied by overproduction of IL-12, IFN-γ and TNF-α. *J. Immunol.* 157, 798–805.

Guglielmetti, C., Le Blon, D., Santermans, E., Salas-Perdomo, A., Daans, J., De Vocht, N., et al. (2016). Interleukin-13 immune gene therapy prevents CNS inflammation and demyelination via alternative activation of microglia and macrophages. *Glia* 64, 2181–2200. doi: 10.1002/glia.23053

Gutierrez-Murgas, Y. M., Skar, G., Ramirez, D., Beaver, M., and Snowden, J. N. (2016). IL-10 plays an important role in the control of inflammation but not in the bacterial burden in S. epidermidis CNS catheter infection. *J. Neuroinflammation* 13:271. doi: 10.1186/s12974-016-0741-1

Gyurkovska, V., and Ivanovska, N. (2016). Distinct roles of TNF-related apoptosis-inducing ligand (TRAIL) in viral and bacterial infections: from pathogenesis to pathogen clearance. *Inflamm. Res.* 65, 427–437. doi: 10.1007/s00011-016-0934-1

He, M., and Liang, P. (2010). IL-24 transgenic mice: *in vivo* evidence of overlapping functions for IL-20, IL-22, and IL-24 in the epidermis. *J. Immunol.* 184, 1793–1798. doi: 10.4049/jimmunol.0901829

Headland, S. E., and Norling, L. V. (2015). The resolution of inflammation: principles and challenges. *Semin. Immunol.* 27, 149–160. doi: 10.1016/j.smim.2015.03.014

Hebenstreit, D., Luft, P., Schmiedlechner, A., Regl, G., Frischauf, A.-M., Aberger, F., et al. (2003). IL-4 and IL-13 induce SOCS-1 gene expression in A549 cells by three functional STAT6-binding motifs located upstream of the transcription initiation site. *J. Immunol.* 171, 5901–5907. doi: 10.4049/jimmunol.171.11.5901

Horiuchi, H., Parajuli, B., Wang, Y., Azuma, Y. T., Mizuno, T., Takeuchi, H., et al. (2015). Interleukin-19 acts as a negative autocrine regulator of activated microglia. *PLoS One* 10:e0118640. doi: 10.1371/journal.pone.0118640

Hosoi, T., Wada, S., Suzuki, S., Okuma, Y., Akira, S., Matsuda, T., et al. (2004). Bacterial endotoxin induces IL-20 expression in the glial cells. *Mol. Brain Res.* 130, 23–29. doi: 10.1016/j.molbrainres.2004.07.005

Hsu, Y.-H., Wu, C.-Y., Hsing, C.-H., Lai, W.-T., Wu, L.-W., and Chang, M.-S. (2015). Anti-IL-20 monoclonal antibody suppresses prostate cancer growth and bone osteolysis in murine models. *PLoS One* 10:e0139871. doi: 10.1371/journal.pone.0139871

Hulshof, S., Montagne, L., De Groot, C. J. A., and Van Der Valk, P. (2002). Cellular localization and expression patterns of interleukin-10, interleukin-4, and their receptors in multiple sclerosis lesions. *Glia* 38, 24–35. doi: 10.1002/glia.10050

Hutchins, A. P., Diez, D., and Miranda-Saavedra, D. (2013). The IL-10/STAT3-mediated anti-inflammatory response: recent developments and future challenges. *Brief. Funct. Genomics* 12, 489–498. doi: 10.1093/bfgp/elt028

Hutchins, A. P., Poulain, S., and Miranda-Saavedra, D. (2012). Genome-wide analysis of STAT3 binding *in vivo* predicts effectors of the anti-inflammatory response in macrophages. *Blood* 119, e110–e119. doi: 10.1182/blood-2011-09-381483

Ichiyama, T., Shoji, H., Takahashi, Y., Matsushige, T., Kajimoto, M., Inuzuka, T., et al. (2008). Cerebrospinal fluid levels of cytokines in non-herpetic acute limbic encephalitis: comparison with herpes simplex encephalitis. *Cytokine* 44, 149–153. doi: 10.1016/j.cyto.2008.07.002

Ikeuchi, H., Kuroiwa, T., Hiramatsu, N., Kaneko, Y., Hiromura, K., Ueki, K., et al. (2005). Expression of interleukin-22 in rheumatoid arthritis: potential role as a proinflammatory cytokine. *Arthritis Rheum.* 52, 1037–1046. doi: 10.1002/art.20965

Iyer, A., Zurolo, E., Prabowo, A., Fluiter, K., Spliet, W. G. M., van Rijen, P. C., et al. (2012). MicroRNA-146a: a key regulator of astrocyte-mediated inflammatory response. *PLoS One* 7:e44789. doi: 10.1371/journal.pone.0044789

Jack, C. S., Arbour, N., Manusow, J., Montgrain, V., Blain, M., McCrea, E., et al. (2005). TLR signaling tailors innate immune responses in human microglia and astrocytes. *J. Immunol.* 175, 4320–4330. doi: 10.4049/jimmunol.175.7.4320

Jackson, S. H., Yu, C.-R., Mahdi, R. M., Ebong, S., and Egwuagu, C. E. (2004). Dendritic cell maturation requires STAT1 and is under feedback regulation by suppressors of cytokine signaling. *J. Immunol.* 172, 2307–2315. doi: 10.4049/jimmunol.172.4.2307

Jeffries, A. M., and Marriott, I. (2017). Human microglia and astrocytes express cGAS-STING viral sensing components. *Neurosci. Lett.* 658, 53–56. doi: 10.1016/j.neulet.2017.08.039

Johnson, M. B., Young, A. D., and Marriott, I. (2017). The therapeutic potential of targeting substance P/NK-1R interactions in inflammatory CNS disorders. *Front. Cell. Neurosci.* 10:296. doi: 10.3389/fncel.2016.00296

Kebir, H., Kreymborg, K., Ifergan, I., Dodelet-Devillers, A., Cayrol, R., Bernard, M., et al. (2007). Human TH17 lymphocytes promote blood-brain barrier disruption and central nervous system inflammation. *Nat. Med.* 13, 1173–1175. doi: 10.1038/nm1651

Khodakheir, T. N., Pourtalebi-firoozabadi, A., and Sangtarash, M. H. (2017). Association between interleukin-19 (IL-19) and interleukin-20 (IL-20) genes polymorphisms with multiple sclerosis in an iranian population. *Gene Cell Tissue* 4:e11957. doi: 10.5812/gct.11957

Klose, J., Schmidt, N. O., Melms, A., Dohi, M., Miyazaki, J., Bischof, F., et al. (2013). Suppression of experimental autoimmune encephalomyelitis by interleukin-10 transduced neural stem/progenitor cells. *J. Neuroinflammation* 10:117. doi: 10.1186/1742-2094-10-117

Koscsó, B., Csóka, B., Selmeczy, Z., Himer, L., Pacher, P., Virág, L., et al. (2012). Adenosine augments interleukin-10 production by microglial cells through an A2B adenosine receptor-mediated process. *J. Immunol.* 188, 445–453. doi: 10.4049/jimmunol.1101224

Kreymborg, K., Etzensperger, R., Dumoutier, L., Haak, S., Rebollo, A., Buch, T., et al. (2007). IL-22 is expressed by Th17 cells in an IL-23-dependent fashion, but not required for the development of autoimmune encephalomyelitis. *J. Immunol.* 179, 8098–8104. doi: 10.4049/jimmunol.179.12.8098

Kumari, S., Bonnet, M. C., Ulvmar, M. H., Wolk, K., Karagianni, N., Witte, E., et al. (2013). Article tumor necrosis factor receptor signaling in keratinocytes triggers interleukin-24-dependent psoriasis-like skin inflammation in mice. *Immunity* 39, 899–911. doi: 10.1016/j.immuni.2013.10.009

Kunz, S., Wolk, K., Witte, E., Witte, K., Doecke, W. D., Volk, H. D., et al. (2006). Interleukin (IL)-19, IL-20 and IL-24 are produced by and act on keratinocytes and are distinct from classical ILs. *Exp. Dermatol.* 15, 991–1004. doi: 10.1111/j.1600-0625.2006.00516.x

Laaksonen, H., Guerreiro-Cacais, A. O., Adzemovic, M. Z., Parsa, R., Zeitelhofer, M., Jagodic, M., et al. (2014). The multiple sclerosis risk gene IL22RA2 contributes to a more severe murine autoimmune neuroinflammation. *Genes Immun.* 15, 457–465. doi: 10.1038/gene.2014.36

Lai, L., Song, Y., Liu, Y., Chen, Q., Han, Q., Chen, W., et al. (2013). MicroRNA-92a negatively regulates toll-like receptor (TLR)-triggered inflammatory response in macrophages by targeting MKK4 kinase. *J. Biol. Chem.* 288, 7956–7967. doi: 10.1074/jbc.m112.445429

Ledeboer, A., Brevé, J. J. P., Poole, S., Tilders, F. J. H., and Dam, A. V. A. N. (2000). Transforming growth factor-β differentially regulate production of pro-inflammatory cytokines and nitric oxide in co-cultures of rat astroglial and microglial cells. *Glia* 142, 134–142. doi: 10.1002/(SICI)1098-1136(200004)30:2<134::AID-GLIA3>3.0.CO;2-3

Ledeboer, A., Brevé, J. J. P., Wierinckx, A., van der Jagt, S., Bristow, A. F., Leysen, J. E., et al. (2002). Expression and regulation of interleukin-10 and interleukin-10 receptor in rat astroglial and microglial cells. *Eur. J. Neurosci.* 16, 1175–1185. doi: 10.1046/j.1460-9568.2002.02200.x

Lee, S., Cho, S., Lee, E., Kim, S., Lee, S., Lim, J., et al. (2013). Interleukin-20 promotes migration of bladder cancer cells through extracellular signal-regulated kinase (ERK) -mediated MMP-9 protein expression leading to nuclear factor (NF-κB) activation by inducing the up-regulation of p21 WAF1 protein expression. *J. Biol. Chem.* 288, 5539–5552. doi: 10.1074/jbc.M112.410233

Lejeune, D., Dumoutier, L., Constantinescu, S., Kruijer, W., Schuringa, J. J., and Renauld, J. C. (2002). Interleukin-22 (IL-22) activates the JAK/STAT, ERK, JNK, and p38 MAP kinase pathways in a rat hepatoma cell line: pathways that are shared with and distinct from IL-10. *J. Biol. Chem.* 277, 33676–33682. doi: 10.1074/jbc.m204204200

Levillayer, F., Mas, M., Levi-Acobas, F., Brahic, M., and Bureau, J. F. (2007). Interleukin 22 is a candidate gene for Tmevp3, a locus controlling

Theiler's virus-induced neurological diseases. *Genetics* 176, 1835–1844. doi: 10.1534/genetics.107.073536

Liang, S. C., Tan, X.-Y., Luxenberg, D. P., Karim, R., Dunussi-Joannopoulos, K., Collins, M., et al. (2006). Interleukin (IL)-22 and IL-17 are coexpressed by Th17 cells and cooperatively enhance expression of antimicrobial peptides. *J. Exp. Med.* 203, 2271–2279. doi: 10.1084/jem.20061308

Lim, S.-H., Park, E., You, B., Jung, Y., Park, A. R., Park, S.-G., et al. (2013). Neuronal synapse formation induced by microglia and interleukin 10. *PLoS One* 8:e81218. doi: 10.1371/journal.pone.0081218

Liu, X., Chauhan, V. S., Young, A. B., and Marriott, I. (2010). NOD2 mediates inflammatory responses of primary murine glia to *Streptococcus pneumoniae*. *Glia* 50, 839–847. doi: 10.1002/glia.20968

Liu, J., Sisk, J. M., Gama, L., Clements, J. E., and Witwer, K. W. (2013). Tristetraprolin expression and microRNA-mediated regulation during simian immunodeficiency virus infection of the central nervous system. *Mol. Brain* 6:40. doi: 10.1186/1756-6606-6-40

Liu, Y. J., Shao, L. H., Zhang, J., Fu, S. J., Wang, G., Chen, F. Z., et al. (2015). The combination of decoy receptor 3 and soluble triggering receptor expressed on myeloid cells-1 for the diagnosis of nosocomial bacterial meningitis. *Ann. Clin. Microbiol. Antimicrob.* 14:17. doi: 10.1186/s12941-015-0078-0

Logsdon, N. J., Deshpande, A., Harris, B. D., Rajashankar, K. R., and Walter, M. R. (2012). Structural basis for receptor sharing and activation by interleukin-20 receptor-2 (IL-20R2) binding cytokines. *Proc. Natl. Acad. Sci. U S A* 109, 12704–12709. doi: 10.1073/pnas.1117551109

Ma, Z., Zhang, E., Yang, D., and Lu, M. (2015). Contribution of Toll-like receptors to the control of hepatitis B virus infection by initiating antiviral innate responses and promoting specific adaptive immune responses. *Cell. Mol. Immunol.* 12, 273–282. doi: 10.1038/cmi.2014.112

Ma, C., Zhao, L.-L., Zhao, H.-J., Cui, J.-W., Li, W., and Wang, N.-Y. (2018). Lentivirus-mediated MDA7/IL24 expression inhibits the proliferation of hepatocellular carcinoma cells. *Mol. Med. Rep.* 17, 5764–5773. doi: 10.3892/mmr.2018.8616

Martin, N. M., and Griffin, D. E. (2017). Interleukin-10 modulation of virus clearance and disease in mice with alphaviral encephalomyelitis. *J. Virol.* 92:e01517-17. doi: 10.1128/jvi.01517-17

Martin, J. C., Wolk, K., Bériou, G., Abidi, A., Witte-Händel, E., Louvet, C., et al. (2017). Limited presence of IL-22 binding protein, a natural IL-22 inhibitor, strengthens psoriatic skin inflammation. *J. Immunol.* 198, 3671–3678. doi: 10.4049/jimmunol.1700021

Martinez Doncel, A., Rubio, A., Arroyo, R., de las Heras, V., Martín, C., Fernandez-Arquero, M., et al. (2002). Interleukin-10 polymorphisms in spanish multiple sclerosis patients. *J. Neuroimmunol.* 131, 168–172. doi: 10.1016/s0165-5728(02)00248-5

McKimmie, C. S., and Fazakerley, J. K. (2005). In response to pathogens, glial cells dynamically and differentially regulate Toll-like receptor gene expression. *J. Neuroimmunol.* 169, 116–125. doi: 10.1016/j.jneuroim.2005.08.006

Mingomataj, E., and Bakiri, A. H. (2016). Regulator versus effector paradigm: interleukin-10 as indicator of the switching response. *Clin. Rev. Allergy Immunol.* 50, 97–113. doi: 10.1007/s12016-015-8514-7

Minkiewicz, J., de Rivero Vaccari, J. P., and Keane, R. W. (2013). Human astrocytes express a novel NLRP2 inflammasome. *Glia* 61, 1113–1121. doi: 10.1002/glia.22499

Mino, T., and Takeuchi, O. (2013). Post-transcriptional regulation of cytokine mRNA controls the initiation and resolution of inflammation. *Biotechnol. Genet. Eng. Rev.* 29, 49–60. doi: 10.1080/02648725.2013.801236

Moidunny, S., Matos, M., Wesseling, E., Banerjee, S., Volsky, D. J., Cunha, R. A., et al. (2016). Oncostatin M promotes excitotoxicity by inhibiting glutamate uptake in astrocytes: implications in HIV-associated neurotoxicity. *J. Neuroinflammation* 13:144. doi: 10.1186/s12974-016-0613-8

Molina-Holgado, E., Vela, J. M., Arévalo-Martin, A., and Guaza, C. (2001). LPS/IFN-g cytotoxicity in oligodendroglial cells: role of nitric oxide and protection by the anti-inflammatory cytokine IL-10. *Eur. J. Neurosci.* 13, 493–502. doi: 10.1046/j.0953-816x.2000.01412.x

Moore, K. W., de Waal Malefyt, R., Coffman, R. L., and O'Garra, A. (2001). Interleukin-10 and the interleukin-10 receptor. *Annu. Rev. Immunol.* 19, 683–765. doi: 10.1146/annurev.immunol.19.1.683

Moser, D. M., and Zhang, X. (2008). Interleukin 10: new perspectives on an old cytokines. *Immunol. Rev.* 226, 205–218. doi: 10.1111/j.1600-065x.2008.00706.x

Myhr, K. M., Vågnes, K. S., Marøy, T. H., Aarseth, J. H., Nyland, H. I., and Vedeler, C. A. (2002). Interleukin-10 promoter polymorphisms in patients with multiple sclerosis. *J. Neurol. Sci.* 202, 93–97. doi: 10.1016/s0022-510x(02)00246-0

Myles, I. A., Fontecilla, N. M., Valdez, P. A., Vithayathil, P. J., Naik, S., Belkaid, Y., et al. (2013). Signaling via the IL-20 receptor inhibits cutaneous production of IL-1 b and IL-17A to promote infection with methicillin-resistant *Staphylococcus aureus*. *Nat. Immunol.* 14, 804–811. doi: 10.1038/ni.2637

Newton, A. H., Cardani, A., and Braciale, T. J. (2016). The host immune response in respiratory virus infection: balancing virus clearance and immunopathology. *Semin. Immunopathol.* 38, 471–482. doi: 10.1007/s00281-016-0558-0

Nikfarjam, B. A., Ebtekar, M., Sabouni, F., Pourpak, Z., and Kheirandish, M. (2014). Detection of Interleukin-19 mRNA in C57BL/6 mice astroglial cells and brain cortex. *Basic Clin. Neurosci.* 5, 88–95.

Norden, D. M., Fenn, A. M., Dugan, A., and Godbout, J. P. (2014). TGFβ produced by IL-10 re-directed astrocytes attenuates microglial activation. *Glia* 62, 881–895. doi: 10.1002/glia.22647

O'Neill, E. J., Day, M. J., and Wraith, D. C. (2006). IL-10 is essential for disease protection following intranasal peptide administration in the C57BL/6 model of EAE. *J. Neuroimmunol.* 178, 1–8. doi: 10.1016/j.jneuroim.2006.05.030

Ouyang, W., Rutz, S., Crellin, N. K., Valdez, P. A., and Hymowitz, S. G. (2011). Regulation and functions of the IL-10 family of cytokines in inflammation and disease. *Annu. Rev. Immunol.* 29, 71–109. doi: 10.1146/annurev-immunol-031210-101312

Papandreou, A., Hedrera-Fernandez, A., Kaliakatsos, M., Chong, W. K., and Bhate, S. (2016). An unusual presentation of paediatric Listeria meningitis with selective spinal grey matter involvement and acute demyelinating polyneuropathy. *Eur. J. Paediatr. Neurol.* 20, 196–199. doi: 10.1016/j.ejpn.2015.08.004

Park, K. W., Lee, H. G., Jin, B. K., and Lee, Y. B. (2007). Interleukin-10 endogenously expressed in microglia prevents lipopolysaccharide-induced neurodegeneration in the rat cerebral cortex *in vivo*. *Exp. Mol. Med.* 39, 812–819. doi: 10.1038/emm.2007.88

Parrish-Novak, J., Xu, W., Brender, T., Yao, L., Jones, C., West, J., et al. (2002). Interleukins 19, 20, and 24 signal through two distinct receptor complexes: differences in receptor-ligand interactions mediate unique biological functions. *J. Biol. Chem.* 277, 47517–47523. doi: 10.1074/jbc.M205114200

Patial, S., Curtis, A. D. II., Lai, W. S., Stumpo, D. J., Hill, G. D., Flake, G. P., et al. (2016). Enhanced stability of tristetraprolin mRNA protects mice against immune-mediated inflammatory pathologies. *Proc. Natl. Acad. Sci. U S A* 113, 1865–1870. doi: 10.1073/pnas.1519906113

Pelegrín, I., Moragas, M., Suárez, C., Ribera, A., Verdaguer, R., Martínez-Yelamos, S., et al. (2014). Listeria monocytogenes meningoencephalitis in adults: analysis of factors related to unfavourable outcome. *Infection* 42, 817–827. doi: 10.1007/s15010-014-0636-y

Pena-Philippides, J. C., Yang, Y., Bragina, O., Hagberg, S., Nemoto, E., and Roitbak, T. (2014). Effect of pulsed electromagnetic field (PEMF) on infarct size and inflammation after cerebral ischemia in mice. *Transl. Stroke Res.* 5, 491–500. doi: 10.1007/s12975-014-0334-1

Perriard, G., Mathias, A., Enz, L., Canales, M., Schluep, M., Gentner, M., et al. (2015). Interleukin-22 is increased in multiple sclerosis patients and targets astrocytes. *J. Neuroinflammation* 12:119. doi: 10.1186/s12974-015-0335-3

Persaud, L., De Jesus, D., Brannigan, O., Richiez-Paredes, M., Huaman, J., Alvarado, G., et al. (2016). Mechanism of action and applications of interleukin 24 in immunotherapy. *Int. J. Mol. Sci.* 17:E869. doi: 10.3390/ijms17060869

Persson, M., Brantefjord, M., Hansson, E., and Rönnbäck, L. (2005). Lipopolysaccharide increases microglial GLT-1 expression and glutamate uptake capacity *in vitro* by a mechanism dependent on TNF-α. *Glia* 51, 111–120. doi: 10.1002/glia.20191

Persson, M., Brantefjord, M., Liljeqvist, J., Bergström, T., Hannson, E., and Rönnbäck, L. (2007). Microglial GLT-1 is upregulated in response to herpes simplex virus infection to provide an antiviral defence via glutathione. *Glia* 55, 1449–1458. doi: 10.1002/glia.20560

Ponomarev, E. D., Veremeyko, T., Barteneva, N., Krichevsky, A. M., and Weiner, H. L. (2011). MicroRNA-124 promotes microglia quiescence and suppresses EAE by deactivating macrophages via the C/EBP-α-PU.1 pathway. *Nat. Med.* 17, 64–70. doi: 10.1038/nm.2266

Qian, L., Wei, S.-J., Zhang, D., Hu, X., Xu, Z., Wilson, B., et al. (2008). Potent anti-inflammatory and neuroprotective effects of TGF- 1 are mediated through the inhibition of ERK and p47phox-Ser345 phosphorylation and translocation in microglia. *J. Immunol.* 181, 660–668. doi: 10.4049/jimmunol.181.1.660

Qin, Z., Wang, P.-Y., Su, D.-F., and Liu, X. (2016). miRNA-124 in immune system and immune disorders. *Front. Immunol.* 7:406. doi: 10.3389/fimmu.2016.00406

Rasley, A., Tranguch, S. L., Rati, D. M., and Marriott, I. (2006). Murine glia express the immunosuppressive cytokine, interleukin-10, following exposure to *Borrelia burgdorferi* or *Neisseria meningitidis*. *Glia* 53, 583–592. doi: 10.1002/glia.20314

Reiss-Mandel, A., Rubin, C., Zayoud, M., Rahav, G., and Regev-Yochay, G. (2018). *Staphylococcus aureus* colonization induces strain-specific suppression of interleukin-17. *Infect. Immun.* 86:e00834-17. doi: 10.1128/iai.00834-17

Rodriguez-Mercado, R., Ford, G. D., Xu, Z., Kraiselburd, E. N., Martinez, M. I., Eterović, V. A., et al. (2012). Acute neuronal injury and blood genomic profiles in a nonhuman primate model for ischemic stroke. *Comp. Med.* 62, 427–438.

Rossi, C., Cusimano, M., Zambito, M., Finardi, A., Capotondo, A., Garcia-Manteiga, J. M., et al. (2018). Interleukin 4 modulates microglia homeostasis and attenuates the early slowly progressive phase of amyotrophic lateral sclerosis article. *Cell Death Dis.* 9:250. doi: 10.1038/s41419-018-0288-4

Rutz, S., Wang, X., and Ouyang, W. (2014). The IL-20 subfamily of cytokines—from host defence to tissue homeostasis. *Nat. Rev. Immunol.* 14, 783–795. doi: 10.1038/nri3766

Sauane, M., Gopalkrishnan, R. V., Lebedeva, I., Mei, M. X., Sarkar, D., Su, Z. Z., et al. (2003). *Mda-7/IL-24* induces apoptosis of diverse cancer cell lines through JAK/STAT-independent pathways. *J. Cell. Physiol.* 196, 334–345. doi: 10.1002/jcp.10309

Schwartz, M., Kipnis, J., Rivest, S., and Prat, A. (2013). How do immune cells support and shape the brain in health, disease, and aging? *J. Neurosci.* 33, 17587–17596. doi: 10.1523/JNEUROSCI.3241-13.2013

Serramía, M. J., Muñoz-fernández, M. Á., and Álvarez, S. (2015). HIV-1 increases TLR responses in human primary astrocytes. *Sci. Rep.* 5:17887. doi: 10.1038/srep17887

Sertorio, M., Hou, X., Carmo, R. F., Dessein, H., Cabantous, S., Abdelwahed, M., et al. (2015). IL-22 and IL-22 binding protein (IL-22BP) regulate fibrosis and cirrhosis in hepatitis C virus and schistosome infections. *Hepatology* 61, 1321–1331. doi: 10.1002/hep.27629

Shah, G. S. (2018). Pyogenic ventriculitis and meningitis caused by streptococcus acidominimus in humans: a case report. *Am. J. Case Rep.* 19, 329–334. doi: 10.12659/ajcr.908000

Sharma, S., Yang, B., Xi, X., Grotta, J. C., Aronowski, J., and Savitz, S. I. (2011). IL-10 directly protects cortical neurons by activating PI-3 kinase and STAT-3 pathways. *Brain Res.* 1373, 189–194. doi: 10.1016/j.brainres.2010.11.096

Shen, H., Kreisel, D., and Goldstein, D. R. (2013). Processes of sterile inflammation. *J. Immunol.* 191, 2857–2863. doi: 10.4049/jimmunol.1301539

Sheng, W. S., Hu, S., Kravitz, F. H., Peterson, P. K., and Chao, C. C. (1995). Tumor necrosis factor α upregulates human microglial cell production of interleukin-10 *in vitro*. *Clin. Diagn. Lab. Immunol.* 2, 604–608.

Sun, Y., Li, N., Zhang, J., Liu, H., Liu, J., Xia, X., et al. (2016). Enolase of *Streptococcus Suis Serotype 2* enhances blood-brain barrier permeability by inducing IL-8 release. *Inflammation* 39, 718–726. doi: 10.1007/s10753-015-0298-7

Sun, Y., Luo, Z.-M., Guo, X.-M., Su, D.-F., and Liu, X. (2015). An updated role of microRNA-124 in central nervous system disorders: a review. *Front. Cell. Neurosci.* 9:193. doi: 10.3389/fncel.2015.00193

Talaat, R. M., Alrefaey, S. A., Bassyouni, I. H., Ashour, M. E., and Raouf, A. A. (2016). Genetic polymorphisms of interleukin 6 and interleukin 10 in Egyptian patients with systemic lupus eythematosus. *Lupus* 25, 255–264. doi: 10.1177/0961203315615219

Tibussek, D., Sinclair, A., Yau, I., Teatero, S., Fittipaldi, N., Richardson, S. E., et al. (2015). Late-onset group B streptococcal meningitis has cerebrovascular complications. *J. Pediatr.* 166, 1187.e1–1192.e1. doi: 10.1016/j.jpeds.2015.02.014

Tsung, A., Tohme, S., and Billiar, T. R. (2014). High-mobility group box-1 in sterile inflammation. *J. Intern. Med.* 276, 425–443. doi: 10.1111/joim.12276

Wang, P., Bai, F., Zenewicz, L. A., Dai, J., Gate, D., Cheng, G., et al. (2012). IL-22 signaling contributes to west nile encephalitis pathogenesis. *PLoS One* 7:e44153. doi: 10.1371/journal.pone.0044153

Wang, M., and Liang, P. (2005). Interleukin-24 and its receptors. *Immunology* 114, 166–170. doi: 10.1111/j.1365-2567.2005.02094.x

Wegenka, U. M. (2010). IL-20: biological functions mediated through two types of receptor complexes. *Cytokine Growth Factor Rev.* 21, 353–363. doi: 10.1016/j.cytogfr.2010.08.001

Werry, E. L., Liu, G. J., Lovelace, M. D., Nagarajah, R., Hickie, I. B., and Bennett, M. R. (2011). Lipopolysaccharide-stimulated interleukin-10 release from neonatal spinal cord microglia is potentiated by glutamate. *Neuroscience* 175, 93–103. doi: 10.1016/j.neuroscience.2010.10.080

Wilbers, R. H. P., van Raaij, D. R., Westerhof, L. B., Bakker, J., Smant, G., and Schots, A. (2017). Re-evaluation of IL-10 signaling reveals novel insights on the contribution of the intracellular domain of the IL-10R2 chain. *PLoS One* 12:e0186317. doi: 10.1371/journal.pone.0186317

Wilson, M. S., Feng, C. G., Barber, D. L., Yarovinsky, F., Cheever, A. W., Sher, A., et al. (2010). Redundant and pathogenic roles for IL-22 in mycobacterial, protozoan, and helminth infections. *J. Immunol.* 184, 4378–4390. doi: 10.4049/jimmunol.0903416

Wolk, K., Kunz, S., Asadullah, K., and Sabat, R. (2002). Cutting edge: immune cells as sources and targets of the IL-10 family members? *J. Immunol.* 168, 5397–5402. doi: 10.4049/jimmunol.168.11.5397

Wolk, K., Witte, E., Warszawska, K., Schulze-Tanzil, G., Witte, K., Philipp, S., et al. (2009). The Th17 cytokine IL-22 induces IL-20 production in keratinocytes: a novel immunological cascade with potential relevance in psoriasis. *Eur. J. Immunol.* 39, 3570–3581. doi: 10.1002/eji.200939687

Xie, W., Fang, L., Gan, S., and Xuan, H. (2016). Interleukin-19 alleviates brain injury by anti-inflammatory effects in a mice model of focal cerebral ischemia. *Brain Res.* 1650, 172–177. doi: 10.1016/j.brainres.2016.09.006

Xin, J., Wainwright, D. A., Mesnard, N. A., Serpe, C. J., Sanders, V. M., and Jones, K. J. (2011). IL-10 within the CNS is necessary for $CD4^+$ T cells to mediate neuroprotection. *Brain Behav. Immun.* 25, 820–829. doi: 10.1016/j.bbi.2010.08.004

Yu, L., Wu, X., Wei, J., Liao, Q., Xu, L., Luo, S., et al. (2015). Preliminary expression profile of cytokines in brain tissue of BALB/c mice with *Angiostrongylus cantonensis* infection. *Parasites and Vectors* 8:328. doi: 10.1186/s13071-015-0939-6

Zenewicz, L. A., and Flavell, R. A. (2008). IL-22 and inflammation: leukin' through a glass onion. *Eur. J. Immunol.* 38, 3265–3268. doi: 10.1002/eji.200838655

Zeng, G., Chen, C. Y., Huang, D., Yao, S., Wang, R. C., and Chen, Z. W. (2011). Membrane-bound IL-22 after de novo production in tuberculosis and anti-*Mycobacterium Tuberculosis* effector function of IL-22^+ $CD4^+$ T cells. *J. Immunol.* 187, 190–199. doi: 10.4049/jimmunol.1004129

Zhang, R., Tan, Z., and Liang, P. (2000). Identification of a novel ligand-receptor pair constitutively activated by ras oncogenes. *J. Biol. Chem.* 275, 24436–24443. doi: 10.1074/jbc.M001958200

Zhao, Y., Bhattacharjee, S., Jones, B. M., Dua, P., Alexandrov, P. N., Hill, J. M., et al. (2013). Regulation of TREM2 expression by an NF-κB-sensitive miRNA-34a. *Neuroreport* 24, 318–323. doi: 10.1097/wnr.0b013e32835fb6b0

Zou, J. Y., and Crews, F. T. (2005). TNF a potentiates glutamate neurotoxicity by inhibiting glutamate uptake in organotypic brain slice cultures: neuroprotection by NF κB inhibition. *Brain Res.* 1034, 11–24. doi: 10.1016/j.brainres.2004.11.014

Conflict of Interest Statement: The authors declare that the research was conducted in the absence of any commercial or financial relationships that could be construed as a potential conflict of interest.

frontiers in Cellular Neuroscience

REVIEW
published: 05 December 2018
doi: 10.3389/fncel.2018.00474

Kinase-Based Taming of Brain Microglia Toward Disease-Modifying Therapy

Sun-Hwa Lee[1] and Kyoungho Suk[2]**

[1] New Drug Development Center, Daegu Gyeongbuk Medical Innovation Foundation, Daegu, South Korea, [2] Department of Pharmacology, Brain Science and Engineering Institute, School of Medicine, Kyungpook National University, Daegu, South Korea

Microglia are the primary immune cells residing in the central nervous system (CNS), where they play essential roles in the health and disease. Depending on the CNS inflammatory milieu, they exist in either resting or activated states. Chronic neuroinflammation mediated by activated microglia is now considered to be a common characteristic shared by many neurodegenerative diseases such as Parkinson's disease, Alzheimer's disease, and amyotrophic lateral sclerosis, which currently pose a significant socioeconomic burden to the global healthcare system. Accumulating evidence has indicated protein kinases (PKs) as important drug targets for therapeutic interventions of these detrimental diseases. Here, we review recent findings suggesting that selected PKs potentially participate in microglia-mediated neuroinflammation. Taming microglial phenotypes by modulating the activity of these PKs holds great promise for the development of disease-modifying therapies for many neurodegenerative diseases.

Keywords: microglia, neuroinflammation, protein kinase, drug target, neurodegenerative disease

OPEN ACCESS

Edited by:
Cinzia Volonté,
Institute of Cell Biology and Neurobiology, CNR, Italy

Reviewed by:
Andrew MacLean,
Tulane University School of Medicine, United States
Cataldo Arcuri,
University of Perugia, Italy

****Correspondence:***
Sun-Hwa Lee
sunhlee@dgmif.re.kr
Kyoungho Suk
ksuk@knu.ac.kr

Received: *22 September 2018*
Accepted: *20 November 2018*
Published: *05 December 2018*

Citation:
Lee S-H and Suk K (2018) Kinase-Based Taming of Brain Microglia Toward Disease-Modifying Therapy. Front. Cell. Neurosci. 12:474. doi: 10.3389/fncel.2018.00474

INTRODUCTION

Human kinases primarily comprise phosphotransferase, which catalyzes the transfer of the γ-phosphoryl group of adenosine triphosphate (ATP) to the hydroxyl group of a tyrosine (Tyr), serine (Ser), threonine (Thr), or histidine (His) residue of proteins and other target molecules including lipids and sugars. The kinases are known to regulate a multitude of cellular signaling pathways such as cell proliferation, survival, growth, apoptosis, differentiation, cytoskeletal rearrangement, metabolism, and angiogenesis. Aberrant kinase activity is linked to a wide range of diseases including neoplastic diseases, central nervous system (CNS) disorders, vascular disorders, and chronic inflammatory diseases. Except for only one protein His kinase and a couple of dual-specificity protein kinases (PKs) capable of phosphorylating both Tyr and Ser/Thr residues on their target molecules, PKs broadly fall into two groups: the protein Tyr kinases (PTKs) and the Ser- and Thr-specific PKs (SPKs) (Rask-Andersen et al., 2014). While the SPKs constitute a majority of the PKs, the PTKs serve as important drug targets due to their strong association of gain and/or loss of function mutations with various diseases. It is noteworthy that most of the US FDA-approved kinase inhibitors are PTK inhibitors for cancer indications, but not for CNS indications (Gunosewoyo et al., 2017).

Microglia are primary immune cells residing in the CNS, where they play key roles in the development and function of a normal healthy brain. Under normal physiological conditions,

ramified microglia constantly monitor the brain microenvironment in search of the presence of tissue damage and pathogen infections by continuously protruding and retracting their long processes. In addition to this surveillant function, microglia exert a phagocytic function to detect and rapidly eliminate degenerating neurons, resulting in the prevention of further detrimental effect on neighboring cells. This microglial phagocytic function is known to be crucial for synapse maturation (Paolicelli et al., 2011; Schafer et al., 2012; Gomez-Nicola and Perry, 2015). Moreover, microglia are directly or indirectly involved in the modulation of neuronal activity at the synapse, and influence myelination and neurogenesis by delivering signals in primary myelinating areas of the developing brain (Wlodarczyk et al., 2017). However, depending on encountered stimuli, microglia are activated and undergo significant changes in their function and morphology. Morphologically, they change to a rounded amoeboid form with shortened processes from a ramified form with long processes. Functionally, they result in either 'classical' pro-inflammatory or 'alternative' anti-inflammatory phenotypes (Arcuri et al., 2017; Kabba et al., 2018). Although neurons, oligodendrocytes, and astrocytes also play important roles in CNS inflammatory responses, it is currently viewed that chronic inflammation mediated by microglia predominantly contributes to many CNS disorders (Glass et al., 2010; Ransohoff, 2016b; Shabab et al., 2017).

Several recent review articles have shed light on the PKs as attractive drug targets for many diseases in the CNS. However, they primarily focused on PKs in neurons (Chico et al., 2009; Martin et al., 2013; Tell and Hilgeroth, 2013; Dzamko et al., 2014; Mehdi et al., 2016; Gunosewoyo et al., 2017), rather than those in microglia (Lee and Suk, 2017). Here, we briefly review recent findings on selected microglial PKs involved in microglia-mediated neuroinflammation (**Figure 1**), a common underlying mechanism of many neurodegenerative diseases including Parkinson's disease (PD), Alzheimer's disease (AD), and amyotrophic lateral sclerosis (ALS).

MICROGLIA-MEDIATED NEUROINFLAMMATION

The incidence of neurodegenerative diseases, including AD, PD, and ALS, is growing worldwide, thereby posing a considerable social and economic burden to the global healthcare system (Gitler et al., 2017). One of the common characteristics shared by these diseases is the loss of a specific population of neurons. AD is caused by the progressive loss of not only pyramidal neurons in the hippocampus and cortex, but cholinergic neurons in the basal forebrain. PD is caused by the progressive degeneration of dopamine neurons in the substantia nigra (SN) pars compacta of the midbrain as well as in other brain areas. ALS is characterized by the loss of motor neurons in the primary motor cortex, brainstem, and spinal cord (Ransohoff, 2016b; Lee and Suk, 2018). However, loss of neurons is not the only characteristic of neurodegenerative diseases. Accumulating evidence implies that neuronal degeneration may activate glial cells such as microglia, astrocytes, and oligodendrocytes, resulting in amplification of neuroinflammation. It is now widely accepted that microglia-mediated chronic inflammation is responsible for the progressive loss of neurons and serves as another hallmark common to neurodegenerative and neurodevelopmental diseases (Glass et al., 2010; Mosher and Wyss-Coray, 2014; Ransohoff, 2016b; Shabab et al., 2017). Furthermore, microglia-induced neurotoxicity as well as oxidative stress are also considered as other common pathological features shared by virtually all neurodegenerative diseases (Lee and Suk, 2018).

Microglial activation is often classified as either 'classical' or 'alternative' (Jha et al., 2016). 'Alternative' activation of microglia is induced by various cytokines [interleukin-4 (IL-4), IL-10, and IL-13], or immune complexes or apoptotic cells, resulting in the production of anti-inflammatory cytokines (IL-10 and transforming growth factor β), neurotrophic and growth factors (Jha et al., 2016; Gosselin et al., 2017). Thus, alternatively activated microglia refers to a beneficial and neuroprotective phenotype, functioning to resolve inflammation, to promote brain repair, and to eliminate cellular debris. In contrast, 'classical' activation of microglia is induced by lipopolysaccharide (LPS), ATP, interferon (IFN)-γ, and granulocyte-macrophage colony-stimulating factor, resulting in the production of pro-inflammatory cytokines [tumor necrosis factor-α (TNF-α), IL-1β, IL-6, and IL-18] and chemokines. In addition, they secrete oxidative stress-related molecules [nitric oxide (NO), reactive oxygen species (ROS), and superoxide anions]. Thus, classically activated microglia often refers to a neurotoxic and destructive phenotype, aggravating neuroinflammation and brain damage (Jha et al., 2016; Lee and Suk, 2018).

While the contributing roles of these two microglial phenotypes in neuroinflammation have been widely presented, microglia exhibit a high degree of heterogeneity (Jha et al., 2016). Depending on the brain area and the disease stages, both microglial phenotypes simultaneously exist in the same pathological brain. Moreover, the presence of more complex and distinct phenotypes of microglia has recently been reported (Bisht et al., 2016; Keren-Shaul et al., 2017; Krasemann et al., 2017). Indeed, *in vivo* activation status of microglia is more likely a continuum of these two phenotypes. Thus, simple classification of microglial activation as either classical or alternative, often referred to as M1 or M2, respectively, does not adequately reflect the complexity of microglial activation. Nonetheless, therapeutic strategies targeting neuroinflammation mediated by microglia are currently focused on the development of glial phenotype modulators (GPMs) that promote the M2 phenotype while suppressing the M1 phenotype of activated microglia (Ransohoff, 2016a; Song and Suk, 2017; Suk, 2017; Lee and Suk, 2018) (**Figure 2**).

PROTEIN KINASES IN MICROGLIA-MEDIATED NEUROINFLAMMATION

For the last two decades, PKs have been intensively pursued by both pharmaceutical industries and academia as attractive

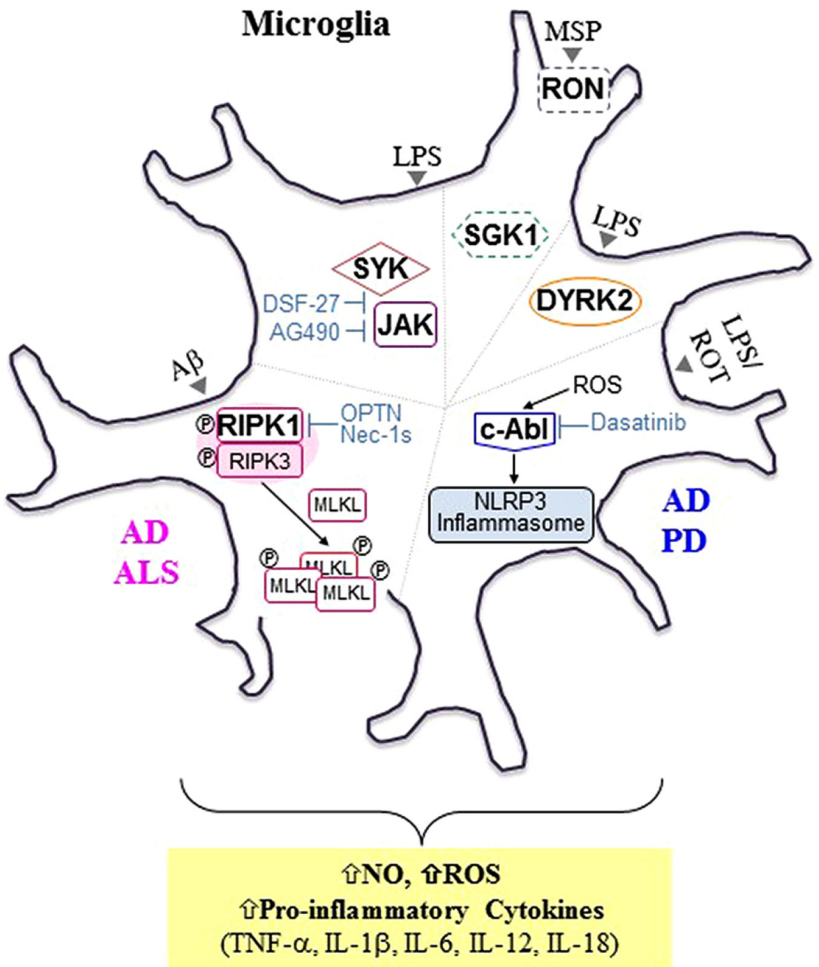

FIGURE 1 | Selected microglial protein kinases involved in microglia-mediated neuroinflammation and neurodegenerative diseases. In addition to progressive neuronal damage and death, it is now evident that chronic neuroinflammation mediated by microglia is another common hallmark shared by neurodegenerative diseases such as Alzheimer's disease (AD), Parkinson's disease (PD), and amyotrophic lateral sclerosis (ALS). Selected protein kinases (PKs) involved in microglia-mediated neuroinflammation are presented here, and these PKs can be targeted to tame microglial phenotypes favorable for disease-modifying treatments. In general, activated receptor interacting protein kinase 1 (RIPK1), a serine (Ser)/threonine (Thr) PK, interacts with and phosphorylates RIPK3, forming a RIPK1/RIPK3-containing complex, which is known as a "ripoptosome." Activated RIPK3, in turn, recruits and phosphorylates mixed lineage kinase domain-like protein (MLKL), promoting MLKL oligomerization and subsequent translocation into the plasma membrane, leading to direct pore formation and the initiation of necroptosis. In animal models of AD [APP/ PS1 transgenic mice] and ALS [optineurin (Optn) knockout mice (KO) and $mSOD^{G93A}$ mice], activated RIPK1 (either by $A\beta_{1-42}$ peptide or by the presence of Optn KO or $mSOD^{G93A}$) mediates inflammatory responses rather than necroptosis in microglia (Ito et al., 2016; Ofengeim et al., 2017). In addition, axonal myelination defects were observed in ALS mouse models and elevated levels of hallmarks of necroptosis were detected in microglia in postmortem cortical samples from AD patients. Treatment with Nec-1s, a highly selective and central nervous system-permeable RIPK inhibitor, was demonstrated to inhibit microglia-mediated inflammation (Ito et al., 2016). Reactive oxygen species (ROS) derived from oxidative stress were found to activate nucleotide oligomerization domain (NOD)-like receptor protein (NLRP3) inflammasome via cellular Abelson murine leukemia viral oncogene homolog 1 (c-Abl) activation, resulting in the release of primarily interleukin (Iβ)-1b and IL-18 (Lawana et al., 2017). Treatment of microglia with dasatinib, a dual c- Abl/c-Src kinase inhibitor, was demonstrated to inhibit NLRP3-mediated release of pro-inflammatory factors including IL-1bβ, IL-18, ROS, nitric oxide (NO), and tumor necrosis factor-α (TNF-α). A strong correlation between inflammasomes and neurological disorders including AD, PD, and multiple sclerosis (MS) has been implicated in many recent studies (Lang et al., 2018). Both spleen tyrosine kinase (SYK) and Janus kinase (JAK), intracellular tyrosine (Tyr) PKs were also found to be associated with microglia-mediated neuroinflammation upon lipopolysaccharide (LPS) stimulation (Zeng et al., 2014). DSF-27, a novel sesquiterpene dimmer isolated from the medicinal plant, *Artemisia argyi*, was demonstrated to inhibit LPS-induced activation of SYK and JAK signaling pathways, resulting in a reduction in TNF-α, IL-1β, IL-6, and NO levels. Treatment with AG490, a specific inhibitor of JAK2, was found to inhibit LPS-induced NO production (Inoue et al., 2016; Asai et al., 2018). Dual-specificity tyrosine phosphorylation-related kinase 2 (DYRK2) is an intracellular Ser/Thr kinase localized in both the nucleus and the cytoplasm. It was demonstrated to translocate to the nucleus and interact with multiple kinases downstream of LPS stimulation, thereby regulating the production of pro-inflammatory molecules such as TNF-α and IL-1β. Unlike the other kinases presented here, the basal activity of both Receptor D'Origine Nantais (RON) and serum- and glucocorticoid-inducible kinase 1 (SGK1), boxed with the dotted line, were demonstrated to be involved in the anti-inflammatory process in microglia. RON, a receptor tyrosine kinase, is activated by its ligand, macrophage-stimulating protein (MSP), resulting in the promotion of anti-inflammatory responses and subsequent tissue repair (Dey et al., 2018). SGK1, an intracellular Ser/Thr kinase, was found to inhibit LPS-induced activation of microglia. Aβ, amyloid beta; ROT, rotenone; APP, Amyloid Precursor Protein; PS1, Presenilin 1; Nec-1s, necrostatin-1s.

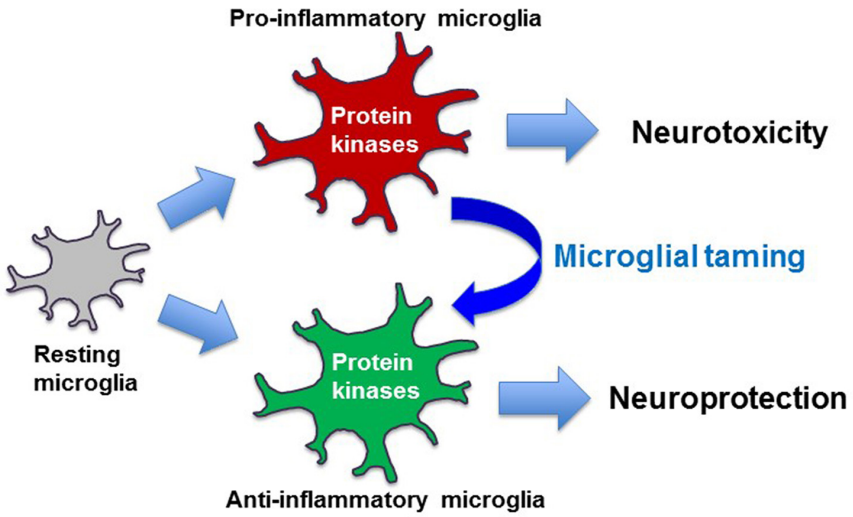

FIGURE 2 | Taming of microglia toward disease-modifying therapy. Pro-inflammatory microglia exert neurotoxic effects, while anti-inflammatory microglia are often neurotrophic and neuroprotective. Protein kinase-based modulation of microglial phenotypes from pro-inflammatory to anti-inflammatory may form the basis of disease-modifying therapy.

drug targets for not only cancer, but also inflammatory, infectious, degenerative, metabolic and cardiovascular diseases. However, most of kinase inhibitors have been approved for cancer indications rather than CNS indications (Gunosewoyo et al., 2017). Nonetheless, an increasing number of PKs have emerged as potential drug targets for CNS disorders (Chico et al., 2009; Gunosewoyo et al., 2017; Lee and Suk, 2017). Thus, this review summarizes selected PKs that are potentially involved in microglial activation and concomitant induction of neuroinflammation (**Figure 1**).

Receptor Interacting Protein Kinases

The receptor interacting protein kinase (RIPK) family contains seven members: RIPK1, RIPK2, RIPK3, RIPK4, RIPK5, RIPK6, and RIPK7. All members of the RIPK family contain an N-terminal Ser/Thr kinase domain (KD) (Ekdahl, 2012). Besides N-terminal KD, RIPK1 has a death domain (DD) and a bridging intermediate domain (ID) harboring an RIP homotypic interaction motif (RHIM) at the C-terminus, while RIPK2 has a caspase activation and recruitment domain (CARD) and ID without an RHIM at the C-terminus. RIPK3 contains a unique C-terminal sequences harboring an RHIM but lacks an ID. Both RIPK4 and RIPK5 contain ankyrin domains and an ID at the C-terminus. Both RIPK6 and RIPK7, which are structurally distant from the other family members, have several unique domains such as leucine-rich repeat (LRR) regions. Thus, RIPK6 and RIPK7 also refer to LRR kinase 1 (LRRK1) and 2 (LRRK2), respectively (Humphries et al., 2015). While there is currently a limited understanding of the physiological functions of RIPK4 – RIPK7, numerous studies have reported the important molecular and physiological roles of RIPK1 – RIPK3 in inflammation and cell death (Ślusarczyk et al., 2018). RIPK1 is now recognized as a master regulator of necroptosis, a regulated cell death characterized by loss of cell membrane integrity, swelling of cytoplasm and organelle, lack of DNA fragmentation, mitochondrial dysfunction and cellular collapse, resulting in deleterious signaling pathways downstream of type 1 TNF- α receptor (TNFR1). Upon TNF-α stimulation, caspase-8 activation is known to induce apoptosis. However, when caspase-8 dependent apoptosis is defective, RIPK1 is recruited to the intracellular DD of TNFR1 and interacts with RIPK3, inducing phosphorylation of RIPK3 and formation of an RIPK1/RIPK3-containing complex, which is known as complex IIb (Cho et al., 2009; He et al., 2009). RIPK3, then, initiates necroptosis by recruiting and phosphorylating mixed lineage kinase domain-like protein (MLKL), which is oligomerized and inserted into the plasma membrane to form pores (**Figure 1**) (Sun et al., 2012; Cai and Liu, 2014; Wang et al., 2014).

Recent studies have demonstrated that microglial RIPK1-mediated necroptosis is closely associated with the pathogenesis of AD and ALS. Ofengeim et al. (2017) reported for the first time that inhibition of RIPK1 kinase activity is effective in alleviating inflammation mediated by microglia *in vitro* and in mouse models of AD. This study demonstrated that elevated levels of RIPK1 were detected in microglia in postmortem cortical samples from AD patients as well as in amyloid precursor protein (APP)/presenilin 1 (PS1) transgenic (Tg) mouse model of AD. In addition, the levels of phosphorylation of RIPK1 on the Ser166 residue, a marker for RIPK1 autophosphorylation and activation, was found to be elevated in primary microglia treated with the $A\beta_{1-42}$ peptide. Either treatment of Nec-1s, a selective and CNS-permeable RIPK1 inhibitor, or by introduction of a kinase dead mutation of RIPK1 ($RIPK1^{D138N/D138N}$) was shown to reduce pro-inflammatory cytokines (TNF-α and IL-6) in primary microglia in response to the $A\beta_{1-42}$ peptide as well as in the CNS of APP/PS1 Tg mice. Interestingly, memory deficits of APP/PS1 Tg mice was significantly improved by

administration of Nec-1s or by genetic inhibition of RIPK1. By analyzing the transcriptional profiles of APP/PS1 microglia, this study revealed that RIPK1 in primary microglia is involved in the upregulation of Cst7 and Ch25h, which were previously identified in adult microglia obtained from animal models of AD (the 5xFAD Tg mice) and ALS (the mSOD1^{G93A} Tg mice), as well as aged mice. Ch25h encodes an enzyme on the cell surface responsible for cholesterol and lipid metabolism, and was previously demonstrated as a point of focus in genome-wide association studies of AD (Wollmer, 2010). Cst7 encodes Cystatin F, an endosomal/lysosomal cathepsin inhibitor, and was recently identified as one of the markers for disease-associated microglia (DAM), which is a newly characterized microglial phenotype found in the diseased brain (Papassotiropoulos et al., 2005; Keren-Shaul et al., 2017). This RIPK1-mediated induction of Cst7 was demonstrated to impair lysosomal trafficking of microglia, resulting in reduced clearing of Aβ. Administration of Nec-1s lowered Cst7 expression levels in APP/PS Tg mice (Ofengeim et al., 2017).

Ito et al. (2016) recently demonstrated that microglial RIPK1 can provoke toxicity of motor neuron axons by using optineurin (Optn) knockout (KO) mice as a model of ALS. The functional loss of OPTN has been associated with both familial and sporadic cases of ALS (Beeldman et al., 2015). The authors found that the Optn N KO mice exhibited enhanced levels of multiple necroptotic markers [RIPK1, RIPK3, phosphorylation of MLKL (p-MLKL), and the complex IIb] both in the spinal cords and in the mouse embryo fibroblasts. Interestingly, it was demonstrated that Optn KO microglia exhibited increased p-RIPK1 on Ser14 and Ser15 residues, indicators of activated RIPK1, compared to that in wild-type (WT) microglia, and that this increased level of p-RIPK1 was inhibited by Nec-1s treatment and by RIPK1$^{D138N/D138N}$. In addition, the Optn KO mice showed elevated levels of several pro-inflammatory cytokines in the spinal cords, but not in those of the Optn KO mice carrying RIPK1$^{D138N/D138N}$. Since microglia express little MLKL, but increased p-RIPK1 levels, the authors suggested that RIPK1 promotes pro-inflammatory signaling, rather than cell death. By performing RNA sequencing on primary microglia obtained from WT, Optn KO mice, and Optn KO mice carrying RIPK1$^{D138N/D138N}$, this study revealed that elevated levels of apoptosis, CD14 and CD86, indicators of the pro-inflammatory state, and axonal myelination defects found in Optn KO mice were not shown in Optn KO mice carrying RIPK1$^{D138N/D138N}$ or by administration of Nec-1s. These results were further confirmed in mSOD^{G93A} Tg mice. Lastly, this study demonstrated that necroptotic markers (RIPK1, MLKL, p-RIPK1, pMLKL, and RIPK3) were also elevated in both microglia and oligodendrocytes in human ALS samples. Collectively, this study suggests that microglial RIPK1 plays a crucial role in inducting inflammatory signaling pathways in ALS.

Given that the level of RIPK1 expression is higher than that of RIPK3 in activated microglia, RIPK1 inhibition may be an effective approach to attenuate microglia-mediated inflammatory responses. In addition, considering that RIPK1 is involved in signaling pathways downstream of TNFR1, rather than TNFR2, inhibiting RIPK1 may provide a novel approach to selectively target the detrimental cellular activities mediated by TNFR1 signaling pathways (Dhib-Jalbut and Kalvakolanu, 2015).

Cellular Abelson Murine Leukemia Viral Oncogene Homolog 1

Cellular abelson murine leukemia viral oncogene homolog 1 (c-Abl) (ABL1) is a member of the Abl family, which also comprises the Abl-related gene (Are or ABL2) as a member. c-Abl is known to be activated by diverse stimuli including oxidative stress, DNA damage, growth factors, and cell adhesion, thereby affecting various cellular activities including cell growth, survival, motility, proliferation, cytoskeleton reorganization, DNA repair, receptor endocytosis, autophagy, and oxidative stress (Gonfloni et al., 2012; Lindholm et al., 2016). Earlier studies have provided evidence that c-Abl plays multiple roles in neuronal development by positively regulating synapse formation, neurulation, and dendrogenesis (Schlatterer et al., 2011), and that aberrant activation of c-Abl is shown to be associated with AD and PD (Derkinderen et al., 2005; Ko et al., 2010; Tremblay et al., 2010; Imam et al., 2011; Gonfloni et al., 2012; Lindholm et al., 2016). Indeed, accumulating evidence has implied the beneficial effect of c-Abl inhibition for patients with AD and PD (Schlatterer et al., 2011; Karuppagounder et al., 2014; Mahul-Mellier et al., 2014; Brahmachari et al., 2016). Nilotinib, an FDA-approved Abl inhibitor for patients with chronic myeloid leukemia, are currently undergoing phase II clinical trials for both AD and PD (Lee and Suk, 2017). Nonetheless, there are limited studies regarding the function of c-Abl in the microglia-mediated neuroinflammatory process in AD and PD (Deleidi et al., 2010; Field et al., 2010; Dhawan and Combs, 2012; Cheng et al., 2017; Lee and Suk, 2017).

Inflammasomes are multiprotein complexes assembled in response to damage signals and invading pathogens. They are presently categorized into two families: the protein family containing pyrin and hematopoietic-interferon-inducible nuclear antigens with 200 amino-acid repeats domain and the nucleotide oligomerization domain (NOD)-like receptor protein (NLR) protein family phylogenetically containing three subfamilies: NODs, IPAF, and NLRPs. Among 14 members of NLPRs, the most well characterized inflammasome is NLRP3 inflammasome consisting of NLRP3, the apoptosis associated speck-like protein containing a CARD domain, and pro-caspase-1 (Rubartelli, 2014; Lang et al., 2018). The NLRP3 inflammasome is tightly controlled and induced by two steps. The first step is the transcriptional induction of pro-IL-1β and NLRP3 by activation of nuclear factor kappa-light-chain-enhancer of activated B cells (NF-κB) via Toll-like receptors (TLRs) or NOD2 signaling. The second step is the formation of the NLRP3 inflammasome complex and subsequent production of mature IL-1β and IL-18 processed by caspase-1 (Ozaki et al., 2015).

Lawana et al. (2017) recently reported that c-Abl is involved in microglial activation of the NLRP3 inflammasome in a BV-2 immortalized murine microglial cell line (Bocchini et al., 1992). This study demonstrated that compared to BV-2 cells treated with either LPS or rotenone (ROT), a

mitochondrial electron transport chain inhibitor, LPS-primed BV-2 cells treated with ROT (LPS/ROT) exhibited a significant increase in NLRP3 inflammasome markers (NLRP3, mature caspase-1, and IL-1β), pro-inflammatory cytokines (TNF-α, IL-1 β, and IL-18), NO and mitochondrial ROS, but a decrease in mitochondrial membrane potential. These results suggest that elevated mitochondrial ROS by LPS/ROT may promote activation of microglia through induction of NLRP3 inflammasome. In addition, this study found that LPS/ROT-treated BV-2 microglial cells displayed a robust induction of both c-Abl phosphorylation on Tyr245 and Tyr412 residues (p-c-Abl), indicators of c-Abl activation, and protein kinase C (PKC)-δ phosphorylation (p-PKC-δ), a downstream mediator of c-Abl activation, while pretreatment with mitochondria-targeted ROS scavengers significantly reduced the levels of p-c-Abl and p-PKC-δ and production of ROS, IL-1β, and IL-18. Interestingly, inhibition of c-Abl by either c-Abl-specific siRNA or pretreatment with dasatinib, a dual kinase inhibitor of both c-Src and c-Abl, reversed the effects of LPS/ROT treatment. Thus, these data suggest that ROT-induced oxidative stress triggers c-Abl activation, leading to exacerbation of LPS-mediated induction of NLRP3 inflammasomes in microglia.

It was also demonstrated that primary microglia stimulated by LPS/ROT exhibited a drastic augmentation of NLRP3 in the mitochondria compared to the control, while dasatinib pretreatment inhibited NLRP3 trafficking to the mitochondria. These data imply that c-Abl inhibition may attenuate ROT-mediated mitochondrial dysfunction, resulting in redistribution of NLRP3 to mitochondria in LPS-primed cells. In addition, this study also showed that LPS/ROT-treated BV-2 cells exhibited a significant increase in NF-κB nuclear translocation and concomitant upregulation of NF-κB-regulated genes including IL-1β, IL-18, and NO, while dasatinib pretreatment markedly attenuated NF-κB activation. These results indicate that the anti-inflammatory effects mediated by dasatinib might, in part, result from inhibition of c-Abl/NF-κB signaling pathways, thereby influencing the NLRP3 inflammasome-mediated pro-inflammatory signaling cascade. Moreover, this study found a sustained and dramatic increase in microtubule-associated proteins 1A/1B light chain 3B, Beclin1, and p62 levels in not only BV-2 cells, but also in primary microglial cells treated with LPS/ROT, compared to that in control cells. However, dasatinib pretreatment and c-Abl siRNA transfection attenuated the increases in these autophagic markers. Furthermore, LPS/ROT-treated BV-2 cells exhibited a marked reduction in lysosomal acidification and transcription factor EB (TFEB) expression levels compared to control cells, while dasatinib pretreatment restored lysosomal acidification and the levels of TFEB expression. These observations suggest that ROT-mediated perturbation of autophagic flux might be further aggravated by LPS. In a neuron-glia co-culture system, it was demonstrated that sequential treatment with LPS/ROT caused a significant increase in p-c-Abl and p-PKC-δ levels and the loss of tyrosine hydroxylase $(TH)^+$ cells, while dasatinib restored the loss of TH levels. In addition, dasatinib administration was shown to reduce the expression of NLRP3, mature caspase-1, IL-1β, and ionized calcium-binding adapter molecule-1 in the SN of LPS-induced neuroinflammatory mouse model of PD. Likewise, LPS-induced hyperphosphorylation of c-Abl kinase and PKC-δ as well as induction of autolysosomal markers were ameliorated by dasatinib treatment in the SN of these mice. Lastly, it was demonstrated that sickness behavior as well as motor function of these mice were also improved by dasatinib treatment.

Taken together, this study for the first time suggested that LPS priming and subsequent ROT stimulation induces ROS-dependent aberrant c-Abl activation, thereby exacerbating NLRP3 inflammasome signaling and amplifying the microglial activation response. Indeed, a study showing that microglial expression of IL-1β and IL-18 depends on NLRP3 inflammasomes supports the findings of this study (Gustin et al., 2015). Moreover, a strong correlation between inflammasomes and neurological disorders including AD, PD, and multiple sclerosis (MS) has been reported in many recent studies (Lang et al., 2018). Thus, targeting c-Abl may be an effective therapeutic option for the modulation of inflammasomes and neurotoxicity.

Spleen Tyrosine Kinase and Janus Kinase 2

Janus kinase 2 (JAK2) belongs to the JAK kinase family comprising four members: JAK1, JAK2, JAK3, and TYK2. It is involved in various cellular signaling activities induced by the activation of diverse receptor families including the type II cytokine receptor family, granulocyte-macrophage colony-stimulating factor receptor family, gp-130 receptor family, and the single chain receptors (Hebenstreit et al., 2005). Spleen tyrosine kinase (SYK), a member of the SYK family comprising SYK and Zeta-chain-associated protein kinase 70, plays a key role in the signaling cascade mediated by immunoreceptors such as B-cell and T-cell receptors (Frommhold et al., 2007; Mócsai et al., 2010). In addition, SYK is known to be recruited to the TLR-associated receptor complex, and thereby contributes to phagocytosis and cytokine expression in various immune cells (Miller et al., 2012). Several previous studies have provided evidence of the involvement of SYK and JAK2 in microglia-mediated inflammatory responses (Combs et al., 1999; Kacimi et al., 2011; Cunningham et al., 2012; Minogue et al., 2012)

A recent study has further indicated the contributing roles of SYK- and JAK-mediated signaling in microglia upon LPS stimulation (Zeng et al., 2014). This study demonstrated that LPS-treated BV-2 cells exhibit an increase in SYK phosphorylation, but pretreatment of DSF-27, a sesquiterpene dimmer compound isolated from *Artemisia argyi*, reversed this increase. In addition, it was found that BV-2 cells treated by either SYK-specific siRNA or DSF-27 pretreatment showed a reduced NO production and phosphorylation of AKT/NF-κB upon LPS stimulation, compared to control cells, suggesting that SYK activation is involved in LPS-mediated AKT/NF-κB activation. In line with these results, DSF-27 pretreatment was shown to inhibit the expression of various inflammatory factors induced by LPS. Considering that both SYK and AKT is potentially involved in the signaling pathways downstream of TREM2, a critical receptor required for DAM activation (Xing et al., 2015;

Mecca et al., 2018), future studies should investigate whether both SYK and AKT may contribute to the function of DAM (Mecca et al., 2018).

The study also demonstrated that phosphorylation of JAK2 and signal transducer and activator of transcription 3 (STAT3) was significantly decreased in LPS-treated BV-2 cells by DSF-27 pretreatment. In addition, treatment with AG490, a specific inhibitor of JAK2, was shown to suppress induction of STAT3 and NO in LPS-treated BV-2 cells. Thus, these data suggest that JAK2 exerts its pro-inflammatory effect on microglia after LPS stimulation, and the anti-inflammatory effect of DSF-27 is in part mediated by inhibition of JAK2. It was also shown that DSF-27 treatment suppressed phosphorylation of both extracellular-signal-regulated kinase (ERK) and p38, and that treatment of BV-2 cells with specific inhibitors of these kinases lowered LPS-induced phosphorylation of JAK2 and STAT3 and release of NO. These results imply that both ERK and p38 may function as potential upstream kinases regulating JAK2/STAT3 signaling pathways in microglia. Lastly, in co-culture systems of primary cortical neurons and microglia as well as midbrain neurons and microglia, this study demonstrated that DSF-27 attenuates neuronal degeneration, suggesting a protective role of DSF-27 against microglia-mediated neuronal injury.

Since IL-6 could activate the JAK2/STAT3 signaling pathway, which could induce TNF-α release, resulting in activation of the SYK/NF-κB signaling pathway, both the SYK and JAK2 pathways could promote activation of each other, thereby enhancing the inflammatory responses. Taken together, this study indicates that regulation of the SYK and JAK2/STAT3 signaling pathways could be an effective therapeutic approach for the containment of microglia-mediated neuroinflammation and neurotoxicity (Chiba et al., 2009).

Serum- and Glucocorticoid-Inducible Kinase 1

Serum- and glucocorticoid-inducible kinase 1 (SGK1) belongs to SGK family comprising three members: SGK1, SGK2, and SGK3. Its expression is regulated by serum and a wide variety of hormones including glucocorticoids (Lang et al., 2006). Although the detailed distribution and function remains unknown, all SGK family members are detected in the CNS (Kobayashi and Cohen, 1999). It has been reported that SGK1 was detected in neurons, astrocytes, oligodendrocytes, and a minor proportion of microglia (Wärntges et al., 2002; Miyata et al., 2011; Slezak et al., 2013). Previous studies have suggested that SGKs play significant roles in neutrophils, Th17 cells, and dendritic cells (Kleinewietfeld et al., 2013; Burgon et al., 2014; Schmid et al., 2014). However, biological functions of SGKs in microglia have been less studied.

Inoue et al. (2016) recently reported that all three members of the SGK family are detected in the mouse cerebral cortex, while SGK1 and SGK3 are detected in several cell lines of microglia including BV-2 and N9. This study revealed that treatment with gsk650394, a pan-SGK inhibitor, significantly inhibited the cellular viability of both BV-2 and N9 cells, suggesting the involvement of basal SGK activity in the maintenance of microglial viability. Pretreatment with gsk650394 further enhanced LPS-mediated translocation of NF-κB and production of pro-inflammatory molecules, including iNOS, NO, and TNF-α in BV-2 cells, and NO production in N9 cells compared to that in untreated control cells. Thus, these results indicate that basal SGK activity is likely associated with the suppression of inflammatory responses of microglial cells.

The same group recently reported the pivotal role of Sgk1 in inhibiting pathological activation of microglia by using Sgk1 KO ($Sgk1^{-/-}$) BV-2 cells, which were created using the clustered regulatory interspaced palindromic repeats/Cas9 system (Asai et al., 2018). This study indicated that functional abolition of Sgk1 in BV-2 cells resulted in amoeboid morphology as well as increased levels of CD68 expression, which are characteristics of activated microglia. Furthermore, LPS-mediated iNOS expression was enhanced in $Sgk1^{-/-}$ BV-2 cells compared with WT BV-2 cells, indicating that disruption of Sgk1 promotes microglial activation. In addition, this study found that $Sgk1^{-/-}$ BV-2 cells proliferate more rapidly than WT BV-2 cells, as demonstrated in a previously study using gsk650394, suggesting that Sgk1 is involved in cellular proliferation. Moreover, compared to that in WT BV-2 cells, $Sgk1^{-/-}$ BV-2 cells exhibited significantly lower AKT phosphorylation and higher ATP susceptibility. Since it has been reported that high doses of ATP repress AKT signaling in microglia and other cells (Bian et al., 2013; Hao et al., 2013), this study assumed that increased susceptibility of $Sgk1^{-/-}$ BV-2 cells to ATP may be at least due to the lower activity of AKT signaling.

Collectively, this study suggests that basal activity of microglial SGK may participate in the inhibition of microglia-mediated neuroinflammation. However, given that SGK1 is implicated in diverse neuronal functions (Lang et al., 2009), preferential targeting of SGK1 in microglia, but not in other cells in the CNS, may clarify the potential *in vivo* role of basal microglial Sgk1 activity in anti-inflammatory responses in the future.

Dual-Specificity Tyrosine Phosphorylation-Related Kinase 2

The dual-specificity kinases are able to catalyze phosphorylation of not only Ser/Thr residues in their substrates, but also a single Tyr residue in their own activation loop (Becker and Joost, 1999). Dual-specificity tyrosine phosphorylation-related kinase 2 (DYRK2) belongs to the dual-specificity tyrosine phosphorylation-related kinase (DYRK) family comprising five members: DYRK1A, DYRK1B, DYRK2, DYRK3, and DYRK4. It has been previously reported that DYRK2 primes c-Jun and c-Myc phosphorylation in cancer cells and controls p53 phosphorylation on the Ser46 residue upon DNA damage (Yoshida, 2008; Taira et al., 2012; Sun et al., 2017). DYRK2 has also been demonstrated to negatively regulate Type I IFN signaling by promoting TNF receptor associated factor family member-associated NF-κB activator-binding kinase 1 (TBK1) degradation via phosphorylation of TBK1 at the Ser527 residue. Since TBK1 is a downstream molecule of TLR4, which is involved in the activation of NF-κB and the induction of pro-inflammatory cytokine expression (Möser et al., 2015), the potential role of DYRK2 in inflammatory responses has been suggested (An et al., 2015).

A recent study explored the potential role of Dyrk2 in LPS-induced activation of microglia (Xu et al., 2018). This study demonstrated that Dyrk2 is localized in the nucleus, but mainly in the cytoplasm of BV-2 cells. In the course of LPS stimulation for 6 h, this study found that the Dyrk2 level was gradually decreased in the cytoplasm, but increased in the nucleus. The phosphorylation of the NF-κB subunit, p65 (p-p65), remained unchanged in the nucleus, but gradually increased in the cytoplasm for 3 h and later decreased. However, the level of p38 phosphorylation (p-p38) was enhanced in both the cytoplasm and the nucleus. This study also demonstrated that Dyrk2 overexpression in BV-2 cells significantly increased the levels of p-p65, p-AKT, and p-p38 after LPS stimulation, implying that DYRK2 is involved in phosphorylation of these molecules. Interestingly, however, it was found that Dyrk2 overexpression reduced the expression of TNF-α and IL-1β. Considering a previous report demonstrating that AKT activation in microglia is associated with anti-inflammatory effects (Kalantari et al., 2017), it is suggested that decreased production of these cytokines by Dyrk2 overexpression is likely due to AKT activation. Since AKT activation also appears to be modulated by TREM2 or CX3CR1 in microglia (Mecca et al., 2018), a contributing role of DYRK2 in AKT activation mediated by these receptors remains to be further studied in the future. It was also found that Dyrk2 selectively interacted with p38 in the nucleus, while it interacted with AKT, p38, and the NF-κB p65 subunit in the cytoplasm of BV-2 cells.

Although the exact mechanisms underlying the direct or indirect influence of DYRK2 on phosphorylation of these molecules and how DYRK2 is activated or translocated to the nucleus upon LPS stimulation remain to be further investigated, this study implies that DYRK2 is likely involved in phosphorylation of multiple molecules downstream of LPS stimulation, and thereby regulates the production of pro-inflammatory molecules.

Receptor D'Origine Nantais

Receptor D'Origine Nantais (RON) is a member of Met proto-oncogene family. It is known to be widely expressed in the neurons and microglia, and is activated by macrophage-stimulating protein (MSP), which functions as a neurotrophic factor (Stella et al., 2001; Yu et al., 2016).

A recent study reported that microglial RON is activated upon binding to MSP, resulting in the promotion of the anti-inflammatory process and subsequent tissue repair (Dey et al., 2018). This study demonstrated that the CNS of mice carrying a deletion of ligand binding domain ($Ron^{-/-}$) exhibited an increase in pro-inflammatory molecules including iNOS, COX2, and TNF-α and tissue degradation factors such as MMP2 and MMP9 compared to that of age-matched WT mice. In addition, $Ron^{-/-}$ mice exhibited exacerbated levels of several metabolic markers of CNS stress (phenylalanine, glutamate, hypoxantine, and choline), but decreased levels of healthy neuron markers (*N*-acetyl aspartate and glutamine). These results imply that RON plays protective roles in the CNS. It also indicated that RON expression was detected in CHME-3 cells, a human fetal microglial cell line, in which MSP stimulation resulted in induction of RON expression and a reduction in LPS-mediated production of TNF-α and IL-1β. Using two disease models, this study further demonstrated the involvement of RON in CNS inflammation. In an experimental autoimmune encephalomyelitis mouse model of MS, loss of Ron led to greater disease severity with elevated tissue inflammation in the CNS compared to that in WT mice. Similarly, it has been shown that loss of Ron resulted in exacerbated CNS inflammation with decreased M2 markers and concomitantly increased M1 markers in the diet-induced obesity mice in comparison to control mice (Frommhold et al., 2007). Currently, it is unknown whether RON activation may also be beneficial in other neurodegenerative diseases. However, this study suggests that induction of RON activation selectively in the CNS could potentially alleviate uncontrolled CNS inflammation.

EPILOG

Microglia are essential for proper brain development and maintenance of CNS homeostasis, such as regulation of synaptic maturation, elimination of damaged or dying neurons, and secretion of neurotrophic modulators. However, microglia lose these physiological functions during the course of many CNS diseases and exhibit distinct phenotypic signatures associated with neurodegenerative diseases, in which microglia-mediated neuroinflammation is one of the key pathologic hallmarks (Butovsky and Weiner, 2018). Thus, taming microglia with GPMs toward both maintaining homeostatic function and inhibiting disease-promoting or inflammatory responses could serve the goal of microglial-targeted therapy (Song and Suk, 2017; Suk, 2017; Lee and Suk, 2018).

A recent analysis reported that the likelihood of US FDA approval for CNS drugs is approximately 50% of that for drugs in other areas and that it takes longer for FDA to approve CNS drugs (Schwartz and Deczkowska, 2016). In addition, gradual and more challenging progress has been made in the development of kinase inhibitors for CNS disorders compared to that for other therapeutic areas such as oncology and chronic inflammation, which appears largely due to the intrinsic complexity linked to CNS drug development and partly to the lack of validated druggable targets. However, an increasing number of PKs have emerged as potential drug targets for CNS disorders (Chico et al., 2009; Gunosewoyo et al., 2017; Lee and Suk, 2017), suggesting better opportunities for the development of CNS drugs in the future. However, the lack of relevant biological systems capable of predicting the efficacy and toxicity of treatment has been stated as the most frequent reason for the clinical failure of CNS dug development. Thus, for the success of developing CNS disease-modifying therapies with GPMs including PKs modulators, we should consider the presence of not only species-specific, but also regional brain differences between human and rodent microglia regarding basic biochemistry, gene expression, transcriptomic profiles, and pharmacologic responses (Melief et al., 2012, 2016; Doorn et al., 2015; Bennett et al., 2016; Grabert et al., 2016; Satoh et al., 2016; Gribkoff and Kaczmarek, 2017). Furthermore, given that genes that are regulated during aging

are critically different between mouse and human microglia, and that transcriptomic and epigenetic signatures of human microglia are heavily influenced by the environmental conditions (Gosselin et al., 2017). Thus, for the translation of microglial research into clinical practice, it is necessary to investigate whether all the features shown in rodent microglia by certain kinase activities are truly applicable to human microglia by incorporating more physiologically relevant assay systems (Hu et al., 2015).

In this review, we summarized recent studies on the potential role of selected PKs in microglial activation and concomitant induction of neuroinflammation. It will not be surprising to find additional PKs relevant to microglia-mediated neuroinflammation in future studies. Targeting more than one PK target may provide effective approaches for the future interventions of many CNS disorders. Alternatively, drug repositioning with FDA-approved protein kinase inhibitors may facilitate the process of drug development for CNS disorders, such as the recently demonstrated beneficial effect of c-Abl inhibitors in AD and PD (Miller et al., 2012). Since neurotoxicity, another hallmark shared by many neurodegenerative diseases, is either directly affected by neuronal kinases or indirectly by signaling pathways mediated by microglial activation via microglial kinases (Lee and Suk, 2018), targeting common PKs shared by both neuron and microglia may serve as promising therapeutic strategies for neurodegenerative diseases.

In conclusion, a growing number of PKs not only in neurons, but also in non-neuronal cells in the CNS, such as microglia, are emerging as important therapeutic targets and there is rapid advancement and growth in the understanding of microglial function. Therefore, taming microglial activation states by modulating the activity of the PKs described in this review holds great promise for curing or alleviating symptoms associated with many neurodegenerative diseases.

AUTHOR CONTRIBUTIONS

S-HL and KS made a substantial intellectual contribution to this work, and wrote the manuscript.

FUNDING

The work was supported by the National Research Foundation of Korea (NRF) grants funded by the Korean government (NRF-2017R1A5A2015391, 2016M3C7A1904148, and 2018R1A2A1A05077118).

ACKNOWLEDGMENTS

We apologize to all authors whose works have not been cited due to space constraints.

REFERENCES

An, T., Li, S., Pan, W., Tien, P., Zhong, B., Shu, H. B., et al. (2015). DYRK2 negatively regulates type I interferon induction by promoting TBK1 degradation via Ser527 phosphorylation. *PLoS Pathog.* 11:e1005179. doi: 10.1371/journal.ppat.1005179

Arcuri, C., Fioretti, B., Bianchi, R., Mecca, C., Tubaro, C., Beccari, T., et al. (2017). Microglia-glioma cross-talk: a two way approach to new strategies against glioma. *Front. Biosci.* 22, 268–309. doi: 10.2741/4486

Asai, H., Inoue, K., Sakuma, E., Shinohara, Y., and Ueki, T. (2018). Potential implication of SGK1-dependent activity change in BV-2 microglial cells. *Int. J. Physiol. Pathophysiol. Pharmacol.* 10, 115–123.

Becker, W., and Joost, H. G. (1999). Structural and functional characteristics of Dyrk, a novel subfamily of protein kinases with dual specificity. *Prog. Nucleic Acid Res. Mol. Biol.* 62, 1–17.

Beeldman, E., van der Kooi, A. J., de Visser, M., van Maarle, M. C., van Ruissen, F., and Baas, F. (2015). A Dutch family with autosomal recessively inherited lower motor neuron predominant motor neuron disease due to optineurin mutations. *Amyotroph. Lateral Scler. Frontotemporal Degener.* 16, 410–411. doi: 10.3109/21678421.2015.1066821

Bennett, M. L., Bennett, F. C., Liddelow, S. A., Ajami, B., Zamanian, J. L., Fernhoff, N. B., et al. (2016). New tools for studying microglia in the mouse and human CNS. *Proc. Natl. Acad. Sci. U.S.A.* 113, E1738–E1746. doi: 10.1073/pnas.1525528113

Bian, S., Sun, X., Bai, A., Zhang, C., Li, L., Enjyoji, K., et al. (2013). P2X7 integrates PI3K/AKT and AMPK-PRAS40-mTOR signaling pathways to mediate tumor cell death. *PLoS One* 8:e60184. doi: 10.1371/journal.pone.0060184

Bisht, K., Sharma, K. P., Lecours, C., Sánchez, M. G., El Hajj, H., Milior, G., et al. (2016). Dark microglia: a new phenotype predominantly associated with pathological states. *Glia* 64, 826–839. doi: 10.1002/glia.22966

Bocchini, V., Mazzolla, R., Barluzzi, R., Blasi, E., Sick, P., and Kettenmann, H. (1992). An immortalized cell line expresses properties of activated microglial cells. *J. Neurosci. Res.* 31, 616–621. doi: 10.1002/jnr.490310405

Brahmachari, S., Ge, P., Lee, S. H., Kim, D., Karuppagounder, S. S., Kumar, M., et al. (2016). Activation of tyrosine kinase c-Abl contributes to alpha-synuclein-induced neurodegeneration. *J. Clin. Invest.* 126, 2970–2988. doi: 10.1172/JCI85456

Burgon, J., Robertson, A. L., Sadiku, P., Wang, X., Hooper-Greenhill, E., Prince, L. R., et al. (2014). Serum and glucocorticoid-regulated kinase 1 regulates neutrophil clearance during inflammation resolution. *J. Immunol.* 192, 1796–1805. doi: 10.4049/jimmunol.1300087

Butovsky, O., and Weiner, H. L. (2018). Microglial signatures and their role in health and disease. *Nat. Rev. Neurosci.* 19, 622–635. doi: 10.1038/s41583-018-0057-5

Cai, Z., and Liu, Z. G. (2014). Execution of RIPK3-regulated necrosis. *Mol. Cell. Oncol.* 1:e960759. doi: 10.4161/23723548.2014.960759

Cheng, J., Liao, Y., Xiao, L., Wu, R., Zhao, S., Chen, H., et al. (2017). Autophagy regulates MAVS signaling activation in a phosphorylation-dependent manner in microglia. *Cell Death Differ.* 24, 276–287. doi: 10.1038/cdd.2016.121

Chiba, T., Yamada, M., and Aiso, S. (2009). Targeting the JAK2/STAT3 axis in Alzheimer's disease. *Expert Opin. Ther. Targets* 13, 1155–1167. doi: 10.1517/14728220903213426

Chico, L. K., Van Eldik, L. J., and Watterson, D. M. (2009). Targeting protein kinases in central nervous system disorders. *Nat. Rev. Drug Discov.* 8, 892–909. doi: 10.1038/nrd2999

Cho, Y. S., Challa, S., Moquin, D., Genga, R., Ray, T. D., Guildford, M., et al. (2009). Phosphorylation-driven assembly of the RIP1-RIP3 complex regulates programmed necrosis and virus-induced inflammation. *Cell* 137, 1112–1123. doi: 10.1016/j.cell.2009.05.037

Combs, C. K., Johnson, D. E., Cannady, S. B., Lehman, T. M., and Landreth, G. E. (1999). Identification of microglial signal transduction pathways mediating a neurotoxic response to amyloidogenic fragments of beta-amyloid and prion proteins. *J. Neurosci.* 19, 928–939. doi: 10.1523/JNEUROSCI.19-03-00928.1999

Cunningham, C. C., Mills, E., Mielke, L. A., O'Farrell, L. K., Lavelle, E., Mori, A., et al. (2012). Osteoarthritis-associated basic calcium phosphate crystals induce pro-inflammatory cytokines and damage-associated molecules

via activation of Syk and PI3 kinase. *Clin. Immunol.* 144, 228–236. doi: 10.1016/j.clim.2012.06.007

Deleidi, M., Hallett, P. J., Koprich, J. B., Chung, C. Y., and Isacson, O. (2010). The Toll-like receptor-3 agonist polyinosinic:polycytidylic acid triggers nigrostriatal dopaminergic degeneration. *J. Neurosci.* 30, 16091–16101. doi: 10.1523/JNEUROSCI.2400-10.2010

Derkinderen, P., Scales, T. M., Hanger, D. P., Leung, K. Y., Byers, H. L., Ward, M. A., et al. (2005). Tyrosine 394 is phosphorylated in Alzheimer's paired helical filament tau and in fetal tau with c-Abl as the candidate tyrosine kinase. *J. Neurosci.* 25, 6584–6593. doi: 10.1523/JNEUROSCI.1487-05.2005

Dey, A., Allen, J. N., Fraser, J. W., Snyder, L. M., Tian, Y., Zhang, L., et al. (2018). Neuroprotective role of the RON receptor tyrosine kinase underlying central nervous system inflammation in health and disease. *Front. Immunol.* 9:513. doi: 10.3389/fimmu.2018.00513

Dhawan, G., and Combs, C. K. (2012). Inhibition of Src kinase activity attenuates amyloid associated microgliosis in a murine model of Alzheimer's disease. *J. Neuroinflammation* 9:117. doi: 10.1186/1742-2094-9-117

Dhib-Jalbut, S., and Kalvakolanu, D. V. (2015). Microglia and necroptosis: the culprits of neuronal cell death in multiple sclerosis. *Cytokine* 76, 583–584. doi: 10.1016/j.cyto.2015.06.004

Doorn, K. J., Brevé, J. J., Drukarch, B., Boddeke, H. W., Huitinga, I., Lucassen, P. J., et al. (2015). Brain region-specific gene expression profiles in freshly isolated rat microglia. *Front. Cell. Neurosci.* 9:84. doi: 10.3389/fncel.2015.00084

Dzamko, N., Zhou, J., Huang, Y., and Halliday, G. M. (2014). Parkinson's disease-implicated kinases in the brain; insights into disease pathogenesis. *Front. Mol. Neurosci.* 7:57. doi: 10.3389/fnmol.2014.00057

Ekdahl, C. T. (2012). Microglial activation - tuning and pruning adult neurogenesis. *Front. Pharmacol.* 3:41. doi: 10.3389/fphar.2012.00041

Field, R., Campion, S., Warren, C., Murray, C., and Cunningham, C. (2010). Systemic challenge with the TLR3 agonist poly I:C induces amplified IFNalpha/beta and IL-1beta responses in the diseased brain and exacerbates chronic neurodegeneration. *Brain Behav. Immun.* 24, 996–1007. doi: 10.1016/j.bbi.2010.04.004

Frommhold, D., Mannigel, I., Schymeinsky, J., Mocsai, A., Poeschl, J., Walzog, B., et al. (2007). Spleen tyrosine kinase Syk is critical for sustained leukocyte adhesion during inflammation in vivo. *BMC Immunol.* 8:31. doi: 10.1186/1471-2172-8-31

Gitler, A. D., Dhillon, P., and Shorter, J. (2017). Neurodegenerative disease: models, mechanisms, and a new hope. *Dis. Model. Mech.* 10, 499–502. doi: 10.1242/dmm.030205

Glass, C. K., Saijo, K., Winner, B., Marchetto, M. C., and Gage, F. H. (2010). Mechanisms underlying inflammation in neurodegeneration. *Cell* 140, 918–934. doi: 10.1016/j.cell.2010.02.016

Gomez-Nicola, D., and Perry, V. H. (2015). Microglial dynamics and role in the healthy and diseased brain: a paradigm of functional plasticity. *Neuroscientist* 21, 169–184. doi: 10.1177/1073858414530512

Gonfloni, S., Maiani, E., Di Bartolomeo, C., Diederich, M., and Cesareni, G. (2012). Oxidative stress, DNA damage, and c-Abl signaling: at the crossroad in neurodegenerative diseases? *Int. J. Cell. Biol.* 2012:683097. doi: 10.1155/2012/683097

Gosselin, D., Skola, D., Coufal, N. G., Holtman, I. R., Schlachetzki, J. C. M., Sajti, E., et al. (2017). An environment-dependent transcriptional network specifies human microglia identity. *Science* 356:eaal3222. doi: 10.1126/science.aal3222

Grabert, K., Michoel, T., Karavolos, M. H., Clohisey, S., Baillie, J. K., Stevens, M. P., et al. (2016). Microglial brain region-dependent diversity and selective regional sensitivities to aging. *Nat. Neurosci.* 19, 504–516. doi: 10.1038/nn.4222

Gribkoff, V. K., and Kaczmarek, L. K. (2017). The need for new approaches in CNS drug discovery: why drugs have failed, and what can be done to improve outcomes. *Neuropharmacology* 120, 11–19. doi: 10.1016/j.neuropharm.2016.03.021

Gunosewoyo, H., Yu, L., Munoz, L., and Kassiou, M. (2017). Kinase targets in CNS drug discovery. *Future Med. Chem.* 9, 303–314. doi: 10.4155/fmc-2016-0214

Gustin, A., Kirchmeyer, M., Koncina, E., Felten, P., Losciuto, S., Heurtaux, T., et al. (2015). NLRP3 inflammasome is expressed and functional in mouse brain microglia but not in astrocytes. *PLoS One* 10:e0130624. doi: 10.1371/journal.pone.0130624

Hao, F., Zhang, N. N., Zhang, D. M., Bai, H. Y., Piao, H., Yuan, B., et al. (2013). Chemokine fractalkine attenuates overactivation and apoptosis of BV-2 microglial cells induced by extracellular ATP. *Neurochem. Res.* 38, 1002–1012. doi: 10.1007/s11064-013-1010-7

He, S., Wang, L., Miao, L., Wang, T., Du, F., Zhao, L., et al. (2009). Receptor interacting protein kinase-3 determines cellular necrotic response to TNF-alpha. *Cell* 137, 1100–1111. doi: 10.1016/j.cell.2009.05.021

Hebenstreit, D., Horejs-Hoeck, J., and Duschl, A. (2005). JAK/STAT-dependent gene regulation by cytokines. *Drug News Perspect.* 18, 243–249. doi: 10.1358/dnp.2005.18.4.908658

Hu, X., Leak, R. K., Shi, Y., Suenaga, J., Gao, Y., Zheng, P., et al. (2015). Microglial and macrophage polarization-new prospects for brain repair. *Nat. Rev. Neurol.* 11, 56–64. doi: 10.1038/nrneurol.2014.207

Humphries, F., Yang, S., Wang, B., and Moynagh, P. N. (2015). RIP kinases: key decision makers in cell death and innate immunity. *Cell Death Differ.* 22, 225–236. doi: 10.1038/cdd.2014.126

Imam, S. Z., Zhou, Q., Yamamoto, A., Valente, A. J., Ali, S. F., Bains, M., et al. (2011). Novel regulation of parkin function through c-Abl-mediated tyrosine phosphorylation: implications for Parkinson's disease. *J. Neurosci.* 31, 157–163. doi: 10.1523/JNEUROSCI.1833-10.2011

Inoue, K., Sakuma, E., Morimoto, H., Asai, H., Koide, Y., Leng, T., et al. (2016). Serum- and glucocorticoid-inducible kinases in microglia. *Biochem. Biophys. Res. Commun.* 478, 53–59. doi: 10.1016/j.bbrc.2016.07.094

Ito, Y., Ofengeim, D., Najafov, A., Das, S., Saberi, S., Li, Y., et al. (2016). RIPK1 mediates axonal degeneration by promoting inflammation and necroptosis in ALS. *Science* 353, 603–608. doi: 10.1126/science.aaf6803

Jha, M. K., Lee, W. H., and Suk, K. (2016). Functional polarization of neuroglia: implications in neuroinflammation and neurological disorders. *Biochem. Pharmacol.* 103, 1–16. doi: 10.1016/j.bcp.2015.11.003

Kabba, J. A., Xu, Y., Christian, H., Ruan, W., Chenai, K., Xiang, Y., et al. (2018). Microglia: housekeeper of the central nervous system. *Cell. Mol. Neurobiol.* 38, 53–71. doi: 10.1007/s10571-017-0504-2

Kacimi, R., Giffard, R. G., and Yenari, M. A. (2011). Endotoxin-activated microglia injure brain derived endothelial cells via NF-kappaB, JAK-STAT and JNK stress kinase pathways. *J. Inflamm.* 8:7. doi: 10.1186/1476-9255-8-7

Kalantari, P., Harandi, O. F., Agarwal, S., Rus, F., Kurt-Jones, E. A., Fitzgerald, K. A., et al. (2017). miR-718 represses proinflammatory cytokine production through targeting phosphatase and tensin homolog (PTEN). *J. Biol. Chem.* 292, 5634–5644. doi: 10.1074/jbc.M116.749325

Karuppagounder, S. S., Brahmachari, S., Lee, Y., Dawson, V. L., Dawson, T. M., and Ko, H. S. (2014). The c-Abl inhibitor, nilotinib, protects dopaminergic neurons in a preclinical animal model of Parkinson's disease. *Sci. Rep.* 4:4874. doi: 10.1038/srep04874

Keren-Shaul, H., Spinrad, A., Weiner, A., Matcovitch-Natan, O., Dvir-Szternfeld, R., Ulland, T. K., et al. (2017). A unique microglia type associated with restricting development of Alzheimer's disease. *Cell* 169, 1276–1290.e17. doi: 10.1016/j.cell.2017.05.018

Kleinewietfeld, M., Manzel, A., Titze, J., Kvakan, H., Yosef, N., Linker, R. A., et al. (2013). Sodium chloride drives autoimmune disease by the induction of pathogenic TH17 cells. *Nature* 496, 518–522. doi: 10.1038/nature11868

Ko, H. S., Lee, Y., Shin, J. H., Karuppagounder, S. S., Gadad, B. S., Koleske, A. J., et al. (2010). Phosphorylation by the c-Abl protein tyrosine kinase inhibits Parkin's ubiquitination and protective function. *Proc. Natl. Acad. Sci. U.S.A.* 107, 16691–16696. doi: 10.1073/pnas.1006083107

Kobayashi, T., and Cohen, P. (1999). Activation of serum- and glucocorticoid-regulated protein kinase by agonists that activate phosphatidylinositide 3-kinase is mediated by 3-phosphoinositide-dependent protein kinase-1 (PDK1) and PDK2. *Biochem. J.* 339(Pt 2), 319–328. doi: 10.1042/bj3390319

Krasemann, S., Madore, C., Cialic, R., Baufeld, C., Calcagno, N., El Fatimy, R., et al. (2017). The TREM2-APOE pathway drives the transcriptional phenotype of dysfunctional microglia in neurodegenerative diseases. *Immunity* 47, 566–581.e9. doi: 10.1016/j.immuni.2017.08.008

Lang, F., Artunc, F., and Vallon, V. (2009). The physiological impact of the serum and glucocorticoid-inducible kinase SGK1. *Curr. Opin. Nephrol. Hypertens.* 18, 439–448. doi: 10.1097/MNH.0b013e32832f125e

Lang, F., Böhmer, C., Palmada, M., Seebohm, G., Strutz-Seebohm, N., and Vallon, V. (2006). (Patho)physiological significance of the serum- and glucocorticoid-inducible kinase isoforms. *Physiol. Rev.* 86, 1151–1178. doi: 10.1152/physrev.00050.2005

Lang, Y., Chu, F., Shen, D., Zhang, W., Zheng, C., Zhu, J., et al. (2018). Role of inflammasomes in neuroimmune and neurodegenerative diseases: a systematic review. *Mediators Inflamm.* 2018:1549549. doi: 10.1155/2018/1549549

Lawana, V., Singh, N., Sarkar, S., Charli, A., Jin, H., Anantharam, V., et al. (2017). Involvement of c-Abl kinase in microglial activation of NLRP3 inflammasome and impairment in autolysosomal system. *J. Neuroimmune Pharmacol.* 12, 624–660. doi: 10.1007/s11481-017-9746-5

Lee, S. H., and Suk, K. (2017). Emerging roles of protein kinases in microglia-mediated neuroinflammation. *Biochem. Pharmacol.* 146, 1–9. doi: 10.1016/j.bcp.2017.06.137

Lee, S. H., and Suk, K. (2018). Identification of glia phenotype modulators based on select glial function regulatory signaling pathways. *Expert Opin. Drug Discov.* 13, 627–641. doi: 10.1080/17460441.2018.1465925

Lindholm, D., Pham, D. D., Cascone, A., Eriksson, O., Wennerberg, K., and Saarma, M. (2016). c-Abl inhibitors enable insights into the pathophysiology and neuroprotection in Parkinson's disease. *Front. Aging Neurosci.* 8:254. doi: 10.3389/fnagi.2016.00254

Mahul-Mellier, A. L., Fauvet, B., Gysbers, A., Dikiy, I., Oueslati, A., Georgeon, S., et al. (2014). c-Abl phosphorylates alpha-synuclein and regulates its degradation: implication for alpha-synuclein clearance and contribution to the pathogenesis of Parkinson's disease. *Hum. Mol. Genet.* 23, 2858–2879. doi: 10.1093/hmg/ddt674

Martin, L., Latypova, X., Wilson, C. M., Magnaudeix, A., Perrin, M. L., Yardin, C., et al. (2013). Tau protein kinases: involvement in Alzheimer's disease. *Ageing Res. Rev.* 12, 289–309. doi: 10.1016/j.arr.2012.06.003

Mecca, C., Giambanco, I., Donato, R., and Arcuri, C. (2018). Microglia and aging: the role of the TREM2-DAP12 and CX3CL1-CX3CR1 axes. *Int. J. Mol. Sci.* 19:E318. doi: 10.3390/ijms19010318

Mehdi, S. J., Rosas-Hernandez, H., Cuevas, E., Lantz, S. M., Barger, S. W., Sarkar, S., et al. (2016). Protein kinases and Parkinson's disease. *Int. J. Mol. Sci.* 17:1585. doi: 10.3390/ijms17091585

Melief, J., Koning, N., Schuurman, K. G., Van De Garde, M. D., Smolders, J., Hoek, R. M., et al. (2012). Phenotyping primary human microglia: tight regulation of LPS responsiveness. *Glia* 60, 1506–1517. doi: 10.1002/glia.22370

Melief, J., Sneeboer, M. A., Litjens, M., Ormel, P. R., Palmen, S. J., Huitinga, I., et al. (2016). Characterizing primary human microglia: a comparative study with myeloid subsets and culture models. *Glia* 64, 1857–1868. doi: 10.1002/glia.23023

Miller, Y. I., Choi, S. H., Wiesner, P., and Bae, Y. S. (2012). The SYK side of TLR4: signalling mechanisms in response to LPS and minimally oxidized LDL. *Br. J. Pharmacol.* 167, 990–999. doi: 10.1111/j.1476-5381.2012.02097.x

Minogue, A. M., Barrett, J. P., and Lynch, M. A. (2012). LPS-induced release of IL-6 from glia modulates production of IL-1beta in a JAK2-dependent manner. *J. Neuroinflammation* 9:126. doi: 10.1186/1742-2094-9-126

Miyata, S., Koyama, Y., Takemoto, K., Yoshikawa, K., Ishikawa, T., Taniguchi, M., et al. (2011). Plasma corticosterone activates SGK1 and induces morphological changes in oligodendrocytes in corpus callosum. *PLoS One* 6:e19859. doi: 10.1371/journal.pone.0019859

Mócsai, A., Ruland, J., and Tybulewicz, V. L. (2010). The SYK tyrosine kinase: a crucial player in diverse biological functions. *Nat. Rev. Immunol.* 10, 387–402. doi: 10.1038/nri2765

Möser, C. V., Stephan, H., Altenrath, K., Kynast, K. L., Russe, O. Q., Olbrich, K., et al. (2015). TANK-binding kinase 1 (TBK1) modulates inflammatory hyperalgesia by regulating MAP kinases and NF-kappaB dependent genes. *J. Neuroinflammation* 12:100. doi: 10.1186/s12974-015-0319-3

Mosher, K. I., and Wyss-Coray, T. (2014). Microglial dysfunction in brain aging and Alzheimer's disease. *Biochem. Pharmacol.* 88, 594–604. doi: 10.1016/j.bcp.2014.01.008

Ofengeim, D., Mazzitelli, S., Ito, Y., DeWitt, J. P., Mifflin, L., Zou, C., et al. (2017). RIPK1 mediates a disease-associated microglial response in Alzheimer's disease. *Proc. Natl. Acad. Sci. U.S.A.* 114, E8788–E8797. doi: 10.1073/pnas.1714175114

Ozaki, E., Campbell, M., and Doyle, S. L. (2015). Targeting the NLRP3 inflammasome in chronic inflammatory diseases: current perspectives. *J. Inflamm. Res.* 8, 15–27. doi: 10.2147/JIR.S51250

Paolicelli, R. C., Bolasco, G., Pagani, F., Maggi, L., Scianni, M., Panzanelli, P., et al. (2011). Synaptic pruning by microglia is necessary for normal brain development. *Science* 333, 1456–1458. doi: 10.1126/science.1202529

Papassotiropoulos, A., Lambert, J. C., Wavrant-De Vrieze, F., Wollmer, M. A., von der Kammer, H., et al. (2005). Cholesterol 25-hydroxylase on chromosome 10q is a susceptibility gene for sporadic Alzheimer's disease. *Neurodegener. Dis.* 2, 233–241. doi: 10.1159/000090362

Ransohoff, R. M. (2016a). A polarizing question: do M1 and M2 microglia exist? *Nat. Neurosci.* 19, 987–991. doi: 10.1038/nn.4338

Ransohoff, R. M. (2016b). How neuroinflammation contributes to neurodegeneration. *Science* 353, 777–783. doi: 10.1126/science.aag2590

Rask-Andersen, M., Zhang, J., Fabbro, D., and Schioth, H. B. (2014). Advances in kinase targeting: current clinical use and clinical trials. *Trends Pharmacol. Sci.* 35, 604–620. doi: 10.1016/j.tips.2014.09.007

Rubartelli, A. (2014). DAMP-mediated activation of NLRP3-inflammasome in brain sterile inflammation: the fine line between healing and neurodegeneration. *Front. Immunol.* 5:99. doi: 10.3389/fimmu.2014.00099

Satoh, J., Kino, Y., Asahina, N., Takitani, M., Miyoshi, J., Ishida, T., et al. (2016). TMEM119 marks a subset of microglia in the human brain. *Neuropathology* 36, 39–49. doi: 10.1111/neup.12235

Schafer, D. P., Lehrman, E. K., Kautzman, A. G., Koyama, R., Mardinly, A. R., Yamasaki, R., et al. (2012). Microglia sculpt postnatal neural circuits in an activity and complement-dependent manner. *Neuron* 74, 691–705. doi: 10.1016/j.neuron.2012.03.026

Schlatterer, S. D., Acker, C. M., and Davies, P. (2011). c-Abl in neurodegenerative disease. *J. Mol. Neurosci.* 45, 445–452. doi: 10.1007/s12031-011-9588-1

Schmid, E., Yan, J., Nurbaeva, M. K., Russo, A., Yang, W., Faggio, C., et al. (2014). Decreased store operated $Ca2^{+}$ entry in dendritic cells isolated from mice expressing PKB/SGK-resistant GSK3. *PLoS One* 9:e88637. doi: 10.1371/journal.pone.0088637

Schwartz, M., and Deczkowska, A. (2016). Neurological disease as a failure of brain-immune crosstalk: the multiple faces of neuroinflammation. *Trends Immunol.* 37, 668–679. doi: 10.1016/j.it.2016.08.001

Shabab, T., Khanabdali, R., Moghadamtousi, S. Z., Kadir, H. A., and Mohan, G. (2017). Neuroinflammation pathways: a general review. *Int. J. Neurosci.* 127, 624–633. doi: 10.1080/00207454.2016.1212854

Slezak, M., Korostynski, M., Gieryk, A., Golda, S., Dzbek, J., Piechota, M., et al. (2013). Astrocytes are a neural target of morphine action via glucocorticoid receptor-dependent signaling. *Glia* 61, 623–635. doi: 10.1002/glia.22460

Ślusarczyk, J., Trojan, E., Głombik, K., Piotrowska, A., Budziszewska, B., Kubera, M., et al. (2018). Targeting the NLRP3 inflammasome-related pathways via tianeptine treatment-suppressed microglia polarization to the M1 phenotype in lipopolysaccharide-stimulated cultures. *Int. J. Mol. Sci.* 19:E1965. doi: 10.3390/ijms19071965

Song, G. J., and Suk, K. (2017). Pharmacological modulation of functional phenotypes of microglia in neurodegenerative diseases. *Front. Aging Neurosci.* 9:139. doi: 10.3389/fnagi.2017.00139

Stella, M. C., Vercelli, A., Repici, M., Follenzi, A., and Comoglio, P. M. (2001). Macrophage stimulating protein is a novel neurotrophic factor. *Mol. Biol. Cell* 12, 1341–1352. doi: 10.1091/mbc.12.5.1341

Suk, K. (2017). Glial phenotype modulators. *Oncotarget* 8, 22309–22310. doi: 10.18632/oncotarget.16245

Sun, L., Wang, H., Wang, Z., He, S., Chen, S., Liao, D., et al. (2012). Mixed lineage kinase domain-like protein mediates necrosis signaling downstream of RIP3 kinase. *Cell* 148, 213–227. doi: 10.1016/j.cell.2011.11.031

Sun, Y., Ge, X., Li, M., Xu, L., and Shen, Y. (2017). Dyrk2 involved in regulating LPS-induced neuronal apoptosis. *Int. J. Biol. Macromol.* 104(Pt A), 979–986. doi: 10.1016/j.ijbiomac.2017.06.087

Taira, N., Mimoto, R., Kurata, M., Yamaguchi, T., Kitagawa, M., Miki, Y., et al. (2012). DYRK2 priming phosphorylation of c-Jun and c-Myc modulates cell cycle progression in human cancer cells. *J. Clin. Invest.* 122, 859–872. doi: 10.1172/JCI60818

Tell, V., and Hilgeroth, A. (2013). Recent developments of protein kinase inhibitors as potential AD therapeutics. *Front. Cell. Neurosci.* 7:189. doi: 10.3389/fncel.2013.00189

Tremblay, M. A., Acker, C. M., and Davies, P. (2010). Tau phosphorylated at tyrosine 394 is found in Alzheimer's disease tangles and can be a product of the Abl-related kinase. *Argic. J. Alzheimers Dis.* 19, 721–733. doi: 10.3233/JAD-2010-1271

Wang, Y., Wang, H., Tao, Y., Zhang, S., Wang, J., and Feng, X. (2014). Necroptosis inhibitor necrostatin-1 promotes cell protection and physiological function

in traumatic spinal cord injury. *Neuroscience* 266, 91–101. doi: 10.1016/j.neuroscience.2014.02.007

Wärntges, S., Friedrich, B., Henke, G., Duranton, C., Lang, P. A., Waldegger, S., et al. (2002). Cerebral localization and regulation of the cell volume-sensitive serum- and glucocorticoid-dependent kinase SGK1. *Pflugers Arch.* 443, 617–624. doi: 10.1007/s00424-001-0737-1

Wlodarczyk, A., Holtman, I. R., Krueger, M., Yogev, N., Bruttger, J., Khorooshi, R., et al. (2017). A novel microglial subset plays a key role in myelinogenesis in developing brain. *EMBO J.* 36, 3292–3308. doi: 10.15252/embj.201696056

Wollmer, M. A. (2010). Cholesterol-related genes in Alzheimer's disease. *Biochim. Biophys. Acta* 1801, 762–773. doi: 10.1016/j.bbalip.2010.05.009

Xing, J., Titus, A. R., and Humphrey, M. B. (2015). The TREM2-DAP12 signaling pathway in Nasu-Hakola disease: a molecular genetics perspective. *Res. Rep. Biochem.* 5, 89–100. doi: 10.2147/RRBC.S58057

Xu, L., Sun, Y., Li, M., and Ge, X. (2018). Dyrk2 mediated the release of proinflammatory cytokines in LPS-induced BV2 cells. *Int. J. Biol. Macromol.* 109, 1115–1124. doi: 10.1016/j.ijbiomac.2017.11.095

Yoshida, K. (2008). Role for DYRK family kinases on regulation of apoptosis. *Biochem. Pharmacol.* 76, 1389–1394. doi: 10.1016/j.bcp.2008.05.021

Yu, S., Allen, J. N., Dey, A., Zhang, L., Balandaram, G., Kennett, M. J., et al. (2016). The RON receptor tyrosine kinase regulates macrophage heterogeneity and plays a protective role in diet-induced obesity. Atherosclerosis, and Hepatosteatosis. *J. Immunol.* 197, 256–265. doi: 10.4049/jimmunol.1600450

Zeng, K. W., Wang, S., Dong, X., Jiang, Y., Jin, H. W., and Tu, P. F. (2014). Sesquiterpene dimmer (DSF-27) inhibits the release of neuroinflammatory mediators from microglia by targeting spleen tyrosine kinase (Syk) and Janus kinase 2 (Jak2): two major non-receptor tyrosine signaling proteins involved in inflammatory events. *Toxicol. Appl. Pharmacol.* 275, 244–256. doi: 10.1016/j.taap.2014.01.014

Conflict of Interest Statement: The authors declare that the research was conducted in the absence of any commercial or financial relationships that could be construed as a potential conflict of interest.

frontiers in Cellular Neuroscience

ORIGINAL RESEARCH
published: 21 December 2018
doi: 10.3389/fncel.2018.00507

Transplantation of Microglia in the Area of Spinal Cord Injury in an Acute Period Increases Tissue Sparing, but Not Functional Recovery

Elvira R. Akhmetzyanova[1], Yana O. Mukhamedshina[1,2], Margarita N. Zhuravleva[1], Luisa R. Galieva[1], Alexander A. Kostennikov[1], Ekaterina E. Garanina[1] and Albert A. Rizvanov[1]*

[1] OpenLab Gene and Cell Technologies, Kazan Federal University, Kazan, Russia, [2] Department of Histology, Cytology and Embryology, Kazan State Medical University, Kazan, Russia

Microglial cells are known as important mediators of inflammation and immune response in the central nervous system (CNS). However, a neuroprotective role of these cells in post-traumatic processes should not be overlooked. Microglial cells are the first to respond to CNS injury and are further involved in all critical events of pathogenesis. When activated microglia clear the cellular debris and release anti- and proinflammatory cytokines and chemokines, nitric oxide, neurotrophins, and antioxidants capable of producing both neurotoxic and neuroprotective effects. The aim of this study was to determine to what extent the phagocytic activity of microglia in an acute period of spinal cord injury (SCI) in rats can effect the post-traumatic processes. For this purpose we implanted genetically modified Ad5-EGFP or Ad5-GDNF microglial cells into the area of acute SCI. Our experiments demonstrate that the area of intact tissue was lower in the group transplanted with Ad5-GDNF-transduced microglial cells with reduced phagocytic activity than that in the group of animals transplanted with Ad5-EGFP-transduced microglia cells which did not affect the cell activity. At the same time, there was no significant difference in the functional recovery index between these groups. Thus, the increased number of microglia cells with good phagocytic activity in the area of acute SCI may contribute to the improved nervous tissue integrity without a significant effect on the functional recovery within 30 days after injury.

Keywords: microglia, spinal cord injury, *egfp*, *gdnf*, adenoviral vector

OPEN ACCESS

Edited by:
Maria Beatrice Passani, Università degli Studi di Firenze, Italy

Reviewed by:
Clara Ballerini, Università degli Studi di Firenze, Italy
Adelaide Fernandes, Universidade de Lisboa, Portugal

****Correspondence:***
Yana O. Mukhamedshina
yana.k-z-n@mail.ru

Received: *23 August 2018*
Accepted: *07 December 2018*
Published: *21 December 2018*

Citation:
Akhmetzyanova ER, Mukhamedshina YO, Zhuravleva MN, Galieva LR, Kostennikov AA, Garanina EE and Rizvanov AA (2018) Transplantation of Microglia in the Area of Spinal Cord Injury in an Acute Period Increases Tissue Sparing, but Not Functional Recovery. Front. Cell. Neurosci. 12:507. doi: 10.3389/fncel.2018.00507

INTRODUCTION

Spinal cord injury (SCI) is characterized by numerous pathologic reactions which involve every cell type of the central nervous system (CNS). It results in neuron and glial cell death, is followed by nerve fiber degeneration, oxidative stress, and other pathological alterations. The activation of microglial cells which are the first to respond to nerve tissue damage is one of the essential events of post-traumatic reactions (Hansson, 2003; Dibaj et al., 2010; Silver et al., 2015). When activated the microglia clear the cellular debris and release anti- and pro-inflammatory cytokines and chemokines, nitric oxide, neurotrophins, and antioxidants capable of exhibiting both neurotoxic and neuroprotective effects (Kreutzberg, 1996; Lai and Todd, 2008; Shechter and Schwartz, 2013).

Lately some approaches to SCI treatment are focusing on modulating microglial reactivity after injury toward a neuroprotective phenotype.

Francos-Quijorna et al. (2016) demonstrated that IL-4 facilitated microglia/macrophages gaining the M2 phenotype, promoting nerve tissue regeneration and functional recovery after SCI. M2a macrophages promoted by IL-4, IL-13, and arginase-1 mainly participate in reducing inflammation, enhancing phagocytosis and differentiation of neural stem cells (NSCs) (Varnum and Ikezu, 2012). The introduction of M2 macrophages into the spinal cord and brain is shown to be effective for the treatment of non-infectious inflammation of the CNS (Weber et al., 2007; Shechter et al., 2013). These studies suggest that modulation of microglial cells toward the neuroprotective phenotype seems to be quite promising in order to stimulate neuroregeneration in SCI.

Our present study was based on the use of GDNF as a potent inhibitor of microglial phagocytic activity to promote the expression of neuroprotective or neurotoxic phenotypes (Rocha et al., 2012; Zhuravleva et al., 2016). The enhancement of the scavenger and phagocytic properties of microglia is supposed to result in early resolution of the initial traumatic events that can improve long-term structural and functional outcome (Redondo-Castro et al., 2013). To test this hypothesis we transplanted genetically modified Ad5-EGFP or Ad5-GDNF microglial cells into the area of acute SCI and followed the animals for 5 weeks, assessing functional improvements and changes in tissue integrity.

MATERIALS AND METHODS

Microglia Isolation and Cultivation

Microglia were isolated from neonatal rat cerebral cortex as described previously (Zhuravleva et al., 2015). Briefly, pups were anesthetized and perfused via the left ventricle with cold DPBS solution supplemented with 5 U/ml sodium heparin. The cortex was isolated, and the pia mater peeled off. Tissue was mechanically homogenized and incubated with an enzyme solution (papain 2 mg/ml, DNAse 50 U/ml, dispase 2.5 U/ml) in DPBS for 30 min at 37°C with shaking at 180 rpm. Cells were separated using a 40 μm cell strainer followed by Optiprep (Sigma) discontinuous density gradient for 40 min at 300 g. Layers were cell suspensions in 19% Optiprep, 9% Optiprep, 7% Optiprep, DPBS. A microglia fraction was obtained from a layer, located between fractions 19 and 9%. The microglia were cultured in DMEM/F12 medium supplemented with granulocyte colony-stimulating factor (G-CSF,5 ng/ml, Sigma, United States), 10% FBS, 2 mM L-Glutamine and Penicillin-Streptomycin (PanEco, Russia) in humidified 5% CO2. Resulting cells were transplanted into the area of SCI after 24 h of culture.

Genetic Modification and Characterization of Microglia

The microglia were transduced with Ad5-EGFP or Ad5-GDNF immediately after the isolation of cells with MOI 40, which provides an optimum level of expression of the transgene and has no cytotoxic effect. The day after transfection, the cells were collected for transplantation. Genetically modified microglia were also analyzed 7 days after transduction by immunocytochemistry (ICC) and flow cytometry (FC) for the detection of the expression of EGFP and GDNF. For ICC, cells were fixed in 4% buffered formalin, washed with 0.1% Triton X-100 in PBS and stained with anti-GDNF antibodies (ab10835, Abcam) at a working dilution of 1:100 for 1 h at RT, washed and stained with Alexa Fluor 647 conjugated anti-goat secondary antibodies A-21447 (Invitrogen) for 30 min at RT. The nuclei were stained with DAPI (d9564, Sigma) for 5 min. The results were analyzed using an AxioObserver Z1 (Carl Zeiss). Briefly, for FC microglial cultures were trypsinized, prefixed with CytoFix (BD Biosciences) and permobilized using Perm 2 (BD Biosciences), incubated with anti-GDNF antibodies (ab10835, Abcam) at a working dilution of 1 μl per 200,000 cells for 30 min at 4°C, washed using centrifugation, stained with Alexa Fluor 555 conjugated anti-goat secondary antibodies (A-21432, Invitrogen) and analyzed using flow cytometer FACS Aria III (BD Biosciences). Ad5-GFP transduced cells were analyzed using FC immediately after trypsinization.

We also analyzed the phenotype of transduced microglia at Day 1, 7, and 14 cultivations. For FC microglia cultures were trypsinized and incubated with antibodies CD11b (101216, BioLegend), CD16 (ab203883, Abcam), CD 40 (ab13545, Abcam), CD 45 (1611525, Sony), CD86 (305420, BioLegend), CD163 (ab182462, Abcam), CD 200 (ab203887, Abcam), CD206 (2205595, Sony) at a working dilution of 1 μl per 200,000 cells for 30 min at 4°C. For CD16, CD40, CD163, and CD200 staining appropriate Alexa Fluor 555 conjugated anti-rabbit secondary antibodies (A-31572, Invitrogen, United States) were used. Stained cells were fixed with CytoFix and analyzed using flow cytometer FACS Aria III. The *in vitro* data were obtained from five independent experiments.

Spinal Cord Injury and Cell Transplantation

All animal protocols were approved by the Kazan Federal University Animal Care and Use Committee (Permit Number: 2 dated on May 5, 2015). Adult male and female Wistar rats (weight of 250–300 g each; Pushchino Laboratory, Russia) were group housed in clear plastic cages (12 h:12 h light/dark cycle) with food and water available *ad libitum*.

Rats were deeply anesthetized by intraperitoneal injection of chloral hydrate (80 mg/ml, 0.4 ml per 100 g, Sigma). After skin incision, the Th8 vertebra was removed by laminectomy. The impact rod (diameter 2 mm, 10 g) of an impactor was centered above Th8 and dropped from a height of 25 mm to induce SCI. Immediately after SCI, 5 μl suspensions of MG+Ad5-GDNF (n = 15) or MG+Ad5-EGFP (n = 15) (containing 1×10^6 cells) were injected into the area of SCI (epicenter) at a depth of 1 mm by using a 5-μl Hamilton syringe. In the control group (SCI) (n = 15), 5 μl 0.9% NaCl were injected into the aforementioned point. After SCI the dorsal back musculature and the skin were sutured. Following surgery the rats received doses of gentamicin (25 mg/kg, Omela, Russian Federation) intramuscularly for seven

consecutive days. Bladders of injured rats were manually emptied twice a day until spontaneous voiding occurred. There was a control group of 10 intact animals.

Behavioral Test

Locomotor recovery was assessed in an open field by using the BBB rating scale. The baseline was obtained three days before SCI. To evaluate differences in functional recovery, a behavioral assessment in all groups was performed before SCI, on day 7, and then every second day. Locomotion was scored simultaneously by two observers who were blinded to the treatment groups. Final scores were obtained by averaging the two scores awarded by the examiners.

Histological Assessment

For histology and immunohistochemistry, 30 days after cell transplantation the rats were anesthetized with chloral hydrate, prior to intracardiac perfusion with 4% paraformaldehyde (PFA, Sigma). After incubation in 30% sucrose, samples were embedded in a tissue freezing medium. Non-fixed tissue was used for RT-PCR. Twenty micrometer transverse tissue sections, obtained with a Microm HM 560 Cryostat, were stained with Azur-eosin for visualizing tissues. Images were captured using a × 20 objective lens and a microscope (APERIOCS2, Leica). The cross-sectional areas of the spared tissue and abnormal cavities were measured on transverse sections of the spinal cord within the midpoint of the lesion center (the epicenter) and in spinal segments 1–5 mm rostral and caudal to the site of injury. The total area of abnormal cavities in the spinal cord cross-section was calculated by adding cavities with an area of not less than 1.500 μm^2. An Aperio imagescope was used to measure the tissue area.

Immunofluorescence Analysis

For immunofluorescence labeling, the sections were blocked with 5% normal goat serum for 1 h at room temperature (RT) and then incubated separately overnight at 4°C with a primary antibody against ionized calcium binding adaptor molecule 1 (Iba1) (Abcam, 1:300) and glial fibrillary acidic protein (GFAP) (Millipore, 1:200). Prior to visualization, the sections were incubated with a fluorophore-conjugated secondary antibody (anti- mouse IgG conjugated with Alexa 546, Invitrogen, 1:200) for 2 h at RT. 4′,6-Diamidino-2-phenylindole (DAPI) (10 μg/mL in PBS, Sigma) was used to visualize nuclei. Coverslips were mounted on slides using a mounting medium (ImmunoHistoMount, Santa Cruz). The sections were examined under a LSM 780 Confocal Microscope (Carl Zeiss, Germany). The total intensity of labeling (semi-quantitative analysis of Iba1 and GFAP) was analyzed using Zen 2012 Software (Carl Zeiss). All sections were imaged in the z-plane using identical confocal settings (laser intensity, gain, and offset). Measurements were obtained from transverse histological sections collected at 5-mm increments extending from the contusion center (observed area, 2 mm^2) of the SCI. The following areas were selected for semiquantitative immunohistochemical evaluation of glial cells: the main corticospinal tract (CST), ventral funiculi (VF), and the ventral horn (VH).

RNA Isolation and Real-Time PCR Analysis

Total RNA from fresh spinal cords (5 mm long segment encompassing the injury site) was isolated using a Yellow Solve Kit (Silex, Russia) according to the manufacturer's recommendations. First strand cDNA synthesis was held using 100 U of RevertAid reverse transcriptase (Thermo Fisher Scientific), 100 pmol of random hexamer primers and 5 U of RNAse inhibitor according to the standard protocol. Quantitative analysis of mRNA of *egfp*, *gdnf*, *irf5*, *iba1* genes was applied using a CFX 96 Real-Time PCR System (Bio-Rad, Hercules, CA, United States). Each PCR reaction contained 100 ng cDNA, 2.5× Reaction mixture B (Syntol, Russia), 200 nM of each primer, and the probe (100 nM) (**Table 1**). The mRNA expression was normalized according to the 18S RNA transcription. To create standard curves plasmid DNA with corresponding inserts was used. The level of mRNA in non-treated spinal cord after injury was considered as 100%.

Statistical Analysis

All statistical analyses were carried out by two independent biostatisticians blinded to the groups. Data are presented as means ± standard deviation. The one-way analysis of variance (ANOVA) with the Tukey's test or two-way analysis of variance (ANOVA) were used for multiple groups. Values of $P < 0.05$ and $P < 0.01$ were considered statistically significant. Data were analyzed using the Origin 7.0 SR0 Software (OriginLab, Northampton, MA, United States).

RESULTS

Analysis of the Expression of EGFP and GDNF *in vitro* and *in vivo* in the Area of SCI

Seven days after microglia transduction with Ad5-EGFP or Ad5-GDNF, EGFP, and GDNF expression was studied *in vitro*

TABLE 1 | Primers and probes for RT-PCR.

Primer	Nucleotide sequence
18S-TM-Forward	gCCgCTAgAggTgAAATTCTTg
18S-TM-Reverse	CATTCTTggCAAATgCTTTCg
18S-TM-Probe	[HEX]ACCgCgCAAgACggACCAg[BH2]
EGFP-TM-Forward	AgCAAAgACCCCAACgAgAA
EGFP-TM-Reverse	ggCggCggTCACgAA
EGFP-TM-Probe	[FAM]CgCgATCACATggTCCTgCTgg[BH1]
GDNF-TM-Forward	CgCTgAgCAgTgACTCAAAT
GDNF-TM-Reverse	CgATTCCgCTCTCTTCTAgg
GDNF-TM-Probe	[FAM]TCCATgACATCATCgAACTgATCAgg[BH1]
Irf5-TM-Forward	AgggCTTCAATgggTCAAC
Irf5-TM-Reverse	gTgTATTTCCCTgTCTCCTTgg
Irf5-TM-Probe	[HEX]ATggTgTTATCTCCgTCCTggCTg[BH2]
Iba1-TM-Forward	ACCAgCgTCTgAggAgCTAT
Iba1-TM-Reverse	AggAAgTgCTTgTTgATCCC
Iba1-TM-Probe	[HEX]CCCTgCAAATCCTTgCTCTggC[BH2]

(**Figure 1**). ICC and FC demonstrated that native microglia expressed GDNF. On day 7 after Ad5-GDNF transduction 50% of microglia demonstrated GDNF overexpression (**Figures 1A,C,F**). Visualized cells by fluorescent microscopy had green fluorescence (MG+Ad5-EGFP) compared to non-transduced/native microglia (**Figures 1B,D**). On day 7 after transduction, 51% of the microglial cells expressed EGFP (**Figure 1E**). mRNA expression in microglia immediately treated with Ad5-EGFP or Ad5-GDNF was 9689 and 6733 times higher relative to non-transduced cells, respectively, at Day 7 after transduction (**Figure 1G**).

We also studied to what extent the transplantation of genetically modified microglia increased the expression of EGFP and GDNF mRNAs in the area of SCI. Thus on day 30 after SCI EGFP mRNA was more than 10000 times higher in the spinal cord of SCI MG+Ad5-EGFP rats than in untreated rats subjected to SCI (**Figure 1H**). The results also demonstrated that the GDNF mRNA expression level was significantly higher

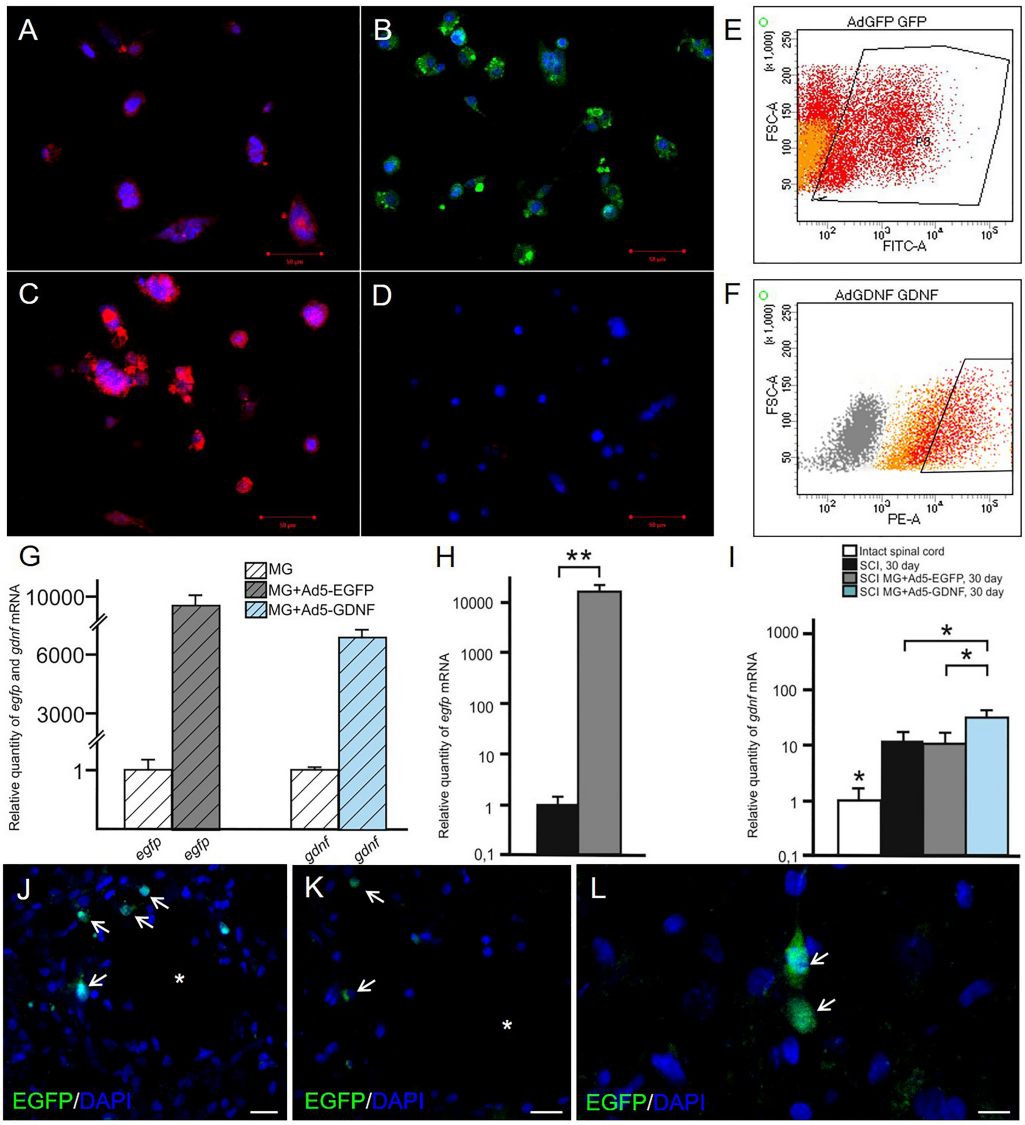

FIGURE 1 | Analysis of the expression of EGFP and GDNF *in vitro* and *in vivo* in the area of SCI. Immunocytochemistry results demonstrate expression GDNF **(A,C)** and EGFP **(B,D)** in transduced by GDNF **(C)** or EGFP **(B)** and non-transduced/native **(A,D)** microglia. Results of flow cytometry are shown **(E,F)**. Based on the flow cytometry data, 51% of the transduced by Ad5-EGFP microglia were EGFP-positive (red color in dot plot, yellow color is for non-transduced cells) **(E)** and 50% of the transduced by Ad5-GDNF microglia demonstrated GDNF overexpression (red color on dot plot, yellow color in dot plot for native cells, gray color is for unstained cells) **(F)**. EGFP and GDNF mRNA expression *in vitro* on cultivation Days 7 **(G)** and *in vivo* at Day 30 after SCI in experimental groups **(H,I)**. The EGFP and GDNF mRNA expression levels in the SCI and Intact controls groups, respectively, were considered 100% **(H,I)**. $^{*}P < 0.05$, $^{**}P < 0.01$, one-way ANOVA followed by a Tukey's *post hoc* test. Ad5-EGFP microglia around the small cavities (asterisks) **(J,K)** and in ventral horns **(L)** at the distance of 3 mm in rostral and 3–4 mm in caudal directions from the injury epicenter, respectively, at Day 30 after SCI and transplantation. Nuclei are stained with DAPI (blue). Scale bar: 20 **(J,K)** and 10 **(L)** μm.

in the group with MG-GDNF transplantation as compared to the other experimental groups ($P < 0.01$) (**Figure 1I**). The lowest expression level was observed in the intact spinal cord, with no reliable difference detected between SCI groups without cell transplantation and those transplanted with MG+Ad5-EGFP. Thus, the data obtained for EGFP and GDNF mRNAs levels in the area of SCI confirmed the efficacy of target gene delivery and possible long-term expression of recombinant gene products.

Distribution and Survival of Transplanted Microglia

Previously in similar experimental conditions, we showed, that MG+Ad5-EGFP survived in the early period of SCI (not less than 14 days), actively expressed recombinant gene *egfp* and migrated up to 5 and 3 mm in the rostral and caudal directions, respectively, from the injection site (Zhuravleva et al., 2015). At Day 30 we observed $EGFP^+$-cells arranged predominantly around the small cavities at the distance of 3–4 mm in both directions from the injury epicenter (**Figures 1J,K**) and up to 1–2 $EGFP^+$-cells in ventral horns in similar directions (**Figure 1L**).

Analysis of Changes in Phenotype and Gene Expression of Microglia *in vitro*

Previously, we showed that 2 week cultured microglia (non-transduced cells) express Iba1, CD68, CD11b/c, and CD45 (Zhuravleva et al., 2015). Microglia had an amoeboid shape initially, but after 2 weeks branched forms of microglia were seen as well. In this study, we estimated the expression level of the following markers (CD11, CD16, CD40, CD45, CD86, CD163, CD200, CD206) in the obtained cultures of transduced microglia at Days 1, 7, and 14 (**Table 2**). At Day 1 we observed maximal levels expression of CD16, CD40, CD86, and CD200 in both culture of transduced microglia without any significant difference in all 8 markers. At Day 7 we observed a significant decline of the expression of CD16, CD40, CD45, CD163, and CD200 without significant differences between microglia transduced by Ad5-EGFP or Ad5-GDNF. Expression of CD11 and CD206 was similar at Day 1 and 7. CD86 only showed consistently high expression levels (more 90%) after 14 days compared to other markers which declined significantly during that time. We observed the only significant difference between two types of transduced microglia for CD45, which had a more than 15-fold increase in microglia transduced by Ad5-EGFP.

We also investigated the expression of pan marker Iba1 and M1 phenotype marker irf5 mRNAs in the microglia at the same time points. The analysis showed that the maximum expression of both Iba1 and irf5 mRNAs was observed on day 14. The irf5 expression gradually increased from 0 to 14 days ($P < 0.05$) (**Figure 2A**). By culture day 1 the Iba1 expression was below that at the time of isolation ($P < 0.05$); however, this parameter consistently increased by culture day 14 ($P < 0.05$) (**Figure 2B**).

Assessment of Microglia in the Area of SCI

To investigate the expression of Iba1 and irf5 mRNAs in injured spinal cord, qRT-PCR was performed on sections obtained from the injury site 30 days post transplantation. When evaluating the Iba1 and irf5 mRNAs levels specific for microglial cells/macrophages, we detected the following pattern in the area of SCI. The Iba1 mRNA level was significantly higher in the group with MG-GDNF transplantation as compared to the other experimental groups. At the same time there was no significant difference in the Iba1 mRNA expression between intact spinal cord group with SCI and transplantation of MG-EGFP ($P < 0.01$) (**Figure 2C**). When evaluating the expression of irf5 mRNA, this value was significantly higher in the SCI group without cell transplantation ($P < 0.01$), than in the other experimental groups, with no reliable differences between them (**Figure 2D**).

Using immunofluorescence we studied the total intensity of Iba1 labeling 5 mm rostrally and caudally from the injury epicenter in selected zones of the white and gray matter. It was significantly higher rostrally from the injury epicenter in all study zones in the group with MG+Ad5-GDNF transplantation ($P < 0.05$) (**Figure 3A**). At the same time, there was no significant difference in the total intensity of Iba1 labeling in the SCI and SCI MG+ Ad5-EGFP groups. A maximum $Iba1^+$-cell concentration was detected in the CST zone of the SCI MG+Ad5-GDNF group in both directions from the site of injury (**Figures 3A–C**). A minimal $Iba1^+$microglial cell concentration was identified in the VF zone (in both directions from the site of injury) in the intact group (**Figure 3C**).

Caudally from the injury epicenter the total intensity of Iba1 labeling in VF and VH zones was higher ($P < 0.05$) in the

TABLE 2 | Results of flow cytometry in microglia culture.

Markers	1 day MG+Ad5-EGFP	1 day MG+Ad5-GDNF	7 day MG+Ad5-EGFP	7 day MG+Ad5-GDNF	14 day MG+Ad5-EGFP	14 day MG+Ad5-GDNF
CD11b	30 ± 5%	25 ± 3%	30 ± 5, 5%	23 ± 1, 5%	18, 5 ± 1, 5%	26 ± 3, 5%
CD16	98 ± 0, 5%	94 ± 3, 5%	45 ± 3%	60 ± 5, 5%	11 ± 0, 5%	11 ± 1, 5%
CD40	99 ± 0, 5%	98 ± 0, 5%	36 ± 4, 5%	22 ± 2, 5%	11 ± 1, 5%	8 ± 0, 5%
CD45	86 ± 5%	83 ± 3%	45 ± 4, 5%	40 ± 2, 5%	15, 5 ± 1, 5%	1 ± 0, 5%*
CD86	99 ± 0, 5%	99 ± 0, 5%	96 ± 0, 5%	94 ± 1, 5%	99 ± 0, 5%	92 ± 0, 5%
CD163	84 ± 5%	76 ± 3, 5%	30 ± 2, 5%	30 ± 2%	11, 5 ± 0, 5%	8 ± 0, 5%
CD200	98 ± 1%	93 ± 2, 5%	40 ± 2, 5%	30 ± 3, 5%	10 ± 0, 5%	10 ± 1%
CD206	35 ± 1, 5%	35 ± 1%	42 ± 2, 5%	35 ± 5, 5%	14 ± 1, 5%	13 ± 1%

*$P < 0.05$, compared to MG+Ad5-EGFP in the relevant period.

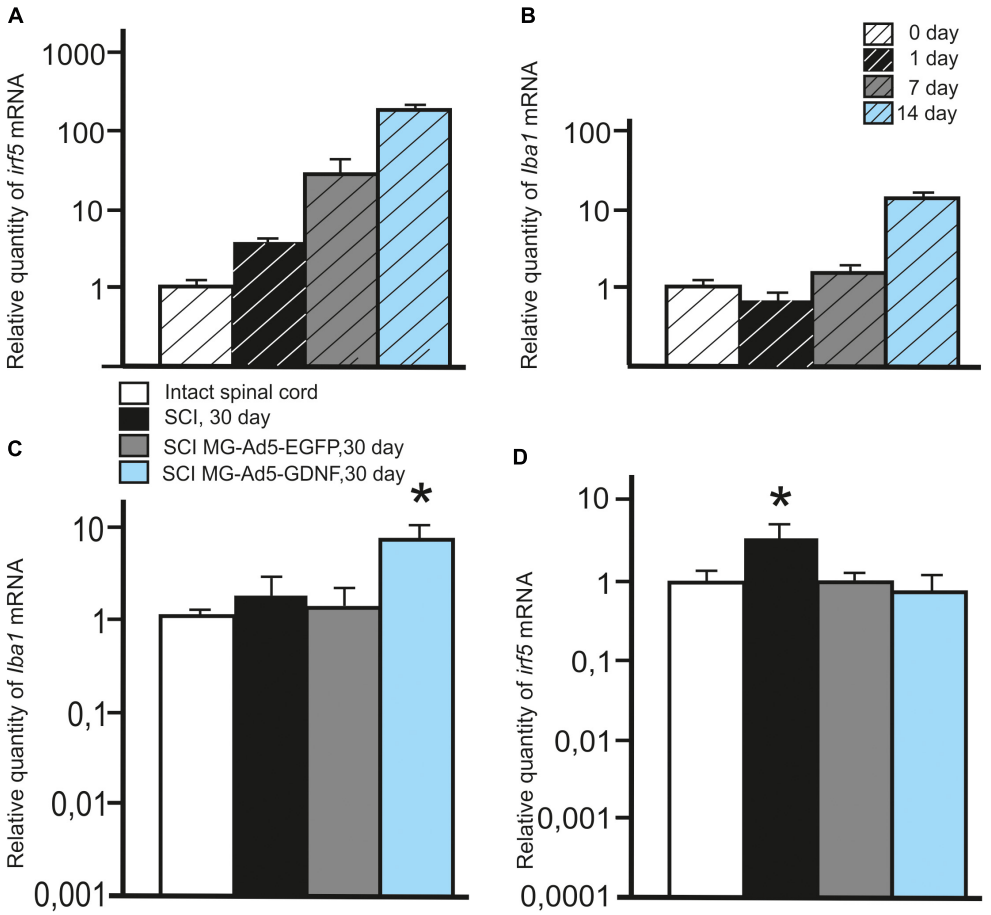

FIGURE 2 | Analysis of the expression of Iba1 and Irf5 mRNA *in vitro* and *in vivo* in the area of SCI. Irf5 **(A)** and Iba1 **(B)** mRNA expression *in vitro* on cultivation Days 0, 1, 7, 14. Irf5 and Iba1 mRNA expression of 0 day group was considered 100%. Differences were statistically significant between all time intervals ($P < 0.05$). Iba1 **(C)** and irf5 **(D)** mRNA expression *in vivo* on day 30 after SCI and cell transplantation. The Iba1 and irf5 mRNA expression levels in Intact controls were considered 100% **(C,D)**. *$P < 0.05$, one-way ANOVA followed by a Tukey's *post hoc* test.

groups with cell transplantation as compared to the SCI group without cell transplantation. Moreover, this parameter in VF zone was significantly higher (twofold) in the group with MG+Ad5-EGFP transplantation as compared to that transplanted with MG+Ad5-GDNF ($P < 0.05$).

Tissue Sparing

Morphometry allowed us to identify differences in the intact tissue area and a total area of abnormal cavities up to 5 mm rostrally and caudally from the injury epicenter in all study groups (**Figure 4**). This analysis demonstrated that within the study range the area of intact tissue was greatest in the SCI MG+Ad5-EGFP group. There was a significant difference at a distance of 2 (>1.85-fold) and 5 mm (>1.26-fold) caudally as compared to the SCI group without cell transplantation (**Figure 4A**) and at a distance of 4 mm (>1.35-fold) rostrally and 1–5 mm (>1.34 to 1.73-folds) caudally as compared to the SCI MG+Ad5-GDNF group (**Figure 4C**). At the same time no significant differences were observed between SCI and SCI MG+Ad5-GDNF groups (**Figure 4B**).

The total area analysis of abnormal cavities revealed no reliable differences between experimental groups (**Figures 4D–F**). There was an only exception at a distance of 3 mm caudally where this value was sevenfold lower in the SCI MG+Ad5-EGFP group than that in the SCI MG+Ad5-GDNF one (**Figure 4F**).

Thus, the morphometric analysis demonstrated that at every distance studied the intact tissue area was greater in the SCI MG+Ad5-EGFP group than in the SCI group without cell transplantation and the SCI MG+Ad5-GDNF group. However, it should be noted that this significant difference was observed in the caudal direction. There was a significant difference in the area of abnormal cavities between SCI MG+Ad5-EGFP and SCI MG+Ad5-GDNF groups in the caudal direction as well.

Assessment of Astrocytes in the Area of SCI

Using the method of immunohistochemistry we studied the total intensity of GFAP labeling 5 mm rostrally and caudally from the injury epicenter in selected zones of the white and gray matter (**Figures 5A,B**). 5 mm rostral to the injury epicenter the

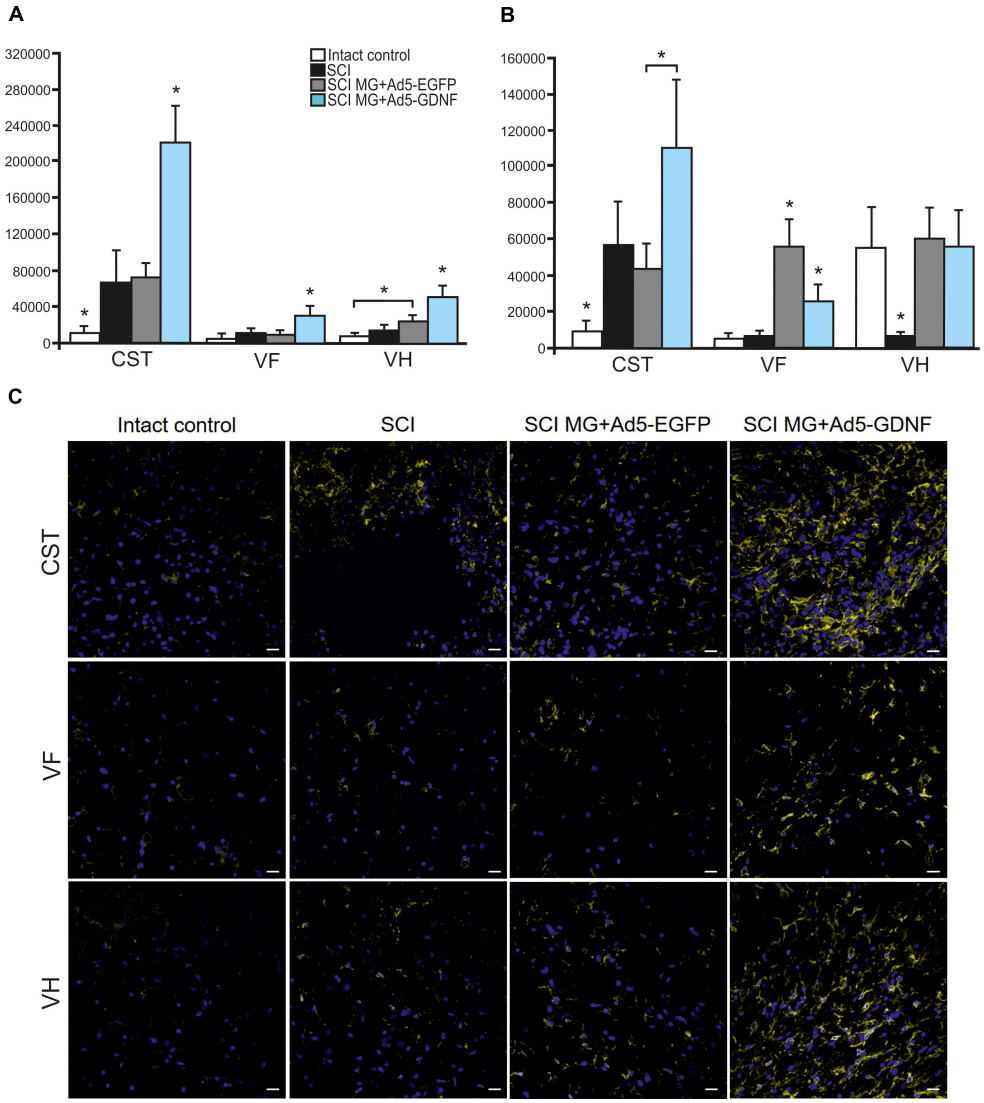

FIGURE 3 | Assessment of microglial cells in the area of SCI. The total intensity of Iba1 labeling 5 mm rostrally **(A)** and caudally **(B)** from the injury epicenter. *$P < 0.05$, one-way ANOVA followed by a Tukey's *post hoc* test. Assessment of microglial cells with Iba1 5 mm rostrally from the injury epicenter within the CST, VF and VH in the experimental groups **(C)**.

GFAP fluorescence intensity was highest in all studied zones in the group with MG+Ad5-EGFP transplantation (**Figure 5C**). This value was 2-fold higher in CST and VH zone ($P < 0.05$) in the SCI MG+Ad5-EGFP group as compared to the SCI MG+Ad5-GDNF one. No significant differences between SCI and SCI MG+Ad5-GDNF groups were observed both rostrally and caudally from the injury epicenter. At the same time, there was a significant difference in the VH zone at a distance of 5 mm rostrally where the total intensity of GFAP labeling was ∼twofold ($P < 0.05$) higher in the SCI MG+Ad5-EGFP group than that in other experimental groups.

Assessment of Locomotor Activity

We assessed locomotor recovery using the BBB rating scale from 7 to 30 days post injury. The motor function scores in the SCI+MG-Ad5-GDNF group were higher than those in the SCI and SCI+MG-Ad5-EGFP groups within 30 days after injury (**Figure 6**). Additionally, there were significant differences ($P < 0.05$) only between the SCI+MG-Ad5-GDNF and SCI groups on Days 14 and 21–30 after injury. We observed no significant differences between SCI and SCI+MG-Ad5-EGFP groups as well as between SCI+MG-Ad5-EGFP and SCI+MG-Ad5-GDNF ones.

DISCUSSION

In our previous study, we showed that glial cell line-derived neurotrophic factor (GDNF), a well-known neuroprotective molecule, decreases phagocytic activity of microglia in an *in vitro*

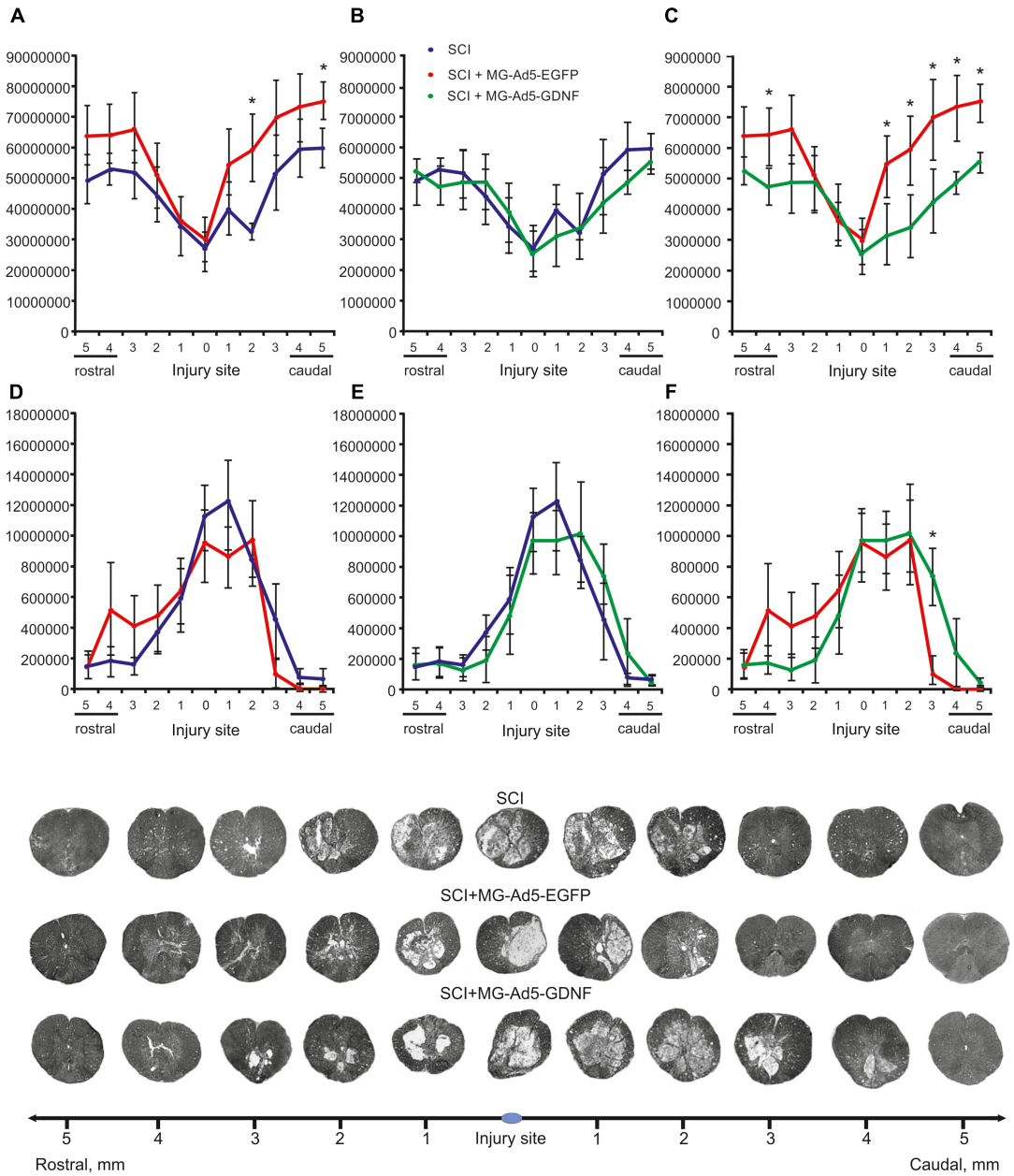

FIGURE 4 | Tissue analysis in experimental groups. An area of the intact tissue **(A–C)** and a total area of abnormal cavities **(D–F)** 5 mm rostrally and caudally from the injury epicenter on Day 30 after SCI and microglia transplantation. $^*P < 0.05$, one-way ANOVA followed by a Tukey's *post hoc* test. Cross sections of the injured spinal cord on Day 30 after SCI in experimental groups (bottom panel). Azur-eosin staining.

model of SCI (Zhuravleva et al., 2016). Ad5-GDNF transducted microglia have shown a similar effect. Therefore, we decided to identify to what extent the microglia phagocytic activity can affect the outcome of post-traumatic processes in the acute period of SCI in rats. Our experiments demonstrated that the intact tissue area was lower in the group with Ad5-GDNF-transduced microglial cell transplantation and had reduced phagocytic activity than that in the group of animals transplanted with microglial cells carrying the gene *egfp*. Interestingly, there were no significant differences in restoring the motor function.

We have previously characterized the microglial transplanted cells (Zhuravleva et al., 2015). Immunocytochemistry demonstrated that immediately after isolation and within 2 weeks of culture the microglial cells expressed Iba1, CD68, CD11b/c, and CD45. In the same time, our results demonstrate that most of the transduced Ad5-EGFP well as Ad5-GDNF microglia predominantly express pan markers Iba1/CD68 and CD86 at all studied culture periods. In their morphologic properties Ad5-EGFP transducted microglia were amoeboid active phagocytic microglia. Amoeboid morphology was shown

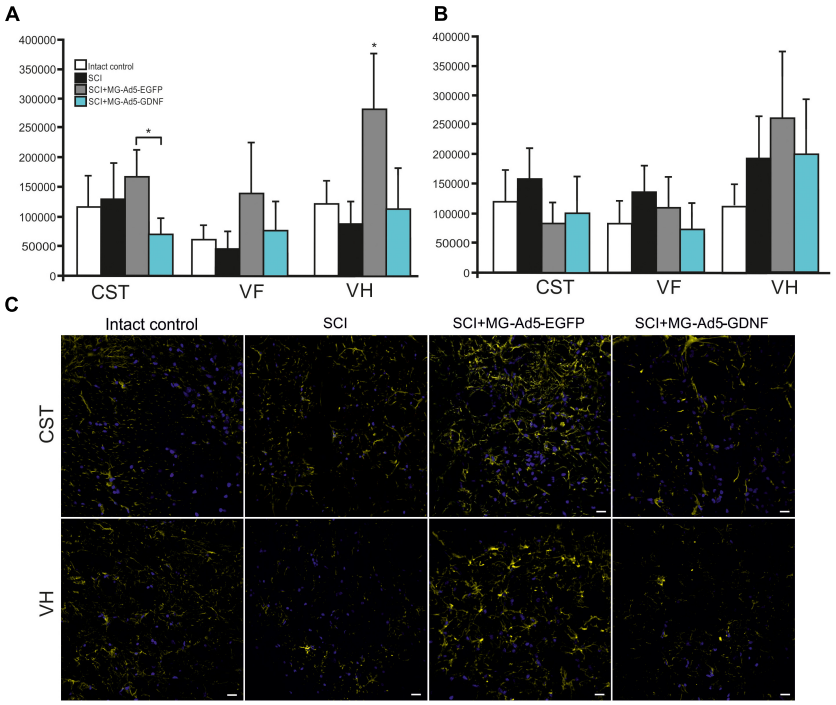

FIGURE 5 | Assessment of astrocytes in the area of SCI. The total intensity of GFAP labeling 5 mm rostrally **(A)** and caudally **(B)** from the injury epicenter. *$P < 0.05$, one-way ANOVA followed by a Tukey's *post hoc* test. Assessment of astrocytes with GFAP 5 mm rostrally from the injury epicenter within the CST and VH in the experimental groups **(C)**.

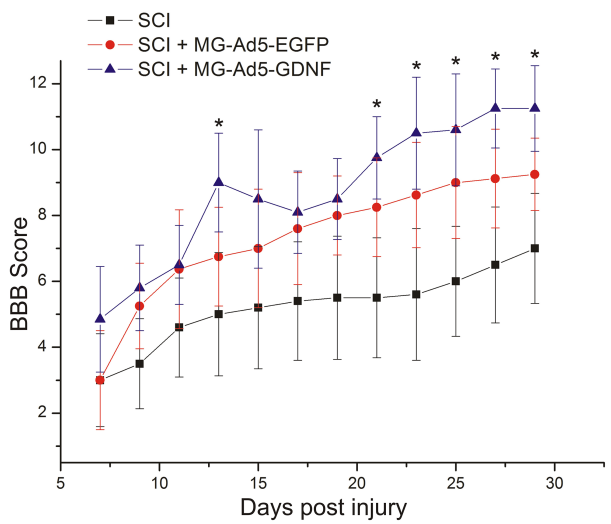

FIGURE 6 | Post-SCI behavioral studies in experimental groups. Assessment of locomotor activity using the BBB rating scale from 7 to 30 days after injury. *$P < 0.05$, one-way ANOVA followed by a Tukey's *post hoc* test.

to reflect a highly active state associated with phagocytosis and a proinflammatory function (Tam and Ma, 2014).

At the same time transduction of microglia with Ad5-GDNF promoted the formation of round, resting non-phagocytic microglia. These findings are in line with the conclusions that GDNF can suppress activation of the microglia in neuroinflammatory processes (Xing et al., 2010; Rickert et al., 2014). Our findings for transplantation effects of active phagocytic and non-phagocytic microglia into the area of SCI are consistent with the assumption made by Redondo-Castro et al. (2013) that the enhancement of the scavenger and phagocytic properties of microglia resulted in was reduction of initial trauma which can improve long-term structural and functional outcome. This positive effect of active phagocytic microglia is due to the removal of dead cells and debris (Boekhoff et al., 2011). Yaguchi et al. (2008) demonstrated that activation of endogenous microglia after SCI improved the integrity of nervous tissue. Moreover, these results are relevant not only to an acute period of injury but also to a chronic one. There is a significant reduction of scar tissue (Hamanoue et al., 2015) with activation of endogenous microglia in the chronic post-traumatic period.

We have previously shown that the microglia transplanted into the area of SCI in an acute period actively migrated rostrally and caudally from the site of injection and survived for at least 14 days with the expression of reporter genes (Zhuravleva et al., 2016). Throughout the whole period of microglia cultivation, the level of Iba1 and irf5 mRNA expression was increased with the maximum value observed on 14 day. This result corresponds to the data that G-CSF (which was added to the culture of microglia) promotes the division of microglia and the maintenance of its functional state (Giulian and Ingeman, 1988). The results obtained in this study provide evidence to the good survival of the microglia implanted into the site of

injury by the expression of Iba1 and irf5 mRNA in the area of SCI at 30 dpi. We demonstrated that the level of irf5 mRNA expression was significantly higher in the SCI group. This result is consistent with the data that after SCI the pool of M1 microglia is increasing (Kigerl et al., 2009) along with irf5 expression (Lawrence and Natoli, 2011). At the same time the level of mRNA Iba1 was significantly higher in groups with microglia transplantation when compared to the other groups. These results seem to be associated with the large number of microglia within the site of injury due to insertion of a donor cell pool in transplantation. It should be noted that the level of mRNA Iba1 (as a pan marker of microglia) was significantly higher in the group with MG-Ad5-GDNF transplantation. The immunohistochemical findings confirmed the results obtained in a real-time PCR analysis and demonstrated a significantly increased Iba1$^+$-cell count predominantly in the rostral direction in the group with MG-Ad5-GDNF transplantation as compared to the other experimental groups. This may be attributed to a supportive GDNF effect on microglial carrier-cells. This is consistent with the previous findings by Salimi et al. (2003) that GDNF promotes cell survival in serum-free cultures of primary rat microglia.

At the same time, immunohistochemical staining for GFAP demonstrated that in most cases an increased intensity of the Iba1 fluorescence was accompanied with decreased intensity of the GFAP fluorescence and vice versa, in the groups with microglia transplantation. This is especially obvious at a distance of 5 mm rostrally where the total intensity of GFAP labeling in all studied zones was higher in the group with MG-Ad5-EGFP transplantation as compared to the SCI+MG-Ad5-GDNF group. Based on these findings it can be concluded that the more microglia in the site of injury, the fewer the number of reactive GFAP$^+$-astrocytes is. The data obtained are consistent with the results of Hamanoue et al. (2015), who demonstrated that activated endogenous microglia within a chronic period alter SCI could lead to significant reduction of scar tissue. Nevertheless, the glial barrier and reactive astrocytes have a positive role in maintaining the structural integrity of spinal cord tissue (Adams and Gallo, 2018). In this regard, an increased astroglial activation can be involved in tissue sparing in the group with MG-Ad5-EGFP transplantation.

We found out that transplantation of MG-Ad5-GDNF into the area of SCI improved recovery of the motor function compared to the SCI group. Nevertheless, there were no significant differences between the groups with microglial transplantation. Higher BBB test scores in the group with MG-Ad5-GDNF transplantation might be due to a supportive effect of GDNF on intact axons and their myelinati; the neuroprotective action maintaining the expression of neurofilament proteins, calcitonin gene-related peptide (CGRP) and axon growth associated protein 43 (GAP-43) (Cheng et al., 2002; Zhang et al., 2009).

Thus, the increased number of active phagocytic microglia in the area of acute SCI might promote improved nerve tissue integrity without a significant effect on functional recovery within 30 days after injury.

AUTHOR CONTRIBUTIONS

YM: conceived and designed the experiments, behavioral study, statistical analysis, and writing the article. EA and MZ: isolation and preparation of rat microglia, histological assessment and immunohistochemical studies. LG: SCI and cell injection. EG: RNA isolation, cDNA synthesis, and real-time PCR. AK: SCI and post-surgical care, behavioral study. AR: development of a research plan and participation in the writing of the article.

FUNDING

This study was supported by Russian Foundation for Basic Research (to EA) (Grant 18-34-00141). AR was supported by the state assignment 20.5175.2017/6.7 ("Leading Researcher") of the Ministry of Education and Science of the Russian Federation. Some of the experiments were conducted using equipment at the Interdisciplinary Center for Analytical Microscopy and Pharmaceutical Research and Education Center, Kazan (Volga Region) Federal University, Kazan, Russia. This work was performed in accordance with the Program of Competitive Growth of the Kazan Federal University and a subsidy allocated to the Kazan Federal University for the state assignment in the sphere of scientific activities.

REFERENCES

Adams, K. L., and Gallo, V. (2018). The diversity and disparity of the glial scar. *Nat. Neurosci.* 21, 9–15. doi: 10.1038/s41593-017-0033-9

Boekhoff, T. M., Ensinger, E. M., Carlson, R., Bock, P., Baumgartner, W., Rohn, K., et al. (2011). Microglial contribution to secondary injury evaluated in a large animal model of human spinal cord trauma. *J. Neurotrauma* 29, 1000–1011. doi: 10.1089/neu.2011.1821

Cheng, H., Wu, J. P., and Tzeng, S. F. (2002). Neuroprotection of glial cell line-derived neurotrophic factor in damaged spinal cords following contusive injury. *J. Neurosci. Res.* 69, 397–405. doi: 10.1002/jnr.10303

Dibaj, P., Nadrigny, F., Steffens, H., Scheller, A., Hirrlinger, J., Schomburg, E. D., et al. (2010). NO mediates microglial response to acute spinal cord injury under ATP control in vivo. *Glia* 58, 1133–1144. doi: 10.1002/glia.20993

Francos-Quijorna, I., Amo-Aparicio, J., Martinez-Muriana, A., and López-Vales, R. (2016). IL-4 drives microglia and macrophages toward a phenotype conducive for tissue repair and functional recovery after spinal cord injury. *Glia* 64, 2079–2092. doi: 10.1002/glia.23041

Giulian, D., and Ingeman, J. E. (1988). Colony-stimulating factors as promoters of ameboid microglia. *J. Neurosci.* 8, 4707–4717.

Hamanoue, M., Morioka, K., Hayakawa, K., Nakajima, K., Ogata, T., and Takamatsu, K. (2015). "Functional recovery from chronic spinal cord injury by the reactivation of endogenous microglia," *Proceedings of the Neuroscience 2015 Chicago Nanosymposium, Spinal Cord, Therapeutic Strategies*, Chicago, IL.

Hansson, E. (2003). Glial neuronal signaling in the central nervous system. *FASEB J.* 17, 341–348. doi: 10.1096/fj.02-0429rev

Kigerl, K. A., Gensel, J. C., Ankeny, D. P., Alexander, J. K., Donnelly, D. J., and Popovich, P. G. (2009). Identification of two distinct macrophage subsets with

divergent effects causing either neurotoxicity or regeneration in the injured mouse spinal cord. *J. Neurosci.* 29, 13435–13444.

Kreutzberg, G. W. (1996). Microglia: a sensor for pathological events in the CNS. *Trends Neurosci.* 19, 312–318. doi: 10.1016/0166-2236(96)10049-7

Lai, A. Y., and Todd, K. G. (2008). Differential regulation of trophic and proinflammatory microglial effectors is dependent on severity of neuronal injury. *Glia* 56, 259–270. doi: 10.1002/glia.20610

Lawrence, T., and Natoli, G. (2011). Transcriptional regulation of macrophage polarization: enabling diversity with identity. *Nat. Rev. Immunol.* 11:750. doi: 10.1038/nri3088

Redondo-Castro, E., Hernández, J., Mahy, N., and Navarro, X. (2013). Phagocytic microglial phenotype induced by glibenclamide improves functional recovery but worsens hyperalgesia after spinal cord injury in adult rats. *Eur. J. Neurosci.* 38, 3786–3798. doi: 10.1111/ejn.12382

Rickert, U., Grampp, S., Wilms, H., Spreu, J., Knerlich-Lukoschus, F., Held-Feindt, J., et al. (2014). Glial cell line-derived neurotrophic factor family members reduce microglial activation via inhibiting p38MAPKs-Mediated inflammatory responses. *J. Neurodegener. Dis.* 2014, 1–10. doi: 10.1155/2014/369468

Rocha, S. M., Cristovão, A. C., Campos, F. L., Fonseca, C. P., and Baltazar, G. (2012). Astrocyte-derived GDNF is a potent inhibitor of microglial activation. *Neurobiol. Dis.* 47, 407–415. doi: 10.1016/j.nbd.2012.04.014

Salimi, K., Moser, K. V., Marksteiner, J., Reindl, M., and Humpel, C. (2003). GDNF and TGF-beta1 promote cell survival in serum-free cultures of primary rat microglia. *Cell Tissue Res.* 312, 135–139. doi: 10.1007/s00441-003-0711-7

Shechter, R., Miller, O., Yovel, G., Rosenzweig, N., London, A., Ruckh, J., et al. (2013). Recruitment of beneficial M2 macrophages to injured spinal cord is orchestrated by remote brain choroid plexus. *Immunity* 38, 555–569. doi: 10.1016/j.immuni.2013.02.012

Shechter, R., and Schwartz, M. (2013). Harnessing monocyte-derived macrophages to control central nervous system pathologies: no longer if' but how'. *J. Pathol.* 229, 332–346. doi: 10.1002/path.4106

Silver, J., Schwab, M. E., and Popovich, P. G. (2015). Central nervous system regenerative failure: role of oligodendrocytes, astrocytes, and microglia. *Cold Spring Harb. Perspect. Biol.* 7:a020602. doi: 10.1101/cshperspect.a020602

Tam, W. Y., and Ma, C. H. E. (2014). Bipolar/rod-shaped microglia are proliferating microglia with distinct M1/M2 phenotypes. *Sci. Rep.* 4:7279. doi: 10.1038/srep07279

Varnum, M. M., and Ikezu, T. (2012). The classification of microglial activation phenotypes on neurodegeneration and regeneration in Alzheimer's disease brain. *Arch. Immunol. Ther. Exp.* 60, 251–266. doi: 10.1007/s00005-012-0181-2

Weber, M. S., Prod'homme, T., Youssef, S., Dunn, S. E., Rundle, C. D., Lee, L., et al. (2007). Type II monocytes modulate T cell-mediated central nervous system autoimmune disease. *Nat. Med.* 13, 935–943. doi: 10.1038/nm1620

Xing, B., Xin, T., Zhao, L., Hunter, R. L., Chen, Y., and Bing, G. (2010). Glial cell line-derived neurotrophic factor protects midbrain dopaminergic neurons against lipopolysaccharide neurotoxicity. *J. Neuroimmunol.* 225, 43–51. doi: 10.1016/j.jneuroim.2010.04.010

Yaguchi, M., Ohta, S., Toyama, Y., Kawakami, Y., and Toda, M. (2008). Functional recovery after spinal cord injury in mice through activation of microglia and dendritic cells after IL-12 administration. *J. Neurosci. Res.* 86, 1972–1980. doi: 10.1002/jnr.21658

Zhang, L., Ma, Z., Smith, G. M., Wen, X., Pressman, Y., Wood, P. M., et al. (2009). GDNF-enhanced axonal regeneration and myelination following spinal cord injury is mediated by primary effects on neurons. *Glia* 57, 1178–1191. doi: 10.1002/glia.20840

Zhuravleva, M., Rizvanov, A., and Mukhamedshina, Y. (2016). Effect of GDNF on morphology, proliferation, and phagocytic activity of rat neonatal cortex isolated microglia. *Bionanoscience* 6, 379–383. doi: 10.1007/s12668-016-0247-4

Zhuravleva, M. N., Mukhamedshina, Y. O., Arkhipova, S. S., Sanatova, E. R., and Rizvanov, A. A. (2015). The morphological and phenotypic characteristics of microglia at different stages of cultivation and transplantation in the area of spinal cord injury in rats. *Genes Cells* 10, 34–39.

Conflict of Interest Statement: The authors declare that the research was conducted in the absence of any commercial or financial relationships that could be construed as a potential conflict of interest.

frontiers in Cellular Neuroscience

ORIGINAL RESEARCH
published: 10 January 2019
doi: 10.3389/fncel.2018.00523

CSF1R Stimulation Promotes Increased Neuroprotection by CD11c+ Microglia in EAE

Agnieszka Wlodarczyk[1,2†], *Anouk Benmamar-Badel*[1,2†], *Oriane Cédile*[1], *Kirstine Nolling Jensen*[1], *Isabella Kramer*[1], *Nick Boe Elsborg*[1] *and Trevor Owens*[1,2*]

[1] *Department of Neurobiology Research, Institute for Molecular Medicine, University of Southern Denmark, Odense, Denmark,* [2] *BRIDGE, Brain Research - Inter-Disciplinary Guided Excellence, Odense, Denmark*

Microglia are resident immune cells of the central nervous system. Their development and maintenance depend on stimulation of Colony Stimulating Factor-1 receptor (CSF1R). Microglia play an important role in neurodevelopment and a population of microglia that expresses the complement receptor CD11c is critical for primary myelination. This population is virtually absent in the healthy adult brain but increases dramatically upon neuroinflammatory conditions, and these microglia are suggested to play a protective role in central nervous system (CNS) diseases. To date, the molecular trigger for their expansion is unknown. Here we showed that stimulation of CSF1R by either of its ligands, CSF1 and interleukin (IL)-34, can induce expansion of CD11c+ microglia. In addition, such stimulation resulted in amelioration of EAE symptoms and decreased demyelination. Treatment with CSF1R ligands also induced expression of the chemokine CCL2, and we showed that experimental overexpression of CCL2 in the brain led to a dramatic increase of CD11c+ microglia, independent of CCR2. Moreover, this led to elevated CSF1 expression, suggesting a positive feedback loop between CSF1R and CCL2. These data provide new insights to microglia biology and open new perspectives for modulating microglial activity in neuroinflammatory diseases such as multiple sclerosis.

Keywords: CD11c, microglia, EAE, CCL2, IL-34, CSF1, CSF1R

OPEN ACCESS

Edited by:
Raquel Ferreira, Universidade da Beira Interior, Portugal

Reviewed by:
Robert Weissert, University of Regensburg, Germany
Adelaide Fernandes, Universidade de Lisboa, Portugal

***Correspondence:**
Trevor Owens
towens@health.sdu.dk

[†] *These authors have contributed equally to this work*

Received: *26 September 2018*
Accepted: *14 December 2018*
Published: *10 January 2019*

Citation:
Wlodarczyk A, Benmamar-Badel A, Cédile O, Jensen KN, Kramer I, Elsborg NB and Owens T (2019) CSF1R Stimulation Promotes Increased Neuroprotection by CD11c+ Microglia in EAE. Front. Cell. Neurosci. 12:523. doi: 10.3389/fncel.2018.00523

INTRODUCTION

Microglia are resident macrophages of the central nervous system (CNS) that primarily mediate surveillance and immunological functions (Nimmerjahn et al., 2005; Kettenmann et al., 2011). Contrary to most tissue macrophages, microglia are long-lived yolk sac-derived cells that maintain their numbers through proliferation without contribution from bone marrow-derived precursor cells in the steady state (Ginhoux et al., 2013; Kierdorf et al., 2013; Prinz and Priller, 2014). Development, maintenance and proliferation of microglia depend on activation of Colony Stimulating Factor-1 receptor (CSF1R), a key signaling pathway in myeloid cell development (Stanley and Chitu, 2014). Activation of CSF1R by its ligands, namely Colony Stimulating Factor-1 (CSF-1) and Interleukin (IL)-34, contributes to microglial proliferation and differentiation, and is critical for microglia development, since a dramatic reduction of microglial numbers is observed in mice lacking IL-34 (Wang et al., 2012). This lack of microglia in IL-34-KO mice leads to severe developmental abnormalities in the CNS (Elmore et al., 2014), underlining the importance of microglia for neurogenesis. Other recent studies point to microglia as key players in neurodevelopment.

Indeed, they participate in establishment of axonal connections (Squarzoni et al., 2014), refinement of synapses in a process called synaptic pruning (Schafer et al., 2012) and they support neuronal survival by production of Insulin-like Growth Factor-1 (IGF1) (Ueno et al., 2013).

We have recently identified a subpopulation of neonatal microglia that transiently expand soon after birth, identified by expression of the integrin complement receptor CD11c (Wlodarczyk et al., 2017). This subpopulation has a unique neurogenic and myelinogenic gene signature and is a major source of IGF1. Importantly, deletion of IGF1 in these cells leads to impaired primary myelination (Wlodarczyk et al., 2017). These findings have been supported by another study showing neonatal microglia importance in the maintenance and maturation of oligodendrocyte progenitors (Hagemeyer et al., 2017). Interestingly, CD11c+ microglia are also found to increase in numbers during neuroinflammation and neurodegeneration, such as in animal models of multiple sclerosis (MS)—experimental autoimmune encephalomyelitis (EAE) and cuprizone induced demyelination, as well as in mouse models for Neuromyelitis Optica and Alzheimer's Disease (AD) (Butovsky et al., 2006a; Remington et al., 2007; Wlodarczyk et al., 2014, 2015). We have shown that although CD11c+ microglia can efficiently present antigen to autoreactive T-cells, they are poor inducers of Th1 and Th17 responses (Wlodarczyk et al., 2014). Moreover, we showed that these microglia produce interferon (IFN)beta and high levels of IGF1 (Wlodarczyk et al., 2015), suggesting that they exert protective rather than detrimental functions in EAE. However, the exact role of CD11c+ microglia and the mechanism for their induction under neuroinflammatory conditions are not fully understood.

Here, we present new insights into the mechanism of induction of CD11c+ microglia. We show that *in vivo* stimulation of CSF1R by IL-34 or CSF1 leads to expansion of CD11c+ microglia, and that this may depend on CCL2 expression. Importantly treatment with CSF1R ligands led to suppression and reduced severity of EAE.

MATERIALS AND METHODS

Mice

C57BL/6j bom female mice aged 7–8 weeks were obtained from Taconic Europe A/S. Female CCL2-KO and CCR2-red fluorescent protein (RFP/RFP) mice were obtained from The Jackson Laboratory and maintained in the Biomedical Laboratory, University of Southern Denmark (Odense). DBA/2-MBP/CCL2 mice that express a mouse CCL2 transgene under control of an MBP promoter (Furtado et al., 2006) were originally obtained from Bristol-Myers Squibb and maintained as a homozygous colony. 2D2 mice, which have CD4+ T cells that express a transgenic Vα3.2β11 TCR specific for myelin oligodendrocyte glycoprotein (MOG) p35-55 (Bettelli et al., 2003) were obtained from Dr. Florian Kurschus (Institute for Molecular Medicine, University Medical Center, Johannes Gutenberg-University, Mainz, Germany, now University Hospital, Heidelberg, Germany) and crossed with DBA/2-MBP/CCL2 to obtain 2D2xMBPCCL2. DBA/2-MBP/CCL2 mice were further backcrossed to C57BL/6j bom to obtain B6-MBP/CCL2. All experiments were approved by the Danish Animal Experiments Inspectorate (approval number 2014-15-0201-00369).

EAE

Seven- to ten-week-old female mice were immunized by subcutaneous injection of 100 μL of an emulsion containing 100 μg of MOGp35–55 (TAG Copenhagen A/S, Frederiksberg, Denmark) in incomplete freunds adjuvant (DIFCO, Alberstslund, Denmark) supplemented with 400 μg heat-killed H37Ra *Mycobacterium tuberculosis* (DIFCO). *Bordetella pertussis* toxin (300 ng; Sigma-Aldrich, Brøndby, Denmark) in 200 μl of PBS was injected intraperitoneally on the same day as and the day after immunization. Animals were monitored daily from day 5 and scored on a 6-point scale as follows: 0, no symptoms; 1, partial loss of tail tonus; 2, complete loss of tail tonus; 3, difficulty walking, 4, paresis in both hind legs; 5, paralysis in both hind legs; 6, front limb weakness. Due to ethical considerations mice were sacrificed when they reached grade 6 or 24 h after hind leg paralysis.

Intrathecal Injections

Adenoviral Overexpression of CCL2

Eight to 10 weeks old CCL2-deficient or CCR2-RFP/RFP mice were anesthetized by means of an intraperitoneal injection of ketamine (Ketalar®, 100 mg/kg of body weight, Intervet International B.V., Bowmeer, the Netherlands) and xylazine (Rompum®, 10 mg/kg of body weight, Bayer, Copenhagen, Denmark). Eight microliters of replication defective adenovirus (10^7 infectious units) in sterile PBS were injected intrathecally at the site of the cisterna magna. Immediately before the injection, mice received a subcutaneous injection of buprenorphine (Temgesic®, 0.1 mg/kg of body weight, Indivior UK limited, Slough, Berkshire, Great Britain). The adenovirus encoding CCL2 was type 5 E1-E3-deleted encoding murine CCL2 gene (AdCCL2), driven by the CMV immediate-early promoter (Buschmann et al., 2012), kindly provided by Dr. J. Gauldie (Pathology & Molecular Medicine, McMaster University, Hamilton, Ontario, Canada). The adenovirus encoding the β-galactosidase gene (AdLacZ) was provided by Dr. J. Nalbantoglu (Montreal Neurological Institute, Montreal, Quebec, Canada).

Seventeen days after injection, mice were lethally anesthetized with sodium pentobarbital (Euthanimal®, 200 mg/kg of body weight, Glostrup sygehusapotek, Glostrup, Denmark), and perfused through the heart with ice-cold PBS before tissues were collected.

IL-34 and CSF1 Treatment

C57BL/6j mice were anesthetized by isoflurane inhalation. Fifty nanograms (Gomez-Nicola et al., 2013) of recombinant mouse IL-34 or recombinant mouse CSF1 (Biolegend, Nordic BioSite ApS, Copenhagen, Denmark) in 10 microliters of sterile PBS were injected in the cisterna magna. Analgesia was performed as described above. This treatment was performed either once or

every 24 h for 3 consecutive days and the mice were sacrificed one day after the last injection. In the EAE experiments, three injections of cytokines were performed, starting at the onset of the disease (grade 2, loss of tail tonus). For each mouse, the day of first injection is referred to as day 0 (D0).

Flow-Cytometry

Mice were anesthetized with sodium pentobarbital and intracardially perfused with ice-cold PBS. Brain tissue was collected and a single cell suspension was generated by forcing through a 70 mm cell strainer (BD Biosciences, Kongens Lyngby, Denmark). Mononuclear cells were collected after centrifugation on 37% Percoll (GE Healthcare Biosciences, Brøndby, Denmark). They were first incubated with anti-Fc receptor (Clone 2.4G2; 1 mg/ml; BD Biosciences) and Syrian hamster IgG (50 mg/ml; Jackson Immuno Research Laboratories Inc., TriChem ApS, Skanderborg, Denmark) in PBS 2% fetal bovine serum (FBS), then with anti-CD45 (Clone 30-F11; Biolegend), anti-CD11b (Clone M1/70; Biolegend), and biotin conjugated anti-CD11c (Clone HL3; BD Pharmingen) antibodies in PBS 2% FBS and finally with streptavidin-APC (Biolegend). Cell populations were gated based on isotype-matched control antibodies as $CD45^{dim}$ $CD11b^{+}$ $CD11c^{-}$ ($CD11c^{-}$ microglia), $CD45^{dim}$ $CD11b^{+}$ $CD11c^{+}$ ($CD11c^{+}$ microglia). Data were collected on an LSRII^{TM} flow cytometer (BD Biosciences) and analyzed using Flowlogic (Inivai, Victoria, Australia).

Immunohistochemistry

DAB Staining

Sixteen-micrometer sections from 4% PFA-fixed, sucrose-cryoprotected frozen spinal cords of PBS-perfused mice were cut on a cryostat and stored at −20°C on Superfrost Plus slides (Fisher Scientific, Roskilde, Denmark). Sections were washed in PBS and endogenous peroxidase was depleted by incubation for 30 min in methanol + 0.2% H_2O_2. Endogenous biotin was blocked using Biotin Blocking system (DAKO, Agilent, Glostrup, Denmark) and incubated for 30 min in 3% BSA in PBS +0.2% Triton X-100 (Merck, Darmstadt, Germany) to prevent unspecific binding. Next, sections were incubated for 1 h at room temperature with biotinylated anti-MOG antibody (protein G affinity-purified supernatant from hybridoma clone Z2 (provided by Prof. Chris Linington, Glasgow University, UK) and IgG2a isotype control from murine myeloma) followed by 1 h incubation at room temperature with streptavidin-horseradish peroxidase (GE Healthcare Biosciences). The sections were developed using 3,3′-diaminobenzidine (DAB, 0.5 mg/ml) (Sigma-Aldrich) and H_2O_2 (0.033%) (Sigma-Aldrich) for 5 min and dehydrated in increasing concentrations of ethanol before clearing in xylene. Mounting was performed in Depex mounting medium (Merck).

Immunofluorescence Staining

Sixteen-micrometer sections from 4% PFA-fixed, sucrose-cryoprotected frozen spinal cords of PBS-perfused mice were cut on a cryostat and stored at −20°C on Superfrost Plus slides (Fisher Scientific). Sections were fixed in acetone for 10 min at room temperature followed by an incubation of 30 min at room temperature in 3% BSA in PBS +0.2% Triton X-100 to prevent non-specific binding. Next, sections were incubated for 1h with anti-NogoA (AB5664P, Millipore, Merck), and then 1 h at room temperature with anti-Rabbit IgG Alexa Fluor 488 secondary antibody (A21206, Invitrogen, Fisher Scientific), or only with anti-GFAP Cy3 conjugated antibody (C9205, Sigma-Aldrich, Merck). Slides were mounted in Fluoresence Mounting Medium (DAKO). Imaging was performed on a FV1000MPE microscope (Olympus).

Semi Quantitative Analysis of Demyelination

Analysis of demyelination was performed by an investigator who was blinded to the study. Five to ten parallel sections of the lumbar part of the spinal cord were graded based on the degree of loss of MOG immunoreactivity on 0–3 point scale where 0 = no lesions, 0.5 = one small lesion, 1 = 1 extended lesion; 1.5 = 2 small lesions; 2 = 2 extended lesions; 2.5 = 3 small lesions; 3 = at least 3 extended lesions. The mean values from all the sections from each animal were plotted as bar graphs.

RT-qPCR

RNA was extracted from brain tissue using TRIzol (Invitrogen, Fisher Scientific) according to the manufacturer's protocol. cDNA was transcribed from 1 μg of total RNA using M-MLV reverse transcriptase (Invitrogen, Fisher Scientific) following the manufacturer's instructions. Quantitative real-time polymerase chain reaction (qPCR) was performed using 1 μL of cDNA combined with 24 μL of Maxima probe/ROX qPCR master mix (Fermentas, Fisher Scientific) with primers and probes (TAG Copenhagen A/S) as follows: *Itgax* (forward primer TGC AGAAGGCCAAGTATTCCTT; reverse primer CAGAGGCCC TGACTCCTGTCT; probe AAGAAAGAGGACCAGCAGT), *Ccl2* (forward primer TGGAGCATCCACGTGTTG; reverse primer ACTCATTGGGATCATCTTGCT; probe CTCAGCCAG ATGCAGTT), *Ifng* (forward primer CATTGAAAGCCTAGA AAGTCTGAATAAC; reverse primer TGGCTCTGCAGGATT TTCATG; probe TCACCATCCTTTTGCCAGTTCCTCCAG), *Il17a* (forward primer CTCCAGAAGGCCCTCAGACTAC; reverse primer TGTGGTGGTCCAGCTTTCC, probe ACTCTC CACCGCAATGA), *Ifnb1* (forward primer GCGTTCCTGCTG TGCTTCTC, reverse primer TTGAAGTCCGCCCTGTAGGT, probe CGGAAATGTCAGGAGCT), *Il10* (forward primer GGT TGCCAAGCCTTATCGGA, reverse primer ACCTGCTCC ACTGCCTTGCT, probe TGAGGCGCTGTCATCGATTTC TCCC). TaqMan® PreAmp Master Mix Kits were used for *Ccr4* (Mm01963217_u1, Applied Biosystems, Fisher Scientific), *Il-34* (Mm01243248_m1, Applied Biosystems, Fisher Scientific) and *Csf1* (Mm00432686_m1, Applied Biosystems, Fisher Scientific).

For *Igf1*, Maxima SYBR Green/ROX qPCR Master Mix (2X) Probe/ROX qPCR Master Mix (Fermentas, Fisher Scientific) with forward and reverse primers (800 nM; from TAG Copenhagen A/S) were used with *Igf1* primers (Forward primer CCG AGG GGC TTT TAC TTC AAC AA; Reverse primer CGG AAG CAA CAC TCA TCC ACA A). qPCRs were performed on a QuantStudio 3 apparatus (Applied Biosystems, Fisher Scientific). Results were expressed relative to 18S rRNA as endogenous control (TaqMan^{TM} Ribosomal RNA control Reagents kit;

Applied Biosystems, Fisher Scientific). One microliters of 1/1,000 diluted cDNA were used for 18S rRNA analysis.

RESULTS

IL-34 and CSF1 Induce CD11c+ Microglia

Since CSF1R signaling is a potent inducer of microglial proliferation, differentiation and maintenance, we asked whether it could play a role in the generation of CD11c+ microglia.

A single intrathecal (i.t) injection of 50 ng of recombinant IL-34 (rIL-34) but not rCSF1via the cisterna magna to otherwise unmanipulated mice (**Figure 1A**) led to a significant increase in numbers of CD11c+ microglia (**Figure 1B**). We were then interested to see if repeated injections of this cytokine could further expand the CD11c+ microglia population. Three daily injections of rIL34 (**Figure 1D**) however sustained CD11c+ microglia increase did not cause further expansion of these cells. Three injections of rCSF1 also resulted in expansion of these cells (**Figure 1E**), indicating that although the pharmacokinetics of these CSF1R ligands differed slightly, their outcomes were equivalent.

The increase of the CD11c+ microglial population that has been described in neuroinflammatory and neurodegenerative models all coincidence with upregulation of the chemokine CCL2. We asked if intrathecal stimulation of CSF1R had an impact on *Ccl2* expression. Analogous to effects on CD11c+ microglial numbers, a single intrathecal injection of rIL-34 but not CSF1 resulted in significantly elevated expression of *Ccl2* mRNA in the brains (**Figure 1C**). We observed an increase in CCL2 expression after 3 consecutive injections of both IL-34 and CSF1 that seemed proportional to observed CD11c+ microglial numbers, although this did not reach statistical significance (**Figure 1F**). We then wished to clarify whether there was a correlation between CCL2 upregulation and CD11c+ microglia increase. Since neither treatment resulted in immune cell infiltration (not shown), we used CD11c gene (*Itgax*) expression as a surrogate for CD11c+ microglia expansion. We showed significant positive correlation between expression of *Ccl2* and *Itgax* mRNA in the brain (**Figure 1G**), indicating that CCL2 expression, however induced, could account for the increase of CD11c+ microglia.

Overexpression of CCL2 Leads to an Increase of CD11c+ Microglia

We then asked if CCL2 plays any role in induction of CD11c+ microglia. We first compared numbers of CD11c+ microglia in the brains of CCL2-deficient and wild-type (WT) mice. Proportions of CD11c+ microglia were significantly reduced in CCL2-deficient brains (**Figure 2A**). We subsequently investigated CD11c microglia proportions in the brains of transgenic mice that overexpressed CCL2 under control of an MBP promoter, on three strain backgrounds (DBA/2-MBP CCL2, DBA/2-MBP CCL2 × 2D2, and B6-MBP-CCL2). Brains of all of these mice contained elevated proportions of CD11c+ microglia, reaching almost 25% of total microglia in case of B6-MBP-CCL2, nearly a 10-fold increase as compared to levels in non-transgenic B6 mice (3%) (**Figure 2B**). We then asked if compensating for lack of CCL2 in CCL2-KO mice by induction of CCL2 expression with an adenoviral vector would restore proportions of CD11c+ microglia. **Figure 2C** shows that this intervention resulted in significantly higher proportion of CD11c+ microglia compared to control virus-infected CCL2-KO mice. To assess whether the induction of CD11c+ microglia was dependent on the CCR2- receptor for CCL2, we overexpressed CCL2 in CCR2 RFP/RFP mice that lack functional CCR2. This overexpression also led to a significant increase of CD11c+ microglia (**Figure 2D**). This increase was noticeably higher than in transfected CCL2-KO, which could be explained by higher overexpression of adenovirus-encoded CCL2 in CCR2 rfp/rfp mice as we previously reported in Cedile et al. (2017). Interestingly, expression of CCL2 in CCL2-KO (**Figure 2E**) as well as CCR2 rfp/rfp (**Figure 2F**) brains resulted in a significant upregulation of *Csf1* but not *Il34* mRNA levels, suggesting a positive feedback loop between CCL2 and CSF1.

Stimulation of CSF1R Leads to Amelioration of EAE

To investigate the role of CD11c+ microglia in neuroinflammation we treated B6 mice that showed first signs of EAE (typically 11–15 days post immunization) daily for 3 consecutive days with 50 ng of rIL-34 or 50 ng of rCSF1, delivered to the cisterna magna as before (**Figure 3A**). Both cytokines effectively suppressed disease progression (**Figure 3B**) and reduced disease severity (**Figure 3C**). The effect was already significant 24 h after first injection of rIL34 and 24 h after second injection of rCSF1. Histological analysis revealed reduced demyelination (**Figures 3D,E**) and reduced loss of oligodendrocytes (**Figure 3F**) in both treated groups in comparison to vehicle-treated controls. We observed no difference in astrocyte activation measured as GFAP gene expression (not shown) and no morphological changes (**Figure 3G**).

Flow-cytometric analysis of the CNS of these mice showed that neither the percentage of infiltrating immune cells (**Figure 4A**) nor the composition of myeloid cells were affected (**Figure 4B**, not shown). However, there was a significant decrease in TCRbeta+ T cells in the spinal cord (SC) upon rIL-34 treatment (**Figure 4C**). Neither treatment induced significant effect on gene expression of pro- (GM-CSF, IL17) or anti-inflammatory (IFNbeta, IL10, IGF1) cytokines in the CNS (not shown), although there was a significant reduction of *Ifng* mRNA levels in the brains of mice that were treated with rIL-34 (**Figure 4D**). Interestingly, CD11c+ microglia expressed higher levels of PDL1 than their CD11c- counterparts (**Figure 4E**), and this was not affected by treatment (not shown), whereas treatment with rCSF1 but not rIL-34 led to a small but significant decrease of MHCII expression on CD11c+ microglia (**Figure 4F**).

DISCUSSION

In this study we show that CSF1R stimulation in the CNS by its ligands leads to expansion of the CD11c+

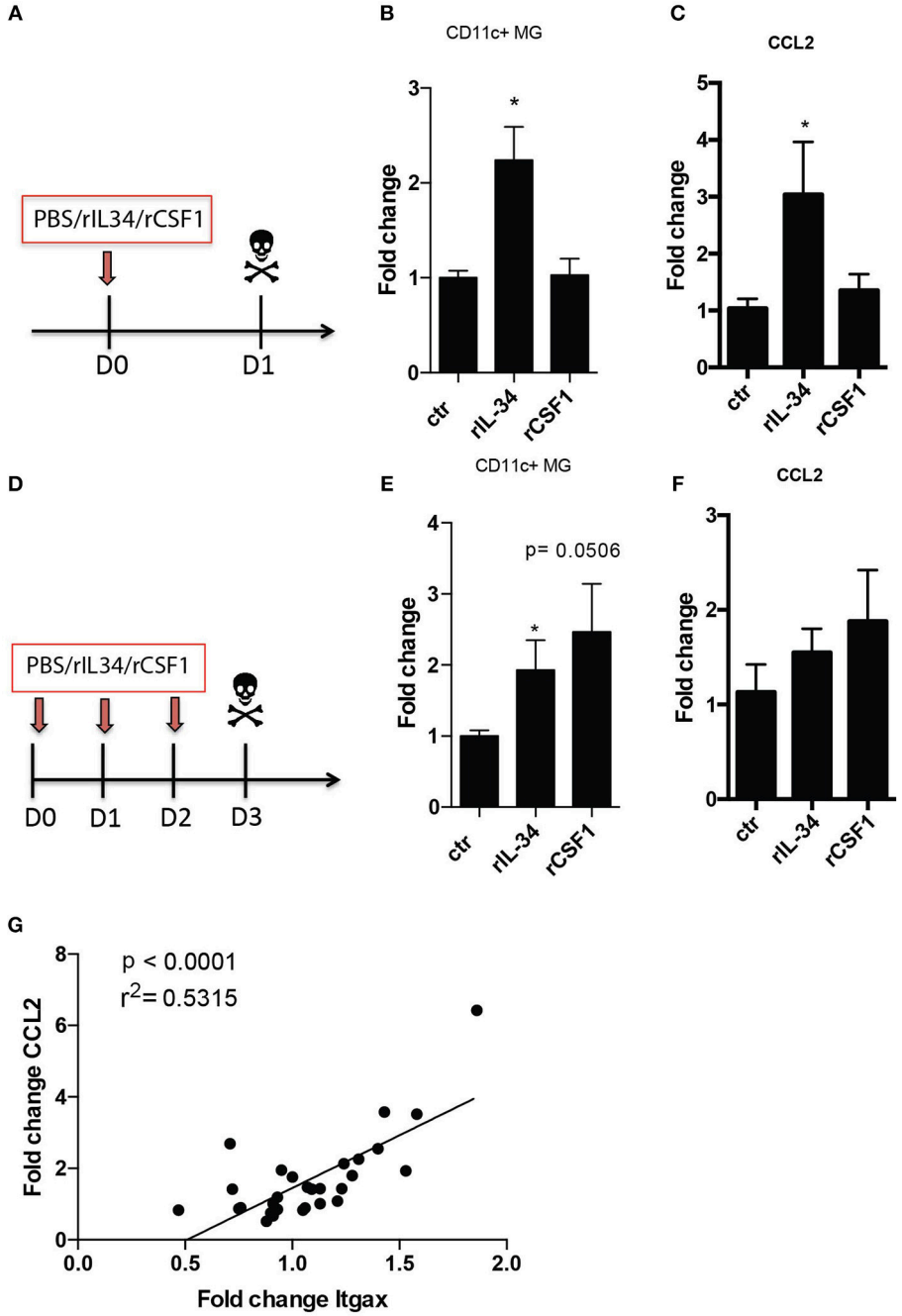

FIGURE 1 | CD11c+ microglia increase due to CSF1R stimulation. B6 mice received one **(A–C)** or three consecutive **(D,E)** i.t injections of 50ng rIL34, 50ng rCSF1 or vehicle (ctr). **(B,E)** Flow cytometry analysis of brains showing fold increase of CD11c+ microglia relative to mean number in ctr animals after single ($n = 8$, $n = 7$, $n = 9$) **(B)** and three consecutive i.t injections ($n = 6$; $n = 6$; $n = 5$). **(C,F)** RT-qPCR analysis of brains showing fold increase of *Ccl2* expression relative to mean expression in ctr animals after single ($n = 4$, $n = 5$, $n = 4$) **(C)** and three consecutive i.t injections: $n = 5$; $n = 6$; $n = 5$ **(F). (G)** *Ccl2* mRNA levels positively correlated with *Itgax* gene expression in brains of mice that received one or three consecutive i.t injections of 50 ng rIL34, 50 ng rCSF1 or ctr ($n = 28$). Data are pooled from at least two individual experiments and presented as means + SEM; $^*p < 0.05$ assessed using Mann–Whitney *U*-test.

microglia subpopulation. Moreover, this population of microglia can also be induced by overexpression of the chemokine CCL2. Interestingly, CSF1R stimulation upregulated CCL2 expression, which correlated with CD11c+ microglia expansion. Moreover, we demonstrated that treatment with CSF1R ligands IL-34 and CSF1 dramatically ameliorated EAE symptoms and reduced demyelination.

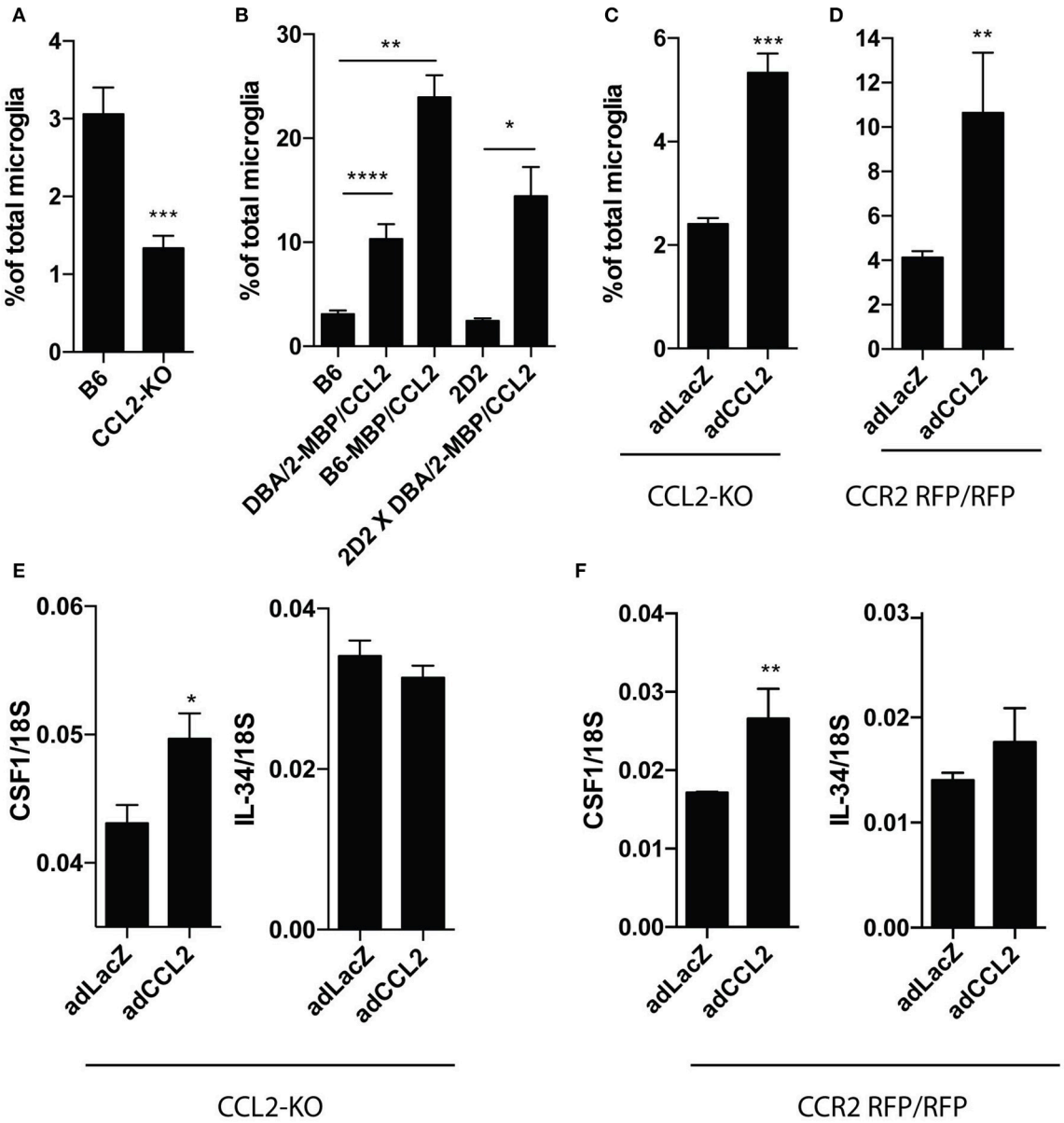

FIGURE 2 | Experimental overexpression of CCL2 leads to expansion of CD11c+ microglia. Results from flow cytometry analysis showing difference in percentage of CD11c+ microglia from total microglia in brains of: B6 ($n = 14$) and CCL2 KO ($n = 6$) mice **(A)**, transgenic mice with over expression of CCL2 and corresponding control animals; B6 ($n = 14$); DBA/2-MBP/CCL2 ($n = 8$); B6-MBP/CCL2 ($n = 3$); 2D2 ($n = 5$); 2D2x DBA/2-MBP/CCL2 ($n = 4$) **(B)**, as well as in CCL2 KO ($n = 7$; $n = 12$) **(C)** and CCR2 RFP/RFP ($n = 5$) **(D)** mice infected with adenoviral vector expressing CCL2 or control vector expressing LacZ. RT-qPCR analysis of brains of CCL2 KO ($n = 5$) **(E)** and CCR2 RFP/RFP ($n = 5$; $n = 6$) **(F)** mice infected with adenoviral vector expressing CCL2 or LacZ, showing expression of CSF1 and IL34, relative to 18S. Data are pooled from at least two individual experiments and presented as means +SEM; $^{*}p < 0.05$; $^{**}p < 0.01$;$^{***}p < 0.001$;$^{****}p < 0.0001$ assessed using Mann–Whitney *U*-test.

The role of microglia in neuroinflammatory conditions such as in EAE is still unclear. Their activation is a hallmark of demyelinated lesions in the MS brain and microglial activity correlates with progression of disability (Rissanen et al., 2018). In EAE, microglial cells were reported to participate in disease aggravation by re-activating T cells that had entered the CNS (Aloisi et al., 1998). Depletion of microglia in EAE proved efficient to repress symptoms (Heppner et al., 2005; Nissen et al., 2018). These findings implicated microglia with negative outcomes in the disease. However, beneficial effects of microglial cells in models of MS have also been reported. In response to demyelination microglia produced anti-inflammatory IFNbeta and cleared myelin debris, so facilitating the process of remyelination that leads to amelioration of the disease (Yamasaki

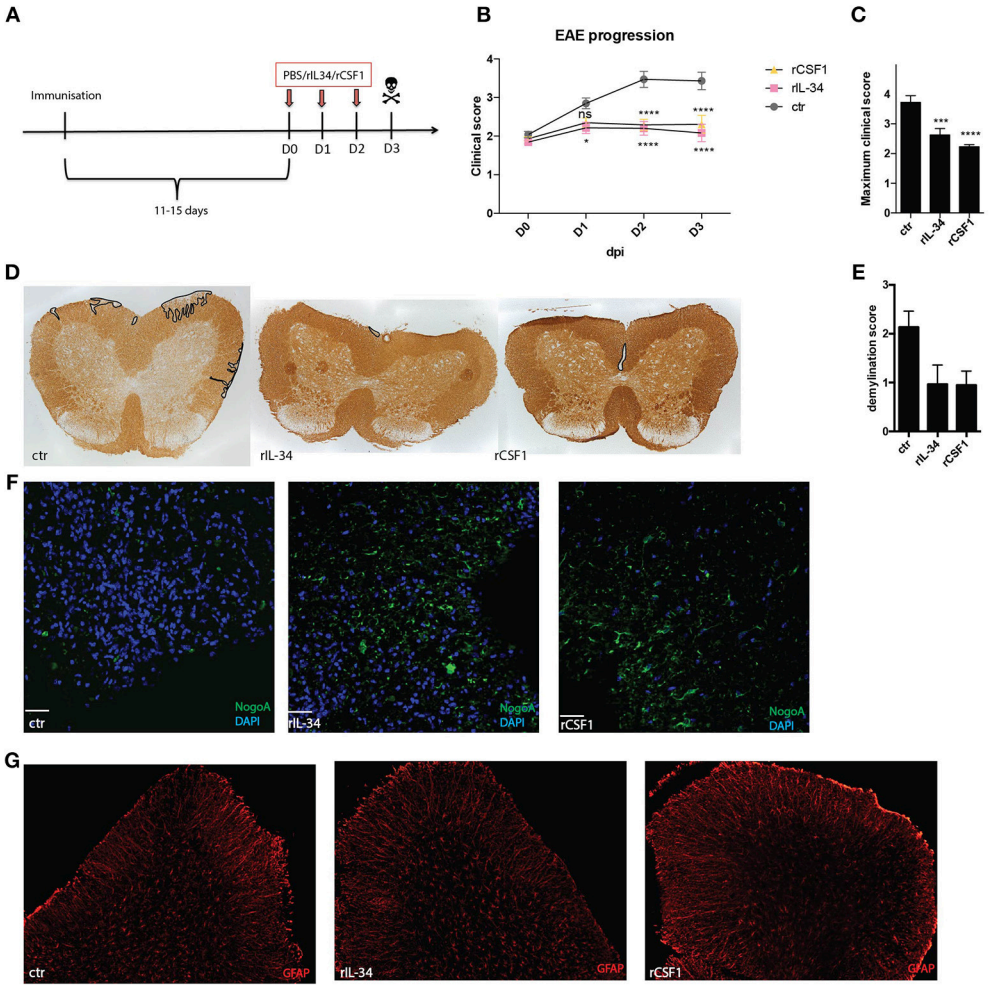

FIGURE 3 | CSF1R stimulation ameliorates EAE. Mice were immunized with MOG35-55+CFA and pertussis toxin. At the onset of the disease (D0, typically 11–15 days post immunization) mice received three consecutive i.t injections of: 50ng rCSF1 ($n = 16$); 50 ng rIL-34 ($n = 20$) or ctr ($n = 22$) at D0, D1, D2, and were sacrificed at D3 **(A)**. Graphs show EAE progression **(B)** and maximum clinical score **(C)** for these mice. Data are pooled from eight individual experiments $^{*}p < 0.05$; $^{***}p < 0.001$;$^{****}p < 0.0001$ assessed using two-way ANOVA **(A)** or student's *t*-test **(B). (D,E)** Representative micrographs **(D)** and semi-quantitative assessment **(E)** of demyelination (defined as loss of MOG immunoreactivity in spinal cord). **(F,G)** Representative micrographs showing NogoA+ oligodendrocytes (green) **(F)** and GFAP+ astrocytes (red) **(G)** in spinal cord. Data are pooled from at least three individual experiments ($n = 3$; $n = 3$; $n = 4$).

et al., 2014; Kocur et al., 2015). It has also been shown that transplantation of microglia pre-stimulated with IL-4 into the CSF resulted in oligodendrogenesis and led to amelioration of EAE (Butovsky et al., 2006b). Recently we have demonstrated that CD11c+ microglia do not polarize T-cells toward a pathogenic phenotype but in turn express neuroprotective and anti-inflammatory factors such as IGF1, SPP1 and IFNbeta (Wlodarczyk et al., 2014, 2015, 2017). Our data here further support an anti-inflammatory phenotype of CD11c+ microglia, showing that they express higher levels of PDL1 in comparison to their CD11c- counterparts. We have previously shown that during EAE both CD11c+ and CD11c- microglia express equal levels of CSF1R and that they expand due to proliferation (Wlodarczyk et al., 2015). It has been shown that IL-34, unlike CSF1, induced neuroprotective properties of microglia in an AD model (Du Yan et al., 1997; Mizuno et al., 2011). This suggests that microglial phenotypes may differ depending on CSF1R ligand stimulation. Here we showed that treatment with CSF1 can modulate phenotype of CD11c+ microglia by decreasing their expression of MHCII. Stimulation of CSF1R by both ligands had a beneficial effect on EAE progression. The faster kinetics in case of rIL-34 treatment is consistent with a delayed induction of CD11c+ microglia by rCSF1. Amelioration of EAE symptoms after rIL-34 and rCSF1 treatment with concomitant reduction of demyelination is in line with a recent study showing beneficial effects of CSF1 in cuprizone-induced demyelination. This intervention led to microglial activation, upregulation of IGF1 as well as reduction of demyelination (Laflamme et al., 2018). Although Laflamme and colleagues showed only marginal effect of CSF1 treatment on infiltrating

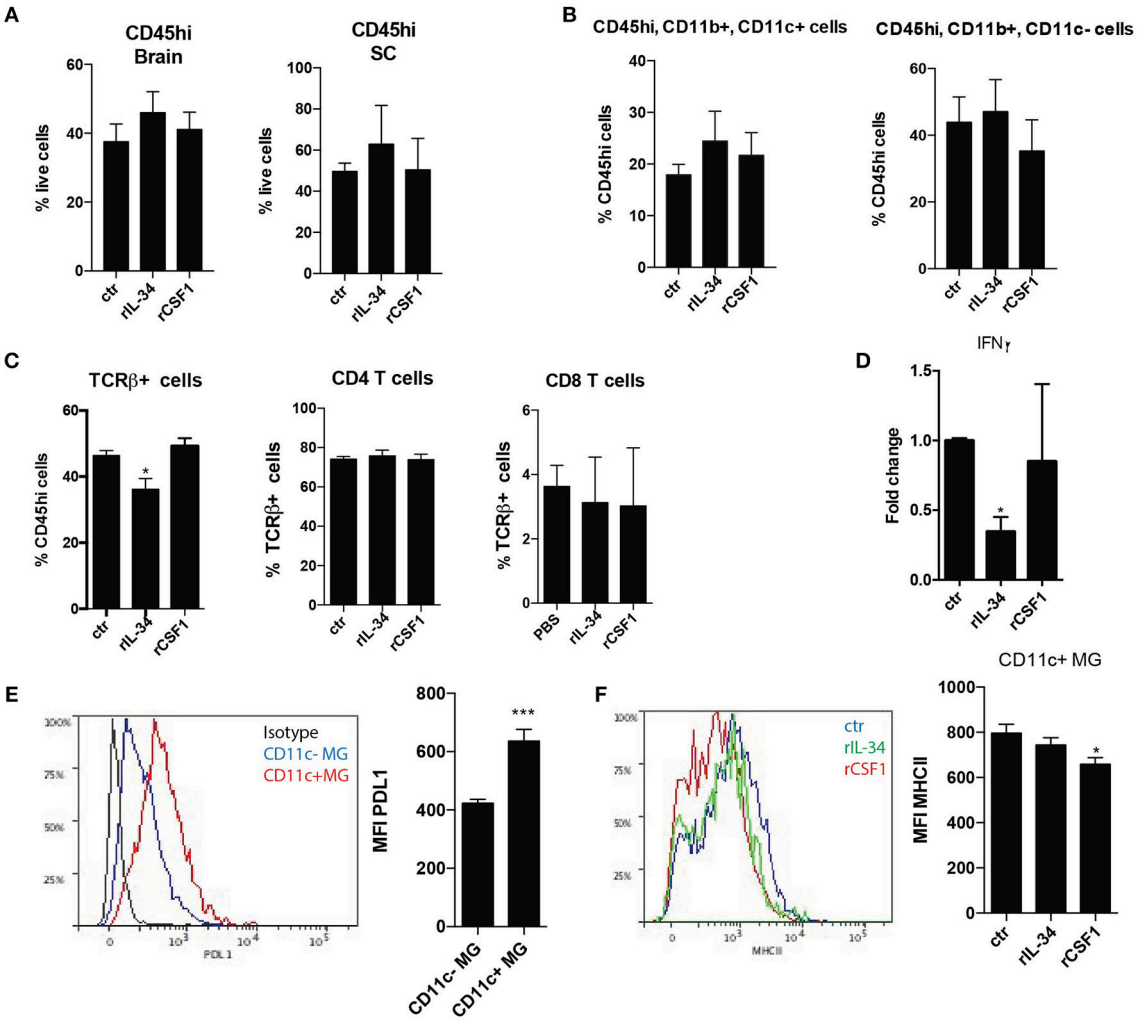

FIGURE 4 | CSF1R stimulation in EAE has no impact on leukocyte infiltration but regulates microglia response. **(A–C)** Flow cytometry analysis of CNS of mice with symptomatic EAE that received three consecutive i.t injections of: 50 ng rCSF1 ($n = 3$), 50 ng rIL-34 ($n = 4$), or ctr ($n = 6$) at D0, D1, and D2 (as in **Figure 3**), showing percentage of infiltrating immune cells gated as CD45high from a live gate in brain and SC **(A)**, and proportions of CD11b+ CD11c+/- myeloid cells **(B)** as well as TCRbeta+ T-cells from CD45high cells and proportions of CD4+ and CD8+ T-cells from CD45high TCRbeta+ cells in the SC **(C). (D,E)** RT-qPCR analysis showing *Ifng* expression in brains: ($n = 4$, $n = 6$, $n = 5$) **(D)**. Representative histogram showing PDL1 expression on CD11c+ (red) and CD11c− (blue) microglia defined as CD45low CD11b+ and an isotype control (black) as well as bar graph showing MFI of PDL1 expression **(E). (F)** Representative histogram showing expression of MHCII in CD11c+ microglia from mice with symptomatic EAE that received three consecutive i.t. injections of: 50 ng rCSF1 (red), 50 ng rIL-34 (green) or ctr (blue) as well as bar graph showing MFI of MHCII **(F)**. Data are pooled from at least 3 individual experiments, presented as means +SEM $^*p < 0.05$; $^{***}p < 0.001$, assessed using Mann–Whitney *U*-test.

leukocytes in the cuprizone model and in our model there were no obvious differences in leukocyte composition, CSF1R is broadly expressed on monocytes/macrophages and we cannot exclude that the CSF1 and IL-34 treatment modulated response of such cells.

CD11c+ microglia are virtually absent in the healthy adult brain, and are mobilized in response to inflammatory cues, demyelination, neurodegeneration (Butovsky et al., 2006a; Remington et al., 2007; Wlodarczyk et al., 2014, 2015). Interestingly, levels of the chemokine CCL2 were elevated in the disease models where these cells have been described such as EAE, cuprizone induced demyelination as well as AD (Mahad and Ransohoff, 2003; Janelsins et al., 2005; Buschmann et al., 2012). Our data show that CCL2 expression positively correlated with expression of *Itgax* mRNA and thus CD11c+ microglia expansion and we could demonstrate that overexpression of CCL2 in the brain induced significant increase of CD11c+ microglia population. Importantly we demonstrated that adenoviral vector-induced expression of CCL2 in CCL2-KO brain restored proportions of CD11c+ microglia to levels similar to those seen in WT animals. It has been reported that CSF1R ligands can induce expression of CCL2 in leukocytes (Eda et al., 2010; Zwicker et al., 2016). Here we confirm these observations showing elevated expression of *Ccl2* upon IL-34 and

CSF1 treatment in the brain. This coincides with an expansion of CD11c+ microglia raising the possibility that CCL2 induction by CSF1R stimulation is directly or indirectly responsible for mobilization of CD11c+ microglia. We also show increase of *Csf1* mRNA following experimental CCL2 upregulation. This is in line with RNA-seq data showing upregulation of CSF1 expression in CD11c+ microglia (Wlodarczyk et al., 2017) and suggests a positive feedback loop between CSF1R ligands and CCL2 that mediates endogenous regulation of microglia activity. The fact that induction of these microglia was not dependent on CCR2 suggests that another receptor for CCL2 may be involved. We have previously identified CCR4 as an alternative receptor for CCL2 in the CNS (Cedile et al., 2017). Whether CCL2 acts directly on microglia via CCR4, or another cell population such as meningeal or perivascular macrophages (Prinz et al., 2017) astrocytes or neurons that also express CCR4 (Cedile et al., 2017) remains to be determined. The CCL2-CCR2 axis is generally considered to be proinflammatory, but here we propose that CCL2 induced via CSFR1 stimulation can promote CNS protection in a CCR2 independent manner.

Taken together we describe here that treatment with CSF1R ligands induces an increase of protective CD11c+ microglia and leads to amelioration of EAE symptoms and reduced demyelination. Moreover, these protective microglia are induced by CCL2 signaling. These data provide new insights in microglia biology that can open new avenues for treatment directed to modulate microglia activity in neuroinflammatory diseases such as MS.

AUTHOR CONTRIBUTIONS

AW, OC, and TO designed the work. AW, AB-B, IK, OC, NE, and KJ performed the experiments. AW and AB-B analyzed the data. AW, AB-B, and TO wrote the manuscript. All authors read and approved the final manuscript.

FUNDING

This work was supported by grants from Lundbeckfonden R209-2015-2724 and R173-2014-717, Danish Council for Independent Research 6110-00064B, Danish MS Society and Warwara Larsens Fond J.2015-415 S.03-16/2015. Novo Nordisk Foundation NNF13OC0006131.

ACKNOWLEDGMENTS

We thank Dina Stæhr Arengoth and Pia Nyborg Nielsen for expert technical assistance, Dr. J. Nalbantoglu and Dr. J. Gauldie for providing viral vectors and Dr. Florian Kurschus for providing 2D2 transgenic mice.

REFERENCES

Aloisi, F., Ria, F., Penna, G., and Adorini, L. (1998). Microglia are more efficient than astrocytes in antigen processing and in Th1 but not Th2 cell activation. *J. Immunol.* 160, 4671–4680.

Bettelli, E., Pagany, M., Weiner, H. L., Linington, C., Sobel, R. A., and Kuchroo, V. K. (2003). Myelin oligodendrocyte glycoprotein-specific T cell receptor transgenic mice develop spontaneous autoimmune optic neuritis. *J. Exp. Med.* 197, 1073–1081. doi: 10.1084/jem.20021603

Buschmann, J. P., Berger, K., Awad, H., Clarner, T., Beyer, C., and Kipp, M. (2012). Inflammatory response and chemokine expression in the white matter corpus callosum and gray matter cortex region during cuprizone-induced demyelination. *J. Mol. Neurosci.* 48, 66–76. doi: 10.1007/s12031-012-9773-x

Butovsky, O., Koronyo-Hamaoui, M., Kunis, G., Ophir, E., Landa, G., Cohen, H., et al. (2006a). Glatiramer acetate fights against Alzheimer's disease by inducing dendritic-like microglia expressing insulin-like growth factor 1. *Proc. Natl. Acad. Sci. U.S.A.* 103, 11784–11789. doi: 10.1073/pnas.0604681103

Butovsky, O., Landa, G., Kunis, G., Ziv, Y., Avidan, H., Greenberg, N., et al. (2006b). Induction and blockage of oligodendrogenesis by differently activated microglia in an animal model of multiple sclerosis. *J. Clin. Invest.* 116, 905–915. doi: 10.1172/JCI26836

Cedile, O., Wlodarczyk, A., and Owens, T. (2017). CCL2 recruits T cells into the brain in a CCR2-independent manner. *APMIS* 125, 945–956. doi: 10.1111/apm.12740

Du Yan, S., Zhu, H., Fu, J., Yan, S. F., Roher, A., Tourtellotte, W. W., et al. (1997). Amyloid-beta peptide-receptor for advanced glycation endproduct interaction elicits neuronal expression of macrophage-colony stimulating factor: a proinflammatory pathway in Alzheimer disease. *Proc. Natl. Acad. Sci. U.S.A.* 94, 5296–5301. doi: 10.1073/pnas.94.10.5296

Eda, H., Zhang, J., Keith, R. H., Michener, M., Beidler, D. R., and Monahan, J. B. (2010). Macrophage-colony stimulating factor and interleukin-34 induce chemokines in human whole blood. *Cytokine* 52, 215–220. doi: 10.1016/j.cyto.2010.08.005

Elmore, M. R., Najafi, A. R., Koike, M. A., Dagher, N. N., Spangenberg, E. E., Rice, R. A., et al. (2014). Colony-stimulating factor 1 receptor signaling is necessary for microglia viability, unmasking a microglia progenitor cell in the adult brain. *Neuron* 82, 380–397. doi: 10.1016/j.neuron.2014.02.040

Furtado, G. C., Pina, B., Tacke, F., Gaupp, S., van Rooijen, N., Moran, T. M., et al. (2006). A novel model of demyelinating encephalomyelitis induced by monocytes and dendritic cells. *J. Immunol.* 177, 6871–6879. doi: 10.4049/jimmunol.177.10.6871

Ginhoux, F., Lim, S., Hoeffel, G., Low, D., and Huber, T. (2013). Origin and differentiation of microglia. *Front. Cell. Neurosci.* 7:45. doi: 10.3389/fncel.2013.00045

Gomez-Nicola, D., Fransen, N. L., Suzzi, S., and Perry, V. H. (2013). Regulation of microglial proliferation during chronic neurodegeneration. *J. Neurosci.* 33, 2481–2493. doi: 10.1523/JNEUROSCI.4440-12.2013

Hagemeyer, N., Hanft, K. M., Akriditou, M. A., Unger, N., Park, E. S., Stanley, E. R., et al. (2017). Microglia contribute to normal myelinogenesis and to oligodendrocyte progenitor maintenance during adulthood. *Acta Neuropathol.* 134, 441–458. doi: 10.1007/s00401-017-1747-1

Heppner, F. L., Greter, M., Marino, D., Falsig, J., Raivich, G., Hovelmeyer, N., et al. (2005). Experimental autoimmune encephalomyelitis repressed by microglial paralysis. *Nat. Med.* 11, 146–152. doi: 10.1038/nm1177

Janelsins, M. C., Mastrangelo, M. A., Oddo, S., LaFerla, F. M., Federoff, H. J., and Bowers, W. J. (2005). Early correlation of microglial activation with enhanced tumor necrosis factor-alpha and monocyte chemoattractant protein-1 expression specifically within the entorhinal cortex of triple transgenic Alzheimer's disease mice. *J. Neuroinflammation* 2:23. doi: 10.1186/1742-2094-2-2

Kettenmann, H., Hanisch, U. K., Noda, M., and Verkhratsky, A. (2011). Physiology of microglia. *Physiol. Rev.* 91, 461–553. doi: 10.1152/physrev.00011.2010

Kierdorf, K., Erny, D., Goldmann, T., Sander, V., Schulz, C., Perdiguero, E. G., et al. (2013). Microglia emerge from erythromyeloid precursors via Pu.1- and Irf8-dependent pathways. *Nat. Neurosci.* 16, 273–280. doi: 10.1038/nn.3318

Kocur, M., Schneider, R., Pulm, A. K., Bauer, J., Kropp, S., Gliem, M., et al. (2015). IFNbeta secreted by microglia mediates clearance of myelin debris in CNS autoimmunity. *Acta Neuropathol. Commun.* 3:20. doi: 10.1186/s40478-015-0192-4

Laflamme, N., Cisbani, G., Prefontaine, P., Srour, Y., Bernier, J., St-Pierre, M. K., et al. (2018). mCSF-induced microglial activation prevents myelin loss and promotes its repair in a mouse model of multiple sclerosis. *Front. Cell. Neurosci.* 12:178. doi: 10.3389/fncel.2018.00178

Mahad, D. J., and Ransohoff, R. M. (2003). The role of MCP-1 (CCL2) and CCR2 in multiple sclerosis and experimental autoimmune encephalomyelitis (EAE). *Semin. Immunol.* 15, 23–32. doi: 10.1016/S1044-5323(02)00125-2

Mizuno, T., Doi, Y., Mizoguchi, H., Jin, S., Noda, M., Sonobe, Y., et al. (2011). Interleukin-34 selectively enhances the neuroprotective effects of microglia to attenuate oligomeric amyloid-beta neurotoxicity. *Am. J. Pathol.* 179, 2016–2027. doi: 10.1016/j.ajpath.2011.06.011

Nimmerjahn, A., Kirchhoff, F., and Helmchen, F. (2005). Resting microglial cells are highly dynamic surveillants of brain parenchyma *in vivo*. *Science* 308, 1314–1318. doi: 10.1126/science.1110647

Nissen, J. C., Thompson, K. K., West, B. L., and Tsirka, S. E. (2018). Csf1R inhibition attenuates experimental autoimmune encephalomyelitis and promotes recovery. *Exp. Neurol.* 307:24–36. doi: 10.1016/j.expneurol.2018.05.021

Prinz, M., Erny, D., and Hagemeyer, N. (2017). Ontogeny and homeostasis of CNS myeloid cells. *Nat. Immunol.* 18, 385–392. doi: 10.1038/ni.3703

Prinz, M., and Priller, J. (2014). Microglia and brain macrophages in the molecular age: from origin to neuropsychiatric disease. *Nat. Rev. Neurosci.* 15, 300–312. doi: 10.1038/nrn3722

Remington, L. T., Babcock, A. A., Zehntner, S. P., and Owens, T. (2007). Microglial recruitment, activation, and proliferation in response to primary demyelination. *Am. J. Pathol.* 170, 1713–1724. doi: 10.2353/ajpath.2007.060783

Rissanen, E., Tuisku, J., Vahlberg, T., Sucksdorff, M., Paavilainen, T., Parkkola, R., et al. (2018). Microglial activation, white matter tract damage, and disability in MS. *Neurol. Neuroimmunol. Neuroinflammation* 5:e443. doi: 10.1212/NXI.0000000000000443

Schafer, D. P., Lehrman, E. K., Kautzman, A. G., Koyama, R., Mardinly, A. R., Yamasaki, R., et al. (2012). Microglia sculpt postnatal neural circuits in an activity and complement-dependent manner. *Neuron* 74, 691–705. doi: 10.1016/j.neuron.2012.03.026

Squarzoni, P., Oller, G., Hoeffel, G., Pont-Lezica, L., Rostaing, P., Low, D., et al. (2014). Microglia modulate wiring of the embryonic forebrain. *Cell Rep.* 8, 1271–1279. doi: 10.1016/j.celrep.2014.07.042

Stanley, E. R., and Chitu, V. (2014). CSF-1 receptor signaling in myeloid cells. *Cold Spring Harb. Perspect. Biol.* 6:a021857. doi: 10.1101/cshperspect.a021857

Ueno, M., Fujita, Y., Tanaka, T., Nakamura, Y., Kikuta, J., Ishii, M., et al. (2013). Layer V cortical neurons require microglial support for survival during postnatal development. *Nat. Neurosci.* 16, 543–551. doi: 10.1038/nn.3358

Wang, Y., Szretter, K. J., Vermi, W., Gilfillan, S., Rossini, C., Cella, M., et al. (2012). IL-34 is a tissue-restricted ligand of CSF1R required for the development of Langerhans cells and microglia. *Nat. Immunol.* 13, 753–760. doi: 10.1038/ni.2360

Wlodarczyk, A., Cedile, O., Jensen, K. N., Jasson, A., Mony, J. T., Khorooshi, R., et al. (2015). Pathologic and protective roles for microglial subsets and bone marrow- and blood-derived myeloid cells in central nervous system inflammation. *Front. Immunol.* 6:463. doi: 10.3389/fimmu.2015.00463

Wlodarczyk, A., Holtman, I. R., Krueger, M., Yogev, N., Bruttger, J., Khorooshi, R., et al. (2017). A novel microglial subset plays a key role in myelinogenesis in developing brain. *EMBO J.* 36, 3292–3308. doi: 10.15252/embj.201696056

Wlodarczyk, A., Lobner, M., Cedile, O., and Owens, T. (2014). Comparison of microglia and infiltrating CD11c(+) cells as antigen presenting cells for T cell proliferation and cytokine response. *J. Neuroinflammation* 11:57. doi: 10.1186/1742-2094-11-57

Yamasaki, R., Lu, H., Butovsky, O., Ohno, N., Rietsch, A. M., Cialic, R., et al. (2014). Differential roles of microglia and monocytes in the inflamed central nervous system. *J. Exp. Med.* 211, 1533–1549. doi: 10.1084/jem.20132477

Zwicker, S., Bureik, D., Bosma, M., Martinez, G. L., Almer, S., and Bostrom, E. A. (2016). Receptor-type protein-tyrosine phosphatase zeta and colony stimulating factor-1 receptor in the intestine: cellular expression and cytokine- and chemokine responses by interleukin-34 and colony stimulating factor-1. *PLoS ONE* 11:e0167324. doi: 10.1371/journal.pone.0167324

Conflict of Interest Statement: The authors declare that the research was conducted in the absence of any commercial or financial relationships that could be construed as a potential conflict of interest.

frontiers in Cellular Neuroscience

ORIGINAL RESEARCH
published: 22 February 2019
doi: 10.3389/fncel.2019.00041

Microglia-Derived Microvesicles Affect Microglia Phenotype in Glioma

Alfonso Grimaldi[1†], Carmela Serpe[2†], Giuseppina Chece[2], Valentina Nigro[3], Angelo Sarra[4], Barbara Ruzicka[3], Michela Relucenti[5], Giuseppe Familiari[5], Giancarlo Ruocco[1], Giuseppe Rubens Pascucci[1], Francesca Guerrieri[1], Cristina Limatola[6,7] and Myriam Catalano[2,7]*

[1] Center for Life Nanoscience, Istituto Italiano di Tecnologia@Sapienza, Rome, Italy, [2] Department of Physiology and Pharmacology, Sapienza University of Rome, Rome, Italy, [3] Department of Physics, Istituto dei Sistemi Complessi del Consiglio Nazionale delle Ricerche, Sapienza University of Rome, Rome, Italy, [4] Department of Science, University of Roma Tre, Rome, Italy, [5] Department of Anatomical, Histological, Forensic Medicine and Orthopedics Sciences, Sapienza University of Rome, Rome, Italy, [6] Department of Physiology and Pharmacology, Laboratory Affiliated to Istituto Pasteur Italia – Fondazione Cenci Bolognetti, Sapienza University of Rome, Rome, Italy, [7] IRCCS Neuromed, Pozzilli, Italy*

Extracellular-released vesicles (EVs), such as microvesicles (MV) and exosomes (Exo) provide a new type of inter-cellular communication, directly transferring a ready to use box of information, consisting of proteins, lipids and nucleic acids. In the nervous system, EVs participate to neuron-glial cross-talk, a bidirectional communication important to preserve brain homeostasis and, when dysfunctional, involved in several CNS diseases. We investigated whether microglia-derived EVs could be used to transfer a protective phenotype to dysfunctional microglia in the context of a brain tumor. When MV, isolated from microglia stimulated with LPS/IFNγ were brain injected in glioma-bearing mice, we observed a phenotype switch of tumor associated myeloid cells (TAMs) and a reduction of tumor size. Our findings indicate that the MV cargo, which contains upregulated transcripts for several inflammation-related genes, can transfer information in the brain of glioma bearing mice modifying microglial gene expression, reducing neuronal death and glioma invasion, thus promoting the recovery of brain homeostasis.

Keywords: microglia, extracellular vesicles, tumor associated myeloid cells, brain tumors, glioma

OPEN ACCESS

Edited by:
Cinzia Volonté, Institute of Cell Biology and Neurobiology, CNR, Italy

Reviewed by:
Marta Fumagalli, University of Milan, Italy
Federica Barbieri, Università di Genova, Italy

***Correspondence:**
Cristina Limatola
cristina.limatola@uniroma1.it

† These authors have contributed equally to this work

Received: *24 October 2018*
Accepted: *25 January 2019*
Published: *22 February 2019*

Citation:
Grimaldi A, Serpe C, Chece G, Nigro V, Sarra A, Ruzicka B, Relucenti M, Familiari G, Ruocco G, Pascucci GR, Guerrieri F, Limatola C and Catalano M (2019) Microglia-Derived Microvesicles Affect Microglia Phenotype in Glioma. Front. Cell. Neurosci. 13:41. doi: 10.3389/fncel.2019.00041

INTRODUCTION

Cellular communication has been recently enriched by a new mechanism, that use the cargo transported by extracellular membrane vesicles (EVs). EVs include exosomes (Exo, 10–100 nm diameter), microvesicles (MV, 100–1000 nm) and apoptotic "blebs" (1–2 mm). EVs are produced by all cell types and their production dynamically changes in number and content in response to specific environmental signals. The content of EVs, considered true metabolic units, is released into the cytoplasm of receiving cells, where they mediate several functional effects (Iraci et al., 2017).

In the brain, EVs modulate synaptic activity and neuronal communication (Korkut et al., 2013; Chivet et al., 2014), and also contribute to spreading disease in several CNS pathologies, such as multiple sclerosis (Carandini et al., 2015), Alzheimer's disease (Aguzzi and Rajendran, 2009; Gouwens et al., 2018), prion disease (Fevrier et al., 2004), and Huntington's disease (Zhang et al., 2016). Neurocentric vision in acute and chronic diseases of the CNS turned out to be insufficient to explain the mechanisms responsible for several disease onset and progression. The role played by

non-neuronal cells, such as astrocytes and microglia, which are in constant communication with neurons to monitor brain parenchyma through their processes, actively contribute to maintain cerebral homeostasis.

EVs released by microglia, similarly to EVs released by macrophages, recapitulate, in their cargo, the inflammatory information of the donor cell (Garzetti et al., 2014; Cunha et al., 2016).

Microglial cells acquire a dysfunctional phenotype in many CNS pathologies, losing their ability to monitor and preserve brain homeostasis. In the context of glioma, tumor associated myeloid cells (TAMs) modify their phenotype and local microenvironment toward a pro-tumor, anti-inflammatory state supporting tumor cell proliferation, survival, and invasion (da Fonseca and Badie, 2013).

In this work, we investigated the role of MV released by polarized microglia on the modulation of microglia state *in vivo*, to verify the hypothesis to use MV to help host microglia to reacquire a homeostatic state in the context of glioma. At this aim EVs, and in particular microvesicles (MV) and exosomes (Exo) released by microglia in inflammatory conditions were isolated and analyzed for their *in vitro* and *in vivo* effects in glioma bearing mice. We demonstrated that *in vitro*, microglia derived LPS/IFNγ-MVs reduced the expression of anti-inflammatory genes in IL4-treated microglia. *In vivo*, LPS/IFNγ-MVs injected in the brain of mice with glioma reduced the anti-inflammatory phenotype of TAMs and significantly reduced tumor size and tumor induced neurotoxicity. We suggest that the cargo of LPS/IFNγ-MV, which contains specific mRNA for inflammatory genes, transfer this information to recipient cells modifying their gene expression profile toward a protective one. Altogether, these findings demonstrate that the administration of exogenous EVs could be a valuable approach to transfer protective signals to TAMs, restoring the homeostatic microglia phenotype.

RESULTS

Dimensional and Morphological Analyses of EVs Derived From Microglia

EVs, in particular microvesicles (MV) and exosomes (Exo), were obtained from BV2 cell line and primary mouse microglia. EV sizes were measured by Dynamic Light Scattering (DLS) performed at a constant temperature of 15°C. The CONTIN distribution demonstrated that BV2-derived MV (**Figure 1A**) had a polydispersity of 20%. The intensity-weighted distribution of hydrodynamic diameter shows that the main population peaked around 300 nm, providing 90% of the total scattered intensity, as evidenced by the integral of the distribution reported in the inset of **Figure 1A**. In MV released by primary microglia (**Figure 1B**) a polydispersity of 30–40% was obtained and two main populations were identified: the first peaked at 250 nm and the second at 880 nm. The distribution integral (inset of **Figure 1B**) highlights that 20% of the total scattered intensity is due to the smallest population, while 50% is due to the largest one. Exo had a polydispersity around 30–40%. Due to their size, the volume-weighted is the most accurate distribution to obtain qualitative information on sample composition. Seventy percent of Exo has a mean size of 34 ± 4 nm (derived from BV2 cells, **Figure 1C**) and of 39 ± 4 nm (derived from primary microglial cells, **Figure 1D**), while larger aggregates provide little contribution to the volume-weighted distribution, as evidenced in the insets of **Figures 1C,D**. For both populations there is a 30% of contribution to the overall scattered intensity due to larger aggregates.

EVs derived from BV2 cells were analyzed at the transmission electron microscopy: data shown in **Figure 1E** identify the typical round vesicle morphology and underlined a scattered composition in size, with the presence of aggregates (**Figure 1E**), that confirmed DLS data above reported.

MV Derived From Microglia Treated With LPS/IFNγ Reduce Migration and Invasion of GL261 Glioma Cells and Are Neuroprotective Against Glioma Excitotoxicity *in vitro*

Cultured primary microglia and BV2 cells were treated with LPS/IFNγ or IL 4. We previously verified microglia polarization by mRNA analysis (Grimaldi et al., 2016); we confirmed these data showing that LPS/IFNγ-treated cells increased NO release and that IL-4-treated cells increased Arg1 expression and activity (**Supplementary Figure S1** and related **Supplementary Methods**). Quantification of MV released by control (C-MV), LPS/IFNγ-treated (LPS/IFNγ-MV), and IL4-treated BV2 cells (IL4-MV) was measured by Laser Transmission Spectroscopy (LTS) (Li et al., 2010). LTS measurements showed that the number (N) of MV/cell in these three conditions was not significantly different (**Figure 2A**). MV were then tested to verify their ability to interfere with glioma cell migration and proliferation. Data shown in **Figure 2B** illustrate that GL261 migration was impaired by LPS/IFNγ-MV, while GL261 migration increased upon IL 4-MV treatment, at 24 and 48 h. In contrast, neither LPS/IFNγ-Exo nor IL 4-Exo (released by primary microglia) affected GL261 migration (**Supplementary Figure S2**). Based on these results, for successive experiments we decided to focus our interest only on the effect of MV. Similarly to migration, results obtained on CXCL12-induced GL261 invasion, demonstrated inhibitory effects of LPS/IFNγ-MV and no effects of IL 4-MV (**Figure 2C**). Note that basal GL261 invasion was significant reduced in the presence of LPS/IFNγ-MV and was significant enhanced in the presence of IL 4-MV. These data indicate that microglia-derived MVs modulate glioma cell movement and invasion.

To investigate the effect of MV on glioma cell viability and proliferation, MTT assay and BrdU staining were performed. Results reported in **Figure 2D** show that neither LPS/IFNγ-MV nor IL 4-MV directly modulate GL261 viability, at 24, 48, 72, or 96 h. Similarly, no changes in proliferation rate were induced by LPS/IFNγ-MV or by IL 4-MV, measured by bromodeoxyuridine (BrdU) staining after 24 h (**Figure 2E**) and 48 h (data not shown). To investigate whether microglia-derived MV could exert indirect effects on glioma, cells were co-cultured with a mixed neuroglia culture in the presence of LPS/IFNγ-MV, for 18 h: in these conditions a reduction of GL261 viability was

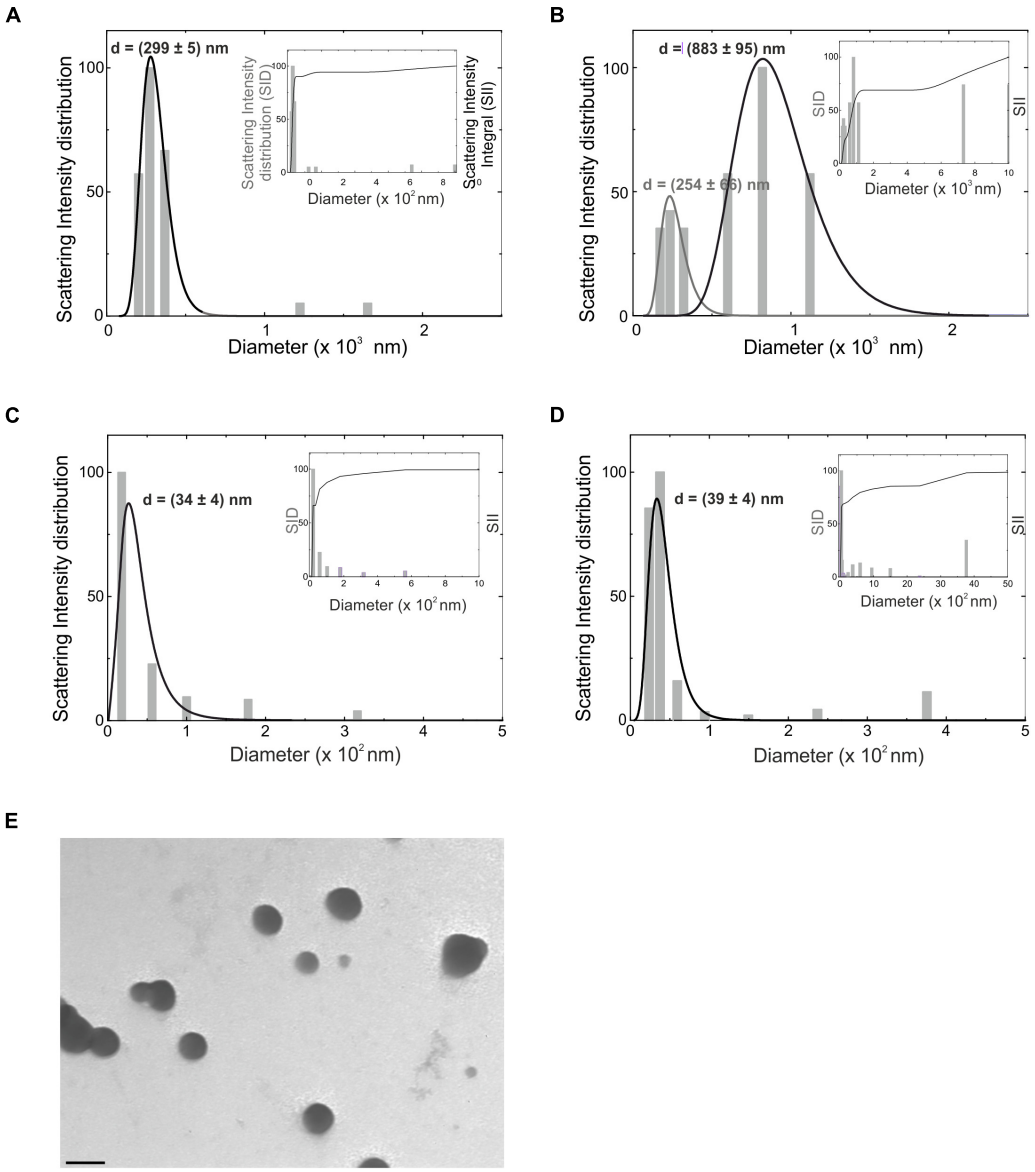

FIGURE 1 | Hydrodynamic diameter distribution (d) as obtained from CONTIN analysis of the intensity autocorrelation curves, for microvesicles obtained from BV2 microglia cell line **(A)** and from primary murine microglia **(B)**, for exosomes from BV2 **(C)** and primary microglia **(D)**, reported as intensity-weighted distribution. The overall normalized integral of the distribution is also reported in the inset of the relative panels (SID, scattering intensity distribution; SII, scattering intensity integral). Gray lines are fits through Log-normal distribution. **(E)** Transmission electron microscopy of EVs derived from BV2 cells. Bar = 100 nm, direct magnification 40000×, print magnification 213000×.

observed (**Figure 2F**), indicating an indirect effect of MV on glioma cell viability. In these same co-culture experiments, we also analyzed the effect of MV on neuron survival and observed (**Figure 2G**) that LPS/IFNγ-MV counteracted GL261-induced neurotoxicity, while IL 4-MV were ineffective.

Microglia-Derived LPS/IFNγ-MV Reduce Tumor Size in Mice

The above reported data prompted us to investigate the effect of LPS/IFNγ-MV in a mouse model of glioma. At this aim, GL261 cells were brain injected in the striatal region of the right hemisphere and, after 7 and 14 days, primary microglia-derived MV were infused in the tumor region via an implanted cannula. Fifteen days after tumor injection (**Figure 3**) LPS/IFNγ-MV treated mice had a significant reduction of tumor size while mice treated with IL 4-MV significantly increased the size of their brain tumors. Similar results were obtained with BV2-derived MV (**Supplementary Figure S3**). To investigate whether these effects on tumor size were mediated by alterations of GL261 cell proliferation, mice treated as in **Figure 3** were given BrdU

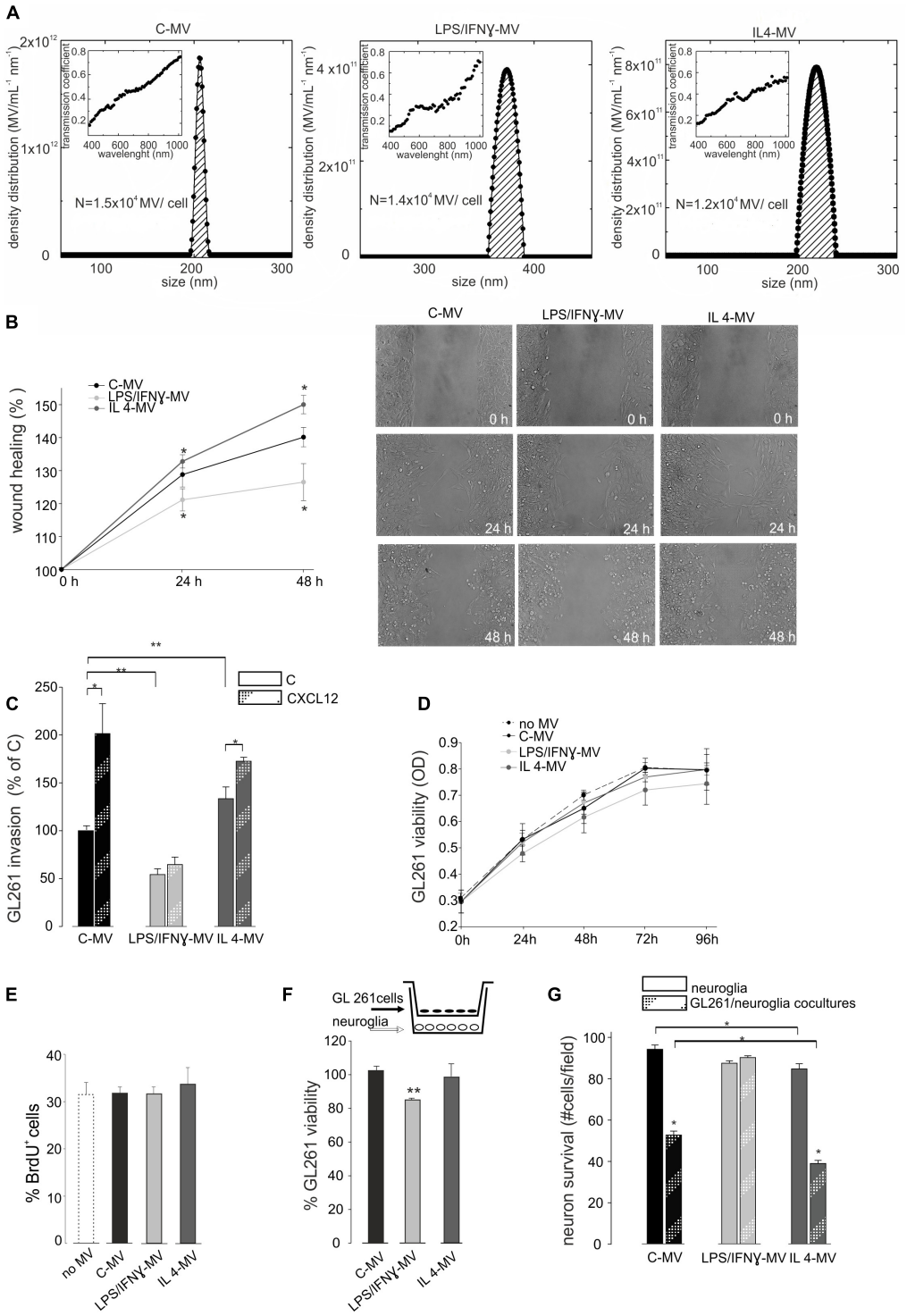

FIGURE 2 | (A) Density distribution of BV2-derived MVs, together with the transmission coefficient as a function of the wavelength (inset). The integral of the density distribution showed the number of MV per ml. Normalizing, the number of vesicles produced by each cell in control condition is $N = 1.5 \times 10^4$ (C-MV), with LPS/IFNγ is $N = 1.4 \times 10^4$ (LPS/IFNγ-MV), with IL4 is $N = 1.2 \times 10^4$ (IL4-MV). **(B)** GL261 glioma cells were treated with MV obtained from untreated microglia (C-MV), microglia treated with LPS/IFNγ (LPS/IFNγ-MV) and IL 4 (IL 4-MV) and a wound healing assay was performed. GL261 migration was measured 24 and 48 h after treatment, data are expressed as mean percentage of wound healing area ± SE, $N = 4$, $^*P < 0.001$ vs. C-MV (one way analysis of variance, Holm-Sidak method). On the right, representative wound healing assay on GL261 cells at 0 h and after 24 and 48 h of C-MV, LPS/IFNγ-MV and IL 4-MV treatment. **(C)** GL261 cells were assayed for basal invasion **(C)** and CXCL12-induced invasion in presence of MV obtained from untreated microglia (C-MV), microglia treated with LPS/IFNγ

(Continued)

FIGURE 2 | Continued
(LPS/IFNγ-MV) and IL 4 (IL 4-MV) in a Boyden chamber system. GL261 invasion was measured as mean percentage ± SE, $N = 4$; $^{*}P < 0.05$ and $^{**}P < 0.001$ (one way analysis of variance, Holm-Sidak method). **(D)** GL261 cells were assayed for cell viability without MV (no-MV), in presence of MV obtained from untreated microglia (C-MV), microglia treated with LPS/IFNγ (LPS/IFNγ-MV) and IL 4 (IL 4-MV) by MTT analysis. Cells were analyzed 0, 24, 48, 72, and 96 h after plating. Viability was reported in optical density (OD) mean ± SE, $N = 4$; no statistical significance vs. C-MV (one way analysis of variance, Holm-Sidak method). **(E)** GL261 cell proliferation was measured as % mean ± SE of $BrdU^{+}$ GL261 cells untreated (no-MV), treated with MV obtained from untreated microglia (C-MV), microglia treated with LPS/IFNγ (LPS/IFNγ-MV) and IL 4 (IL 4-MV) for 24 h, $N = 4$, no statistical significance vs. C-MV (one way analysis of variance, Holm-Sidak method). **(F)** GL261 cells, co-cultured with hippocampal neuroglial cultures (as depicted in the inset) were treated for 18 h with MV obtained from untreated microglia (C-MV), microglia treated with LPS/IFNγ (LPS/IFNγ-MV) and IL 4 (IL 4-MV), were analyzed for viability by trypan Blue staining. Data are expressed as number of viable cells/field ± SE, $N = 3$; $^{**}P < 0.05$, Student's *t*-test. **(G)** Hippocampal neuroglial cultures alone or co-cultured with GL261 cells (as depicted in the inset of panel **F**) were treated with MV obtained from untreated microglia (C-MV), microglia treated with LPS/IFNγ (LPS/IFNγ-MV) and IL 4 (IL 4-MV) for 18 h and were analyzed for neuronal viability. Data are expressed as number of viable cells/field ± SE, $N = 3$, $^{*}P < 0.001$, Student's *t*-test.

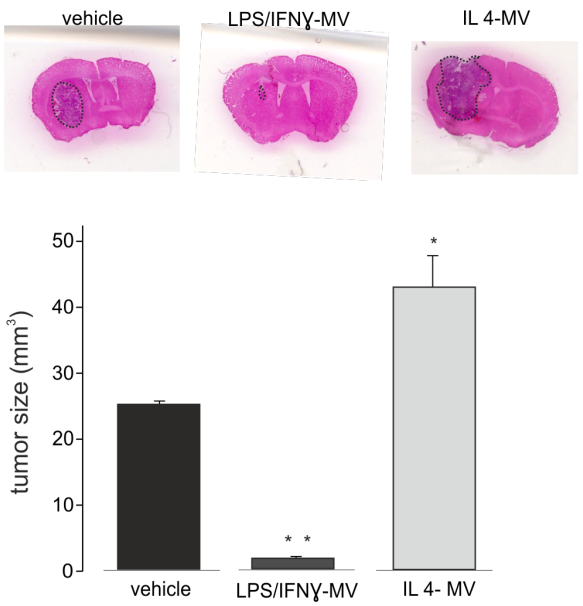

FIGURE 3 | Tumor size in the brain of GL261-bearing mice treated with vehicle or MV obtained from microglia treated with LPS/IFNγ (LPS/IFNγ-MV) and IL 4 (IL 4-MV). Tumor size (in mm^3) was reported as mean ± SE, $N = 7$/experimental group, $^{*}P < 0.05$, $^{**}p \leq 0.001$ vs. vehicle, Student's *t*-test. On the top, representative coronal brain sections of GL261-bearing mice treated as above, stained with hematoxylin-eosin; tumor area in the dashed line.

2 h before euthanasia. Quantification of BrdU-labeled cells, normalized for tumor area, revealed a significant reduction of cell proliferation in the tumoral region (**Figure 4A**) of LPS/IFNγ-MV treated mice. Treatment with LPS/IFNγ-MV also reduced glioma cell migration *in vivo*, as reported in **Figure 4B**, where tumor cell invasion was calculated as the number of cells protruding more than 150 μm from the main tumor mass. In the peritumor region, we evaluated neuronal death by Fluoro Jade staining, comparing mice treated with LPS/IFNγ-MV with control mice. Data shown in **Figure 4C** demonstrate that neuronal death was significant reduced in LPS/IFNγ-MV treated mice, demonstrating *in vivo* a neuroprotective effect of LPS/IFNγ-MV against tumor-induced excitotoxicity.

All these data demonstrated that LPS/IFNγ-MV carry anti-tumor information that are effective in reducing tumor size *in vivo*.

Microglia-Derived LPS/IFNγ-MVs Modify the Phenotype of Tumor-Associated Microglia

To understand the mechanisms of action of the injected MVs, we first decided to investigate their cellular localization upon brain injection. At this aim, MVs derived from primary microglia, were stained with the membrane-selective dye PKH26 and brain injected in glioma bearing mice. Cerebral slices obtained from the tumoral region show the presence of PKH26-MV on both $Iba1^{-}$ and $Iba1^{+}$ cells (**Figure 5A**). We never observed PKH26 staining outside the tumor area. It is known that a high amount of tumor associated microglia/macrophages (TAMs) are present in glioma, and may represent up to 50% of tumor mass (Hambardzumyan et al., 2016). TAMs exert tumor supporting function releasing factors that facilitate tumor proliferation and migration (Fonseca et al., 2012). We wonder whether the interaction of MVs with TAMs could modulate their pro-tumor activity, and investigated the effect of LPS/IFNγ-MV on gene expression of $CD11^{+}$ cells isolated from the brains of glioma-bearing mice. As shown in **Figure 5B**, the expression of *arg1*, *cd163*, *cd206*, *fizz1*, and *ym1* genes all correlated with an anti-inflammatory, pro-tumor phenotype, were up-regulated in $CD11b^{+}$ cells in the ipsilateral hemisphere of glioma bearing mice and were significant reduced upon LPS/IFNγ-MV treatment (with the exception of *fizz1*). Similar modulatory effects were observed *in vitro*: as shown in **Figure 5D**, LPS/IFNγ-MV (derived from primary microglia) significant reduced the microglial expression of all analyzed genes (*arg1*, *cd163*, *cd206*, *ym1*, and *fizz1*) except *ym1*, indicating a direct modulation likely induced by MV cargo that enter microglia also *in vitro* (**Figure 5C**).

All these data suggest that LPS/IFNγ-MVs might directly signal to microglia and instruct these cells toward an antitumor phenotype.

mRNA Analyses of Microglia-Derived LPS/IFNγ-MV

To investigate the nature of the cargo transported by LPS/IFNγ-MV that could help the understanding of the above described mechanisms, the mRNA content of MVs

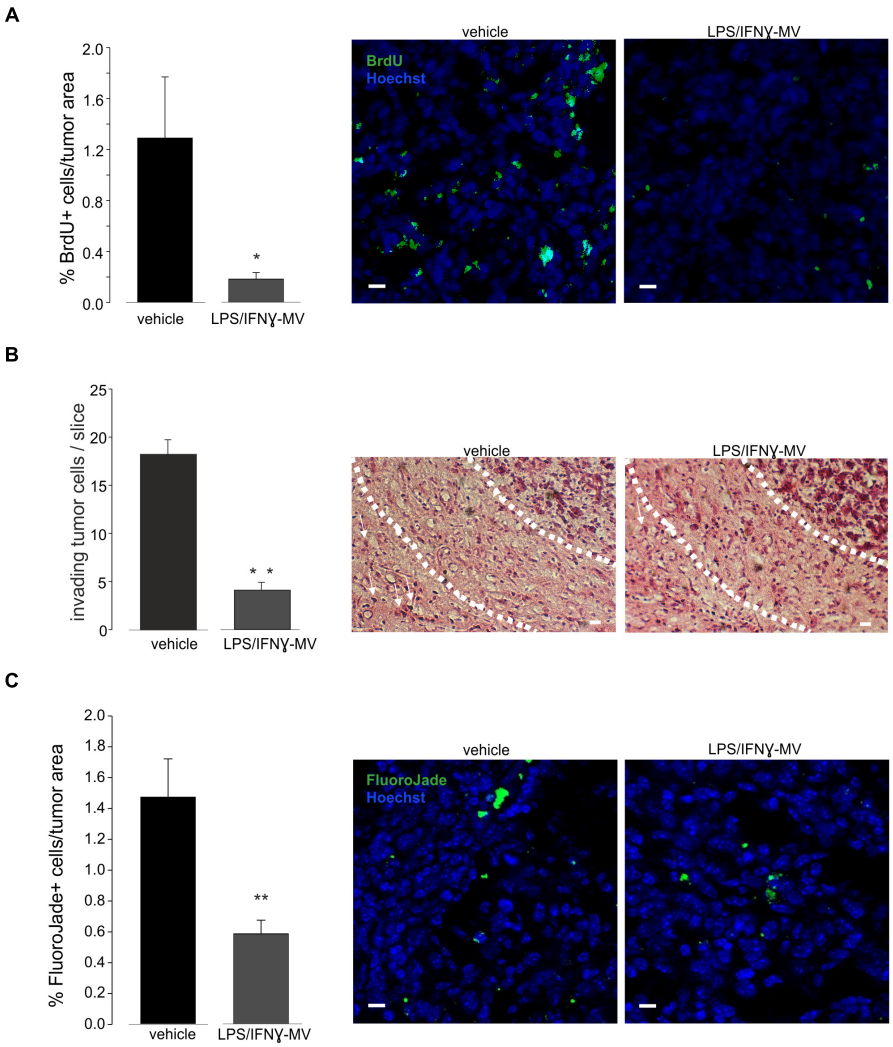

FIGURE 4 | (A) Cell proliferation, measured as BrdU$^+$ cell area/tumor area in GL261-bearing mice treated with vehicle or MV obtained from microglia treated with LPS/IFNγ (LPS/IFNγ-MV), data are expressed as mean percentage ± SE, $N = 3$, $^{**}P \leq 0.001$ vs. vehicle, Student's *t*-test. On the right: representative immunofluorescence on coronal brain slices of GL261-bearing mice treated as above (BrdU in green; Hoechst in blue), scale bars, 20 μm. **(B)** Glioma cells invading the brain parenchyma for more than 150 μm beyond tumor border 17 days after glioma cell transplantation in GL261-bearing mice treated with vehicle or MV obtained from microglia treated with LPS/IFNγ (LPS/IFNγ-MV), data are expressed as mean cell number ± SE, $N = 3$/experimental group, $^{**}P \leq 0.001$, Student's *t*-test vs. vehicle. On the right, representative brain peritumoral sections stained with haematoxylin/eosin; white arrows indicate glioma cells invading the brain parenchyma beyond the main tumor border for more than 150 μm (dashed line); scale bars, 20 μm. **(C)** Neuronal death, measured as Fluoro Jade$^+$ cells/tumor area in GL261-bearing mice treated with vehicle or MV obtained from microglia treated with LPS/IFNγ (LPS/IFNγ-MV), data are expressed as mean percentage ± SE, $N = 3$, $^{**}P \leq 0.001$ vs. vehicle, Student's *t*-test. On the right: representative immunofluorescence on coronal brain slices of GL261-bearing mice treated as above (Fluoro Jade in green; Hoechst in blue), scale bars, 20 μm.

released by primary microglia was analyzed by NanoString chip for the expression of 243 key inflammation-related genes and compared with MVs released by control, unstimulated microglia. As shown on **Figure 6A**, 18 genes were significantly up-regulated in LPS/IFNγ-MV. Data were confirmed by RT-PCR for *tnf*-α and *il1b* genes (**Figure 6B**), validating the immune panel system.

Pathway analysis, performed on the 10 most significant functional categories defined by the Gene Ontology Biological process (**Figure 6C**) indicated that LPS/IFNγ-MV contain 12% of genes involved in inflammatory responses (*c3*, *ccl4*, *ccl5*, *cxcl2*, *cxcl9*, *tnf*, *ptgs2*, *ccl7*, *il1b*, *ccl2*, *ccl3*, *il1rn*, *hif1a*), 14% of genes involved in defense responses (*irf7*, *c3*, *ccl4*, *ccl5*, *cxcl2*, *cxcl9*, *tnf*, *ptgs2*, *mx1*, *ccl7*, *il1b*, *ccl2*, *ccl3*, *il1rn*, *hif1a*), 12% of genes involved in responses to wounding (*c3*, *ccl4*, *ccl5*, *cxcl2*, *cxcl9*, *tnf*, *ptgs2*, *ccl7*, *il1b*, *ccl2*, *ccl3*, *il1rn*, *hif1a*), 12% of genes involved in immune responses (*irf7*, *c3*, *ccl4*, *ccl5*, *cxcl2*, *cxcl9*, *tnf*, *mx1*, *ccl7*, *il1b*, *ccl2*, *ccl3*, *csf3*), 4% of genes involved in regulation of natural killer cell chemotaxis (*ccl7*, *ccl4*, *ccl3*, *ccl2*, *ccl5*), 8% of genes involved in positive regulation of response to external stimuli (*c3*, *ccl4*, *ccl5*, *tnf*, *ccl7*, *ptgs2*, *il1b*, *ccl2*, *ccl3*), 10% of genes involved in regulation of cytokine production (*irf7*, *c3*, *ccl4*, *ccl5*, *tnf*, *ptgs2*, *il1b*, *ccl2*, *ccl3*, *hif1a*, *cebpb*), 13% of genes involved in immune system process

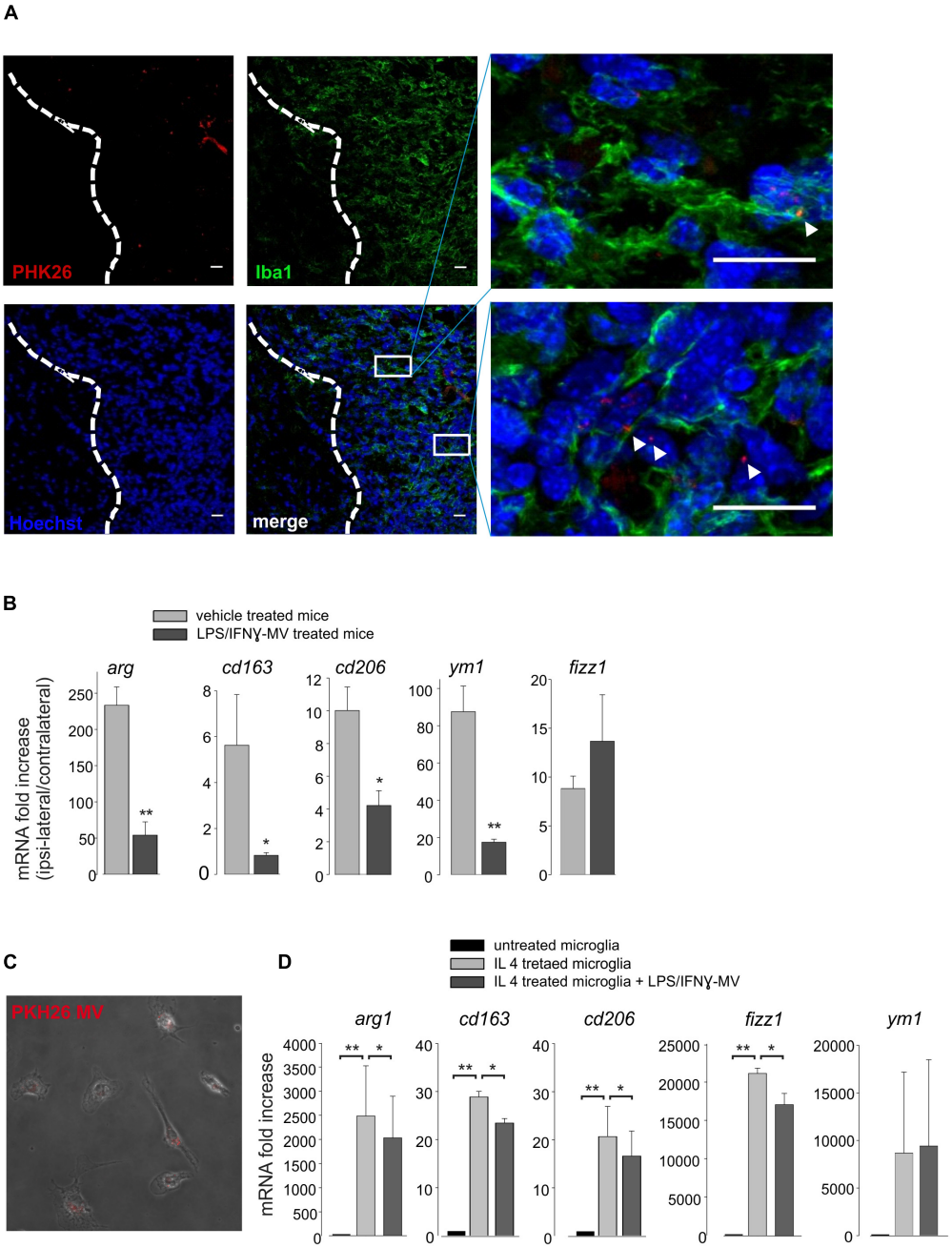

FIGURE 5 | (A) Immunofluorescence analysis for Iba1 (in green) of coronal brain sections from GL261-bearing mice treated with PKH26-stained MV (in red; Hoechst in blue) obtained from microglia. Tumor region at the right of the dashed line. In the merge, identification of two tumor regions shown at higher magnification. Scale bar: 20 μm **(B)** RT-PCR of anti-inflammatory genes (*arg1*, *cd163*, *cd206*, *ym1*, and *fizz1*) in CD11b$^+$ cells extracted from brains of GL261-bearing mice treated with vehicle or MV obtained from microglia treated with LPS/IFNγ (LPS/IFNγ-MV). Data are the mean ± SE of fold increase (normalized vs. contralateral cerebral hemisphere of each animal; gene expression was normalized vs. *gapdh*), $N = 5$, $^{**}P < 0.001$, $^{*}P < 0.05$ vs. vehicle treated mice, Student's *t*-test. **(C)** Merged of bright and fluorescence fields of microglia treated with IL 4 and incubated with PKH26-stained MV (in red) obtained from LPS/IFNγ-treated microglia. **(D)** RT-PCR on mRNAs of untreated or IL 4-treated microglia incubated with or without MV obtained from LPS/IFNγ-treated microglia, and analyzed for the expression of anti-inflammatory genes (*arg1*, *cd163*, *cd206*, *fizz1*, and *ym1*). Data are the mean ± SE of fold increase (normalized vs. *gapdh*), $N = 3$, $^{**}P < 0.001$, $^{*}P < 0.05$, Student's *t*-test.

(*irf7*, *c3*, *ccl4*, *ccl5*, *cxcl2*, *cxcl9*, *tnf*, *mx1*, *ccl7*, *il1b*, *ccl2*, *ccl3*, *hif1a*, *csf3*), 8% of genes involved in positive regulation of cytokine production (*irf7*, *c3*, *ccl4*, *ccl5*, *tnf*, *ptgs2*, *il1b*, *ccl3*, *hif1a*), and 7% of genes involved in leukocyte migration (*ccl4*, *ccl5*, *cxcl2*, *tnf*, *ccl7*, *il1b*, *ccl2*, *ccl3*). These data demonstrated that the MV mRNA content is highly complex, covering genes coding for proteins

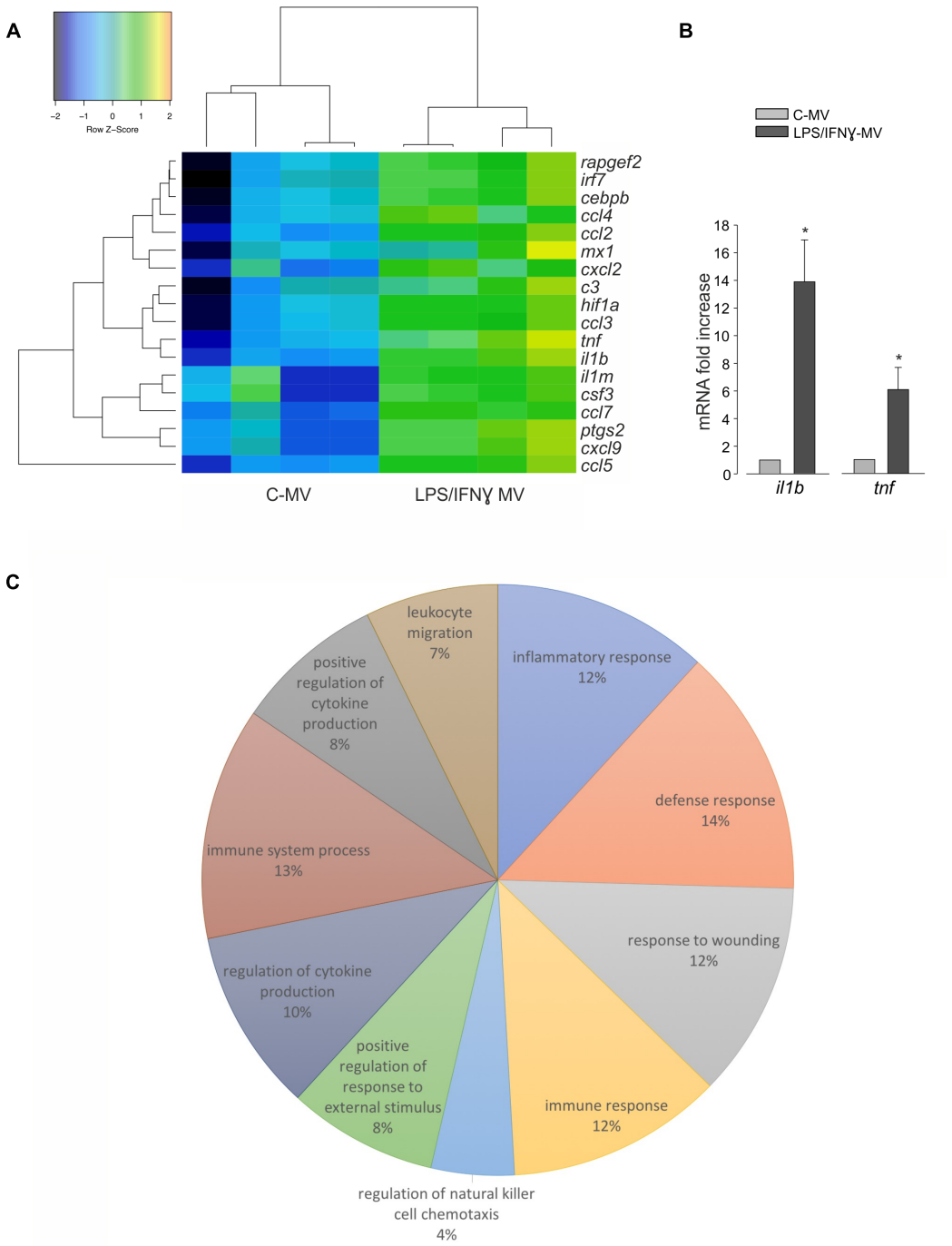

FIGURE 6 | (A) mRNAs isolated from MV released by untreated microglia (C-MV) or microglia treated with LPS/IFNγ (LPS/IFNγ-MV) were analyzed by NanoString. Heat map analysis of NanoString data show hierarchical clustering of 18 differentially expressed genes between C-MV and LPS/IFNγ-MV, $N = 4$. The signals were normalized and transformed to the log2 scale. The color scale indicates the gene expression standard deviations from the mean, with black/blue for low expression and green/orange for the high expression levels. Eighteen genes (listed on the right) were considered significant because with at least 2.8-fold changes with $P < 0.05$ (Wilcoxon test) at the 95% confidence level. Dendrograms illustrate the relationship-distance between samples and genes. **(B)** RT-PCR on mRNAs isolated from MV derived from untreated microglia (C-MV) or microglia treated with LPS/IFNγ (LPS/IFNγ-MV) analyzed for the expression of *il1b* and *tnf* genes. Data are the mean ± SE of fold increase (normalized vs. *gapdh*), $N = 3$, $^*P < 0.05$, Student's *t*-test vs. C-MV. **(C)** The pie chart illustrates the distribution of the 18 differentially expressed genes across the 10 most significant functional categories defined by the Gene Ontology Biological process. The percentage numbers represent the frequency of genes in each category. Data were analyzed using FIDEA tool.

related to different pathways of the inflammatory process, and that their delivery to TAM might contribute to re-activate the immune response, which oppose glioma growth.

MATERIALS AND METHODS

Primary Brain Cells Cultures

Neuroglial cultures were prepared from 0- to 2-day-old (p0–p2) C57BL/6N mice as already described (Lauro et al., 2010); neurons-astrocytes-microglia ratio is 60-35-5%. Microglia cultures were obtained as already reported (Grimaldi et al., 2016) and were 98% Iba1$^+$ positive (Lauro et al., 2010).

Cell Lines

BV2 murine microglial cells and GL261 murine glioma cells were cultured in DMEM supplemented with 10–20% heat-inactivated FBS, 100 IU/ml penicillin G, 100 μg/ml streptomycin, 2.5 μg/ml amphotericin B and grown at 37°C in a 5% CO_2 and humidified atmosphere.

Microglia Stimulation (Polarization)

Primary microglia and BV2 cells were treated for 24 hours with IFN-γ (20 ng/ml) and LPS (100 ng/ml), or with IL-4 (20 ng/ml) or with EVs.

Extraction of EVs

Cytokine-treated microglia were stimulated for 30 min with ATP (1 mM) in KRH (125 mM NaCl; 5 mM KCl; 1.2 mM $MgSO_4$; 1.2 mM KH_2PO_4; 2 mM $CaCl_2$; 6 mM D-glucose; 25 mM HEPES/NaOH, pH = 7.4). Cell supernatant was collected and centrifuged at 800 *g* for 5 min to remove cell debris. The obtained supernatant was centrifuged at 10000 *g* for 30 min at 4°C and the resulting pellet, containing MVs, was re-suspended in KRH buffer for DLS, LTS and transmission electron microscopy, in PBS for *in vivo* experiments or in serum-free DMEM for microglia stimulation, MTT, wound healing and BrDU proliferation assays. Remaining supernatant underwent ultracentrifugation at 100,000 *g* for 1-h at 4°C. The Exo, present in this second pellet, were re-suspended in KRH buffer for DLS measures and in serum free DMEM for wound healing assay. The same protocol permits to eliminate EVs from the medium used to re-suspend MVs and Exo and guarantees that the EVs obtained only derived from polarized microglial cells. In some experiments, EVs were labeled with PKH26, a lipophilic membrane red fluorescent dye (PKH26 GL-1KT, Sigma-Aldrich) according to manufacturer protocol. Briefly, PKH26 dye was re-suspended in diluent C to a final concentration of 0.6 μM (dye solution). MV were re-suspended in 500 μL of dye solution and incubated for 5 min, while mixed with gentle pipetting. Excess dye was bound with 500 μL EVs-depleted bovine serum albumin (1%, Sigma-Aldrich). MV pellet, obtained by centrifugation (10000 × *g*, 30 min, 4°C) was washed twice in PBS. PKH26-stained MV were re-suspended in PBS for *in vivo* administration and in serum-free DMEM for *in vitro* treatment. In all the experiments, the same procedure of staining minus MV was performed as control condition.

Dynamic Light Scattering and Data Analysis

Dynamic light scattering (DLS) measurements were performed using a standard optical setup. The monochromatic and polarized beam emitted from a He-Ne laser (10 mW at λ = 632.8 nm) was focused on the sample placed in a capillary of 2 mm of diameter positioned in a cylindrical VAT for index matching and temperature control. The scattered intensity was collected at a scattering angle θ = 90°that, according to the relation $Q = (4\pi n/\lambda)\sin(\theta/2)$, corresponds to a scattering vector Q = 0.0187 nm^{-1}. A single mode optical fiber collected the scattered light as a function of time and the signal was detected by a photomultiplier. In this way the normalized intensity autocorrelation function $g_2(Q,t) = <I(Q,t)I(Q,0)>/<I(Q,0)>^2$ with a high coherence factor close to the ideal unit value was measured. Measurements were performed at fixed temperature around 15°C. Reproducibility has been tested by repeating measurements several times on different samples. The intensity correlation curves obtained from DLS experiments have been analyzed with the Laplace inversion through the CONTIN algorithm weighted as overall contribution to the scattered intensity. However, the scattered intensity depends on the squared volume of the scattering particle, thus leading to an overestimation of the large particles. Therefore, this approach has good reliability for samples of EVs, whose hydrodynamic diameter is expected in the range D_h = 100÷1000 nm. On the other hand, small particles are under-represented in the intensity-weighted distribution and Laplace transformation can be very inaccurate. To represent the hydrodynamic diameter distribution of Exo with size expected in the range D_h = 10÷100 nm the volume-weighted distribution has been chosen. The mean size of each population has been calculated by fitting the scattering intensity distribution with a Log-normal function.

Laser Transmission Spectroscopy

Laser Transmission Spectroscopy (LTS) allows to obtain the density of MV in suspension by measuring the transmission of laser light (at zero angle with respect to the incoming beam) through the suspension as a function of wavelength (Li et al., 2010). The transmission of light through the MV sample (re-suspended in KRH) is recorded along with that of KRH. The fundamental data-acquisition process involves measuring the wavelength-dependent transmission of light through an aqueous suspension of vesicles. Given the extinction information, and the known wavelength-dependent properties of the vesicles, Mie theory can be used to accurately determine their density distribution as a function of diameter. The extinction data are analyzed and inverted by a mean square root-based algorithm that outputs the particle size distribution. The integral of the density distribution provides the number of MV per ml of solution and the absolute number (N) of MV per cell is calculated

as the ratio between the number of MV in a given volume and the total number of MV donor cells.

Transmission Electron Microscopy

Microvesicles derived from BV2 cells (extracted as above) were fixed by glutaraldehyde 2.5% in PBS buffer pH 7.4 at least 2 h and gently resuspended in PBS buffer. A drop of the solution was put on a Formvar copper grid 200 mesh for 10 min. After drying with filter paper, uranyl acetate aqueous solution (1%, 1 min) was used for negative staining. Samples were observed with a ZEISS EM 10 transmission electron microscope equipped with a Gatan CCD camera at 60 kw.

Neuronal Viability Assay

Neuroglial cultures at 9–11 days *in vitro* were co-cultured with GL261 cells (5×10^4/well) in the presence or absence of EVs with a ratio of donor:target cells 1:1. After 18 h, cells were treated with detergent-containing buffer and counted in a haemocytometer as already described (Lauro et al., 2010).

MTT Cell Viability Assay

GL261 cells were seeded into 24-well plates and treated with vehicle (untreated), IFN-γ /LPS- or IL 4-MV for 3 days. MTT (500 μg/ml) was added into each well for 1.5 h. DMSO was then added to stop the reaction and the formazan produced was measured at 570 nm. Viability of cells was expressed relative to absorbance.

Wound-Healing Assay

GL261 cells (5×10^5/ml) were seeded into the inner wells of cell culture inserts (ibidi, Germany) placed in a Petri dish. Once attached to the substratum, the inserts were removed, leaving a central 500 μm cell-free septum in which cells could migrate. Cell medium with MV released by IFN-γ /LPS- or IL 4-treated microglia (ratio 1:1 = donor: target cells) was added. Cells were incubated with a cell cycle blocker (cytarabine, 10 μM) to prevent GL261 proliferation for all the time of the experiment. Dishes were maintained at 37°C, 5% CO_2. Pictures of the starting point (0 h) and 24 and 48 h after treatment were taken at a phase contrast microscope (Nikon) and processed through MetaMorph 7.6.5.0 software (Molecular Device). GL261 migration was evaluated by the area between the two cell fronts (by ImageJ software) and data are expressed as % of area occupied by cells.

Invasion Assay

GL261 cells (7×10^3 cells/cm^2) were plated on matrigel-coated polycarbonate membranes (8 μm diameter pores, Corning) of a Boyden Chamber system in presence of IFN-γ /LPS-MV or IL 4-MV (ratio 1:1 donor:target cells) and incubated for 48 h at 37°C with CXCL12 (100 nM, Peprotech) in the lower chamber as chemoattractant. The experiments were performed in presence of cytarabine (10 μM). Cells adhering to the upper side of the membranes were scraped off, whereas cells that have invaded through the pores were stained with a solution containing 50% isopropanol, 1% formic acid, and 0.5% (wt/vol) brilliant blue R 250 and counted in more than 20 fields with a 20× objective.

In vivo Experiments

Experiments were approved by the Italian Ministry of Health, in accordance with the ethical guidelines on use of animals from the EC Council Directive 2010/63/EU. Eight-week-old male C57BL/6N mice were injected with GL261, as previously described (Grimaldi et al., 2016), in the right striatal brain region. During surgery, a guide cannula was placed 2 mm deep in the striatum and it was fixed with quick-setting cement. After 7 and 14 days, mice were infused via cannula with MVs obtained from 1×10^6 microglia cells re-suspended in 4 μl PBS). The day after the second infusion, animals were sacrificed and analyzed for tumor size (Grimaldi et al., 2016). Alternatively, mice were deeply anesthetized and CD11b$^+$ cells were isolated as already described (Grimaldi et al., 2016). Obtained cells were lysed in Trizol reagent (Invitrogen, Milan, Italy) for RNA extraction and Real Time PCR analysis.

BrdU Proliferation Assay

GL261 cells were grown on glass coverslips (1.5×10^4 cells/cm^2) in 24-well plates for 18 h. Cells were exposed to vehicle or EV for 24 h, cellular proliferation was analyzed adding BrdU (10 μM, Sigma-Aldrich, B5002) for 30 min. Cells were washed in PBS, fixed (4% PFA, 30 min), permeabilized (1% Triton X-100, 15 min), blocked (1% BSA, 1 h) at RT and incubated overnight with anti-BrdU (1:200, Novusbio, NB500-169). Hoechst was used to stain all nuclei. BrdU positive cells were counted out of 800 cells for condition. Proliferation rate is calculated as BrdU$^+$ cells respect to Hoechst stained cells. *In vivo*, 15 days after glioma cell injection, BrdU was i.p. injected (50 mg/kg). Two hours later, mice were killed and their brains processed for immunofluorescence.

Immunofluorescence

Coronal brain sections (20 μm) were washed in PBS, blocked (3% goat serum in 0.3% Triton X-100) for 1h at RT and incubated with anti-Iba1 (1:500, Wako, 019-19741, 4°C) or anti-BrdU (1:200, Novusbio, NB500-169, RT). Brain slices were stained with the fluorophore-conjugated secondary antibodies (1 h, RT) and Hoechst for nuclei visualization and analyzed using a fluorescence microscope. For Fluoro Jade-C staining, we followed the manufacturer instructions (Millipore, AG325).

Real Time PCR

RNAs extracted from all samples were quantified and retro-transcribed using IScriptTM Reverse Transcription Supermix (Bio-Rad). Real time PCR (RT-PCR) was carried out in an I-Cycler IQ Multicolor RT-PCR Detection System (Bio-Rad) using SsoFast Eva Green Supermix (Bio-Rad). The PCR protocol consisted of 40 cycles of denaturation at 95°C for 30 s and annealing/extension at 58°C for 30 s. The Ct values from each gene were normalized to the Ct value of GAPDH. Relative quantification was performed using the $2^{-\Delta\Delta Ct}$ method and expressed as fold increase. Primer sequences: arg1, forward: CTCCAAGCCAAAGTCCTTAGAG, reverse: AGGAGCTGTCATTAGGGACATC; cd163 forward: GCTAGACGAAGTCATCTGCACTGGG, reverse: TCAGCCT

CAGAGACATGAACTCGG; cd206 fw: CAAGGAAGGTTGG CATTTGT, reverse: CCTTTCAGTCCTTTGCAAGT; ym1 forward: CAGGTCTGGCAATTCTTCTGAA, reverse: GTCT TGCTCATGTGTGTAAGTGA; fizz1 forward: CCAATCCA GCTAACTATCCCTCC, reverse: ACCCAGTAGCAGTCA TCCCA; gapdh forward: TCGTCCCGTAGACAAAATGG, reverse: TTGAGGTCAATGAAGGGGTC.

RNA Isolation and NanoString nCounter Analysis

Total RNA was isolated from microglia-derived MV by Total Exosome RNA Protein Isolation Kit (# 4478545, Invitrogen) and concentrated using the Microcon10 centrifugal filters (#MRCPRT010, Merck Millipore). Gene expression raw data were normalized considering housekeeping genes via nSolver Software (NanoString). Statistical analysis was conducted in R (version 3.5.0) with RStudio (version 1.1.383[1]). On normalized and log2-transformed data, differential expression was tested applying the Wilcoxon test ($P < 0.05$) and filtering by log2FC > 1.5. All differentially expressed genes were classified into several catalogs according to the Gene Ontology (GO) annotation. The over-representation analyses of GO terms, including biological process and molecular function, were performed using the FIDEA tool[2].

Statistical Analysis

Statistical analyses were performed using SigmaPlot 11.0 Software unless otherwise stated.

DISCUSSION

The present study demonstrated that microglia-derived LPS/IFNγ-MV transfer a protective-antitumor phenotype to the brain of glioma bearing mice. We demonstrated that LPS/IFNγ-MV, which contain the transcripts for a number of inflammation-related genes, can modify TAMs phenotype reducing the expression of anti-inflammatory genes, exert protective effects on neurons and reduce glioma cell proliferation and invasion in surrounding parenchyma.

We have shown that LPS/IFNγ-MV contain 18 genes upregulated in comparison with MV isolated by unstimulated microglia. The majority of these genes referred to the immune response that could underlie the robust effect of MV on the modification of microglia phenotype. It is known that many solid tumors, such as colon-rectal, epithelial ovarian, brain and lung cancers, release EVs which are involved in supporting TAM reprogramming toward an anti-inflammatory, tumor-supporting phenotype (Fabbri et al., 2012; Challagundla et al., 2015; Neviani and Fabbri, 2015; Chen et al., 2017; Shinohara et al., 2017; Cooks et al., 2018). Our findings demonstrated that in the context of a brain tumor, microglia-derived MV can be used in reverse, as a tool to contrast glioma progression, modulating local microenvironment.

[1]http://www.rstudio.com/

[2]http://circe.med.uniroma1.it/fidea/

Previous reports described that EVs released from LPS stimulated BV2 cell line contain cytokines such as TNF-α and IL-6, as well as ribosome, focal adhesion, extracellular matrix, and membrane proteins (Yang et al., 2018). BV2-derived EVs expressing the cytokine IL-4, delivered in a mouse model of multiple sclerosis, propagated an anti-inflammatory response, upregulating microglia and macrophage expression of chitinase 3-like 3 (ym1) and arginase (arg-1), which reduced neuroinflammation with protective effects on tissues (Casella et al., 2018). Consistently, we observed that the EVs released by cytokine-stimulated microglia maintain the phenotype of the donor cells. This result is in line with the evidence that vesicles released by macrophages and dendritic cells reflect the inflammatory state of original cells (Kim et al., 2005; Viaud et al., 2009; Garzetti et al., 2014).

Microvesicle are supposed to transfer their cargo by docking at the plasma membrane of target cells, nevertheless the exact mechanism is not fully revealed. This interaction is neither stochastic nor unspecific because MV do recognize the target cells (Losche et al., 2004). The recognition takes place by activation of specific surface receptors (Gasser and Schifferli, 2004; Bianco et al., 2005), or by transfer of membrane receptors, as demonstrated for the chemokine receptor CCR5 (Mack et al., 2000) and the growth factor receptor EGFRvIII (Al-Nedawi et al., 2008). MV could function as messengers, being enriched in specific miRNA, mRNA, and proteins, to start an angiogenic program (Deregibus et al., 2007), to spread a danger signal through HMGB1 (Tucher et al., 2018) or to induce a developmental program (Ratajczak et al., 2006). In our experiments, we measured mRNA content of microglia released LPS/IFNγ-MV, but we cannot exclude additional transfer elements (such as membrane or signal proteins) from MV to glioma and TAM, responsible for the antitumor effects.

In addition to a modulation of TAM phenotype, we observed that LPS/IFNγ-MV affect glioma cell properties. We observed direct effects on glioma cell migration and invasion capability, and indirect effects on tumor cell viability, which requires the presence of parenchymal cells, likely microglia, as preferential target of microglia-derived EVs (Verderio et al., 2012). The effects of microglia-derived MV on GL261 cells could reflect the transfer of cell-donor information as reported for the first time for antigen-presenting cells that secrete exosomes able to stimulate T cell proliferation (Raposo et al., 1996) or, more recently in Alzheimer disease, for microglia released MV that exert toxicity on neurons (Joshi et al., 2014). In our experiments, EV-mediated reduction of tumor mass could be the cause of the EV-induced decreased neurotoxicity in the presence of glioma. However, we cannot exclude that EVs also directly target neurons, as shown by other authors (Antonucci et al., 2012; Chivet et al., 2014), but the lack of detectable PKH26-MV staining in extra tumoral regions of glioma bearing mice would suggest a direct or local paracrine effect. In addition, *in vitro* experiments demonstrated that microglia-derived MVs did not directly affect neuron viability.

The dimensional analyses of EVs extracted by primary mouse microglia and BV2 cell line reflect data reported on nervous system-released vesicles (Basso and Bonetto, 2016;

Zappulli et al., 2016) and underline the similarity between primary microglia and cell lines, at least for EV dimension. Our TEM analysis shows that single particles have a spherical morphology; in addition to single EV, multiple aggregates are observed confirming size and shape already reported for EVs derived from microglial cells (Turola et al., 2012; Gouwens et al., 2018). In comparison with more physiological conditions (*in vivo* or *ex vivo*), cell lines and primary cultures of microglia display many differences in term of gene expression and response to stimuli (Horvath et al., 2008; Henn et al., 2009). However, there are evident advantages in using EVs derived from microglia cells lines, such as the possibility to obtain sufficient EVs for potential therapeutic application and the similar results obtained with MV from BV2 or from freshly isolated microglia encourage in this direction. However, a detailed analysis of the cargo differences in MV obtained from cell lines, cultured or freshly obtained microglial cells is lacking.

The choice to deliver MV *in situ* into the tumor region allowed us to use a relatively small amount of vesicles per infusion and to observe a direct effect on tumor mass. Different brain delivery of EVs, as into the cisterna magna (Casella et al., 2018), would give additional information on the effects of EVs in the contralateral hemisphere, for the multicellular targets of EVs. Additional delivery methods were tested for EVs, such as the intravenous (Alvarez-Erviti et al., 2011) and intra-nasal (Zhuang et al., 2011) approach. Intravenous administration permits indirect access of MV to the brain through the initial absorption in different cells (Laso-García et al., 2018). Intranasal delivery might reduce the final brain concentration due to lungs and gastrointestinal tract dilution. Nevertheless, both delivering routes would be easily reproduced in humans, while intratumor transfer would be only possible upon surgery procedures during glioma removal. For that reason, alternative EV injection routes, in glioma models, need further investigations. For brain tumor treatment, EVs have been tested to convey specific molecules such as small interference RNAs for TGF beta 1 and VEGF (Zhang et al., 2014; Yang et al., 2017), pro-apoptotic peptides (Ye et al., 2018), and chemotherapeutic drugs (Tang et al., 2012; Yang et al., 2015). EVs are preferred to artificial nanoparticles for their low toxicity (Lewinski et al., 2008; Shvedova et al., 2010).

To our knowledge, this is the first evidence that, in the context of a brain glioma, microglia-derived MVs can be used to transfer a cargo of molecular information that reach TAM restoring a neuroprotective phenotype, modulating their inflammatory state and re-establishing a homeostatic brain microenvironment.

AUTHOR CONTRIBUTIONS

AG, CS, and MC conceived the study and performed the experiments. GC provided technical support for primary mouse cultures and cannulae implantation. VN, AS, BR, and GR performed the DLS and LTS experiments, and analyzed the results. MR and GF performed the TEM experiments and analyzed the results. GRP and FG performed the NanoString experiments and analyzed the results. CL and MC conceived the study and wrote the manuscript. All authors reviewed and approved the final manuscript.

FUNDING

This work was supported by grants from AIRC (IG2015-16699 to CL), from the Italian Ministry of Research (PRIN 2015E8EMCM_001 to CL), from the Italian Ministry of Health (H2020 Euronanomed2 "Nanoglio" to CL), and from Ateneo 2016 to CM; CL is part of the H2020 Twinning Project "SynaNet".

ACKNOWLEDGMENTS

The authors wish to thank the Imaging Facility at Center for Life Nano Science, Istituto Italiano di Tecnologia, for support and technical advice.

SUPPLEMENTARY MATERIAL

The Supplementary Material for this article can be found online at: https://www.frontiersin.org/articles/10.3389/fncel.2019.00041/full#supplementary-material

REFERENCES

Aguzzi, A., and Rajendran, L. (2009). The transcellular spread of cytosolic amyloids, prions, and prionoids. *Neuron* 64, 783–790. doi: 10.1016/j.neuron.2009.12.0162009

Al-Nedawi, K., Meehan, B., Micallef, J., Lhotak, V., May, L., Guha, A., et al. (2008). Intercellular transfer of the oncogenic receptor EGFRvIII by microvesicles derived from tumour cells. *Nat. Cell Biol.* 5, 619–624. doi: 10.1038/ncb1725

Alvarez-Erviti, L., Seow, Y., Yin, H., Betts, C., Lakhal, S., and Wood, M. J. (2011). Delivery of siRNA to the mouse brain by systemic injection of targeted exosomes. *Nat. Biotechnol.* 29, 341–345. doi: 10.1038/nbt.1807

Antonucci, F., Turola, E., Riganti, L., Caleo, M., Gabrielli, M., Perrotta, C., et al. (2012). Microvesicles released from microglia stimulate synaptic activity via enhanced sphingolipid metabolism. *EMBO J.* 31, 1231–1240. doi: 10.1038/emboj.2011.489

Basso, M., and Bonetto, V. (2016). Extracellular vesicles and a novel form of communication in the brain. *Front. Neurosci.* 10:127. doi: 10.3389/fnins.2016.00127

Bianco, F., Pravettoni, E., Colombo, A., Schenk, U., Möller, T., Matteoli, M., et al. (2005). Astrocyte-derived ATP induces vesicle shedding and IL-1 beta release from microglia. *J. Immunol.* 174, 7268–7277. doi: 10.4049/jimmunol.174.11.7268

Carandini, T., Colombo, F., Finardi, A., Casella, G., Garzetti, L., Verderio, C., et al. (2015). Microvesicles: what is the role in multiple sclerosis? *Front. Neurol.* 6:111. doi: 10.3389/fneur.2015.00111

Casella, G., Colombo, F., Finardi, A., Descamps, H., Ill-Raga, G., Spinelli, A., et al. (2018). Extracellular vesicles containing IL-4 modulate neuroinflammation in a mouse model of multiple sclerosis. *Mol. Ther.* 26, 2107–2118. doi: 10.1016/j.ymthe.2018.06.024

Challagundla, K. B., Wise, P. M., Neviani, P., Chava, H., Murtadha, M., Xu, T., et al. (2015). Exosome-mediated transfer of microRNAs within the tumor

microenvironment and neuroblastoma resistance to chemotherapy. *J. Natl. Cancer. Inst.* 107:djv135. doi: 10.1093/jnci/djv135

Chen, Z., Feng, X., Herting, C. J., Garcia, V. A., Nie, K., Pong, W. W., et al. (2017). Cellular and molecular identity of tumor-associated macrophages in glioblastoma. *Cancer Res.* 77, 2266–2278. doi: 10.1158/0008-5472.CAN-16-2310

Chivet, M., Javalet, C., Laulagnier, K., Blot, B., Hemming, F. J., and Sadoul, R. (2014). Exosomes secreted by cortical neurons upon glutamatergic synapse activation specifically interact with neurons. *J. Extracell. Vesicles* 3:24722. doi: 10.3402/jev.v3.24722

Cooks, T., Pateras, I. S., Jenkins, L. M., Patel, K. M., Robles, A. I., Morris, J., et al. (2018). Mutant p53 cancers reprogram macrophages to tumor supporting macrophages via exosomal miR-1246. *Nat. Commun.* 9:771. doi: 10.1038/s41467-018-03224-w

Cunha, C., Gomes, C., Vaz, A. R., and Brites, D. (2016). Exploring new inflammatory biomarkers and pathways during LPS-Induced M1 Polarization. *Mediat. Inflamm.* 2016:6986175. doi: 10.1155/2016/6986175

da Fonseca, A. C., and Badie, B. (2013). Microglia and macrophages in malignant gliomas: recent discoveries and implications for promising therapies. *Clin. Dev. Immunol.* 2013:264124. doi: 10.1155/2013/264124

Deregibus, M. C., Cantaluppi, V., Calogero, R., Lo Iacono, M., Tetta, C., Biancone, L., et al. (2007). Endothelial progenitor cell derived microvesicles activate an angiogenic program in endothelial cells by a horizontal transfer of mRNA. *Blood* 110, 2440–2448. doi: 10.1182/blood-2007-03-078709

Fabbri, M., Paone, A., Calore, F., Galli, R., Gaudio, E., Santhanam, R., et al. (2012). MicroRNAs bind to toll-like receptors to induce prometastatic inflammatory response. *Proc. Natl. Acad. Sci. U.S.A.* 109, E2110–E2116. doi: 10.1073/pnas.1209414109

Fevrier, B., Vilette, D., Archer, F., Loew, D., Faigle, W., Vidal, M., et al. (2004). Cells release prions in association with exosomes. *Proc. Natl. Acad. Sci. U.S.A.* 101, 9683–9688. doi: 10.1073/pnas.0308413101

Fonseca, A. C., Romão, L., Amaral, R. F., Assad Kahn, S., Lobo, D., Martins, S., et al. (2012). Microglial stress inducible protein 1 promotes proliferation and migration in human glioblastoma cells. *Neuroscience* 200, 130–141. doi: 10.1016/j.neuroscience.2011.10.025

Garzetti, L., Menon, R., Finardi, A., Bergami, A., Sica, A., Martino, G., et al. (2014). Activated macrophages release microvesicles containing polarized M1 or M2 mRNAs. *J. Leukoc. Biol.* 95, 817–825. doi: 10.1189/jlb.0913485

Gasser, O., and Schifferli, J. A. (2004). Activated polymorphonuclear neutrophils disseminate anti-inflammatory microparticles by ectocytosis. *Blood* 104, 2543–2548. doi: 10.1182/blood-2004-01-0361

Gouwens, L. K., Ismail, M. S., Rogers, V. A., Zeller, N. T., Garrad, E. C., Amtashar, F. S., et al. (2018). Aβ42 protofibrils interact with and are trafficked through microglial-derived microvesicles. *ACS Chem. Neurosci.* 9, 1416–1425. doi: 10.1021/acschemneuro.8b00029

Grimaldi, A., D'Alessandro, G., Golia, M. T., Grössinger, E. M., Di Angelantonio, S., Ragozzino, D., et al. (2016). KCa3.1 inhibition switches the phenotype of glioma-infiltrating microglia/macrophages. *Cell Death Dis.* 7, e2174. doi: 10.1038/cddis.2016.73

Hambardzumyan, D., Gutmann, D. H., and Kettenmann H. (2016). The role of microglia and macrophages in glioma maintenance and progression. *Nat. Neurosci.* 19, 20–27. doi: 10.1038/nn.4185

Henn, A., Lund, S., Hedtjarn, M., Schrattenholz, A., Porzgen, P., and Leist, M. (2009). The suitability of BV2 cells as alternative model system for primary microglia cultures or for animal experiments examining brain inflammation. *ALTEX* 26, 83–94. doi: 10.14573/altex.2009.2.83

Horvath, R. J., Nutile-McMenemy, N., Alkaitis, M. S., and Deleo, J. A. (2008). Differential migration, LPS-induced cytokine, chemokine, and NO expression in immortalized BV-2 and HAPI cell lines and primary microglial cultures. *J. Neurochem.* 107, 557–569. doi: 10.1111/j.1471-4159.2008.05633.x

Iraci, N., Gaude, E., Leonardi, T., Costa, A. S. H., Cossetti, C., Peruzzotti-Jametti, L., et al. (2017). Extracellular vesicles are independent metabolic units with asparaginase activity. *Nat. Chem. Biol.* 9, 951–955. doi: 10.1038/nchembio.2422

Joshi, P., Turola, E., Ruiz, A., Bergami, A., Libera, D. D., Benussi, L., et al. (2014). Microglia convert aggregated amyloid-β into neurotoxic forms through the shedding of microvesicles. *Cell Death Differ.* 21, 582–593. doi: 10.1038/cdd.2013.180

Kim, S. H., Lechman, E. R., Bianco, N., Menon, R., Keravala, A., Nash, J., et al. (2005). Exosomes derived from IL-10-treated dendritic cells can suppress inflammation and collagen-induced arthritis. *J. Immunol.* 174, 6440–6448. doi: 10.4049/jimmunol.174.10.6440

Korkut, C., Li, Y., Koles, K., Brewer, C., Ashley, J., Yoshihara, M., et al. (2013). Regulation of postsynaptic retrograde signaling by presynaptic exosome release. *Neuron* 77, 1039–1046. doi: 10.1016/j.neuron.2013.01.013

Laso-García, F., Ramos-Cejudo, J., Carrillo-Salinas, F. J., Otero-Ortega, L., Feliú, A., Gómez-de Frutos, M., et al. (2018). Therapeutic potential of extracellular vesicles derived from human mesenchymal stem cells in a model of progressive multiple sclerosis. *PLoS One* 13:e0202590. doi: 10.1371/journal.pone.0202590

Lauro, C., Cipriani, R., Catalano, M., Trettel, F., Chece, G., Brusadin, V., et al. (2010). Adenosine A1 receptors and microglial cells mediate CX3CL1-induced protection of hippocampal neurons against Glu-induced death. *Neuropsychopharmacology* 35, 1550–1559. doi: 10.1038/npp.2010.26

Lewinski, N., Colvin, V., and Drezek, R. (2008). Cytotoxicity of nanoparticles. *Small* 4, 26–49. doi: 10.1002/smll.2007005954

Li, F., Schafer, R., Hwang, C., Tanner, C. E., and Ruggiero, S. T. (2010). High-precision sizing of nanoparticles by laser transmission spectroscopy. *Appl. Opt.* 49, 6602–6611. doi: 10.1364/AO.49.006602

Losche, W., Scholz, T., Temmler, U., Oberle, V., and Claus, R. A. (2004). Platelet-derived microvesicles transfer tissue factor to monocytes but not to neutrophils. *Platelets* 15, 109–115. doi: 10.1080/09537100310001649885

Mack, M., Kleinschmidt, A., Brühl, H., Klier, C., Nelson, P. J., Cihak, J., et al. (2000). Transfer of the chemokine receptor CCR5 between cells by membrane-derived microparticles: a mechanism for cellular human immunodeficiency virus 1 infection. *Nat. Med.* 6, 769–775. doi: 10.1038/77498

Neviani, P., and Fabbri, M. (2015). Exosomic microRNAs in the tumor microenvironment. *Front. Med.* 2:47. doi: 10.3389/fmed.2015.00047

Raposo, G., Nijman, H. W., Stoorvogel, W., Liejendekker, R., Harding, C. V., Melief, C. J., et al. (1996). B lymphocytes secrete antigen-presenting vesicles. *J. Exp. Med.* 183, 1161–1172. doi: 10.1084/jem.183.3.1161

Ratajczak, J., Miekus, K., Kucia, M., Zhang, J., Reca, R., Dvorak, P., et al. (2006). Embryonic stem cell-derived microvesicles reprogram hematopoietic progenitors: evidence for horizontal transfer of mRNA and protein delivery. *Leukemia* 20, 847–856. doi: 10.1038/sj.leu.2404132

Shinohara, H., Kuranaga, Y., Kumazaki, M., Sugito, N., Yoshikawa, Y., Takai, T., et al. (2017). Regulated polarization of tumor-associated macrophages by miR-145 via colorectal cancer-derived extracellular vesicles. *J. Immunol.* 199, 1505–1515. doi: 10.4049/jimmunol.1700167

Shvedova, A. A., Kagan, V. E., and Fadeel, B. (2010). Close encounters of the small kind: adverse effects of man-made materials interfacing with the nano-cosmos of biological systems. *Annu. Rev. Pharmacol. Toxicol.* 50, 63–88. doi: 10.1146/annurev.pharmtox.010909.105819

Tang, K., Zhang, Y., Zhang, H., Xu, P., Liu, J., Ma, J., et al. (2012). Delivery of chemotherapeutic drugs in tumour cell-derived microparticles. *Nat. Commun.* 3:1282. doi: 10.1038/ncomms2282

Tucher, C., Bode, K., Schiller, P., Claßen, L., Birr, C., Souto-Carneiro, M. M., et al. (2018). Extracellular vesicle subtypes released from activated or apoptotic T-lymphocytes carry a specific and stimulus-dependent protein cargo. *Front. Immunol.* 9:534. doi: 10.3389/fimmu.2018.00534

Turola, E., Furlan, R., Bianco, F., Matteoli, M., and Verderio, C. (2012). Microglial microvesicle secretion and intercellular signaling. *Front. Physiol.* 3:149. doi: 10.3389/fphys.2012.00149

Verderio, C., Muzio, L., Turola, E., Bergami, A., Novellino, L., Ruffini, F., et al. (2012). Myeloid microvesicles are a marker and therapeutic target for neuroinflammation. *Ann. Neurol.* 72, 610–624. doi: 10.1002/ana.23627

Viaud, S., Terme, M., Flament, C., Taieb, J., André, F., Novault, S., et al. (2009). Dendritic cell-derived exosomes promote natural killer cell activation and

proliferation: a role for NKG2D ligands and IL-15Ralpha. *PLoS One* 4:e4942. doi: 10.1371/journal.pone.0004942

Yang, T., Fogarty, B., LaForge, B., Aziz, S., Pham, T., Lai, L., et al. (2017). Delivery of small interfering RNA to inhibit vascular endothelial growth factor in zebrafish using natural brain endothelia cell-secreted exosome nanovesicles for the treatment of brain cancer. *AAPS J.* 19, 475–486. doi: 10.1208/s12248-016-0015-y

Yang, T. Z., Martin, P., Fogarty, B., Brown, A., Schurman, K., Phipps, R., et al. (2015). Exosome delivered anticancer drugs across the blood-brain barrier for brain cancer therapy in Danio Rerio. *Pharm. Res.* 32, 2003–2014. doi: 10.1007/s11095-014-1593-y

Yang, Y., Boza-Serrano, A., Dunning, C. J. R., Clausen, B. H., Lambertsen, K. L., and Deierborg, T. (2018). Inflammation leads to distinct populations of extracellular vesicles from microglia. *J. Neuroinflammation* 15:168. doi: 10.1186/s12974-018-1204-7

Ye, Z., Zhang, T., He, W., Jin, H., Liu, C., Yang, Z., et al. (2018). Methotrexate-loaded extracellular vesicles functionalized with therapeutic and targeted peptides for the treatment of glioblastoma multiforme. *ACS Appl. Mater. Interfaces* 10, 12341–12350. doi: 10.1021/acsami.7b18135

Zappulli, V., Friis, K. P., Fitzpatrick, Z., Maguire, C. A., and Breakefield, X. O. (2016). Extracellular vesicles and intercellular communication within the nervous system. *J. Clin. Invest.* 126, 1198–1207. doi: 10.1172/JCI81134

Zhang, X., Abels, E. R., Redzic, J. S., Margulis, J., Finkbeiner, S., and Breakefield, X. O. (2016). Potential transfer of polyglutamine and CAG-repeat RNA in extracellular vesicles in Huntington's disease: background and evaluation in cell culture. *Cell. Mol. Neurobiol.* 36, 459–470. doi: 10.1007/s10571-016-0350-7

Zhang, Y., Li, L., Yu, J., Zhu, D., Zhang, Y., Li, X., et al. (2014). Microvesicle-mediated delivery of transforming growth factor beta1 siRNA for the suppression of tumor growth in mice. *Biomaterials* 35, 4390–4400. doi: 10.1016/j.biomaterials.2014.02.003

Zhuang, X., Xiang, X., Grizzle, W., Sun, D., Zhang, S., Axtell, R. C., et al. (2011). Treatment of brain inflammatory diseases by delivering exosome encapsulated anti-inflammatory drugs from the nasal region to the brain. *Mol. Ther.* 19, 1769–1779. doi: 10.1038/mt.2011.164

Conflict of Interest Statement: The authors declare that the research was conducted in the absence of any commercial or financial relationships that could be construed as a potential conflict of interest.

frontiers in Cellular Neuroscience

ORIGINAL RESEARCH
published: 01 March 2019
doi: 10.3389/fncel.2019.00067

Neuroglial Involvement in Abnormal Glutamate Transport in the Cochlear Nuclei of the *Igf1*$^{-/-}$ Mouse

Veronica Fuentes-Santamaría[1]*, *Juan C. Alvarado*[1], *Lourdes Rodríguez-de la Rosa*[2,3,4], *José M. Juiz*[1] and *Isabel Varela-Nieto*[2,3,4]*

[1]Instituto de Investigación en Discapacidades Neurológicas (IDINE), Facultad de Medicina, Universidad de Castilla-La Mancha, Albacete, Spain, [2]Grupo de Neurobiología de la Audición, Instituto de Investigaciones Biomédicas Alberto Sols, Consejo Superior de Investigaciones Científicas-Universidad Autónoma de Madrid, Madrid, Spain, [3]Centro de Investigación Biomédica en Red de Enfermedades Raras (CIBERER), CIBER MP, Instituto de Salud Carlos III, Madrid, Spain, [4]Instituto de Investigación Sanitaria del Hospital Universitario La Paz (IdiPAZ), Madrid, Spain

Insulin-like growth factor 1 (IGF-1) is a powerful regulator of synaptic activity and a deficit in this protein has a profound impact on neurotransmission, mostly on excitatory synapses in both the developing and mature auditory system. Adult *Igf1*$^{-/-}$ mice are animal models for the study of human syndromic deafness; they show altered cochlear projection patterns into abnormally developed auditory neurons along with impaired glutamate uptake in the cochlear nuclei, phenomena that probably reflect disruptions in neuronal circuits. To determine the cellular mechanisms that might be involved in regulating excitatory synaptic plasticity in 4-month-old *Igf1*$^{-/-}$ mice, modifications to neuroglia, astroglial glutamate transporters (GLTs) and metabotropic glutamate receptors (mGluRs) were assessed in the cochlear nuclei. The *Igf1*$^{-/-}$ mice show significant decreases in IBA1 (an ionized calcium-binding adapter) and glial fibrillary acidic protein (GFAP) mRNA expression and protein accumulation, as well as dampened mGluR expression in conjunction with enhanced glutamate transporter 1 (GLT1) expression. By contrast, no differences were observed in the expression of glutamate aspartate transporter (GLAST) between these *Igf1*$^{-/-}$ mice and their heterozygous or wildtype littermates. These observations suggest that congenital IGF-1 deficiency may lead to alterations in microglia and astrocytes, an upregulation of GLT1, and the downregulation of groups I, II and III mGluRs. Understanding the molecular, biochemical and morphological mechanisms underlying neuronal plasticity in a mouse model of hearing deficits will give us insight into new therapeutic strategies that could help to maintain or even improve residual hearing when human deafness is related to IGF-1 deficiency.

Keywords: hearing loss, cochlear nucleus, IGF-1, glutamate receptors, astrocytes, microglia

OPEN ACCESS

Edited by:
Raquel Ferreira, Universidade da Beira Interior, Portugal

Reviewed by:
Hadley Wilson Horch, Bowdoin College, United States
Yu-Feng Wang, Harbin Medical University, China

***Correspondence:**
Veronica Fuentes-Santamaría
veronica.fuentes@uclm.es
Isabel Varela-Nieto
i.varela.nieto@csic.es

Received: *08 November 2018*
Accepted: *11 February 2019*
Published: *01 March 2019*

Citation:
Fuentes-Santamaría V, Alvarado JC, Rodríguez-de la Rosa L, Juiz JM and Varela-Nieto I (2019) Neuroglial Involvement in Abnormal Glutamate Transport in the Cochlear Nuclei of the Igf1$^{-/-}$ Mouse. Front. Cell. Neurosci. 13:67. doi: 10.3389/fncel.2019.00067

INTRODUCTION

Gene knockout studies in mice have demonstrated that insulin-like growth factor 1 (IGF-1), a growth promoting hormone, is essential for the proper functioning of the inner ear (Magariños et al., 2012; Varela-Nieto et al., 2013; Yamahara et al., 2015). A loss of this factor causes significant anomalies in the development of cochlear circuits during postnatal development, which impairs

peripheral function in these animals (Camarero et al., 2001, 2002; Cediel et al., 2006; Riquelme et al., 2010). Indeed, immature patterns of cochlear innervation persist in postnatal day 20 (P20) knockout mice and the spiral ganglion is abnormal, phenomena that are associated with increased auditory thresholds between the ages of 1–12 months and that ultimately result in severe sensorineural deafness (Murillo-Cuesta et al., 2011). Consequently, there is hypotrophy and hypoplasia in the cochlear nucleus of adult *Igf1*$^{-/-}$ mice, which develops in parallel with higher wave II amplitudes in auditory brainstem responses (ABRs). The lack of IGF-1 also modifies excitatory but not inhibitory synapses in the cochlear nuclei, evident as an upregulation in the vesicular glutamate-transporter 1 (VGluT1; Fuentes-Santamaría et al., 2016). This modulation involves myocyte enhancer factor-2 (MEF2) transcription factors, which are downregulated in the IGF-1-deficient cochlea and cochlear nucleus, and that play a pivotal role in regulating excitatory synapses (Flavell et al., 2006; Ruffle et al., 2006; Sanchez-Calderon et al., 2010; Rashid et al., 2014).

Glia are closely associated with synapses and they are key regulators of synaptic neurotransmission in the central nervous system (CNS; Bacci et al., 1999; Hansson and Rönnbäck, 2003; Ullian et al., 2004; Slezak et al., 2006). In the healthy brain, quiescent microglial cells are very dynamic, and they act as sensors to maintain environmental homeostasis in the CNS. Along with their well-established role as modulators of brain inflammation, responsive microglia monitor neuronal excitability and they regulate synapse formation, maturation and pruning by secreting factors that affect synaptic responses (Eroglu and Barres, 2010). Under pathological conditions, these non-neuronal cells also represent the first line of defense in the CNS, responding quickly to signals released by injured neurons and by synapses, by modifying their structural appearance and physiology (Wolf et al., 2017). Studies based on glia-free culture of isolated cortex, retinal ganglion cells or spinal motor neurons have revealed that astrocytes also contribute to the formation, maturation and stability of synapses (Nakanishi et al., 1994; Pfrieger and Barres, 1996; Ullian et al., 2001). When extracellular glutamate levels increase, accumulation of this neurotransmitter is avoided by the clearance of glutamate from the synaptic cleft by excitatory amino acid transporters (EAATs) on astrocytes, preventing excess receptor activation and hence, glutamate excitotoxicity (Danbolt, 2001). These non-neuronal cells express both the EAAT1/glutamate aspartate transporter (GLAST) and EAAT2/GLT1 human/rodent carrier subtypes, and although their expression is region-selective (Lehre et al., 1995), GLT1 appears to be responsible for most of the glutamate uptake at excitatory synapses (Rothstein, 1996; Lehre and Danbolt, 1998). More specifically, GLAST and not GLT1 is expressed strongly by inner supporting cells in the developing and adult mouse cochlea (Furness and Lehre, 1997; Furness and Lawton, 2003; Jin et al., 2011), and it is responsible for glutamate removal at the synapse between inner hair cells and Type I spiral ganglion neurons (Glowatzki et al., 2006). Fibrocytes in the spiral ligament and spiral limbus also express high levels of GLAST, suggesting that these cells also regulate cochlear glutamate uptake (Furness et al., 2009). The fact that GLAST-deficient mice accumulate glutamate in the perilymph in response to acoustic overstimulation led to the proposal that this carrier protects against noise-induced hearing loss (Hakuba et al., 2000; Chen et al., 2010). Ultrastructural studies in the mouse have also provided evidence that both Na^+-dependent glutamate transporters (GLTs) are expressed strongly in the cochlear nucleus, where they might modulate synaptic function (Josephson and Morest, 2003). GLT1 is also expressed by primary auditory neurons and glial cells in the spiral ganglion (Rebillard et al., 2003).

By competing for neurotransmitter binding and/or uptake, GLTs also modify the activation state of receptor populations at nearby synapses (Huang et al., 2004; Galik et al., 2008; Benediktsson et al., 2012). As such, electrophysiological recordings in acute hippocampal slices demonstrate that selective pharmacologic inhibition of astrocyte GLTs modifies the access of mGluRs to glutamate released at interneuron synapses (Huang et al., 2004; Nicoletti et al., 2011). These mGluRs are G-protein coupled receptors (GCPRs) that activate multiple signaling pathways to drive slow neuronal excitation in the brain (Niswender and Conn, 2010). Based on their specific properties, these receptors have been divided into groups I (mGluR1 and mGluR5), II (mGluR2 and mGluR3) and III (mGluR4, mGluR6, mGluR7, mGluR8), each of which seems to be involved in modulating cell excitability and synaptic transmission (Ferraguti and Shigemoto, 2006). The expression of mGluRs in the mammalian and avian auditory system has been seen to vary depending on the specific nucleus and the cell types they contain (Petralia et al., 2000; Lu, 2014). For example, mGluR1 and mGluR2 mRNA and protein has been detected in both the dorsal and ventral subdivisions of the cochlear nuclei, most intensely in the dorsal cochlear nucleus (DCN) where they seem to be located both pre- and post-synaptically (Bilak and Morest, 1998; Petralia et al., 2000; Kemmer and Vater, 2001; Nicholas and Hyson, 2004; Diaz et al., 2009; Martinez-Galan et al., 2010; Carzoli and Hyson, 2011, 2014). However, there is some controversy regarding the expression of the mGluR4 and mGluR7 subunits, and little information is available about mGluR3, mGluR5, mGluR6 and mGluR8 (Lu, 2014).

In the present study, we have assessed whether IGF-1-dependent alterations in synaptic neurotransmission in the cochlear nuclei involve glial cell dysfunction. Given that neuroglia actively participates in regulating synaptic transmission, the expression of ionized calcium-binding adaptor 1 (IBA1) and glial fibrillary acidic protein (GFAP) mRNA and protein was evaluated in mice lacking the *Igf1* gene as markers of microglial and astrocytes, respectively. In addition, as the activity of the glutamatergic system is impaired in *Igf1*$^{-/-}$ mice, possible abnormalities in the expression of the astroglial glutamate carriers (GLT1 and GLAST) and metabotropic glutamate receptors (mGluR1–5) were also investigated.

MATERIALS AND METHODS

Mouse Handling and Genotyping

Mice heterozygous for the *Igf1* gene (*Igf1*$^{+/-}$) were maintained on a hybrid MF1 and 129/sv genetic background to increase

the survival of *Igf1*$^{-/-}$ animals (Liu et al., 1993). *Igf1*$^{-/-}$ mice mortality before adulthood is high, although between 20%–30% survived. Male and female *Igf1*$^{-/-}$, *Igf1*$^{+/-}$ and *Igf1*$^{+/+}$ mice littermates were used in this study, aged 4 months (n = 24), and they were genotyped as described previously (Sanchez-Calderon et al., 2010). The mice were fed tap water and a standard diet, and they were housed following recommendations of the Federation of European Laboratory Animal Science Associations. Animal experimentation was carried out in accordance with Spanish and European legislation (RD 53/2013; EU directive 2010/63/EU), and the protocols were approved by the Animal Care and Use Committees of Spanish National Research Council (CSIC).

Cytoarchitecture of the Mouse Cochlear Nuclei

The nomenclature used to define the cochlear nucleus complex was based on previous studies in the mouse (Mugnaini et al., 1980; Martin and Rickets, 1981; Lambert and Schwartz, 1982; Webster and Trune, 1982). The criteria for the classification of cochlear nucleus neurons were based on cell size, shape and location within the nucleus. As in other mammals, the cochlear nuclei can be divided into two major regions termed the DCN and the ventral cochlear nucleus. *The DCN* is a laminated structure composed of three layers; the superficial molecular layer (ml, layer 1), the granule/fusiform cell layer (grl, layer 2) and the deep layer or central region (cr, layer 3) of the nucleus. *The layer 1* is composed of small stellate cells, cartwheel cells, granule cell axons and fusiform cell dendrites. *The layer 2* is made up of diverse neuron types including fusiform cells, also known as pyramidal or principal cells, many granule cells and cartwheel cells while *the layer 3* contains mostly giant cells and tuberculoventral cells. *The ventral cochlear nucleus* is further divided by the cochlear nerve root into posteroventral cochlear nucleus (PVCN) and anteroventral cochlear nucleus (AVCN) subdivisions. According to their size and morphology, there are three main types of ventral cochlear nucleus neurons: (1) globular and spherical bushy cells are mainly located in the AVCN; (2) multipolar cells are present in both the AVCN and the PVCN; and (3) octopus cells are found exclusively in the PVCN. *The cochlear granule cell domain* is a continuous sheet of tightly packed granule cells which covers the dorsal and ventral regions of the ventral cochlear nucleus and the granule/fusiform layer of the DCN. A lamina of these cells also extends medially and ventrally to separate the DCN from the PVCN.

RNA Isolation and Reverse Transcription Quantitative PCR

Mice were sacrificed by barbiturate overdose (Dolethal®, 40–90 mg/kg i/p), decapitated and a midline incision was made in the skin of the head to flip it over the eyes and free the skull. Next, a frontal bone cross-section in the skull in front of the olfactory bulbs and a caudal cross-section by the interparietal bone were made. Both sections were joined by a longitudinal section along the sagittal suture, which facilitated partial removal of the frontal and parietal bones and exposure of the encephalon. To locate the cochlear nuclei, different anatomical landmarks including the cerebellum, the inferior cerebellar peduncle and the spinal trigeminal tract were used as reference points (Franklin and Paxinos, 2013). After removal of the overlying cerebellar flocculus, the dorsal and ventral cochlear nuclei of *Igf1*$^{+/+}$, *Igf1*$^{+/-}$ and *Igf1*$^{-/-}$ mice (at least n = 3 per genotype) were dissected off the dorsolateral part of the brainstem (Ryugo and Willard, 1985; Juiz et al., 2000; Fuentes-Santamaria et al., 2005; Caminos et al., 2015). Tissue samples were conveniently stabilized using *RNAlater*® and disrupted with a *TissueLyser* system. Total RNA was isolated and genomic DNA efficiently removed using the *RNeasy Plus Mini Kit*® automated on a QIAcube (QIAGEN), according to manufacturer's instructions. Quality and quantity of RNA was further assessed by using the Agilent 2100 bioanalyzer, only samples with a RIN > 8.5 were used. Using equal quantities of this RNA from each individual mouse as a template, cDNAs were generated by reverse transcription (RT: *High-Capacity cDNA Reverse Transcription Kit*; Thermo Fisher Scientific) and amplified by quantitative PCR (qPCR) in a 7900HT System (ThermoFisher Scientific) as described previously (Fuentes-Santamaría et al., 2016). TaqMan® Gene Expression Assays[1] (Life Technologies) were used to detect *Iba1* (Mm00479862_g1), *Gfap* (Mm01253033_m1), *Glast* (Mm00600697_m1), *Glt1* (Mm00441457_m1), *mGluR1* (Mm01187089_m1), *mGluR2* (Mm01235831_m1), *mGluR4* (Mm01306128_m1) and *mGluR7* (Mm01189424_m1). All probes used span exon/exon boundaries with the exception of *Iba1* (Mm00479862_g1). Randomly, control reactions were carried out to secure the quality of the reagents used (no cDNA) and purity of RNA preparations (no RT). Hypoxanthine phosphoribosyltransferase 1 (*Hprt1*) and ribosomal protein lateral stalk subunit P0 (*Rplp0*) were used as endogenous reference genes for normalization, and the relative quantity (RQ) was calculated against calibrator samples, as determined by the $2^{-\Delta\Delta Ct}$ method (Livak and Schmittgen, 2001). The data are presented as the mean RQ.

Characterization of Primary Antibodies

Information about the primary antibodies used in this study is summarized in **Table 1**. The *anti- NeuN* antibody was produced from the nuclei of mouse brain cells and as described previously (Mullen et al., 1992; Lind et al., 2005), it detects a single 48 kDa band in western blots of mouse brain tissue. It has been used as a neuronal maker as it recognizes the neuron-specific NeuN protein, which is widely expressed in peripheral and central neurons (Rasmussen et al., 2007). The staining pattern described here for the cochlear nuclei matches previous descriptions (Fuentes-Santamaría et al., 2012). The *anti-calretinin (CR)* antibody was raised against the human CR protein and its specificity has been assessed in Western blots of membrane fractions from the cochlear nucleus, recognizing a single specific 31 kDa band (Fuentes-Santamaria et al., 2005). The *IBA1* antibody was raised against a synthetic peptide corresponding to the C-terminal fragment of rat protein, N-PTGPPAKKAISELP-C (Imai et al., 1996). This antibody recognizes a single band with an estimated molecular weight of 17 kDa, and it stains microglia and macrophages in the peripheral

[1] https://bioinfo.appliedbiosystems.com/genome-database/gene-expression.html

TABLE 1 | List of primary antibodies.

Primary antibody	Immunogen	Host	Code/clone	Dilution	Manufacturer
NeuN	Recombinant mouse NeuN	Guinea Pig	ABN90	1:2,000	Millipore, Billerica, MA, USA
CR	Recombinant human CR	Rabbit	7699/3H	1:1,500	Swant, Bellinzona, Switzerland
Iba-1	C-terminus of Iba1′ (N′-PTGPPAKKAISELP-C′)	Rabbit	019-19741	1:2,000	Wako Pure Chemical Industries, Neuss, Germany
GFAP	Cow spinal cord GFAP	Rabbit	Z0334	1:2,000	Dako, Glostrup, Denmark
GLAST	C-terminus of EAAT1 of human origin	Goat	SC-7757	1:100	Santa cruz Biotechnology, Inc. Germany
GLT-1	Carboxy-terminus of rat GLT-1	Guinea pig	AB1783	1:200	Millipore, Billerica, MA, USA
mGluR1α	Mouse mGluR1a, 945–11277aa	Rabbit	G046-mGluR1a-AG	1:1,000	Frontier Institute, Japan

and central auditory system (Ito et al., 1998; Sasaki et al., 2001; Fuentes-Santamaría et al., 2012). The *GFAP* antibody was raised against GFAP from bovine spinal cord and it recognizes a single 50 kDa band in western blots that corresponds to the GFAP protein (Debus et al., 1983). GFAP is an intermediate filament protein and it mainly stains astrocytes in the mature CNS. It is important to note that GFAP is a reliable marker to label reactive protoplasmic and fibrous astrocytes but since some resting astrocytes express this marker only weakly, they might not be detected by immunohistochemistry (Sofroniew and Vinters, 2010). GFAP staining in the mouse cochlear nuclei with this antibody was consistent with previous studies in rodents (Fuentes-Santamaría et al., 2017). The *anti-EAAT1 (GLAST)* antibody was raised against a peptide mapping to the C-terminus of human EAAT1 and it detects a single band at approximately 65 kDa in Western blots of rat brain tissue. EAAT1 is an excitatory amino acid transporter expressed mainly in astrocytes and staining of the mouse cochlear nucleus with this antibody matched previous observations (Furuta et al., 1997; Schmitt et al., 1997). The *anti-EAAT2 (GLT1)* antibody was raised against a synthetic peptide from the carboxy-terminus of rat GLT1 and its target is also an excitatory amino acid transporter mainly located in astrocytes. Its specificity and staining pattern have been described elsewhere (Furuta et al., 1997; Atoji and Islam, 2009).

Immunohistochemistry

Under deep ketamine hydrochloride anesthesia (0.12 mg/g injected i.p.—intraperitoneal), mice (n = 15) were transcardially perfused with a 0.9% saline solution, followed by a solution of 4% paraformaldehyde (PFA) in 0.1 M phosphate buffer (PB; pH 7.3). The brain of the mice was removed and incubated overnight in 30% sucrose in PB, and coronal sections (40 μm) were then obtained on a sliding microtome. The brain tissue from each genotype was processed simultaneously. The sections were rinsed in Tris-buffered saline (TBS, pH 7.4) containing 0.2% Triton X-100 (Tx) and incubated overnight (with agitation) at 4°C with a primary antibody raised against IBA1, GFAP, GLT1, GLAST or mGluR1α. After several rinses in TBS-Tx 0.2%, antibody binding was detected over 2 h with the corresponding biotinylated secondary antibodies (1:200; Vector Laboratories, Burlingame, CA, USA), and the antigen-antibody complex was visualized by incubating for 1 h in ABC reagent (PK-6100, vector laboratories, Burlingame, CA, USA) at room temperature and performing diaminobenzidine histochemistry. Finally, the sections were mounted onto gelatin-coated slides, air-dried and coverslipped using Cytoseal (Stephens Scientific, Camden, NJ, USA) for light microscopy analysis. Control experiments were performed by omitting either the primary or secondary antibody, or the ABC reagent, resulting in no staining.

Double Immunofluorescence Labeling

An alternate set of brain sections from these same animals was rinsed several times in PBS-Tx 0.2% and incubated overnight in the corresponding cocktail of primary antibodies. Sections were double-labeled with a solution containing primary antibodies against IBA1and NeuN, GFAP and NeuN, GLAST and calretinin (CR), or mGluR1α and NeuN, and single-labeled with GLT1 (**Table 1**). After four 15 min rinses in TBS-Tx (0.2%), the secondary antibodies (1:200) were applied for 2 h at room temperature: donkey anti-goat conjugated to Alexa 488 and donkey anti-rabbit conjugated to Alexa 594 for GLAST and CR; goat anti-rabbit conjugated to Alexa 488 and goat anti-guinea pig conjugated to Alexa 594 for IBA1/NeuN, GFAP/NeuN and mGluR1α/NeuN; goat anti-guinea pig conjugated to Alexa 594 for GLT1 (Molecular Probes, Eugene, OR, USA). These sections were then counterstained with DAPI (4′,6-diamidino-2-phenylindole; Molecular Probes, Eugene, OR, USA) and mounted.

Morphometric Analysis of Microglia Branching: Skeleton Analysis

To evaluate the possible modifications in the ramification of microglia in the cochlear nuclei due to IGF-1 deficiency, a skeleton analysis was performed using NIH ImageJ software (Schneider et al., 2012). The analysis of each nucleus was done on four sections from three mice per genotype. Images were captured with a 40× objective, converted into 16-bit scale and by using the thresholding function, the immunostained microglia were counted using a cell counter plug-in. The 16-bit scale images were then transformed into binary images that were subsequently, skeletonized (**Figure 1**). The Analyze Skeleton plug-in (version 3.1.3[2], Arganda-Carreras et al., 2010), was used to calculate the endpoints and the processes length in each field. The obtained values were normalized and expressed as endpoints/cell and process length/cell (Morrison and Filosa, 2013; Turlejski et al., 2016; Morrison et al., 2017). The following parameters were evaluated: *(1) the number of microglial cells per field; (2) the number of microglia process endpoints per cell; and (3) the microglia process length per cell (μm)*. The endpoints/cell give us an estimate of the number of branch points of microglia, while the process length/cell gives us the

[2]https://imagej.net/AnalyzeSkeleton

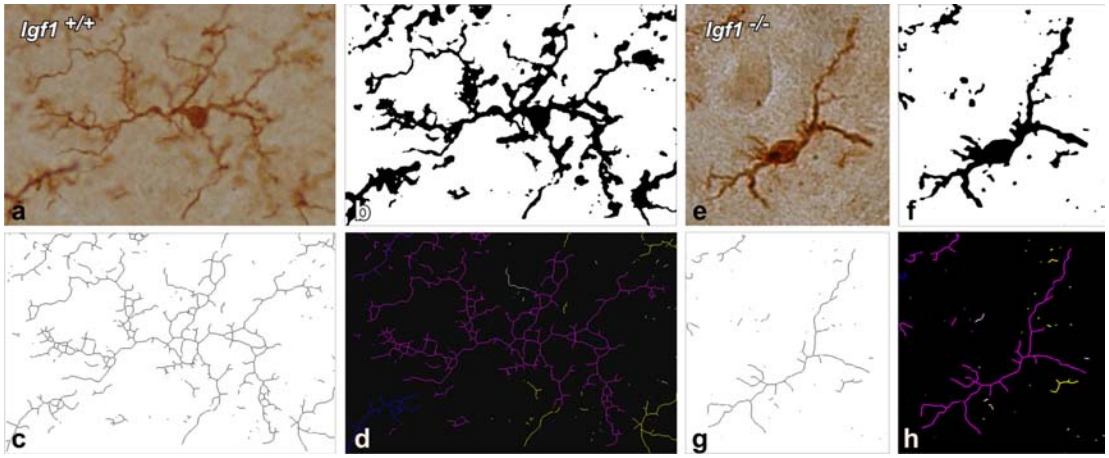

FIGURE 1 | Morphometric analysis of microglial branching. For the skeleton analysis, digital images of IBA1 immunostained cells were captured with a 40× objective **(A,E)**, converted into binary images **(B,F)** and then skeletonized **(C,G)**. To evaluate microglial morphology parameters, skeletonized images were processed using the Analyze Skeleton plugin for Image J. Each glial cell is identified with a different color. The representative glia is shown in purple, and part of the skeleton of the other glial cells is shown in yellow, blue and white **(D,H)**.

mean length of microglial branches (Morrison and Filosa, 2013; Turlejski et al., 2016; Morrison et al., 2017). It is possible, at least in some instances that, after generating the skeleton, a few loops could be detected by the software in the resultant images. For pruning these loops, the software compares the original and the resulting skeleton images and by using, in our case, the method of the lowest intensity voxel, it excludes any voxel with intensities below the threshold. In that way, any possible loop/s that could affect the measurement will be eliminated. Similar to the densitometric analysis, and to avoid bias, all measurements were performed by the same experimenter blinded to the mouse genotype.

Evaluation and Quantification of the Immunostaining

Light Microscopy

The brains that were processed for light microscopy were analyzed with brightfield illumination using a Nikon Eclipse photomicroscope equipped with a 40× objective. Images were captured with a DXM 1200C digital camera attached to the microscope. This study evaluates qualitatively and quantitatively the immunostaining produced by different antibodies used to label microglia, astrocytes, astroglial GLTs and mGluRs in the mouse cochlear nuclei. The qualitative parameters used to assess the immunostaining were: (1) *cell morphology* (ramified vs. bipolar), *staining intensity* (weak, moderate, or strong) and *immunopositive profiles (cell/puncta) area*. The quantitative analysis was provided through the use of custom-made macros that were written in a Pascal-like language (Xu et al., 2000; Alvarado et al., 2004). Captured color images of each selected field were digitized and the ensuing 8-bit images had a grayscale of pixel intensities that ranged from 0 (white) to 255 (black). Three animals of each genotype were used to evaluate the immunostaining in the DCN, PVCN and AVCN. In each coronal section, three microscopic fields (36.85 × 10^3 μm^2; dorsal, middle and ventral) were sampled 160 μm apart using a 40× objective and a total of four sections per mouse were analyzed. To quantify the immunostaining, images containing grayscale values from 0 to 255 were normalized, and then, an automatic threshold was set as two standard deviations above the value of the field. Profiles exceeding the threshold for detection were considered as labeled. *The mean gray level of the immunostaining* and *the immunostained area* were used as indicators of the protein levels and cell/puncta immunostained area, respectively (Fuentes-Santamaria et al., 2005; Alvarado et al., 2007b, 2014; Adams et al., 2008). The *immunostained area* gave us an estimate of the area occupied by stained profiles and it was calculated as the sum of all the immunostained cellular elements present in the field (Benson et al., 1997; Fuentes-Santamaría et al., 2012, 2013). To avoid bias, all measurements were performed by the same experimenter blinded to the animal conditions.

Confocal Microscopy

The brains from each genotype were processed simultaneously and the cochlear nuclei photographed under similar conditions. For appropriate image acquisition and interpretation, the following parameters were controlled: laser intensity, detector gain, pinhole aperture, number of optical sections and Z-stacking. For each dye, optical sections every 2.5 μm through the thickness of each nucleus were captured sequentially with 40× or 63× Plan Apo oil-immersion objectives, merged and saved as TIFF files using the ZEN 2009 Light Edition software. Fluorescent sections were examined with a laser scanning confocal microscope (LSM 710: Zeiss, Germany) with excitation laser lines at 405, 488 and 594 nm.

Image Processing and Statistical Analysis

Photoshop CS3 (Adobe) and Canvas X (Deneba) were used to adjust the size, brightness and contrast of the images. The immunohistochemical and qPCR data were expressed as the

means ± SD, and the statistical comparisons among genotypes were made using a one-factor analysis of variance and Scheffé's *post hoc* analysis as necessary. A p-value < 0.05 was considered statistically significant, and the significance levels (α) and power (β) were set to 0.05 and 95%, respectively. Significant differences among animal groups are indicated by asterisks: $^{*}p < 0.05$; $^{**}p < 0.01$; and $^{***}p < 0.001$.

RESULTS

Altered Microglial Morphology and IBA1 Downregulation in *Igf1*$^{-/-}$ Mice

As alterations to microglia may lead to neuronal and synaptic dysfunction (Kettenmann et al., 2013; Wu et al., 2015), the morphology of these non-neuronal cells and their IBA1 expression was studied in the cochlear nuclei of *Igf1*$^{-/-}$ mice and compared to heterozygous and wild-type mice. Regardless of the genotype, microglia in both cochlear nucleus subdivisions had a resting phenotype, characterized by a small round cell body with ramified processes (**Figures 2**, **3**). Qualitative observations showed that, when compared to the other genotypes, *Igf1*$^{-/-}$ mice exhibited more lightly stained microglia, which was coupled to an apparent decrease in both cell number and microglia ramification in all the nuclei analyzed (arrows in **Figures 2C–E**, **3E–G,K–M**). To further assess the branching of microglia, reconstructed Z-stack confocal images of IBA1 stained microglia were also evaluated for each nucleus and genotype (arrows in **Figures 2F–H**, **3H–J,N–Q**). This analysis of the confocal images also demonstrated that microglia in *Igf1*$^{-/-}$ mice had shorter processes, which covered a smaller surface area than in *Igf1*$^{+/+}$ and *Igf1*$^{+/-}$ mice. These observations were corroborated by analyses of variance (ANOVA), which demonstrated a significant effect of IGF-1 deficiency over the mean gray levels of IBA1 immunostaining in the DCN ($F_{(2,22)} = 10.35$, $p < 0.001$), PVCN ($F_{(2,15)} = 13.86$, $p < 0.001$) and AVCN ($F_{(2,18)} = 13.81$, $p < 0.001$), as well as over the immunostained areas in the DCN ($F_{(2,22)} = 10.77$, $p < 0.001$), PVCN ($F_{(2,15)} = 9.94$, $p < 0.01$) and AVCN ($F_{(2,18)} = 12.15$, $p < 0.001$). Further analysis using a Scheffé's *post hoc* test

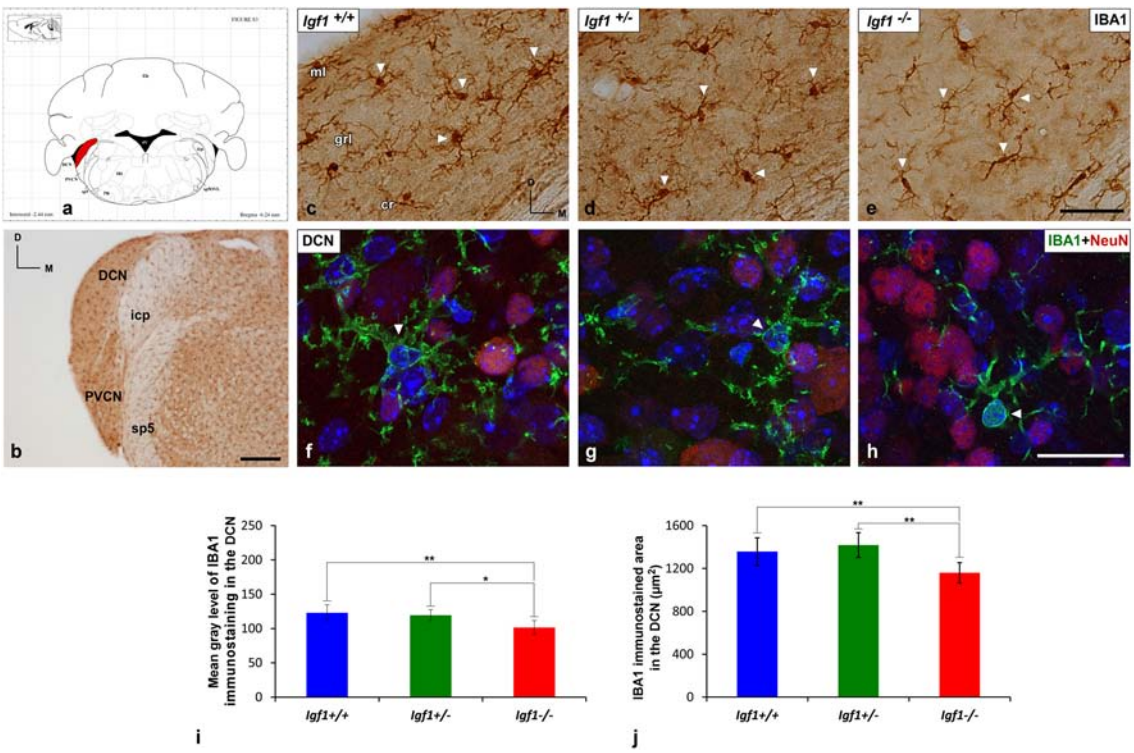

FIGURE 2 | IBA1 immunostaining in the DCN of *Igf1*$^{-/-}$ mice. **(A)** Coronal section of a wild-type mouse brain taken from the Franklin and Paxinos (2013) mouse brain atlas, to show the location of the DCN (red) and PVCN. **(B)** Representative coronal section of the cochlear nuclei in the wild-type genotype immunostained with IBA1. In *Igf1*$^{-/-}$ mice, cells with multipolar or bipolar morphology were stained more weakly, and they had shorter processes than in *Igf1*$^{+/+}$ and *Igf1*$^{+/-}$ mice (arrows in **C–E**). The maximum intensity projections of confocal images of the DCN illustrate a reduction in microglial branching in *Igf1*$^{-/-}$ mice (arrow in **H**) when compared to the other genotypes (arrows in **F**,**G**). Quantification of the immunostaining showed the significant decrease in the mean gray levels **(I)** and the immunostained areas **(J)** in the *Igf1*$^{-/-}$ mouse when compared to the other genotypes. Arrows point to IBA1 immunostained cells. Cell nuclei in **(F–H)** are stained with DAPI (blue). The error bars indicate the standard deviations of the mean. Statistically significant differences among the animal groups were evaluated by one-factor analyses of variance (ANOVA; $^{*}p < 0.05$; $^{**}p < 0.01$). Abbreviations: Cb, Cerebellum; cr, central region of the dorsal cochlear nucleus (DCN); grl, granule/fusiform layer; IBA1, ionized-calcium-binding adaptor; icp, inferior cerebellar peduncle; IRt, intermediate reticular nucleus; ml, molecular layer; NeuN, neuronal marker; PVCN, posteroventral cochlear nucleus; sp5, spinal trigeminal nucleus; sp5OVL, spinal trigeminal nucleus, oral part, ventrolateral division; 4V, 4th ventricle; 7N, facial nucleus. Scale bars: 250 µm in **(B)**; 50 µm in (**C**; it also applies to **C**,**D**); 20 µm in (**H**; it also applies to **F**,**G**).

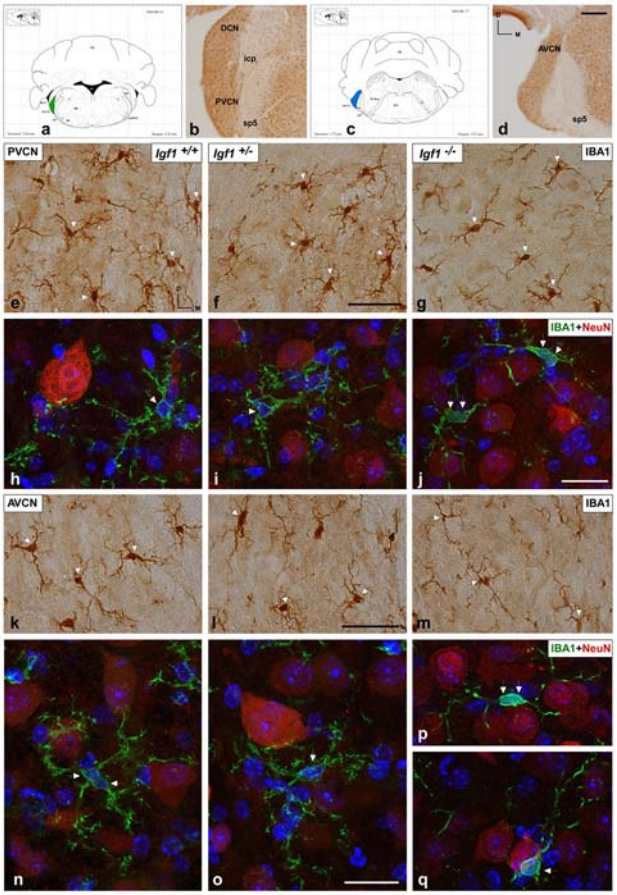

FIGURE 3 | IBA1 immunostaining in the PVCN and AVCN of *Igf1*$^{-/-}$ mice. **(A,C)** Coronal sections of a wild-type mouse brain, taken from Franklin and Paxinos (2013) mouse brain atlas, showing the location of the PVCN (green) and AVCN (blue). **(B,D)** Representative coronal sections of the ventral cochlear nucleus in the wild-type genotype immunostained with IBA1. In the PVCN and AVCN of *Igf1*$^{-/-}$ mice, there was less staining (**G,J,M,P,Q**) relative to the *Igf1*$^{+/+}$ **(E,H,K,N)** and *Igf1*$^{+/-}$ mice (**F,I,L,O**). Maximum intensity projections of confocal images from the PVCN and AVCN show the reduced microglial arborization in *Igf1*$^{-/-}$ mice as compared to the other genotypes (**H–J,N–Q** for the PVCN and AVCN; respectively). Arrows point to IBA1 immunostained cells. Cell nuclei are stained with DAPI (blue). Abbreviations: AVCN, anteroventral cochlear nucleus; Cb, Cerebellum; IBA1, ionized-calcium-binding adaptor; icp, inferior cerebellar peduncle; IRt, intermediate reticular nucleus; NeuN, neuronal marker; PnC, pontine reticular nucleus, caudal part; PVCN, posteroventral cochlear nucleus; sp5, spinal trigeminal nucleus; sp5OVL, spinal trigeminal nucleus, oral part, ventrolateral division; 4V, 4th ventricle; 7n, facial nerve; 7N, facial nucleus; 8n, vestibulocochlear nerve. Scale bars: 250 μm in (**D**; it also applies to **B**); 50 μm in (**F,J**; it also applies to **E,G,H,I**); 20 μm in (**L,O**; it also applies to **K**,**M**,**N**,**P,Q**).

determined that the mean gray levels in the *Igf1*$^{-/-}$ mice were significantly lower than in the *Igf1*$^{+/+}$ ($p < 0.01$ for the DCN, $p < 0.001$ for the PVCN and AVCN) and *Igf1*$^{+/-}$ ($p < 0.05$ for the DCN and AVCN, $p < 0.01$ for the PVCN) mice (**Figures 2I**, **4**). Similar decreases were observed for the immunostained areas relative to the *Igf1*$^{+/+}$ ($p < 0.01$ for the DCN, $p < 0.05$ for the PVCN and AVCN) and *Igf1*$^{+/-}$ ($p < 0.01$ for the DCN and PVCN, $p < 0.001$ for the AVCN) mice (**Figures 2J**, **4**). Moreover, a one-way ANOVA analysis also identified an IGF-1 dependent effect on microglial ramification. Accordingly, the morphometric analysis of microglial branching revealed statistically significant decreases in the number of microglia/field in the DCN, PVCN and AVCN of *Igf1*$^{-/-}$ mice compared to *Igf1*$^{+/+}$ and *Igf1*$^{+/-}$ mice, as well as in the microglia process endpoints/cell and microglia process length/cell (**Tables 2**, **3**; also see **Figure 1**). In accordance with the immunohistochemical data, qPCR gene expression studies detected weaker *Iba1* mRNA expression levels in the cochlear nuclei of *Igf1*$^{-/-}$ mice relative to the other genotypes ($p < 0.05$, **Figure 4E**).

Downregulation of GFAP Expression in *Igf1*$^{-/-}$ Mice

Excitatory synaptic neurotransmission appears to be altered in the cochlear nucleus of *Igf1*$^{-/-}$ mice (Fuentes-Santamaría et al., 2016). Since astrocytes are modulators of mature and functional synapses, and they are crucial for the maintenance of synapses (Chung et al., 2006), the astrocytic expression of GFAP in the cochlear nuclei was examined. In all genotypes evaluated, GFAP protein was located in the cytoplasm and processes of astrocytes that were highly ramified (**Figures 5**, **6**). Specifically, in the granule cell domain, immunostained astrocytes were densely packed and intensely stained (asterisks in **Figures 5A–C**). In agreement with previous observations in rodents (Burette et al., 1998; Insausti et al., 1999), GFAP immunostaining in the DCN of all genotypes, was distributed in a dorso-ventral gradient, whereby the molecular layer was more intensely stained than the intermediate granule/fusiform layer and the central region of the DCN (insets in **Figures 5A–C**) where astrocytes organized into patches characterized by multiple cells (arrows in **Figures 5A,B**). In all of the mice analyzed, irrespective of the genotype, astrocytes were associated with neurons in the cochlear nucleus, as well as with other astrocytes (**Figures 5D–F**). In IGF-1 deficient mouse, the immunostaining in the intermediate and deep layers of the DCN, but not in the superficial layer (ml), seemed to be weaker than in the other animal groups (**Figures 5A–F**). Similarly, a reduction in the immunostaining was also detected in the PVCN and AVCN of *Igf1*$^{-/-}$ mice (**Figures 5G–L**, **6A–F**). These decreases were confirmed by ANOVA, which showed that there was a significant effect of the IGF-1 deficiency on the mean gray levels of GFAP immunostaining in the DCN ($F_{(2,13)} = 5.32$, $p < 0.05$), PVCN ($F_{(2,18)} = 17.32$, $p < 0.001$) and AVCN ($F_{(2,12)} = 14.99$, $p < 0.001$), and on the immunostained areas in the DCN ($F_{(2,13)} = 17.88$, $p < 0.001$), PVCN ($F_{(2,18)} = 13.37$, $p < 0.001$) and AVCN ($F_{(2,12)} = 18.33$, $p < 0.001$; **Figures 5M–P**, **6G,H**). Similarly, there was significantly less *Gfap* mRNA in the *Igf1*$^{-/-}$ mice than in the *Igf1*$^{+/+}$ and *Igf1*$^{+/-}$ mice ($p < 0.01$, **Figure 6I**).

IGF-1 Dependent Alterations to Astrocyte Glutamate Transporters

To determine possible abnormalities in astrocyte GLTs that might contribute to abnormal excitatory synaptic activity in the cochlear nucleus circuits of *Igf1*$^{-/-}$ mice, as reported previously (Fuentes-Santamaría et al., 2016), the expression of GLT1 and GLAST was investigated.

TABLE 2 | Morphometric analysis of microglial ramification in the dorsal cochlear nucleus (DCN).

	DCN		
Genotype	**Microglia/field**	**Microglia process endpoints/cell**	**Microglia process length/cell (μm)**
Igf1$^{+/+}$ (1)	7.75 ± 0.48	45.00 ± 1.09	47.48 ± 1.08
Igf1$^{+/-}$ (2)	7.25 ± 0.25	46.23 ± 2.19	49.36 ± 2.79
Igf1$^{-/-}$ (3)	5.50 ± 0.29	38.22 ± 0.49	38.58 ± 1.69
$F_{(2,9)}$ =	11.67 (**)	8.95 (**)	8.43 (**)
Statistical comparison	**Significance levels**		
1 vs. 2	NS	NS	NS
1 vs. 3	**	*	*
2 vs. 3	*	**	**

*Values are means ± standard errors. Statistically significant differences among the animal groups were evaluated by one-factor analyses of variance (ANOVA; *$p < 0.05$; **$p < 0.01$; NS, No significant).*

TABLE 3 | Morphometric analysis of microglial ramification in the posteroventral cochlear nucleus (PVCN) and anteroventral cochlear nucleus (AVCN).

	PVCN		
Genotype	**Microglia/field**	**Microglia process endpoints/cell**	**Microglia process length/cell (μm)**
Igf1$^{+/+}$ (1)	10.00 ± 0.41	52.36 ± 3.00	54.00 ± 3.98
Igf1$^{+/-}$ (2)	10.75 ± 0.63	46.94 ± 2.29	52.92 ± 1.79
Igf1$^{-/-}$ (3)	8.00 ± 0.41	40.67 ± 1.92	38.95 ± 2.85
$F_{(2,9)}$ =	8.31 (**)	4.12 (*)	4.94 (*)
Statistical comparison	**Significance levels**		
1 vs. 2	NS	NS	NS
1 vs. 3	*	*	*
2 vs. 3	**	*	*
	AVCN		
Genotype	**Microglia/field**	**Microglia process endpoints/cell**	**Microglia process length/cell (μm)**
Igf1$^{+/+}$ (1)	10.75 ± 0.63	46.80 ± 1.13	49.38 ± 1.12
Igf1$^{+/-}$ (2)	10.50 ± 0.87	48.54 ± 2.30	51.83 ± 2.93
Igf1$^{-/-}$ (3)	7.50 ± 0.29	40.51 ± 0.52	40.49 ± 1.79
$F_{(2,9)}$ =	7.98 (**)	7.81 (**)	7.57 (**)
Statistical comparison	**Significance levels**		
1 vs. 2	NS	NS	NS
1 vs. 3	**	*	*
2 vs. 3	*	**	**

Values are means ± standard errors. Statistically significant differences among the animal groups were evaluated by one-factor ANOVA ($p < 0.05$; **$p < 0.01$; NS, No significant).*

Upregulation of EAAT2/GLT1 Expression in *Igf1*$^{-/-}$ Mice

Regardless of the genotype, GLT1 immunostaining was evident as dense punctate labeling that was similarly distributed throughout the cochlear nuclei (**Figures 7**, **8**). In the DCN, the GLT1 stained puncta were distributed throughout the molecular layer, granule/fusiform layer and the central region of the DCN (**Figures 7A–C**). Similar diffuse punctate neuropil staining was also observed in the PVCN (**Figures 8A–C**) and AVCN (**Figures 8F–H**). Although the distribution of GLT1 immunostaining was similar in the different genotypes, the GLT1 puncta in *Igf1*$^{-/-}$ mice were apparently more strongly stained and they seemed to occupy a larger extension in both subdivisions of the cochlear nucleus (**Figures 7**, **8**). These qualitative immunohistochemical appreciations were confirmed by ANOVA, which showed a significant effect of the absence of IGF-1 on the mean gray level of GLT1 in the DCN ($F_{(2,10)} = 15.94$, $p < 0.001$), PVCN ($F_{(2,10)} = 61.48$, $p < 0.001$) and AVCN ($F_{(2,9)} = 32.92$, $p < 0.001$) and also on the immunostained areas in the DCN ($F_{(2,10)} = 28.16$, $p < 0.001$), PVCN ($F_{(2,10)} = 41.85$, $p < 0.001$) and AVCN ($F_{(2,9)} = 28.66$, $p < 0.001$). As demonstrated using Scheffé's *post hoc* test, the mean gray levels in the *Igf1*$^{-/-}$ mice were significantly higher than in the *Igf1*$^{+/+}$ ($p < 0.001$ for DCN, PVCN and AVCN) and *Igf1*$^{+/-}$ ($p < 0.01$ for DCN and AVCN, $p < 0.001$ for PVCN) mice (**Figures 7D**, **8D,I**). Likewise, the GLT1 immunostained areas were also larger in the *Igf1*$^{-/-}$ mice than in the *Igf1*$^{+/+}$ ($p < 0.001$ for all nuclei) and *Igf1*$^{+/-}$ ($p < 0.001$ for DCN and PVCN; $p < 0.01$ for AVCN) mice (**Figures 7E**, **8E,J**). Corroborating the protein expression data, *Glt1* mRNA expression in the *Igf1*$^{-/-}$ mice cochlear nuclei was significantly stronger than in the other genotypes ($p < 0.001$; **Figure 7F**).

GLAST Expression in *Igf1*$^{-/-}$ Mice

Like GLT1, a dense network of GLAST immunostained puncta was evident in the neuropil and around the soma of DCN, PVCN and AVCN neurons in *Igf1*$^{+/+}$, *Igf1*$^{+/-}$ and *Igf1*$^{-/-}$ mice (**Figure 9**). However, in contrast to GLT1 there appeared to be no significant differences in the immunostaining among the distinct mouse genotypes, in either the mean gray levels of

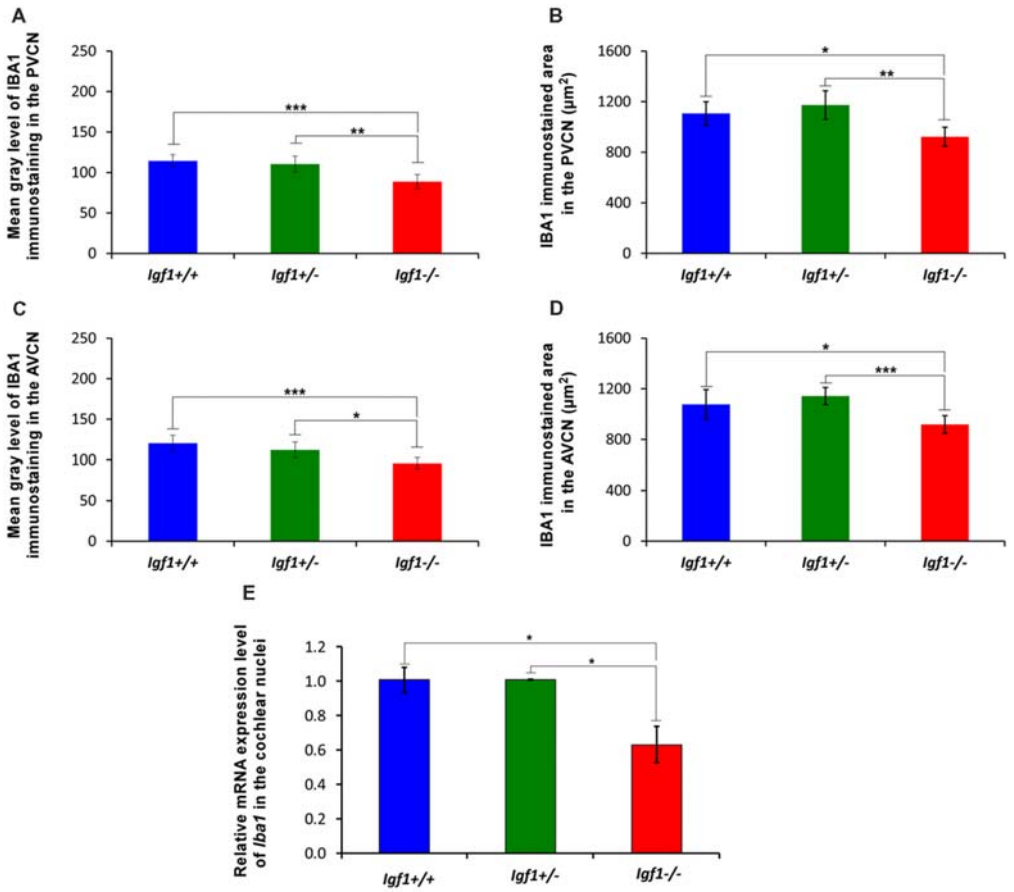

FIGURE 4 | Insulin-like growth factor 1 (IGF-1) deficiency leads to *Iba1* downregulation in *Igf1*$^{-/-}$ mice. Bar graphs showing decreases in the mean gray levels **(A,B)** and immunostained areas **(C,D)** in the *Igf1*$^{-/-}$ mouse cochlear nuclei when compared to *Igf1*$^{+/+}$ and *Igf1*$^{+/-}$ mice. Similar reductions in *Iba1* expression were also detected by RT-quantitative PCR (qPCR; **E**). Error bars indicate the standard deviations of the mean. Statistically significant differences among the animal groups were evaluated by one-factor ANOVA (*$p < 0.05$; **$p < 0.01$, ***$p < 0.001$). Abbreviations: AVCN, anteroventral cochlear nucleus; PVCN, posteroventral cochlear nucleus.

GLAST immunostaining in the DCN ($F_{(2,7)}$ = 0.94, NS), PVCN ($F_{(2,9)}$ = 1.01, NS) and AVCN ($F_{(2,11)}$ = 1.56, NS) or in the immunostained areas in the DCN ($F_{(2,7)}$ = 0.24, NS), PVCN ($F_{(2,9)}$ = 1.56, NS) and AVCN ($F_{(2,11)}$ = 0.93, NS; **Figure 10**). In accordance with these immunohistochemical findings, there were also no differences in *Glast* gene expression in the cochlear nuclei of *Igf1*$^{-/-}$ mice relative to the *Igf1*$^{+/-}$ and *Igf1*$^{-/-}$ mice (**Figure 9J**).

Downregulation of mGluRs in *Igf1*$^{-/-}$ Mice

As the upregulated GLT1 expression is suggestive of abnormal glutamate uptake, the mRNA and protein expression of mGluRs were also examined in the *Igf1*$^{-/-}$ mice cochlear nuclei. As mGluR1α is expressed abundantly in the cochlear nuclei (Lu, 2014), its expression was evaluated at both the mRNA and protein levels, whereas the expression of *mGluR2*, *mGluR*4 a*nd mGluR7* was only based on qPCR analyses. mGluR1α staining was detected in the DCN of *Igf1*$^{+/+}$, *Igf1*$^{+/-}$ and *Igf1*$^{-/-}$ mice, mostly in the neuropil of the molecular layer and on the dendrites of fusiform and cartwheel cells in the granule/fusiform layer (**Figures 11A–C**), (Bilak and Morest, 1998; Petralia et al., 2000). Regardless of the genotype, the immunostaining in the PVCN and AVCN was observed in globular and stellate cells which were identified according to their location within the nucleus, as shown previously (Bilak and Morest, 1998; **Figures 11D–I**). In *Igf1*$^{-/-}$ mice, the mGluR1α staining levels in the dorsal and ventral cochlear nucleus subdivisions were weaker than in the other genotypes (**Figure 11**). When quantified, immunostaining revealed a significant effect of the lack of IGF-1 on the mean gray level of mGluR1α in the DCN ($F_{(2,13)}$ = 18.17, $p < 0.001$), PVCN ($F_{(2,14)}$ = 51.59, $p < 0.001$) and AVCN ($F_{(2,9)}$ = 56.55, $p < 0.001$) and also on the immunostained areas in the DCN ($F_{(2,13)}$ = 18.17, $p < 0.001$), PVCN ($F_{(2,14)}$ = 16.03, $p < 0.01$) and AVCN ($F_{(2,9)}$ = 19.91, $p < 0.001$). According to the *post hoc* test, the mean gray levels in the *Igf1*$^{-/-}$ mice were significantly lower than in the *Igf1*$^{+/+}$ ($p < 0.01$ for the DCN, $p < 0.001$ for the PVCN and AVCN) and *Igf1*$^{+/-}$ ($p < 0.001$ for all nuclei) mice (**Figures 11J,L,N**). Likewise, the immunostained areas of mGluR1α were also smaller in

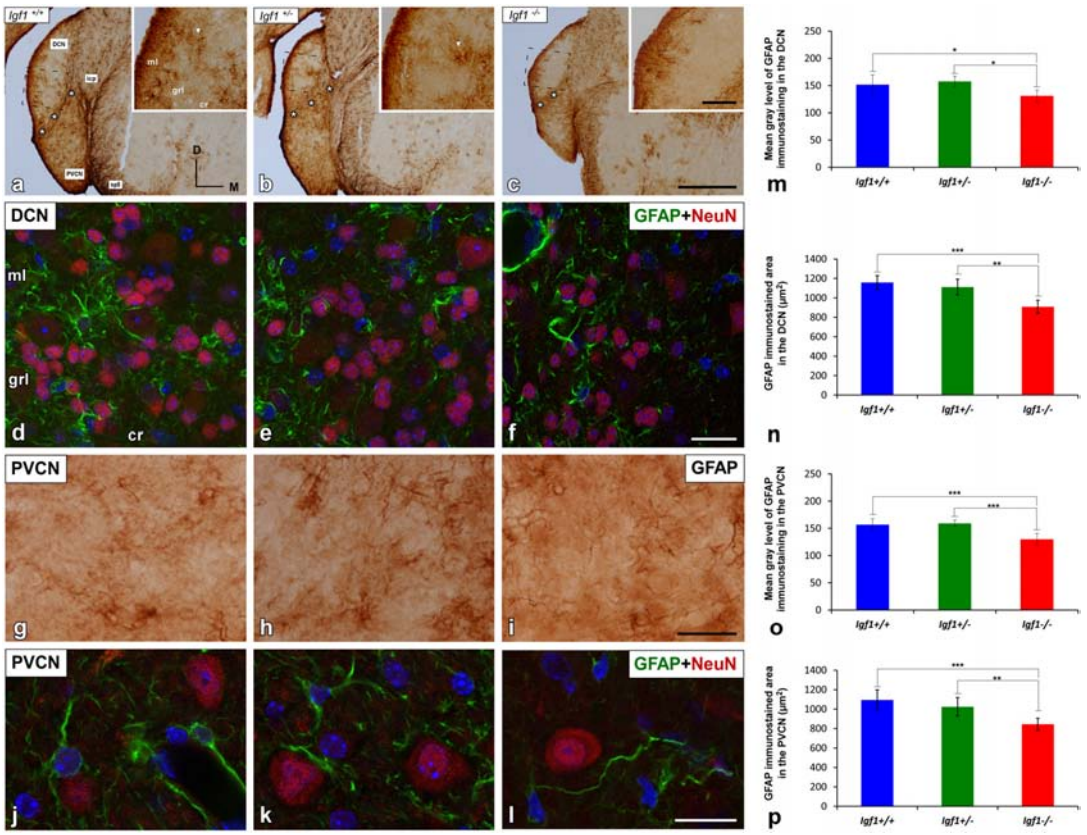

FIGURE 5 | GFAP immunostaining in the DCN and PVCN of *Igf1*$^{-/-}$ mice. GFAP immunostaining was distributed throughout the different DCN layers in all the genotypes analyzed **(A–F)**. GFAP-immunostained astrocytes were strongly stained in the molecular layer while only a few astrocytes were observed in the intermediate layer and central region of the DCN **(A–C)**. Note that some of these astrocytes group together forming patches of immunostaining (arrows in **A,B**). In the *Igf1*$^{-/-}$ mice, GFAP immunostaining was apparently weaker in the deeper layers (grl and cr) of the DCN and in the PVCN than in *Igf1*$^{+/+}$ and *Igf1*$^{+/-}$ mice **(A–C,G–I)**. The spatial relationship between neurons and astrocytes in all genotypes is shown in Z-stack confocal microscopy images of the DCN **(D–F)** and PVCN **(J–L)**. Quantification of the mean gray levels **(M,O)** and stained areas **(N,P)** in these nuclei corroborated the decreases in the immunostaining. Asterisks in **(A–C)** indicate GFAP immunostaining in the granule cell domain. Statistically significant differences among the mouse genotypes were evaluated by one-factor ANOVA (*$p < 0.05$, **$p < 0.01$, ***$p < 0.001$). Cell nuclei in **(D–F)** and **(J–L)** are stained with DAPI (blue). The square boxes in **(A–C)** indicate the location of the higher magnification images shown in **(A–C**; insets). Abbreviations: cr, central region of the dorsal cochlear nucleus (DCN); GFAP, glial fibrillary acidic protein; grl, granule/fusiform layer; ml, molecular layer; NeuN, neuronal marker; PVCN, posteroventral cochlear nucleus; sp5, spinal trigeminal nucleus. Scale bars: 500 μm in (**C**; it also applies to **A,B**); 100 μm in the inset in (**C**; it also applies to insets in **A,B**); 20 μm in (**F,I**; it also applies to **D,E,G,H**) and 50 μm in (**L**; it also applies to **J,K**).

the *Igf1*$^{-/-}$ mice than in the *Igf1*$^{+/+}$ ($p < 0.001$ for the DCN, $p < 0.01$ for the PVCN and AVCN) and *Igf1*$^{+/-}$ ($p < 0.01$ for all nuclei) mice (**Figures 11K,M,O**). Significant decreases in *mGluR1, mGluR2* and *mGluR4* gene expression were detected in the *Igf1*$^{-/-}$ mouse cochlear nucleus relative to the wild-type mice. Although *mGluR7* expression also appeared to be weaker, this difference did not reach statistical significance (**Figure 12**).

DISCUSSION

The present study demonstrates that IGF-1 deficiency leads to alterations in glial morphology, a decreased expression and protein accumulation in IBA1 and GFAP, an upregulation of GLT1 but not GLAST, and the downregulation of groups I, II and III mGluRs. Our previous findings in *Igf1*$^{-/-}$ mice demonstrated that primary cochlear afferents upregulate their VGluT1 protein but not the vesicular GABA transporter (VGAT), suggesting that presynaptic excitatory neurotransmission may be impaired. This synaptic plasticity might be mediated by MEF2 proteins, which are downregulated in both the cochlea and the cochlear nucleus, and which may reflect enhanced synaptic efficacy (Fuentes-Santamaría et al., 2016). As an activity-dependent factor, rapid elevations of IGF-1 within neurons in response to modifications in cochlear activity have been associated with synaptic rearrangements in the rat cochlear nucleus (Alvarado et al., 2007a; Fuentes-Santamaría et al., 2007, 2012, 2013). In other brain structures like the hippocampus, IGF-1 is also a regulator of excitatory synaptic transmission (Ramsey et al., 2005; Xing et al., 2007; Deak and Sonntag, 2012). Indeed, the effects of a reduced density of glutamatergic terminals in the hippocampus of mice with low-serum IGF-1 levels is ameliorated by continued systemic IGF-1 administration (Trejo et al., 2007).

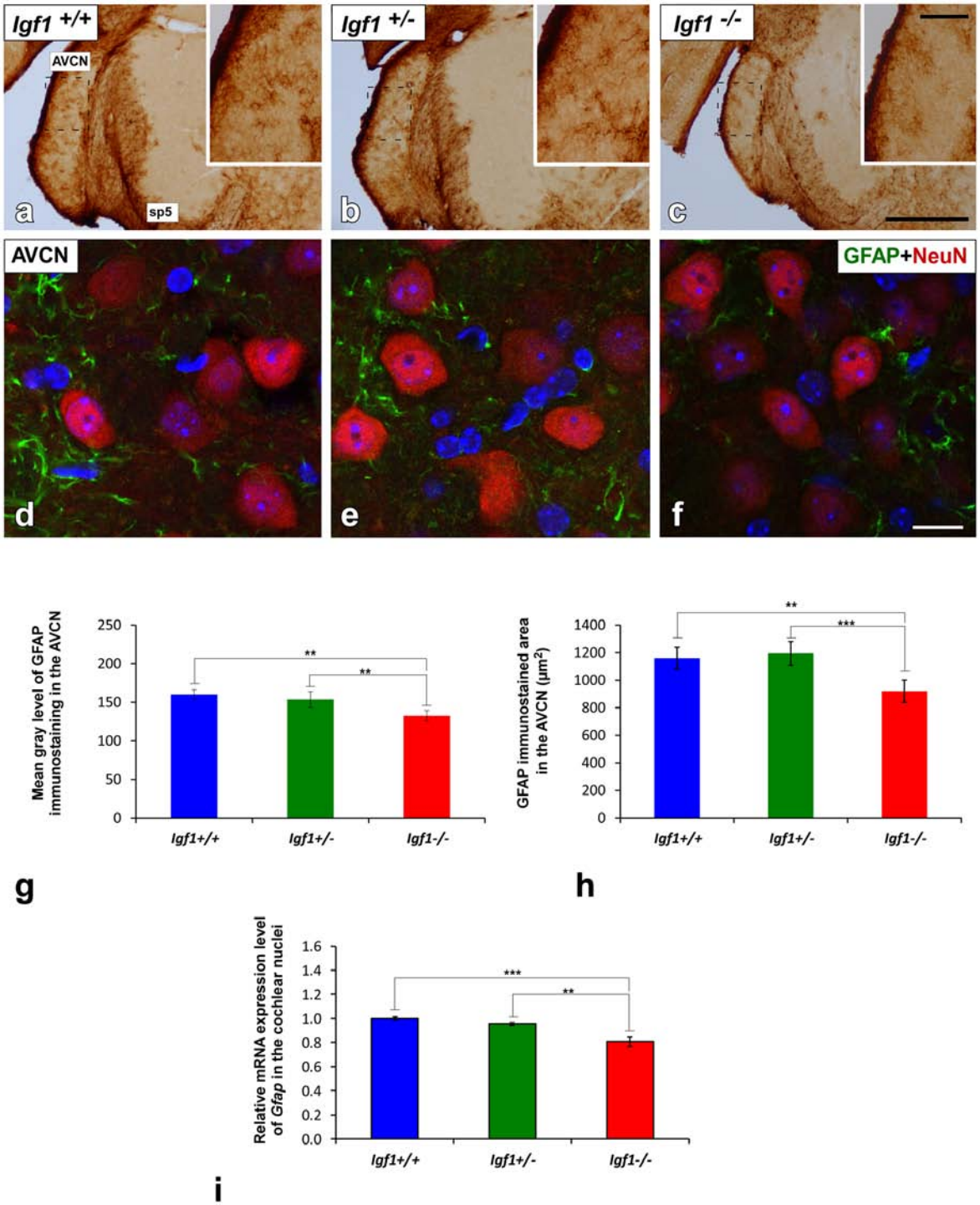

FIGURE 6 | GFAP immunostaining in the AVCN of *Igf1*$^{-/-}$ mice. Analysis of GFAP immunostaining in the *Igf1*$^{-/-}$ mice showed that there were fewer astrocytes and they were less intensely stained **(C,F)** when compared to *Igf1*$^{+/+}$ **(A,D)** and *Igf1*$^{+/-}$ mice **(B,E)**. Z-stack confocal microscopy images of GFAP and NeuN double-labeling are shown for all genotypes **(D–F)**. The apparent decrease in GFAP immunostaining in the *Igf1*$^{-/-}$ mouse was corroborated by quantifying the mean gray levels **(G)** and the stained areas **(H)**. The qualitative and quantitative data were confirmed when RT-qPCR data showed decreased *Gfap* expression in the *Igf1*$^{-/-}$ mouse cochlear nuclei **(I)**. The error bars indicate the standard deviations of the mean. Statistically significant differences among the animal groups were evaluated by one-factor ANOVA (**$p < 0.01$, ***$p < 0.001$). Cell nuclei are stained with DAPI (blue). The square boxes in a-c indicate the location of the higher magnification images shown in (**A–C**; insets). Abbreviations: AVCN, anteroventral cochlear nucleus; GFAP, glial fibrillary acidic protein; NeuN, neuronal marker; sp5, spinal trigeminal nucleus. Scale bars: 500 µm in (**C**; it also applies to **A,B**); 100 µm in the inset in (**C**; it also applies to insets in **A,B**) and 20 µm in (**F**; it also applies to **D,E**).

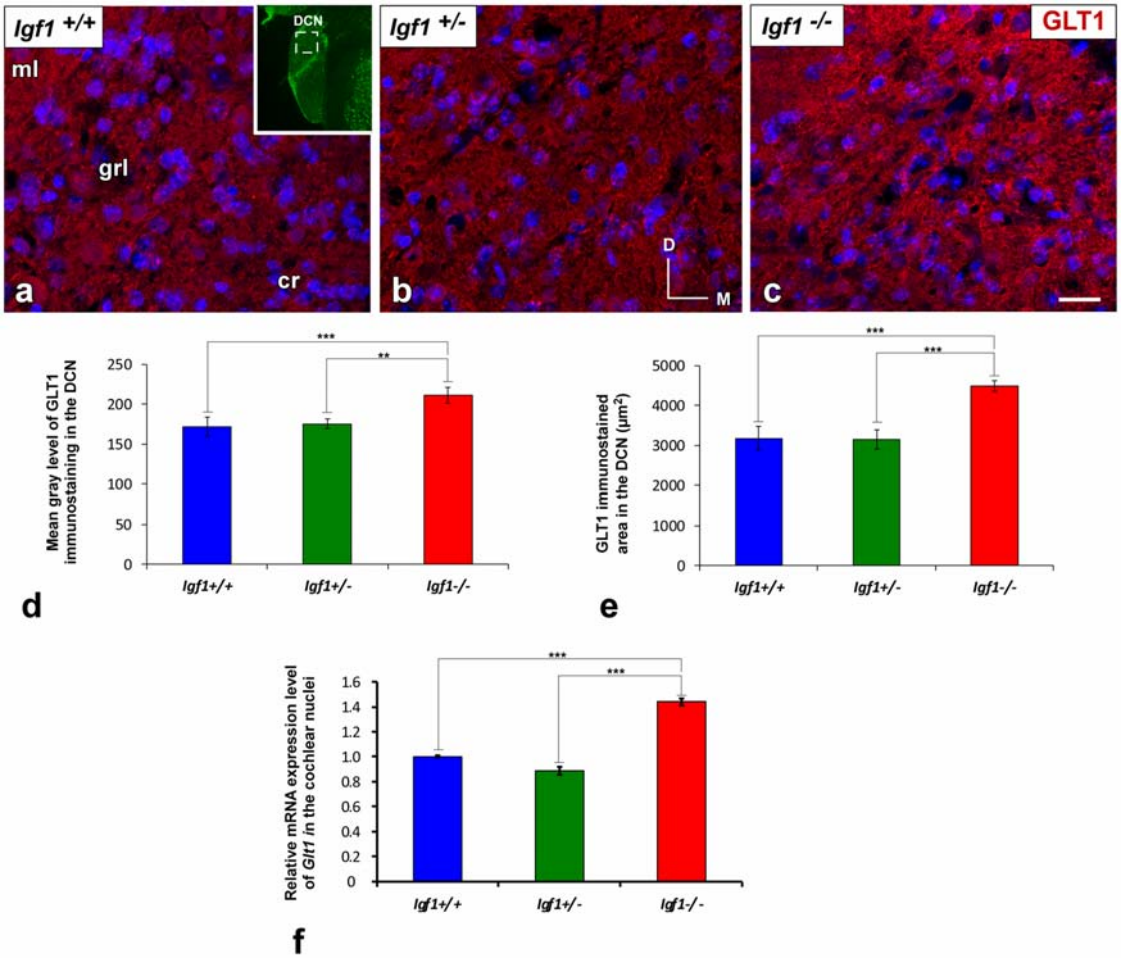

FIGURE 7 | Upregulation of GLT1 in the DCN of *Igf1*$^{-/-}$ mice. In the *Igf1*$^{-/-}$ mouse, the strongly GLT1 immunostained puncta (red) were found in all layers of the nucleus and presumptively occupied a larger area **(C)** than in the other genotypes **(A,B)**. These qualitative observations were corroborated by significant increases in the mean gray levels and the immunostained areas **(D,E)**. Similar increases in the IGF-1 deficient DCN were also detected by quantifying *Glt1* mRNA expression **(F)**. The inset in (**A**; pseudo-colored green for higher contrast) indicates the approximate location of the fields shown in **(A–C)**. Error bars indicate the standard deviations of the mean. Statistically significant differences among the animal groups were evaluated by one-factor ANOVA (**$p < 0.01$, ***$p < 0.001$). Cell nuclei are stained with DAPI (blue). Abbreviations: cr, central region of the dorsal cochlear nucleus (DCN); GLT1, glutamate transporter 1; grl, granule/fusiform layer; ml, molecular layer. Scale bar: 20 μm in (**C**; it also applies to **A**,**B**).

The effects of IGF-1 on glial cells have been studied in different systems. When non-astrocytic inner retinal glia-like cells are stimulated by IGF-1 in the avian retina, retinal neurons and Müller glia are more vulnerable to excitotoxic damage (Fischer et al., 2010). In the mouse retina, IGF-1 deficiency causes age-associated retinal gliosis (Arroba et al., 2018). In cerebellar cultures, blocking the IGF-1 receptor in astrocytes reduces their capacity to rescue neurons damaged by oxidative stress, suggesting that this growth factor is crucial for these non-neuronal cells to exert their protective effects (Genis et al., 2014). Moreover, transgenic mice overexpressing IGF-1 in the retina develop gliosis and microgliosis, along with impaired glutamate recycling, which leads to cell death. Hence, glial cells appear to be involved in the regulation of excitatory synaptic function (Villacampa et al., 2013). Our data demonstrate that *Igf1*$^{-/-}$ mice have less *Iba1* mRNA and, consequently, lower IBA1 protein levels along with decreases in the mean gray levels of IBA1 immunostaining and immunostained areas in both cochlear nucleus subdivisions. *Igf1*$^{-/-}$ mice display structural modifications of microglia including decreases in the number of cells per field, shorter processes length and a reduction in microglial branching as compared to heterozygous and wildtype mice. The contribution of microglia to the adaptive responses that take place in the auditory nuclei in response to cochlear damage induced by acoustic trauma or cochlear ablation has been well documented (Fuentes-Santamaría et al., 2012; Dinh et al., 2014; Janz and Illing, 2014; Baizer et al., 2015). In this regard, lesion-induced microglial activation may exert regulatory influences on cochlear nucleus synapses, contributing to structural and functional remodeling. Recent data from microglia depletion models indicated that the loss of microglia during brain development leads to defective

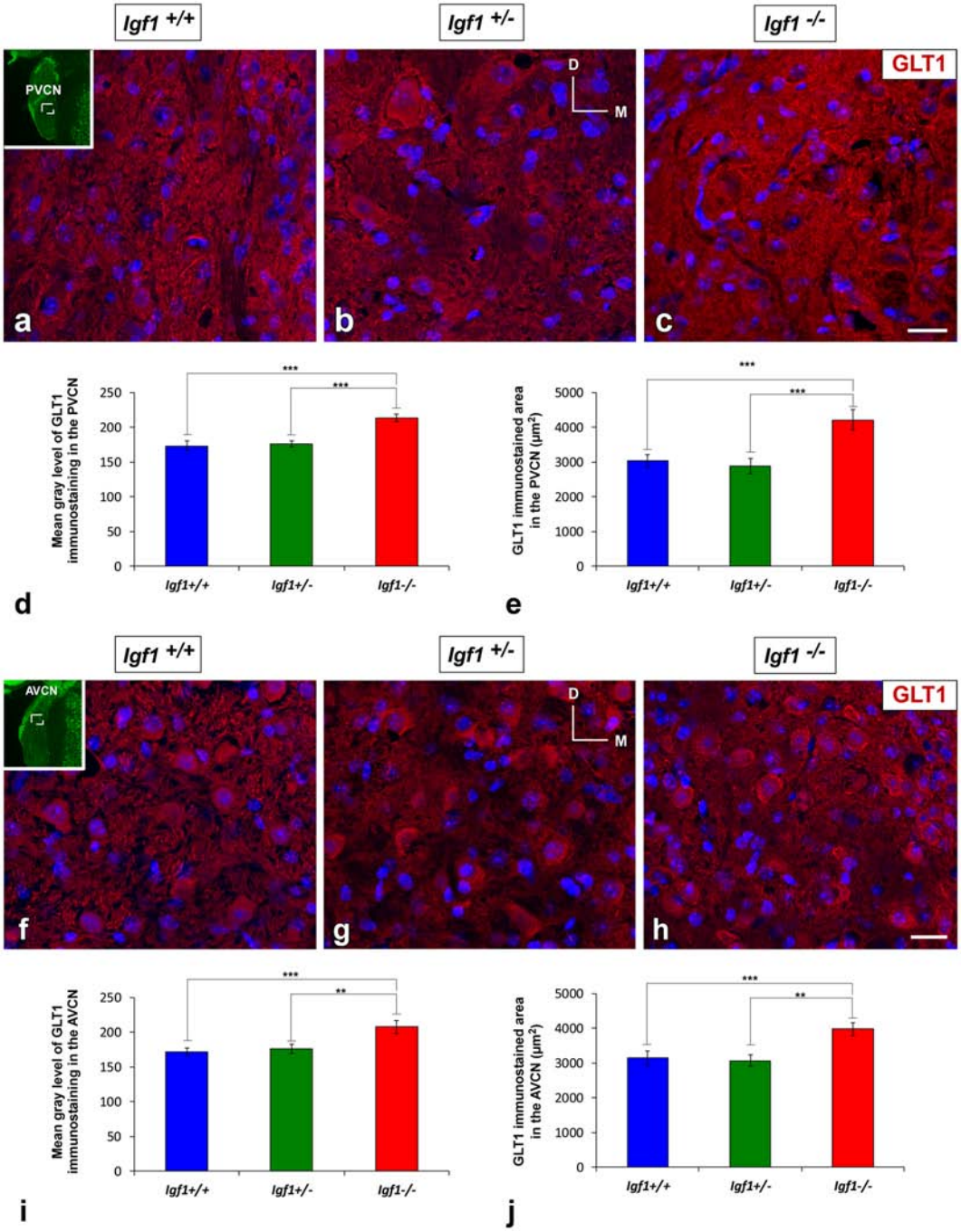

FIGURE 8 | Upregulation of GLT1 in the ventral cochlear nuclei of *Igf1*$^{-/-}$ mice. Z-stack confocal microscopy images show enhanced GLT1 immunostaining (red) in the IGF-1 deficient ventral cochlear nucleus **(C,H)** relative to the *Igf1*$^{+/+}$ **(A,F)** and *Igf1*$^{+/-}$ mice **(B,G)**. Quantification of the immunostaining confirmed this upregulation in both the PVCN **(D,E)** and AVCN **(I,J)**. The inset in (**A,F**; pseudo-colored green for higher contrast) indicates the approximate location of the fields shown in **(A–C,F–H)**; for the PVCN and AVCN, respectively. The error bars indicate the standard deviations of the mean. Statistically significant differences among the animal groups were evaluated by one-factor ANOVA (**$p < 0.01$, ***$p < 0.001$). Cell nuclei are stained with DAPI (blue). Abbreviations: AVCN, anteroventral cochlear nucleus; GLT1, glutamate transporter 1; PVCN, posteroventral cochlear nucleus. Scale bar: 20 µm in (**C,H**; it also applies to **A,B,F,G**).

glial-synapse communication and aberrant synaptic maturation (Paolicelli and Ferretti, 2017). Indeed, the absence of IGF-1 leads to an ineffective refinement of cochlear synapses during postnatal maturation, which results in dysfunctional excitatory connections in the adult cochlear nucleus (Camarero et al., 2001; Riquelme et al., 2010; Fuentes-Santamaría et al., 2016). Given that microglial motility is primarily involved in reshaping neuronal circuits during development, and in supporting and maintaining

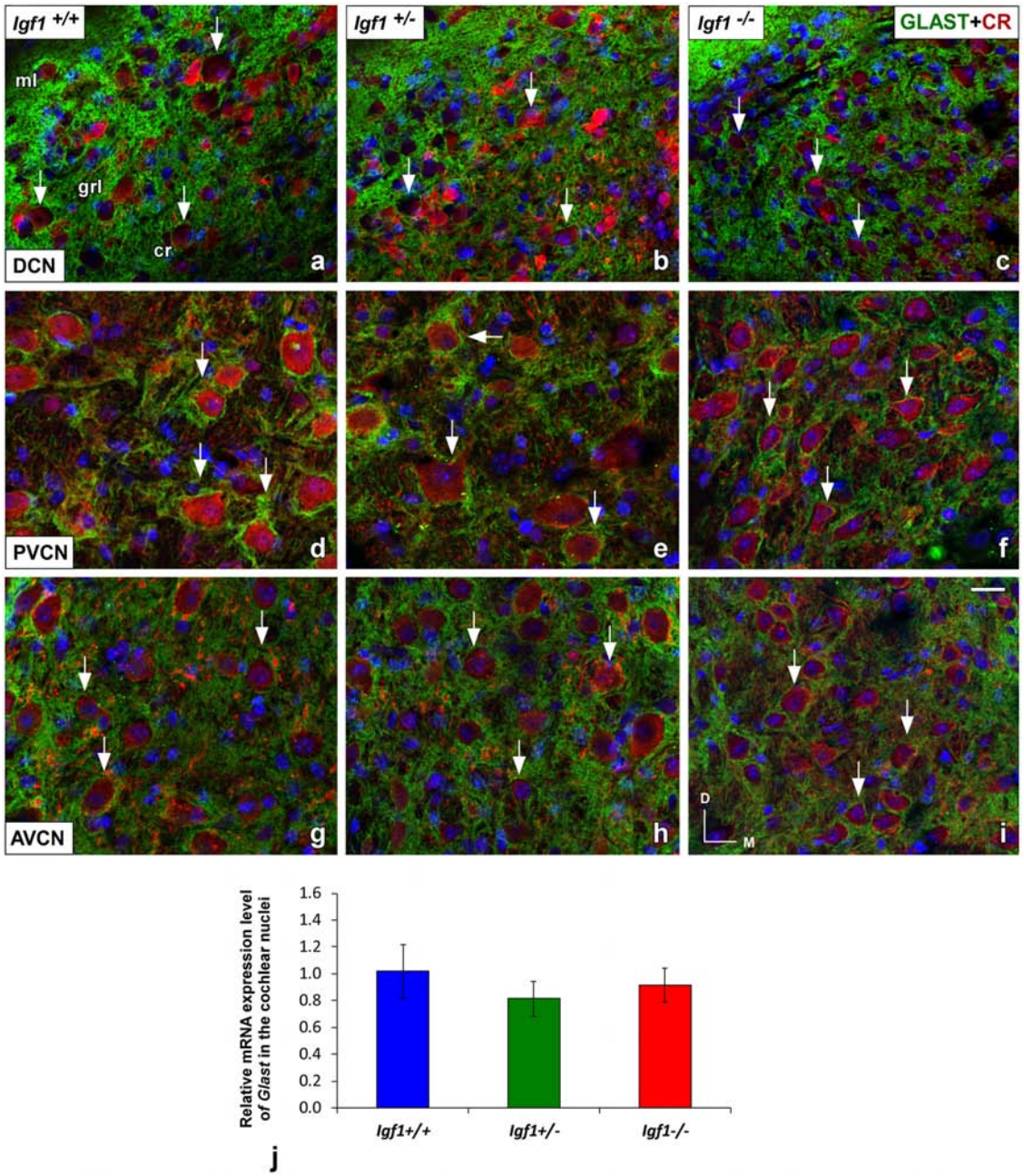

FIGURE 9 | Glutamate aspartate transporter (GLAST) immunostaining in the *Igf1*$^{-/-}$ mice cochlear nuclei. In all genotypes, GLAST stained puncta (green) were densely distributed throughout the neuropil and on the soma of DCN **(A–C)**, PVCN **(D–F)** and AVCN **(G–I)** neurons immunostained with CR (red). No differences were observed in the distribution of the immunostaining among the three groups. The analysis of *Glast* expression levels by RT-qPCR confirmed these immunohistochemical results **(J)**. The error bars indicate the standard deviations of the mean. Arrows point to CR-immunostained cells. Cell nuclei are stained with DAPI (blue). Abbreviations: AVCN, anteroventral cochlear nucleus; cr, central region of the DCN (dorsal cochlear nucleus); CR, calretinin; GLAST, glutamate aspartate transporter; grl, granule/fusiform layer; ml, molecular layer; PVCN, posteroventral cochlear nucleus. Scale bar: 20 μm in (**I**; it also applies to **A–H**).

active synapses in the adult brain, limited microglial branching due to IGF-1 deficiency may produce defective neuronal-glial communication and consequently, abnormal synaptic transmission in auditory nuclei.

Astrocytes continuously exchange signals with pre- and postsynaptic elements at the tripartite synapse, and they are also crucial for the formation and maintenance of glutamatergic synapses due to their dynamic involvement in the processing and integration of synaptic information (Ricci et al., 2009; Villalba and Smith, 2011; Kim et al., 2017; Papouin et al., 2017). Our data in the *Igf1*$^{-/-}$ mouse reveal a significant decrease in GFAP protein and mRNA, as well as reductions in astrocyte

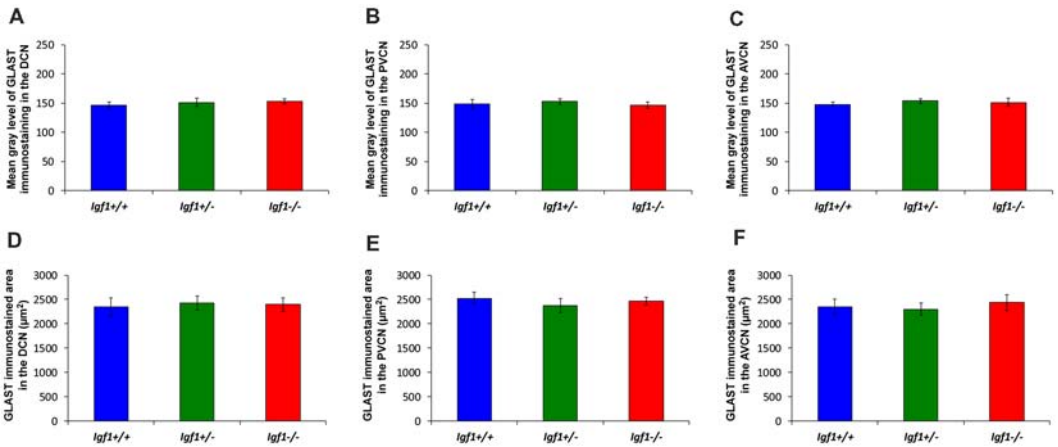

FIGURE 10 | Histograms showing the mean gray levels of GLAST immunostaining and the immunostained areas in the cochlear nuclei of *Igf1*$^{-/-}$, *Igf1*$^{+/-}$ and *Igf1*$^{+/+}$ mice. Analysis of the immunostaining indicated that there were no significant differences among the genotypes in either the mean gray levels of immunostaining **(A–C)** or in the immunostained areas **(D–F)** in the DCN, PVCN and AVCN. The error bars indicate the standard deviations of the mean. Abbreviations: DCN, dorsal cochlear nucleus; PVCN, posteroventral cochlear nucleus; AVCN, anteroventral cochlear nucleus.

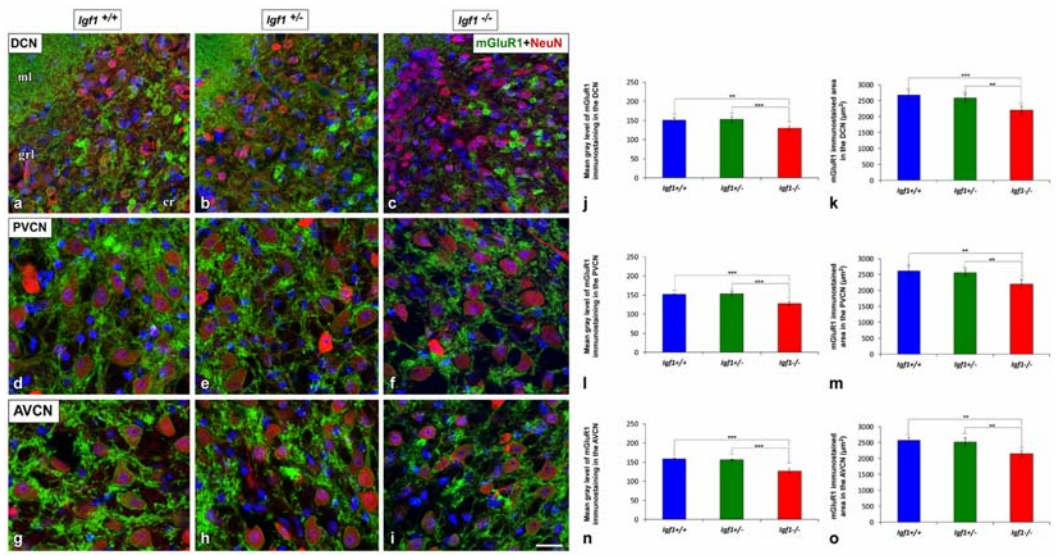

FIGURE 11 | Downregulation of mGluR1α in the cochlear nuclei of *Igf1*$^{-/-}$ mice. In the *Igf1*$^{-/-}$ mice, there was less mGluR1α staining (green) in the molecular and granule layers of the DCN than in the other genotypes **(A–C)**. Similar decreases were also detected in *Igf1*$^{-/-}$ mouse PVCN **(D–F)** and AVCN **(G–I)**. Quantification confirmed these qualitative decreases in the *Igf1*$^{-/-}$ mouse relative to the *Igf1*$^{+/+}$ and *Igf1*$^{+/-}$ mice **(J–O)**. The error bars indicate the standard deviations of the mean. Statistically significant differences among the animal groups were evaluated by one-factor ANOVA (**$p < 0.01$, ***$p < 0.001$). Neurons are stained with NeuN antibody (red) and cell nuclei are stained with DAPI (blue). Abbreviations: AVCN, anteroventral cochlear nucleus; cr, central region of the dorsal cochlear nucleus (DCN); grl, granule/fusiform layer; ml, molecular layer; mGluR1, metabotropic glutamate receptor 1; NeuN, neuronal marker; PVCN, posteroventral cochlear nucleus. Scale bar: 20 μm in (**I**; it also applies to **A–H**).

density. In this regard, the loss of GFAP in *Igf1*$^{-/-}$ mice results in increased synaptic plasticity and altered GLT activity, suggesting that GFAP expression is essential to correctly regulate glutamatergic neurotransmission (Hughes et al., 2004). It is worth noting that the morphological and functional plasticity of the astrocyte is achieved through polymerization/assembly and depolymerization/disassembling of GFAP which acts a scaffolding network for the translocation of GFAP-associated functional molecules (Wang and Parpura, 2018), such as the GLTs. Accordingly, it has been proposed that the glutamate-mediated localization of GLT1 and GLAST in the astrocyte membrane is highly dependent on the actin cytoskeleton of this glial cell (Duan et al., 1999; Zhou, 2004). Astrocyte dysfunction may modify the coverage of neurons by glia, increasing neuronal communication and influencing glutamate concentrations and therefore, the activity of carriers and receptors. GLT1 and GLAST

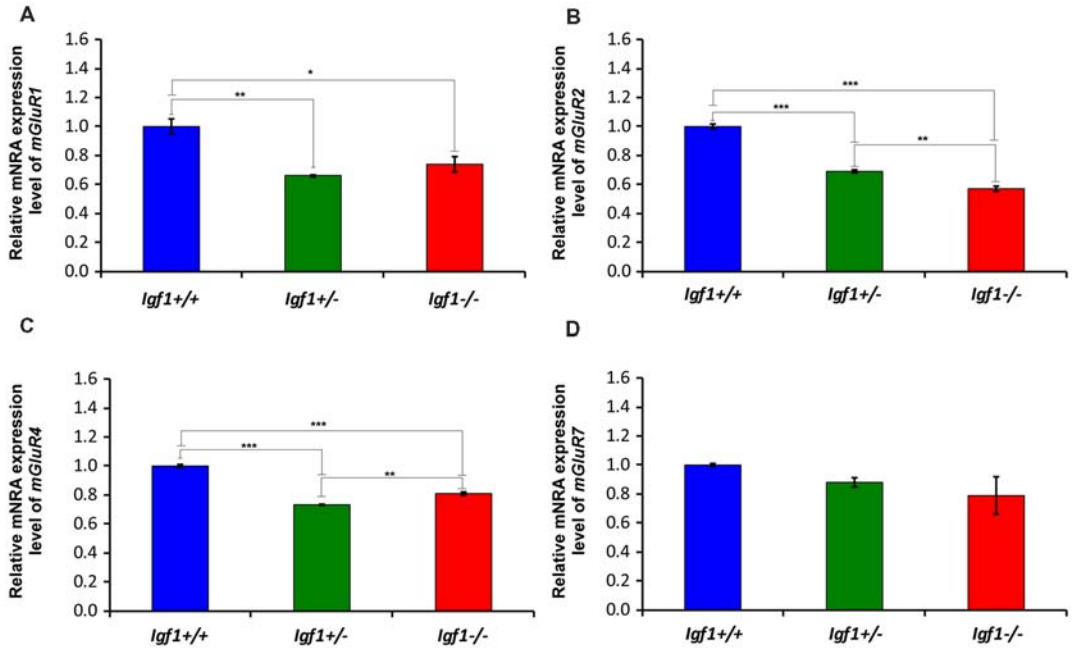

FIGURE 12 | The loss of IGF-1 leads to *mGluR1α, mGluR2α, mGluR4α and mGluR7α* downregulation. The *mGluR1α, mGluR2α, mGluR4α and mGluR7α* mRNA expression was determined by RT-qPCR in 4-month-old *Igf1*$^{-/-}$, *Igf1*$^{+/-}$ and *Igf1*$^{+/+}$ mice. The results demonstrate a decline in *mGluR1α* **(A)**, *mGluR2α* **(B)**, *mGluR4α* **(C)** and *mGluR7α* **(D)** expression in the *Igf1*$^{-/-}$ mouse when compared with *Igf1*$^{+/-}$ and *Igf1*$^{+/+}$ mice. Note that the decrease in *mgluR7α* expression in the *Igf1*$^{-/-}$ mice was not statistically significant. Also, they show a significant downregulation of *mGluR1α* **(A)**, *mGluR2α* **(B)** and *mGluR4α* in heterozygous mice compared with their age-matched control mice. The error bars indicate the standard deviations of the mean. Statistically significant differences among the animal groups were evaluated by one-factor ANOVA (*$p < 0.05$; **$p < 0.01$, ***$p < 0.001$).

are both high-affinity, sodium-dependent GLTs located on perisynaptic processes of astrocytes and closely associated with excitatory synapses. In cultures of chick cerebellar Bergmann glia cells, GLT1 activity is modulated by IGF-1 signaling (Gamboa and Ortega, 2002) and thus, the absence of this factor may alter excitatory signaling.

GLT1 dysfunction has been linked to several neurological disorders in which glutamate homeostasis is impaired (Verkhratsky et al., 2012; Soni et al., 2014). For instance, upregulation of GLT1 expression improves signs of Huntington's disease in symptomatic R6/2 mice (Miller et al., 2008) and enhanced GLT1 expression also has been detected in the prefrontal cortex of schizophrenic patients, suggesting impaired glutamatergic transmission in this disease (Matute et al., 2005). GLT1 also appears to be upregulated in *Igf1*$^{-/-}$ mice, the predominant glial GLT, while the expression and accumulation of the GLAST protein were not modified. In line with these observations, GLT1 immunoreactivity is enhanced in cerebellar synaptosomal preparations of *Gfap*$^{-/-}$ mice when compared to wild-type animals (Hughes et al., 2004). Such upregulation in cerebellar synaptic GLT1 protein expression may facilitate the rapid uptake of synaptic glutamate through the activation of mGluRs, suggesting a pivotal role for GFAP in trafficking GLTs. Based on these observations, our results provide evidence of IGF-1-dependent regulation of astrocytes, that alters glial glutamate transport capacity and therefore, excitatory synapses. Although the number of astrocytes and/or transporters per cell was not assessed for each genotype in the current study, it is plausible to postulate that an upregulation in GLT1 in the mutant mouse would contribute to clear excessive glutamate resultant from increased neuronal interactions in response to astrocytes loss and/or dysfunction. Indeed, GLT1 is responsible for most of the glutamate uptake (90%) around excitatory synapses (Lehre and Danbolt, 1998), although the mechanisms that drive the increase in GLT1 in the *Igf1*$^{-/-}$ mice are still unclear.

GLT1 overexpression near synapses could have important consequences for the kinetics of glutamate uptake and hence, on mGluR levels in the cochlear nuclei. For instance, an upregulation in GLT1 in the *Igf1*$^{-/-}$ cochlear nuclei will reduce the amount of glutamate available in the synaptic cleft, thus resulting in decreased glutamate binding to mGluRs (Huang et al., 2004). This decrease, in turn, would lead to significantly dampen the gene expression levels of *mGluR1*, *mGluR2*, *mGluR4* and *mGluR7*, as demonstrated in this study. In accordance with our data, previous studies have demonstrated that *mGluR1* is detected in the DCN of rodents under normal physiological conditions, particularly on unipolar brush cells and cartwheel cells, and also in globular bushy cells and stellate cells in the PVCN and AVCN (Bilak and Morest, 1998; Kemmer and Vater, 2001). Although the mGluR1 in the cochlear nuclei is mostly found post-synaptically, it has also been detected in presynaptic elements (Petralia et al., 1996; Wright et al., 1996). mGluR2 is also expressed in

the cochlear nuclei while the expression of mGluR4 and mGluR7 remains unclear (Lu, 2014). *In vivo* and *in vitro* studies in the chick cochlear nucleus, nucleus magnocellularis, have demonstrated that pharmacological blockade of groups I and II mGluR activation provokes neuronal degeneration, suggesting a pivotal role for these receptors in regulating neuronal survival (Nicholas and Hyson, 2004; Diaz et al., 2009; Carzoli and Hyson, 2011, 2014). The activation of these receptors also regulates glutamate uptake at the cochlear nucleus-auditory nerve synapse, preventing the excitotoxic accumulation of extracellular glutamate (Carzoli and Hyson, 2014). Whole cell recordings in brain slice preparations demonstrated that the activity of mGluRs suppresses GABAergic transmission (Lu, 2007), highlighting their role in achieving balanced excitation and inhibition in the nucleus magnocellularis.

In summary, adult *Igf1*$^{-/-}$ mice show modifications in the morphological features of the glutamatergic synapses (presynaptic and postsynaptic components) that lead to excitatory synaptic plasticity, which involves not only auditory neurons but also glial cells. Although the role of microglia in this process is unclear, their reduced arborization may result in more prolonged microglia response times and therefore, lead to decreased modulation of neuronal activity. On the other hand, the reduction in the fine astrocytic processes may facilitate neuronal interactions that, along with an enhanced expression of GLT1, would contribute to regulation of synaptic glutamate resulting from excessive neuronal activation.

CONCLUSION

The results presented here suggest that absence of IGF-1 leads to central adaptive events in the adult *Igf1*$^{-/-}$ cochlear nuclei, which include structural impairment of microglia and astrocytes, upregulation in GLT1 expression, and downregulation of mGluRs. These morphological alterations may contribute to adaptation of auditory neurons and their synaptic connections to changing levels of activity, due to the imbalances in neurotransmission. Determining the molecular, biochemical and morphological mechanisms underlying neuronal plasticity in a mouse model of hearing deficits will give us insight into new therapeutic strategies that could help to maintain or even improve residual hearing when human deafness is related to IGF-1 deficiency.

AUTHOR CONTRIBUTIONS

All authors had full access to all the data in the study and take responsibility for the integrity of the data and the accuracy of the data analysis. VF-S, JA and IV-N: study concept and design. VF-S, JA and LR-R: acquisition of data, statistical analysis and interpretation of data. VF-S and JA: drafting of the manuscript. VF-S, JA, LR-R, IV-N and JJ: critical revision of the manuscript for important intellectual content. IV-N, VF-S and JJ: obtaining funding.

FUNDING

This work was supported by the Spanish Ministerio de Economía y Competitividad (MINECO; SAF2016-788898-C2-1R) to JJ and VF-S; Seventh Framework Programme (FP7)-HEALTH-2012-INNOVATON (#304925) to JJ; CIBERER/FEDER ACCI-ER16P5AC7091 and ER17P5AC7612 to LR-R; and Spanish MINECO/FEDER (SAF2014-53979-R), FP7-PEOPLE-2013-IAPP TARGEAR, CIBERER/FEDER (ACCI-ER16P5AC7091 and ER17P5AC7612) to IV-N. LR-R holds a contract supported by CIBERER (Institute of Health Carlos III) co-financed with FEDER funds.

ACKNOWLEDGMENTS

We would like to thank Maria Cruz Gabaldón for her excellent technical assistance and the Neurobiology of Hearing group (IIBm, CSIC-UAM) for sharing procedures, information and helpful discussions.

REFERENCES

Adams, M. M., Shi, L., Linville, M. C., Forbes, M. E., Long, A. B., Bennett, C., et al. (2008). Caloric restriction and age affect synaptic proteins in hippocampal CA3 and spatial learning ability. *Exp. Neurol.* 211, 141–149. doi: 10.1016/j.expneurol.2008.01.016

Alvarado, J. C., Fuentes-Santamaría, V., Franklin, S. R., Brunso-Bechtold, J. K., and Henkel, C. K. (2007a). Synaptophysin and insulin-like growth factor-1 immunostaining in the central nucleus of the inferior colliculus in adult ferrets following unilateral cochlear removal: a densitometric analysis. *Synapse* 61, 288–302. doi: 10.1002/syn.20373

Alvarado, J. C., Stanford, T. R., Vaughan, J. W., and Stein, B. E. (2007b). Cortex mediates multisensory but not unisensory integration in superior colliculus. *J. Neurosci.* 27, 12775–12786. doi: 10.1523/jneurosci.3524-07.2007

Alvarado, J. C., Fuentes-Santamaría, V., Gabaldón-Ull, M. C., Blanco, J. L., and Juiz, J. M. (2014). Wistar rats: a forgotten model of age-related hearing loss. *Front. Aging Neurosci.* 6:29. doi: 10.3389/fnagi.2014.00029

Alvarado, J. C., Fuentes-Santamaría, V., Henkel, C. K., and Brunso-Bechtold, J. K. (2004). Alterations in calretinin immunostaining in the ferret superior olivary complex after cochlear ablation. *J. Comp. Neurol.* 470, 63–79. doi: 10.1002/cne.11038

Arganda-Carreras, I., Fernández-González, R., Muñoz-Barrutia, A., and Ortiz-De-Solorzano, C. (2010). 3D reconstruction of histological sections: application to mammary gland tissue. *Microsc. Res. Tech.* 73, 1019–1029. doi: 10.1002/jemt.20829

Arroba, A. I., Campos-Caro, A., Aguilar-Diosdado, M., and Valverde, Á. M. (2018). IGF-1, inflammation and retinal degeneration: a close network. *Front. Aging Neurosci.* 10:203. doi: 10.3389/fnagi.2018.00203

Atoji, Y., and Islam, M. R. (2009). Distribution of glutamate transporter 1 mRNA in the central nervous system of the pigeon (*Columba livia*). *J. Chem. Neuroanat.* 37, 234–244. doi: 10.1016/j.jchemneu.2009.03.002

Bacci, A., Verderio, C., Pravettoni, E., and Matteoli, M. (1999). The role of glial cells in synaptic function. *Philos. Trans. R. Soc. Lond. B Biol. Sci.* 354, 403–409. doi: 10.1098/rstb.1999.0393

Baizer, J. S., Wong, K. M., Manohar, S., Hayes, S. H., Ding, D., Dingman, R., et al. (2015). Effects of acoustic trauma on the auditory system of the rat: the role of microglia. *Neuroscience* 303, 299–311. doi: 10.1016/j.neuroscience.2015.07.004

Benediktsson, A. M., Marrs, G. S., Tu, J. C., Worley, P. F., Rothstein, J. D., Bergles, D. E., et al. (2012). Neuronal activity regulates glutamate transporter dynamics in developing astrocytes. *Glia* 60, 175–188. doi: 10.1002/glia.21249

Benson, C. G., Gross, J. S., Suneja, S. K., and Potashner, S. J. (1997). Synaptophysin immunoreactivity in the cochlear nucleus after unilateral

cochlear or ossicular removal. *Synapse* 25, 243–257. doi: 10.1002/(SICI)1098-2396(199703)25:3<243::AID-SYN3>3.0.CO;2-B

Bilak, S. R., and Morest, D. K. (1998). Differential expression of the metabotropic glutamate receptor mGluR1α by neurons and axons in the cochlear nucleus: in situ hybridization and immunohistochemistry. *Synapse* 28, 251–270. doi: 10.1002/(SICI)1098-2396(199804)28:4<251::AID-SYN1>3.0.CO;2-8

Burette, A., Jalenques, I., and Romand, R. (1998). Developmental distribution of astrocytic proteins in the rat cochlear nucleus. *Dev. Brain Res.* 107, 179–189. doi: 10.1016/S0165-3806(97)00212-5

Camarero, G., Avendano, C., Fernandez-Moreno, C., Villar, A., Contreras, J., de Pablo, F., et al. (2001). Delayed inner ear maturation and neuronal loss in postnatal Igf-1-deficient mice. *J. Neurosci.* 21, 7630–7641. doi: 10.1523/jneurosci.21-19-07630.2001

Camarero, G., Villar, M. A., Contreras, J., Fernández-Moreno, C., Pichel, J. G., Avendaño, C., et al. (2002). Cochlear abnormalities in insulin-like growth factor-1 mouse mutants. *Hear. Res.* 170, 2–11. doi: 10.1016/s0378-5955(02)00447-1

Caminos, E., Vaquero, C. F., and Martinez-Galan, J. R. (2015). Relationship between rat retinal degeneration and potassium channel KCNQ5 expression. *Exp. Eye Res.* 131, 1–11. doi: 10.1016/j.exer.2014.12.009

Carzoli, K. L., and Hyson, R. L. (2011). *In vivo* analysis of the role of metabotropic glutamate receptors in the afferent regulation of chick cochlear nucleus neurons. *Hear. Res.* 272, 49–57. doi: 10.1016/j.heares.2010.10.020

Carzoli, K. L., and Hyson, R. L. (2014). Activation of metabotropic glutamate receptors regulates ribosomes of cochlear nucleus neurons. *PloS One* 9:e111243. doi: 10.1371/journal.pone.0111243

Cediel, R., Riquelme, R., Contreras, J., Díaz, A., and Varela-Nieto, I. (2006). Sensorineural hearing loss in insulin-like growth factor I-null mice: a new model of human deafness. *Eur. J. Neurosci.* 23, 587–590. doi: 10.1111/j.1460-9568.2005.04584.x

Chen, Z., Kujawa, S. G., and Sewell, W. F. (2010). Functional roles of high-affinity glutamate transporters in cochlear afferent synaptic transmission in the mouse. *J. Neurophysiol.* 103, 2581–2586. doi: 10.1152/jn.00018.2010

Chung, H. J., Jan, Y. N., and Jan, L. Y. (2006). Polarized axonal surface expression of neuronal KCNQ channels is mediated by multiple signals in the KCNQ2 and KCNQ3 C-terminal domains. *Proc. Natl. Acad. Sci. U S A* 103, 8870–8875. doi: 10.1073/pnas.0603376103

Danbolt, N. C. (2001). Glutamate uptake. *Prog. Neurobiol.* 65, 1–105. doi: 10.1016/s0301-0082(00)00067-8

Deak, F., and Sonntag, W. E. (2012). Aging, synaptic dysfunction, and insulin-like growth factor (IGF)-1. *J. Gerontol. A Biol. Sci. Med. Sci.* 67, 611–625. doi: 10.1093/gerona/gls118

Debus, E., Weber, K., and Osborn, M. (1983). Monoclonal antibodies specific for glial fibrillary acidic (GFA) protein and for each of the neurofilament triplet polypeptides. *Differ. Res. Biol. Divers.* 25, 193–203. doi: 10.1111/j.1432-0436.1984.tb01355.x

Diaz, C., Martinez-Galan, J. R., and Juiz, J. M. (2009). Development of glutamate receptors in auditory neurons from long-term organotypic cultures of the embryonic chick hindbrain. *Eur. J. Neurosci.* 29, 213–230. doi: 10.1111/j.1460-9568.2008.06578.x

Dinh, M. L., Koppel, S. J., Korn, M. J., and Cramer, K. S. (2014). Distribution of glial cells in the auditory brainstem: normal development and effects of unilateral lesion. *Neuroscience* 278, 237–252. doi: 10.1016/j.neuroscience.2014.08.016

Duan, S., Anderson, C. M., Stein, B. A., and Swanson, R. A. (1999). Glutamate induces rapid upregulation of astrocyte glutamate transport and cell-surface expression of GLAST. *J. Neurosci.* 19, 10193–10200. doi: 10.1523/jneurosci.19-23-10193.1999

Eroglu, C., and Barres, B. A. (2010). Regulation of synaptic connectivity by glia. *Nature* 468, 223–231. doi: 10.1038/nature09612

Ferraguti, F., and Shigemoto, R. (2006). Metabotropic glutamate receptors. *Cell Tissue Res.* 326, 483–504. doi: 10.1007/s00441-006-0266-5

Fischer, A. J., Scott, M. A., Zelinka, C., and Sherwood, P. (2010). A novel type of glial cell in the retina is stimulated by insulin-like growth factor 1 and may exacerbate damage to neurons and Müller glia. *Glia* 58, 633–649. doi: 10.1002/glia.20950

Flavell, S. W., Cowan, C. W., Kim, T.-K., Greer, P. L., Lin, Y., Paradis, S., et al. (2006). Activity-dependent regulation of MEF2 transcription factors suppresses excitatory synapse number. *Science* 311, 1008–1012. doi: 10.1126/science.1122511

Franklin, K. B. J., and Paxinos, G. (2013). *Paxinos and Franklin's The Mouse Brain in Stereotaxic Coordinates*. 4th Edn. Amsterdam: Academic Press, an imprint of Elsevier.

Fuentes-Santamaría, V., Alvarado, J. C., Gabaldón-Ull, M. C., and Juiz, J. M. (2013). Upregulation of insulin-like growth factor and interleukin 1β occurs in neurons but not in glial cells in the cochlear nucleus following cochlear ablation. *J. Comp. Neurol.* 521, 3478–3499. doi: 10.1002/cne.23362

Fuentes-Santamaría, V., Alvarado, J. C., Henkel, C. K., and Brunso-Bechtold, J. K. (2007). Cochlear ablation in adult ferrets results in changes in insulin-like growth factor-1 and synaptophysin immunostaining in the cochlear nucleus. *Neuroscience* 148, 1033–1047. doi: 10.1016/j.neuroscience.2007.07.026

Fuentes-Santamaría, V., Alvarado, J. C., and Juiz, J. M. (2012). Long-term interaction between microglial cells and cochlear nucleus neurons after bilateral cochlear ablation. *J. Comp. Neurol.* 520, 2974–2990. doi: 10.1002/cne.23088

Fuentes-Santamaría, V., Alvarado, J. C., Melgar-Rojas, P., Gabaldón-Ull, M. C., Miller, J. M., and Juiz, J. M. (2017). The role of glia in the peripheral and central auditory system following noise overexposure: contribution of TNF-α and IL-1β to the pathogenesis of hearing loss. *Front. Neuroanat.* 11:9. doi: 10.3389/fnana.2017.00009

Fuentes-Santamaría, V., Alvarado, J. C., Rodríguez-de la Rosa, L., Murillo-Cuesta, S., Contreras, J., Juiz, J. M., et al. (2016). Erratum to: IGF-1 deficiency causes atrophic changes associated with upregulation of VGluT1 and downregulation of MEF2 transcription factors in the mouse cochlear nuclei. *Brain Struct. Funct.* 221:1205. doi: 10.1007/s00429-014-0945-z

Fuentes-Santamaria, V., Alvarado, J. C., Taylor, A. R., Brunso-Bechtold, J. K., and Henkel, C. K. (2005). Quantitative changes in calretinin immunostaining in the cochlear nuclei after unilateral cochlear removal in young ferrets. *J. Comp. Neurol.* 483, 458–475. doi: 10.1002/cne.20437

Furness, D. N., and Lawton, D. M. (2003). Comparative distribution of glutamate transporters and receptors in relation to afferent innervation density in the mammalian cochlea. *J. Neurosci.* 23, 11296–11304. doi: 10.1523/jneurosci.23-36-11296.2003

Furness, D. N., Lawton, D. M., Mahendrasingam, S., Hodierne, L., and Jagger, D. J. (2009). Quantitative analysis of the expression of the glutamate-aspartate transporter and identification of functional glutamate uptake reveal a role for cochlear fibrocytes in glutamate homeostasis. *Neuroscience* 162, 1307–1321. doi: 10.1016/j.neuroscience.2009.05.036

Furness, D. N., and Lehre, K. P. (1997). Immunocytochemical localization of a high-affinity glutamate-aspartate transporter, GLAST, in the rat and guinea-pig cochlea. *Eur. J. Neurosci.* 9, 1961–1969. doi: 10.1111/j.1460-9568.1997.tb00763.x

Furuta, A., Rothstein, J. D., and Martin, L. J. (1997). Glutamate transporter protein subtypes are expressed differentially during rat CNS development. *J. Neurosci.* 17, 8363–8375. doi: 10.1523/jneurosci.17-21-08363.1997

Galik, J., Youn, D.-H., Kolaj, M., and Randić, M. (2008). Involvement of group I metabotropic glutamate receptors and glutamate transporters in the slow excitatory synaptic transmission in the spinal cord dorsal horn. *Neuroscience* 154, 1372–1387. doi: 10.1016/j.neuroscience.2008.04.059

Gamboa, C., and Ortega, A. (2002). Insulin-like growth factor-1 increases activity and surface levels of the GLAST subtype of glutamate transporter. *Neurochem. Int.* 40, 397–403. doi: 10.1016/s0197-0186(01)00106-1

Genis, L., Dávila, D., Fernandez, S., Pozo-Rodrigálvarez, A., Martínez-Murillo, R., and Torres-Aleman, I. (2014). Astrocytes require insulin-like growth factor I to protect neurons against oxidative injury. *F1000Res.* 3:28. doi: 10.12688/f1000research.3-28.v2

Glowatzki, E., Cheng, N., Hiel, H., Yi, E., Tanaka, K., Ellis-Davies, G. C. R., et al. (2006). The glutamate-aspartate transporter GLAST mediates glutamate uptake at inner hair cell afferent synapses in the mammalian cochlea. *J. Neurosci.* 26, 7659–7664. doi: 10.1523/jneurosci.1545-06.2006

Hakuba, N., Koga, K., Gyo, K., Usami, S. I., and Tanaka, K. (2000). Exacerbation of noise-induced hearing loss in mice lacking the glutamate transporter GLAST. *J. Neurosci.* 20, 8750–8753. doi: 10.1523/jneurosci.20-23-08750.2000

Hansson, E., and Rönnbäck, L. (2003). Glial neuronal signaling in the central nervous system. *FASEB J.* 17, 341–348. doi: 10.1096/fj.02-0429rev

Huang, Y. H., Sinha, S. R., Tanaka, K., Rothstein, J. D., and Bergles, D. E. (2004). Astrocyte glutamate transporters regulate metabotropic glutamate receptor-mediated excitation of hippocampal interneurons. *J. Neurosci.* 24, 4551–4559. doi: 10.1523/jneurosci.5217-03.2004

Hughes, E. G., Maguire, J. L., McMinn, M. T., Scholz, R. E., and Sutherland, M. L. (2004). Loss of glial fibrillary acidic protein results in decreased glutamate transport and inhibition of PKA-induced EAAT2 cell surface trafficking. *Mol. Brain Res.* 124, 114–123. doi: 10.1016/j.molbrainres.2004.02.021

Imai, Y., Ibata, I., Ito, D., Ohsawa, K., and Kohsaka, S. (1996). A novel gene iba1 in the major histocompatibility complex class III region encoding an EF hand protein expressed in a monocytic lineage. *Biochem. Biophys. Res. Commun.* 224, 855–862. doi: 10.1006/bbrc.1996.1112

Insausti, A. M., Cruz-Orive, L. M., Jáuregui, I., Manrique, M., and Insausti, R. (1999). Stereological assessment of the glial reaction to chronic deafferentation of the cochlear nuclei in the macaque monkey (*Macaca fascicularis*). *J. Comp. Neurol.* 414, 485–494. doi: 10.1002/(SICI)1096-9861(19991129)414:4<485::AID-CNE5>3.0.CO;2-W

Ito, D., Imai, Y., Ohsawa, K., Nakajima, K., Fukuuchi, Y., and Kohsaka, S. (1998). Microglia-specific localisation of a novel calcium binding protein, Iba1. *Mol. Brain Res.* 57, 1–9. doi: 10.1016/s0169-328x(98)00040-0

Janz, P., and Illing, R.-B. (2014). A role for microglial cells in reshaping neuronal circuitry of the adult rat auditory brainstem after its sensory deafferentation. *J. Neurosci. Res.* 92, 432–445. doi: 10.1002/jnr.23334

Jin, D., Ohlemiller, K. K., Lei, D., Dong, E., Role, L., Ryugo, D. K., et al. (2011). Age-related neuronal loss in the cochlea is not delayed by synaptic modulation. *Neurobiol. Aging* 32, 2321.e13–2321.e23. doi: 10.1016/j.neurobiolaging.2010.05.011

Josephson, E. M., and Morest, D. K. (2003). Synaptic nests lack glutamate transporters in the cochlear nucleus of the mouse. *Synapse* 49, 29–46. doi: 10.1002/syn.10201

Juiz, J. M., Luján, R., Domínguez del Toro, E., Fuentes, V., Ballesta, J. J., and Criado, M. (2000). Subcellular compartmentalization of a potassium channel (Kv1.4): preferential distribution in dendrites and dendritic spines of neurons in the dorsal cochlear nucleus: Kv1.4 channels in dendrites and dendritic spines. *Eur. J. Neurosci.* 12, 4345–4356. doi: 10.1111/j.1460-9568.2000.01335.x

Kemmer, M., and Vater, M. (2001). Cellular and subcellular distribution of AMPA-type glutamate receptor subunits and metabotropic glutamate receptor 1α in the cochlear nucleus of the horseshoe bat (*Rhinolophus rouxi*). *Hear. Res.* 156, 128–142. doi: 10.1016/s0378-5955(01)00266-0

Kettenmann, H., Kirchhoff, F., and Verkhratsky, A. (2013). Microglia: new roles for the synaptic stripper. *Neuron* 77, 10–18. doi: 10.1016/j.neuron.2012.12.023

Kim, S. K., Nabekura, J., and Koizumi, S. (2017). Astrocyte-mediated synapse remodeling in the pathological brain. *Glia* 65, 1719–1727. doi: 10.1002/glia.23169

Lambert, P. R., and Schwartz, I. R. (1982). A longitudinal study of changes in the cochlear nucleus in the CBA mouse. *Otolaryngol. Head Neck Surg.* 90, 787–794. doi: 10.1177/019459988209000620

Lehre, K. P., and Danbolt, N. C. (1998). The number of glutamate transporter subtype molecules at glutamatergic synapses: chemical and stereological quantification in young adult rat brain. *J. Neurosci.* 18, 8751–8757. doi: 10.1523/JNEUROSCI.18-21-08751.1998

Lehre, K. P., Levy, L. M., Ottersen, O. P., Storm-Mathisen, J., and Danbolt, N. C. (1995). Differential expression of two glial glutamate transporters in the rat brain: quantitative and immunocytochemical observations. *J. Neurosci.* 15, 1835–1853. doi: 10.1523/JNEUROSCI.15-03-01835.1995

Lind, D., Franken, S., Kappler, J., Jankowski, J., and Schilling, K. (2005). Characterization of the neuronal marker NeuN as a multiply phosphorylated antigen with discrete subcellular localization. *J. Neurosci. Res.* 79, 295–302. doi: 10.1002/jnr.20354

Liu, J. P., Baker, J., Perkins, A. S., Robertson, E. J., and Efstratiadis, A. (1993). Mice carrying null mutations of the genes encoding insulin-like growth factor I (Igf-1) and type 1 IGF receptor (Igf1r). *Cell* 75, 59–72. doi: 10.1016/s0092-8674(05)80084-4

Livak, K. J., and Schmittgen, T. D. (2001). Analysis of relative gene expression data using real-time quantitative PCR and the $2^{-\Delta\Delta C_T}$ method. *Methods* 25, 402–408. doi: 10.1006/meth.2001.1262

Lu, Y. (2007). Endogenous mGluR activity suppresses GABAergic transmission in avian cochlear nucleus magnocellularis neurons. *J. Neurophysiol.* 97, 1018–1029. doi: 10.1152/jn.00883.2006

Lu, Y. (2014). Metabotropic glutamate receptors in auditory processing. *Neuroscience* 274, 429–445. doi: 10.1016/j.neuroscience.2014.05.057

Magariños, M., Contreras, J., Aburto, M. R., and Varela-Nieto, I. (2012). Early development of the vertebrate inner ear. *Anat. Rec.* 295, 1775–1790. doi: 10.1002/ar.22575

Martin, M. R., and Rickets, C. (1981). Histogenesis of the cochlear nucleus of the mouse. *J. Comp. Neurol.* 197, 169–184. doi: 10.1002/cne.901970113

Martinez-Galan, J. R., Perez-Martinez, F. C., and Juiz, J. M. (2010). Differences in glutamate-mediated calcium responses in the ventral cochlear nucleus and inferior colliculus of the developing rat. *Hear. Res.* 267, 46–53. doi: 10.1016/j.heares.2010.03.089

Matute, C., Melone, M., Vallejo-Illarramendi, A., and Conti, F. (2005). Increased expression of the astrocytic glutamate transporter GLT-1 in the prefrontal cortex of schizophrenics. *Glia* 49, 451–455. doi: 10.1002/glia.20119

Miller, B. R., Dorner, J. L., Shou, M., Sari, Y., Barton, S. J., Sengelaub, D. R., et al. (2008). Up-regulation of GLT1 expression increases glutamate uptake and attenuates the Huntington's disease phenotype in the R6/2 mouse. *Neuroscience* 153, 329–337. doi: 10.1016/j.neuroscience.2008.02.004

Morrison, H. W., and Filosa, J. A. (2013). A quantitative spatiotemporal analysis of microglia morphology during ischemic stroke and reperfusion. *J. Neuroinflammation* 10:4. doi: 10.1186/1742-2094-10-4

Morrison, H., Young, K., Qureshi, M., Rowe, R. K., and Lifshitz, J. (2017). Quantitative microglia analyses reveal diverse morphologic responses in the rat cortex after diffuse brain injury. *Sci. Rep.* 7:13211. doi: 10.1038/s41598-017-13581-z

Mugnaini, E., Osen, K. K., Dahl, A. L., Friedrich, V. L. Jr., and Korte, G. (1980). Fine structure of granule cells and related interneurons (termed Golgi cells) in the cochlear nuclear complex of cat, rat and mouse. *J. Neurocytol.* 9, 537–570. doi: 10.1007/bf01204841

Mullen, R. J., Buck, C. R., and Smith, A. M. (1992). NeuN, a neuronal specific nuclear protein in vertebrates. *Development* 116, 201–211.

Murillo-Cuesta, S., Rodríguez-de la Rosa, L., Cediel, R., Lassaletta, L., and Varela-Nieto, I. (2011). The role of insulin-like growth factor-I in the physiopathology of hearing. *Front. Mol. Neurosci.* 4:11. doi: 10.3389/fnmol.2011.00011

Nakanishi, K., Okouchi, Y., Ueki, T., Asai, K., Isobe, I., Eksioglu, Y. Z., et al. (1994). Astrocytic contribution to functioning synapse formation estimated by spontaneous neuronal intracellular Ca^{2+} oscillations. *Brain Res.* 659, 169–178. doi: 10.1016/0006-8993(94)90876-1

Nicholas, A. H., and Hyson, R. L. (2004). Group I and II metabotropic glutamate receptors are necessary for the activity-dependent regulation of ribosomes in chick auditory neurons. *Brain Res.* 1014, 110–119. doi: 10.1016/j.brainres.2004.03.066

Nicoletti, F., Bockaert, J., Collingridge, G. L., Conn, P. J., Ferraguti, F., Schoepp, D. D., et al. (2011). Metabotropic glutamate receptors: from the workbench to the bedside. *Neuropharmacology* 60, 1017–1041. doi: 10.1016/j.neuropharm.2010.10.022

Niswender, C. M., and Conn, P. J. (2010). Metabotropic glutamate receptors: physiology, pharmacology, and disease. *Annu. Rev. Pharmacol. Toxicol.* 50, 295–322. doi: 10.1146/annurev.pharmtox.011008.145533

Paolicelli, R. C., and Ferretti, M. T. (2017). Function and dysfunction of microglia during brain development: consequences for synapses and neural circuits. *Front. Synaptic Neurosci.* 9:9. doi: 10.3389/fnsyn.2017.00009

Papouin, T., Dunphy, J., Tolman, M., Foley, J. C., and Haydon, P. G. (2017). Astrocytic control of synaptic function. *Philos. Trans. R. Soc. Lond. B Biol. Sci.* 372:20160154. doi: 10.1098/rstb.2016.0154

Petralia, R. S., Rubio, M. E., Wang, Y. X., and Wenthold, R. J. (2000). Differential distribution of glutamate receptors in the cochlear nuclei. *Hear. Res.* 147, 59–69. doi: 10.1016/s0378-5955(00)00120-9

Petralia, R. S., Wang, Y. X., Zhao, H. M., and Wenthold, R. J. (1996). Ionotropic and metabotropic glutamate receptors show unique postsynaptic, presynaptic, and glial localizations in the dorsal cochlear nucleus. *J. Comp. Neurol.* 372, 356–383. doi: 10.1002/(sici)1096-9861(19960826)372:3<356::aid-cne3>3.3.co;2-#

Pfrieger, F. W., and Barres, B. A. (1996). New views on synapse-glia interactions. *Curr. Opin. Neurobiol.* 6, 615–621. doi: 10.1016/s0959-4388(96)80093-6

Ramsey, M. M., Adams, M. M., Ariwodola, O. J., Sonntag, W. E., and Weiner, J. L. (2005). Functional characterization of des-IGF-1 action at excitatory synapses in the CA1 region of rat hippocampus. *J. Neurophysiol.* 94, 247–254. doi: 10.1152/jn.00768.2004

Rashid, A. J., Cole, C. J., and Josselyn, S. A. (2014). Emerging roles for MEF2 transcription factors in memory. *Genes Brain Behav.* 13, 118–125. doi: 10.1111/gbb.12058

Rasmussen, S., Wang, Y., Kivisäkk, P., Bronson, R. T., Meyer, M., Imitola, J., et al. (2007). Persistent activation of microglia is associated with neuronal dysfunction of callosal projecting pathways and multiple sclerosis-like lesions in relapsing—remitting experimental autoimmune encephalomyelitis. *Brain* 130, 2816–2829. doi: 10.1093/brain/awm219

Rebillard, G., Ruel, J., Nouvian, R., Saleh, H., Pujol, R., Dehnes, Y., et al. (2003). Glutamate transporters in the guinea-pig cochlea: partial mRNA sequences, cellular expression and functional implications. *Eur. J. Neurosci.* 17, 83–92. doi: 10.1046/j.1460-9568.2003.02429.x

Ricci, G., Volpi, L., Pasquali, L., Petrozzi, L., and Siciliano, G. (2009). Astrocyte-neuron interactions in neurological disorders. *J. Biol. Phys.* 35, 317–336. doi: 10.1007/s10867-009-9157-9

Riquelme, R., Cediel, R., Contreras, J., la Rosa Lourdes, R. D., Murillo-Cuesta, S., Hernandez-Sanchez, C., et al. (2010). A comparative study of age-related hearing loss in wild type and insulin-like growth factor I deficient mice. *Front. Neuroanat.* 4:27. doi: 10.3389/fnana.2010.00027

Rothstein, J. D. (1996). Excitotoxicity hypothesis. *Neurology* 47, S19–S25; discussion S26. doi: 10.1212/wnl.47.4_suppl_2.19s

Ruffle, R. A., Mapley, A. C., Malik, M. K., Labruzzo, S. V., Chabla, J. M., Jose, R., et al. (2006). Distribution of constitutively expressed MEF-2A in adult rat and human nervous systems. *Synapse* 59, 513–520. doi: 10.1002/syn.20266

Ryugo, D. K., and Willard, F. H. (1985). The dorsal cochlear nucleus of the mouse: a light microscopic analysis of neurons that project to the inferior colliculus. *J. Comp. Neurol.* 242, 381–396. doi: 10.1002/cne.902420307

Sanchez-Calderon, H., Rodriguez-de la Rosa, L., Milo, M., Pichel, J. G., Holley, M., and Varela-Nieto, I. (2010). RNA microarray analysis in prenatal mouse cochlea reveals novel IGF-I target genes: implication of MEF2 and FOXM1 transcription factors. *PLoS One* 5:e8699. doi: 10.1371/journal.pone.0008699

Sasaki, Y., Ohsawa, K., Kanazawa, H., Kohsaka, S., and Imai, Y. (2001). Iba1 is an actin-cross-linking protein in macrophages/microglia. *Biochem. Biophys. Res. Commun.* 286, 292–297. doi: 10.1006/bbrc.2001.5388

Schmitt, A., Asan, E., Püschel, B., and Kugler, P. (1997). Cellular and regional distribution of the glutamate transporter GLAST in the CNS of rats: nonradioactive in situ hybridization and comparative immunocytochemistry. *J. Neurosci.* 17, 1–10. doi: 10.1523/JNEUROSCI.17-01-00001.1997

Schneider, C. A., Rasband, W. S., and Eliceiri, K. W. (2012). NIH Image to ImageJ: 25 years of image analysis. *Nat. Methods* 9, 671–675. doi: 10.1038/nmeth.2089

Slezak, M., Pfrieger, F. W., and Soltys, Z. (2006). Synaptic plasticity, astrocytes and morphological homeostasis. *J. Physiol. Paris* 99, 84–91. doi: 10.1016/j.jphysparis.2005.12.082

Sofroniew, M. V., and Vinters, H. V. (2010). Astrocytes: biology and pathology. *Acta Neuropathol.* 119, 7–35. doi: 10.1007/s00401-009-0619-8

Soni, N., Reddy, B. V. K., and Kumar, P. (2014). GLT-1 transporter: an effective pharmacological target for various neurological disorders. *Pharmacol. Biochem. Behav.* 127, 70–81. doi: 10.1016/j.pbb.2014.10.001

Trejo, J. L., Piriz, J., Llorens-Martin, M. V., Fernandez, A. M., Bolós, M., LeRoith, D., et al. (2007). Central actions of liver-derived insulin-like growth factor I underlying its pro-cognitive effects. *Mol. Psychiatry* 12, 1118–1128. doi: 10.1038/sj.mp.4002076

Turlejski, T., Humoud, I., Desai, R., Smith, K. J., and Marina, N. (2016). Immunohistochemical evidence of tissue hypoxia and astrogliosis in the rostral ventrolateral medulla of spontaneously hypertensive rats. *Brain Res.* 1650, 178–183. doi: 10.1016/j.brainres.2016.09.012

Ullian, E. M., Christopherson, K. S., and Barres, B. A. (2004). Role for glia in synaptogenesis. *Glia* 47, 209–216. doi: 10.1002/glia.20082

Ullian, E. M., Sapperstein, S. K., Christopherson, K. S., and Barres, B. A. (2001). Control of synapse number by glia. *Science* 291, 657–661. doi: 10.1126/science.291.5504.657

Varela-Nieto, I., Murillo-Cuesta, S., Rodríguez-de la Rosa, L., Lassatetta, L., and Contreras, J. (2013). IGF-I deficiency and hearing loss: molecular clues and clinical implications. *Pediatr. Endocrinol. Rev.* 10, 460–472. Available on line at: http://www.pediatricendoreviews.com/#!volume-104/c12kb

Verkhratsky, A., Sofroniew, M. V., Messing, A., deLanerolle, N. C., Rempe, D., Rodríguez, J. J., et al. (2012). Neurological diseases as primary gliopathies: a reassessment of neurocentrism. *ASN Neuro* 4:e00082. doi: 10.1042/an20120010

Villacampa, P., Ribera, A., Motas, S., Ramírez, L., García, M., de la Villa, P., et al. (2013). Insulin-like growth factor I (IGF-I)-induced chronic gliosis and retinal stress lead to neurodegeneration in a mouse model of retinopathy. *J. Biol. Chem.* 288, 17631–17642. doi: 10.1074/jbc.m113.468819

Villalba, R. M., and Smith, Y. (2011). Neuroglial plasticity at striatal glutamatergic synapses in Parkinson's disease. *Front. Syst. Neurosci.* 5:68. doi: 10.3389/fnsys.2011.00068

Wang, Y.-F., and Parpura, V. (2018). Astroglial modulation of hydromineral balance and cerebral edema. *Front. Mol. Neurosci.* 11:204. doi: 10.3389/fnmol.2018.00204

Webster, D. B., and Trune, D. R. (1982). Cochlear nuclear complex of mice. *Am. J. Anat.* 163, 103–130. doi: 10.1002/aja.1001630202

Wolf, S. A., Boddeke, H. W. G. M., and Kettenmann, H. (2017). Microglia in physiology and disease. *Annu. Rev. Physiol.* 79, 619–643. doi: 10.1146/annurev-physiol-022516-034406

Wright, D. D., Blackstone, C. D., Huganir, R. L., and Ryugo, D. K. (1996). Immunocytochemical localization of the mGluR1 α metabotropic glutamate receptor in the dorsal cochlear nucleus. *J. Comp. Neurol.* 364, 729–745. doi: 10.1002/(sici)1096-9861(19960122)364:4<729::aid-cne10>3.0.co;2-k

Wu, Y., Dissing-Olesen, L., MacVicar, B. A., and Stevens, B. (2015). Microglia: dynamic mediators of synapse development and plasticity. *Trends Immunol.* 36, 605–613. doi: 10.1016/j.it.2015.08.008

Xing, C., Yin, Y., Chang, R., Gong, X., He, X., and Xie, Z. (2007). Effects of insulin-like growth factor 1 on synaptic excitability in cultured rat hippocampal neurons. *Exp. Neurol.* 205, 222–229. doi: 10.1016/j.expneurol.2007.01.029

Xu, Y. H., Sattler, G. L., Edwards, H., and Pitot, H. C. (2000). Nuclear-labeling index analysis (NLIA), a software package used to perform accurate automation of cell nuclear-labeling index analysis on immunohistochemically stained rat liver samples. *Comput. Methods Programs Biomed.* 63, 55–70. doi: 10.1016/s0169-2607(00)00075-4

Yamahara, K., Yamamoto, N., Nakagawa, T., and Ito, J. (2015). Insulin-like growth factor 1: a novel treatment for the protection or regeneration of cochlear hair cells. *Hear. Res.* 330, 2–9. doi: 10.1016/j.heares.2015.04.009

Zhou, J. (2004). Glutamate transporter cluster formation in astrocytic processes regulates glutamate uptake activity. *J. Neurosci.* 24, 6301–6306. doi: 10.1523/JNEUROSCI.1404-04.2004

Conflict of Interest Statement: The authors declare that the research was conducted in the absence of any commercial or financial relationships that could be construed as a potential conflict of interest.

frontiers in Cellular Neuroscience

ORIGINAL RESEARCH
published: 14 March 2019
doi: 10.3389/fncel.2019.00090

Galectin-3 (MAC-2) Controls Microglia Phenotype Whether Amoeboid and Phagocytic or Branched and Non-phagocytic by Regulating the Cytoskeleton

*Fanny Reichert and Shlomo Rotshenker**

Department of Medical Neurobiology, Institute for Medical Research Israel-Canada (IMRIC), Faculty of Medicine, Hebrew University, Jerusalem, Israel

Myelin surrounding central nervous system (CNS) axons breaks down in multiple sclerosis (MS) and following traumatic axonal injury. Myelin-debris so produced is harmful to repair since it impedes remyelination in MS and the regeneration of traumatized axons. These devastating outcomes are largely due to inefficient removal by phagocytosis of myelin-debris by microglia. Therefore, revealing mechanisms that control phagocytosis is vital. We previously showed that in phagocytosis, filopodia and lamellipodia extend/engulf and then retract/internalize myelin-debris. Moreover, cofilin activates phagocytosis by advancing the remodeling of actin filaments (i.e., existing filaments disassemble and new filaments assemble in a new configuration), causing filopodia/lamellipodia to protrude, and furthermore, Galectin-3 (formally named MAC-2) activates phagocytosis by enhancing K-Ras.GTP/PI3K signaling that leads to actin/myosin-based contraction, causing filopodia/lamellipodia to retract. To understand further how Galectin-3 controls phagocytosis we knocked-down (KD) Galectin-3 expression in cultured primary microglia using Galectin-3 small-hairpin RNA (Gal-3-shRNA). KD Galectin-3 protein levels reduced phagocytosis extensively. Further, inhibiting nucleolin (NCL) and nucleophosmin (NPM), which advance K-Ras signaling as does Galectin-3, also reduced phagocytosis. Strikingly and unexpectedly, knocking down Galectin-3 resulted in a dramatic transformation of microglia morphology from "amoeboid-like" to "branched-like," rearrangement of actin filaments and inactivation of cofilin. Thus, Galectin-3 may control microglia morphology and phagocytosis by regulating the activation state of cofilin, which, in turn, affects how actin filaments organize and how stable they are. Furthermore, our current and previous findings together suggest that Galectin-3 activates phagocytosis by targeting the cytoskeleton twice: first, by advancing cofilin activation, causing filopodia/lamellipodia to extend/engulf myelin-debris. Second, by advancing actin/myosin-based contraction through K-Ras.GTP/PI3K signaling, causing filopodia/lamellipodia to retract/internalize myelin-debris.

Keywords: microglia, Galectin-3, phagocytosis, myelin, cytoskeleton, actin, cofilin, K-Ras

OPEN ACCESS

Edited by:
Raquel Ferreira, Universidade da Beira Interior, Portugal

Reviewed by:
Andrew Chan, University Hospital Bern, Switzerland
Ruben Lopez-Vales, Autonomous University of Barcelona, Spain

****Correspondence:***
Shlomo Rotshenker
shlomor@ekmd.huji.ac.il

Received: *31 October 2018*
Accepted: *22 February 2019*
Published: *14 March 2019*

Citation:
Reichert F and Rotshenker S (2019) Galectin-3 (MAC-2) Controls Microglia Phenotype Whether Amoeboid and Phagocytic or Branched and Non-phagocytic by Regulating the Cytoskeleton. Front. Cell. Neurosci. 13:90. doi: 10.3389/fncel.2019.00090

INTRODUCTION

Microglia are a self-maintained population of innate immune cells unique to the central nervous system (CNS) parenchyma (Rio-Hortega, 1932; Sierra et al., 2016; Tay et al., 2016; Norris and Kipnis, 2018). Microglia differ by origin and molecular signature from CNS associated macrophages (i.e., perivascular, choroid plexus and meningeal) and from circulating monocytes (Ajami et al., 2007; Butovsky et al., 2014; Goldmann et al., 2016). Moreover, the intact blood brain barrier (BBB) separates microglia from CNS associated macrophages and circulating monocytes; yet, monocytes may enter the CNS parenchyma through dysfunctional BBB in trauma and disease (Mildner et al., 2007).

Microglia populate the developing CNS parenchyma during embryogenesis and further proliferate during the neonatal period. At that period, microglia display "amoeboid" morphology and phagocytic activity that enables them to remove apoptotic cells and eliminate/strip/prune synapses, shaping the CNS neuronal circuitry (Tremblay et al., 2010; Schafer et al., 2012; Kettenmann et al., 2013). Towards adulthood, microglia morphology transforms to "branched" and their phagocytic activity subsides. Upon injury and disease, microglia revert to amoeboid morphology and phagocytic activity resumes, enabling them to remove tissue debris (Rio-Hortega, 1932; Sierra et al., 2016; Norris and Kipnis, 2018). Thus, the notion that phagocytic activity correlates mostly with amoeboid morphology and non-phagocytic activity with branched morphology is long standing. Nonetheless, the molecular mechanisms that control the transformation from one phenotype to the other have remained largely unknown. It has been suggested that transcription factor Runx1 controls the *in vivo* postnatal conversion of forebrain microglia morphology from amoeboid to branched; yet, the involvement of Runx1 in phagocytosis was not tested (Zusso et al., 2012). It has further been shown that microglia were amoeboid and phagocytic when cultured in the presence of serum/FCS but branched and non-phagocytic when cultured in the absence of FCS; yet, the molecular mechanisms that induced each phenotype were not studied (Bohlen et al., 2017).

Our present study focuses on the phagocytosis of myelin-debris (often referred to as degenerated myelin). Myelin produced by oligodendrocytes surrounds CNS axons, enabling neuronal function through fast conduction of electrical activity. Myelin breaks down in demyelinating diseases such as multiple sclerosis (MS) and in Wallerian degeneration that traumatic axonal injury induces distal to lesion sites (e.g., spinal cord injury). Myelin-debris so produced is harmful to repair since it blocks remyelination in MS (Kotter et al., 2006; Lassmann et al., 2007) and impedes the regeneration/growth of traumatized axons (Yiu and He, 2006; Vargas and Barres, 2007). These devastating outcomes are largely due to inefficient removal by phagocytosis of myelin-debris, highlighting the significance of understanding mechanisms that control phagocytosis.

We previously showed that filopodia and lamellipodia extend/engulf and then retract/internalize myelin-debris in phagocytosis (Hadas et al., 2012). Mechanical forces generated by the cytoskeleton drive these structural changes. Protrusion of filopodia/lamellipodia requires that filaments of actin (F-actin) undergo remodeling, i.e., existing F-actin disassemble and new F-actin assemble in a new configuration, causing plasma membranes to protrude (Oser and Condeelis, 2009; Bernstein and Bamburg, 2010). We previously showed that cofilin, a member of the actin depolymerizing factor (ADF) family that advances filopodia/lamellipodia production by disassembling F-actin, activates phagocytosis (Hadas et al., 2012; Gitik et al., 2014), and further, that actin/myosin-based contraction drives filopodia/lamellipodia to retract/internalize myelin-debris (Gitik et al., 2010).

We further previously suggested two mechanisms that impede the phagocytosis of myelin-debris. In the first, myelin-debris itself attenuates its own phagocytosis. In this regard, CD47 on myelin binds SIRPα (CD172a) on microglia and macrophages, and in turn, SIRPα generates "don't eat me" signaling in which cofilin is inactivated, the remodeling of F-actin is obstructed, and phagocytosis is reduced (Gitik et al., 2011, 2014). This could be the case in MS since the removal by phagocytosis of myelin-debris is inefficient in MS (Kotter et al., 2006; Lassmann et al., 2007). The second mechanism could play a role in CNS Wallerian degeneration (i.e., distal to but not including the lesion site), where microglia fail to phagocytose myelin-debris altogether. We suggested that this failure results mostly from microglia failing to upregulate the expression of the β-galactoside-binding lectin Galectin-3 (formally named MAC-2; Rotshenker et al., 2008; Rotshenker, 2009).

Many normal and malignant cells produce and secrete Galectin-3, a member of a large family of galectins. Galectin-3 takes part in numerous functions in health and disease; e.g., pre-mRNA splicing in the nucleus, signaling pathways in cytoplasm, and activation of surface receptors extracellularly (Ruvolo, 2016; Thiemann and Baum, 2016; Mèndez-Huergo et al., 2017). Amongst functions that relate to our current project, Galectin-3 advances K-Ras signaling in the cytoplasm. K-Ras is a member of the Ras family of small GTPases K-, H- and N-Ras that are active when GTP bound and inactive when GDP bound. Galectin-3 binds and stabilizes active K-Ras.GTP at the inner surface of cell membranes, prolonging K-Ras dependent signaling (Tian et al., 2010). Of further interest to us are nucleolin (NCL) and nucleophosmin (NPM) since, amongst their various functions, the two advance K-Ras dependent signaling by chaperoning and stabilizing K-Ras.GDP at the inner surface of plasma membranes where it needs to be activated (Inder et al., 2010). Further, NCL is present at low levels in plasma membranes of some normal cells (e.g., microglia) and at much higher levels in some malignant cells (Hirano et al., 2005; Bates et al., 2009; Ozawa et al., 2013). As a cell surface receptor, NCL binds and is instrumental in endocytosing particulate material.

We previously showed that Galectin-3 expression correlates with myelin-debris phagocytosis in microglia. In adult mice, non-phagocytosing microglia did not express Galectin-3 in intact CNS nor in CNS Wallerian degeneration, i.e., distal to but not including the lesion site. In contrast, and along

with activating phagocytosis, microglia upregulated Galectin-3 expression *in vivo* at lesion sites and in experimental allergic encephalomyelitis (EAE), and in cultured primary microglia (Reichert and Rotshenker, 1996, 1999). We further showed that Galectin-3 activated phagocytosis by binding and stabilizing K-Ras.GTP, prolonging the activity of K-Ras.GTP/PI3K signaling (Rotshenker et al., 2008; Rotshenker, 2009), leading to PI3K/PLC/PKC signaling (Makranz et al., 2004; Cohen et al., 2006), and then to actin/myosin-based contraction (Gitik et al., 2010).

Our aims in this project have been to further understand and validate the role of Galectin-3 as a key regulator of myelin-debris phagocytosis. First, we infected cultured primary microglia with Galectin-3 small-hairpin RNA (Gal-3-shRNA) to reduce/knockdown (KD) Galectin-3 protein levels, generating Gal-3-KD microglia. Second, we aimed to determine whether NCL and NPM activate phagocytosis as predicted from their ability to advance K-Ras signaling as Galectin-3 does. Third, we aimed to reveal which cytoskeletal molecules regulated by Galectin-3 activate phagocytosis. Our current findings suggest that Galectin-3 controls both microglia morphology and phagocytosis by targeting the cytoskeleton.

MATERIALS AND METHODS

Animals

Balb/C wild-type mice (Harlan Sprague-Dawley, Inc., Israel) and transgenic Galectin-3 knockout (Gal-3$^{-/-}$) mice (provided by Prof. Yoel Kloog; Levy et al., 2011) were used in accordance with the National Research Council's guide for the care and use of laboratory animals and with the approval of the institutional ethics committee Hebrew University Faculty of Medicine.

Media Products

DMEM, DMEM/F12, FCS, HI-FCS, Gentamicin sulfate and L-Glutamine obtained from Biological Industries (Beit-Haemek, Israel).

Isolation of Primary Microglia

Microglia were isolated from brains of neonate mice as previously described (Reichert and Rotshenker, 2003). In brief, brains were stripped of their meninges, enzymatically dissociated, cells plated on poly-L-lysine coated flasks for 1 week, replated for 1- to 2-h on bacteriological plates and non-adherent cells washed away. The vast majority of adherent cells are microglia judged by morphology and expression of P2Y12 (Butovsky et al., 2014), and Galectin-3, complement receptor-3 (CR-3) and F4/80 (Reichert and Rotshenker, 1996, 1999). Microglia were maintained in DMEM/10% HI-FCS and 10% medium conditioned by the L-cell line that produces CSF-1 (American Type Culture Collection, Rockville, VA, USA).

Generation of Microglia With Stable Reduced Galectin-3 Protein Expression

Knocking down Galectin-3 protein expression was achieved through lentiviral infection of wild-type Balb/C microglia with shRNA directed against mouse Galectin-3 mRNA (Gal-3-shRNA) using pLKO.1 puro plasmids (Sigma-Aldrich, St. Louis, MO, USA). We tested three different shRNA sequences and finally used sequence 5′-GCAGTACAACCATCGGATGAA-3′. The plasmid was transfected into a 293T-based packaging cell line and the resulting culture supernatant used for lentiviral infection. Infected microglia were selected based on their resistance to puromycin brought by the pLKO.1 plasmid and levels of Galectin-3 protein were monitored by immunoblot. We refer to these microglia as Gal-3-KD microglia. As a control, microglia were infected in a similar way with the shRNA sequence 5′-CTTACGCTGAGTACTTCGA-3′ against the non-target firefly Luciferase gene. We refer to these microglia as control or control Luciferase (Con-Luc) microglia.

Isolation of Myelin

Myelin isolation from mouse brains was performed as previously described (Slobodov et al., 2001) and visualized (Gitik et al., 2010). Isolated myelin is "myelin-debris" since isolation involves breakdown of intact myelin.

Phagocytosis of Myelin-Debris

Microglia were plated in 96-well tissue culture plates at a density that minimizes cell-cell contact (0.25–1.5 $\times$ 10^4/well) in the presence of DMEM/F12 supplemented by 10% FCS. Non-adherent microglia were washed out after 2-h and adherent microglia left to rest overnight. Next, phagocytes were washed and myelin-debris added in the presence of 10% FCS for the indicated periods, unphagocytosed myelin-debris washed out, and levels of phagocytosis determined by ELISA. For testing the role of NCL and NPM in phagocytosis, microglia were pre-incubated overnight in 10 μM NCL inhibitor GRO (AS1411) aptamer and its control CRO (inactive oligomer; Integrated DNA Technologies, Coralville, IA, USA) or 2-h in 4 μM of NPM inhibitor NSC348884 (Cayman Chemicals, Ann Arbor, MI, USA). Then, 1-h of phagocytosis was assayed.

Quantifying Myelin-Debris Phagocytosis by ELISA

We quantified phagocytosis as previously detailed (Slobodov et al., 2001). The assay is based on the detection of myelin basic protein (MBP) in microglia lysates. Since MBP is unique to myelin and not produced by microglia, MBP levels in microglia cytoplasm are proportional to levels of phagocytosed myelin-debris. In brief, after washing unphagocytosed myelin-debris, microglia were lysed (0.05 M carbonate buffer, pH 10), lysates transferred to high protein absorbance plates (Nalge Nunc International, Rochester, NY, USA) and levels of MBP determined by ELISA using rat anti-MBP mAb and matching control IgG (Bio-Rad Laboratories Inc., Hercules, CA, USA).

When phagocytosis by Gal-3-KD microglia was compared to phagocytosis by control (Con-Luc) microglia, phagocytosis by each population was first normalized to the respective number of microglia counted in 1-mm^2 area at the center of wells. Normalizing phagocytosis to cell number is required since Gal-3-KD and control microglia may differ in their adherence

properties, thus resulting in different number of adherent microglia even when the same number of cells was initially seeded. To this end, microglia in replicate plates were fixed, stained and counted. Phagocytosis by Gal-3-KD microglia was calculated as percentage of phagocytosis by control microglia normalized to 100%. Phagocytosis in the presence of NCL and NPM inhibitors was calculated as percentage of phagocytosis in the presence of their respective controls, each control normalized to 100%.

Immunoblot Analysis

Microglia were plated in 10-cm tissue culture plates at a density that minimizes cell-cell contact (3×10^6 cells per plate) in the presence of DMEM supplemented by 10% FCS, and left to rest overnight. Phagocytes were washed in fresh DMEM supplemented by 10% FCS, myelin-debris added in the presence of serum for the indicated periods and unphagocytosed myelin-debris washed out. For lysis, microglia were washed in PBS and lysed in ice-cold lysis buffer (Tris HCL 1 M pH 7.5, $MgCl_2$ 1 M, NaCl 4 M, 0.5% NP-40, 0.1% DTT, 0.1% NaVa), supplemented with protease and phosphatase inhibitors cocktails (Sigma-Aldrich, St. Louis, MO, USA), cellular debris was removed by centrifugation, and total protein content determined using Bradford reagent (Sigma-Aldrich, St. Louis, MO, USA). Equal protein content from whole cell lysates was separated on SDS-PAGE. Proteins were blotted to nitrocellulose membranes, blocked with 10% non-fat milk or 5% BSA in Tris-buffered saline (TBS) for 1-h at RT, incubated over night at 4^0C in the presence of rat anti-mouse Galectin-3/MAC-2 M3/38 mAb (American Type Collection, Rockville, MD, USA), rabbit anti-cofilin, rabbit anti-pS^3-cofilin-1, and rabbit anti-β-tubulin (Santa Cruz Biotechnology, Santa Cruz, CA, USA). Blots were washed with TBST and incubated with respective secondary Abs donkey anti-rat and goat anti-rabbit conjugated to HRP (Jackson ImmunoResearch, West Grove, PA, USA) for 40-min at RT. Proteins were visualized with EZ-ECL kit for HRP detection (Beit Haemek, Israel). The intensities of immunoblot bands were determined by ImageJ software.

Confocal Fluorescence Microscopy

Microscopy was carried out in Olympus FluoView FV1000 confocal microscope. Alexa Fluor 488 labeled phalloidin (Invitrogen, Carlsbad, CA, USA) was used to visualize F-actin. CR3 was visualized using two rat anti-mouse CR3 mAbs produced by hybridoma cell lines: mAb M1/70 (Developmental Studies Hybridoma Bank, Iowa City, IA, USA) and mAb 5C6 (American Type Culture Collection, Rockville, VA, USA) followed by Cy3-conjugated rabbit anti-rat IgG (Jackson ImmunoResearch, West Grove, PA, USA). Optical slices, 1 μm thick, were scanned sequentially and then used to reconstruct whole images.

Statistical Analysis and Data Presentation

Parametric statistics were used after verifying that all data values follow a Gaussian distribution. The D'Agostino-Pearson normality test, unpaired *t*-test and one- and two way ANOVA were carried out using GraphPad Prism software as detailed in figure legends.

RESULTS

Galectin-3 Activates the Phagocytosis of Myelin-Debris

We previously showed that Galectin-3 activates the phagocytosis of myelin-debris in cultured primary microglia by binding and stabilizing K-Ras.GTP and so enhancing K-Ras.GTP/PI3K signaling (Rotshenker et al., 2008; Rotshenker, 2009). We reached this understanding based on the findings that levels of K-Ras.GTP alone and levels of the K-Ras.GTP/Galectin-3 complex increased during phagocytosis, and further, that disrupting the K-Ras.GTP/Galectin-3 complex pharmacologically reduced K-Ras.GTP levels, PI3K activity and phagocytosis. To validate the key role Galectin-3 plays in activating phagocytosis, we presently KD Galectin-3 protein levels in cultured primary microglia through lentiviral infection with Gal-3-shRNA, generating Gal-3-KD microglia. We used microglia infected with non-target Luciferase-shRNA as control. Gal-3-KD microglia displayed about 70% reductions in both Galectin-3 protein levels and myelin-debris phagocytosis compared with control microglia (**Figure 1**). This finding conforms to our previous observations that disrupting the K-Ras.GTP/Galectin-3 complex pharmacologically reduced phagocytosis by 70% (Rotshenker et al., 2008). Thus, our present and previous findings validate the key role that Galectin-3 plays in activating phagocytosis.

Nucleolin (NCL) and Nucleophosmin (NPM) Activate the Phagocytosis of Myelin-Debris

Our previous findings suggest that Galectin-3 activates the phagocytosis of myelin-debris by advancing K-Ras signaling (Rotshenker et al., 2008; Rotshenker, 2009). Since NCL and NPM also advance K-Ras signaling (Inder et al., 2010), we hypothesized that NCL and NPM could activate phagocytosis as does Galectin-3. We tested this prediction using specific NCL and NPM inhibitors (**Figure 2**). NCL inhibitor AS14111 reduced phagocytosis by about 30% and NPM inhibitor NSC38884 reduced phagocytosis by about 25%. This contrasts with about 70% reduced phagocytosis caused by knocking down Galectin-3 protein levels in Gal-3-KD microglia (**Figure 1**) and about 70% reduced phagocytosis caused by disrupting the K-Ras.GTP/Galectin-3 complex pharmacologically (Rotshenker et al., 2008; Rotshenker, 2009). This discrepancy could result, in part, from the different mechanism by which the three advance K-Ras signaling. Galectin-3 does so by stabilizing K-Ras.GTP (i.e., already activated K-Ras) and NCL and NPM by stabilizing K-Ras.GDP that yet needs to undergo activation at the inner surface of cell membranes (Inder et al., 2010; Tian et al., 2010).

Galectin-3 Controls Microglia Morphology and the Organization of Actin Filaments

Strikingly and unexpectedly, the morphology of cultured Gal-3-KD microglia differed dramatically from that of cultured control microglia (**Figure 3**). Control microglia were mostly oval/ellipsoid and fine filopodia projected from them. In

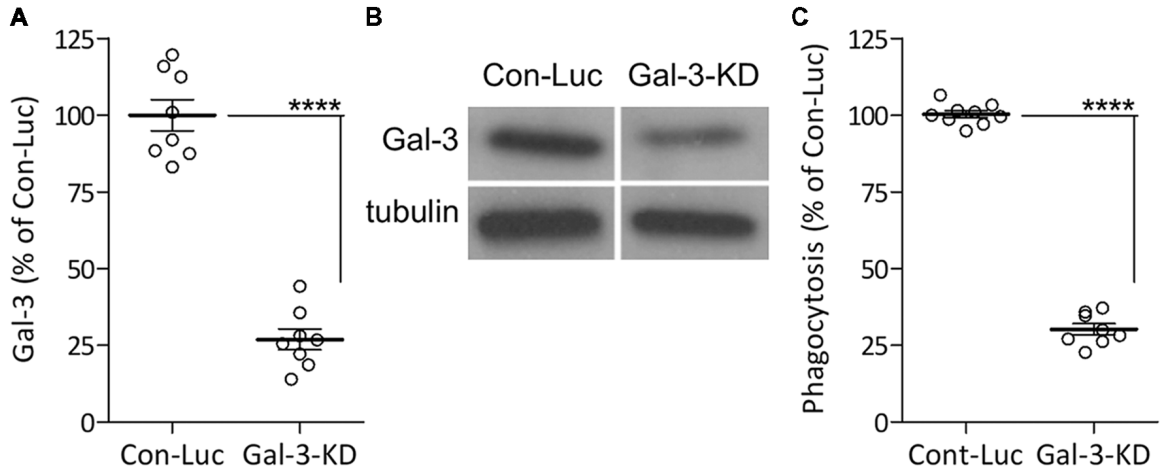

FIGURE 1 | The phagocytosis of myelin-debris is reduced in microglia expressing reduced levels of Galectin-3 protein. **(A,B)** Galectin-3 (Gal-3) protein levels were reduced/knocked-down (KD) in microglia infected with Gal-3-small-hairpin RNA (shRNA; Gal-3-KD microglia) compared with control microglia infected with non-target Luciferase-shRNA (Con-Luc microglia). **(A)** Quantification of Gal-3 protein levels based on **(B)** immunoblot analysis. **(A)** Gal-3 levels in Gal-3-KD microglia were calculated as percentage of Gal-3 levels in control microglia (Con-Luc) normalized to 100%. Values from individual blots and averages ± SE are given. Significance of difference, $^{****}p < 0.0001$, by unpaired *t*-test. **(C)** Phagocytosis of myelin-debris is reduced in Gal-3-KD microglia. Phagocytosis by Gal-3-KD microglia was calculated as percentage of phagocytosis by control microglia (Con-Luc) normalized to 100%. Values of individual experiments and averages ± SE are given. Significance of difference, $^{****}p < 0.0001$, by unpaired *t*-test.

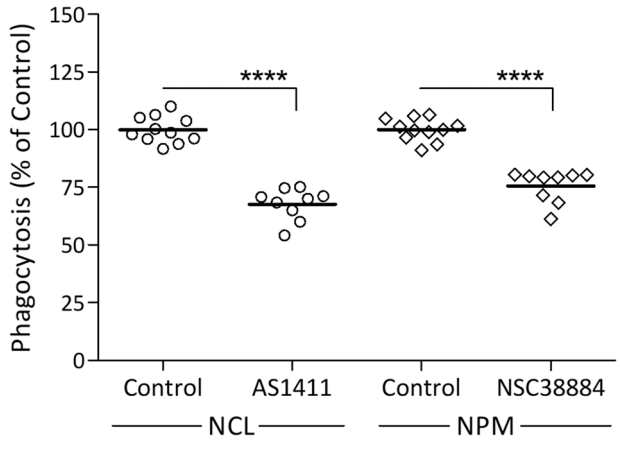

FIGURE 2 | Nucleolin (NCL) and nucleophosmin (NPM) inhibitors reduce the phagocytosis of myelin-debris. Wild-type microglia were pre-incubated in NCL inhibitor AS1411, NPM inhibitor NSC38884 and their respective controls, myelin-debris added for 1-h and phagocytosis assayed. Phagocytosis in the presence of each inhibitor was calculated as percentage of phagocytosis in its respective control normalized to 100%. Values of individual experiments and averages ± SE are given. Significance of difference, $^{****}p < 0.0001$, by unpaired *t*-test.

contrast, Gal-3-KD microglia extended thick branches that varied from short to very long. Some of these primary branches gave rise to secondary thick branches and filopodia projected from both primary and secondary branches. The morphology of control and Gal-3-KD microglia was very similar to that of cultured microglia obtained from wild-type and Galectin-3 knockout (Gal-$3^{-/-}$) mice (**Figure 5**). We refer to the morphology of Gal-3-KD microglia as being "branched-like" and that of control microglia as being "amoeboid-like" since the two reminded us of the "branched" and "amoeboid" morphologies described by Rio-Hortega (1932) in the intact and injured CNS parenchyma, respectively (Rio-Hortega, 1932; Sierra et al., 2016).

Moreover, the organization of actin filaments (F-actin) in control microglia differed strikingly from that in Gal-3-KD microglia (**Figure 3**). In control microglia, F-actin appeared in fine filamentous structures at the cell center and in closely packed filamentous structures at the cell cortex. In contrast, in Gal-3-KD microglia, F-actin appeared predominantly in highly dense deposits that varied from punctate to massive, and furthermore, fine filamentous structures were barely detected, if at all. The organization of F-actin in control and Gal-3-KD microglia was similar to that in cultured microglia from wild-type and Gal-$3^{-/-}$ mice (**Figure 5**). Thus, knocking down and knocking out Galectin-3 resulted in a dramatic change in both the morphology of microglia and the organization of F-actin in microglia, raising the possibility that Galectin-3 controls microglia morphology by regulating the organization of F-actin.

Galectin-3 Advances the Activation of Cofilin

Changing the organization of F-actin in cells requires that existing F-actin disassemble and new F-actin assemble in a different configuration from before (i.e., remodeling of F-actin). Active unphosphorylated cofilin (cofilin) initiates remodeling by causing F-actin to disassemble whereas inactive phosphorylated cofilin (p-cofilin) advances F-acting stabilization by obstructing the disassembly of F-actin (Oser and Condeelis, 2009; Bernstein and Bamburg, 2010). This understanding led us to hypothesize

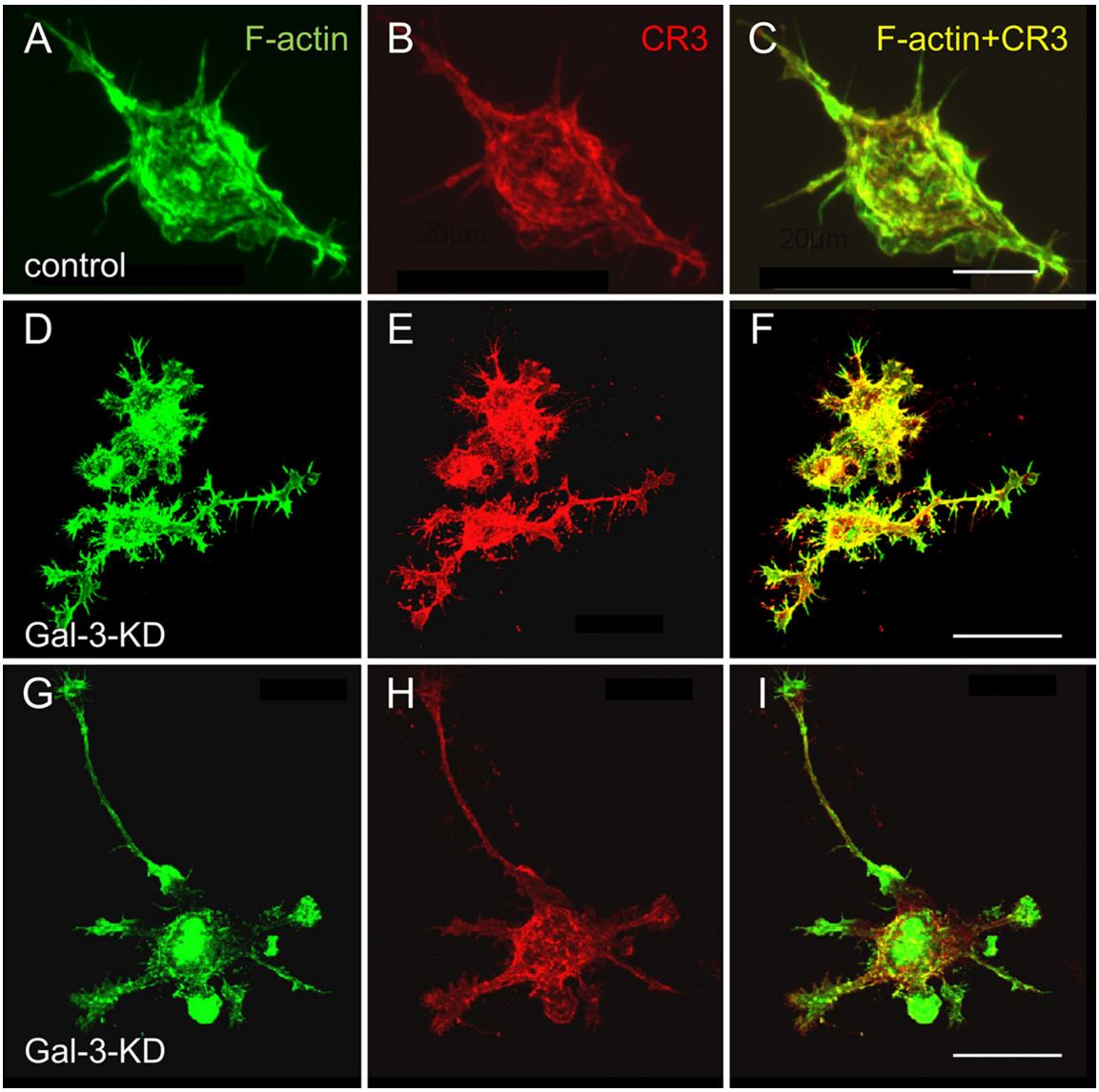

FIGURE 3 | Control microglia display amoeboid-like morphology and organization of filaments of actin (F-actin) in filamentous structures whereas Gal-3-KD microglia display branched-like morphology and organization of F-actin in dense punctate and massive deposits. Immunofluorescence confocal microscopy images of **(A–C)** a control microglia and **(D** through **I)** two fields of Gal-3-KD microglia. **(A,D,G)** F-actin is visualized by Alexa Fluor 488 labeled phalloidin (green). **(B,E,H)** Complement receptor-3 (CR3), a principal phagocytic receptor that mediates the phagocytosis of myelin-debris (Rotshenker, 2003), is visualized by anti-CR3 mAbs M1/70 and 5C6 (red). **(C,F,I)** F-actin/CR3 overlap (yellow). As seen, the images of Gal-3-KD microglia in (**D** through **I**) are reduced by a factor of five compared with the images of the control microglia in **(A–C)**. Bars: 10 μm in **(C)** for control microglia and 40 μm in **(F,I)** for Gal-3-KD microglia.

that cofilin could be instrumental in changing the organization of F-actin in control and wild-type microglia from that in Gal-3-KD and Gal-3$^{-/-}$ microglia (**Figures 3**, **5**). Further, we showed before that active cofilin activated and inactive p-cofilin inhibited phagocytosis in which filopodia/lamellipodia engulf myelin-debris (Hadas et al., 2012; Gitik et al., 2014). Taken all in consideration, could Galectin-3 control microglia morphology, F-actin organization, and phagocytosis by regulating the activation state of cofilin?

We addressed this issue by analyzing the activation state of cofilin before and during phagocytosis in control and Gal-3-KD microglia (**Figure 4**). Levels of inactive cofilin (i.e., p-cofilin), which advances the stabilization of F-actin, were higher in non-phagocytosing Gal-3-KD microglia than in non-phagocytosing control microglia. Then, during phagocytosis, in agreement with our previous findings (Hadas et al., 2012; Gitik et al., 2014), control microglia displayed transient activation of cofilin (i.e., transient reduction in p-cofilin levels). In contrast, levels of inactive p-cofilin remained high throughout phagocytosis in Gal-3-KD microglia. Taken altogether, it is very likely that knocking down Galectin-3 prompted structural changes in non-phagocytosing Gal-3-

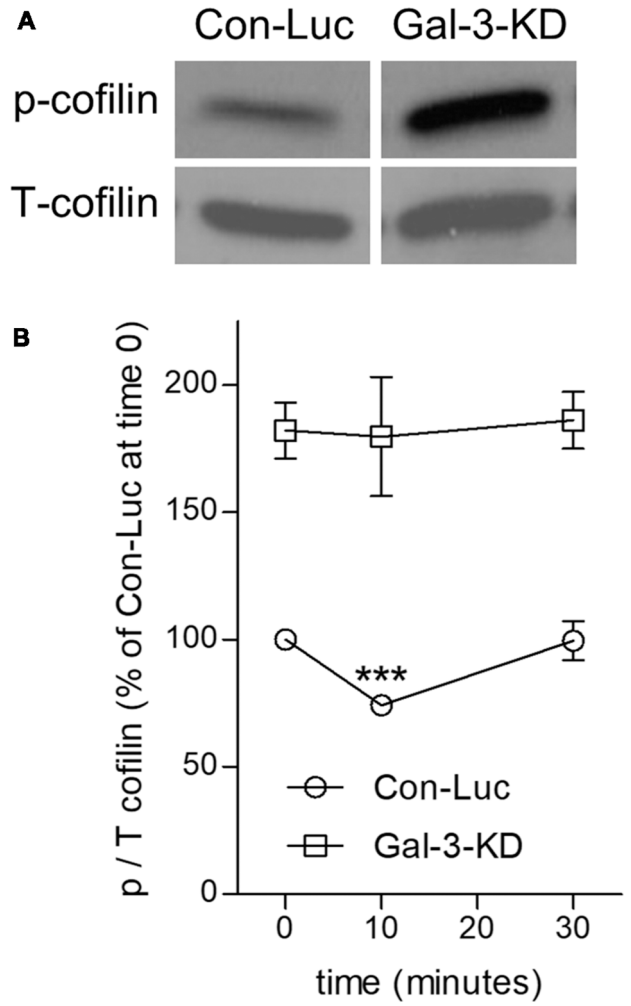

FIGURE 4 | Knocking down Galectin-3 advances the inactive state of cofilin (cofilin → p-cofilin) in non-phagocytosing and phagocytosing Galectin-3-KD microglia. **(A)** Levels of inactive p-cofilin are higher in non-phagocytosing Gal-3-KD than in non-phagocytosing control (Con-Luc) microglia. A representative immunoblot (one of six) of phosphorylated and total cofilin-1 (p- and T-cofilin). The western blot images were cropped for illustration purposes in **Supplementary Figure S1**. **(B)** Cofilin is transiently activated (i.e., transient reduction in p-cofilin) in control (Con-Luc) microglia but not in Gal-3-KD microglia. Quantitation of the ratio p/T cofilin based on immunoblots of microglia lysates taken before (time 0) and after 10 and 30 min of phagocytosis. The ratio p/T cofilin in non-phagocytosing control (Con-Luc) microglia (time 0 as in **A**) was defined 100%. Then, p/T in all other non-phagocytosing and phagocytosing microglia was calculated as percentage of p/T in control (Con-Luc) microglia at time 0. Average values ± SEM of six experiments, each performed in duplicates, are given. Significance of differences between initial values at 0 min and those at 10 and 30 min was calculated for control (Con-Luc) and Gal-3-KD microglia separately by one-way ANOVA and the Dunnett post-test. Activation of cofilin is significant, $^{***}p < 0.001$, in control (Con-Luc) microglia at 10 min. The difference between control (Con-Luc) and Gal-3-KD microglia is significant at all-time points (0, 10 and 30 min), $p < 0.001$ for each time point, by two way ANOVA and the Bonferroni posttest (not marked on the graph).

KD microglia and further reduced their phagocytic activity by advancing the inactive state of cofilin (i.e., increasing p-cofilin levels).

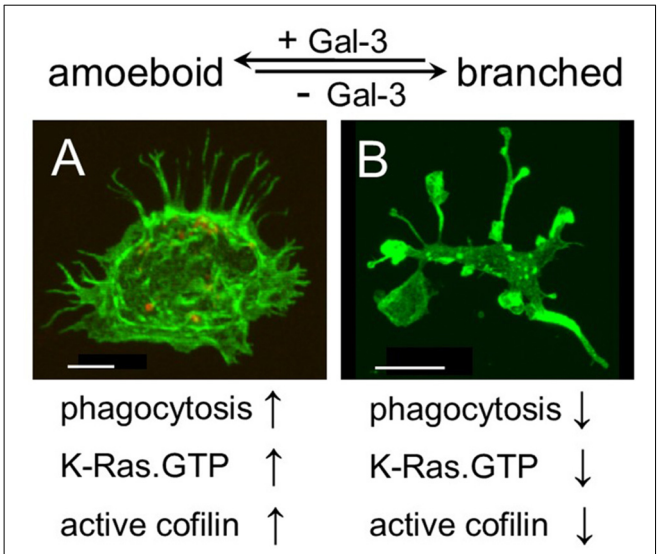

FIGURE 5 | Galectin-3 controls microglia phenotype whether amoeboid and phagocytic or branched and non-phagocytic by regulating the cytoskeleton. Immunofluorescence confocal microscopy images of cultured **(A)** wild-type and **(B)** Gal-$3^{-/-}$ microglia. F-actin is visualized by Alexa Fluor 488 labeled phalloidin (green). As seen, the image of the Gal-$3^{-/-}$ microglia in **(B)** is reduced by a factor of 6.4 compared with the image of the wild-type microglia in **(A)**. Bars: 5 μm in **(A)** and 20 μm in **(B)**.

DISCUSSION

Our findings are the first to suggest a molecular mechanism that controls both the morphology and the phagocytic activity of microglia, namely, that Galectin-3, by regulating the cytoskeleton, controls microglia phenotype whether amoeboid and phagocytic or branched and non-phagocytic. We reached this understanding based on the findings that amoeboid microglia were rich in Galectin-3, they displayed productive phagocytosis and F-actin organized in them in filamentous structures readily accessible for remodeling by active cofilin. In contrast, branched microglia were deficient in Galectin-3, they displayed unproductive phagocytosis, F-actin organized in them in punctate and/or massive deposits stabilized by inactive cofilin and the appearance of F-actin in filamentous structures was scarce. Thus consistent with the realization that the cytoskeleton controls cell morphology, the presence or absence of Galectin-3 could determine microglia morphology, whether amoeboid or branched, by controlling the activation state of cofilin and so affecting how F-actin is organized and how stable any particular organization is. Consistent with the realization that cofilin driven remodeling of F-actin advances the protrusion of filopodia/lamellipodia (Oser and Condeelis, 2009; Bernstein and Bamburg, 2010) and our previous findings that cofilin activates phagocytosis in which filopodia/lamellipodia engulf myelin-debris (Hadas et al., 2012; Gitik et al., 2014), Galectin-3 could activate phagocytosis by advancing the activation of cofilin. Taken altogether, it is most probable that Galectin-3 controls microglia phenotype whether amoeboid/phagocytic or branched/non-phagocytic by regulating the activation state of

cofilin, which, in turn, affects the organization and stability of F-actin (**Figure 5**).

Galectin-3 activating the phagocytosis of myelin-debris through cofilin, as we show here, adds to our previous findings that Galectin-3 activated phagocytosis by enhancing K-Ras.GTP/PI3K signaling (Rotshenker et al., 2008; Rotshenker, 2009), leading to PI3K/PLC/PKC signaling (Makranz et al., 2004; Cohen et al., 2006) and then to actin/myosin-based contraction, causing filopodia/lamellipodia to retract/internalize myelin-debris (Gitik et al., 2010). Our present findings that NCL and NPM activated phagocytosis, albeit less than Galectin-3, agree with and further support the concept that Galectin-3 activates phagocytosis by advancing K-Ras signaling since also NCL and NPM advance K-Ras signaling (Inder et al., 2010; Tian et al., 2010). Nonetheless, as we currently show, Galectin-3 dominated over NCL and NPM in this regard. Thus, our present and previous findings together suggest that Galectin-3 activates phagocytosis by targeting the cytoskeleton twice: first, by advancing the active state of cofilin, leading to F-actin remodeling, and second, by advancing K-Ras.GTP/PI3K signaling, leading to actin/myosin-based contraction (**Figure 5**).

It is most probable that our proposition that Galectin-3 controls microglia phenotype whether amoeboid/phagocytic or branched/non-phagocytic, which we base on findings in cultured microglia, applies to the *in vivo* scenario. The concept of Galectin-3 activated phagocytosis is supported by our previous findings that the expression of Galectin-3 (named MAC-2 in some of our previous studies) correlated with myelin-debris phagocytosis in microglia *in vivo*. In adult mice, non-phagocytosing microglia did not express Galectin-3 protein in intact CNS nor in CNS Wallerian degeneration, i.e., distal to lesion sites. In contrast, and along with activating phagocytosis, microglia upregulated Galectin-3 expression at sites of trauma and in EAE (Reichert and Rotshenker, 1996, 1999). With regard to Galectin-3 controlling microglia morphology, two reports are of interest to us. First, that transcription factors Runx1 and Runx2 regulate Galectin-3 expression in human pituitary tumors (Zhang et al., 2009). Second, that amoeboid microglia in neonate mice but not branched microglia in adult mice expressed Runx1, and further, that Runx1 is upregulated in spinal cord microglia activated by nerve injury in adult mice (Zusso et al., 2012). If in mice, as in human pituitary tumors, Runx1 controls Galectin-3 protein expression, then Runx1 controls microglia morphology *in vivo* through Galectin-3 as our present findings suggest. Lastly, Galectin-3 may also be involved in the pruning of synapses during the neonatal period and in the early loss of synapses in Alzheimer diseases (Schafer et al., 2012; Hong et al., 2016). We base this suggestion on the findings that in these two instances CR3 mediated the phagocytosis of synaptic elements in microglia and that CR3 is the principal phagocytic receptor that mediated the phagocytosis of myelin-debris in microglia in our studies (Reichert and Rotshenker, 2003; Rotshenker, 2003). Thus, Galecin-3 could activate CR3 mediated phagocytosis of synaptic elements as it activated CR3 mediated phagocytosis of myelin-debris. Taken altogether, Galectin-3 may control microglia morphology and phagocytic activity *in vivo* as *in vitro*.

AUTHOR CONTRIBUTIONS

SR designed and supervised experiments conducted by FR.

FUNDING

This work was supported by grant number 1658/14 from the Israel Science Foundation, and The Charles Wolfson Charitable Trust.

ACKNOWLEDGMENTS

We thank Rachel Klinehause for her participation in some experiments and Dr. Sara Leven for reviewing and commenting on the manuscript.

SUPPLEMENTARY MATERIAL

The Supplementary Material for this article can be found online at: https://www.frontiersin.org/articles/10.3389/fncel.2019.00090/full#supplementary-material

FIGURE S1 | Levels of inactive p-cofilin are higher in non-phagocytosing control (Con-Luc)microglia than in non-phagocytosing Gal-3-KD microglia. **(A,B)** Two separateimmunoblots were carried out using replicate lysate samples from non-phagocytosing control(Con-Luc) and Gal-3-KD microglia. In **(A)**, p-cofilin was visualized and in **(B)**, T-cofilin wasvisualized. The marked images were cropped and used for illustration in manuscript **Figure 4**.

REFERENCES

Ajami, B., Bennett, J. L., Krieger, C., Tetzlaff, W., and Rossi, F. M. (2007). Local self-renewal can sustain CNS microglia maintenance and function throughout adult life. *Nat. Neurosci.* 10, 1538–1543. doi: 10.1038/nn2014

Bates, P. J., Laber, D. A., Miller, D. M., Thomas, S. D., and Trent, J. O. (2009). Discovery and development of the G-rich oligonucleotide AS1411 as a novel treatment for cancer. *Exp. Mol. Pathol.* 86, 151–164. doi: 10.1016/j.yexmp.2009.01.004

Bernstein, B. W., and Bamburg, J. R. (2010). ADF/cofilin: a functional node in cell biology. *Trends Cell Biol.* 20, 187–195. doi: 10.1016/j.tcb.2010.01.001

Bohlen, C. J., Bennett, F. C., Tucker, A. F., Collins, H. Y., Mulinyawe, S. B., and Barres, B. A. (2017). Diverse requirements for microglial survival, specification and function revealed by defined-medium cultures. *Neuron* 94, 759–773. doi: 10.1016/j.neuron.2017.04.043

Butovsky, O., Jedrychowski, M. P., Moore, C. S., Cialic, R., Lanser, A. J., Gabriely, G., et al. (2014). Identification of a unique TGF-β-dependent molecular and functional signature in microglia. *Nat. Neurosci.* 17, 131–143. doi: 10.1038/nn.3599

Cohen, G., Makranz, C., Spira, M., Kodama, T., Reichert, F., and Rotshenker, S. (2006). Non-PKC DAG/Phorbol-Ester receptor(s) inhibit complement receptor-3 and nPKC inhibit scavenger receptor-AI/II-mediated myelin phagocytosis but cPKC, PI3k and PLC gamma activate myelin phagocytosis by both. *Glia* 53, 538–550. doi: 10.1002/glia.20304

Gitik, M., Kleinhaus, R., Hadas, S., Reichert, F., and Rotshenker, S. (2014). Phagocytic receptors activate and immune inhibitory receptor SIRPα inhibits phagocytosis through paxillin and cofilin. *Front. Cell Neurosci.* 8:104. doi: 10.3389/fncel.2014.00104

Gitik, M., Liraz Zaltsman, S., Oldenborg, P. -A., Reichert, F., and Rotshenker, S. (2011). Myelin down-regulates myelin phagocytosis by microglia and

macrophages through interactions between CD47 on myelin and SIRPα (signal regulatory protein-α) on phagocytes. *J. Neuroinflammation* 8:24. doi: 10.1186/1742-2094-8-24

Gitik, M., Reichert, F., and Rotshenker, S. (2010). Cytoskeleton plays a dual role of activation and inhibition in myelin and zymosan phagocytosis by microglia. *FASEB J.* 24, 2211–2221. doi: 10.1096/fj.09-146118

Goldmann, T., Wieghofer, P., Jordão, M. J. C., Prutek, F., Hagemeyer, N., Frenzel, K., et al. (2016). Origin, fate and dynamics of macrophages at central nervous system interfaces. *Nat. Immunol.* 17, 797–805. doi: 10.1038/ni.3423

Hadas, S., Spira, M., Hanisch, U. K., Reichert, F., and Rotshenker, S. (2012). Complement receptor-3 negatively regulates the phagocytosis of degenerated myelin through tyrosine kinase Syk and cofilin. *J. Neuroinflammation* 9:166. doi: 10.1186/1742-2094-9-166

Hirano, K., Miki, Y., Hirai, Y., Sato, R., Itoh, T., Hayashi, A., et al. (2005). A multifunctional shuttling protein nucleolin is a macrophage receptor for apoptotic cells. *J. Biol. Chem.* 280, 39284–39293. doi: 10.1074/jbc.m505275200

Hong, S., Beja-Glasser, V. F., Nfonoyim, B. M., Frouin, A., Li, S., Ramakrishnan, S., et al. (2016). Complement and microglia mediate early synapse loss in Alzheimer mouse models. *Science* 352, 712–716. doi: 10.1126/science.aad8373

Inder, K. L., Hill, M. M., and Hancock, J. F. (2010). Nucleophosmin and nucleolin regulate K-Ras signaling. *Commun. Integr. Biol.* 3, 188–190. doi: 10.4161/cib.3.2.10923

Kettenmann, H., Kirchhoff, F., and Verkhratsky, A. (2013). Microglia: new roles for the synaptic stripper. *Neuron* 77, 10–18. doi: 10.1016/j.neuron.2012.12.023

Kotter, M. R., Li, W. -W., Zhao, C., and Franklin, R. J. (2006). Myelin impairs CNS remyelination by inhibiting oligodendrocyte precursor cell differentiation. *J. Neurosci.* 26, 328–332. doi: 10.1523/jneurosci.2615-05.2006

Lassmann, H., Brück, W., and Lucchinetti, C. F. (2007). The immunopathology of multiple sclerosis: an overview. *Brain Pathol.* 17, 210–218. doi: 10.1111/j.1750-3639.2007.00064.x

Levy, R., Biran, A., Poirier, F., Raz, A., and Kloog, Y. (2011). Galectin-3 mediates cross-talk between K-Ras and Let-7c tumor suppressor microRNA. *PLoS One* 6:e27490. doi: 10.1371/journal.pone.0027490

Makranz, C., Cohen, G., Baron, A., Levidor, L., Kodama, T., Reichert, F., et al. (2004). Phosphatidylinositol 3-kinase, phosphoinositide-specific phospholipase-Cγ and protein kinase-C signal myelin phagocytosis mediated by complement receptor-3 alone and combined with scavenger receptor-AI/II in macrophages. *Neurobiol. Dis.* 15, 279–286. doi: 10.1016/j.nbd.2003.11.007

Mèndez-Huergo, S. P., Blidner, A. G., and Rabinovich, G. A. (2017). Galectins: emerging regulatory checkpoints linking tumor immunity and angiogenesis. *Curr. Opin. Immunol.* 45, 8–15. doi: 10.1016/j.coi.2016.12.003

Mildner, A., Schmidt, H., Nitsche, M., Merkler, D., Hanisch, U. K., Mack, M., et al. (2007). Microglia in the adult brain arise from Ly-6C^{hi}CCR2^{+} monocytes only under defined host conditions. *Nat. Neurosci.* 10, 1544–1553. doi: 10.1038/nn2015

Norris, G. T., and Kipnis, J. (2018). Immune cells and CNS physiology: microglia and beyond. *J. Exp. Med.* 216, 60–70. doi: 10.1084/jem.20180199

Oser, M., and Condeelis, J. (2009). The cofilin activity cycle in lamellipodia and invadopodia. *J. Cell. Biochem.* 108, 1252–1262. doi: 10.1002/jcb.22372

Ozawa, D., Nakamura, T., Koike, M., Hirano, K., Miki, Y., and Beppu, M. (2013). Shuttling protein nucleolin is a microglia receptor for amyloid beta peptide 1–42. *Biol. Pharm. Bull.* 36, 1587–1593. doi: 10.1248/bpb.b13-00432

Reichert, F., and Rotshenker, S. (1996). Deficient activation of microglia during optic nerve degeneration. *J. Neuroimmunol.* 70, 153–161. doi: 10.1016/s0165-5728(96)00112-9

Reichert, F., and Rotshenker, S. (1999). Galectin-3/MAC-2 in experimental allergic encephalomyelitis. *Exp. Neurol.* 160, 508–514. doi: 10.1006/exnr.1999.7229

Reichert, F., and Rotshenker, S. (2003). Complement-receptor-3 and scavenger-receptor-AI/II mediated myelin phagocytosis in microglia and macrophages. *Neurobiol. Dis.* 12, 65–72. doi: 10.1016/s0969-9961(02)00008-6

Rio-Hortega, P. D. (1932). "Microglia," in *Cytology and Cellular Pathology of the Nervous System*, ed. W. Penfield (New York, NY: Hafner Publishing Company), 483–534.

Rotshenker, S. (2003). Microglia and macrophage activation and the regulation of complement-receptor-3 (CR3/MAC-1)-mediated myelin phagocytosis in injury and disease. *J. Mol. Neurosci.* 21, 65–72. doi: 10.1385/jmn:21:1:65

Rotshenker, S. (2009). The role of galectin-3/MAC-2 in the activation of the innate-immune function of phagocytosis in microglia in injury and disease. *J. Mol. Neurosci.* 39, 99–103. doi: 10.1007/s12031-009-9186-7

Rotshenker, S., Reichert, F., Gitik, M., Haklai, R., Elad-Sfadia, G., and Kloog, Y. (2008). Galectin-3/MAC-2, Ras and PI3K activate complement receptor-3 and scavenger receptor-AI/II mediated myelin phagocytosis in microglia. *Glia* 56, 1607–1613. doi: 10.1002/glia.20713

Ruvolo, P. P. (2016). Galectin 3 as a guardian of the tumor microenvironment. *Biochim. Biophys. Acta* 1863, 427–437. doi: 10.1016/j.bbamcr.2015.08.008

Schafer, D. P., Lehrman, E. K., Kautzman, A. G., Koyama, R., Mardinly, A. R., Yamasaki, R., et al. (2012). Microglia sculpt postnatal neural circuits in an activity and complement-dependent manner. *Neuron* 74, 691–705. doi: 10.1016/j.neuron.2012.03.026

Sierra, A., de, C. F., Del Río-Hortega, J., Rafael Iglesias-Rozas, J., Garrosa, M., and Kettenmann, H. (2016). The "Big-Bang" for modern glial biology: translation and comments on Pío del Río-Hortega 1919 series of papers on microglia. *Glia* 64, 1801–1840. doi: 10.1002/glia.23046

Slobodov, U., Reichert, F., Mirski, R., and Rotshenker, S. (2001). Distinct inflammatory stimuli induce different patterns of myelin phagocytosis and degradation in recruited macrophages. *Exp. Neurol.* 167, 401–409. doi: 10.1006/exnr.2000.7559

Tay, T. L., Hagemeyer, N., and Prinz, M. (2016). The force awakens: insights into the origin and formation of microglia. *Curr. Opin. Neurobiol.* 39, 30–37. doi: 10.1016/j.conb.2016.04.003

Thiemann, S., and Baum, L. G. (2016). Galectins and immune responses—just how do they do those things they do? *Annu. Rev. Immunol.* 34, 243–264. doi: 10.1146/annurev-immunol-041015-055402

Tian, T., Plowman, S. J., Parton, R. G., Kloog, Y., and Hancock, J. F. (2010). Mathematical modeling of K-Ras nanocluster formation on the plasma membrane. *Biophys. J.* 99, 534–543. doi: 10.1016/j.bpj.2010.04.055

Tremblay, M.-È., Lowery, R. L., and Majewska, A. K. (2010). Microglial Interactions with Synapses Are Modulated by Visual Experience. *PLoS Biol.* 8:e1000527. doi: 10.1371/journal.pbio.1000527

Vargas, M. E., and Barres, B. A. (2007). Why is Wallerian degeneration in the CNS so slow? *Annu. Rev. Neurosci.* 30, 153–179. doi: 10.1146/annurev.neuro.30.051606.094354

Yiu, G., and He, Z. (2006). Glial inhibition of CNS axon regeneration. *Nat. Rev. Neurosci.* 7, 617–627. doi: 10.1038/nrn1956

Zhang, H.-Y., Jin, L., Stilling, G. A., Ruebel, K. H., Coonse, K., Tanizaki, Y., et al. (2009). RUNX1 and RUNX2 upregulate Galectin-3 expression in human pituitary tumors. *Endocrine* 35, 101–111. doi: 10.1007/s12020-008-9129-z

Zusso, M., Methot, L., Lo, R., Greenhalgh, A. D., David, S., and Stifani, S. (2012). Regulation of postnatal forebrain amoeboid microglial cell proliferation and development by the transcription factor Runx1. *J. Neurosci.* 32, 11285–11298. doi: 10.1523/jneurosci.6182-11.2012

Conflict of Interest Statement: The authors declare that the research was conducted in the absence of any commercial or financial relationships that could be construed as a potential conflict of interest.

frontiers in Cellular Neuroscience

ORIGINAL RESEARCH
published: 09 April 2019
doi: 10.3389/fncel.2019.00109

Phenotypic Effects of Wild-Type and Mutant SOD1 Expression in N9 Murine Microglia at Steady State, Inflammatory and Immunomodulatory Conditions

Ana Rita Vaz[1,2], *Sara Pinto*[1], *Catarina Ezequiel*[1], *Carolina Cunha*[1], *Luís A. Carvalho*[1], *Rui Moreira*[1,3] *and Dora Brites*[1,2]*

[1]Research Institute for Medicines (iMed.ULisboa), Faculty of Pharmacy, University of Lisbon, Lisbon, Portugal, [2]Department of Biochemistry and Human Biology, Faculty of Pharmacy, University of Lisbon, Lisbon, Portugal, [3]Department of Pharmaceutical Chemistry and Therapeutics, Faculty of Pharmacy, University of Lisbon, Lisbon, Portugal

Accumulation of mutated superoxide dismutase 1 (mSOD1) in amyotrophic lateral sclerosis (ALS) involves injury to motor neurons (MNs), activation of glial cells and immune unbalance. However, neuroinflammation, besides its detrimental effects, also plays beneficial roles in ALS pathophysiology. Therefore, the targeting of microglia to modulate the release of inflammatory neurotoxic mediators and their exosomal dissemination, while strengthening cell neuroprotective properties, has gained growing interest. We used the N9 microglia cell line to identify phenotype diversity upon the overexpression of wild-type (WT; hSOD1^{WT}) and mutated G93A (hSOD1^{G93A}) protein. To investigate how each transduced cell respond to an inflammatory stimulus, N9 microglia were treated with lipopolysaccharide (LPS). Glycoursodeoxycholic acid (GUDCA) and dipeptidyl vinyl sulfone (VS), known to exert neuroprotective properties, were tested for their immunoregulatory properties. Reduced Fizz1, IL-10 and TLR4 mRNAs were observed in both transduced cells. However, in contrast with hSOD1^{WT}-induced decreased of inflammatory markers, microglia transduced with hSOD1^{G93A} showed upregulation of pro-inflammatory (TNF-α/IL-1β/HMGB1/S100B/iNOS) and membrane receptors (MFG-E8/RAGE). Importantly, their derived exosomes were enriched in HMGB1 and SOD1. When inflammatory-associated miRNAs were evaluated, increased miR-146a in cells with overexpressed hSOD1^{WT} was not recapitulated in their exosomes, whereas hSOD1^{G93A} triggered elevated exosomal miR-155/miR-146a, but no changes in cells. LPS stimulus increased M1/M2 associated markers in the naïve microglia, including MFG-E8, miR-155 and miR-146a, whose expression was decreased in both hSOD1^{WT} and hSOD1^{G93A} cells treated with LPS. Treatment with GUDCA or VS led to a decrease of TNF-α, IL-1β, HMGB1, S100B and miR-155 in hSOD1^{G93A} microglia. Only GUDCA was able to increase cellular IL-10, RAGE and TLR4, together with miR-21, while decreased exosomal miR-155 cargo. Conversely, VS reduced MMP-2/MMP-9 activation, as well as upregulated MFG-E8 and miR-146a, while producing miR-21

OPEN ACCESS

Edited by:
Raquel Ferreira, Universidade da Beira Interior, Portugal

Reviewed by:
Adrian Israelson, Ben-Gurion University of the Negev, Israel
Hermona Soreq, Hebrew University of Jerusalem, Israel

***Correspondence:**
Dora Brites
dbrites@ff.ulisboa.pt

Received: *31 October 2018*
Accepted: *05 March 2019*
Published: *09 April 2019*

Citation:
Vaz AR, Pinto S, Ezequiel C, Cunha C, Carvalho LA, Moreira R and Brites D (2019) Phenotypic Effects of Wild-Type and Mutant SOD1 Expression in N9 Murine Microglia at Steady State, Inflammatory and Immunomodulatory Conditions. Front. Cell. Neurosci. 13:109. doi: 10.3389/fncel.2019.00109

shuttling into exosomes. The current study supports the powerful role of overexpressed hSOD1^{WT} in attenuating M1/M2 activation, and that of hSOD1^{G93A} in switching microglia from the steady state into a reactive phenotype with low responsiveness to stimuli. This work further reveals GUDCA and VS as promising modulators of microglia immune response by eliciting common and compound-specific molecular mechanisms that may promote neuroregeneration.

Keywords: amyotrophic lateral sclerosis, mutant SOD1^{G93A}, microglia reactivity, inflammatory-associated microRNAs, glycoursodeoxycholic acid, vinyl sulfone

INTRODUCTION

Amyotrophic lateral sclerosis (ALS) is a fatal motor neuron (MN) disease that affects both upper MNs, in the motor cortex, and lower MNs, in the brainstem and spinal cord. The major hallmark of this disease is the accumulation of intracellular protein inclusions in MNs, thought to be caused by mutations, protein damage such as oxidation, or protein seeding (Chiò et al., 2013; Robberecht and Philips, 2013). Among the several genes linked to ALS, there is evidence supporting a pathogenic role for Cu/Zn superoxide dismutase 1 (SOD1) in 20% of familial ALS cases and 3% of sporadic cases (Krüger et al., 2016). In fact, mutations in SOD1 are associated with a toxic gain of function that leads to protein misfolding and aggregation of the protein intracellularly (Rotunno and Bosco, 2013). More importantly, the uptake of misfolded and aggregated mutant SOD1 by other cells induces aggregation of endogenous mutant SOD1 and wild-type (WT) SOD1 protein (Münch et al., 2011; Sundaramoorthy et al., 2013). Small extracellular vesicles, here also designated as exosomes, have particular relevance as part of the cell-to-cell signaling mechanisms. Actually, once released, these vesicles can be taken up by nearby cells or travel long distances, affecting cellular function in either physiological or pathological ways (Sarko and McKinney, 2017). Misfolded and mutant SOD1 can be released *via* exocytosis, upon apoptosis or, as recently reported, inside exosomes (Gomes et al., 2007; Basso et al., 2013; Silverman et al., 2016). Once released into the extracellular space, mutant SOD1 activates microglia (Zhao et al., 2010) and we recently showed that the engulfment of exosomes released from mutant SOD1 MNs by microglia leads to the activation of inflammatory signaling pathways and loss of their phagocytic ability (Pinto et al., 2017). Despite decades of research and several studies pointing to SOD1 toxic function as the main player in ALS pathogenesis, the exact role of SOD1^{WT} and the impact of the mutated form in microglia function remains unclear. The relevance of microglia in the onset and progression of ALS is increasingly recognized and different polarized activated phenotypes were found in several models of ALS. In the majority of the studies using mutated SOD1 models, microglia overactivation was shown to contribute for ALS progression (Beers et al., 2006; Boillée et al., 2006). Two types of microglial activation have been considered, the classical M1 phenotype associated with the release of pro-inflammatory molecules and activation of receptors, and the M2 phenotype related with the secretion of anti-inflammatory mediators and growth factors, contributing to the repair and neuroprotection (Brites and Fernandes, 2015; Komine and Yamanaka, 2015). However, the latest knowledge points to the coexistence of different heterogeneous states and mixed phenotypes (Tang and Le, 2016; Pinto et al., 2017), and anti-inflammatory strategies have been replaced by the concept of active immunomodulation (Pena-Altamira et al., 2016). Actually, microglia activation was described as having both beneficial and injurious effects in ALS, depending on the relative prevalence of harmful and protective genes, on the ALS disease model and on the state of disease progression (Liao et al., 2012; Brites and Vaz, 2014; Gravel et al., 2016). In this sense, while the reduction of microgliosis was shown to slow ALS progression in the mutated SOD1 mice (Martínez-Muriana et al., 2016), reactive microglia was protective to MN degeneration in a mouse model of TDP-43 proteinopathy (Spiller et al., 2018), reinforcing the relevance of microglia reactivity and function in the ALS context.

Inflammatory-associated microRNAs (inflamma-miRNAs) are without doubt a new paradigm for understanding immunoregulation and inflammation. They showed to be important mediators of macrophages/microglia polarization and were found as part of microglia exosomal cargo, thus being able to modulate other cells (Alexander et al., 2015; Cardoso et al., 2016; Cunha et al., 2016; Fernandes et al., 2018). One of the miRNAs that gained particular attention in ALS is miRNA(miR)-155, already described in fALS and sALS patients (Koval et al., 2013), and also in the pre-symptomatic mutated superoxide dismutase 1 (mSOD1) mice, even before MN loss (Cunha et al., 2018), pointing this miRNA as a promising biomarker in ALS. Interestingly, targeting of miR-155 restored microglial proper functions in mSOD1 mice and prolonged mice survival (Butovsky et al., 2015), suggesting the benefits of molecules targeting miR-155 levels to be used as therapeutic strategies.

Currently, there are still no specific targets and effective therapies for ALS, due to the involvement of several multifactorial pathophysiological mechanisms. The only available treatments licensed by the Food and Drug Administration (FDA) are riluzole, since 1996, and the new compound, Edaravone (Abe et al., 2017; Cruz, 2018). Our previous studies have demonstrated that glycoursodeoxycholic acid (GUDCA), a conjugated bile acid, has antioxidant, anti-inflammatory and neuroprotective effects in a cellular model of mutant SOD1 neurodegeneration (Vaz et al., 2015). Lately, we also showed that dipeptidyl vinyl sulfone (VS), a small molecule with inhibitory cysteine protease activity, was able to prevent amyloid-β(Aβ)-induced microglia-inflammatory signaling pathways in the N9 microglia cell line, by inhibiting high

mobility group box protein 1 (HMGB1) and interleukin(IL)-1β production (Falcão et al., 2017). Surprisingly, VS was also able to rescue miR-155 overexpression, thus indicating its potential in miR-155 immunoregulation.

Mice overexpressing human $SOD1^{WT}$ have been used as controls, but some studies revealed the existence of abnormalities in the cerebellum (Afshar et al., 2017) and others that hastened the disease in G85R transgenic mice (Wang et al., 2009), highlighting that exaggerated expression of SOD1 is clearly not physiological. In fact, overexpression of both *SOD1* and *SOD1G93A* genes account for an elevation of SOD1 protein levels and changes in iron metabolism genes expression (Gajowiak et al., 2015). However, in the N9 murine microglia, SOD1 overexpression decreased the release of tumor necrosis factor α (TNF-α) and IL-6 upon stimulation with lipopolysaccharide (LPS; Dimayuga et al., 2007), and that of mutant SOD1 in BV-2 microglial cell lines increased TNF-α secretion and their neurotoxic potential (Liu et al., 2009). It is thus essential to significantly expand our knowledge on the molecular mechanisms involved in ALS microglia dysfunctional properties to target key steps with novel drugs. In the present study, we assessed the inflammatory phenotype diversity of N9 murine microglia upon transduction to promote the overexpression of human SOD1, WT ($hSOD1^{WT}$) or mutated G93A ($hSOD1^{G93A}$) protein, relatively to naïve cells. To have a better insight on how such transduction may differently compromise the microglia response to an inflammatory stimulus, we treated these cells with LPS and evaluated a set of inflammatory and anti-inflammatory mediators, as well as inflamma-miRNAs. Finally, we assessed the potential immunoregulatory properties of GUDCA and VS.

Data revealed that both $hSOD1^{WT}$ and $hSOD1^{G93A}$ overexpression in N9-microglia induced morphological shape alterations and reduction of M2 markers, compatible with an activated cell. Major inflammatory genes were only increased in the $hSOD1^{G93A}$ cells, which released exosomes enriched in miR-155 and miR-146a, as well as in HMGB1 and SOD1 mRNAs. Interestingly, transduced cells showed a defective stimulus-response to LPS, in contrast with the naïve cells that presented exacerbated inflammatory markers. We also provide evidence that GUDCA and VS exert immunomodulatory properties over the $hSOD1^{G93A}$ microglia, but that their benefits are mediated by molecular pathways that are specific of each compound. Thus, we may conclude that depending on the key molecular cascades to be modulated towards neuroprotection, GUDCA and VS can be effective therapeutic strategies to restore microglial function in ALS.

MATERIALS AND METHODS

N9 Cell Line Transduction: Lentiviral Production and Generation of N9 Cells Expressing $hSOD1^{WT}$-GFP and $hSOD1^{G93A}$-GFP Protein

We used the N9 microglial cell line (Cunha et al., 2016; Pinto et al., 2017). These cells are reported to present features similar to microglia in primary cultures, such as phagocytosis and inflammation-related features (Righi et al., 1989; Bruce-Keller et al., 2000; Fleisher-Berkovich et al., 2010). Lentiviral particles were produced by co-transfections of HEK293T cells with the packaging plasmids pGal-pol and pRev, the envelope plasmid pVSV-G and the lentiviral expression vectors plvAcGFP-hSOD1wt/plvAcGFP-hSOD1G93A (plasmids #27138 and #27142, respectively, Addgene, Cambridge, USA; Stevens et al., 2010), at a ratio of 3:2:1:4, using X-tremeGene HP, according to the manufacturer's instructions (Roche, Mannhein, Germany; Simões et al., 2015; Pereira et al., 2016). Twenty-four hours after transfection, cell media was changed. Supernatants containing lentiviral particles were collected after 48 and 72 h, filtered using a 0.22 μm sterile filter and stored at −80°C. To stably overexpress $hSOD1^{WT}$ and $hSOD1^{G93A}$ in N9 microglia cell line, cells were seeded in 6-well plates at a density of 3×10^5 cells/well and, 24 h after plating, cells were transduced by adding the supernatants containing lentiviral particles. Media was changed 4–5 times to eliminate all the lentiviral particles (Simões et al., 2015; Pereira et al., 2016). Stable cell lines were purified by cell sorting of green fluorescent protein (GFP) expression (BDFACSAria, BD Biosciences) and the percentage of GFP-positive cells was monitored in the GUAVA flow cytometer. The percentage of GFP-expressing cells was >80% in all experiments (**Figure 1**). Cells were maintained in Roswell Park Memorial Institute (RPMI) medium supplemented with 10% fetal bovine serum (FBS), 1% L-glutamine and 1% Penicillin/Streptomycin. For each experiment, cells were plated at a concentration of 1×10^5 cells/ml (Cunha et al., 2016). RPMI was purchased from Sigma-Aldrich (St. Louis, MO, USA). FBS, L-glutamine and Penicillin/Streptomycin were purchased from Biochrom AG (Berlin, Germany).

N9 Cells Incubation

After 24 h of plating, cellular media was changed and either $hSOD1^{WT}$ and $hSOD1^{G93A}$ cells were maintained for 48 h, treated or not with LPS (300 ng/ml). Non-transduced N9 cells (naïve) were used as controls, and also treated or not with LPS. In another set of experiments, $hSOD1^{G93A}$ cells were incubated with GUDCA (50 μM) or with VS (10 μM), also during 48 h.

Exosome Isolation

Exosomes were obtained from the extracellular media of N9 naïve, $hSOD1^{WT}$ and N9 $hSOD1^{G93A}$ cells, according to our previous publication (Pinto et al., 2017). Briefly, after the time of incubation, extracellular media was centrifuged at 1,000 *g* for 10 min, to remove cell debris. Then, the supernatant was transferred to a different tube and centrifuged at 16,000 *g* for 1 h to pellet microvesicles. The recovered supernatant was filtered in a 0.22 μm pore filter, transferred to an ultracentrifuge tube and centrifuged at 100,000 *g* for 2 h, to pellet exosomes. Afterward, the pellet of exosomes was resuspended in phosphate-buffered saline (PBS) and centrifuged one last time at 100,000 *g* for 2 h, in order to wash the pellet. All the procedure was performed at 4°C. Exosome pellet was resuspended in lysis buffer for further RNA isolation.

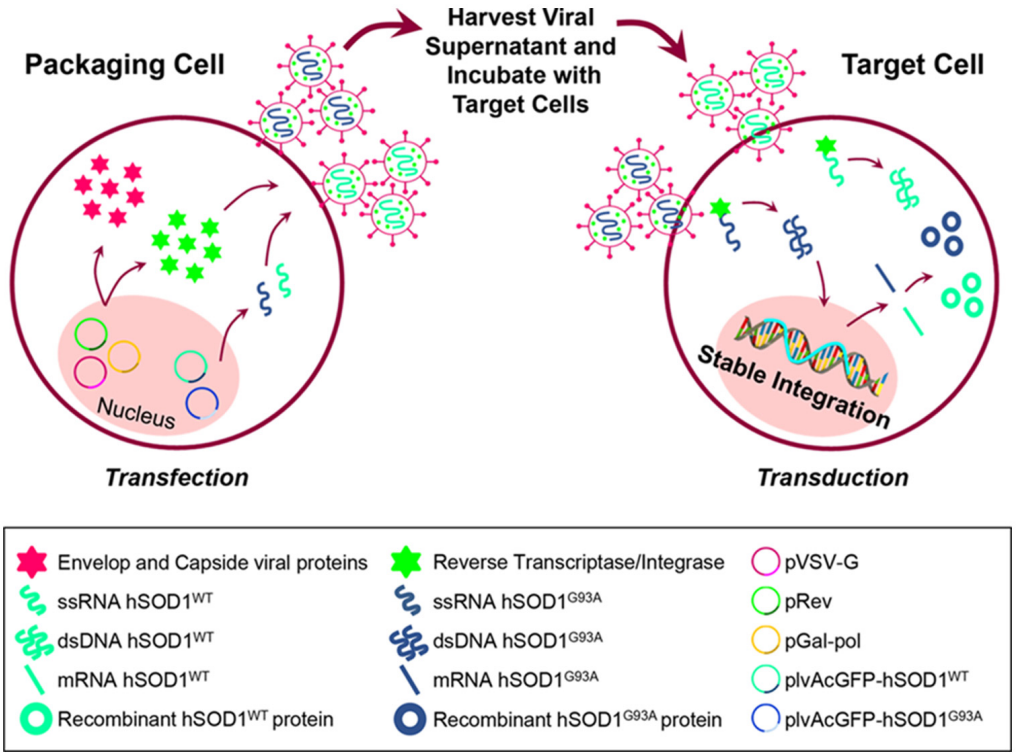

FIGURE 1 | Schematic representation of cell transfection for lentiviral production and further generation of N9 cells expressing hSOD1^{WT}-green fluorescent protein (GFP) and hSOD1^{G93A}-GFP protein. HEK293T cells were incubated with the packaging plasmids pGal-pol and pRev, the envelop plasmid pVSV-G and the lentiviral expression vectors plvAcGFP-hSOD1^{WT} and plvAcGFP-hSOD1^{G93A}, in order to produce lentivirus carrying single-strand RNAs (ssRNA) containing the sequence for human superoxide dismutase 1 wild-type (WT; hSOD1^{WT}), and carrying the G93A mutation (hSOD1^{G93A}). Cell supernatants were collected and incubated with N9 naïve cells, then reverse transcriptase converted the ssRNA into double-strand RNA (dsRNA) that entered the cell nucleus and stably integrated the genome.

Negative-Staining Transmission Electron Microscopy

Exosomes were visualized by transmission electron microscopy (TEM); for negative staining TEM, 10 μL of samples were mounted on Formvar/carbon film-coated mesh nickel grids (Electron Microscopy Sciences, Hatfield, PA, USA) and left standing for 2 min. The liquid in excess was removed with filter paper, and 10 μL of 1% uranyl acetate was added on to the grids and left standing for 10 s, after which, the liquid in excess was removed with filter paper. Visualization was carried out on a JEOL JEM 1400 TEM at 120 kV (Tokyo, Japan). Images were digitally recorded using a CCD digital camera Orious 1100W Tokyo, Japan at the HEMS/i3S of the University of Porto.

Western Blot

Cells were collected in Cell Lysis Buffer and protein concentration was determined using a protein assay kit (Bio-Rad, Hercules, CA, USA) according to manufacturer's specifications. Then, 50 μg of protein were separated in a 12% polyacrylamide electrophoresis gel (SDS-PAGE) and transferred to a nitrocellulose membrane. After blocking with 5% (w/v) nonfat milk solution, membranes were incubated with the following primary antibodies: rabbit anti-SOD1 (1:500), mouse anti-GFP (1:1,000 both from Santa Cruz Biotechnology®) or anti-β-actin (1:5,000), from Sigma, all diluted in 5% (w/v) BSA overnight at 4°C, followed by the secondary antibodies goat anti-rabbit or goat anti-mouse, respectively, both HRP-linked (1:5,000 Santa Cruz Biotechnology®) diluted in blocking solution. Chemiluminescence detection was performed by using Western Bright™ Sirius (K- 12043-D10, Advansta, Menlo Park, CA, USA) and bands were visualized in the ChemiDoc™ XRS System (Bio-Rad; Vaz et al., 2015). In parallel, we performed western blot analysis in isolated exosomes to evaluate the expression of Alix, Flotillin-1 and CD63 by using the same procedure, 20 μg of total protein and specific antibodies (mouse anti-Alix, Cell Signaling, mouse anti-flotillin-1, BD Biosciences, goat anti-CD63, Santa Cruz Biotechnology). In this case, we used Amido Black staining as the loading control.

Quantitative Real Time-PCR

Total RNA was extracted from N9 microglia using TRIzol® (LifeTechnologies, Carlsbad, CA, USA), according to manufacturer's instructions. RNA inside exosomes was extracted using miRCURY Isolation Kit—Cell (#300110, Exiqon, Vedbaek, Denmark). Total RNA was quantified

using Nanodrop ND-100 Spectrophotometer (NanoDrop Technologies, Wilmington, DE, USA) and conversion to cDNA was performed with GRS cDNA Synthesis Master Mix (GRiSP, Porto, Portugal). Quantitative Real Time-PCR (qRT-PCR) was performed on a QuantStudio 7 Flex Real-Time PCR System (Applied Biosystems) using an Xpert Fast Sybr Blue (GRiSP). qRT-PCR was accomplished under optimized conditions: 50°C for 2 min followed by 95°C for 2 min and finally 50 cycles at 95°C for 5 s and 62°C for 30 s. In order to verify the specificity of the amplification, a melt-curve analysis was performed, immediately after the amplification protocol. Non-specific products of PCR were not found in any case. Results were normalized to β-actin and expressed as fold change. The sequences used for primers are represented in **Supplementary Table S1**. For miRNA analysis, conversion of cDNA was achieved with the universal cDNA Synthesis Kit (#203301, Exiqon; Cunha et al., 2018). The Power SYBR® Green PCR Master Mix (Applied Biosystems) was used in combination with predesigned primers (Exiqon), represented in **Supplementary Table S1**, using SNORD110, U6 and RNU1A1 as reference genes. The reaction conditions consisted of polymerase activation/denaturation and well-factor determination at 95°C for 10 min, followed by 50 amplification cycles at 95°C for 10 s and 60°C for 1 min (ramp-rate 1.6°/s). Relative mRNA and miRNA concentrations were calculated using the ΔΔCT equation and quantification of target miRNAs was made in comparison to the geometric average of the three reference genes. In addition, we used the synthetic RNA template spike-in (UniSp6) as a positive control to ensure the quality of the reaction and subsequent evaluations. All samples were measured in duplicate.

Assessment of Gelatinases (MMP-2 and MMP-9) by Gelatin Zymography

Activities of MMP-2 and MMP-9 were determined in the N9 extracellular media, either alone or after incubation with LPS, GUDCA or VS, by performing a SDS-PAGE zymography in 0.1% gelatin-10% acrylamide gels, under non-reducing conditions (Silva et al., 2010). Briefly, after electrophoresis, the gels were washed for 1 h in a solution containing 2.5% Triton-X-100 to remove SDS and to renature the MMP species in the gel and then incubated at 37°C to induce gelatin lysis (buffer: 50 mM Tris pH 7.4, 5 mM $CaCl_2$, 1 μM $ZnCl_2$) overnight. Gels were then stained with 0.5% Coomassie Brilliant Blue R-250 (Sigma-Aldrich) and destained in 30% ethanol/10% acetic acid/H_2O (v/v). Gelatinase activity, detected as a white band on a blue background, was measured using the Image Lab™ analysis software (Bio-Rad).

Quantification of Nitrite Levels

Levels of nitric oxide (NO) were estimated by measuring the concentration of nitrites (NO_2^-), a product of NO metabolism, in the extracellular media of N9 cells. Extracellular medium, free from cellular debris, was mixed with Griess reagent [1% (w/v) sulfanilamide in 5% H_3PO_4 and 0.1% (w/v) N-1 naphtylethylenediamine, all from Sigma-Aldrich, in a proportion of 1:1 (v/v)] in 96-well tissue culture plates for 10 min in the dark, at room temperature (Vaz et al., 2015). The absorbance at 540 nm was determined using a microplate reader (Bio-Rad Laboratories; Hercules, CA, USA). A calibration curve was used for each assay. All samples were measured in duplicate.

Statistical Analysis

Results of at least three independent experiments were expressed as mean ± SEM. Comparisons between N9 naïve and N9 naïve incubated with LPS were made using unpaired two-tailed Student's *t*-test. Comparisons between the different groups were made by one-way ANOVA followed by multiple comparisons Bonferroni *post hoc* correction using GraphPad Prism 7 (GraphPad Software, San Diego, CA, USA). *P*-values of 0.05 were considered statistically significant.

RESULTS

Overexpression of Human WT and Mutant SOD1 in N9 Microglia Does Not Produce Significant Alterations in Cellular Viability or Phagocytic Ability and Neither in the Number of Cell-Derived Exosomes

To achieve SOD1 overexpression in microglia, N9 naïve cells were transduced with $hSOD1^{WT}$ and $hSOD1^{G93A}$ coupled with a GFP tail, as detailed in the methods section, which allowed us to monitor protein expression over time. As previously observed in our group, Western blot analysis showed the presence of mouse SOD1 protein expression at 16 kDa in all samples (Vaz et al., 2015). In N9 $hSOD1^{WT}$ and $hSOD1^{G93A}$ microglia, hSOD1 expression was verified at ∼48 kDa, consistent with the weight of hSOD1 coupled with the GFP tail (**Figure 2A**). In addition, the 27 kDa band corresponding to GFP alone (indicated in additional supporting information) was only detected in cells transduced with GFP alone upon incubation with anti-GFP antibody. To note that, although appearing slightly higher in N9 $hSOD1^{WT}$ microglia, we did not find significant differences between $hSOD1^{WT}$ and $hSOD1^{G93A}$ expression, also confirmed by the percentage of GFP-positive cells checked routinely in the GUAVA flow cytometer, as well as by immunocytochemistry (**Figure 2B**). We additionally evaluated cellular morphology, phagocytic ability and cell viability to assess the impact of hSOD1 transduction in these cells. However, no differences were found between $hSOD1^{WT}$ and $hSOD1^{G93A}$ cells (**Supplementary Figure S1**).

In our previous work, we demonstrated that neuronal exosomes from $hSOD1^{G93A}$ cells carry a content of inflamma-miRNAs similar to the cells of origin, facilitating the shuttle of miR-124 from neuron to microglia, while induce phenotypic alterations and cellular reactivity in recipient microglia cells (Pinto et al., 2017). Therefore, in the current study, we isolated exosomes from N9, either naïve or overexpressing $hSOD1^{WT}$ or $hSOD1^{G93A}$. We have confirmed the presence of Alix, Flotillin-1 and the tetraspanin CD63 in exosomal lysates (**Figure 3A**). Diameter exosome size was ∼100 nm and cup-shape morphology was obtained by TEM (**Figure 3B**).

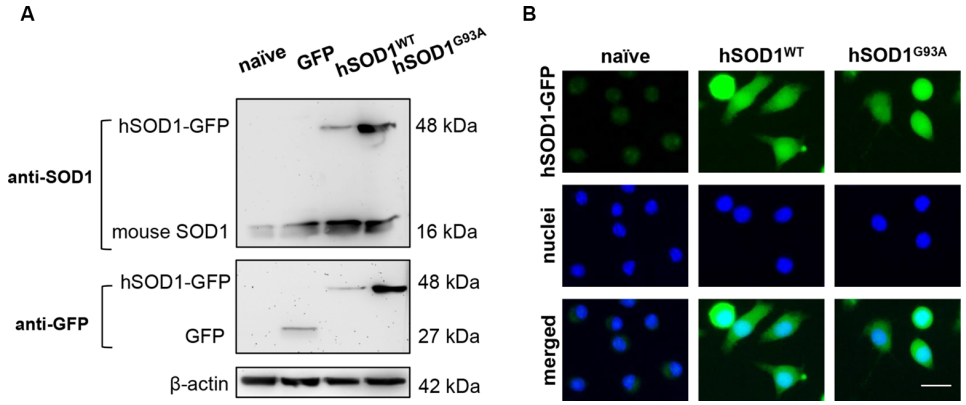

FIGURE 2 | Transduced N9 microglia efficiently express the human SOD1 protein. The presence of hSOD1 WT and carrying the G93A mutation ($hSOD1^{WT}$ and $hSOD1^{G93A}$, respectively), coupled with the green fluorescent protein tail (hSOD1-GFP), as well as the expression of GFP was confirmed by Western blot and immunocytochemistry. **(A)** Western blot analysis indicates the presence of mouse SOD1, as well as hSOD1-GFP at a higher weight, while GFP expression in only observed for cells transduced with GFP not fused with hSOD1. Representative results from one blot are shown and β-actin was used as a loading control. Samples ran in the same gel at the same conditions. **(B)** Expression of hSOD1-GFP was confirmed by immunocytochemistry (green fluorescence). Nuclear staining was achieved with Hoechst dye (in blue). Representative results of one experiment are shown. Scale bar represents 20 μm.

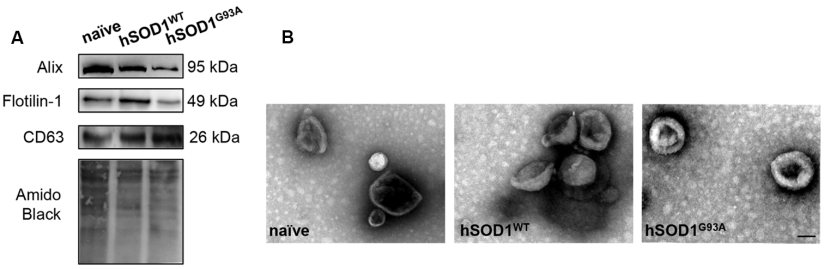

FIGURE 3 | Exosomes released by N9 cells, either naïve or expressing $hSOD1^{WT}$ or $hSOD1^{G93A}$ show similar markers, size and shape. Exosomes were isolated from the extracellular media of N9 cells, either naïve or overexpressing human $hSOD1^{WT}$ and $hSOD1^{G93A}$, as described in methods. **(A)** Western blot analysis indicates the presence of common exosome markers Alix, Flotillin-1, and CD63. **(B)** Representative images obtained by negative-staining transmission electron microscopy (TEM) of exosomes are depicted evidencing cup shape morphology and that the majority of vesicles have a diameter of close to 100 nm. Scale bar represents 100 nm.

N9 $hSOD1^{WT}$ Microglia Show Downregulated Anti-/Pro-inflammatory Genes, While N9 $hSOD1^{G93A}$ Cells Express Upregulated MFG-E8, RAGE and Pro-inflammatory Genes, and Release Exosomes Enriched in HMGB1 and SOD1

Although SOD1 mutations are reported in fALS cases (Barber and Shaw, 2010), the effect of mutant $SOD1^{G93A}$ specifically in microglia is not completely clarified. Recently, reactive microglia evidenced to exert neuroprotective functions in a mouse model of TDP-43 proteinopathy (Spiller et al., 2018), highlighting the beneficial role that microglia activation may also have in neurodegenerative diseases. To explore the reactive signature of WT and mutant SOD1 in N9 microglia, we evaluated the gene expression of specific inflammatory markers in naïve and in transduced cells overexpressing hSOD1. When compared to naïve cells, N9 $hSOD1^{WT}$ microglia showed decreased levels of pro-inflammatory markers (usually associated to the M1 phenotype, TNF-α/IL-1β/S100B/iNOS), as well as anti-inflammatory markers (related to the M2 phenotype, Arg1/SOCS1/Fizz1/IL-10; **Figures 4A,B**). Although some anti-inflammatory markers were similar to naïve cells (Arg1 and SOCS1) or reduced in a similar way to those observed in N9 $hSOD1^{WT}$ microglia (Fizz1 and IL-10), N9 $hSOD1^{G93A}$ cells showed an increase in the pro-inflammatory markers that were studied. More importantly, some of these markers (TNF-α, IL-1β and HMGB1) were not only above the levels obtained in N9 $hSOD1^{WT}$ cells, but also above those of naïve cells, which indicate a stressed microglia that may contribute to either a depressed or exacerbated response, depending on the inflammatory stimulus (**Figures 4A,B**). Since we did not find significant differences between the levels of such markers in N9 transduced with GFP alone (**Supplementary Figure S2**), we may assume that the changes observed are due to the presence of $hSOD1^{WT}$ or $hSOD1^{G93A}$ and not because of the lentiviral infection. Moreover, increased expression of membrane surface receptors, like MFG-E8 and RAGE, was only evident in N9 $hSOD1^{G93A}$ microglia, when compared to N9 $hSOD1^{WT}$ microglia, while TLR-4 expression was reduced in both cells

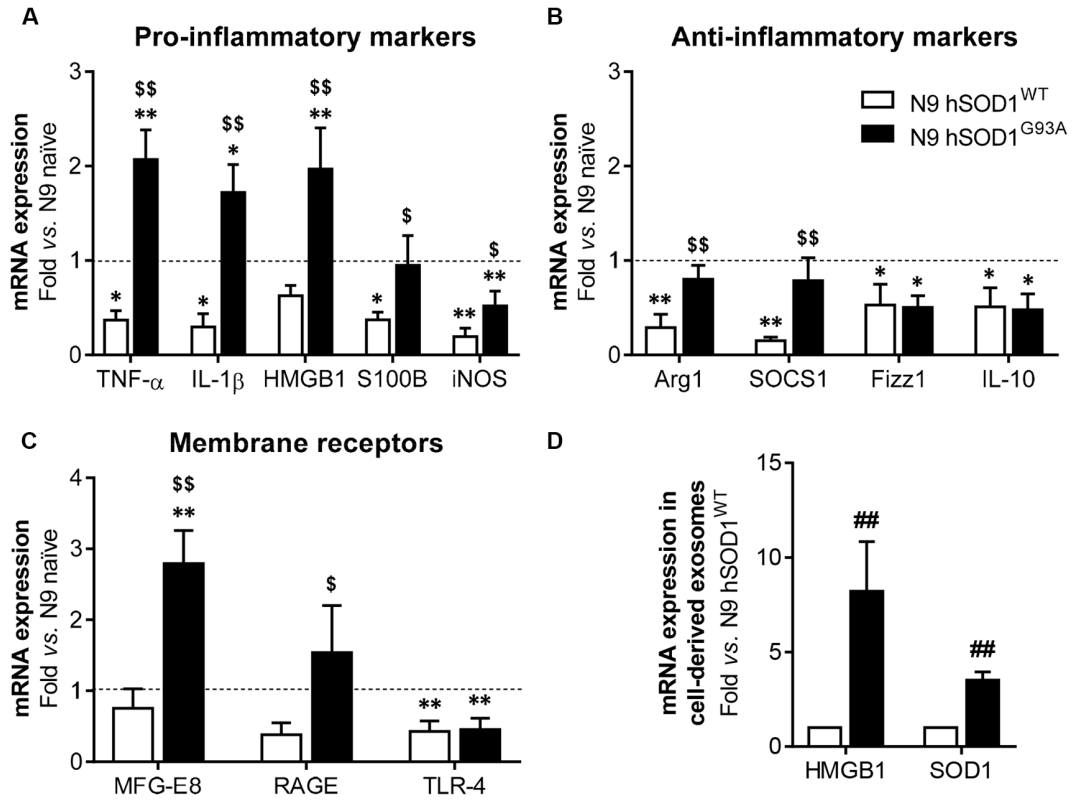

FIGURE 4 | N9 hSOD1^{G93A} microglia have a pro-inflammatory phenotype with an exacerbated MFG-E8 and RAGE gene expression, and originate exosomes enriched in HMGB1 and SOD1. Cellular mRNA expression of pro-inflammatory markers **(A)**, anti-inflammatory markers **(B)** and membrane surface receptors **(C)** was assessed by quantitative Real-Time PCR (qRT-PCR). The dashed line represents the average value (N9 naïve cells). **(D)** mRNA expression was also evaluated in exosomes by qRT-PCR and N9 hSOD1^{WT} cells were used as a control. Results are mean (± SEM) from at least three independent experiments. $^{*}p < 0.05$ and $^{**}p < 0.01$ vs. N9 naïve microglia; $^{\$}p < 0.05$ and $^{\$\$}p < 0.01$ vs. N9 hSOD1^{WT} microglia; one-way ANOVA (Bonferroni *post hoc* correction). $^{\#\#}p < 0.01$ vs. N9 hSOD1^{WT} cells; unpaired Student's *t*-test (two-tailed).

(**Figure 4C**). Interestingly, we observed that exosomes may also be involved in the propagation of the alarmin HMGB1 and the SOD1 protein, whose gene levels were found elevated in N9 hSOD1^{G93A} microglia, thus contrasting with N9 hSOD1^{WT} cells (**Figure 4D**). This result is consistent with previous findings where SOD1 was described to be transported into the extracellular media in exosomes and further collected by other cells (Silverman et al., 2016). This finding suggests that mutated microglia also contribute to chronic inflammatory status through the transport of HMGB1 in their released exosomes, never described to be carried by microglial-derived exosomes.

N9 hSOD1^{WT} Microglia Show a Specific miR-146a Upregulation Not Recapitulated in Their Exosomes, While Those From hSOD1^{G93A} Cells Are Unique as Mediators of Neuroinflammation by Their Elevated miR-155 and miR-146a Cargo

Inflamma-miRNAs are reported to have a modulatory role in microglia activation (Cardoso et al., 2012; Saba et al., 2012) and to circulate as part of exosomal cargo (Alexander et al., 2015; Fernandes et al., 2018). In this study, we were mainly interested in assessing for the first time the differential expression of miR-155, miR-146a, miR-125b and miR-21 in N9 cells transduced with WT and mutant SOD1 relatively to the naïve ones, which are known to mediate macrophage polarization (Essandoh et al., 2016), CNS inflammation (Su et al., 2016) and to be expressed in the spinal cord of SOD1^{G93A} mice at the symptomatic stage (Cunha et al., 2018). Decreased levels of miR-125b and miR-21, when compared with the naïve cells (as well as cells transduced with GFP, **Supplementary Figure S2**), were found in WT and mutated microglia (**Figure 5A**), and may account to a compromised response to an inflammatory stimulus (Tili et al., 2007; Parisi et al., 2016), thus turning microglia more susceptible to activation (Barnett et al., 2016; Cardoso et al., 2016). Regarding the pro-inflammatory miR-155 and its negative regulator miR-146a, only the last one was increased in N9 hSOD1^{WT} microglia. While upregulated levels of miR-146a in hSOD1^{WT} cells may act as a negative regulator of miR-155 increase, thus accounting for their normal content in exosomes, selective release of miR-155 and miR-146a from hSOD1^{G93A} N9 cells into exosomes (**Figure 5B**) may drive disease progression in the mSOD1 ALS model.

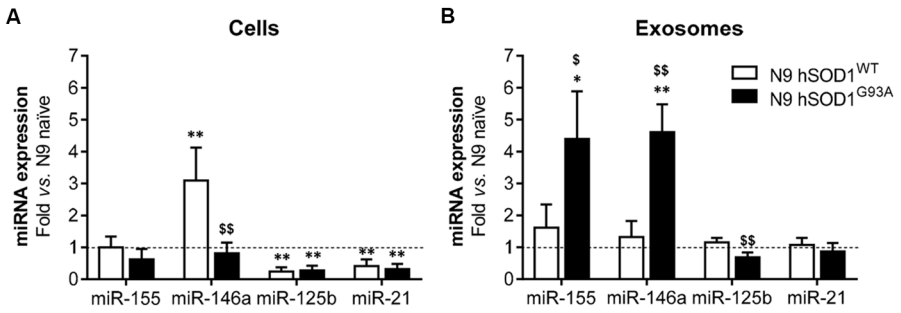

FIGURE 5 | N9 hSOD1^{WT} microglia highly express miR-146a, while N9 hSOD1^{G93A} cells actively package miR-155 and miR-146a into their exosomes. Inflammatory microRNAs (miRNA, miR) expression in both cells **(A)** and exosomes **(B)** were analyzed by qRT-PCR. N9 naïve cells were used as a control and the dashed line represents the average value. Results are mean (± SEM) from at least three independent experiments. $^{*}p < 0.05$ and $^{**}p < 0.01$ vs. N9 naïve microglia; $^{\$}p < 0.05$ and $^{\$\$}p < 0.01$ vs. N9 hSOD1^{WT} microglia; one-way ANOVA (Bonferroni *post hoc* correction).

MiRNAs that are overrepresented in exosomes in comparison to levels in the cell indicate a selective exported mechanism (Bell and Taylor, 2017).

Overexpression of Human WT and Mutant SOD1 in N9 Microglia Leads to a Defective Inflammatory Gene Response to LPS Stimulation, With an Increased miR-155 Sorting in Exosomes From WT Cells

It was demonstrated that SOD1^{WT} overexpression decreases ROS production and reduces neurotoxic inflammatory markers, even in the presence of LPS (Dimayuga et al., 2007). Therefore, we thought that would be interesting to further explore differences in hSOD1 microglia reactivity towards LPS treatment relatively to naïve cells, to better understand microglial behavior when facing an inflammatory environment in the context of ALS. As indicated in **Table 1**, incubation of naïve cells with LPS induced an activated phenotype with increased TNF-α, HMGB1 and S100B, but not of IL-1β or iNOS gene expression. Upregulation of Fizz1 and MFG-E8 was notorious, together with increased extracellular MMP-9 activation and NO production. Curiously, we found a decrease in the gene expression of S100B and RAGE. Stimulation with LPS also upregulated miR-155, miR-146a and miR-21, and downregulated miR-125b in cells. Interestingly, they were all found reduced in respective cell-derived exosomes, with the exception of miR-146a. However, either hSOD1^{WT} or hSOD1^{G93A} cells revealed lower expression of pro- and anti-inflammatory genes upon LPS challenge, than naïve N9 microglia.

It is important to note that GFP-transduced cells were able to respond to LPS in a similar manner to naïve N9 in terms of pro- or anti-inflammatory markers we used, as well as in miRNAs expression (**Supplementary Figure S2**), indicating that the differences in transduced cells do not derive from lentiviral transduction or GFP expression. In a similar way, MFG-E8 and RAGE mRNA levels were found downregulated in both transduced cells, in comparison with the LPS-treated naïve ones, while no significant differences were obtained for extracellular MMP-9, MMP-2 and NO levels. The same defective pattern was observed for inflamma-miRNAs, though an increase of miR-21 was observed in LPS-treated hSOD1^{WT} cells and of miR-125b in hSOD1^{G93A} transduced microglia. To highlight, however, that the selective exported mechanism of miR-155 into exosomes was notorious in the hSOD1^{WT} cells, contrasting with its low expression in mSOD1 cells and their exosomes after stimulation with LPS, further attesting their increased inability to develop an inflammatory response against damage.

Mitigation of Pro-inflammatory Genes and Regulation of Inflamma-miRNAs in N9 hSOD1^{G93A} Microglia by GUDCA and VS Is Mediated by Common and Compound-Specific Molecular Mechanisms

The alterations observed in the expression of pro- and anti-inflammatory-associated genes and miRNAs, as well as the inability to mount an inflammatory response when facing an inflammatory stimulus in the microglia transduced with hSOD1^{G93A}, led us to test two different compounds described as immunomodulators in glial cells (Fernandes et al., 2007; Falcão et al., 2017). Neither of them caused identifiable changes in cell viability (**Supplementary Figure S3**) and both were similarly efficient in decreasing the expression of genes associated to a pro-inflammatory response, such as TNF-α, IL-1β, HMGB1 and S100B (**Figure 6A**). Interestingly, we found that MMP-2 and MMP-9 activation was merely downregulated by VS in hSOD1^{G93A} cells (**Figure 6B**), supporting its specificity over that of GUDCA to inhibit these pro-inflammatory mediators. This may have therapeutic relevance since the elevation of MMP-9/-2 expression was observed in the spinal cord of SOD1^{G93A} mice (Fang et al., 2010), and that of MMP-9 in NSC-34 MNs overexpressing hSOD1^{G93A} (Vaz et al., 2015). Though that both VS and GUDCA showed to reduce the expression of the anti-inflammatory associated genes Arg1 and SOCS1, only GUDCA significantly enhanced the expression of IL-10 mRNA (**Figure 6C**), revealing its potential to counteract

TABLE 1 | Differences in gene and miRNA expression, as well as in soluble factors, after exposure of naïve and transduced N9 microglia to lipopolysaccharide (LPS).

Markers	N9 naïve with LPS (fold change vs. N9 naïve)	N9 hSOD1^{WT} with LPS (fold change vs. N9 naïve with LPS)	N9 hSOD1^{G93A} with LPS (fold change vs. N9 naïve with LPS)
Genes			
Pro-inflammatory markers			
TNF-α	$10.56 \pm 3.87^{++}$	$0.45 \pm 0.10^{**}$	$0.49 \pm 0.21^{*}$
IL-1β	8.03 ± 5.05	0.74 ± 0.33	0.40 ± 0.12
HMGB1	$1.69 \pm 0.28^{++}$	$0.56 \pm 0.16^{**}$	$0.38 \pm 0.06^{**}$
S100B	$0.40 \pm 0.12^{++}$	1.14 ± 0.41	$0.34 \pm 0.12^{\$}$
iNOS	1.56 ± 0.68	$0.34 \pm 0.15^{**}$	$0.20 \pm 0.04^{**}$
Anti-inflammatory markers			
Arg1	1.41 ± 0.45	$0.33 \pm 0.11^{**}$	$0.23 \pm 0.06^{**}$
SOCS1	$0.31 \pm 0.09^{++}$	$0.46 \pm 0.12^{**}$	$0.51 \pm 0.14^{**}$
Fizz1	$7.40 \pm 1.83^{++}$	$0.33 \pm 0.13^{**}$	$0.26 \pm 0.06^{**}$
IL-10	3.10 ± 1.75	$0.32 \pm 0.15^{**}$	$0.29 \pm 0.06^{**}$
Receptors			
MFG-E8	$3.41 \pm 0.99^{+}$	$0.40 \pm 0.17^{**}$	$0.44 \pm 0.12^{**}$
RAGE	$0.46 \pm 0.26^{+}$	$0.46 \pm 0.18^{**}$	$0.31 \pm 0.11^{**}$
TLR4	2.00 ± 0.65	2.97 ± 1.42	$0.40 \pm 0.10^{\$}$
Soluble factors			
MMP-9	$2.23 \pm 0.34^{++}$	1.66 ± 0.42	1.16 ± 0.14
MMP-2	1.20 ± 0.15	0.97 ± 0.06	1.04 ± 0.14
NO	$2.31 \pm 0.23^{+}$	3.68 ± 1.25	2.96 ± 0.71
MicroRNAs			
miR-155	$6.28 \pm 1.95^{++}$	$0.41 \pm 0.15^{**}$	$0.40 \pm 0.19^{*}$
miR-146a	$5.34 \pm 1.10^{++}$	$0.44 \pm 0.17^{**}$	$0.35 \pm 0.15^{**}$
miR-125b	$0.25 \pm 0.12^{++}$	$0.37 \pm 0.11^{*}$	$1.18 \pm 0.38^{\$\$}$
miR-21	$5.01 \pm 1.66^{+}$	$2.04 \pm 0.44^{*}$	$0.63 \pm 0.24^{\$\$}$
In exosomes			
miR-155	$0.34 \pm 0.34^{+}$	$7.88 \pm 2.82^{*}$	$0.30 \pm 0.12^{\$}$
miR-146a	1.25 ± 0.36	1.04 ± 0.30	1.02 ± 0.57
miR-125b	$0.48 \pm 0.07^{++}$	1.39 ± 0.52	0.49 ± 0.15
miR-21	$0.36 \pm 0.11^{++}$	2.53 ± 1.60	0.50 ± 0.20

Results are expressed as fold change (MEAN ± SEM) from at least three independent experiences for LPS-treated naïve cells vs. non-treated N9 naïve cells and for LPS-treated N9 hSOD1^{WT} and N9 hSOD1^{G93A} microglia vs. LPS-treated naïve cells. Comparisons between N9 naïve and N9 naïve with LPS were made using an unpaired two-tailed Student's t-test. Comparisons between the three different groups (N9 naïve with LPS, N9 hSOD1^{WT} with LPS and N9 hSOD1^{G93A} with LPS) were made by One-way ANOVA followed by multiple comparisons Bonferroni post hoc correction. $^{+}p < 0.05$ and $^{++}p < 0.01$ vs. N9 naïve microglia; $^{*}p < 0.05$ and $^{**}p < 0.01$ vs. N9 naïve with LPS; $^{\$}p < 0.05$ and $^{\$\$}p < 0.01$ vs. N9 hSOD1^{WT} with LPS.

inflammation whenever it is exacerbated. Unique potential therapeutic benefits of VS were also found for its ability in increasing the gene expression of MFG-E8 (**Figure 6D**), a protein that has been described as promoting microglia phagocytosis (Lei et al., 2013). Further studies should elucidate whether activation of RAGE and TLR-4 by GUDCA, as we here observed, will have benefits in restoring the immune response of hSOD1^{G93A} cells. Additionally, both VS and GUDCA showed to be equally efficient in decreasing intracellular miR-155, while miR-21 was selectively enhanced by GUDCA and miR-146a by VS (**Figure 7A**), again reinforcing their action through distinct pathways. Sorting into exosomes was also different considering that GUDCA was again effective in sustaining dissemination of miR-155 and inflammation by exosomes released from hSOD1^{G93A} cells. In addition, exosome-shuttling of miR-21, indicated to have protective effects against oxidative stress (Shi et al., 2018), merely occurred by VS treatment (**Figure 7B**).

These novel data provide clear evidence of the beneficial contribution of VS and GUDCA as immunoregulatory compounds in the hSOD1^{G93A} N9 microglia, by sharing similar modulatory properties, but overall by additionally counteracting distinct inflammatory signaling pathways.

DISCUSSION

The role of glial cells in neurodegenerative diseases, particularly in ALS, has been thoroughly investigated and discussed, with evidences that these cells are key contributors to the neuroinflammation processes and disease progression (Lasiene and Yamanaka, 2011). In this study, we focused on microglia since they have a deregulated inflammatory profile when expressing mutant SOD1 (Beers et al., 2006; Boillée et al., 2006). To create an ALS cellular model based in SOD1 mutations, we transduced the N9 microglia cell line in order to overexpress the hSOD1^{WT} or hSOD1^{G93A} gene. Although some studies have pointed that elevated and not physiological levels of SOD1^{WT} may cause the neurodegeneration and disease onset in the SOD1 ALS mouse model (Wang et al., 2009; Afshar et al., 2017), the transduction process of WT and mutant hSOD1 in our cellular model did not cause any loss of cell viability. Furthermore, N9 hSOD1^{WT} cells presented a higher viability when compared to N9 naïve cells, which may derive from the antioxidant properties of SOD1 protein, thus conferring increased resistance to cell death.

A study using the N9 microglia cell line demonstrated that SOD1 overexpression was able to decrease superoxide and NO

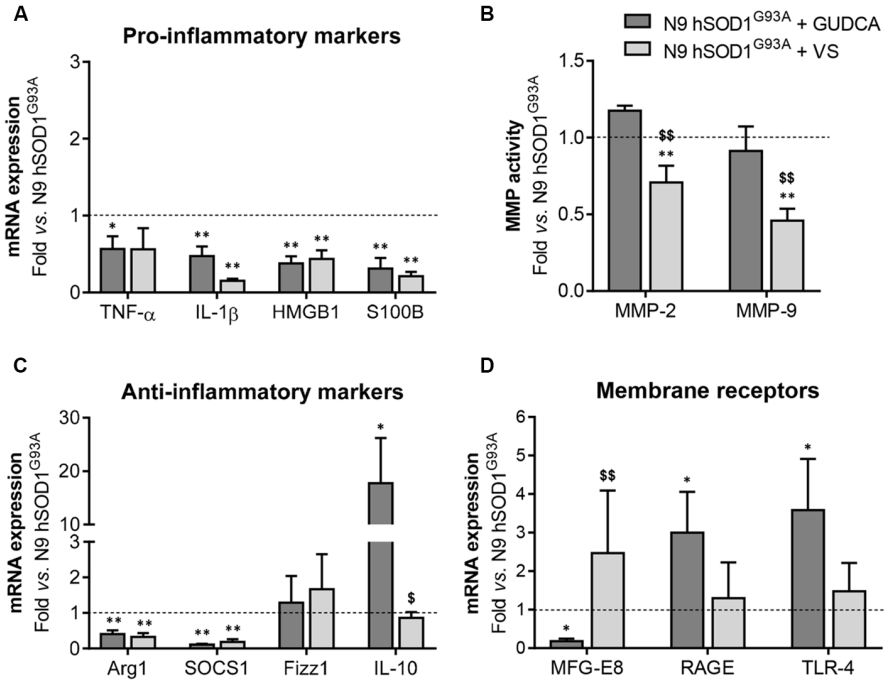

FIGURE 6 | Pro-inflammatory markers in N9 hSOD1^{G93A} microglia are downregulated by glycoursodeoxycholic acid (GUDCA) and dipeptidyl vinyl sulfone (VS), with GUDCA specifically upregulating IL-10, RAGE and TLR-4 genes, and VS promoting the increase of MFG-E8 and the decrease of MMP-2 and MMP-9 activation. N9 hSOD1^{G93A} microglia were incubated with 50 μM of GUDCA or 10 μM of VS for 48 h. Cellular mRNA expression of pro-inflammatory markers **(A)**, anti-inflammatory markers **(C)** and membrane surface receptors **(D)** was evaluated by qRT-PCR. **(B)** Activation of MMP-2 and MMP-9 was assessed by gelatin zymography assay. The intensity of the bands was quantified using computerized image analysis (Image Lab^{TM} software). Non-treated mutant cells were used as control and the dashed line represents average values. Results are mean (± SEM) from at least three independent experiments. $^{*}p < 0.05$ and $^{**}p < 0.01$ vs. N9 hSOD1^{G93A} microglia; $^{\$}p < 0.05$ and $^{\$\$}p < 0.01$ vs. N9 hSOD1^{G93A} + GUDCA; one-way ANOVA (Bonferroni *post hoc* correction).

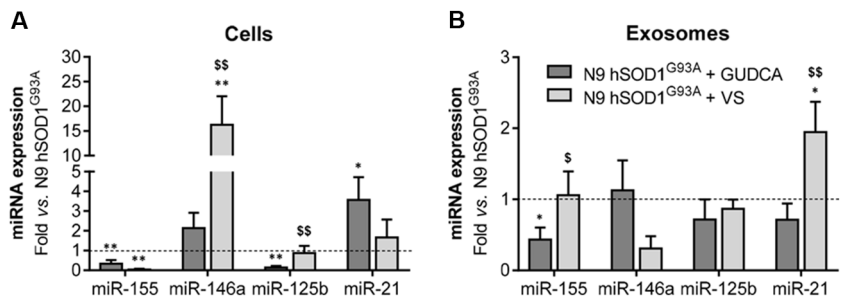

FIGURE 7 | Treatment of N9 hSOD1^{G93A} microglia with glycoursodeoxycholic acid (GUDCA) and dipeptidil vinyl sulfone (VS) decreases miR-155, with GUDCA specifically upregulating miR-21 in cells, and VS promoting the increase of miR-146a in cells and of miR-21 in exosomes. After 48 h incubation of N9 hSOD1^{G93A} microglia with 50 μM of GUDCA or 10 μM of VS, inflammatory microRNAs (miRNA, miR) in both cells **(A)** and exosomes **(B)** were analyzed by qRT-PCR. Non-treated mutant cells were used as control and the dashed line represents the average values. Results are mean (± SEM) from at least three independent experiments. $^{*}p < 0.05$ and $^{**}p < 0.01$ vs. N9 hSOD1^{G93A} microglia; $^{\$}p < 0.05$ and $^{\$\$}p < 0.01$ vs. N9 hSOD1^{G93A} + GUDCA; one-way ANOVA (Bonferroni *post hoc* correction).

production, as well as to attenuate the ability of activated microglia to induce toxicity in cultured neurons (Dimayuga et al., 2007). Here, we observed a decrease in the selected pro- and anti-inflammatory genes evaluated upon hSOD1^{WT} expression, reflecting a deactivation process of the N9 microglia. The same was not observed in the case of hSOD1^{G93A} overexpression, which led to heterogeneous activation and polarization of the cells. In fact, microglia isolated from the spinal cord of the mSOD1 model is characterized by an M1/M2 dichotomy (Chiu et al., 2013), but no clear information was provided regarding the cortical brain microglia (Righi et al., 1989), as the N9 model used in our study. In addition, a recent study showed that microglia activation leads to increased expression of pro-inflammatory genes that is accompanied by the expression of some anti-inflammatory genes, as well (Lively and Schlichter, 2018). Interestingly, when looking at the

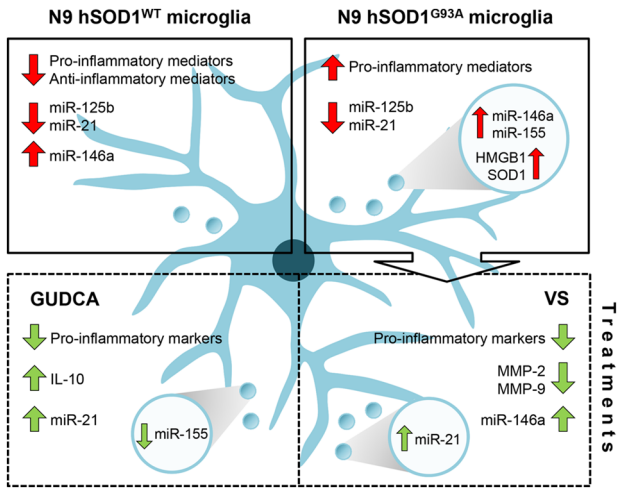

FIGURE 8 | Schematic representation of the dysregulated inflammatory-associated mediators and immunomodulation benefits by GUDCA or VS in N9 cells transduced with hSOD1^{WT} and hSOD1^{G93A} protein. Overexpression of hSOD1^{WT} causes a downregulation of pro- and anti-inflammatory genes in N9 cells and upregulation of miR-146a. In contrast, hSOD1^{G93A} transduction causes increased gene expression of pro-inflammatory mediators, thus leading to an activated microglia population. Both transduced cells reveal a decrease of miR-125b and miR-21. To note that the release of exosomes containing miR-155 and miR-146a, as well as HMGB1 and SOD1 by N9 hSOD1^{G93A} cells may determine the propagation of inflammation. Treatment with GUDCA or VS effectively modulates the gene expression of pro-inflammatory molecules, together with the increase of anti-inflammatory miRNAs. GUDCA increases IL-10 and cellular miR-21, with a substantial reduction of exosomal miR-155, while VS decreases MMP-2 and MMP-9 activation and determines the shuttle of miR-21 into exosomes. In sum, GUDCA and VS are relevant immunoregulators of the dysfunctional microglia in mutated superoxide dismutase 1 (mSOD1) ALS, and their differential target specificity may be envisaged as very promising to recover specific disease-related subtypes. GUDCA, glycoursodeoxycholic acid; HMGB1, high mobility group box protein 1; miR, microRNA; MMP, matrix metalloproteinase; SOD1, superoxide dismutase 1; VS, dipeptidyl vinyl sulfone.

miRNA profile of transduced cells, miR-146a was only found increased in N9 hSOD1^{WT} cells, which may determine the inhibition of the inflammatory response by targeting the NF-κB pathway with consequent downregulation of the alarmin S100B and the pro-inflammatory cytokines. Since NF-κB activation is necessary for the induction of several miRNAs, such as miR-125b and miR-21, this can explain the reduced levels of these miRNAs in N9 hSOD1^{WT} cells. On the other hand, their downregulation in hSOD1^{G93A} N9 microglia may reveal that cells became reactive and lose their ability to counteract an additional stress stimulus, considering the anti-inflammatory role of these miRNAs (Tili et al., 2007; Ma et al., 2011; Cardoso et al., 2016). In accordance with these findings, N9 hSOD1^{G93A} cells revealed an overexpression of the RAGE receptor. Such result may derive from the activated inflammatory cascade subsequent to the binding of HMGB1 to RAGE, based on the elevated gene expression of such alarmin in these cells, with consequent increased expression of TNF-α, and IL-1β, as here observed by us. Indeed, increased expression of pro-inflammatory mediators in SOD1^{G93A} mice has already been described (Hensley et al., 2006; Jeyachandran et al., 2015) and mutant SOD1^{G93A} microglia was reported to be more neurotoxic than WT microglia, also due to the increased production of ROS and TNF-α pro-inflammatory cytokine (Liu et al., 2009). Additionally, WT and mutated SOD1 overexpression cause a decrease in Fizz1 and IL-10 expression genes, suggesting a delayed response of the transduced microglia toward repair mechanisms during neuroinflammation.

Furthermore, in the mutant SOD1 mouse model, as well as in fALS and sALS patients, miR-155 was found to be elevated and its targeting revealed to restore the dysfunctional microglia and to attenuate disease progression in the ALS mouse model (Koval et al., 2013; Butovsky et al., 2015; Cunha et al., 2018). In N9 hSOD1^{G93A} microglia, despite the similar endogenous levels of miR-155 and miR-146a relatively to naïve cells, these miRNAs were found to be shuttled into exosomes, similarly to our previous observations on N9 microglia polarization by LPS (Cunha et al., 2016). Our findings in hSOD1^{G93A} overexpressing cells highlight the exacerbated expression of inflammatory genes indicating that cells carrying such mutation are more reactive than the N9 hSOD1^{WT} microglia, probably influencing the surrounding cells and contributing to an overall inflammatory environment. In accordance, gene expression analysis in exosomes from mutated cells also revealed that HMGB1 and SOD1 are transported as part of their cargo, together with miR-155 and miR-146a, contributing to the dissemination of inflammatory mediators and aggravating the neuroinflammation status. These results are supported by previous studies showing that mutant/misfolded SOD1 is released into exosomes and is propagated to different cells, while also inducing exosome formation and release from cells (Basso et al., 2013; Grad et al., 2014; Silverman et al., 2016). HMGB1 is described as being secreted either in apoptotic bodies (Bell et al., 2006; Buzas et al., 2014), or in cell-derived exosomes (Sheller-Miller et al., 2017), but never mentioned to be carried in microglia-derived exosomes, as we now report. Although MFG-E8 is not a typical pro-inflammatory mediator, activated microglia upregulate MFG-E8, which has been related with the phagocytosis of viable neurons (Fricker et al., 2012) and with the production of pro-inflammatory cytokines (Liu et al., 2013). However, MFG-E8 role appears to be dose-dependent, since it is also proposed that a high concentration of MFG-E8 blocks the binding between apoptotic cells and microglia/macrophages, thus leading to the inhibition of phagocytosis (Yamaguchi et al., 2008). This may indicate that, in an inflammatory state, in which these cells appear to be, N9 hSOD1^{G93A} microglia can either cause neuronal death or be unable to restore the homeostatic balance, contributing to ALS pathogenesis.

Overexpression of hSOD1^{WT} and hSOD1^{G93A}, although useful to understand ALS underlying mechanisms, are not physiological models. In this sense, only the transduced cells with GFP stimulated with LPS reproduced the M1 polarization found in the naïve cells after 24 h treatment (Cunha et al., 2016), while a defective stimulation and depressed resolving capacity after LPS pro-inflammatory activation was found in the transduced N9 hSOD1^{WT} and hSOD1^{G93A} microglia.

We may then hypothesize that these microglia may become inefficient protectors of the brain against endogenous damage and pathogens. Actually, when compared with the response of the naïve cells towards LPS, hSOD1^{WT} and hSOD1^{G93A} N9 microglia clearly revealed a decrease in the majority of pro- and anti-inflammatory mediators. Moreover, intracellular inflammatory-associated miRNAs were downregulated, including miR-155 and miR-146a, which are both involved in the NF-κB pathway, by being upregulated upon inflammatory stimulus, and by acting as a negative feedback regulator, respectively (Mann et al., 2017). Though SOD1 overexpression was indicated to reduce neurotoxic inflammatory signaling in microglia (Dimayuga et al., 2007), we could still observe an increased exosomal content in miR-155 meaning that immunomodulatory effects were conserved, a finding not observed in exosomes from the mutated N9 microglia. Instead, their enrichment in miR-125b was shown to account for decreased MN survival in ALS, once miR-125b was found to be neurotoxic and to be upregulated in the lumbar spinal cord of SOD1^{G93A} mice (Parisi et al., 2016).

After concluding that hSOD1^{G93A} N9 microglia show upregulated pro-inflammatory markers, downregulated resolving genes, and exosomal enriched cargo in HMGB1 and SOD1, we tested the immunoregulatory properties of GUDCA and VS in rescuing the dysfunctional phenotype of the mutated microglia towards a more neuroprotective one, based on previous results (Vaz et al., 2015; Falcão et al., 2017). Our data demonstrate that both GUDCA and VS promote inflammatory resolution leading to a reduction of TNF-α, IL-1β, HMGB1, S100B and miR-155 expression, corroborating their anti-inflammatory properties (Fernandes et al., 2007; Vaz et al., 2015; Ko et al., 2017) in other cells and disease models. Interestingly, we observed a significant increase of the anti-inflammatory cytokine IL-10, together with miR-21 and membrane receptors RAGE and TLR-4 only in GUDCA-treated cells. This is not without precedent, since GUDCA was demonstrated to inhibit the production of TNF-α and IL-1β in astroglial cells by preventing the maturation of these cytokines and their consequent release in an experimental model of jaundice, thus preventing astroglial reactivity (Fernandes et al., 2007). Also, miR-21 was reported to promote an anti-inflammatory response by increasing IL-10 production (Sheedy et al., 2010). In this way, GUDCA may be acting through the activation of the receptor TLR-4, leading to the expression of this miRNA that, consequently, promotes an anti-inflammatory response. The decrease of miR-155 encapsulation in exosomes by GUDCA may further concur to attenuate the stimulation produced by the hSOD1^{G93A} overexpression in N9 cells. Regarding VS, similarly to what we observed in N9-microglia exposed to Aβ peptide (Falcão et al., 2017), this compound showed its anti-inflammatory properties by reducing miR-155, HMGB1 and IL-1β, as well as MMP-2 and MMP-9 activation. Additionally, VS increased the cellular expression of miR-146a and decreased that of miR-155, probably as a consequence of NF-κB pathway inhibition and its immunoregulatory properties (Su et al., 2016). Furthermore, VS significantly promoted the expression of MFG-E8 that drives microglia phagocytosis (Liu et al., 2013) and the shuttle of miR-21 into exosomes in hSOD1^{G93A} N9 microglia, which was reported to negatively regulate the secondary inflammatory response of microglia (Wang et al., 2018) by acting in recipient cells. The inhibition of the pro-inflammatory response by miR-146a upregulation may also favor the specific downregulation of MMP-2 and MMP-9 (Könnecke and Bechmann, 2013), potentially resulting in the restoration of immune homeostasis and highlighting VS as a microglia-targeted candidate in ALS. We may then conclude that, although through different mechanisms of action, both GUDCA and VS show beneficial therapeutic properties for immunomodulation towards neuroprotection in ALS. Importantly, because each of the compounds showed specificity to unique microglia targets, that may open new possibilities to modulate precise microglia subtypes.

Overall, and as schematically represented in **Figure 8**, our findings clarify the importance of hSOD1^{WT} in the host cell, by having calming and antioxidant effects. Besides inducing the expression of pro-inflammatory genes, hSOD1^{G93A} protein decreased the expression of anti-inflammatory genes, thus increasing the reactivity of the cell. In addition, by decreasing microglia repairing ability in damaging conditions, the expression of the mutated protein may further contribute to compromised homeostatic balance and failure in neuroregenerative processes. Finally, we propose that GUDCA and VS are potential pharmacological approaches in single or combined therapeutic strategies for ALS, due to their multi-target effects and active microglia immunomodulation.

AUTHOR CONTRIBUTIONS

DB and AV conceived and designed the experiments. AV and CC implemented and optimized the transduction procedures. RM supervised the chemical synthesis of dipeptidyl vinyl sulfone. AV, SP, CE and LC carried out the experiments. SP, AV and DB analyzed the data and wrote the manuscript. DB critically reviewed the content and approved the final version for publication.

FUNDING

This work was funded by Research Grant of the Santa Casa Scientific Research Program on ALS (SCML-Project ELA-2015-002 to DB), by Fundação para a Ciência e a Tecnologia (FCT), through project PTDC/MED-NEU/31395/2017 (to DB) and grant UID/DTP/04138/2013 (to iMed.ULisboa), as well as by the Programa Operacional Regional de Lisboa and the Programa Operacional Competitividade e Internacionalização (LISBOA-01-0145-FEDER-031395 to DB), and individual fellowship (SFRH/BPD/76590/2011 to AV).

ACKNOWLEDGMENTS

We thank Diane Pereira and Inês Moranguinho from iMed.ULisboa, for providing plasmids that allowed us to produce the lentiviral particles; Dr. Elsa Rodrigues, iMed.ULisboa, for the anti-GFP antibody and for helping in the interpretation of

the data obtained with such antibody. We also thank Dr. Rui Fernandes and A.R. Malheiro, i3S—Instituto de Investigação e Inovação em Saúde and HEMS/IBMC—Histology and Electron Microscopy Service, Universidade do Porto for acquisition and analysis of TEM images.

SUPPLEMENTARY MATERIAL

The Supplementary Material for this article can be found online at: https://www.frontiersin.org/articles/10.3389/fncel.2019.00109/full#supplementary-material

REFERENCES

Abe, K., Aoki, M., Tsuji, S., Itoyama, Y., Sobue, G., Togo, M., et al. (2017). Safety and efficacy of edaravone in well defined patients with amyotrophic lateral sclerosis: a randomised, double-blind, placebo-controlled trial. *Lancet Neurol.* 16, 505–512. doi: 10.1016/S1474-4422(17)30115-1

Afshar, P., Ashtari, N., Jiao, X., Rahimi-Balaei, M., Zhang, X., Yaganeh, B., et al. (2017). Overexpression of human SOD1 leads to discrete defects in the cerebellar architecture in the mouse. *Front. Neuroanat.* 11:22. doi: 10.3389/fnana.2017.00022

Alexander, M., Hu, R., Runtsch, M. C., Kagele, D. A., Mosbruger, T. L., Tolmachova, T., et al. (2015). Exosome-delivered microRNAs modulate the inflammatory response to endotoxin. *Nat. Commun.* 6, 7321–7321. doi: 10.1038/ncomms8321

Barber, S. C., and Shaw, P. J. (2010). Oxidative stress in ALS: key role in motor neuron injury and therapeutic target. *Free Radic. Biol. Med.* 48, 629–641. doi: 10.1016/j.freeradbiomed.2009.11.018

Barnett, R. E., Conklin, D. J., Ryan, L., Keskey, R. C., Ramjee, V., Sepulveda, E. A., et al. (2016). Anti-inflammatory effects of miR-21 in the macrophage response to peritonitis. *J. Leukoc. Biol.* 99, 361–371. doi: 10.1189/jlb.4A1014-489R

Basso, M., Pozzi, S., Tortarolo, M., Fiordaliso, F., Bisighini, C., Pasetto, L., et al. (2013). Mutant copper-zinc superoxide dismutase (SOD1) induces protein secretion pathway alterations and exosome release in astrocytes: implications for disease spreading and motor neuron pathology in Amyotrophic Lateral Sclerosis. *J. Biol. Chem.* 288, 15699–15711. doi: 10.1074/jbc.m112.425066

Beers, D. R., Henkel, J. S., Xiao, Q., Zhao, W., Wang, J., Yen, A. A., et al. (2006). Wild-type microglia extend survival in PU.1 knockout mice with familial amyotrophic lateral sclerosis. *Proc. Natl. Acad. Sci. U S A* 103, 16021–16026. doi: 10.1073/pnas.0607423103

Bell, C. W., Jiang, W., Reich, C. F. III., and Pisetsky, D. S. (2006). The extracellular release of HMGB1 during apoptotic cell death. *Am. J. Physiol. Cell Physiol.* 291, C1318–C1325. doi: 10.1152/ajpcell.00616.2005

Bell, E., and Taylor, M. A. (2017). Functional roles for exosomal MicroRNAs in the tumour microenvironment. *Comput. Struct. Biotechnol. J.* 15, 8–13. doi: 10.1016/j.csbj.2016.10.005

Boillée, S., Yamanaka, K., Lobsiger, C. S., Copeland, N. G., Jenkins, N. A., Kassiotis, G., et al. (2006). Onset and progression in inherited ALS determined by motor neurons and microglia. *Science* 312, 1389–1392. doi: 10.1126/science.1123511

Brites, D., and Fernandes, A. (2015). Neuroinflammation and depression: microglia activation, extracellular microvesicles and microRNA dysregulation. *Front. Cell. Neurosci.* 9:476. doi: 10.3389/fncel.2015.00476

Brites, D., and Vaz, A. R. (2014). Microglia centered pathogenesis in ALS: insights in cell interconnectivity. *Front. Cell. Neurosci.* 8, 117–117. doi: 10.3389/fncel.2014.00117

Bruce-Keller, A. J., Keeling, J. L., Keller, J. N., Huang, F. F., Camondola, S., and Mattson, M. P. (2000). Antiinflammatory effects of estrogen on microglial activation. *Endocrinology* 141, 3646–3656. doi: 10.1210/en.141.10.3646

Butovsky, O., Jedrychowski, M. P., Cialic, R., Krasemann, S., Murugaiyan, G., Fanek, Z., et al. (2015). Targeting miR-155 restores abnormal microglia and attenuates disease in SOD1 mice. *Ann. Neurol.* 77, 75–99. doi: 10.1002/ana.24304

Buzas, E. I., György, B., Nagy, G., Falus, A., and Gay, S. (2014). Emerging role of extracellular vesicles in inflammatory diseases. *Nat. Rev. Rheumatol.* 10, 356–364. doi: 10.1038/nrrheum.2014.19

Cardoso, A. L., Guedes, J. R., and de Lima, M. C. P. (2016). Role of microRNAs in the regulation of innate immune cells under neuroinflammatory conditions. *Curr. Opin. Pharmacol.* 26, 1–9. doi: 10.1016/j.coph.2015.09.001

Cardoso, A. L., Guedes, J. R., Pereira de Almeida, L., and Pedroso de Lima, M. C. (2012). miR-155 modulates microglia-mediated immune response by down-regulating SOCS-1 and promoting cytokine and nitric oxide production. *Immunology* 135, 73–88. doi: 10.1111/j.1365-2567.2011.03514.x

Chiò, A., Traynor, B. J., Collins, J., Simeone, J. C., Goldstein, L. A., and White, L. A. (2013). Global epidemiology of amyotrophic lateral sclerosis: a systematic review of the published literature. *Neuroepidemiology* 41, 118–130. doi: 10.1159/000351153

Chiu, I. M., Morimoto, E. T., Goodarzi, H., Liao, J. T., O'Keeffe, S., Phatnani, H. P., et al. (2013). A neurodegeneration-specific gene-expression signature of acutely isolated microglia from an amyotrophic lateral sclerosis mouse model. *Cell Rep.* 4, 385–401. doi: 10.1016/j.celrep.2013.06.018

Cruz, M. P. (2018). Edaravone (Radicava): a novel neuroprotective agent for the treatment of amyotrophic lateral sclerosis. *PT* 43, 25–28.

Cunha, C., Gomes, C., Vaz, A. R., and Brites, D. (2016). Exploring new inflammatory biomarkers and pathways during LPS-induced M1 polarization. *Mediators Inflamm.* 2016:6986175. doi: 10.1155/2016/6986175

Cunha, C., Santos, C., Gomes, C., Fernandes, A., Correia, A. M., Sebastiao, A. M., et al. (2018). Downregulated glia interplay and increased miRNA-155 as promising markers to track ALS at an early stage. *Mol. Neurobiol.* 55, 4207–4224. doi: 10.1007/s12035-017-0631-2

Dimayuga, F. O., Wang, C., Clark, J. M., Dimayuga, E. R., Dimayuga, V. M., and Bruce-Keller, A. J. (2007). SOD1 overexpression alters ROS production and reduces neurotoxic inflammatory signaling in microglial cells. *J. Neuroimmunol.* 182, 89–99. doi: 10.1016/j.jneuroim.2006.10.003

Essandoh, K., Li, Y., Huo, J., and Fan, G. C. (2016). MiRNA-mediated macrophage polarization and its potential role in the regulation of inflammatory response. *Shock* 46, 122–131. doi: 10.1097/SHK.0000000000000604

Falcão, A. S., Carvalho, L. A. R., Lidónio, G., Vaz, A. R., Lucas, S. D., Moreira, R., et al. (2017). Dipeptidyl vinyl sulfone as a novel chemical tool to inhibit HMGB1/NLRP3-inflammasome and inflamma-miRs in Aβ-mediated microglial inflammation. *ACS Chem. Neurosci.* 8, 89–99. doi: 10.1021/acschemneuro.6b00250

Fang, L., Teuchert, M., Huber-Abel, F., Schattauer, D., Hendrich, C., Dorst, J., et al. (2010). MMP-2 and MMP-9 are elevated in spinal cord and skin in a mouse model of ALS. *J. Neurol. Sci.* 294, 51–56. doi: 10.1016/j.jns.2010.04.005

Fernandes, A., Ribeiro, A. R., Monteiro, M., Garcia, G., Vaz, A. R., and Brites, D. (2018). Secretome from SH-SY5Y APPSwecells trigger time-dependent CHME3 microglia activation phenotypes, ultimately leading to miR-21 exosome shuttling. *Biochimie* 155, 67–82. doi: 10.1016/j.biochi.2018.05.015

Fernandes, A., Vaz, A. R., Falcão, A. S., Silva, R. F. M., Brito, M. A., and Brites, D. (2007). Glycoursodeoxycholic acid and interleukin-10 modulate the reactivity of rat cortical astrocytes to unconjugated bilirubin. *J. Neuropathol. Exp. Neurol.* 66, 789–798. doi: 10.1097/nen.0b013e3181461c74

Fleisher-Berkovich, S., Filipovich-Rimon, T., Ben-Shmuel, S., Hülsmann, C., Kummer, M. P., and Heneka, M. T. (2010). Distinct modulation of microglial amyloid β phagocytosis and migration by neuropeptides. *J. Neuroinflammation* 7:61. doi: 10.1186/1742-2094-7-61

Fricker, M., Neher, J. J., Zhao, J. W., Théry, C., Tolkovsky, A. M., and Brown, G. C. (2012). MFG-E8 mediates primary phagocytosis of viable neurons during neuroinflammation. *J. Neurosci.* 32, 2657–2666. doi: 10.1523/JNEUROSCI.4837-11.2012

Gajowiak, A., Styś, A., Starzyński, R. R., Bednarz, A., Lenartowicz, M., Staroń, R., et al. (2015). Mice overexpressing both non-mutated human SOD1 and mutated SOD1(G93A) genes: a competent experimental model for studying iron metabolism in amyotrophic lateral sclerosis. *Front. Mol. Neurosci.* 8:82. doi: 10.3389/fnmol.2015.00082

Gomes, C., Keller, S., Altevogt, P., and Costa, J. (2007). Evidence for secretion of Cu,Zn superoxide dismutase via exosomes from a cell model of amyotrophic lateral sclerosis. *Neurosci. Lett.* 428, 43–46. doi: 10.1016/j.neulet.2007.09.024

Grad, L. I., Yerbury, J. J., Turner, B. J., Guest, W. C., Pokrishevsky, E., O'Neill, M. A., et al. (2014). Intercellular propagated misfolding of wild-type

Cu/Zn superoxide dismutase occurs via exosome-dependent and -independent mechanisms. *Proc. Natl. Acad. Sci. U S A* 111, 3620–3625. doi: 10.1073/pnas.1312245111

Gravel, M., Béland, L. C., Soucy, G., Abdelhamid, E., Rahimian, R., Gravel, C., et al. (2016). IL-10 controls early microglial phenotypes and disease onset in ALS caused by misfolded superoxide dismutase 1. *J. Neurosci.* 36, 1031–1048. doi: 10.1523/JNEUROSCI.0854-15.2016

Hensley, K., Abdel-Moaty, H., Hunter, J., Mhatre, M., Mou, S., Nguyen, K., et al. (2006). Primary glia expressing the G93A-SOD1 mutation present a neuroinflammatory phenotype and provide a cellular system for studies of glial inflammation. *J. Neuroinflammation* 3:2. doi: 10.1186/1742-2094-3-2

Jeyachandran, A., Mertens, B., McKissick, E. A., and Mitchell, C. S. (2015). Type I Vs. type II cytokine levels as a function of sod1 g93a mouse amyotrophic lateral sclerosis disease progression. *Front. Cell. Neurosci.* 9:462. doi: 10.3389/fncel.2015.00462

Ko, W. K., Lee, S. H., Kim, S. J., Jo, M. J., Kumar, H., Han, I. B., et al. (2017). Anti-inflammatory effects of ursodeoxycholic acid by lipopolysaccharide-stimulated inflammatory responses in RAW 264.7 macrophages. *PLoS One* 12:e0180673. doi: 10.1371/journal.pone.0180673

Komine, O., and Yamanaka, K. (2015). Neuroinflammation in motor neuron disease. *Nagoya J. Med. Sci.* 77, 537–549.

Könnecke, H., and Bechmann, I. (2013). The role of microglia and matrix metalloproteinases involvement in neuroinflammation and gliomas. *Clin. Dev. Immunol.* 2013:914104. doi: 10.1155/2013/914104

Koval, E. D., Shaner, C., Zhang, P., du Maine, X., Fischer, K., Tay, J., et al. (2013). Method for widespread microRNA-155 inhibition prolongs survival in ALS-model mice. *Hum. Mol. Genet.* 22, 4127–4135. doi: 10.1093/hmg/ddt261

Krüger, S., Battke, F., Sprecher, A., Munz, M., Synofzik, M., Schöls, L., et al. (2016). Rare variants in neurodegeneration associated genes revealed by targeted panel sequencing in a german ALS cohort. *Front. Mol. Neurosci.* 9:92. doi: 10.3389/fnmol.2016.00092

Lasiene, J., and Yamanaka, K. (2011). Glial cells in amyotrophic lateral sclerosis. *Neurol. Res. Int.* 2011, 718987–718987. doi: 10.1155/2011/718987

Lei, C., Lin, S., Zhang, C., Tao, W., Dong, W., Hao, Z., et al. (2013). High-mobility group box1 protein promotes neuroinflammation after intracerebral hemorrhage in rats. *Neuroscience* 228, 190–199. doi: 10.1016/j.neuroscience.2012.10.023

Liao, B., Zhao, W., Beers, D. R., Henkel, J. S., and Appel, S. H. (2012). Transformation from a neuroprotective to a neurotoxic microglial phenotype in a mouse model of ALS. *Exp. Neurol.* 237, 147–152. doi: 10.1016/j.expneurol.2012.06.011

Liu, Y., Hao, W., Dawson, A., Liu, S., and Fassbender, K. (2009). Expression of amyotrophic lateral sclerosis-linked SOD1 mutant increases the neurotoxic potential of microglia via TLR2. *J. Biol. Chem.* 284, 3691–3699. doi: 10.1074/jbc.M804446200

Liu, Y., Yang, X., Guo, C., Nie, P., Liu, Y., and Ma, J. (2013). Essential role of MFG-E8 for phagocytic properties of microglial cells. *PLoS One* 8:e55754. doi: 10.1371/journal.pone.0055754

Lively, S., and Schlichter, L. C. (2018). Microglia responses to pro-inflammatory stimuli (LPS, IFNγ+TNFα) and reprogramming by resolving cytokines (IL-4, IL-10). *Front. Cell. Neurosci.* 12:215. doi: 10.3389/fncel.2018.00215

Ma, X., Becker Buscaglia, L. E., Barker, J. R., and Li, Y. (2011). MicroRNAs in NF-kappaB signaling. *J. Mol. Cell Biol.* 3, 159–166. doi: 10.1093/jmcb/mjr007

Mann, M., Mehta, A., Zhao, J. L., Lee, K., Marinov, G. K., Garcia-Flores, Y., et al. (2017). An NF-κB-microRNA regulatory network tunes macrophage inflammatory responses. *Nat. Commun.* 8:851. doi: 10.1038/s41467-017-00972-z

Martínez-Muriana, A., Mancuso, R., Francos-Quijorna, I., Olmos-Alonso, A., Osta, R., Perry, V. H., et al. (2016). CSF1R blockade slows the progression of amyotrophic lateral sclerosis by reducing microgliosis and invasion of macrophages into peripheral nerves. *Sci. Rep.* 6:25663. doi: 10.1038/srep25663

Münch, C., O'Brien, J., and Bertolotti, A. (2011). Prion-like propagation of mutant superoxide dismutase-1 misfolding in neuronal cells. *Proc. Natl. Acad. Sci. U S A* 108, 3548–3553. doi: 10.1073/pnas.1017275108

Parisi, C., Napoli, G., Amadio, S., Spalloni, A., Apolloni, S., Longone, P., et al. (2016). MicroRNA-125b regulates microglia activation and motor neuron death in ALS. *Cell Death Differ.* 23, 531–541. doi: 10.1038/cdd.2015.153

Pena-Altamira, E., Prati, F., Massenzio, F., Virgili, M., Contestabile, A., Bolognesi, M. L., et al. (2016). Changing paradigm to target microglia in neurodegenerative diseases: from anti-inflammatory strategy to active immunomodulation. *Expert Opin. Ther. Targets* 20, 627–640. doi: 10.1517/14728222.2016.1121237

Pereira, D. M., Simões, A. E. S., Gomes, S. E., Castro, R. E., Carvalho, T., Rodrigues, C. M. P., et al. (2016). MEK5/ERK5 signaling inhibition increases colon cancer cell sensitivity to 5-fluorouracil through a p53-dependent mechanism. *Oncotarget* 7, 34322–34340. doi: 10.18632/oncotarget.9107

Pinto, S., Cunha, C., Barbosa, M., Vaz, A. R., and Brites, D. (2017). Exosomes from NSC-34 cells transfected with hSOD1–G93A are enriched in mir-124 and drive alterations in microglia phenotype. *Front. Neurosci.* 11:273. doi: 10.3389/fnins.2017.00273

Righi, M., Mori, L., De Libero, G., Sironi, M., Biondi, A., Mantovani, A., et al. (1989). Monokine production by microglial cell clones. *Eur. J. Immunol.* 19, 1443–1448. doi: 10.1002/eji.1830190815

Robberecht, W., and Philips, T. (2013). The changing scene of amyotrophic lateral sclerosis. *Nat. Rev. Neurosci.* 14, 248–264. doi: 10.1038/nrn3430

Rotunno, M. S., and Bosco, D. A. (2013). An emerging role for misfolded wild-type SOD1 in sporadic ALS pathogenesis. *Front. Cell. Neurosci.* 7:253. doi: 10.3389/fncel.2013.00253

Saba, R., Gushue, S., Huzarewich, R. L. C. H., Manguiat, K., Medina, S., Robertson, C., et al. (2012). MicroRNA 146a (miR-146a) is over-expressed during prion disease and modulates the innate immune response and the microglial activation state. *PLoS One* 7:e30832. doi: 10.1371/journal.pone.0030832

Sarko, D. K., and McKinney, C. E. (2017). Exosomes: origins and therapeutic potential for neurodegenerative disease. *Front. Neurosci.* 11:82. doi: 10.3389/fnins.2017.00082

Sheedy, F. J., Palsson-McDermott, E., Hennessy, E. J., Martin, C., O'Leary, J. J., Ruan, Q., et al. (2010). Negative regulation of TLR4 via targeting of the proinflammatory tumor suppressor PDCD4 by the microRNA miR-21. *Nat. Immunol.* 11, 141–147. doi: 10.1038/ni.1828

Sheller-Miller, S., Urrabaz-Garza, R., Saade, G., and Menon, R. (2017). Damage-associated molecular pattern markers HMGB1 and cell-free fetal telomere fragments in oxidative-stressed amnion epithelial cell-derived exosomes. *J. Reprod. Immunol.* 123, 3–11. doi: 10.1016/j.jri.2017.08.003

Shi, B., Wang, Y., Zhao, R., Long, X., Deng, W., and Wang, Z. (2018). Bone marrow mesenchymal stem cell-derived exosomal miR-21 protects C-kit+ cardiac stem cells from oxidative injury through the PTEN/PI3K/Akt axis. *PLoS One* 13:e0191616. doi: 10.1371/journal.pone.0191616

Silva, S. L., Vaz, A. R., Barateiro, A., Falcão, A. S., Fernandes, A., Brito, M. A., et al. (2010). Features of bilirubin-induced reactive microglia: from phagocytosis to inflammation. *Neurobiol. Dis.* 40, 663–675. doi: 10.1016/j.nbd.2010.08.010

Silverman, J. M., Fernando, S. M., Grad, L. I., Hill, A. F., Turner, B. J., Yerbury, J. J., et al. (2016). Disease mechanisms in ALS: misfolded sod1 transferred through exosome-dependent and exosome-independent pathways. *Cell. Mol. Neurobiol.* 36, 377–381. doi: 10.1007/s10571-015-0294-3

Simões, A. E. S., Pereira, D. M., Gomes, S. E., Brito, H., Carvalho, T., French, A., et al. (2015). Aberrant MEK5/ERK5 signalling contributes to human colon cancer progression via NF-κB activation. *Cell Death Dis.* 6:e1718. doi: 10.1038/cddis.2015.83

Spiller, K. J., Restrepo, C. R., Khan, T., Dominique, M. A., Fang, T. C., Canter, R. G., et al. (2018). Microglia-mediated recovery from ALS-relevant motor neuron degeneration in a mouse model of TDP-43 proteinopathy. *Nat. Neurosci.* 21, 329–340. doi: 10.1038/s41593-018-0083-7

Stevens, J. C., Chia, R., Hendriks, W. T., Bros-Facer, V., van Minnen, J., Martin, J. E., et al. (2010). Modification of superoxide dismutase 1 (SOD1) properties by a GFP tag—implications for research into amyotrophic lateral sclerosis (ALS). *PLoS One* 5:e9541. doi: 10.1371/journal.pone.0009541

Su, W., Aloi, M. S., and Garden, G. A. (2016). MicroRNAs mediating CNS inflammation: small regulators with powerful potential. *Brain Behav. Immun.* 52, 1–8. doi: 10.1016/j.bbi.2015.07.003

Sundaramoorthy, V., Walker, A. K., Yerbury, J., Soo, K. Y., Farg, M. A., Hoang, V., et al. (2013). Extracellular wildtype and mutant SOD1 induces ER-Golgi pathology characteristic of amyotrophic lateral sclerosis in neuronal cells. *Cell. Mol. Life Sci.* 70, 4181–4195. doi: 10.1007/s00018-013-1385-2

Tang, Y., and Le, W. (2016). Differential roles of M1 and M2 microglia in neurodegenerative diseases. *Mol. Neurobiol.* 53, 1181–1194. doi: 10.1007/s12035-014-9070-5

Tili, E., Michaille, J.-J., Cimino, A., Costinean, S., Dumitru, C. D., Adair, B., et al. (2007). Modulation of miR-155 and miR-125b levels following lipopolysaccharide/TNF-α stimulation and their possible roles in regulating the response to endotoxin shock. *J. Immunol.* 179, 5082–5089. doi: 10.4049/jimmunol.179.8.5082

Vaz, A. R., Cunha, C., Gomes, C., Schmucki, N., Barbosa, M., and Brites, D. (2015). Glycoursodeoxycholic acid reduces matrix metalloproteinase-9 and caspase-9 activation in a cellular model of superoxide dismutase-1 neurodegeneration. *Mol. Neurobiol.* 51, 864–877. doi: 10.1007/s12035-014-8731-8

Wang, L., Deng, H. X., Grisotti, G., Zhai, H., Siddique, T., and Roos, R. P. (2009). Wild-type SOD1 overexpression accelerates disease onset of a G85R SOD1 mouse. *Hum. Mol. Genet.* 18, 1642–1651. doi: 10.1093/hmg/ddp085

Wang, M., Mungur, R., Lan, P., Wang, P., and Wan, S. (2018). MicroRNA-21 and microRNA-146a negatively regulate the secondary inflammatory response of microglia after intracerebral hemorrhage. *Int. J. Clin. Exp. Pathol.* 11, 3348–3356.

Yamaguchi, H., Takagi, J., Miyamae, T., Yokota, S., Fujimoto, T., Nakamura, S., et al. (2008). Milk fat globule EGF factor 8 in the serum of human patients of systemic lupus erythematosus. *J. Leukoc. Biol.* 83, 1300–1307. doi: 10.1189/jlb.1107730

Zhao, W., Beers, D. R., Henkel, J. S., Zhang, W., Urushitani, M., Julien, J.-P., et al. (2010). Extracellular mutant SOD1 induces microglial-mediated motoneuron injury. *Glia* 58, 231–243. doi: 10.1002/glia.20919

Conflict of Interest Statement: The authors declare that the research was conducted in the absence of any commercial or financial relationships that could be construed as a potential conflict of interest.

frontiers in Cellular Neuroscience

ORIGINAL RESEARCH
published: 30 July 2019
doi: 10.3389/fncel.2019.00308

Microglia Express Insulin-Like Growth Factor-1 in the Hippocampus of Aged $APP_{swe}/PS1_{\Delta E9}$ Transgenic Mice

*Christa Løth Myhre[1], Camilla Thygesen[1,2,3†], Birgitte Villadsen[1,2†], Jeanette Vollerup[1,2], Laura Ilkjær[1], Katrine Tækker Krohn[1,2], Manuela Grebing[1], Shuainan Zhao[1,2], Asif Manzoor Khan[1], Lasse Dissing-Olesen[1], Morten Skovgaard Jensen[4], Alicia A. Babcock[1] and Bente Finsen[1,2]**

[1] Department of Neurobiology, Institute of Molecular Medicine, University of Southern Denmark, Odense, Denmark, [2] Brain Research – Inter-Disciplinary Guided Excellence, Department of Clinical Research, University of Southern Denmark, Odense, Denmark, [3] Department of Biochemistry and Molecular Biology, University of Southern Denmark, Odense, Denmark, [4] Department of Biomedicine, Aarhus University, Aarhus, Denmark

OPEN ACCESS

Edited by:
Raquel Ferreira,
University of Beira Interior, Portugal

Reviewed by:
Daniela Tropea,
Trinity College Dublin, Ireland
Aline Stephan,
Université de Strasbourg, France

***Correspondence:**
Bente Finsen
bfinsen@health.sdu.dk

†Share second authorship

Specialty section:
This article was submitted to Non-Neuronal Cells, a section of the journal Frontiers in Cellular Neuroscience

Received: 23 November 2018
Accepted: 24 June 2019
Published: 30 July 2019

Citation:
Myhre CL, Thygesen C, Villadsen B, Vollerup J, Ilkjær L, Krohn KT, Grebing M, Zhao S, Khan AM, Dissing-Olesen L, Jensen MS, Babcock AA and Finsen B (2019) Microglia Express Insulin-Like Growth Factor-1 in the Hippocampus of Aged $APP_{swe}/PS1_{\Delta E9}$ Transgenic Mice. Front. Cell. Neurosci. 13:308. doi: 10.3389/fncel.2019.00308

Insulin-like growth factor-1 (IGF-1) is a pleiotropic molecule with neurotrophic and immunomodulatory functions. Knowing the capacity of chronically activated microglia to produce IGF-1 may therefore show essential to promote beneficial microglial functions in Alzheimer's disease (AD). Here, we investigated the expression of IGF-1 mRNA and IGF-1 along with the expression of tumor necrosis factor (TNF) mRNA, and the amyloid-β (Aβ) plaque load in the hippocampus of 3- to 24-month-old $APP_{swe}/PS1_{\Delta E9}$ transgenic (Tg) and wild-type (WT) mice. As IGF-1, in particular, is implicated in neurogenesis we also monitored the proliferation of cells in the subgranular zone (sgz) of the dentate gyrus. We found that the Aβ plaque load reached its maximum in aged 21- and 24-month-old $APP_{swe}/PS1_{\Delta E9}$ Tg mice, and that microglial reactivity and hippocampal IGF-1 and TNF mRNA levels were significantly elevated in aged $APP_{swe}/PS1_{\Delta E9}$ Tg mice. The sgz cell proliferation decreased with age, regardless of genotype and increased IGF-1/TNF mRNA levels. Interestingly, IGF-1 mRNA was expressed in subsets of sgz cells, likely neuroblasts, and neurons in both genotypes, regardless of age, as well as in glial-like cells. By double *in situ* hybridization these were shown to be IGF1 $mRNA^+$ CD11b $mRNA^+$ cells, i.e., IGF-1 mRNA-expressing microglia. Quantification showed a 2-fold increase in the number of microglia and IGF-1 mRNA-expressing microglia in the molecular layer of the dentate gyrus in aged $APP_{swe}/PS1_{\Delta E9}$ Tg mice. Double-immunofluorescence showed that IGF-1 was expressed in a subset of Aβ plaque-associated $CD11b^+$ microglia and in several subsets of neurons. Exposure of primary murine microglia and BV2 cells to $A\beta_{42}$ did not affect IGF-1 mRNA expression. IGF-1 mRNA levels remained constant in WT mice with aging, unlike TNF mRNA levels which increased with aging. In conclusion, our results suggest that the increased IGF-1 mRNA levels can be ascribed to a larger number of IGF-1 mRNA-expressing microglia

in the aged $APP_{swe}/PS1_{\Delta E9}$ Tg mice. The finding that subsets of microglia retain the capacity to express IGF-1 mRNA and IGF-1 in the aged $APP_{swe}/PS1_{\Delta E9}$ Tg mice is encouraging, considering the beneficial therapeutic potential of modulating microglial production of IGF-1 in AD.

Keywords: neuroinflammation, tumor necrosis factor, insulin-like growth factor, cerebral amyloidosis, aging, neurogenesis

INTRODUCTION

Alzheimer's disease (AD) is an age-associated progressive neurodegenerative disease and the most common cause of dementia. Histopathological changes include accumulation of beta-amyloid (Aβ) in plaques and a chronic microglial reaction, that takes its onset years before a diagnosis can be made (Cagnin et al., 2001; Heneka et al., 2015; Heppner et al., 2015). Knowing microglial capacity to produce neurotrophic and immunomodulatory factors, such as the insulin-like growth factor-1 (IGF-1) (Fernandez and Torres-Alemán, 2012), as well as factors with potential deleterious functions, such as the pleiotrophic cytokine tumor necrosis factor (TNF) (Arnett et al., 2001; Lambertsen et al., 2009), is therefore essential to promote beneficial and ameliorate detrimental microglial functions. While it is well-known that microglia are a major source of TNF in transgenic mouse models of AD (Hickman et al., 2008; Minogue et al., 2014; Babcock et al., 2015), there is less information about microglia as a significant local source of IGF-1. To our knowledge, the first evidence of microglia being a source of IGF-1 in the adult CNS was the finding of a transient deafferentation-induced up-regulation of IGF-1 mRNA in the perforant pathway innervated parts of the dentate gyrus in young, adult rats which functionally was suggested to be involved in deafferentation-induced axonal sprouting (Guthrie et al., 1995). This up-regulation of IGF-1 mRNA was reported to be attenuated in aged rats (Woods et al., 1998).

IGF-1 is a member of the insulin gene family. It is a 70 amino acid long growth factor hormone with potent anabolic effects during development (Arroba et al., 2018). Deficiency in IGF-1 leads to microcephalus and mental retardation in the human (Woods et al., 1996). IGF-1 is transiently expressed in high levels in central projection neurons during development (Bondy, 1991; Bondy et al., 1992), consistent with an important role in brain development and neuroplasticity (Dyer et al., 2016). Additionally, an IGF-1 mRNA-expressing microglial subset was recently reported to support myelinogenesis during development (Wlodarczyk et al., 2017). IGF-1 binds with high affinity to the IGF-1 receptor (IGF-1R) as well as the insulin receptor (lower affinity), which are both tyrosine kinase receptors, sharing signaling molecules and trophic activities (Fernandez and Torres-Alemán, 2012). While the expression of IGF-1 declines with development, the IGF-1R, remains expressed at high level in the adult brain (Bondy et al., 1992).

Aβ plaque load has been shown to follow a sigmoidal path in the neocortex of both AD patients (Serrano-Pozo et al., 2011; Jack et al., 2013) and in the $APP_{swe}/PS1_{\Delta E9}$ transgenic (Tg) mouse (Jankowsky et al., 2004; Babcock et al., 2015), eventually stabilizing and reaching a plateau. Whether the same phenomenon occurs in the hippocampus is unknown. Aβ plaques appear in the hippocampus during early stages of AD (Thal et al., 2002), especially within the target zone of the perforant pathway carrying information from the entorhinal cortex into the hippocampus (Hyman et al., 1986; Pooler et al., 2013). Unlike in normal aging, AD patients lose hippocampal CA1 neurons (West et al., 1994), and hippocampal atrophy is associated with the development of AD (Bobinski et al., 2000; Nelson et al., 2012; Huijbers et al., 2015). The hippocampus is also a site of neurogenesis, which involves proliferation of cells in the subgranular zone (sgz) of the dentate gyrus (Eriksson et al., 1998; Kempermann et al., 2004). Studies report both an increase (Jin et al., 2004) and a decrease (Ziabreva et al., 2006; Crews et al., 2010) in sgz cell proliferation in AD brains, indicating that neurogenesis may be deregulated. Contradictory results on sgz cell proliferation have also been reported in different transgenic mouse models of AD (Chuang, 2010). The $APP_{swe}/PS1_{\Delta E9}$ Tg mouse, which develops Aβ plaques in the hippocampus from 3 months of age (Hamilton and Holscher, 2012), has been reported to have more pronounced loss of sgz cell proliferation with age than age-matched wild-type (WT) mice by some groups (Demars et al., 2010; Valero et al., 2011; Hamilton and Holscher, 2012). Results by us showed a reduced number of neuroblasts in the sgz of male 18-month-old $APP_{swe}/PS1_{\Delta E9}$ Tg mice, while sgz cell proliferation was unaffected by genotype (Olesen et al., 2017).

Neurogenesis has been reported to be regulated by both systemic (Foster et al., 2011) and locally-produced IGF-1 (Anderson et al., 2002; Stranahan et al., 2009), and it is reduced during normal aging (Kuhn et al., 1996; Knoth et al., 2010; Spalding et al., 2013). In the case of TNF, small amounts of TNF have been shown to increase sgz cell proliferation, while higher TNF levels can induce apoptosis (Iosif et al., 2006). Decreased serum levels of IGF-1 (Ramsey et al., 2004; Sonntag et al., 2005; Duron et al., 2014), and increased serum levels of TNF in AD patients (Perry et al., 2001; Holmes et al., 2009; Swardfager et al., 2010), might potentially impair hippocampal neurogenesis and/or neuroblast survival and differentiation.

The $APP_{swe}/PS1_{\Delta E9}$ Tg mouse exhibits changes in both the IGF-1 and TNF system (Zhang et al., 2013; Francois et al., 2014; Minogue et al., 2014; Babcock et al., 2015). Using this mouse model, we recently showed that TNF mRNA levels in the neocortex correlate to the age-dependent increase in Aβ plaque-load as well as aging, and additionally, that microglial production of TNF was functionally correlated to microglial

uptake of Aβ (Babcock et al., 2015). We here expanded this study to include an investigation of the accumulation of Aβ plaques, microglial reactivity, and expression of IGF-1 mRNA and IGF-1 as well as TNF mRNA progression with age in the hippocampus of $APP_{swe}/PS1_{\Delta E9}$ Tg mice. We additionally used double *in situ* hybridization (*ISH*) to investigate whether or not IGF-1 mRNA might co-localize to CD11b $mRNA^+$ microglia, besides being expressed in neurons. Finally, we investigated how Aβ pathology and age affected proliferation of sgz cells in the neurogenic niche of the hippocampus. Our results show that a subset of microglia in the aging $APP_{swe}/PS1_{\Delta E9}$ Tg mouse retain the capacity to express IGF-1 mRNA, suggesting that the increased IGF-1 mRNA levels in the aged $APP_{swe}/PS1_{\Delta E9}$ Tg mice may be ascribed to microglia. This finding attracts attention to the perspectives of modulating microglial synthesis of IGF-1 in AD.

MATERIALS AND METHODS

Mice and Experimental Material

Female $APP_{swe}/PS1_{\Delta E9}$ Tg mice that expressed humanized APP (Mo/HuAPP695sweK595N/M596L) and mutant human $PS1_{\Delta E9}$ in neurons (Jankowsky et al., 2004) and WT littermates were bred and maintained on a hybrid (C57BL/6 × C3H/HeN; B6C3) background. Additionally, three 24-26-month-old $APP_{swe}/PS1_{\Delta E9}$ Tg and two 26-month-old WT littermate bred on a C57BL/6 background and two postnatal day 5 (P5) C57BL/6 pups were used for *ISH* and IGF-1 protein detection. All mice were housed and bred in the Biomedical Laboratory, University of Southern Denmark. $APP_{swe}/PS1_{\Delta E9}$ Tg and WT mice on a hybrid background were perfused with phosphate-buffered saline (PBS) and analyzed at 3, 6, 9, 12, 15, 18, 21, and 24 months of age (n = 6–10 per group). Sections (20-μm-thick) were cut from fresh frozen left hemispheres, on a cryostat, and used for immunohistochemistry (IHC) and *ISH*. This experimental material was previously used to quantify changes in Aβ plaque load and TNF $mRNA^+$ and interleukin-1β $mRNA^+$ cells in the neocortex (Babcock et al., 2015). The hippocampus was dissected from the right hemisphere, and stored in Trizol at −80°C for polymerase chain reaction (qPCR) analysis. Additional mice used for *ISH* were euthanized by decapitation and the brains processed in 20-μm-thick cryostat sections. WT and $APP_{swe}/PS1_{\Delta E9}$ Tg mice used for double immunofluorescence staining were perfused with Sorensen's buffer, followed by 4% paraformaldehyde (PFA). After 2 h post-fixation in 4% PFA and overnight immersion in 20% sucrose, these brains were frozen in CO_2 snow and cut as 20-μm-thick horizontal sections on a cryostat. The proliferation of sgz cells was evaluated in groups of 3-, 9-, and 15-month-old Tg and WT mice receiving 90 mg/kg BrdU i.p. at 2, 12, and 22 h prior to PBS-perfusion (n = 6–8 per group). Hippocampi were isolated, immersion-fixed in 4% PFA, followed by 1% PFA and 20% sucrose in each solution overnight at 4°C, and then frozen in CO_2 snow. Hippocampi were cut into 30-μm-thick cryostat sections. Experiments were conducted according to permission from the Danish Ethical Animal Care Committee (Permissions no. 2011/562-67 and 2011/561-1950).

Primary Microglia and Microglial BV2 Cells

Primary murine microglia were cultured and isolated as described in Thygesen et al. (2018). Primary microglia were harvested from mixed glia cultures and plated in 24-well culture plates at a density of 1.5×10^5 cells/mL. The BV2 murine microglial cell line was kindly provided by Jan Thorleif Pedersen, Lundbeck A/S, Denmark. Cells were grown in Dulbecco's modified eagle medium, 10% fetal bovine serum (FBS), 1% penicillin/glutamine/streptomycin in 5% CO_2 at 37°C and plated in 24-well culture plates at a density of 0.75×10^5 cells/mL. After plating, cells were allowed to settle for 24 h after which they were stimulated with 1 μM $A\beta_{42}$ (Anaspec) for 24 h in 5% CO_2 at 37°C. The $A\beta_{42}$ peptide solution was prepared according to Stine et al. (2003). Briefly, a lyophilized peptide stock of 0.1 mg was dissolved in dimethyl sulfoxide to a final concentration of 5 mM and diluted to 100 μM in Dulbecco's modified eagle medium, 10% FBS, 1% penicillin/glutamine/streptomycin, and left 24 h at 37°C to allow peptide aggregation prior to cell stimulation.

Immunohistochemistry (IHC) and Immunofluorescence Staining

Antibodies and Isotype Controls

Biotinylated mouse anti-human $A\beta_{1-16}$, (clone 6e10, Covance), rat anti-mouse CD11b (clone 5C6, Serotec), rat anti-BrdU (clone BU1/75 (ICR1), Abcam), and rabbit anti-IGF-1 (ab9572, Abcam) were used as primary antibodies. Biotinylated goat anti-rat IgG (GE Healthcare United Kingdom limited) and biotinylated goat anti-rat IgG (Thermo) were used as secondary antibodies for BrdU and CD11b IHC, respectively, while an alkaline phosphatase (AP)-conjugated goat-anti rabbit antibody was used for IGF-1 (Sigma, A3812) IHC. Horseradish peroxidase-conjugated streptavidin (HRP-SA) (Dako) was applied after biotinylated antibodies were bound. Biotinylated mouse IgG1 (Caltag), rat IgG2b (Biosite), rat IgG2a (BioLegend), and rabbit IgG (DAKO) were used as isotype or IgG controls.

BrdU-Pretreatment

Sections from immersion-fixed hippocampi were stained for BrdU. After post-fixing sections for 10 min in 4% PFA, sections were rinsed with 2 × saline sodium citrate (2 × SSC) and 49% formamide in tris-buffered saline (TBS) for 2 h at 60°C. Sections were then rinsed with 2 × SSC at 60°C for 2 h and incubated with 2N HCl for 2 h at 37°C. Finally, sections were rinsed with 0.1 M sodium borate buffer (pH = 8.5) for 10 min, before proceeding with the IHC protocol.

Protocol Aβ, CD11b, and BrdU

IHC was performed as previously described (Babcock et al., 2015). All sections were acclimatized for 30 min at room temperature (RT). Fresh frozen sections to be stained for CD11b were fixed in 4% buffered formalin (pH 7.0) for 2 min, then immersed in 50% acetone, 100% acetone, and 50% acetone for 2 min in each solution, and for Aβ, sections were fixed in 4% PFA overnight. All sections for Aβ, CD11b and BrdU IHC were then rinsed with TBS and TBS + 1% Triton X-100. Non-specific

binding was blocked by incubation in TBS containing 10% FBS for 30 min. Primary antibodies or isotype controls were prepared in TBS with 10% FBS and applied for 1 h at RT, followed by 4°C overnight. After acclimatization and rinsing in TBS, endogenous peroxidase was blocked in sections prepared for Aβ and CD11b IHC using 10% methanol and 10% H_2O_2 in TBS for 10 min. After rinsing in TBS, secondary antibodies for CD11b and BrdU staining were added for 1 h at RT in TBS containing 10% FBS. SA-conjugated horseradish peroxidase diluted in TBS containing 10% FBS (1:200) was added for 1 h at RT, and then sections were rinsed in TBS and developed with 0.05% diaminobenzidine (DAB) in TBS containing 0.01% H_2O_2. Sections were further rinsed in TBS, dehydrated in graded ethanol, cleared in xylene, and coverslipped with Depex mounting medium. BrdU-stained sections and a parallel series of sections were stained with Toluidine blue (pH 7.4), and rinsed three times with H_2O before dehydration and mounting. No staining was observed in sections stained with isotype controls (data not shown).

IHC for IGF-1

IHC for IGF-1 was performed as described for TNF in Lambertsen et al. (2001), however, sections were fixed in 4% PFA overnight, or as described above for CD11b, by use of an AP-conjugated secondary antibody.

Immunofluorescence

Immunofluorescence staining was performed in tissue sections from PFA-perfused mice, using a combination of antibodies directed against Aβ (clone 6e10) and CD11b (clone 5C6). The staining procedure was largely as described for IHC (section "Protocol Aβ, CD11b, and BrdU"), except that primary antibodies were applied in combination and steps to block endogenous peroxidase activity were omitted. The bound primary antibodies were detected by incubating sections with SA-TRITC (AbDSerotec) and AlexaFluor488-labeled goat-anti rat IgG (Invitrogen) simultaneously. Sections were kept in the dark after application of secondary reagents. Sections incubated with isotype controls (biotinylated mouse IgG1 (Caltag) or rat IgG2b (Biosite) instead of primary antibodies, showed no staining (data not shown). Immunofluorescence for IGF-1 and CD11b (clone 5C6) was performed on fresh frozen tissue sections from 24-month-old $APP_{swe}/PS1_{\Delta E9}$ (n = 2) and 26-month-old WT (n = 1) mice. Sections were brought to RT for 30 min, fixed as described for CD11b, and dried 60 min at RT. The staining was performed as described above, however, using AlexaFluor488-labeled goat-anti rabbit IgG (Invitrogen) and AlexaFluor568 goat-anti rat IgG (Invitrogen) simultaneously as secondary reagents. Specificity was controlled by substitution of the primary antibodies with rabbit IgG and isotype and rat IgG2b. Sections were mounted with DAKO fluorescence mounting medium. Immunofluorescence images were captured with an Olympus BX63 upright, automated fluorescence microscope installed with an Olympus DP80 camera, X-cite 120LED system with the following filter cubes (U-FBNA FL Ex.BP470- 495 Em.BA510-550, U-FGNA FL Ex.BP540-550 EM.BA575-625, U-FMCHE FL Ex.BP 565-585 Em.BA600-690, and U-FUNA FL Ex.BP360-370 EmBA420-460), and objectives (UPLSAPO2 10X/0.4, UPLSAPO2 40X/0.95, PLAPON0 60X/1.42, and UPLSAPO 100X/1.4), using the CellSens Software (Thygesen et al., 2018).

Estimation of % Aβ Plaque Load and Measurement of Hippocampal Volume

% Aβ Plaque Load

The % Aβ plaque load was quantified by estimating the area of the hippocampus covered by Aβ plaques using unbiased stereological principles. This was carried out using the same Aβ-stained sections previously used for quantifying neocortical Aβ plaque load (Babcock et al., 2015). All Aβ plaques were counted by the same person (CM) using an Olympus BX 50-microscope (Olympus, Germany) fitted with a U-PMTVC Japan color camera (Olympus, Germany), a Proscan Prior motorized specimen stage, and a Heidenhain MT12 microcator connected to a PC installed with the CAST-2 Software (Visiopharm, Denmark). The hippocampus in the left hemisphere was delineated in Aβ-stained sections using anatomical borders. After delineation, the software determined the area of the hippocampus that was used for the sampling (A_{HC}). We used a point-counting method with a 286.5 μm × 216 μm frame and 36-crosses, each corresponding to an area of 1,714.5 μm^2, which produced an acceptable coefficient of error (CE) of <0.10 in a 9-month-old $APP_{swe}/PS1_{\Delta E9}$ Tg mouse with moderate Aβ plaque formation. Only Aβ plaques marked by a counting cross in the hippocampus were counted. Counting was carried out systematically in 5–8 sections per mouse. The percentage of hippocampus covered by plaques, % Aβ plaque load, was calculated as previously described (Babcock et al., 2015). The CE for individual mice and the average CE for each age group were calculated as outlined in West et al. (1996). The coefficient of variation, CV, is calculated as SD/Mean. CV and average CE are shown in **Supplementary Table S1** for each age group.

Hippocampal Volume Estimation

We estimated the volume of the left hippocampus based on the hippocampal areas (A_{HC}) delineated during Aβ quantification (section "% Aβ Plaque Load"). For each mouse, hippocampal volume (V_{HC}) was determined using volumetric principles, based on typically four systematically sampled sections, and was calculated using the following equation: $V_{HC} = A_{HC} \times d$, where A_{HC} is the area of the hippocampus (see section "% Aβ Plaque Load") and d is the distance between sections (960 μm). The CV (SD/mean) values for individual age groups are included in **Supplementary Table S1**.

qPCR

RNA was isolated using the Trizol method and then converted into cDNA (Babcock et al., 2006; Wirenfeldt et al., 2007). The quantitative PCR (qPCR) reaction was carried out in triplicate in 96-well plates using an Applied Biosystems PRISM 7300 Real time PCR machine (Babcock et al., 2006). Primer and probe sequences used were: for HPRT (F′ GTT AAG CAG TAC AGC CCC AAA ATG, R′ AAA TCC AAC AAA GTC TGG CCT GTA and probe: Fam-AGC TTG CTG GTG AAA AGG ACC TCT CGA AGT); GAPDH (F′ TGT CAA GCT CAT TTC CTG

GTA TGA, R′ CTT ACT CCT TGG AGG CCA TGT AG and probe: FAM-TCC ACC ACC CTG TTG CTG TAG CCG); TNF (F′ TGG CCT CCC TCT CAT CAG TTC, R′ CCA CTT GGT GGT TTG CTA CGA and probe: 5′-FAM-TGG CCC AGA CCC TCA CAC TCA GAT CAT C) (Fenger et al., 2006; Meldgaard et al., 2006); IGF-1 (F′ CCG AGG GGC TTT TAC TTC AAC AA, R′CGG AAG CAA CAC TCA TCC ACA A); and brain-derived neurotrophic factor (BDNF) (F′ GGC CCA ACG AAG AAA ACC AT, R′ AGC ATC ACC CGG GAA GTG T). Maxima Probe Master (Fermentas) was used as master mix for TaqMan qPCR (TNF, HPRT, GAPDH) and Maxima Sybr Green Master (Fermentas) as master mix for Sybr Green qPCR (IGF-1, BDNF). In the case of the hippocampal tissue, the qPCR results were calibrated relative to spleen cDNA and were normalized using HPRT, which is stably expressed in mice under pathological conditions in brain tissue (Meldgaard et al., 2006). In the case of the *in vitro* experiments, RNA was isolated with the RNeasy mini kit and the qPCR results were normalized using two reference genes (GAPDH and HPRT), as done in Thygesen et al. (2018). The relative qPCR values on the hippocampal data are shown as fold-increases versus the 3-month-old WT group, on primary microglia as fold-increases compared to whole neocortex, and as Aβ-stimulated versus un-stimulated cells.

ISH

AP-Labeled Probes and Controls

ISH was performed on fresh frozen cryostat sections using a *de novo* synthesized AP-labeled oligo DNA probe specific for IGF-1 mRNA (5′/AP/CCC CTC GGT CCA CAC ACG AAC TGA AGA) or a mixture of two AP-labeled oligo DNA probes specific for TNF mRNA (5′/AP/CG TAG TCG GGG CAG CCT TGT CCC TTG AA and 5′/AP/CT TCT CAT CCC TTT GGG GAC CGA TCA CC) (Gregersen et al., 2000; Lambertsen et al., 2009; Babcock et al., 2015). The IGF-1 probe was designed in Oligo v. 6 to target both IGF-1 isoforms and with sequence specificity verified by BLAST. No specific signal was detected for either system when a series of negative controls was performed. This included pre-treatment of sections with RNAse prior to hybridization in order to control for binding to RNA, hybridization with 100-fold excess of unlabelled probe to control for non-specific binding of the AP-linker arm, and buffer controls (Clausen et al., 2013). A probe for GAPDH mRNA was included as a control for the *ISH* procedure and to know the tissue quality.

ISH protocol

Fresh frozen sections were dried at 55°C for 10 min, then dehydrated in 96% Ethanol for 3 h at RT and dried 1 h at RT. Probes mixed in hybridization buffer were applied to sections with coverslips and allowed to hybridize overnight in a dark hybridization chamber at 37°C. Sections were rinsed three times 30 min with 1 × SSC (pH = 9.5) in 55°C preheated holders and rinsed twice with Tris–HCL buffer for 10 min at RT. Sections were developed with Nitro blue tetrazolium (NBT) + 5-bromo-4-chloro-3-indolyl-phosphate (BCIP), for 3 days in the dark at RT. The sections were rinsed in 25°C distilled water for 1 h to stop development, and then mounted with Aquatex.

Double-ISH

ViewRNA Tissue Assay Kit (Affymetrix) and probes specific for IGF-1 mRNA (VB1-20972 (Probe 1-AP)) and CD11b (Itgam) mRNA (VB6-15396 (Probe 6-AP)) (Affymetrix) were used for co-expression analysis which, with smaller modifications, was performed according to the QuantiGene ViewRNA ISH Tissue 2-Plex Assay Protocol by Affymetrix as described in Grebing et al. (2016). After ISH the sections were counterstained with hematoxylin (Sigma-Aldrich), rinsed in tap water three times, dried for 1 h and coverslipped in Ultramount (Dako).

Counting of BrdU$^+$ Cells

BrdU$^+$ cells were systematically counted in every 10th section of the hippocampus (typically 12–18 sections per mouse), using an Olympus BX 41-microscope (Olympus, Denmark) equipped with a 20 × objective. BrdU$^+$ cells were only counted if their nucleus was located in the sgz. The total number of sections containing the hippocampus was determined in a parallel series of Toluidine Blue-stained sections. Data are presented as the mean number of BrdU$^+$ cells per hippocampal section.

Counting of IGF-1 mRNA$^+$ CD11b mRNA$^+$ Cells

All hematoxylin-stained nuclei were counted manually in the region of interest (ROI) which was either the lateral or medial blade of the molecular layer in the dentate gyrus, together with all CD11b mRNA$^+$ and/or IGF-1 mRNA$^+$ cells. Quantification was performed in 5 hippocampi in three sections from 3 Tg mice and 3 hippocampi in two sections from 2 WT mice by the use of a 40 × high numerical objective (NA 0.95) and an Olympus BX41 microscope. For a cell to be counted as an either IGF-1 or CD11b mRNA$^+$ cell, or as an IGF-1 mRNA$^+$ CD11b mRNA$^+$ cell, the cell defined by its hematoxylin-stained nucleus, should display one or more red and/or blue puncta, each puncta reflecting the presence of an IGF-1 or CD11b mRNA molecule. To calculate the cellular density the area within which the cells were counted was measured using a microscope Olympus DP80 Dual Color Monochrome CCD camera mounted on a motorized BX63 Olympus microscope and the Olympus CellSens software.

Statistics

Data are presented graphically with indication of the medians and 25 and 75% quartiles. All statistical analyses were performed using Prism (GraphPad Software, version 6). The % Aβ plaque load and volumetric data were analyzed by Kruskal–Wallis test followed by Dunn's multiple comparison test, and with linear regression and Boltzmann sigmoidal curve fitting. qPCR and BrdU data were analyzed by Kruskal–Wallis test followed by Dunn's multiple comparison test. Pearson correlation was performed to investigate relationships between Aβ plaque load, age, and cytokine mRNA levels. Mann–Whitney test was used for comparisons of two groups. Statistically significant differences are indicated as $p < 0.05^{*}$, $p < 0.01^{**}$, $p < 0.001^{***}$, and $p < 0.0001^{****}$.

RESULTS

Aβ Plaque Load Follows a Sigmoidal Trajectory in the Hippocampus With Age

We first examined the accumulation of Aβ plaques in the hippocampus of $APP_{swe}/PS1_{\Delta E9}$ Tg mice with age. We visualized Aβ plaques in 3-, 6-, 9-, 12-, 15-, 18-, 21-, and 24-month-old mice using IHC (**Figure 1A**). Very few Aβ plaques were observed in the hippocampus at 3 months of age. At 6 months of age, Aβ plaques were observed in the molecular layer of the dentate gyrus, with most Aβ plaques located in the terminal area of the perforant pathway, and essentially no Aβ plaques in the dentate hilus or stratum radiatum of the hippocampus proper (**Figure 1A**). From 9 and 12 months of age, Aβ plaques increased moderately, remaining most frequent in areas innervated by the perforant pathway, with still very few Aβ plaques in the hilus. In the oldest mice, Aβ plaques were found in all hippocampal regions (**Figure 1A**). To quantify % Aβ plaque load in the entire hippocampus, we used unbiased stereology. Stereological point-counting confirmed our observations of an age-dependent increase in Aβ plaque load (Kruskal–Wallis test, $P < 0.0001$) (**Figure 1B**). The largest increase in % Aβ plaque load occurred between 12 and 15 months of age, increasing from 2.2 to 4.5% of the hippocampus now covered by Aβ plaques. The maximal % Aβ plaque load was 6% at 21 and 24 months. A sigmoidal trajectory in % Aβ plaque load was determined using non-linear regression ($R^2 = 0.86$, **Figure 1B**), which is consistent with observations in the neocortex in both AD (Serrano-Pozo et al., 2011; Jack et al., 2013) and $APP_{swe}/PS1_{\Delta E9}$ Tg mice (Babcock et al., 2015). Statistically significant increases in % Aβ plaque load were observed from 15 months of age, compared to 3-month-old mice (**Figure 1B**, asterisks). No significant differences in hippocampal volume were observed in Tg mice between 3 to 24 months of age (**Figure 1C**). As expected, no Aβ plaques were observed in WT mice at any age (data not shown).

Microglia Accumulate at Aβ Plaques in the Hippocampus of $APP_{swe}/PS1_{\Delta E9}$ Tg Mice

We next analyzed changes in microglial reactivity. The IHC staining for the microglial surface β-integrin CD11b was homogeneously distributed in the hippocampus of WT mice, reflecting an even distribution of microglia even in 24-month-old mice (**Figures 2A–C**). In contrast, changes in microglial CD11b immunoreactivity were readily apparent in the hippocampus in $APP_{swe}/PS1_{\Delta E9}$ Tg mice (**Figure 2A**). Aggregates of $CD11b^+$ microglia were clearly visible in the hippocampus of Tg mice at 6 months and were more numerous at 12, 18, and 24 months (**Figure 2A**). These aggregates seemed to coincide temporally with the appearance of Aβ plaques (**Figure 1A**), initially forming in areas innervated by the perforant pathway before becoming prominent in the dentate hilus and other hippocampal regions in aged $APP_{swe}/PS1_{\Delta E9}$ Tg mice (**Figure 2A**). In double-stained sections, CD11b aggregates in these regions overlapped with Aβ plaques (**Figure 2B**), with microglia clustering around Aβ plaques (**Figure 2C**), as also reported for microglia in the neocortex of the same mice (Babcock et al., 2015).

IGF-1 mRNA Levels Increase With Age in the Hippocampus of $APP_{swe}/PS1_{\Delta E9}$ Tg Mice

To assess the expression of IGF-1 mRNA relative to age and genotype, we examined IGF-1 mRNA levels in contralateral hippocampi from the 3- to 24-month-old $APP_{swe}/PS1_{\Delta E9}$ Tg mice used for Aβ plaque load estimation, and from age-matched WT mice. We detected significant, but less than 2-fold increases in IGF-1 mRNA levels in 15- and 24-month-old Tg mice compared to young, 3-month-old Tg mice (Kruskal–Wallis test, $P < 0.05$, both age groups) (**Figure 3A**). In the $APP_{swe}/PS1_{\Delta E9}$ Tg mice the 15-month-old mice showed significantly higher IGF-1 mRNA levels compared to age-matched WT mice (Dunn's test, $P < 0.05$, both age groups) (**Figure 3A**). In accordance with these results, IGF-1 mRNA levels were significantly correlated with % Aβ plaque load ($r = 0.56$, $P < 0.0001$) and age ($r = 0.54$, $P < 0.001$) in Tg mice, while no correlation to age was observed in the WT mice (**Table 1**). In conclusion, the aging $APP_{swe}/PS1_{\Delta E9}$ Tg mice showed a significant increase in IGF-1 mRNA levels, which correlated to the age-dependent increase in % Aβ plaque load in these mice.

TNF mRNA Levels Increase With Age in the Hippocampus of $APP_{swe}/PS1_{\Delta E9}$ Tg and WT Mice

Next, we assessed whether and how hippocampal TNF mRNA levels might change relative to age and genotype (**Figure 3B**). We detected significant, up to 3–4-fold increases in TNF mRNA levels in 21- and 24-month-old WT mice compared to young, 3-month-old WT mice (Kruskal–Wallis test, $P < 0.01$, both age groups) (**Figure 3B**). In $APP_{swe}/PS1_{\Delta E9}$ Tg mice, TNF mRNA levels showed a 7–8-fold increase at 21 and 24 months, compared to 3-month-old Tg mice (Kruskal–Wallis test, $P < 0.01$ and $P < 0.001$, respectively) (**Figure 3B**). Due to the age-associated increases in TNF mRNA levels also in the WT mice, TNF mRNA levels were maximally 2.5-fold higher in Tg mice compared to WT mice at a given age (**Figure 3B**). In the $APP_{swe}/PS1_{\Delta E9}$ Tg mice the 15- and 24-month-old mice showed significantly higher TNF mRNA levels compared to age-matched WT mice (Dunn's test, $P < 0.01$, both age groups) (**Figure 3B**). As suggested by these results, TNF mRNA levels across all mouse groups correlated to both the % Aβ plaque load ($r = 0.63$, $P < 0.0001$) as well as age ($r = 0.73$, $P < 0.0001$) in $APP_{swe}/PS1_{\Delta E9}$ Tg mice (**Table 1**), and to age in WT mice ($r = 0.68$, $P < 0.0001$). Having previously shown rare TNF $mRNA^+$ cells in the neocortex of the same mice (Babcock et al., 2015), we also analyzed the expression of TNF mRNA in the hippocampus. TNF $mRNA^+$ cells were scarce even in the 24-month-old WT and $APP_{swe}/PS1_{\Delta E9}$ Tg mice (**Supplementary Figure S1**). TNF $mRNA^+$ cells were observed in all hippocampal subregions, regardless of age and genotype (data not shown).

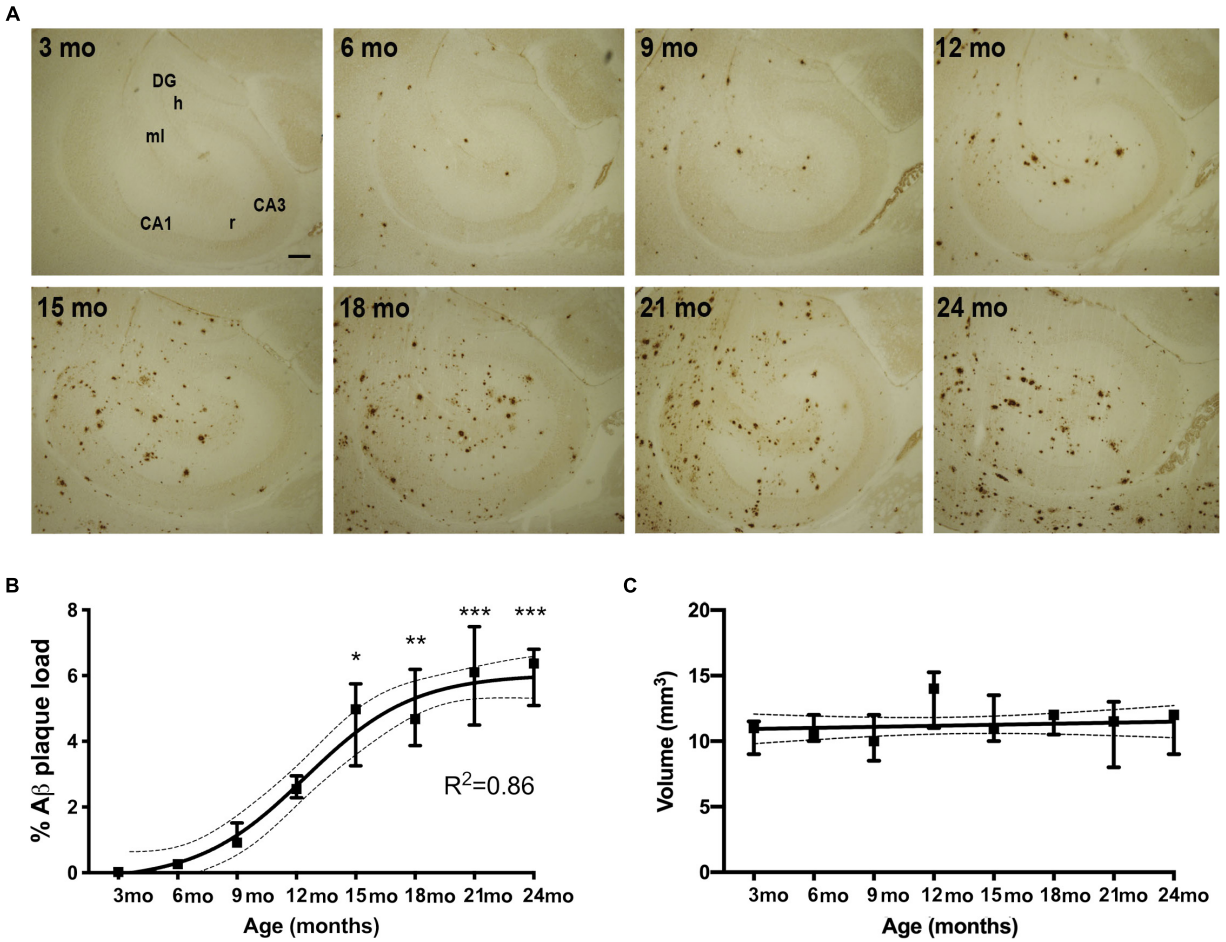

FIGURE 1 | % Aβ plaque load follows a sigmoidal trajectory with age in the hippocampus of $APP_{swe}/PS1_{\Delta E9}$ Tg mice. **(A)** IHC staining for Aβ shows an age-dependent increase in Aβ plaques in the hippocampus of Tg mice. Initially plaques become abundant in the perforant pathway innervated parts or the hippocampus. CA1, CA3, regio superior and inferior hippocampus, respectively; DG, dentate gyrus; h, hilus; ml, molecular layer; r, stratum radiatum. Scale bar: 100 μm. **(B,C)** Stereological quantification showing that hippocampal % Aβ plaque load increases significantly from 15 months of age and follows a sigmoidal trajectory, based on non-linear regression analyses **(B)**, whereas hippocampal volume is not significantly changed with age in Tg mice **(C)**. 95% confidence intervals are included. Data points show medians and 25 and 75% quartiles for each group [n = 6/group except for n = 4 for 15-month-old mice in **(B)**, and n = 5 or 6/group except for n = 4 for 15-month-old mice and n = 3 for 24-month-old mice in **(C)**]. Asterisks represent statistically significant increases in % Aβ plaque load versus 3-month-old mice as determined by Dunn's test. *$p < 0.05$, **$p < 0.01$, ***$p < 0.001$.

Cellular and Regional Expression of IGF-1 mRNA in the Hippocampus of $APP_{swe}/PS1_{\Delta E9}$ Tg Mice

To know the distribution and the source of the IGF-1 mRNA-expressing cells, we next hybridized sections parallel to those used for Aβ plaque load estimation using an AP-conjugated probe specific for IGF-1 mRNA. We observed numerous IGF-1 $mRNA^+$ neuronal-like cells throughout the hippocampus of the adult and aging $APP_{swe}/PS1_{\Delta E9}$ Tg and WT mice, with predilection to the sgz, defining the border between the granule cell layer and the dentate hilus (**Figure 4A**). IGF-1 $mRNA^+$ neuronal-like cells were also relatively abundant in the stratum radiatum of CA3 and CA1 (data not shown). Besides the neuronal-like cells, a more widespread punctuate staining was observed in the neural tissue, corresponding to a low baseline expression of IGF-1 mRNA by both neurons and glia (data not shown). Despite of the increased microglial reactivity in the Tg mice (**Figures 2A,B**), we observed no clear differences in *ISH* signal between Tg and WT mice using the AP-conjugated probe (**Figure 4A**). Therefore the expression level of IGF-1 mRNA was also analyzed in primary murine microglia from C57BL/6 mice by use of qPCR. The mRNA levels of IGF-1 and CD11b were determined relative to the expression level in neocortex of 3-month-old C57BL/6 mice. IGF-1 and CD11b mRNA levels were respectively, 3- and 2-fold higher in primary microglia compared to whole neocortex tissue (**Figure 4B**).

Next, we hybridized tissues from P5 mouse pups, which are known to contain high numbers of IGF-1 mRNA-expressing microglia (Hammond et al., 2019), showing a predilection to locate in the developing corpus callosum (Wlodarczyk et al., 2017), which was confirmed by our *ISH*

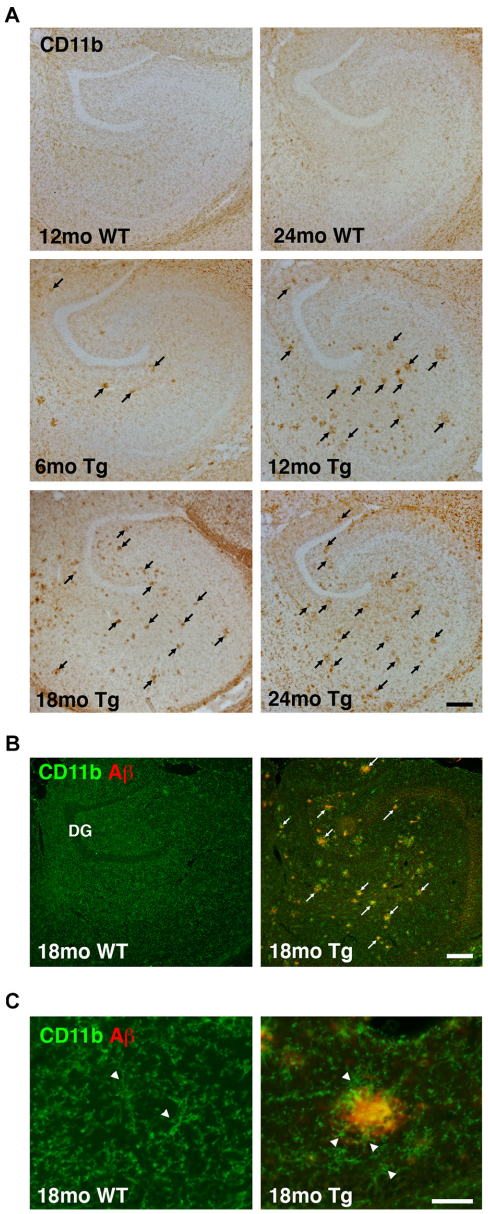

FIGURE 2 | Altered microglial distribution in the hippocampus of $APP_{swe}/PS1_{\Delta E9}$ Tg mice. **(A)** Low magnification panels show changes in CD11b immunoreactivity in the hippocampus of 6-, 12-, 18-, and 24-month-old Tg mice. The hippocampus from 12- and 24-month-old WT mice is shown for comparison. **(B,C)** Combined immunofluorescence staining for CD11b and Aβ shows increased CD11b immunoreactivity near Aβ plaques in low magnification images from 18-month-old Tg mice **(B)**. No plaques are observed in age-matched WT mice **(B)**. Arrowheads in **(C)** point to $CD11b^+$ microglia. Microglial cells are clustered around Aβ plaques in Tg mice, but not in WT mice. The photomicrographs in **(C)** were both obtained in the dentate molecular layer. DG, dentate gyrus. Scale bars: 200 μm **(A,B)**, 500 μm **(C)**.

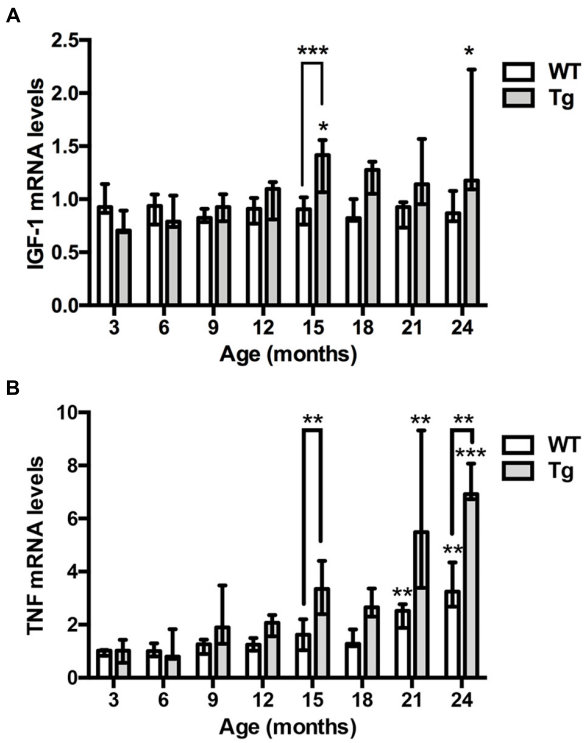

FIGURE 3 | IGF-1 and TNF mRNA levels are elevated in the hippocampus of aging $APP_{swe}/PS1_{\Delta E9}$ Tg mice. **(A)** Quantitative PCR analysis shows significantly increased hippocampal IGF-1 mRNA levels with age in Tg mice (gray bars), but not WT mice (white bars). Bars represent medians with 25 and 75% quartiles (n = 6–10 per group, except for n = 4 for 18-month-old Tg mice). **(B)** Quantitative PCR analysis shows significantly increased TNF mRNA levels with age in the hippocampus of both Tg mice (gray bars) and WT mice (white bars). Bars represent medians with 25 and 75% quartiles (n = 6–10 per group). *$p < 0.05$, **$p < 0.01$, ***$p < 0.001$, ***$p < 0.0001$, based on Kruskal–Wallis test followed by Dunn's multiple comparison test.

(**Supplementary Figure S2A**). With their round nuclei these cells ressembled amoeboid microglia (Dalmau et al., 2003). IGF-1 mRNA was also expressed in amoeboid-like cells in the developing angular bundle (**Supplementary Figure S2A**), and in cells with a neuronal morphology, which were observed throughout the hippocampus, including the stratum radiatum of CA3 and CA1 and the sgz in the dentate gyrus (**Supplementary Figure S2A**). Additionally, the cerebellar Purkinje cells expressed high levels IGF-1 mRNA (data not shown). Compared to the hybridized sections, sections pre-treated with RNAse A prior to hybridization or hybridized with an excess of unlabelled probe (competition control) were devoid of signal (**Supplementary Figure S2B**).

In combination, the detection of high levels of IGF-1 mRNA in primary microglia and the *in situ* detection of IGF-1 mRNA in amoeboid-like microglia in developing white matter raised the possibility that we might also be able to detect IGF-1 mRNA in activated microglia in the aged $APP_{swe}/PS1_{\Delta E9}$ Tg mice.

More Microglia Express IGF-1 mRNA in the Dentate Molecular Layer in Aged $APP_{swe}/PS1_{\Delta E9}$ Tg Than WT Mice

We then investigated if the increased levels of IGF-1 mRNA in the hippocampus of the aged $APP_{swe}/PS1_{\Delta E9}$ Tg mice might

TABLE 1 | Pearson correlations between cytokine mRNA levels, and age and % Aβ plaque load, in the hippocampus of 3–24-month-old WT and $APP_{swe}/PS1_{\Delta E9}$ Tg mice.

Genotype and variable / Cytokine mRNA levels	WT	$APP_{swe}/PS1_{\Delta E9}$	
	Age	Age	% Aβ plaque load
TNF mRNA levels	r 0.68, $P < 0.0001$	r 0.73, $P < 0.0001$	r 0.63, $P < 0.0001$
IGF-1 mRNA levels	r 0.00, ns	r 0.54, $P < 0.0001$	r 0.56, $P < 0.0001$

be ascribed to microglia expressing IGF-1 mRNA. We therefore tried to co-localize IGF-1 mRNA to CD11b $mRNA^+$ microglia in aged Tg mice and WT mice (n = 2–3/group) using the sensitive View-RNA *ISH* technique (Grebing et al., 2016). As expected, neuronal-like IGF-1 $mRNA^+$ sgz cells were readily observed in overview images of the dentate gyrus (**Figure 4C**). High magnification images, showed co-localization of IGF-1 mRNA to CD11b $mRNA^+$ microglia in both WT and Tg mice (**Figure 4D**). Quantitative analysis showed that the density of IGF-1 $mRNA^+$ CD11b $mRNA^+$ microglia was higher in hippocampi from Tg compared to WT mice (**Figure 4E** and **Supplementary Table S2**). Since the number of CD11b $mRNA^+$ microglia was also higher (**Figure 4E**), the percentage of IGF-1 $mRNA^+$ microglia was comparable in Tg and WT mice (15.9% and 14.5%, respectively). Taken together, this suggest that the increased levels of IGF-1 mRNA in the aged $APP_{swe}/PS1_{\Delta E9}$ Tg mice can be attributed to an increased number of IGF-1 $mRNA^+$ microglia in these mice.

IGF-1 Immunoreactivity Is Abundant in Neurons and Can Be Detected in Microglia in Aged $APP_{swe}/PS1_{\Delta E9}$ Tg Mice

To examine whether Aβ plaque-associated microglia produce IGF-1 protein in the aged $APP_{swe}/PS1_{\Delta E9}$ Tg mice, we next stained sections parallel to those used for co-expression analysis for IGF-1 mRNA and CD11b mRNA by IHC for IGF-1. IGF-1 immunoreactivity was abundant in subsets of neurons in the hippocampal formation (**Figures 5A–C**), especially in layer II of the entorhinal cortex (**Figure 5C**), and in fiber-like structures in the CA3 pyramidal cell layer (**Figures 5A–C**). IGF-1 immunoreactivity was also observed in scattered neurons in the dentate hilus (**Figure 5B**) and in the neocortex (data not shown), and it was abundant in the Purkinje cells in the cerebellum (**Supplementary Figure 3A**). In addition to the neuronal IGF-1 immunoreactivity, an Aβ plaque-associated punctuate IGF-1 immunoreactivity was observed in the Tg mice (**Figure 5D**). This type of IGF-1 immunoreactivity was most abundant in the entorhinal cortex and in neocortex, but could also be seen in the dentate gyrus (**Figure 5D**). Frequently, IGF-1 immunoreactivity was also observed on fiber-like structures in association with the plaques (data not shown). Importantly, substitution of the primary antibody with inert rabbit IgG abolished all staining (**Figure 5D** and **Supplementary Figure S3B**).

Next, to clarify whether the punctuate IGF-1 staining might co-localize to microglia we performed double-immunofluorescence staining for IGF-1 and CD11b. Punctuate IGF-1 immunofluorescence signal could be detected in a subset of $CD11b^+$ microglia associated with the Aβ plaques (**Figure 5E**, orthogonal views in **Supplementary Figures S4**, **S5**, **S6**) and fiber-like structures in the plaques (**Figure 5E**). As described above, IGF-1 immunofluorescence was abundant in entorhinal layer II neurons, fibers in the CA3 pyramidal cell layer as well as in cerebellar Purkinje cells (**Supplementary Figure S7**). Substitution control revealed unspecific binding of the secondary AlexaFluor568 goat-anti rat IgG to the vasculature in our specimens (**Supplementary Figure S7**). However, due to the morphological characteristics of the microglia this did, however, not interfere with interpretation of the double-immunofluorescence staining. In conclusion, IGF-1 is abundantly expressed in subsets of neurons in both genotypes and in a subset of Aβ plaques-associated microglia in aged $APP_{swe}/PS1_{\Delta E9}$ Tg mice.

IGF-1 mRNA Expression in Microglial BV2 Cells Is Unaffected by Addition of $Aβ_{42}$

Microglial content of Aβ was previously shown to be functionally correlated to microglial cytokine expression *in vivo* (Babcock et al., 2015). To clarify whether Aβ might impact microglial expression of IGF-1 mRNA, we examined the effect of $Aβ_{42}$ on the IGF-1 mRNA expression in microglial BV2 cells. For the stimulation was used $Aβ_{42}$ which is more prevalent than $Aβ_{40}$ in the hippocampus and neocortex of aging Tg mice (Babcock et al., 2015; von Linstow et al., 2017). As a reference was included CD11b mRNA. $Aβ_{42}$ exposure of microglial BV2 cells for 24 h had no impact on neither IGF-1 nor CD11b mRNA expression (**Figures 6A,B**). In support, $Aβ_{42}$ exposure for 24 h of primary microglia from newborn C57BL/6 mice did not impact IGF-1 or CD11b mRNA expression either (**Figures 6C,D**).

Cell Proliferation in the sgz Decreases With Age

We finally asked whether the increased Aβ plaque load in the female $APP_{swe}/PS1_{\Delta E9}$ Tg mice might contribute to age-related differences in cellular proliferation in the dentate gyrus. We therefore quantified proliferating ($BrdU^+$) cells in the sgz of the dentate gyrus where neural precursors are located (Zhao et al., 2008). To assess changes relevant to our assessment of the Aβ plaque-induced changes in cytokine mRNA levels, we included groups of 3-, 9-, and 15-month-old Tg and WT mice. At 3 months of age, we observed clusters of $BrdU^+$ cells in

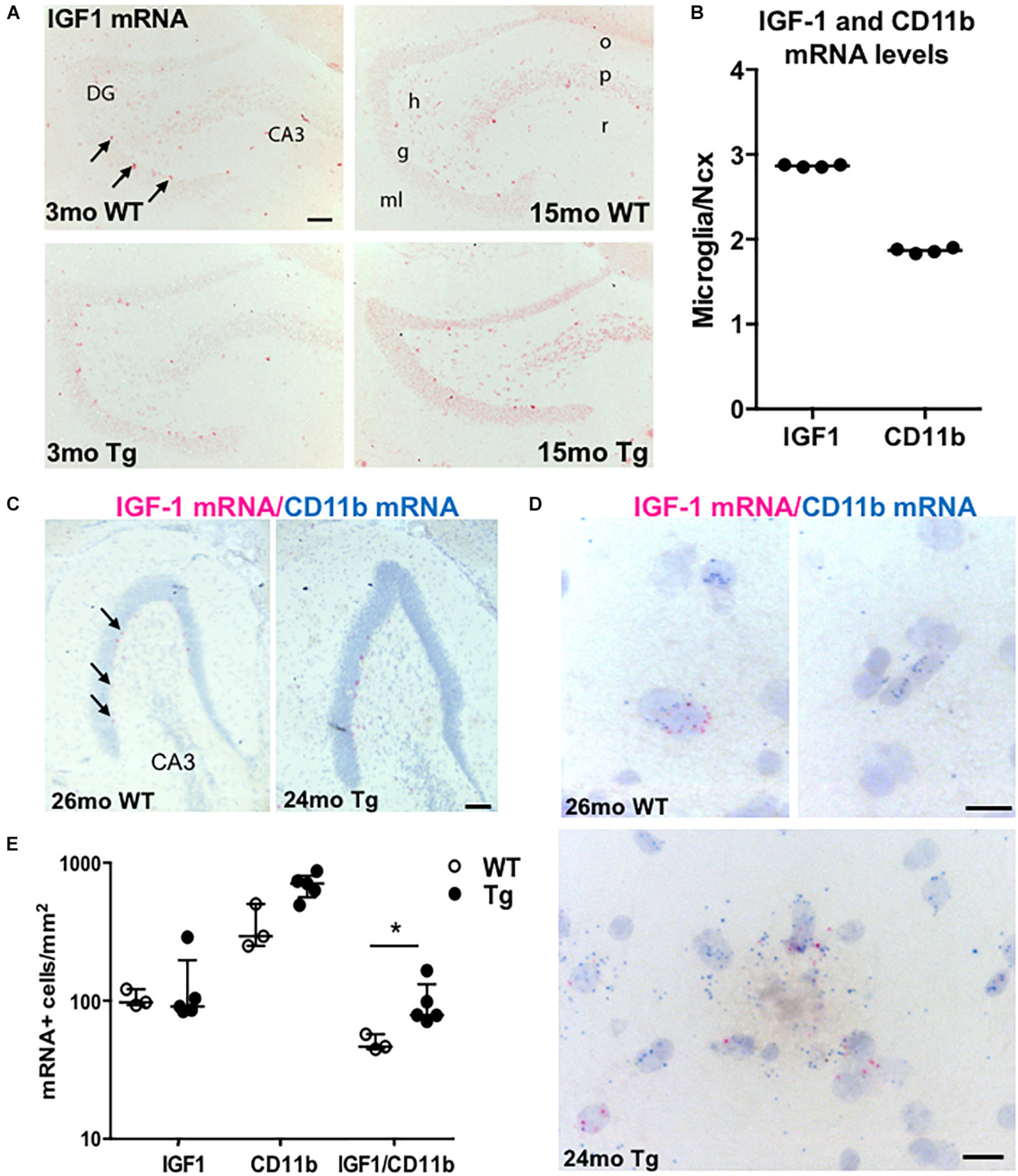

FIGURE 4 | IGF-1 mRNA is expressed in microglia as well as neurons in $APP_{swe}/PS1_{\Delta E9}$ Tg mice. **(A)** *ISH* showing IGF-1 $mRNA^+$ cells in the hippocampus of 3- and 15-month-old WT and Tg mice. *ISH* was performed with AP-conjugated probes. The only clearly visible cells are sgz cells bordering the granular cell layer (arrows) and scattered neurons in the dentate hilus and stratum radiatum of CA3. **(B)** Scatter-plot showing IGF-1 and CD11b mRNA levels in primary microglia relative to Ncx samples from 3-month-old C57BL/6 mice. Each data point represents one microglial culture from the same experiment. The horizontal bar represents the median. Both genes are more abundantly expressed in primary microglia than in whole Ncx tissue. **(C,D)** View-RNA double ISH for IGF-1 mRNA (red) and CD11b mRNA (blue) in approx. two-year-old WT and Tg mice. Arrows in **(C)** point at sgz cells expressing IGF-1 mRNA, as also observed in **(A)**. High magnifications in **(D)** show single cells expressing IGF-1 mRNA and/or CD11b mRNA in a WT mouse (top panels) and in a Tg mouse (bottom panel). Note the amorphous material in the bottom panel reflecting the presence of an amyloid plaque. **(E)** Scatter-plot showing the number of IGF-1 $mRNA^+$, CD11b $mRNA^+$, and IGF mRNA-expressing CD11b $mRNA^+$ microglia in WT and Tg mice. Bars represent medians **(B,E)** with 25 and 75% quartiles **(E)**. CA3, regio inferior hippocampus; DG, dentate gyrus; h, hilus; g, granule cell layer; ml, molecular layer; o, stratum oriens; p, pyramidal cell layer; and r, stratum radiatum. $^*p < 0.05$, Mann–Whitney, unpaired, and two-tailed. Scale bars: 100 μm **(A,C)**, 20 μm **(D)**.

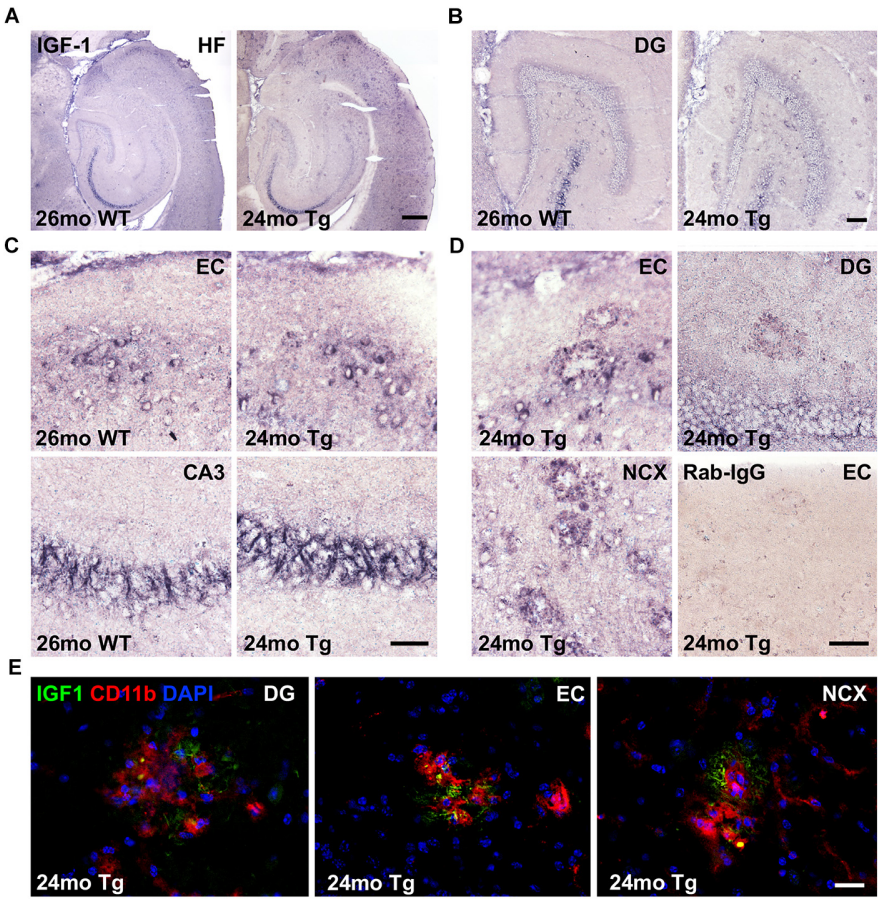

FIGURE 5 | IGF-1 is expressed in neurons and a subset of microglia in $APP_{swe}/PS1_{\Delta E9}$ Tg mice. **(A–C)** IHC of sections from 24-month-old $APP_{swe}/PS1_{\Delta E9}$ Tg and 26-month-old WT mice showing IGF-1 immunoreactivity in the hippocampal formation **(A)** and dentate gyrus **(B)**, with higher magnification of neurons in the entorhinal cortex and fiber-like structures in CA3 **(C)**. **(D)** High magnifications from Tg mice showing amyloid plaque-associated punctuate IGF-1 immunoreactivity in dentate gyrus, entorhinal cortex, and neocortex. Substitution control performed with inert rabbit IgG showed no staining. CA3, regio inferior hippocampus; DG, dentate gyrus; EC, entorhinal cortex; HF, hippocampal formation; and NCX, neocortex. **(E)** Double immunofluorescence for IGF-1 (green) and CD11b (red), and nuclear staining with DAPI (blue). Co-localization of IGF-1 to $CD11b^+$ microglia is visualized by the punctuate yellow staining, whereas the $IGF\text{-}1^+$ fiber-like structures in the plaques remain green. Scale-bars: 400 μm **(A)**, 100 μm **(B)**, 50 μm **(C,D)**, and 20 μm **(E)**.

the sgz in both Tg and WT mice (**Figure 7A**, data shown for WT mice). These clearly decreased at 9 months of age, and at 15 months almost no $BrdU^+$ cells were observed in either Tg or WT mice (**Figure 7A**). Quantification showed a significant age-dependent reduction in $BrdU^+$ cells in both Tg and WT mice (Kruskal–Wallis test, $P < 0.001$, both genotypes) (**Figure 7B**). Statistically significant decreases in number of $BrdU^+$ were observed at 15 months of age, compared to 3-month-old mice in both genotypes (**Figure 7B**, asterisks). We did not observe any significant differences between WT and Tg mice in any age group. Four out of 6 WT mice and one out of 6 Tg belonging to group of 3-mo-old mice showed very low cell numbers, which might be attributed to suboptimal BrdU-staining. Finally, hippocampal mRNA levels of brain derived neurotrophic factor (BDNF), which is known to promote neurogenesis (Lichtenwalner and Parent, 2006), remained constant across ages in both Tg and WT mice (**Supplementary Figure S8**).

DISCUSSION

The main results of this study showed that hippocampal IGF-1 mRNA levels are increased close to two-fold in aged $APP_{swe}/PS1_{\Delta E9}$ Tg mice, that approx. 15% of microglia in the molecular layer of the dentate gyrus in aged Tg as well as WT mice express IGF-1 mRNA, and that a subset of microglia in aged Tg mice express IGF-1 protein. Since microglial density was approx. two-fold higher in Tg mice compared to WT mice, the Tg mice also harbored two-fold more IGF-1 mRNA-expressing microglia. Thus, the increased hippocampal IGF-1 mRNA levels may be ascribed to an increased number of IGF-1-expressing microglia. Still, the most predominant cell types expressing IGF-1 mRNA, were neurons, including neuroblast-like cells in the sgz. Neurogenesis, given by the number of proliferating cells in the sgz, declined with age in both genotypes, regardless of the genotype-associated differences in hippocampal IGF-1 mRNA levels. The strength, limitations and perspectives of these

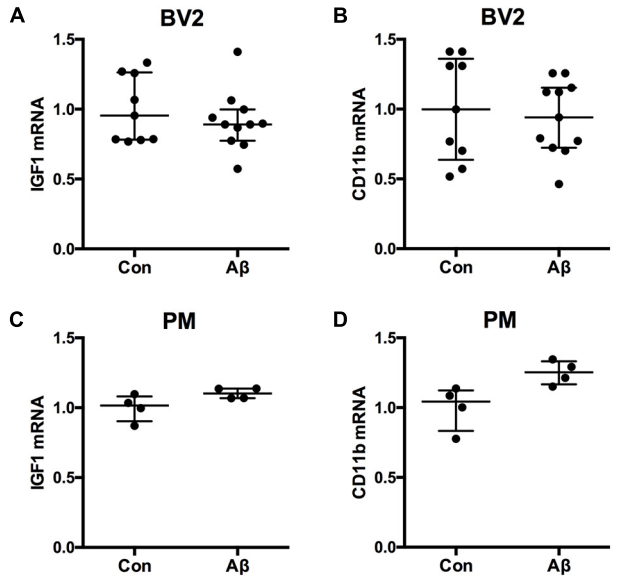

FIGURE 6 | IGF-1 mRNA is unchanged in BV2 cells and primary microglia after $A\beta_{42}$ exposure. The BV2 cell line and primary microglia from newborn mice were stimulated 24 h with 1 μM $A\beta_{42}$ whereafter, RNA was isolated, reverse transcribed and used for qPCR for IGF-1 mRNA **(A,C)** and CD11b mRNA **(B,D)**. Levels of IGF-1 mRNA **(A,C)** and CD11b mRNA **(B,D)** were unchanged after $A\beta_{42}$ exposure. Each dot represents 1 experiment. Bars indicate the medians and the error bars the 25 and 75% quartiles.

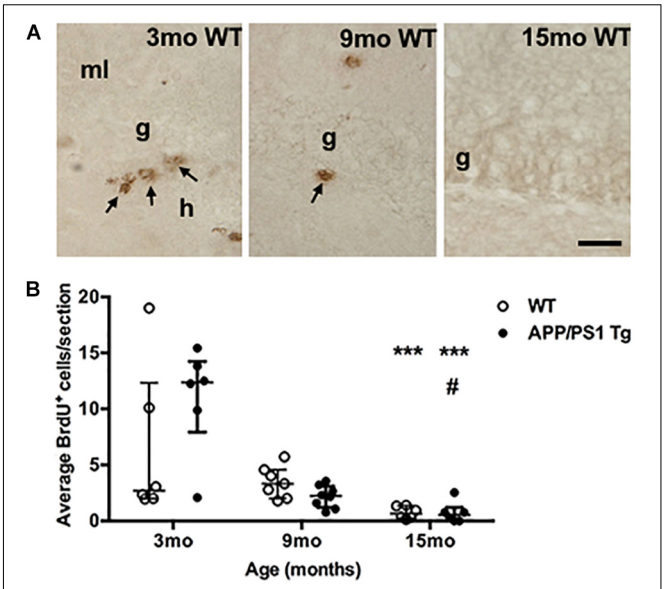

FIGURE 7 | Cell proliferation in the subgranular zone of both genotypes decreases with age. **(A)** Immunohistochemical staining of proliferating $BrdU^+$ cells (arrows) in the subgranular zone of 3-, 9-, and 15-month-old WT mice. The BrdU-staining was performed on sections from post-fixed, isolated hippocampi. In general, fewer $BrdU^+$ cells were observed in the subgranular zone at 9 months of age, and at 15 months, almost no $BrdU^+$ cells were observed in either Tg (not shown), or WT mice. g, granular cell layer; h, hilus; and ml, molecular layer. Scale bar: 20 μm. **(B)** Scatter-plot showing the average number of $BrdU^+$ cells in the sgz 3-, 9-, and 15-month-old WT and $APP_{swe}/PS1_{\Delta E9}$ Tg mice. Despite of a large variation in the number of $BrdU^+$ cells in 3-month-old mice (see text for details) there was a significant age-dependent reduction in $BrdU^+$ cells in both $APP_{swe}/PS1_{\Delta E9}$ Tg and WT mice by 15 months of age. Data are expressed as the mean number of $BrdU^+$ cells per section and are shown as mean ± sem for each group (n = 6–8 per group). No significant differences were observed between WT and Tg mice. #$p < 0.05$ (vs. 9-month-old Tg mice), ***$p < 0.0001$ (vs. 3-month-old mice).

findings, and of our results on the genotype- and age-associated changes in hippocampal TNF mRNA levels, are discussed below.

We found that % Aβ plaque load increased with age in the hippocampus of $APP_{swe}/PS1_{\Delta E9}$ Tg mice and reached a maximum in 21-month-old mice. The resulting sigmoidal curve corresponds to observations in the neocortex in AD patients (Serrano-Pozo et al., 2011; Jack et al., 2013) and the same $APP_{swe}/PS1_{\Delta E9}$ Tg mice (Babcock et al., 2015). This apparent maximum limit for hippocampal Aβ-load might explain why Aβ plaque load is not well correlated with cognitive symptoms in AD patients (Nelson et al., 2012; Jack et al., 2013). Cognitive symptoms appear to be a consequence of neurodegeneration, whereas Aβ deposition is an "upstream" event (Jack et al., 2013). Since $APP_{swe}/PS1_{\Delta E9}$ Tg mice are not genetically modified to produce neurofibrillary tangles, which may trigger neuronal death (Braak and Braak, 1995; Eckermann et al., 2007), we did not expect to see marked changes in hippocampal volume. Although a modest neuronal loss around plaques has been reported in aged $APP_{swe}/PS1_{\Delta E9}$ Tg mice (Radde et al., 2006; Rupp et al., 2011), no global loss of hippocampal CA1 neurons was observed in $APP_{swe}/PS1_{\Delta E9}$ Tg mice at 12 months of age (West et al., 2009). We observed no age- or genotype-associated changes in neocortex volume in our former study (Babcock et al., 2015).

We found that a subset of microglia in aged $APP_{swe}/PS1_{\Delta E9}$ Tg mice synthesized IGF-1 mRNA and IGF-1 protein. These findings are in line with reports of microglial expression of IGF-1 mRNA after perforant pathway deafferentation in rats (Guthrie et al., 1995), overlapping with zones where we found Aβ plaque load to be prominent. Deposition of Aβ can induce modest damage to axons (Liu et al., 2008; Nikolajsen et al., 2011), dendrites and neuronal somata (Radde et al., 2006; Rupp et al., 2011). In addition, Aβ plaques were also prominent in the entorhinal cortex giving rise to the perforant pathway. Microglia may sense degenerating neurons and Aβ via the same cell surface receptors (Babcock et al., 2006; Jana et al., 2008), and Aβ, potentially in combination with Aβ plaque-associated neuronal damage, may provoke a response similar to perforant pathway axonal degeneration. The microglial population increases two- to four-fold in the outer part of the dentate molecular layer in response to perforant pathway axonal degeneration in mice (Dissing-Olesen et al., 2007; Wirenfeldt et al., 2007). In the present study, we found that microglial density was two-fold higher in the molecular layer in $APP_{swe}/PS1_{\Delta E9}$ Tg mice compared to WT mice, and that the Tg mice also harbored two-fold more IGF-1 mRNA-expressing microglia. Whether individual microglia express more IGF-1 mRNA per cell in aged Tg compared to WT mice requires more comprehensive studies, also addressing differences in IGF-1 mRNA expression between the different IGF-1 mRNA-expressing cell types in the

dentate gyrus and hippocampus proper, as well as the effect on aging. Microglia isolated from the brains of aged C57BL/6 mice were previously reported to express higher IGF-1 mRNA levels than microglia from young mice (Hickman et al., 2013). The reason for the absence of effect of Aβ42 on the IGF-1 mRNA expression by the BV2 cells and the primary microglia could be that these cells already express high levels of IGF-1 mRNA, which the published data from the P5 pubs (Wlodarczyk et al., 2017; Hammond et al., 2019) and our own *ISH* data indicate. Another reason could be that a combination of Aβ42 and Aβ40 might be more efficient in stimulating microglial IGF-1 mRNA expression than Aβ42.

IGF-1 has previously been shown to modulate hippocampal neurogenesis (Aberg et al., 2000, 2003; Anderson et al., 2002), and the cell type showing the most intense *ISH* signal for IGF-1 mRNA, across ages and genotypes, were the neuroblast-like cells in the sgz. With their characteristic distribution and morphology these cells resembled the doublecortin-expressing neuroblasts which we showed are reduced in 18-month-, but not 9- or 3-month-old male $APP_{swe}/PS1_{\Delta E9}$ Tg mice (Olesen et al., 2017). Enhancing microglial expression of IGF-1 in 9- to 10-month-old $APP_{K95N,\ M591L}/PS1_{\Delta E9}$ Tg mice by glatiramer acetate treatment was previously suggested as a mechanism to enhance neurogenesis and counteract learning deficits (Butovsky et al., 2006). In comparison, in our present study the elevated hippocampal IGF-1 mRNA levels in the aged $APP_{swe}/PS1_{\Delta E9}$ Tg mice did not influence neurogenesis, which was similarly low in the 15-month-old female and the 18-month-old male Tg and littermate WT mice (the present study and Olesen et al., 2017, respectively). Importantly, although the changes we observed were less than two-fold, IGF-1 mRNA was expressed at relatively high levels in the hippocampus of both WT and $APP_{swe}/PS1_{\Delta E9}$ Tg mice, typically detected by qPCR at 8–10 cycle thresholds before TNF. The fact that baseline-level of IGF-1 mRNA is relatively high in the hippocampus, and that several cellular sources, including neurons, microglia, as well as sgz cells, produce IGF-1 mRNA, calls for caution in the interpretation of the contribution of microglial versus non-microglial cells as sources of the functionally important IGF-1. Additionally, increased expression of IGF-1 mRNA may be counteractive, since Aβ can reduce neuronal sensitivity to IGF-1 by decreasing neuronal IGF-1Rs (Giuffrida et al., 2012). Reduced IGF-1 sensitivity in $APP_{swe}/PS1_{\Delta E9}$ Tg mice has been observed (Zhang et al., 2013), as has deregulated IGF-1 signaling (Zemva and Schubert, 2014).

We also observed increased TNF mRNA levels in $APP_{swe}/PS1_{\Delta E9}$ as well as WT mice with age. Increased hippocampal TNF mRNA and protein have previously been reported in aged $APP_{swe}/PS1_{\Delta E9}$ Tg mice (Francois et al., 2014; Minogue et al., 2014). Though the cell source of TNF mRNA in hippocampus was not determined by double-ISH, as done for IGF-1 mRNA and CD11b mRNA, we have previously shown that neocortical microglia produce TNF in aging WT and $APP_{swe}/PS1_{\Delta E9}$ Tg mice (Babcock et al., 2015). Also, the age-related increase in hippocampal TNF mRNA fits well with the reported increase in TNF mRNA expression in microglia from aged C57BL/6 mice (Hickman et al., 2013). TNF might also be produced by infiltrating macrophages (Clausen et al., 2008; Lambertsen et al., 2009) as immigrating cells can be detected in the hippocampus of chimeric $APP_{swe}/PS1_{\Delta E9}$ Tg mice, though greatly outnumbered by microglia (Babcock et al., 2015). As expected based on our quantitative studies of TNF $mRNA^+$ cells in the neocortex of the same $APP_{swe}/PS1_{\Delta E9}$ Tg mice (Babcock et al., 2015), we found very low numbers of TNF $mRNA^+$ cells, distributed sporadically throughout the hippocampus, though absent from the neurogenic niche in the sgz in both genotypes. This suggests that fold-increases in TNF mRNA measured at the whole hippocampus level by qPCR may reflect individual cells expressing high levels of TNF mRNA.

In this study, we used IHC staining for CD11b for visualization of microglial activation. Changes in CD11b immunoreactivity could be observed in all hippocampal subregions of $APP_{swe}/PS1_{\Delta E9}$ Tg mice with $CD11b^+$ cellular aggregates coinciding with Aβ plaques, as previously reported (Bolmont et al., 2008; Minogue et al., 2014; Babcock et al., 2015), and with Aβ plaques and microglial aggregates in the dentate hilus, in close association with the sgz. Although microglial phagocytosis of apoptotic new-born neurons is maintained during aging and acute inflammation (Sierra et al., 2010), the additional challenge of being exposed to and to take up Aβ could change how efficiently microglia can support this key physiological process during neurogenesis. A significant subpopulation of microglia in $APP_{swe}/PS1_{\Delta E9}$ Tg mice has a high Aβ load (Babcock et al., 2015), and having to clear Aβ interfered with phagocytic uptake of beads in the hippocampus of another Tg mouse model (Krabbe et al., 2013). Interestingly, microglial capacity for phagocytosis appears to be related to the cytokine profile (Babcock et al., 2015), however, while we know that the microglial subset expressing TNF is poor in taking up Aβ, we have no data on whether microglial expression of IGF-1 impacts their uptake of Aβ. Recently, we showed by the use of proteomics that $CD11b^+$ myeloid cells (mainly microglia) isolated from 24-month-old $APP_{swe}/PS1_{\Delta E9}$ Tg mice have lower expression of IGF binding protein 2 (IGFBP2) compared to $CD11b^+$ myeloid cells from 24-month-old WT mice (Thygesen et al., 2018). IGFBP2 is also expressed in microglia in active lesions in multiple sclerosis cases (Chesik et al., 2004). Secretion of IGFBP2 is important for transport of IGF-1 to its receptors. While we did not identify IGF-I as being differentially regulated in our proteomics study (Thygesen et al., 2018), likely due to the technical limitation on low molecular protein identification by mass spectrometry (Nilsson et al., 2010), we in the present study found IGF-1 co-localized to a subset of plaques-associated $CD11b^+$ microglia. Taking into consideration that the double-immunofluorescence staining was a compromise regarding fixation protocols, to allow simultaneous detection of CD11b and IGF-1, the frequency of $IGF\text{-}1^+$ microglia is likely underestimated. Indeed, IGF-1 mRNA was shown to be among the significantly upregulated genes in microglia from 6-month-old male 5XFAD mice in recent single-cell RNA-sequencing studies, classifying the IGF-1 $mRNA^+$ microglia as homeostatic microglia (Keren-Shaul et al., 2017).

Decreased sgz cell proliferation in normal aging is well-documented in both humans (Spalding et al., 2013) and rodents (Kuhn et al., 1996; Demars et al., 2010; Valero et al., 2011;

Villeda et al., 2011; Hamilton and Holscher, 2012; Olesen et al., 2017). In comparison, in AD, sgz proliferation has been reported to be both increased (Jin et al., 2004) and decreased (Ziabreva et al., 2006; Crews et al., 2010), similar to inconsistencies described in different mouse models of AD (Chuang, 2010). Several studies reported more pronounced decreases in $APP_{swe}/PS1_{\Delta E9}$ Tg than WT mice (Butovsky et al., 2006; Demars et al., 2010; Valero et al., 2011; Hamilton and Holscher, 2012). We recently reported that sgz cell proliferation decreased to the same extent in $APP_{swe}/PS1_{\Delta E9}$ Tg and littermate WT mice at 18 months of age, while we did observe a larger reduction in the number of doublecortin immunoreactive neuroblasts in the $APP_{swe}/PS1_{\Delta E9}$ Tg mice (Olesen et al., 2017).

CONCLUSION

In conclusion, the results suggest that the increased IGF-1 mRNA levels observed in aged $APP_{swe}/PS1_{\Delta E9}$ Tg mice can be ascribed to a larger number of IGF-1 mRNA-expressing microglia, and additionally that IGF-1 mRNA is translated into IGF-1 protein in a subset of Aβ-plaque-associated microglia. The finding that microglia retain the capacity to produce IGF-1 in the aged $APP_{swe}/PS1_{\Delta E9}$ Tg mice is interesting, since this may provide a potentially modifiable local cellular source of IGF-1 in the Aβ plaque-burdened brain in individuals with AD.

ETHICS STATEMENT

Experiments were conducted according to permission from the Danish Ethical Animal Care Committee (Permission Nos. 2011/562-67 and 2011/561-1950).

AUTHOR CONTRIBUTIONS

CM conceptualized processing of mice, hippocampal plaque-load estimation, BrdU staining/quantification, qPCR, ISH, and writing of the manuscript. CT and BV performed cell culture work, qPCR, IHC of tissue, and quantitation of ISH. LI, JV, KK, MG, SZ, AK, and LD-O carried out the processing of mice and *ISH*. MJ, AB, and BF guided and supervised the study. BF initiated the project. All authors read, edited, and approved the manuscript.

FUNDING

This work was supported by the Augustinus Foundation; Aase og Ejnar Danielsens Fond; The Carlsberg Foundation, Grosserer M. Brogaard og Hustrus Mindefond, Odense; Kathrine og Vigo Skovgaards Fond; Fonden til Lægevidenskabens Fremme; the Lundbeck Foundation; The Novo Nordisk Foundation; Overlægerådets Legatudvalg; the Sino-Danish Center for Education and Research; the University of Southern Denmark; the Danish Alzheimer's Society; the Danish Medical Research Council, Direktor Ejnar Jonassens Fond, and SDU2020, a research initiative by the University of Southern Denmark.

ACKNOWLEDGMENTS

We would like to thank Dr. Christina Fenger for assisting in the *ISH* probe design of IGF-1 and Sussanne Petersen, Janne Skalshøi, Lene Jørgensen, Inger Nissen, and Alice Lundsgaard Larsen for outstanding technical assistance.

SUPPLEMENTARY MATERIAL

The Supplementary Material for this article can be found online at: https://www.frontiersin.org/articles/10.3389/fncel.2019.00308/full#supplementary-material

FIGURE S1 | *ISH* showing representative TNF $mRNA^+$ cells in the hippocampus of 12- and 24-month-old WT and $APP_{swe}/PS1_{\Delta E9}$ Tg mice. Scale bar: 10 μm.

FIGURE S2 | Distribution of IGF-1 $mRNA^+$ cells in postnatal day five (P5) old mouse pups. *ISH* of horizontal sections of P5 C57BL/6 mouse pups with AP-conjugated probe for IGF-1 mRNA. **(A)** High power photomicrograph of IGF-1 $mRNA^+$ cells with the morphology of amoeboid microglia in the corpus callosum. Overview of the hippocampal formation (HF), and high power of IGF-1 $mRNA^+$ cells in the angular bundle and IGF-1 $mRNA^+$ sgz cells at the border between the granule cell layer and the dentate hilus (DG). **(B)** ISH showing IGF-1 $mRNA^+$ cells in the hippocampus (higher magnification of section shown in **(A)**, and blank RNAse control (RNAse) and competition control (Comp) in parallel sections from the same mouse. ab, angular bundle; BS, brain stem; CA1, CA3, regio superior and inferior hippocampus, respectively; cc, corpus callosum; DG, dentate gyrus; ec, external capsule; f, fimbria-fornix; h, hilus; g, granule cell layer; ml, molecular layer; and Th, thalamus. Scale bars: 150 μm **(A,C,D)**, 250 μm **(B)**, 250 μm **(E–G)**.

FIGURE S3 | IGF-1 expression in cerebellar and hippocampal neurons. IHC for IGF-1 on sections from 24-month-old $APP_{swe}/PS1_{\Delta E9}$ Tg and 26-month-old WT mice. IHC was performed by use of a two-step protocol using AP-conjugated anti-rabbit antibody for the detection of the primary rabbit-anti-IGF-1 antibody. **(A)** IGF-1 is expressed in high levels in cerebellar Purkinje cells. **(B)** In the hippocampal formation, IGF-1 immunoreactivity is most abundant in entorhinal layer II neurons and in fibre-like structures in the CA3 pyramidal cell layer. Substitution control performed with inert rabbit IgG abolished all staining. CA3, regio superior hippocampus; CB, cerebellum; and HF, hippocampal formation. Scale bars: 50 μm (**A**,bottom), 100 μm (**A**, top and **B**, bottom), and 400 μm (**A**, top).

FIGURE S4 | Double-immunofluorescence staining for IGF-1 and microglial CD11b in dentate gyrus. **(A)** Single-layers showing of the immunofluorescence signal for CD11b (red) and IGF-1 (green) in the dentate gyrus (DG) of 24-month-old $APP_{swe}/PS1_{\Delta E9}$, corresponding to **Figure 5B**. Nuclei are stained with DAPI (blue). Fresh frozen sections were used for the double-immunofluorescence stainings. Pictures were obtained using a 40 × objective creating a z-stack through the section. **(B)** Orthogonal views of the z-stack showing overlap of IGF-1 and CD11b immunofluorescense signal (yellow). Scale bars: 20 μm.

FIGURE S5 | Double-immunofluorescence staining for IGF-1 and microglial CD11b in the entorhinal cortex. **(A)** Single-layers showing of the immunofluorescence signal for CD11b (red) and IGF-1 (green) in the entorhinal cortex (EC) of 24-month-old $APP_{swe}/PS1_{\Delta E9}$, corresponding to **Figure 5B**. Nuclei are stained with DAPI (blue). Fresh frozen sections were used for the double-immunofluorescence stainings. Pictures were obtained using a 40 × objective creating a z-stack through the section. **(B)** Orthogonal views of the z-stack showing overlap of IGF-1 and CD11b immunofluorescense signal (yellow). Scale bars: 20 μm.

FIGURE S6 | Double-immunofluorescence staining for IGF-1 and microglial CD11b in the neocortex. **(A)** Single-layers showing of the immunofluorescence

signal for CD11b (red) and IGF-1 (green) in neocortex (NCX) of 24-month-old $APP_{swe}/PS1_{\Delta E9}$, corresponding to **Figure 5B**. Nuclei are stained with DAPI (blue). Fresh frozen sections were used for the double-immunofluorescence stainings. Pictures were obtained using a 40 × objective creating a z-stack through the section. **(B)** Orthogonal views of the z-stack showing overlap of IGF-1 and CD11b immunofluorescense signal (yellow). Scale bars: 20 μm.

FIGURE S7 | Double-immunofluorescence stainings for IGF-1 and CD11b in sections from 24-month-old $APP_{swe}/PS1_{\Delta E9}$ mice. IGF-1 (green), CD11b (red), and nuclei are stained with DAPI (blue). **(A)** Amyloid-plaque-associated aggregates of $CD11b^+$ microglia (arrows) are abundant in the entorhinal cortex. Note, the high levels of IGF-1 expression in entorhinal layer II neurons. **(B)** Substitution control performed on section to the one used for the photomicrographs shown in **(A,C,D)**. Substitution of both primary antibodies with inert rabbit IgG and rat IgG2b, respectively, did not abolish all signal, but left behind a faint vascular staining from the secondary AlexaFluor568 goat-anti rat IgG. **(C)** Cerebellar cortex with IGF-1 expression in the Purkinje cells (arrows). **(D)** IGF-1 immunoreactive fibre-like structures between the CA3 pyramidal cells. CB, cerebellum; EC, entorhinal cortex; g, granule cell layer; ml, molecular layer; o, stratum oriens; p, pyramical cell layer; r, stratum radiatum; and wm, white matter. Scale bars: 100 μm **(A)**, 100 μm **(B)**, and 20 μm **(C,D)**.

FIGURE S8 | BDNF mRNA levels do not change with age in $APP_{swe}/PS1_{\Delta E9}$ Tg and WT mice. Quantitative PCR analysis shows that levels of BDNF mRNA are not significantly different with age in hippocampus of either Tg mice (gray bars) or WT mice (white bars). Specific age groups are indicated on the graph. Bars represent medians with 25 and 75% quartiles (n = 6–10 per group).

TABLE S1 | Summary of stereology data on % Aβ plaque load and hippocampal volume in $APP_{swe}/PS1_{\Delta E9}$ Tg mice.

TABLE S2 | IGF-1 mRNA expression by CD11b $mRNA^+$ microglia in the molecular layer of aged WT and $APP_{swe}/PS1_{\Delta E9}$ Tg mice.

REFERENCES

Aberg, M. A., Aberg, N. D., Hedbacker, H., Oscarsson, J., and Eriksson, P. S. (2000). Peripheral infusion of IGF-I selectively induces neurogenesis in the adult rat hippocampus. *J. Neurosci.* 20, 2896–2903. doi: 10.1523/jneurosci.20-08-02896.2000

Aberg, M. A., Aberg, N. D., Palmer, T. D., Alborn, A. M., Carlsson-Skwirut, C., Bang, P., et al. (2003). IGF-I has a direct proliferative effect in adult hippocampal progenitor cells. *Mol. Cell. Neurosci.* 24, 23–40. doi: 10.1016/s1044-7431(03)00082-4

Anderson, M. F., Aberg, M. A., Nilsson, M., and Eriksson, P. S. (2002). Insulin-like growth factor-I and neurogenesis in the adult mammalian brain. *Brain Res. Dev. Brain Res.* 134, 115–122. doi: 10.1016/s0165-3806(02)00277-8

Arnett, H. A., Mason, J., Marino, M., Suzuki, K., Matsushima, G. K., Ting, J. P., et al. (2001). TNF alpha promotes proliferation of oligodendrocyte progenitors and remyelination. *Nat. Neurosci.* 4, 1116–1122. doi: 10.1038/nn738

Arroba, A. I., Compos-Caro, A., Aguilar-Diosdado, M., and Valverde, A. M. (2018). IGF-1, inflammation and retinal inflammation: a close network. *Front. Aging Neurosci.* 5:203. doi: 10.3389/fnagi.2018.00203

Babcock, A. A., Ilkjær, L., Clausen, B., Villadsen, B., Dissing-Olesen, L., Bendixen, A. T. M., et al. (2015). Cytokine-producing microglia have an altered beta-amyloid load in aged APP/PS1 Tg mice. *Brain Behav. Immun.* 48, 86–101. doi: 10.1016/j.bbi.2015.03.006

Babcock, A. A., Wirenfeldt, M., Holm, T., Nielsen, H. H., Dissing-Olesen, L., Toft-Hansen, H., et al. (2006). Toll-like receptor 2 signaling in response to brain injury: an innate bridge to neuroinflammation. *J. Neurosci.* 26, 12826–12837. doi: 10.1523/jneurosci.4937-05.2006

Bobinski, M., de Leon, M. J., Wegiel, J., Desanti, S., Convit, A., Louis, L. A., et al. (2000). The histological validation of post mortem magnetic resonance imaging-determined hippocampal volume in Alzheimer's disease. *Neuroscience* 95, 721–725. doi: 10.1016/s0306-4522(99)00476-5

Bolmont, T., Haiss, F., Eicke, D., Radde, R., Mathis, C. A., Klunk, W. E., et al. (2008). Dynamics of the microglial/amyloid interaction indicate a role in plaque maintenance. *J. Neurosci.* 28, 4283–4292. doi: 10.1523/JNEUROSCI.4814-07.2008

Bondy, C. A. (1991). Transient IGF-1 gene expression during the maturation of functionally related central projection neurons. *J. Neurosci.* 11, 3442–3455. doi: 10.1523/jneurosci.11-11-03442.1991

Bondy, C. A., Werner, H., Roberts, C. T. Jr., and LeToith, D. (1992). Cellular pattern of type-1 insulin-like growth factor receptor gene expression during maturation of the rat brain: comparison with insulin-like growth factors I and II. *Neuroscience* 4, 909–923. doi: 10.1016/0306-4522(92)90193-6

Braak, H., and Braak, E. (1995). Staging of Alzheimer's disease-related neurofibrillary changes. *Neurobiol. Aging* 16, 271–278; discussion 278–284.

Butovsky, O., Koronyo-Hamaoui, M., Kunis, G., Ophir, E., Landa, G., and Cohen, H. (2006). Glatiramer acetate fights against Alzheimer's disease by inducing dendritic-like microglia expressing insulin-like growth factor 1. *Proc. Natl. Acad. Sci. U.S.A.* 103, 11784–11789. doi: 10.1073/pnas.0604681103

Cagnin, A., Brooks, D. J., Kennedy, A. M., Gunn, R. N., Myers, R., Turkheimer, F. E., et al. (2001). In-vivo measurment of activated microglia in dementia. *Lancet* 358, 461–467.

Chesik, D., De Keyser, J., and Wilczak, N. (2004). Involvement of insulin-like growth factor binding protein-2 in activated microglia as assessed in post mortem human brain. *Neurosci. Lett.* 362, 14–16. doi: 10.1016/j.neulet.2004.01.039

Chuang, T. T. (2010). Neurogenesis in mouse models of Alzheimer's disease. *Biochim. Biophys. Acta* 1802, 872–880. doi: 10.1016/j.bbadis.2009.12.008

Clausen, B., Fenger, C., and Finsen, B. (2013). In situ hybridization of cytokine mRNA using alkaline phosphatase-labelled oligodeoxynucleotide probes. *Methods Mol. Biol.* 1041, 83–91. doi: 10.1007/978-1-62703-520-0_10

Clausen, B. H., Lambertsen, K. L., Babcock, A. A., Holm, T. H., Dagnaes-Hansen, F., and Finsen, B. (2008). Interleukin-1beta and tumor necrosis factor-alpha are expressed by different subsets of microglia and macrophages after ischemic stroke in mice. *J. Neuroinflamm.* 5:46. doi: 10.1186/1742-2094-5-46

Crews, L., Adame, A., Patrick, C., Delaney, A., Pham, E., Rockenstein, E., et al. (2010). Increased BMP6 levels in the brains of Alzheimer's disease patients and APP transgenic mice are accompanied by impaired neurogenesis. *J. Neurosci.* 30, 12252–12262. doi: 10.1523/JNEUROSCI.1305-10.2010

Dalmau, I., Vela, J. M., González, B., Finsen, B., and Castellano, B. (2003). Dynamics of microglia in the developing rat brain. *J. Comp. Neurol.* 458, 144–157. doi: 10.1002/cne.10572

Demars, M., Hu, Y. S., Gadadhar, A., and Lazarov, O. (2010). Impaired neurogenesis is an early event in the etiology of familial Alzheimer's disease in transgenic mice. *J. Neurosci. Res.* 88, 2103–2117. doi: 10.1002/jnr.22387

Dissing-Olesen, L., Ladeby, R., Nielsen, H. H., Toft-Hansen, H., Dalmau, I., Finsen, B., et al. (2007). Axonal lesion-induced microglial proliferation and microglial cluster formation in the mouse. *Neuroscience* 149, 112–122. doi: 10.1016/j.neuroscience.2007.06.037

Dyer, A. H., Vahdatpour, C., Sanfeliu, A., and Tropea, D. (2016). The role of insulin-like growth factor-1 (IGF-1) in brain development, maturation and neuroplasticity. *Neuroscience* 325, 89–99. doi: 10.1016/j.neuroscience.2016.03.056

Duron, E., Vidal, J. S., Funalot, B., Brunel, N., Viollet, C., Seux, M. L., et al. (2014). Insulin-like growth factor I, insulin-like growth factor binding protein 3, and atrial fibrillation in the elderly. *J. Gerontol. A Biol. Sci. Med. Sci.* 69, 1025–1032. doi: 10.1093/gerona/glt206

Eckermann, K., Mocanu, M. M., Khlistunova, I., Biernat, J., Nissen, A., Hofmann, A., et al. (2007). The beta-propensity of Tau determines aggregation and synaptic loss in inducible mouse models of tauopathy. *J. Biol. Chem.* 282, 31755–31765. doi: 10.1074/jbc.m705282200

Eriksson, P. S., Perfilieva, E., Bjork-Eriksson, T., Alborn, A. M., Nordborg, C., Peterson, D. A., et al. (1998). Neurogenesis in the adult human hippocampus. *Nat. Med.* 4, 1313–1317.

Fenger, C., Drojdahl, N., Wirenfeldt, M., Sylvest, L., Jorgensen, O. S., Meldgaard, M., et al. (2006). Tumor necrosis factor and its p55 and p75 receptors are not required for axonal lesion-induced microgliosis in mouse fascia dentata. *Glia* 54, 591–605. doi: 10.1002/glia.20405

Fernandez, A. M., and Torres-Alemán, I. (2012). The many faces of insulin-like peptide signalling in the brain. *Nat. Rev. Neurosci.* 13, 225–239. doi: 10.1038/nrn3209

Foster, P. P., Rosenblatt, K. P., and Kuljis, R. O. (2011). Exercise-induced cognitive plasticity, implications for mild cognitive impairment and Alzheimer's disease. *Front. Neurol.* 2:28. doi: 10.3389/fneur.2011.00028

Francois, A., Rioux Bilan, A., Quellard, N., Fernandez, B., Janet, T., Chassaing, D., et al. (2014). Longitudinal follow-up of autophagy and inflammation in brain of APPswePS1dE9 transgenic mice. *J. Neuroinflamm.* 11:139. doi: 10.1186/s12974-014-0139-x

Giuffrida, M. L., Tomasello, F., Caraci, F., Chiechio, S., Nicoletti, F., Copani, A., et al. (2012). Beta-amyloid monomer and insulin/IGF-1 signaling in Alzheimer's disease. *Mol. Neurobiol.* 46, 605–613. doi: 10.1007/s12035-012-8313-6

Grebing, M. M., Nielsen, H. H., Fenger, C. D., Jensen, K. T., von Linstow, C. U., Clausen, B. H., et al. (2016). Myelin specific T cells induce interleukin-1beta expression in activated microglia in zones of axonal degeneration. *Glia* 64, 407–424. doi: 10.1002/glia.22937

Gregersen, R., Lambertsen, K., and Finsen, B. (2000). Microglia and macrophages are the major source of tumor necrosis factor in permanent middle cerebral artery occlusion in mice. *J. Cereb. Blood Flow Metab.* 20, 53–65. doi: 10.1097/00004647-200001000-00009

Guthrie, K. M., Nguyen, T., and Gall, C. M. (1995). Insulin-like growth factor-1 mRNA is increased in deafferented hippocampus: spatiotemporal correspondence of a trophic event with axon sprouting. *J. Comp. Neurol.* 352, 147–160. doi: 10.1002/cne.903520111

Hamilton, A., and Holscher, C. (2012). The effect of ageing on neurogenesis and oxidative stress in the APP(swe)/PS1(deltaE9) mouse model of Alzheimer's disease. *Brain Res.* 1449, 83–93. doi: 10.1016/j.brainres.2012.02.015

Hammond, T. R., Dufort, C., Dissing-Olesen, L., Giera, S., Young, A., Wysoker, A., et al. (2019). Single-cell RNA sequencing of microglia throughout the mouse lifespan and in the injured brain reveals complex cell-state changes. *Immunity* 50, 253–271. doi: 10.1016/j.immuni.2018.11.004

Heppner, F. L., Ransohoff, R. M., and Becher, B. (2015). Immune attack: the role of inflammation in Alzheimer disease. *Nat. Rev. Neurosci.* 16, 358–372. doi: 10.1038/nrn3880

Heneka, M. T., Carson, M. J., Khoury, J. E., Landreth, G. E., Brosseron, F., Feinstein, D. L., et al. (2015). Neuroinflammation in Alzheimer's disease. *Lancet Neurol.* 14, 389–405.

Hickman, S. E., Allison, E. K., and El Khoury, J. (2008). Microglial dysfunction and defective beta-amyloid clearance pathways in aging Alzheimer's disease mice. *J. Neurosci.* 28, 8354–8360. doi: 10.1523/JNEUROSCI.0616-08.2008

Hickman, S. E., Kingery, N. D., Ohsumi, T. K., Borowsky, M. L., Wang, L. C., Means, T. K., et al. (2013). The microglial sensome revealed by direct RNA sequencing. *Nat. Neurosci.* 16, 1896–1905. doi: 10.1038/nn.3554

Holmes, C., Cunningham, C., Zotova, E., Woolford, J., Dean, C., Kerr, S., et al. (2009). Systemic inflammation and disease progression in Alzheimer disease. *Neurology* 73, 768–774. doi: 10.1212/WNL.0b013e3181b6bb95

Huijbers, W., Mormino, E. C., Schultz, A. P., Wigman, A., Ward, A. M., Larvie, M., et al. (2015). Amyloid-b deposition in mild cognitive impairment is associated with increased hippocampal activity, atrophy and clinical progression. *Brain* 138, 1023–1035. doi: 10.1093/brain/awv007

Hyman, B. T., Van Hoesen, G. W., Kromer, L. J., and Damasio, A. R. (1986). Perforant pathway changes and the memory impairment of Alzheimer's disease. *Ann. Neurol.* 20, 472–481. doi: 10.1002/ana.410200406

Iosif, R. E., Ekdahl, C. T., Ahlenius, H., Pronk, C. J., Bonde, S., Kokaia, Z., et al. (2006). Tumor necrosis factor receptor 1 is a negative regulator of progenitor proliferation in adult hippocampal neurogenesis. *J. Neurosci.* 26, 9703–9712. doi: 10.1523/jneurosci.2723-06.2006

Jack, C. R. Jr., Wiste, H. J., Lesnick, T. G., Weigand, S. D., Knopman, D. S., Vemuri, P., et al. (2013). Brain beta-amyloid load approaches a plateau. *Neurology* 80, 890–896. doi: 10.1212/WNL.0b013e3182840bbe

Jana, M., Palencia, C. A., and Pahan, K. (2008). Fibrillar amyloid-beta peptides activate microglia via TLR2: implications for Alzheimer's disease. *J. Immunol.* 181, 7254–7262. doi: 10.4049/jimmunol.181.10.7254

Jankowsky, J. L., Fadale, D. J., Anderson, J., Xu, G. M., Gonzales, V., Jenkins, N. A., et al. (2004). Mutant presenilins specifically elevate the levels of the 42 residue beta-amyloid peptide in vivo: evidence for augmentation of a 42-specific gamma secretase. *Hum. Mol. Genet.* 13, 159–170. doi: 10.1093/hmg/ddh019

Jin, K., Peel, A. L., Mao, X. O., Xie, L., Cottrell, B. A., Henshall, D. C., et al. (2004). Increased hippocampal neurogenesis in Alzheimer's disease. *Proc. Natl. Acad. Sci. U.S.A.* 101, 343–347.

Kempermann, G., Wiskott, L., and Gage, F. H. (2004). Functional significance of adult neurogenesis. *Curr. Opin. Neurobiol.* 14, 186–191. doi: 10.1016/j.conb.2004.03.001

Keren-Shaul, H., Spinrad, A., Weiner, A., Matcovitch-Natan, O., Dvir-Szternfeld, R., Ullan, T. K., et al. (2017). A unique microglia type associated with restricting development of Alzheimer's disease. *Cell* 169, 1276–1290. doi: 10.1016/j.cell.2017.05.018

Knoth, R., Singec, I., Ditter, M., Pantazis, G., Capetian, P., Meyer, R. P., et al. (2010). Murine features of neurogenesis in the human hippocampus across the lifespan from 0 to 100 years. *PLoS One* 5:e8809. doi: 10.1371/journal.pone.0008809

Krabbe, G., Halle, A., Matyash, V., Rinnenthal, J. L., Eom, G. D., Bernhardt, U., et al. (2013). Functional impairment of microglia coincides with Beta-amyloid deposition in mice with Alzheimer-like pathology. *PLoS One* 8:e60921. doi: 10.1371/journal.pone.0060921

Kuhn, H. G., Dickinson-Anson, H., and Gage, F. H. (1996). Neurogenesis in the dentate gyrus of the adult rat: age-related decrease of neuronal progenitor proliferation. *J. Neurosci.* 16, 2027–2033. doi: 10.1523/jneurosci.16-06-02027.1996

Lambertsen, K. L., Clausen, B. H., Babcock, A. A., Gregersen, R., Fenger, C., Nielsen, H. H., et al. (2009). Microglia protect neurons against ischemia by synthesis of tumor necrosis factor. *J. Neurosci.* 29, 1319–1330. doi: 10.1523/JNEUROSCI.5505-08.2009

Lambertsen, K. L., Gregersen, R., Lomholt, N. D., Owens, T., and Finsen, B. (2001). A specific and sensitive protocol for detection of tumor necrosis factor in the murine central nervous system. *Brain Res. Protoc.* 7, 175–191. doi: 10.1016/s1385-299x(01)00062-9

Lichtenwalner, R. J., and Parent, J. M. (2006). Adult neurogenesis and the ischemic forebrain. *J. Cereb. Blood Flow Metab.* 26, 1–20. doi: 10.1038/sj.jcbfm.9600170

Liu, Y., Yoo, M.-J., Savonenko, A., Stirling, W., Price, D. L., Borchelt, D. R., et al. (2008). Amyloid pathology is associated with progressive monoaminergic neurodegeneration in a transgenic mouse model of alzheimer's disease. *J. Neurosci.* 28, 13805–13814. doi: 10.1523/jneurosci.4218-08.2008

Meldgaard, M., Fenger, C., Lambertsen, K. L., Pedersen, M. D., Ladeby, R., Finsen, B., et al. (2006). Validation of two reference genes for mRNA level studies of murine disease models in neurobiology. *J. Neurosci. Methods* 156, 101–110. doi: 10.1016/j.jneumeth.2006.02.008

Minogue, A. M., Jones, R. S., Kelly, R. J., McDonald, C. L., Connor, T. J., Lynch, M. A., et al. (2014). Age-associated dysregulation of microglial activation is coupled with enhanced blood-brain barrier permeability and pathology in APP/PS1 mice. *Neurobiol. Aging* 35, 1442–1452. doi: 10.1016/j.neurobiolaging.2013.12.026

Nelson, P. T., Alafuzoff, I., Bigio, E. H., Bouras, C., Braak, H., Cairns, N. J., et al. (2012). Correlation of Alzheimer disease neuropathologic changes with cognitive status: a review of the literature. *J. Neuropathol. Exp. Neurol.* 71, 362–381. doi: 10.1097/NEN.0b013e31825018f7

Nilsson, T., Mann, M., Aebersold, R., Yates, J. R., Bairoch, A., Bergeron, et al. (2010). Mass spectrometry in high-throughput proteomics: ready for the big time. *Nat. Methods* 7, 681–685. doi: 10.1038/nmeth0910-681

Nikolajsen, G. N., Jensen, M. S., and West, M. J. (2011). Cholinergic axon length reduced by 300 meters in the brain of an Alzheimer mouse model. *Neurobiol. Aging* 32, 1927–1931. doi: 10.1016/j.neurobiolaging.2011.05.006

Olesen, L. Ø, Sivasaravanaparan, M., Severino, M., Babcock, A. A., Bouzinova, E. V., West, M. J., et al. (2017). Neuron number and neurogenesis in the dentate gyrus of aged APPswe/PS1dE9 transgenic mice: effect of long-term treatment with paroxetine. *Neurobiol. Aging* 104, 50–60. doi: 10.1016/j.nbd.2017.04.021

Perry, R. T., Collins, J. S., Wiener, H., Acton, R., and Go, R. C. (2001). The role of TNF and its receptors in Alzheimer's disease. *Neurobiol. Aging* 22, 873–883. doi: 10.1016/s0197-4580(01)00291-3

Pooler, A. M., Polydoro, M., Wegmann, S. K., Pitstick, R., Kay, K. R., Sanchez, L., et al. (2013). Tau-amyloid interactions in the rTgTauEC model of early Alzheimer's disease suggest amyloid-induced disruption of axonal projections and exacerbated axonal pathology. *J. Comp. Neurol.* 521, 4236–4248. doi: 10.1002/cne.23411

Ramsey, M. M., Weiner, J. L., Moore, T. P., Carter, C. S., and Sonntag, W. E. (2004). Growth hormone treatment attenuates age-related changes in hippocampal short-term plasticity and spatial learning. *Neuroscience* 129, 119–127. doi: 10.1016/j.neuroscience.2004.08.001

Radde, R., Bolmont, T., Kaeser, S. A., Coomaraswamy, J., Lindau, D., Stoltze, L., et al. (2006). Aβ42-driven cerebral amyloidosis in transgenic mice reveals early and robust pathology. *EMBO Rep.* 7, 940–946. doi: 10.1038/sj.embor.7400784

Rupp, N. J., Wegenast-Braun, B. M., Radde, R., Calhoun, M. E., and Jucker, M. (2011). Early onset amyloid lesions lead to severe neuritic abnormalities and local, but not global neuron loss in APPPS1 transgenic mice. *Neurobiol. Aging* 32, 2324.e1–2324.e6. doi: 10.1016/j.neurobiolaging.2010.08.014

Serrano-Pozo, A., Mielke, M. L., Gomez-Isla, T., Betensky, R. A., Growdon, J. H., Frosch, M. P., et al. (2011). Reactive glia not only associates with plaques but also parallels tangles in Alzheimer's disease. *Am. J. Pathol.* 179, 1373–1384. doi: 10.1016/j.ajpath.2011.05.047

Sierra, A., Encinas, J. M., Deudero, J. J., Chancey, J. H., Enikolopov, G., Overstreet-Wadiche, L. S., et al. (2010). Microglia shape adult hippocampal neurogenesis through apoptosis-coupled phagocytosis. *Cell Stem Cell* 7, 483–495. doi: 10.1016/j.stem.2010.08.014

Sonntag, W. E., Carter, C. S., Ikeno, Y., Ekenstedt, K., Carlson, C. S., Loeser, R. F., et al. (2005). Adult-onset growth hormone and insulin-like growth factor I deficiency reduces neoplastic disease, modifies age-related pathology, and increases life span. *Endocrinology* 146, 2920–2932. doi: 10.1210/en.2005-0058

Spalding, K. L., Bergmann, O., Alkass, K., Bernard, S., Salehpour, M., Huttner, H. B., et al. (2013). Dynamics of hippocampal neurogenesis in adult humans. *Cell* 153, 1219–1227. doi: 10.1016/j.cell.2013.05.002

Stine, W. B., Dahlgren, K. N. Jr., Krafft, G. K., and LaDu, M. J. (2003). In vitro characterization of conditions for amyloid-beta peptide oligomerization and fibrillogenesis. *J. Biol. Chem.* 278, 11612–11622. doi: 10.1074/jbc.m210207200

Stranahan, A. M., Zhou, Y., Martin, B., and Maudsley, S. (2009). Pharmacomimetics of exercise: novel approaches for hippocampally-targeted neuroprotective agents. *Curr. Med. Chem.* 16, 4668–4678. doi: 10.2174/092986709789878292

Swardfager, W., Lanctot, K., Rothenburg, L., Wong, A., Cappell, J., Herrmann, N., et al. (2010). A meta-analysis of cytokines in Alzheimer's disease. *Biol. Psychiatry* 68, 930–941. doi: 10.1016/j.biopsych.2010.06.012

Thal, D. R., Rub, U., Orantes, M., and Braak, H. (2002). Phases of A beta-deposition in the human brain and its relevance for the development of AD. *Neurology* 58, 1791–1800. doi: 10.1212/wnl.58.12.1791

Thygesen, C., Ilkjær, C., Kempf, S. J., Hemdrup, A. L., von Linstow, C. U., Babcock, A. A., et al. (2018). Diverse protein profiles in CNS myeloid cells and CNS tissue from lipopolysaccharide- and vehicle-injected APPSWE/PS1ΔE9 transgenic mice implicate cathepsin Z in Alzheimer's disease. *Front. Cell. Neurosci.* 12:397. doi: 10.3389/fncel.2018.00397.

Valero, J., Espana, J., Parra-Damas, A., Martin, E., Rodriguez-Alvarez, J., Saura, C. A., et al. (2011). Short-term environmental enrichment rescues adult neurogenesis and memory deficits in APP(Sw,Ind) transgenic mice. *PLoS One* 6:e16832. doi: 10.1371/journal.pone.0016832

Villeda, S. A., Luo, J., Mosher, K. I., Zou, B., Britschgi, M., Bieri, G., et al. (2011). The ageing systemic milieu negatively regulates neurogenesis and cognitive function. *Nature* 477, 90–94. doi: 10.1038/nature10357

von Linstow, C. U., Waider, J., Grebing, M., Metaxas, A., Lesch, K. P., and Finsen, B. (2017). Serotonin augmentation therapy by escitalopram has minimal effects on amyloid-β levels in early-stage Alzheimer's-like disease in mice. *Alzheimer's Res. Ther.* 9:74. doi: 10.1186/s13195-017-0298-y

West, M. J. (2012). The precision of estimates in stereological analyses. *Cold Spring Harb. Protoc.* 2012, 937–949. doi: 10.1101/pdb.top071050

West, M. J., Bach, G., Soderman, A., and Jensen, J. L. (2009). Synaptic contact number and size in stratum radiatum CA1 of APP/PS1DeltaE9 transgenic mice. *Neurobiol. Aging* 30, 1756–1776. doi: 10.1016/j.neurobiolaging.2008.01.009

West, M. J., Coleman, P. D., Flood, D. G., and Troncoso, J. C. (1994). Differences in the pattern of hippocampal neuronal loss in normal ageing and Alzheimer's disease. *Lancet* 344, 769–772. doi: 10.1016/s0140-6736(94)92338-8

West, M. J., Østergaard, K., Andreassen, O., and Finsen, B. (1996). Counting in situ hybridized neurons with modern unbiased stereological methods. *J. Comp. Neurol.* 370, 11–22.

Wirenfeldt, M., Dissing-Olesen, L., Anne Babcock, A., Nielsen, M., Meldgaard, M., Zimmer, J., et al. (2007). Population control of resident and immigrant microglia by mitosis and apoptosis. *Am. J. Pathol.* 171, 617–631. doi: 10.2353/ajpath.2007.061044

Wlodarczyk, A., Holtman, I. F., Krueger, M., Yogev, N., Bruttger, J., Khorooshi, R., et al. (2017). A novel microglial subset plays a key role in myelinogenesis in developing brain. *EMBO J.* 36, 3292–3308. doi: 10.15252/embj.201696056

Woods, K. A., Camacho-Hübner, C., Savage, M. O., and Clark, A. J. (1996). Intrauterine growth retardation and postnatal growth failure associated with deletion of the insulin-like growth factor I gene. *New Engl. J. Med.* 335, 1363–1367. doi: 10.1056/nejm199610313351805

Woods, A. G., Guthrie, K. M., Kurlawalla, M. A., and Gall, C. M. (1998). Deafferentation-induced increases in hippocampal insulin-like growth factor-1 messenger RNA expression are severely attenuated in middle aged and aged rats. *Neuroscience* 83, 663–668.

Zemva, J., and Schubert, M. (2014). The role of neuronal insulin/insulin-like growth factor-1 signaling for the pathogenesis of Alzheimer's disease: possible therapeutic implications. *CNS Neurol. Disord. Drug Targets* 13, 322–337. doi: 10.2174/18715273113126660141

Zhang, B., Tang, X. C., and Zhang, H. Y. (2013). Alternations of central insulin-like growth factor-1 sensitivity in APP/PS1 transgenic mice and neuronal models. *J. Neurosci. Res.* 91, 717–725. doi: 10.1002/jnr.23201

Zhao, C., Deng, W., and Gage, F. H. (2008). Mechanisms and functional implications of adult neurogenesis. *Cell* 132, 645–660. doi: 10.1016/j.cell.2008.01.033

Ziabreva, I., Perry, E., Perry, R., Minger, S. L., Ekonomou, A., Przyborski, S., et al. (2006). Altered neurogenesis in Alzheimer's disease. *J. Psychosom. Res.* 61, 311–316.

Conflict of Interest Statement: The authors declare that the research was conducted in the absence of any commercial or financial relationships that could be construed as a potential conflict of interest.

frontiers in Molecular Neuroscience

DATA REPORT
published: 24 October 2019
doi: 10.3389/fnmol.2019.00248

Intra-CA1 Administration of Minocycline Alters the Expression of Inflammation-Related Genes in Hippocampus of CCI Rats

*Li He[1†], Rui Xu[1†], Yuanshou Chen[1], Xiaohong Liu[1], Youfu Pan[2], Song Cao[3], Tao Xu[1], Hong Tian[1] and Junwei Zeng[1]**

[1] Department of Physiology, Zunyi Medical University, Zunyi, China, [2] Department of Genetics, Zunyi Medical University, Zunyi, China, [3] Department of Pain Medicine, Affiliated Hospital of Zunyi Medical Univerisity, Zunyi, China

Keywords: neuropathic pain, hippocampus, microglia, toll-like receptor, chemokines

Some recent evidence suggests that microglia activation and inflammatory cytokine production in the hippocampus are associated with the development of pain behavior following peripheral nerve injury. We observed sciatic nerve chronic constriction injury (CCI)-induced inflammation-related gene expression changes that are modulated by minocycline in rat hippocampus. Intra-CA1 administration of minocycline was applied after nerve injury. Genome-wide mRNA expression in the hippocampus was evaluated to monitor the fundamental gene expression levels. We found that minocycline treatment produces a pronounced inhibition of CCI-induced mechanical allodynia. We identified 790 genes differentially expressed in CCI vs. sham rats. Among these changed genes, the 425 differentially expressed genes showed a significantly different effect in CCI vs. minocycline-treated rats. Moreover, 390 transcripts were characterized by an increase in mRNA abundance after nerve injury, and minocycline treatment reduced the level of these changes. Only 35 transcripts were characterized by a decrease in mRNA after nerve injury, and minocycline treatment reversed the decrease in the hippocampus. Noteworthily, cytokine-cytokine receptor interaction and the toll-like receptor signaling pathway are the top two most significantly enriched KEGG (kyoto encyclopedia of genes and genomes) terms in comparing the sham vs. CCI group and CCI vs. minocycline-treated group. Nine kinds of transcription factor gene transcripts (Runx3, Tfec, Pax-1, Batf3, Sp5, Hlx, Nfkbiz, Spil, Fli1) increased in abundance after nerve injury, and minocycline treatment reversed these changes. Afterwards, we selected some genes for further validation by using quantitative PCR: interleukins (Il1β), chemokines (Cxcl13, Cxcl1, Ccl2, Cxcl11, Ccl7, Ccl20), toll-like receptors (Tlr8 and Tlr1), and transcription factors (Runx3, Nfkbiz and Spil). We suggested that the transcriptional changes of these inflammation-related genes are strongly related to the processes of microglia activation underlying neuropathic pain development.

OPEN ACCESS

Edited by:
Liliana Bernardino, University of Beira Interior, Portugal

Reviewed by:
Antonio J. Herrera, University of Seville, Spain
Muddanna Sakkattu Rao, Kuwait University, Kuwait

***Correspondence:**
Junwei Zeng
junweizeng@sohu.com

[†] *These authors have contributed equally to this work*

Received: 18 October 2018
Accepted: 26 September 2019
Published: 24 October 2019

Citation:
He L, Xu R, Chen Y, Liu X, Pan Y, Cao S, Xu T, Tian H and Zeng J (2019) Intra-CA1 Administration of Minocycline Alters the Expression of Inflammation-Related Genes in Hippocampus of CCI Rats. Front. Mol. Neurosci. 12:248. doi: 10.3389/fnmol.2019.00248

INTRODUCTION

Neuropathic pain is a chronic pain condition that is usually induced by peripheral nerve injury. Recent reports suggest that the inflammation-related cytokines accumulation in dorsal root ganglion, dorsal spinal cord, hippocampus, thalamus, and somatosensoric cortex are paralleled by pain responses in different animal models of neuropathic pain (Al-Amin et al., 2011; Sun et al., 2016; Chang et al., 2018; Liu et al., 2018). In the chronic constriction injury (CCI) and the spared nerve injury models of neuropathic pain in rats, an increase in interleukin 1 beta (IL-1β), interleukin 6 (IL-6), nerve growth factor (NGF), and glial cell-derived neurotrophic factor (GDNF) was observed in most brain regions (Al-Amin et al., 2011). The overproduction of tumor necrosis factor-α (TNF-α) may regulate synaptic plasticity in the rat hippocampus through microglia-dependent mechanism after spared nerve injury of the sciatic nerve (Liu et al., 2017).

However, it is not clear whether other inflammation-related neuroactive substances will be affected after microglia activation in the rat hippocampus after peripheral nerve injury.

It is clear that many kinds of toll-like receptors (TLRs) are expressed in the hippocampus and act as a type of pattern-recognition receptor that participate in inflammatory responses. TLR1 expression in the hippocampus was increased in the neurons, microglia, and astrocytes in seizure mice (Wang et al., 2015). TLR (2, 3, 4, 7, and 9) expression was upregulated in the hippocampus of restraint stressed rats (Timberlake et al., 2018). TLR2 and TLR4 in the rat hippocampus are related to the lipopolysaccharide (LPS)-induced neuron cell death (He et al., 2013; Henry et al., 2014). That TLR3-induces the increased expression of IL-1β in the rat hippocampus was suggested by Henry et al. (2014). TLR8, expressed in most regions of the brain, is associated with injury and neurite outgrowth (Ma et al., 2006). It is well known that TLR-dependent signaling is often associated with the overproduction and release of inflammatory cytokines in many different types of cells. However, the relationship between the changes of TLRs expression and microglia activation in hippocampus of CCI rats is not known.

Previous studies reveal that chemokine production is enhanced in some neuroimmunological diseases accompanied by pathological pain (Cartier et al., 2005). CXCL13 is obviously upregulated in the spinal cord after spinal nerve ligation and induces astrocyte activation via its receptor CXCR5 (Zhang et al., 2017). Chemokine CCL2 (C-C motif ligand 2) in the rostral ventromedial medulla is related to the descending pain facilitation in nerve-injured rats (Guo et al., 2012). Expression of chemokines CCL2 and CCL3 was increased in the thalamus and hippocampus after severe spinal cord injuries (Knerlich-Lukoschus et al., 2011). The overproduction of IL-1β and CCL2 was found in the hippocampus of CCI rats (Fiore and Austin, 2018). Moreover, Lanfranco et al. reported that CCL5 gene expression was found in neurons and glial cells in the rat hippocampus (Lanfranco et al., 2018). However, no evidence directly addresses the relationship between microglia activation and chemokine accumulation in neuropathic hypersensitivity.

It is clear that minocycline is an important modulator of the immune response and easily permeates the blood-brain barrier (Stolp et al., 2007; Vonder Haar et al., 2014). Clinically, minocycline can be administered by the intravenous route in patients with traumatic brain injury (Rojewska et al., 2014). More recent evidence suggest that minocycline is effective at reducing the spontaneous pain behavior in animal models of neuropathic pain, and that means it appears to be a promising analgesic drug (LeBlanc et al., 2011; Rojewska et al., 2014). In the present study, minocycline is applied to identify what inflammation-related genes at the hippocampus are closely related to the increased microglia activity in CCI-induced neuropathic pain rats.

MATERIALS AND METHODS

Experimental Animals

In the experiments, adult male Sprague-Dawley (SD) rats (200–220 g) were housed under a 12: 12 h revised light/dark cycle. The protocol was prepared from SD rats in accordance with the National Institutes of Health guidelines in a manner that minimized animal suffering and animal numbers. All experiments involving animals were approved by the Zunyi Medical University Committee on Ethics in the Care and Use of Laboratory Animals.

Intra-hippocampal Injection

Rats were anesthetized by pentobarbital sodium (40 mg/kg, i.p.) and mounted in a David Kopf stereotaxic frame (Model 1900, Tujunga, CA, USA) with a flat skull position. An incision was made along the midline and the scalp was retracted. The area surrounding the bregma was cleaned. Stainless steel guide cannulae were unilaterally implanted 1 mm above the CA1 according to rat brain atlases. Two holes were drilled through the skull and two stainless steel needles (28 gauge) were inserted through the holes (A/P-3.3 mm caudal to the bregma, L/R ± 2.0 mm lateral to the midline, D/V2.8 mm ventral to the skull surface) (Paxinos and Watson, 1998). These rats were allowed to recover for 6 days before CCI operation. A total of 0.5 μl of either PBS or minocycline was infused (0.167 μl/min, 3 min) (Zhang et al., 2016). After infusion, needles remained in place for an additional 3 min to avoid reflux. After nerve injury, the rats received bilateral intra-hippocampal treatment of 0.5 μl of either vehicle or minocycline (1, 2, 5, 10, and 15 μg/μl, twice a day) for 7 days consecutively.

The Chronic Constriction Injury (CCI) Model

Rats were anesthetized with pentobarbital sodium (40 mg/kg, i.p.), and the sciatic nerve (left) was exposed. The left sciatic nerve was exposed and a 15-mm length of sciatic nerve proximal to the sciatic trifurcation was dissected. Four loose ligatures (4.0 braided silk) were made around the sciatic nerve at 1-mm intervals. Sham rats underwent the same procedure but without nerve ligation. After surgery, rats were housed in separate cages (at room temperature for 24 h) to avoid scratching each other (Safakhah et al., 2017; Liu et al., 2018). Rats that exhibited motor deficits such as hind-limb paralysis, impaired righting reflexes, and hind-limb dragging were excluded. That is to say, after implantation of a cannula into the hippocampus, the hind limb function of rats used for CCI and behavioral testing was not to be impaired (Huang et al., 2018). Hernández-López et al. also reported that stereotactic surgery for cannula placement in the dorsal hippocampus does not impair the motor coordination of rats (Hernández-López et al., 2017). In addition, rats not exhibiting pain hypersensitivity after nerve injury were excluded.

Behavioral Assessment

Mechanical withdrawal threshold (MWT) was recorded to assess the response of the paw to mechanical stimulus. An electronic von Frey plantar aesthesiometer (IITC, Wood Dale, IL, USA) was used (Huang et al., 2018). After habituation to the test environment, the measurements were made. Baseline values were obtained before surgery. Mechanical stimulation was applied against the mid-plantar area of the left hind paw, and brisk withdrawal or paw flinching was considered to be positive behavior. The MWT was recorded and the cut-off force was set at 60 g. Three successive stimuli were applied, and MWT was represented by the mean values.

Transcriptional Profile Analysis

Male SD rats were divided into Sham, CCI+0.01M PBS and CCI+ Minocycline groups ($n = 3$ per group). Three subjects from each group who met all inclusion criteria (see below) were subjected to microarray analyses. At 7 days following CCI or sham surgery, the rats were anesthetized with pentobarbital sodium (40 mg/kg, i.p.). The hippocampus of rats was dissected, flash-frozen (in liquid nitrogen) and stored at −80°C for analysis. According to the procedures described in the manual, total RNA was isolated from hippocampal tissue using TRI Reagent (Sigma Aldrich, USA). RNA degradation and contamination were checked by gel electrophoresis. The quantity of each RNA sample obtained was checked using the NanoPhotometer® spectrophotometer (IMPLEN, CA, USA) with pass criteria of absorbance ratios of A260/A280 ≥ 1.8 and A260/A230 ≥ 1.6. RNA concentrations were assessed using Qubit® RNA Assay Kit in Qubit® 2.0 Fluorometer (Life Technologies, CA, USA). A total amount of 2 μg RNA per sample was used to construct the cDNA library.

First-strand cDNA was synthesized using a HiFiScript gDNA Removal cDNA Synthesis Kit (CWBIO, Beijing, China) according to the standard protocols. Quantitative real-time PCR was carried out using a QuantStudio™ 6 Flex Real-Time System (Applied Biosystems, USA) with UltraSYBR Mixture (CWBIO, Beijing, China). The following PCR amplification program was used: 95°C for 2 min, followed by 40 cycles of 95°C for 10 s, 50–54°C (changed according to the primer sequences) for 20 s and 72°C for 20 s. A dissociation curve was performed (55–95°C) after the last PCR cycle to ascertain the specificity of the amplification reactions. The abundance of each mRNA was normalized with respect to the endogenous housekeeping gene β-actin, and the relative gene expression levels were determined by the $^{2-\Delta\Delta}$Ct method.

Microarray experiments were performed to determine gene-expression profiles in rat hippocampus. Based on the differentially expressed gene (DEG) results, the heat maps were constructed using Multiexperiment Viewer (MeV; http://mev.tm4.org/). Gene ontology (GO) and pathway enrichment analyses were carried out with the aid of the NCBI COG (http://www.ncbi.nlm.nih.gov/COG/), Gene Ontology Database (http://www.geneontology.org/) and KEGG pathway database (http://www.genome.jp/kegg/).

The DEGs were ascertained using the DESeq R package (1.10.1) as detailed in a previous study (Wang et al., 2010). False discovery rate (FDR) was used to correct the results for *P*-value. FDR ≤ 0.05 and an absolute value of log2 (fold-change) ≥1 were used as the threshold for screening DEGs. Pathway functional enrichment analysis was performed using the "phyper" function in R. The *P*-value calculating formula is:

$$P = 1 - \sum_{i=0}^{m-1} \frac{\binom{M}{i}\binom{N-M}{n-i}}{\binom{N}{n}}$$

Here, M is the number of genes in the pathway, N is the total number of genes in the genome, m is the number of target gene candidates in M and n is the number of differentially expressed genes. In addition, i =1, 2, 3, … (M-1) where M represents the number of genes in the pathway. The Fisher's score indicates the ratio of genes (number m) belonging to the functional pathway out of the total differentially expressed genes (number n) (Zhang et al., 2018). Subsequently we calculate the value of FDR. FDR ≤ 0.01 is considered as significantly enriched.

RT-PCR

Male SD rats were divided into Sham, Sham+Minocycline, CCI+0.01M PBS and CCI+ Minocycline groups ($n = 6$ per group). The changes in the abundance of some gene transcripts in the rat hippocampus after nerve injury and the modulatory effects of minocycline should be further investigated by PCR analysis of samples independent from those used for the microarray studies. According to the methods mentioned above, four groups of animals were treated and killed by cutting their necks. Brain tissue was quickly dissected on the ice platform and was immersed and washed with phosphate buffered solution (PBS). The hippocampus was isolated and rapidly transferred into separate RNase-free 1.5 ml Eppendorf tubes. Total RNA was immediately isolated using the TRIzol Reagent (MRC Co., Cincinnati, USA). The concentration and purity of RNA samples were measured using Spectrophotometer (Thermo Fisher Scientific). The ratios of OD260/OD280 were between 1.9 and 2.1. cDNA was synthesized from RNA by reverse transcription reaction using the SuperScript II reverse transcriptase kit (Invitrogen). All primers are shown in **Table 1**. qPCR was performed in a final volume of 20 μl (8 μl H_2O, 10 μl mastermix, 1 μl assay-mix, and 1 μl cDNA) on a Linegene Real-time PCR detection system (Bioer Technology, China). PCR reaction conditions were as follows: (1) 95°C 8 min 1 Cycle; (2) 95°C 15 s and 60°C 1 min, 40 Cycles. The experimental data analysis was carried out using the $^{2-\Delta\Delta}$Ct method (Livak and Schmittgen, 2001).

Statistical Analysis

All data were presented as mean ± standard deviation (SD.). The behavioral and PCR data were analyzed by one- (compared within the group) or two-way (compared between groups) ANOVA. If significance was established, *post-hoc* Dunnett or Bonferroni's multiple comparisons were performed. All statistical tests were carried out using SPSS 18.0 software (IBM, Armonk, NY). The level of significance was set as $p < 0.05$.

RESULTS

Intra-CA1 Administration of Minocycline Attenuates CCI-Induced Mechanical Allodynia

To investigate the antinociceptive effect of minocycline on the mechanical nociceptive threshold in neuropathic pain rats, the MWT was recorded on the day before and after surgery (at POD 1, 3, 5, and 7). A total of five doses (1, 2, 5, 10, and 15 μg/μl, twice a day) were administered. We compared the changes of MWT between the different time points (**Figure 1**). Application

TABLE 1 | Primers used for RT-PCR.

Gene	Forward	Reverse
Cxcl13 (NM-001017496.1)	5′-TTTGGTAACCATCTGGCAGTA-3′	5′-GCTCGACCTTTATCAATCTAAT-3′
Cxcl1 (NM-030845.1)	5′-TGGCTATGACTTCGGTTTGGGT-3′	5′-GGCAGGGATTCACTTCAAGAACA-3′
Ccl2 (NM-031530.1)	5′-GTGCTGAAGTCCTTAGGGTTG-3′	5′-GTCGGCTGGAGAACTACAAGA-3′
Cxcl11 (NM-182952.2)	5′-CCAGGCACCTTTGTCCTTTAT-3′	5′-GGTTCCAGGCTTCGTTATGTT-3′
Ccl7 (NM-001007612.1)	5′-CACCGACTACTGGTGATCTTTC-3′	5′-TTCATCCACTTGCTGCTATGT-3′
Ccl20 (NM-019233.1)	5′-GACAAGACCACTGGGACA-3′	5′-AGCCTAAGAACCAAGAAG-3′
Iba-1 (NM-017196.3)	5′-CAAGGATTTGCAGGGAGGA-3′	5′-CAGCATTCGCTTCAAGGACATA-3′
Cd68 (NM-001031638.1)	5′-TCAAACAGGACCGACATCAGA-3′	5′- ATTGCTGGAGAAAGAACTATGCT-3′
iNOS (NM-012611.3)	5′-GATGTGCTGCCTCTGGTCCT-3′	5′-GAGCTCCTGGAACCACTCGT-3′
IL-1β (NM-031512.2)	5′-CAGCCTTACTGGCCTGCTAC-3′	5′-CTGCTACCACGACAGCCATA-3′
Tlr8 (NM-001101009.1)	5′-TGCTTCATTTGGGATTTG-3′	5′-TGGCATTTACACGCTCAC-3′
Tlr1 (NM-001172120.2)	5′-CAGTTTCTGGGATTGAGCGGT-3′	5′-TAATGTGCTGAAGACACTTGGGATC-3′
Runx3 (NM-130425.1)	5′-GGCTTTGGTCTGGTCCTCTATC-3′	5′-GCAACGCTTCCGCTGTCA-3′
Nfkbiz (NM-001107095.1)	5′-CCGTAGAAGTAAGCGAGGTT-3′	5′-GAGCATGATCGTGGACAAG-3′
Spil (NM-001005892.2)	5′-CAATCTTTGCTCCTCTTT-3′	5′-CTACCAATCCTGGCTTCA-3′
β-actin (NM-031144.3)	5′-AGCCATGTACGTAGCCATCC-3′	5′-ACCCTCATAGATGGGCACAG-3′

of minocycline at 1, 2, and 5 μg/μl for 30 min showed increased MWT in comparison to CCI rats ($P < 0.05$). Application of minocycline at 1, 2, and 5 μg/μl for 1 h also showed more significant increase in MWT (vs. CCI rats: $P < 0.01$; vs. 30 min: $P < 0.05$). Application of minocycline at 10 and 15 μg/μl for 30 min showed a slight increase but was not significantly different from that of the vehicle-treated CCI group. Application of minocycline at 10 μg/μl for 1 h showed obvious increased MWT (vs. CCI rats: $P < 0.05$; vs. 30 min: $P < 0.05$). Application of minocycline at 15 μg/μl for 1 h also showed increased MWT (vs. CCI rats: $P < 0.05$). Application of minocycline at 5 μg/μl for 2 h showed slightly increased MWT (vs. CCI rats: $P < 0.05$; vs. 1 h: $P < 0.01$). These results suggest that minocycline produced a reversal of MWT, with maximal effect at 1 h after minocycline administration.

As shown in **Figure 1B**, decreased MWT was observed in rats on day 1 after surgery compared to sham rats ($P < 0.05$), and the allodynia was sustained throughout the experimental period. Compared to the vehicle-treated CCI rats, minocycline at 1 μg/μl induced significant analgesic effect ($P < 0.05$). Minocycline at doses of 2 and 5 μg/μl showed better analgesic effects in comparison with minocycline at dose 1 μg/μl ($P < 0.05$). We also noticed that minocycline at a dose of 5 μg/μl showed apparent elevations of the mechanical pain threshold in comparison with minocycline at a dose of 2 μg/μl ($P < 0.05$). On the other hand, minocycline at 10 μg/μl produced moderate antinociceptive effect in CCI rats. Minocycline at 15 μg/μl induced a slight but significant antinociceptive effect in CCI rats. Minocycline at a dose of 5 μg/μl showed better analgesic effects in comparison with minocycline at doses of 10 and 15 μg/μl ($P < 0.05$). In a short, three main conclusions can be drawn: (1) The decreased MWT in CCI rats and the analgesic effect of minocycline in minocycline-treated CCI rats are maintained over 7 days; (2) a greater analgesic effect of minocycline occurs 1 h after its administration; (3) the highest analgesic effect of minocycline occurs at a dose of 5 μg/μl. Then, the minimum dose of minocycline (5 μg/μl) showing maximum effect was selected in the following experiments.

Identification of Differentially Expressed Genes Between Different Groups

To explore the possible role of microglia activation and inflammation within the hippocampus in the development of peripheral neuropathic pain, the DEGs between different groups were identified. According to the results, in the rat hippocampus, there were 790 DEGs between the sham group and the CCI

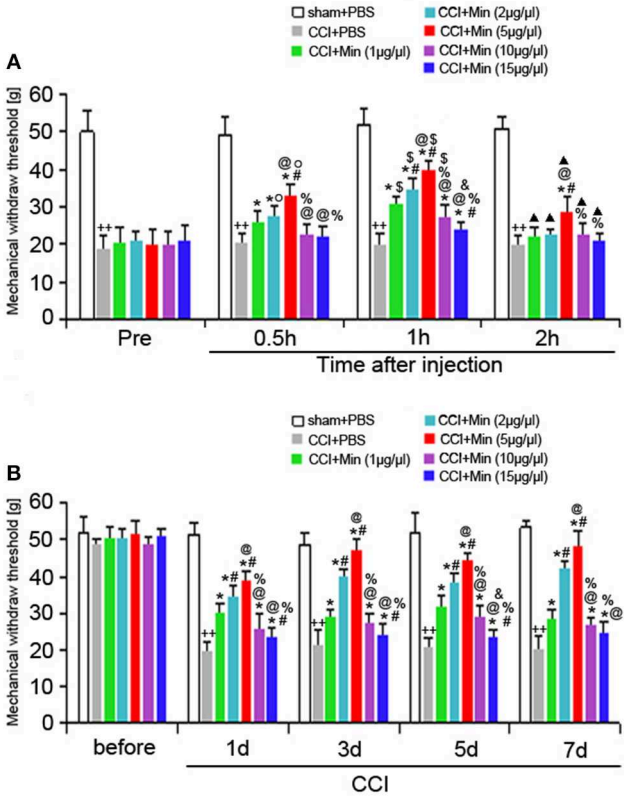

FIGURE 1 | MWT was determined in different groups. All values represent mean ± SD ($n = 8$). **(A)** Decreased MWT was exhibited in the CCI rats on day 1 after surgery compared to sham rats ($^{++}P < 0.01$). Compared with CCI rats, minocycline (1, 2, 5, 10, and 15 μg/μl) treatment exerted anti-hyperalgesic effects ($^{*}P < 0.05$). Minocycline treatment showed obvious increased MWT (vs. 1 μg/μl: $^{\#}P < 0.05$; vs. 2 μg/μl: $^{@}P < 0.05$; vs. 5 μg/μl: $^{\%}P < 0.05$; vs. 10 μg/μl: $^{\&}P < 0.05$). Greater analgesic effect of minocycline occurs 1 h after its administration (vs. Pre: $^{\circ}P < 0.05$; vs. 30 min: $^{\$}P < 0.05$; vs. 1 h: $^{\blacktriangle}P < 0.05$); **(B)** The MWT was measured at 1, 3, 5, and 7 days after surgery. Decreased MWT was exhibited in the CCI rats on days 1, 3, 5, and 7 after nerve injury compared to sham rats ($^{++}P < 0.01$). Compared with CCI rats, minocycline (1, 2, 5, 10, and 15 μg/μl) treatment exerted anti-hyperalgesic effects ($^{*}P < 0.05$). Minocycline treatment showed the more obvious increase in MWT (vs. 1 μg/μl: $^{\#}P < 0.05$; vs. 2 μg/μl: $^{@}P < 0.05$; vs. 5 μg/μl: $^{\%}P < 0.05$; vs. 10 μg/μl: $^{\&}P < 0.05$).

group. Among them, 613 genes were increased and 177 were decreased (as shown in **Figure 2A** and **Table S1**). There were 840 DEGs between the CCI group and minocycline-treated group, among them 143 genes were increased and 697 were decreased (as shown in **Figure 2B** and **Table S2**). Between the sham group vs. CCI group and minocycline-treated group vs. CCI group, 448 DEGs were shared (as shown in **Figure 2D** and **Table S3**). Among these 448 DEGs, 398 transcripts were characterized by an increase in mRNA abundance after nerve injury, and minocycline application decreased the level of these changes. Only 34 transcripts were characterized by a decrease in mRNA after nerve injury, and minocycline treatment reversed the decrease in hippocampus of CCI rats (as shown in **Table S3**). It seems that these 432 genes may be associated with the effect of minocycline in CCI rats. In addition, only two transcripts were upregulated in CCI and upregulated by minocycline. Fourteen transcripts were downregulated in CCI and downregulated by minocycline. We also found that there were 766 DEGs between the sham group and the minocycline-treated group. Among them 342 genes were increased and 424 were decreased (as shown in **Figure 2C** and **Table S4**). Between the sham group vs. CCI group and sham group vs. minocycline-treated group, 252 DEGs were shared, among them 86 genes were increased and 166 were decreased (as shown in **Figure 2D** and **Table S5**).

Differential Expression Analysis at the Gene Ontology Annotation Level

The DEGs were annotated covering molecular biological function, cellular component and biological process. As shown in **Figure 3**, the DEGs in the sham, CCI and minocycline-treated groups can be mostly classified into biological processes. The five most enriched GO terms of the DEGs for biological process were the cellular process, biological regulation, regulation of biological process, response to stimulus, and metabolic process. The five most enriched GO terms of the DEGs for the cellular component were cell, cell part, organelle, membrane, and membrane part. The five most enriched GO terms of the DEGs for molecular function were binding, catalytic activity, signal transducer activity and molecular function regulator. Compared with the sham group, the differentially expressed annotated genes in biological process, molecular function, and cellular component were mainly increased in CCI rats (**Figure 3A**). As far as the minocycline-treated and CCI groups were concerned, the differentially expressed annotated genes in biological process, molecular function, and cellular component were mainly decreased in the minocycline-treated group (**Figure 3B**). As a result, as shown in **Figure 3C**, between sham and minocycline-treated group, the numbers of DEGs in biological process, molecular function, and cellular component are decreased.

KEGG Pathway Analysis of Differentially Expressed Genes

Compared with the sham-operated group, the CCI group had 20 differential gene-involved significant pathways. DEGs contained in these pathways (top 14) are shown in **Table 2**. Some pathogenic microorganism infection-related pathways (herpes simplex infection, tuberculosis, influenza A, malaria, Pertussis, and Leishmaniasis infection) were also involved in the process. As far as the sham and CCI groups were concerned, the most enriched KEGG pathways were the cytokine-cytokine receptor interaction pathway and the TLR signaling pathway. The cytokine-cytokine receptor interaction pathway was significantly affected, with 31 increased genes and 1 decreased gene involved in the hippocampus of CCI rats. The TLR signaling pathway was significantly affected, with 17 increased genes and 2 decreased genes involved in the hippocampus of CCI rats.

We also noticed that the minocycline-treated group had 20 differential gene-involved significant pathways in comparison with the CCI group. DEGs contained in these pathways (top 14)

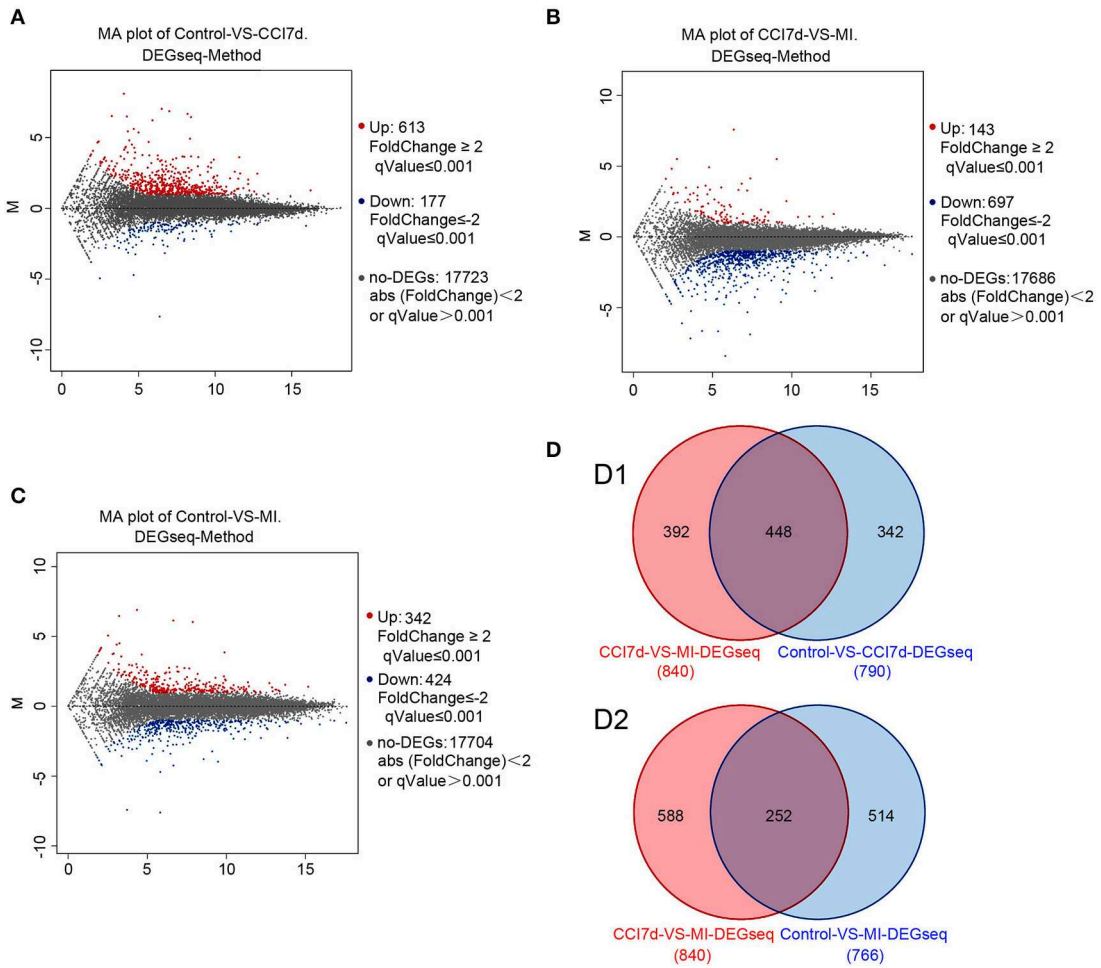

FIGURE 2 | The DEGs were identified. In **(A–C)**, red dots represent increased DEGs and blue dots represent decreased DEGs. In addition, gray dots represent non-DEGs. **(A)** MA plot for DEG analysis between sham and CCI groups. **(B)** MA plot of DEGs among the hippocampus between the CCI and minocycline-treated group. **(C)** MA plot of DEGs among the hippocampus between sham and minocycline-treated group. **(D)** Comparisons of the number and overlapping DEGs between different experimental groups (the Venn diagram of DEGs). (D1) Blue circle represents number of DEGs between sham and CCI group; red circle represents number of DEGs between CCI and minocycline-treated group; the overlapping area represents shared DEGs of two comparable groups. (D2) Blue circle represents number of DEGs between sham group and minocycline-treated group; red circle represents number of DEGs between CCI group and minocycline-treated group; the overlapping area represents shared DEGs of two comparable groups.

are also shown in **Table 2**. These results reveal that minocycline administration can regulate the expression of genes in these pathways, and reversing the gene expression changes in these pathways may be considered as one of the important mechanisms of minocycline against CCI-induced neuropathic pain. Some pathogenic microorganism infection-related pathways were also significantly downregulated. As far as the CCI and minocycline-treated groups were concerned, the most enriched KEGG pathways were the cytokine-cytokine receptor interaction pathway and the TLR signaling pathway. Among them, the cytokine-cytokine receptor interaction pathway was obviously affected, with 33 decreased genes involved. The TLR signaling pathway was significantly affected, with 16 decreased genes and 2 increased genes involved in the hippocampus of minocycline-treated CCI rats.

mRNA Expression Profile of Inflammation-Related Genes in Rat Hippocampus

Cytokines and chemokines were originally identified as essential mediators for inflammatory and immune responses in the formation of neuropathic pain (White and Wilson, 2008; Totsch and Sorge, 2017). As shown in **Table 3**, in the rat hippocampus, higher transcript levels of Cxcl13, Cxcl1, Ccl2, Cxcl11, Ccl7, Ccl20, Ccl3, Ccl6, Ccl5, and Cxcl16 (Top 10 upregulated chemokine genes) were found in the CCI group as compared with sham rats. Except for Cxcl1, this upregulation of chemokine genes was almost diminished after repeated treatment with minocycline. We noticed that pro-inflammatory biomarker Il1β and iNOS are robustly upregulated at the transcriptional level after nerve injury. After minocycline treatment, iNOS and

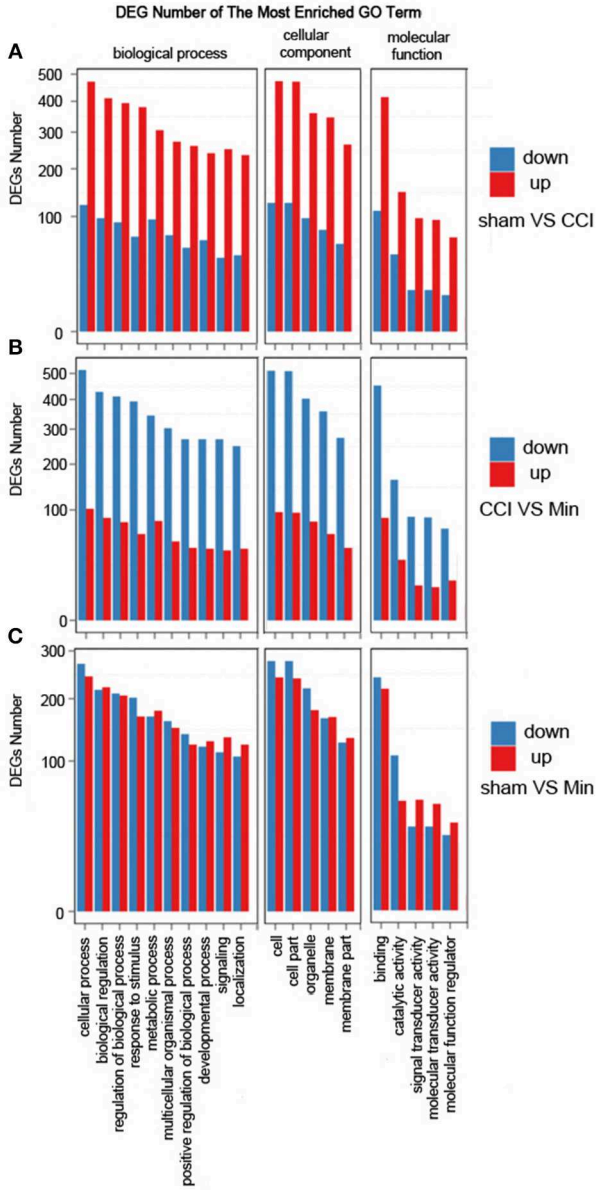

FIGURE 3 | GO term classification of increased and decreased genes on DEGs for each pairwise. X axis represents GO term. Y axis represents the number of increased/decreased genes. **(A)** The most enriched GO terms between the sham and CCI groups. **(B)** The most enriched GO terms between the CCI and minocycline-treated groups. **(C)** The most enriched GO terms between the sham and minocycline-treated groups.

Il1β were obviously downregulated as compared with CCI rats. Il-18rap (rCG22315) transcript was also upregulated in the hippocampus, and minocycline suppressed upregulation in CCI rats.

In addition, cytokine signaling-3 ($SOCS_3$) and TLR gene transcripts were upregulated in the hippocampus, and minocycline suppressed the upregulation of SOCSs and Tlr8, Tlr1, Tlr13, Tlr7, Tlr2, and Tlr9 gene transcripts in CCI rats. We found that, after nerve injury, Tlr4 transcripts were only upregulated by <1 fold (Tlr4: fold = 0.56, FDR = 0.0167). The Tnf-α and Nlrp3 transcripts were upregulated by >1 fold (Tnf-α: fold = 1.492, FDR = 0.037; Nlrp3: fold = 1.21, FDR = 4.18E-23) in the hippocampus of CCI rats. Moreover, the upregulated Tnf-α and Nlrp3 gene transcripts were only moderately suppressed by minocycline (Tnf-α: fold = 0.469, FDR = 0.275; Nlrp3: fold = 0.79, FDR = 5.55E-12). Besides, Nlrp1a gene transcripts were only slightly upregulated (Nlrp1a: fold = 0.29, FDR = 0.007). For these reasons, the changes of Tnf-α, Tlr4, and Nlrp gene transcripts are not listed in **Table 3**. At last, we noted that C3, Ptges, Mt1, Il20rb, Il21r, Il2rb, Hpgds, Il1r1, Tlr8, Card11, P2ry6, Casp4, Fas, and Tifab were upregulated in the CCI group as compared with sham rats. Afterward, the upregulation of these gene transcripts was almost diminished after repeated treatment with minocycline.

More studies have suggested that Cd68, Iba-1 (ionized calcium-binding adaptor molecule-1, involved in microglial motility), Ox-42 (Cd11b, involved in microglial plasticity and motility), Msr-1(macrophage scavenger receptor 1, involved in phagocytosis), and Mhc-II (major histocompatibility complex II) are common markers of microglia activation (Booth and Thomas, 1991; Minett et al., 2016). As shown in **Table 3**, we found that, compared with sham rats, the Cd68, Msr-1, and Iba-1 transcripts were upregulated by >1 fold in hippocampus of CCI rats. After repeated treatment with minocycline, the Cd68, Msr-1, and Iba-1 transcripts were all obviously downregulated by >1 fold as compared with CCI rats. To our surprise, the Cd11b transcripts were upregulated by <1 fold (fold = 0.72, FDR = 9.34E-30) as compared with sham rats. Moreover, after minocycline treatment, the Cd11b transcripts were only downregulated by <1 fold (fold = 0.55, FDR = 7.70E-19) as compared with CCI rats.

It is clear that microglia/macrophages respond to acute brain injury by becoming activated and developing a pro-inflammatory profile of M1-like or anti-inflammatory profile of M2-like phenotypes (Perego et al., 2013; Luo et al., 2018). According to previous studies, M1 polarization could be determined by the expression levels of Cd86, as well as Il1β, Ccl2, Ccl3, and iNOS. M2 polarization could be ascertained by the increased expression of Arg1, Tgfβ1 (transforming growth factor beta 1), and Il4rα (Pusic et al., 2014; Wu et al., 2014; Ji et al., 2018; Luo et al., 2018). Cd206 (mannose receptor 1, Mrc1) is present in M1 and M2a microglia (Pusic et al., 2014; Wu et al., 2014; Ji et al., 2018; Luo et al., 2018). We noticed that peripheral nerve injury increased the expression of Cd86, Il1β, iNos, Ptges, Ccl2, Ccl3, and Mrc-1. At the same time, we also observed the increased expression of Tgfβ1, Il4rα, and Socs3. However, the expression of Arg1, another M2 marker, is decreased. It appears that minocycline obviously inhibits M1 activation (decreased expression of Cd86, Il1β, iNos, Ptges, and Mrc-1), thus reducing production of cytokines including Il1β, NO, PGs, Ccl2, and Ccl3 in CCI rats. On the other hand, as shown in **Table 3**, we found that, compared with sham rats, the Tgfβ1 and Il4rα transcripts were upregulated >1 fold (Tgfβ1: fold = 1.16, FDR = 2.58 E-49; Il4rα: fold = 1.03, FDR = 5.18 E-70) in the hippocampus of CCI rats. After repeated treatment with minocycline, the Tgfβ1 and IL4rα transcripts were downregulated by <1 fold as compared

TABLE 2 | The top 14 most significant KEGG pathways identified with increased and decreased genes among different groups.

Pathway (FDR ≤ 0.01)	CCI group vs. sham group	Minocycline-treated group vs. CCI group
Cytokine-cytokine receptor interaction	**Increased:** Cxcl11, Cxcl13, Cxcl16, Cxcl4, Ccl2, Ccl3, Ccl7, Ccl5, Ccr2, Ccr5, Osmr, Csf3, Csf3r, Il4r, Il13ra1, Csf2rb, Il2ra, Il2rb, Il2rg, Csf1r, Il10rb, IL20rb, Sf1b, Sf1a, Sf14, Fas, Cd40, Tgfβ1, Il1β, Il1r1, Il18r, Ap **Decreased:** Tnfsf15	**Decreased:** Il8ra, Cxcr3, Cxcl11, Cxcl13, Cxcl16, Cxcl4, Ccr7, Ccl2, Ccl3, Ccl5, Ccl7, Osmr, Bsf3, Csf3, Csf2rb, Il2rb, Il2ra, Il2rg, Il4r, Il21r, Il10ra, Il20rb, Ltb, Sf1b, Sf1a, Sf14, Fas, Sf9, Tnfsf4, Tnfsf13b, Il-1b, Il1r1, Il18rap
Toll-like receptor signaling pathway	**Increased:** Tlr1, Tlr2, Tlr6, Md2, P13k, Tlr7. Tlr9, Trif, Opn, Tp12, Il1β, Rantes, Mip1α, Cd40, Cd86, Itac **Decreased:** Mkk3,Irf7	**Increased:** Mkk3, Mkk6 **Decreased:** Lbp, Tlr1, Tlr2, Tlr6, Cd14, Md-2, Tlr7, Tlr8, Tlr9, Tab1, Iκbα, Il-1β, Ccl5, Mip-1α, Cd86, I-Tac
Phagosome	**Increased:** Mhcl, MhcII, Fcyr, Ic3b, collectins, Tlr2, Cd14, Tlr6, Mr, Dectin1, Sra1, Tuba, Tubb, Cyba, Nox1, Ncf1, Ncf2, Ncf4, **Decreased:** Tap, Stx7	**Increased:** Stx7 **Decreased:** Mhcl, MhcII, Tuba, Tubb, M6pr, Fcyr, C3, Tsp, Tlr2, Tlr6, Cd14, Mr, Dectin1, Sra1, P22phox, Gp91, P67phox, P40phox
Fc gamma R-mediated Phagocytosis	**Increased:** Fcgr2b, Cd45, Src, Lat, Pi3k, Fcyri, Fcgr2a, Plcy, Sphk, Cpkc, Ncf1, Wasp, Arpc5, Vav, Rac, Dock2, Pag3 **Decreased:** Crk	**Increased:** CrkII **Decreased:** Fcgr2b, Cd45, Fcyri, FcyrIIa, Src,Pld, Vav, CrkII, Sphk,Rac, Pag3, Wasp, Arp2, Arp3, Gsn
TNF signaling pathway	**Increased:** Tnfr1, Ciap1/2, Tp12, Rip3, Mlkl, Ccl2, Ccl5, Cxcl1, Cxcl2, Cxcl3, Fas, Il1β, Bcl3, Socs3, Ifi47, Tnfr2 **Decreased:** Mkk3	**Increased:** Mkk3, Mkk6 **Decreased:** Tnfr1, Ciap1, Ciap2, Tab1, Tab2, Tab3, Iκba, C/ebpb, Rip3, Mlkl, Ccl2, Ccl5, Cxc11, Cxc12, Cxc13, Fas, Il-1β, Bcl3, Nfkbia, Socs3, Ifl47, Icam1, Tnfr2,
Complement and coagulation cascades	**Increased:** Tfpi, F10, Vwf, Par3, A2m, Pai, C3, Fd, Fb, C1qrs, C1inh, Mbl, C2, C4, C6, Cr4, C5ar1 **Decreased:** Klkb1, Tfpi, Fh	**Increased:** F5, Fh, A2m, Fga **Decreased:** F10, Par3, Par4, A2m, Pai, Upar, Bdkrb1, Bdkrb2, Cfi, Cfb, Cfd, C3, C6, C7, C8,C9, C1qa, C1inh C2, C4, C3ar1, Cr4, C5ar1
Cell adhesion molecules	**Increased:** Cd86, MhcII, Mhcl, Pvrl2, Cd40, Itgal, Cd2, Cd4, Cd8, Cd6, Ptprc, Selp, Sell, Sdc, Pvrl1 **Decreased:** Cntnap2, Mpz, Mhc1	**Increased:** Cldn, Cdh2, Cdh41 **Decreased:** Cd2, Cd86, Icos, MhcII, Mhcl, Cd8, Cd6. Itgal, Icam3, PtprC, Selp, Icam1, Icam2, Ngl1, Sdc, Mag
Natural killer cell mediated cytotoxicity	**Increased:** Bid, Fas, Trailr, Itgal, Shp1, Dap12, Fcer1y, FcyrIII, Nkp30, Lat, Vav, Rac, Pi3k, Plcy, Pkc	**Increased:** Rae-1 **Decreased:** Icam1, Icam2, Trailr, Fas, Itgal, FcyrIII, Shp-1, Dap-12, Fcer1g, Sap, Vav, Rac
NF-κB signaling pathway	**Increased:** Il1β, Il1r, Lyn, Lat, Btk, Plcy2, Cd14, Md2, Cd40, Trif, Ciap1/2, Carma, Bcl2a1, Baff	**Decreased:** Il1β, Il-1r, Tnf-r1, Lbp, Cd14, Md-2, Ltb, Baff, Btk, Ciap1, Ciap2, Tab, Carma, Iκbα, Il1β, Icam
Chemokine signaling pathway	**Increased:** Ac, Chemokine, Cxcr2, Gnb1, Src, Pi3k, Dock2, Rac, Vav, Wasp, Ncf1 **Decreased:** Ac, Gnb1, Crk	**Increased:** Gnb1, Crk **Decreased:** Gro, Cxcr2, Gnb1, Src, Vav, Crk,Rac, Wasp, Iκb
Osteoclast differentiation	**Increased:** Ii-1, Tgfb, Il-1r, Tnfr1, Oscar, Fcry, Dap12, Btk, Socs1, Plcy, Pi3k, Nadph, Spi1	**Decreased:** Ii-1, Il-1r, Tnfr1, Oscar, Fcry, Dap12, Btk, Socs1, Socs3, Tab1, Tab2, Nadph, Iκb, Spl1
B cell receptor signaling pathway	**Increased:** Cd72, Shp1, Lyn, Btk, FcgrIIb, Leu13, Vav, Plc-y2, Calma, Rac, Pi3k **Decreased:** Bam32	**Decreased:** Iga, Cd72, Shp1, Fcgr2b, Leu13, Btk, Vav, Rac, Card11, Iκb
Primary immunodeficiency	**Increased:** Yc, Btk, Cd45, Cd4, Cd8, Cd8α, CIIta, Cd40 **Decreased:** Tap2,Rfxap	**Decreased:** Cd3e, Il2rg, Iga, Btk, Cd45, Cd4, Cd8, Rfxap, CIIta, Cd8a, Rfxap, CIIta, Icos
Platelet activation	**Increased:** Collagen, Vwf, Par1, Fcry, Lyn, Pi3k, Btk, Plcy2, Ac, Kind3, Fcgr2a, Tbxas **Decreased:** Ac,Collagen	**Increased:** Col1a,Fg **Decreased:** CIl1a, Par1, Par4, P2x1, Fcry, Pi3k, Btk, Tbxas1, Fermt3, Fcgr2a

with CCI rats. Compared with sham rats, the Arg1 transcripts were downregulated by >1 fold in the hippocampus of CCI rats. Treatment with minocycline only slightly upregulated the transcriptional level of Arg1.

It is well known that some transcription factors have been shown to be directly or indirectly associated with the expression of inflammation-related cytokine genes. Compared with the sham group, the upregulated transcription factor genes were maff, Elf4, Nr2f2, Vgl13, Lst1, Runx3, Tfec, Sp5, Nfkbiz, Hlx, Spi1 (Pu.1), Fli1, Batf3, and Pax-1. Among them, we would like to mention that the levels of gene transcripts of Runx3, Tfec, Sp5, Nfkbiz, Hlx, Spi1, Fli1, Batf3, and Pax-1 were largely suppressed by minocycline. It is noteworthy that gene transcripts of Tfec, Nfkbiz, Hlx, Spil, Fli1, and Batf3 and Pax-1 were obviously increased in the CCI group compared with those of sham rats, and the expression of these genes returned to normal level after minocycline administration. On the other hand, as shown in **Table 3**, we found that, compared with sham rats, the Maff, Elf4, Vgl13, and Nr2f2 transcripts were upregulated by >1 fold in the hippocampus of CCI rats. After repeated treatment with minocycline, the Maff, Elf4, Vgl13, and Nr2f2 transcripts were slightly downregulated by <1 fold as compared with CCI rats. In addition, compared with sham rats, the Cartpt, Six3, Meox1, Tfap-2c, Ebf3, Mkx, and Mei4 transcripts were downregulated by >1 fold in the hippocampus of CCI rats. Among these transcripts, the Meox1 were obviously reversed by

TABLE 3 | mRNA expression profile of inflammation-related genes among different groups.

Gene symbol	Sham vs. CCI		CCI vs. minocycline		Sham vs. minocycline	
	Fold change	FDR	Fold change	FDR	Fold change	FDR
Cxcl13	+7.03	7.02E-236	−8.42	2.75 E-207	−1.39	0.13
Cxcl1	+5.44	2.07E-31	−1.87	1.75 E-13	+3.57	2.18E-08
Ccl2	+5.35	1.35E-48	−6.65	1.77 E-47	−1.30	0.26
Cxcl11	+4.80	2.95E-26	−4.45	2.75 E-25	+0.35	0.72
Ccl7	+4.27	1.02E-17	−7.25	4.73E-18	0	0
Ccl20	+3.46	0.003003	−3.44	0.0029	0.02	0.99
Ccl3	+2.40	0.000603	−3.38	4.47 E-05	−0.98	0.42
Ccl6	+2.22	3.47E-12	−3.20	2.39 E-17	−0.98	0.07
Ccl5	+1.61	3.03E-07	−3.48	6.45 E-16	−1.87	0
Cxcl16	+1.27	6.02E-31	−1.88	1.70 E-53	−0.61	5.23E-05
INos	+5.46	2.72E-06	−5.44	2.67 E-06	0	0
Il1β	+4.34	9.98E-19	−3.15	4.47E-15	+1.19	0.15
Il18rap	+4.13	6.00 E-16	−6.11	2.35 E-17	−1.98	0.17
Socs3	+3.67	2.94 E-243	−3.08	5.23E-209	+0.58	0
C3	+3.61	0	−3.83	0	−0.22	0
Tlr8	+3.49	1.05E-11	−4.20	4.72 E-13	−0.71	0.49
Ptges	+3.47	4.28E-49	−2.48	2.02 E-35	+0.99	0
Mt1	+2.15	4.94E-228	−1.81	5.21E-181	+0.34	0
Il20rb	+2.08	1.32 E-18	−1.11	3.61 E-08	+0.97	0
Tlr1	+1.93	1.91E-09	−2.12	1.57 E-10	−0.18	0.66
Il21r	+1.92	1.10E-18	−2.01	1.21 E-19	−0.09	0.77
Il2rb	+1.69	2.99 E-06	−1.78	1.14 E-16	−0.10	0.84
Tnfrsf1b	+1.66	5.44E-32	−1.20	6.16 E-20	+0.46	0.01
Hpgds	+1.64	1.35E-07	−1.56	3.59 E-07	+0.08	0.84
Tlr13	+1.61	8.94E-20	−1.37	1.03 E-15	+0.24	0.27
I11r1	+1.48	8.55E-62	−1.15	6.06 E-42	+0.32	0
Irf8	+1.57	7.14E-85	−1.35	5.28 E-27	+0.23	0.03
Card11	+1.49	1.38E-28	−1.65	9.27 E-33	−0.16	0.36
P2ry6	+1.49	4.35E-44	−1.33	8.20 E-37	+0.17	0.21
Tlr7	+1.48	7.32E-34	−1.15	4.02 E-23	+0.33	0.02
Casp4	+1.38	3.52E-14	−1.34	1.52 E-13	+0.04	0.86
Fas	+1.22	1.79E-05	−1.37	2.68 E-06	−0.15	0.68
Tlr2	+1.06	1.61E-19	−1.05	3.82 E-19	+0.10	0.94
Tlr9	+1.06	0.0001	−1.65	8.08 E-08	−0.60	0.10
Tifab	+1.01	8.91 E-29	−1.05	4.44 E-30	−0.03	0.76
Cd68	+3.45	9.91E-95	−2.90	1.19E-80	+0.54	0.05
Msr-1	+2.01	7.93E-21	−1.94	7.27 E-20	0.07	0.82
Iba-1	+1.16	3.94E-46	−1.16	1.28E-45	0	0.98
Ox-42 (Cd11b)	+0.72	9.34E-30	−0.55	7.70E-19	+0.17	0.01
Ptges	+3.47	4.28E-49	−2.48	2.02 E-35	+0.99	0.01
Mrc1	+2.85	4.43 E-129	−2.71	6.94 E-122	+0.13	0.48
Cd86	+1.46	1.41E-07	−1.86	3.20 E-10	−0.41	0.27
Tgfβ1	+1.16	2.58 E-49	−0.96	4.06E-36	+0.20	0.03
Arg1	−1.06	8.19 E-17	+0.43	0	−0.62	5.18E-08
IL4r	+1.03	5.18 E-70	−0.14	0	+0.90	3.18E-51
Runx3	+6.39	7.42 E-11	−3.79	1.51 E-09	0	0
Tfec	+3.95	5.47 E-17	−5.25	7.13 E-19	−1.30	0.26
Pax-1	+3.70	0.0009	−4.68	0.0004	0	0
Batf3	+2.67	0.0005	−1.03	4.69 E-08	−0.11	0.62
Sp5	+2.17	6.15 E-06	−1.42	0.00076	+0.76	0.20
Hlx	+1.58	9.94 E-28	−1.26	1.85 E-11	+0.32	0.18
Nfkbiz	+1.46	9.25E-28	−2.02	1.12 E-42	−0.56	0
Spi1 (Pu.1)	+1.33	2.57E-34	−1.19	1.12 E-28	+0.15	0.27

(Continued)

TABLE 3 | Continued

Gene symbol	Sham vs. CCI		CCI vs. minocycline		Sham vs. minocycline	
	Fold change	FDR	Fold change	FDR	Fold change	FDR
Fli1	+1.21	3.04 E-35	−1.11	1.33 E-30	+0.10	0.39
Lst1	+2.39	0.0001	−1.29	0.01	+1.10	0.14
Maff	+1.67	1.72 E-09	−0.45	0.04	+1.23	2.50E-05
Elf4	+1.39	6.46 E-11	−0.95	1.93E-06	+0.45	0.07
Vgl13	+1.38	3.40 E-51	+0.66	2.52E-24	+2.04	2.25E-140
Nr2f2	+1.12	2.89 E-144	+0.59	1.82E-71	+1.72	0
Cartpt	−2.30	2.14 E-70	+0.17	0.23	−2.13	0
Six3	−1.68	6.84 E-06	−0.57	0.20	−2.25	1.48E-08
Meox1	−1.64	7.13 E-05	+1.11	0.01	−0.53	0.10
Tfap-2c	−1.55	1.84 E-05	+0.28	0.31	−1.27	0
Ebf3	−1.40	2.05 E-05	−0.44	0.22	−1.84	7.32E-08
Mkx	−1.12	2.27 E-08	−0.003	0.49	−1.12	7.17E-09
Mei4	−1.00	2.91 E-05	+0.09	0.4	−0.91	6.09E-05

Cxcl13, C-X-C motif chemokine ligand 13; Cxcl1, C-X-C motif chemokine ligand 1; Ccl2, C-C motif chemokine ligand 2; Cxcl11, C-X-C motif chemokine ligand 11; Ccl7, C-C motif chemokine ligand 7; Ccl20, C-C motif chemokine ligand 20; Ccl3, C-C motif chemokine ligand 3; Ccl6, C-C motif chemokine ligand 6; Ccl5, C-C motif chemokine ligand 5; Cxcl16, C-X-C motif chemokine ligand 16; Nos, nitric oxide synthase 2; Il1β, interleukin 1 beta; Il18rap, interleukin 18 receptor accessory protein; Socs3, suppressor of cytokine signaling 3; C3, complement C3; Tlr8, toll-like receptor 8; Ptges, prostaglandin E synthase; Mt1, metallothionein 1; Il20rb, interleukin 20 receptor subunit beta; Tlr1, toll-like receptor 1; Il21r, interleukin 21 receptor; Il2rb, interleukin 2 receptor subunit beta; Tnfrsf1b, TNF receptor superfamily member 1B; Hpgds, hematopoietic prostaglandin D synthase; Tlr13, toll-like receptor 13; Il1r1, interleukin 1 receptor type 1; Irf8, interferon regulatory factor 8; Card11, caspase recruitment domain family, member 11; P2ry6, pyrimidinergic receptor P2Y6; Tlr7, toll-like receptor 7; Casp4, caspase 4; Fas, Fas cell surface death receptor; Tlr2, toll-like receptor 2; Tlr9, toll-like receptor 9; Tifab, TIFA inhibitor; Cd68, Cd68 molecule; Msr-1, macrophage scavenger receptor 1; Iba-1, ionized calcium binding adaptor molecule 1; Cd11b, Complement receptor 3; Mrc1, mannose receptor, C type 1; Cd86, CD86 molecule; Tgfβ1, transforming growth factor, beta 1; Arg1, arginase 1; IL4rα, interleukin 4 receptor; Runx3, runt-related transcription factor 3; Pax-1, paired box 1; Batf3, basic leucine zipper ATF-like transcription factor 3; Sp5, Sp5 transcription factor; Hlx, H2.0-like homeobox; Nfkbiz, NFKB inhibitor zeta; Spi1, Spi-1 proto-oncogene; Fli1, Fli-1 proto-oncogene; Lst1, leukocyte specific transcript 1; Maff, MAF bZIP transcription factor F; Elf4, E74 like ETS transcription factor 4; Vgl13, vestigial-like family member 3; Nr2f2, nuclear receptor subfamily 2; Cartpt, CART prepropeptide; Six3, SIX homeobox 3; Meox1, mesenchyme homeobox 1; Tfap-2c, transcription factor AP-2 gamma; Ebf3, EBF transcription factor 3; Mkx, mohawk homeobox; Mei4, meiotic double-stranded break formation protein 4).

minocycline by >1 fold in the hippocampus of minocycline-treated CCI rats. However, the Cartpt, Six3, Tfap-2c, Ebf3, mkx, and Mei4 transcripts were not obviously reversed by <1 fold in minocycline-treated CCI rats. Individual genes in each category are listed below:

1) only upregulated in CCI rats: Maff, Elf4, Nr2f2, Vgl13, Lst1;
2) only downregulated in CCI rats: Cartpt, Six3, Ap-2c, Ebf3, Mei4;
3) upregulated in CCI and downregulated by minocycline: Runx3, Tfec, Sp5, Nfkbiz, Hlx, Spi1 (Pu.1), Fli1, Batf3, Pax-1; and
4) downregulated in CCI and upregulated by minocycline: Meox1.

Validation of Microarray Results

Many of the genes that were identified by microarray analysis should be subject to validation by RT-PCR. As shown in **Figure 4**, we observed that there has been a tacit agreement between the microarray and the PCR gene expression data in terms of changes in both magnitude and direction. The PCR data show that CCI induced the increased expression of cytokines (CXCL13, CXCL1, CCL2, CXCL11, CCL7, and CCL20), TLRs (TLR8 and TLR1), Iba-1 and M1 polarization markers (Cd68, iNOS, IL-1β), and transcription factors (Runx3, Nfkbiz, and Spil). The administration of minocycline did not change the expression of these inflammation-related genes in sham-operated rats (**Figure 4**). In agreement with the microarray data, minocycline treatment obviously suppressed the elevation in mRNA levels of these genes. Minocycline significantly diminished the upregulated Cd68, iNOS, and Il1β. It appears that transcription factors Runx3, Nfkbiz, and Spil may be involved in the minocycline-mediated analgesic effect and the increased production of inflammation-related cytokines in the hippocampus of neuropathic pain rats. Finally, we found that, between sham and minocycline-treated CCI rats, the expression of the inflammatory-related cytokines (Cxcl13, Ccl2, Cxcl11, Ccl7, and Ccl20), TLRs (Tlr8 and Tlr1), Iba-1 and M1 polarization markers (Cd68, iNOS, and Il1β), and transcription factor (Nfkbiz and Spil) have no statistical significance (**Figure 4**), which imply that, after minocycline treatment, the upregulated gene expression in CCI rats has returned to normal. On the other hand, between sham and minocycline-treated CCI rats, the expression of Cxcl1 and Runx3 was only partly suppressed by minocycline, which implies that these two genes' expression may be only partly modulated by microglia activity.

DISCUSSION

We reported here the hippocampal genome-wide transcriptome profiling of rats in neuropathic pain status to elucidate minocycline-mediated analgesic effect at the molecular level. It is well known that the CCI model of neuropathic pain displays

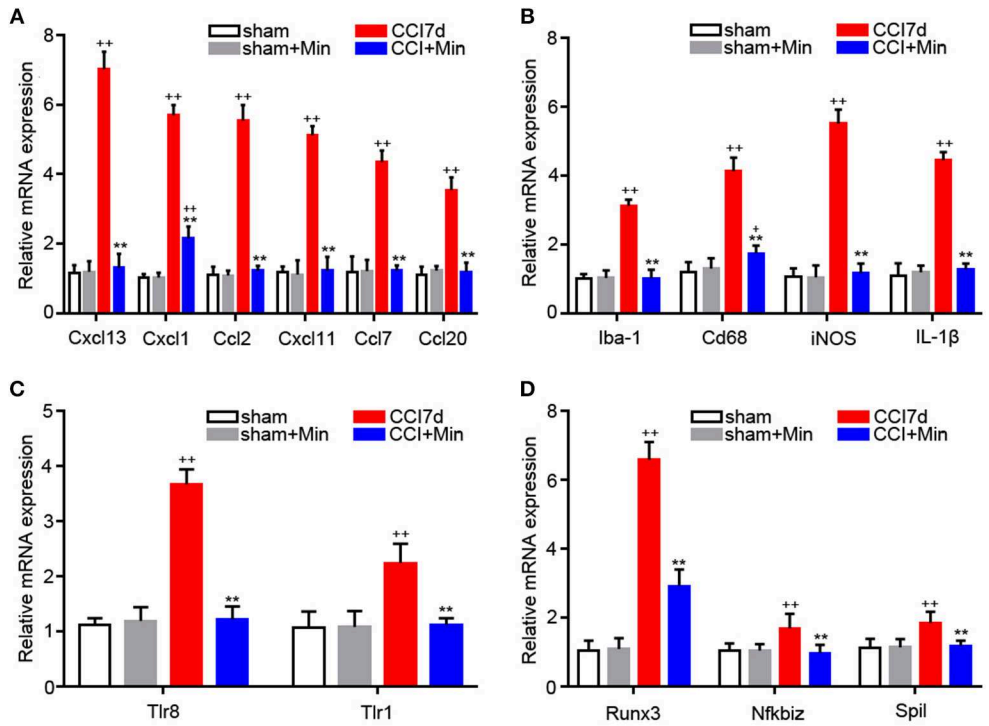

FIGURE 4 | RT-PCR showing the expression of Cxcl13, Cxcl1, Ccl2, Cxcl11, Ccl7, Ccl20, Iba-1, CD68, iNOS, IL-1β, TLR8, TLR1, Runx3, Nfkbiz, and Spil mRNA in the rat hippocampus ($n = 6$). $^{+}P < 0.05$ and $^{++}P < 0.01$, compared with both the sham and sham+Minocyclyne groups; $^{**}P < 0.01$, compared with the CCI 7d group; this applies for all the genes. **(A)** The expression of CXCL13, CXCL1, CCL2, CXCL11, CCL7, CCL20 in the hippocampus. **(B)** The expression of Iba-1, CD68, iNOS, and IL-1β in the hippocampus. **(C)** The expression of TLR8 and TLR1 in the hippocampus. **(D)** The expression of Runx3, Nfkbiz, and Spil in the hippocampus.

some symptoms that are very common in neuropathic pain patients including mechanical and thermal allodynia. Then, we screened the hippocampus of the CCI rats for DEGs.

It has also been proved that minocycline exerts an anti-nociceptive effect in different pain models. Recent studies revealed that the hippocampal CA1 region is more sensitive to ischemic injury and peripheral inflammatory stimulation (Sun et al., 2016; Song et al., 2018). In the present study, CCI operation reduced the threshold of paw withdrawal to a mechanical stimulation. After minocycline treatment, this mechanical allodynia was progressively reduced from 1 to 7 days, which suggests that minocycline reduced pain hypersensitivity by modulating the microglia function within the hippocampus at the early stage of neuropathic pain. On the other hand, it was reported that the onset of depressive-like behavior in CCI animals was 2 weeks following peripheral nerve injury (Xie et al., 2017; Gong et al., 2018). Moreover, minocycline treatment suppressed hippocampal cytokine accumulation and depression-like behaviors in different animal models of chronic pain, such as posttraumatic stress disorder-pain comorbidity (Sun et al., 2016), visceral pain (Zhang et al., 2016), bone Cancer Pain (Dai et al., 2019), and infant nerve injury (Gong et al., 2018). For this reason, we may propose here that minocycline treatment might reduce the risk of nerve injury-induced depression. More studies should be performed to detect the relationship between depression and chronic pain and the effects of minocycline.

We observed that minocycline at 1 μg/μl induced significant analgesic effect in comparison to CCI rats. Minocycline at doses of 2 and 5 μg/μl showed better analgesic effects in comparison to minocycline at a dose of 1 μg/μl. Minocycline at a dose of 5 μg/μl showed apparent elevations of the MWT in comparison with minocycline at a dose of 2 μg/μl. On the other hand, minocycline at 10 μg/μl produced a moderate antinociceptive effect in CCI rats. Minocycline at 15 μg/μl produced a slight but significant nociceptive effect. It seems the minimum dose of minocycline at 5 μg/μl shows the maximum analgesic effect. Recently, several studies also showed the negative action of minocycline in animal or cellular models for nervous system disorders. Similarly to what we observed in CCI rats, Matsukawa et al. also support the idea that neuroprotection is dose-dependent, in that only low doses of minocycline inhibit neuronal cell death cascades at the acute stroke phase, whereas high doses exacerbate ischemic injury (Matsukawa et al., 2009). A low dose of minocycline (25 mg/kg) showed protective effects, with reduced retinal ganglion cell loss and microglial activation, while a high dose of minocycline (100 mg/kg) showed damage effects, with more retinal ganglion cell loss and microglial activation in mice with retinal ischemia-reperfusion injury (Huang et al., 2018). An *in vivo* experiment from Li et al. also showed that intraperitoneal minocycline treatment (45 mg/kg) may induce delayed activation of microglia in aged rats and thus cannot prevent postoperative cognitive dysfunction (Li et al., 2018). For

this reason, although our results do not directly investigate the influence and relevant mechanism of high doses of minocycline (10 and 15 μg/μl) on the neuronal excitability or synaptic strength, the present study suggests the possibility that a high dose of minocycline might regulate cell function in neuronal or non-neuronal cells within the hippocampus of CCI rats. In our experiments, the molecular weight of minocycline hydrochloride was 493.94. Then, 494 μg/μl corresponds to 1 M and 5 μg/μl to 10^4 μM, 10 μg/μl corresponds to 2×10^4 μM and 15 μg/μl corresponds to 3×10^4 μM. Pinkernelle et al. reported that application of 10 μM minocycline (24 h) was deleterious for spinal motor neuron survival (Pinkernelle et al., 2013). Incubation with 50 μM minocycline (24 h) resulted in increased cell metabolic activity in primary glial cultures. Application of 100 μM minocycline inhibited astroglia migration (24 h) and upregulated the elevated Cx43 protein expression (72 h) in rat spinal cord slices (Pinkernelle et al., 2013). A high dose of minocycline attenuated reductions in O1- and O4-positive oligodendrocyte progenitor cells and myelin content in hypoxia-ischemia-induced neuroinflammation and white matter injury in rats (Carty et al., 2008). However, we also noticed that 10 and 15 μg/μl showed poor analgesic effects within 2 h after minocycline treatment. A study on the protective effect of minocycline on ischemic stroke from Matsukawa et al. indicated that 75 min incubation with 10 μM minocycline induced increased Bcl-2 protein expression in striatum neurons. Moreover, application of 10 or 100 μM minocycline for 4 h displayed toxicity to both neurons and astrocytes in the striatum (Matsukawa et al., 2009). We also noticed that minocycline (30 min, 1 h, and 2 h after its injection) at doses of 10 and 15 μg/μl showed poor analgesic effects in comparison with minocycline at a dose of 5 μg/μl, and the poor effect was sustained for 7 days. It seems that the adverse effects of minocycline on neurons or non-neuronal cells may have occurred in a short period of time. Of course, the influence of different doses of minocycline on neurons or non-neuronal cells in the hippocampus remains to be further studied.

We found that, in the sham group vs. CCI group and minocycline-treated group vs. CCI group, the top 2 items of KEGG pathway are cytokine-cytokine receptor interaction and TLR pathway, which indicates that minocycline administration can regulate the expression of genes in these two pathways, and reversing these gene expression changes may be considered as one of the important reasons for minocycline-mediated analgesic effect. Nerve damage leads to glial activation and thus facilitates the production and release of pronociceptive factors such as interleukins and chemokines from glial cells. We noticed that, after sciatic nerve injury, IL-1β was the most striking interleukin that increased most seriously in hippocampus of CCI rats. Moreover, the increased gene expression of CXCL13, CXCL1, CCL2, CXCL11, and CCL7 in the rat hippocampus was observed after nerve damage. The increased chemokine expression was obviously suppressed by intra-hippocampal injection of minocycline. It appears that minocycline was able to reduce microglia activity efficiently, which led to the decreased expression of these genes. In addition, the increased expression of interleukins and chemokines should be regulated by some transcription factors. For example, the elevated expression of IL-1β was associated with binding of transcription factor Spil/Pu.1 to IL-1β promoter in activated inflammatory macrophage (Vanoni et al., 2017). Spil/Pu.1 can also bind to the CCL2 promoter and stimulate its expression (Sarma et al., 2014). Runx3 knockdown can induce the downregulation of CXCL11 in lung cancer cells (Kim et al., 2015). IκBz can function as a transcriptional activator of CXCL1 and CCL2, which are involved in inflammatory responses (Hildebrand et al., 2013; Brennenstuhl et al., 2015). Similarly, we also found that, compared to sham rats, IL-1β, CXCL1, CXCL11, CCL2, and transcription factor (Spil/Pu.1, Runx3, and IκBz) are obviously elevated at 7 days following nerve injury. After treatment with minocycline, these interleukins and chemokines and transcription factor were obviously decreased. It seems that the increased expression of interleukins and chemokines may be regulated by these transcription factors in the rat hippocampus after nerve injury.

In addition, nerve injury evoked the elevated expression of many different kinds of TLRs (TLR8, TLR1, TLR13, TLR7, TLR2, and TLR9) in the rat hippocampus. After treatment with minocycline, the elevated expression of these TLRs in the hippocampus was significantly lower compared to the CCI group. More recent studies suggest that TLRs play an important role in immune response by producing inflammatory cytokines and chemokines under pathological conditions. For example, TLR1, TLR2, TLR7, and TLR9 activation stimulated the production of IL-1β and MCP-1 in B cells (Agrawal and Gupta, 2011). TLR2 activation led to the accumulation of IL-1β and chemokines (CCL7, CCL8, CCL9, CXCL1, CXCL2, CXCL4, and CXCL5) in primary mouse microglial cells (Aravalli et al., 2005). TLR7 and TLR9 stimulation led to the accumulation of IL-1β, CCL2, CCL3, CXCL1, CXCL9, and CXCL10 in mouse brain (Butchi et al., 2011). It is reasonable to speculate that, in the hippocampus of CCI rats, activation of TLR signaling in the hippocampus by peripheral nerve injury may partially participate in the increased expression of these inflammatory cytokines or chemokines.

Some previous studies demonstrate that IκBz can serve as a nuclear inhibitor of NF-κB and is thought to have a key role in inflammatory responses. On the other hand, IκBz is induced quickly in monocytes and macrophages after LPS stimulation (Yamazaki et al., 2001). In the present experiments, the CCI-induced increased expression of IκBz was completely impaired in minocycline-treated CCI rats, suggesting a role for microglia activation in upregulated IκBz expression. It was reported that IκBz is obviously induced in macrophages after TLR or IL-1R stimulation (Hanihara et al., 2013). In chronic lymphocytic leukemia cells, TLR9 activation can lead to the increased IκBz expression and IgM release (Fonte et al., 2017). Inhibition of TLR1/TLR2 signaling suppressed D39-evoked IκBz expression in human monocyte (Sundaram et al., 2016). On the other hand, promoting IκBz degradation inhibits TLR-mediated inflammation and disorders (Hanihara-Tatsuzawa et al., 2014). Similarly, the absence of IκBz obviously suppressed B-cell activation and proliferation after TLR activation (Kimura et al., 2018). We also noted that TLR8, TLR1, TLR13, TLR7, TLR2, TLR9, and IκBz gene expression robustly increased in

the hippocampus, and the expression was obviously impaired in minocycline-treated CCI rats. One possible explanation is that the upregulated IκBz gene expression may be associated with the increased TLR expression. In addition, microglia-mediated inflammatory reaction plays a double role in some nervous diseases due to two distinct phenotypes, including the neurotoxic reactive phenotype (M1) and neuroprotective M2 (Kobayashi et al., 2013; Tang and Le, 2016). In the present study, minocycline inhibits M1 activation, thus leading to decreased expression of inflammatory factors including IL-1β, CCL2, CCL3, and iNOS. Thus, it can be seen that dampening of M1 polarization is another possible mechanism of minocycline-medicated analgesia.

In summary, the DEGs were identified, and many inflammation-related genes including TLRs and chemokines were considered as important genes in the formation of neuropathic pain through pathway analysis of microarray data, which may help us to further understand the underlying molecular mechanisms of chronic pain. After the bioinformatics analysis of gene expression profiles, the expression of inflammation-related genes was further identified via the RT-PCR method. Although the results obtained from our experiments indicate that intra-hippocampal injection of minocycline exerts an analgesic effect and many inflammation-related genes may be involved in the formation of neuropathic pain, the study we conducted also has certain limitations that should be considered in future studies. In other words, further studies are required to further explore the roles of these inflammation-related genes in the hippocampus, where it is implicated in the formation of the neuropathic pain.

DATA AVAILABILITY STATEMENT

Publicly available datasets were analyzed in this study. This data can be found here: https://pan.baidu.com/s/1dZ4ImpqLIEqWkF3gN2llDw.

ETHICS STATEMENT

The protocol was prepared from SD rats in accordance with the National Institutes of Health guidelines in a manner that minimized animal suffering and animal numbers. All experiments were carried out in accordance with China animal welfare legislation and were approved by the Zunyi Medical University Committee on Ethics in the Care and Use of Laboratory Animals.

AUTHOR CONTRIBUTIONS

JZ, YC, and XL: conceived and designed the experiments. LH, RX, and HT: animal experiment. LH and TX: behavioral assessment of pain. LH, RX, YP, and SC: analyzed the data. JZ, LH, and XL: wrote the paper.

FUNDING

This work was supported by the National Natural Science Foundation of China (No. 31860291) and the Program for Major research projects for innovation groups in Guizhou Province [(2018)025].

ACKNOWLEDGMENTS

We are very grateful to the staff of the Department of Physiology, the Department of Pharmacology, and the Department of Clinical Pharmacotherapeutics of School of Pharmacy in Zunyi Medical University.

SUPPLEMENTARY MATERIAL

The Supplementary Material for this article can be found online at: https://www.frontiersin.org/articles/10.3389/fnmol.2019.00248/full#supplementary-material

REFERENCES

Agrawal, S., and Gupta, S. (2011). TLR1/2, TLR7, and TLR9 signals directly activate human peripheral blood naive and memory B cell subsets to produce cytokines, chemokines, and hematopoietic growth factors. *J. Clin. Immunol.* 31, 89–98. doi: 10.1007/s10875-010-9456-8

Al-Amin, H., Sarkis, R., Atweh, S., Jabbur, S., and Saadé, N. (2011). Chronic dizocilpine or apomorphine and development of neuropathy in two animal models II: effects on brain cytokines and neurotrophins. *Exp. Neurol.* 228, 30–40. doi: 10.1016/j.expneurol.2010.11.005

Aravalli, R. N., Hu, S., Rowen, T. N., Palmquist, J. M., and Lokensgard, J. R. (2005). Cutting edge: TLR2-mediated proinflammatory cytokine and chemokine production by microglial cells in response to herpes simplex virus. *J. Immunol.* 175, 4189–4193. doi: 10.4049/jimmunol.175.7.4189

Booth, P. L., and Thomas, W. E. (1991). Evidence for motility and pinocytosis in ramified microglia in tissue culture. *Brain. Res.* 548, 163–171. doi: 10.1016/0006-8993(91)91118-K

Brennenstuhl, H., Armento, A., Braczysnki, A. K., Mittelbronn, M., and Naumann, U. (2015). IκBζ, an atypical member of the inhibitor of nuclear factor kappa B family, is induced by γ-irradiation in glioma cells, regulating cytokine secretion and associated with poor prognosis. *Int. J. Oncol.* 47, 1971–1980. doi: 10.3892/ijo.2015.3159

Butchi, N. B., Woods, T., Du, M., Morgan, T. W., and Peterson, K. E. (2011). TLR7 and TLR9 trigger distinct neuroinflammatory responses in the CNS. *Am. J. Pathol.* 179, 783–794. doi: 10.1016/j.ajpath.2011.04.011

Cartier, L., Hartley, O., Dubois-Dauphin, M., and Krause K H. (2005). Chemokine receptors in the central nervous system: role in brain inflammation and neurodegenerative diseases. *Brain Res. Rev.* 48, 16–42. doi: 10.1016/j.brainresrev.2004.07.021

Carty, M. L., Wixey, J. A., Colditz, P., B., Buller, K. M (2008). Post-insult minocycline treatment attenuates hypoxia-ischemia-induced neuroinflammation and white matter injury in the neonatal rat: a comparison of two different dose regimens. *Int. J. Dev. Neurosci.* 26, 477–485. doi: 10.1016/j.ijdevneu.2008.02.005

Chang, L., Ye, F., Luo, Q., Tao, Y., and Shu, H. (2018). Increased hyperalgesia and proinflammatory cytokines in the spinal cord and dorsal root ganglion after surgery and/or fentanyl administration in rats. *Anesth. Analg.* 126, 289–297. doi: 10.1213/ANE.0000000000002601

Dai, J., Ding, Z., Zhang, J., Xu, W., Guo, Q., Zou, W., et al. (2019). Minocycline relieves depressive-like behaviors in rats with bone cancer

pain by inhibiting microglia activation in hippocampus. *Anesth. Analg.* doi: 10.1213/ANE.0000000000004063. [Epub ahead of print].

Fiore, N T., and Austin, P. J. (2018). Glial-cytokine-neuronal adaptations in the ventral hippocampus of rats with affective behavioral changes following peripheral nerve injury. *Neuroscience* 390, 119–140. doi: 10.1016/j.neuroscience.2018.08.010

Fonte, E., Vilia, M. G., Reverberi, D., Sana, I., Scarfò, L., Ranghetti, P., et al. (2017). Toll-like receptor 9 stimulation can induce IκBζ expression and IgM secretion in chronic lymphocytic leukemia cells. *Haematologica* 102, 1901–1912. doi: 10.3324/haematol.2017.165878

Gong, X., Chen, Y., Chang, J., Huang, Y., Cai, M., and Zhang, M. (2018). Environmental enrichment reduces adolescent anxiety- and depression-like behaviors of rats subjected to infant nerve injury. *J. Neuroinflammation* 15:262. doi: 10.1186/s12974-018-1301-7

Guo, W., Wang, H., Zou, S., Dubner, R., and Ren, K. (2012). Chemokine signaling involving chemokine (C-C motif) ligand 2 plays a role in descending pain facilitation. *Neurosci. Bull.* 28, 193–207. doi: 10.1007/s12264-012-1218-6

Hanihara, F., Takahashi, Y., Okuma, A., Ohba, T., and Muta, T. (2013). Transcriptional and post-transcriptional regulation of IκB-ζ upon engagement of the BCR, TLRs and FcγR. *Int. Immunol.* 25, 531–544. doi: 10.1093/intimm/dxt017

Hanihara-Tatsuzawa, F., Miura, H., Kobayashi, S., Isagawa, T., Okuma, A., Manabe, I., et al. (2014). Control of Toll-like receptor-mediated T cell-independent type 1 antibody responses by the inducible nuclear protein IκB-ζ. *J. Biol. Chem.* 289, 30925–30936. doi: 10.1074/jbc.M114.553230

He, Y., Zhou, A., and Jiang, W. (2013). Toll-like receptor 4-mediated signaling participates in apoptosis of hippocampal neurons. *Neural. Regen. Res.* 8, 2744–2753. doi: 10.3969/j.issn.1673-5374.2013.29.006

Henry, R. J., Kerr, D. M., Finn, D. P., and Roche, M. (2014). FAAH-mediated modulation of TLR3-induced neuroinflammation in the rat hippocampus. *J. Neuroimmunol.* 276, 126–134. doi: 10.1016/j.jneuroim.2014.09.002

Hernández-López, F., Rodríguez-Landa, J. F., Puga-Olguín, A., Germán-Ponciano, L. J., Rivadeneyra- Domínguez, E., and Bernal-Morales, B. (2017). Analysis of activity and motor coordination in rats undergoing stereotactic surgery and implantation of a cannula into the dorsal hippocampus. *Neurologia* 32, 579–586. doi: 10.1016/j.nrleng.2016.03.002

Hildebrand, D. G., Alexander, E., Hörber, S., Lehle, S., Obermayer, K., Münck, N. A., et al. (2013). IκBζ is a transcriptional key regulator of CCL2/MCP-1. *J. Immunol.* 190, 4812–4820. doi: 10.4049/jimmunol.1300089

Huang, D., Yang, J., Liu, X., He, L., Luo, X., Tian, H., et al. (2018). P2Y6 receptor activation is involved in the development of neuropathic pain induced by chronic constriction injury of the sciatic nerve in rats. *J. Clin. Neurosci.* 56, 156–162. doi: 10.1016/j.jocn.2018.07.013

Ji, J., Xue, T. F., Guo, X. D., Yang, J., Guo, R. B., Wang, J., et al. (2018). Antagonizing peroxisome proliferator-activated receptor γ facilitates M1-to-M2 shift of microglia by enhancing autophagy via the LKB1-AMPK signaling pathway. *Aging Cell* 17:e12774. doi: 10.1111/acel.12774

Kim, H. J, Park, J., Lee, S. K., Kim, K. R., Park, K. K., and Chung, W. Y. (2015). Loss of RUNX3 expression promotes cancer-associated bone destruction by regulating CCL5, CCL19 and CXCL11 in non-small cell lung cancer. *J. Pathol.* 237, 520–531. doi: 10.1002/path.4597

Kimura, A., Kitajima, M., Nishida, K., Serada, S., Fujimoto, M., Naka, T., et al. (2018). NQO1 inhibits the TLR-dependent production of selective cytokines by promoting IκB-ζ degradation. *J. Exp. Med.* 215, 2197–2209. doi: 10.1084/jem.20172024

Knerlich-Lukoschus, F., Noack, M., von der Ropp-Brenner, B., Lucius, R., Mehdorn, H. M., and Held-Feindt, J. (2011). Spinal cord injuries induce changes in CB1 cannabinoid receptor and C-C chemokine expression in brain areas underlying circuitry of chronic pain conditions. *J. Neurotrauma* 28, 619–634. doi: 10.1089/neu.2010.1652

Kobayashi, K., Imagama, S., Ohgomori, T., Hirano, K., Uchimura, K., Sakamoto, K., et al. (2013). Minocycline selectively inhibits M1 polarization of microglia. *Cell Death Dis.* 4:e525. doi: 10.1038/cddis.2013.54

Lanfranco, M. F., Mocchetti, I., Burns, M. P., and Villapol, S. (2018). Glial- and neuronal-specific expression of CCL5 mRNA in the rat brain. *Front. Neuroanat.* 11:137. doi: 10.3389/fnana.2017.00137

LeBlanc, B. W., Zerah, M. L., Kadasi, L. M., Chai, N., and Saab, C. Y. (2011). Minocycline injection in the ventral posterolateral thalamus reverses microglial reactivity and thermal hyperalgesia secondary to sciatic neuropathy. *Neurosci. Lett.* 498, 138–142. doi: 10.1016/j.neulet.2011.04.077

Li, W., Chai, Q., Zhang, H., Ma, J., Xu, C., Dong, J., et al. (2018). High doses of minocycline may induce delayed activation of microglia in aged rats and thus cannot prevent postoperative cognitive dysfunction. *J. Int. Med. Res.* 46, 1404–1413. doi: 10.1177/0300060517754032

Liu, Y., Zhang, Y., Pan, R., Chen, M., Wang, X. Kong, E., et al. (2018). Lentiviral-mediated inducible silencing of TLR4 attenuates neuropathic pain in a rat model of chronic constriction injury. *Mol. Med. Rep.* 18, 5545–5551. doi: 10.3892/mmr.2018.9560

Liu, Y., Zhou, L. J., Wang, J., Li, D., Ren, W. J., Peng, J., et al. (2017). TNF-α differentially regulates synaptic plasticity in the hippocampus and spinal cord by microglia-dependent mechanisms after peripheral nerve injury [J]. *J. Neurosci.* 37, 871–881. doi: 10.1523/JNEUROSCI.2235-16.2016

Livak, K.J., and Schmittgen, T.D. (2001). Analysis of relative gene expression data using real-time quantitative PCR and the $2^{-\Delta\Delta}$CT method. *Methods* 25, 402–408. doi: 10.1006/meth.2001.1262

Luo, X. Q., Li, A., Yang, X., Xiao, X., Hu, R., Wang, T. W., et al. (2018). Paeoniflorin exerts neuroprotective effects by modulating the M1/M2 subset polarization of microglia/macrophages in the hippocampal CA1 region of vascular dementia rats via cannabinoid receptor 2. *Chin. Med.* 13:14. doi: 10.1186/s13020-018-0173-1

Ma, Y., Li, J., Chiu, I., Wang, Y., Sloane, J. A., Lü, J., et al. (2006). Toll-like receptor 8 functions as a negative regulator of neurite outgrowth and inducer of neuronal apoptosis. *J. Cell Biol.* 175, 209–215. doi: 10.1083/jcb.200606016

Matsukawa, N., Yasuhara, T., Hara, K., Xu, L., Maki, M., Yu, G., et al. (2009). Therapeutic targets and limits of minocycline neuroprotection in experimental ischemic stroke. *BMC Neurosci.* 10:126. doi: 10.1186/1471-2202-10-126

Minett, T., Classey, J., Matthews, F. E., Fahrenhold, M., Taga, M., Brayne, C., et al. (2016). Ince PG5, Nicoll JA, Boche D; MRC CFAS. Microglial immunophenotype in dementia with Alzheimer's pathology. *J. Neuroinflammation* 13:135. doi: 10.1186/s12974-016-0601-z

Paxinos, G., and Watson, C. R. (1998). *The Rat Brain in Stereotaxic Coordinates*. New York, NY: Academic. Press.

Perego, C., Fumagalli, S., and De Simoni, M. G. (2013). Three-dimensional confocal analysis of microglia/macrophage markers of polarization in experimental brain injury. *J. Vis. Exp.* e50605. doi: 10.3791/50605

Pinkernelle, J., Fansa, H., Ebmeyer, U., and Keilhoff, G. (2013). Prolonged minocycline treatment impairs motor neuronal survival and glial function in organotypic rat spinal cord cultures. *PLoS ONE* 8:e73422. doi: 10.1371/journal.pone.0073422

Pusic, K. M., Pusic, A. D., Kemme, J., and Kraig, R. P. (2014). Spreading depression requires microglia and is decreased by their M2a polarization from environmental enrichment. *Glia* 62, 1176–1194. doi: 10.1002/glia.22672

Rojewska, E., Korostynski, M., Przewlocki, R., Przewlocka, B., and Mika, J. (2014). Expression profiling of genes modulated by minocycline ina rat model of neuropathic pain. *Mol. Pain* 10:47. doi: 10.1186/1744-8069-10-47

Safakhah, H. A, Moradi, Kor. N., Bazargani, A., Bandegi, A. R., Gholami Pourbadie, H., Khoshkholgh-Sima, B., et al. (2017). Forced exercise attenuates neuropathic pain in chronic constriction injury of male rat: an investigation of oxidative stress and inflammation. *J. Pain Res.* 10, 1457–1466. doi: 10.2147/JPR.S135081

Sarma, N. J., Tiriveedhi, V., Crippin, J. S., Chapman, W. C., and Mohanakumar, T. (2014). Hepatitis C virus-induced changes in microRNA 107 (miRNA-107) and miRNA-449a modulate CCL2 by targeting the interleukin-6 receptor complex in hepatitis. *J. Virol.* 88, 3733–3743. doi: 10.1128/JVI.03060-13

Song, Q., Fan, C., Wang, P., Li, Y., Yang M, and Yu, S. Y. (2018). Hippocampal CA1 βCaMKII mediates neuroinflammatory responses via COX-2/PGE2 signaling pathways in depression. *J. Neuroinflammation* 15:338. doi: 10.1186/s12974-018-1377-0

Stolp, H. B., Ek, C. J., Johansson, P. A., Dziegielewska, K. M., Potter, A. M., Habgood, M. D., et al. (2007). Effect of minocycline on inflammation-induced damage to the blood-brain barrier and white matter during development. *Eur. J. Neurosci.* 26, 3465–3474. doi: 10.1111/j.1460-9568.2007.05973.x

Sun, R., Zhang, Z., Lei, Y., Liu, Y., Lu, C., Rong, H., et al. (2016). Hippocampus activation of microglia may underlie the shared neurobiology of comorbid posttraumatic stress disorder and chronic pain. *Mol. Pain* 12:1744806916679166. doi: 10.1177/1744806916679166

Sundaram, K., Rahman, M. A., Mitra, S., Knoell, D. L., Woodiga, S. A., King, S. J., et al. (2016). IκBζ regulates human monocyte pro-inflammatory responses induced by *Streptococcus pneumoniae*. *PLoS ONE* 11:e0161931. doi: 10.1371/journal.pone.0161931

Tang, Y., and Le, W. (2016). Differential roles of M1 and M2 microglia in neurodegenerative diseases. *Mol. Neurobiol.* 53, 1181–1194. doi: 10.1007/s12035-014-9070-5

Timberlake, M., Prall, K., Roy, B., and Dwivedi, Y. (2018). Unfolded protein response and associated alterations in toll-like receptor expression and interaction in the hippocampus of restraint rats. *Psychoneuroendocrinology* 89, 185–193. doi: 10.1016/j.psyneuen.2018.01.017

Totsch, S. K., and Sorge, R. E. (2017). Immune system involvement in specific pain conditions. *Mol. Pain* 13:1744806917724559. doi: 10.1177/1744806917724559

Vanoni, S., Tsai, Y. T., Waddell, A., Waggoner, L., Klarquist, J., Divanovic, S., et al. (2017). Myeloid-derived NF-κB negative regulation of PU.1 and c/EBP-β-driven pro-inflammatory cytokine production restrains LPS-induced shock. *Innate Immun*. 23, 175–187. doi: 10.1177/1753425916681444

Vonder Haar, C., Anderson, G. D., Elmore, B. E., Moore, L. H., Wright, A. M., Kantor, E. D., et al. (2014). Comparison of the effect of minocycline and simvastatin on functional recovery and geneexpression in a rat traumatic brain injury model. *J. Neurotrauma.* 31, 961–975. doi: 10.1089/neu.2013.3119

Wang, F. X., Liu, S. Y., Zheng, X., Chen, X., Lu, L. X., Chen B., et al. (2015). TLR1 expression in mouse brain was increased in a KA-induced seizure model. *Inflamm. Res*. 64, 487–495. doi: 10.1007/s00011-015-0828-7

Wang, L., Feng, Z., Wang, X., Wang, X., and Zhang, X. (2010). DEGseq: an R package for identifying differentially expressed genes from RNA-seq data. *Bioinformatics* 26, 136–138. doi: 10.1093/bioinformatics/btp612

White, F. A., and Wilson, N. M. (2008). Chemokines as pain mediators and modulators. *Curr. Opin. Anaesthesiol.* 21, 580–585. doi: 10.1097/ACO.0b013e32830eb69d

Wu, J., Zhao, Z., Sabirzhanov, B., Stoica, B. A., Kumar, A., Luo, T., et al. (2014). Spinal cord injury causes brain inflammation associated with cognitive and affective changes: role of cell cycle pathways. *J. Neurosci.* 34, 10989–1006. doi: 10.1523/JNEUROSCI.5110-13.2014

Xie, Z. M., Wang, X. M., Xu, N., Wang, J., Pan, W., Tang, X. H., et al. (2017) Alterations in the inflammatory cytokines and brain-derived neurotrophic factor contribute to depression-like phenotype after spared nerve injury: improvement by ketamine. *Sci. Rep*. 7:3124. doi: 10.1038/s41598-017-03590-3

Yamazaki, S., Muta, T., and Takeshige, K. (2001). A novel IkappaB protein, IkappaB-zeta, induced by proinflammatory stimuli, negatively regulates nuclear factor-kappaB in the nuclei. *J. Biol. Chem*. 276, 27657–27662. doi: 10.1074/jbc.M103426200

Zhang, G., Zhao, B. X., Hua, R., Kang, J., Shao, B. M., Carbonaro, T. M., et al. (2016). Hippocampal microglial activation and glucocorticoid receptor down-regulation precipitatevisceral hypersensitivity induced by colorectal distension in rats. *Neuropharmacology* 102, 295–303. doi: 10.1016/j.neuropharm.2015.11.028

Zhang, W., Cui, Q., Qu, W., Ding, X., Jiang, D., and Liu, H. (2018). TRIM58/cg26157385 methylation is associated with eight prognostic genes in lung squamous cell carcinoma. *Oncol. Rep*. 40, 206–216. doi: 10.3892/or.2018.6426

Zhang, Z. J., Jiang, B. C., and Gao, Y. J. (2017). Chemokines in neuron-glial cell interaction and pathogenesis of neuropathic pain. *Cell Mol. Life Sci*. 74, 3275–3291. doi: 10.1007/s00018-017-2513-1

Conflict of Interest: The authors declare that the research was conducted in the absence of any commercial or financial relationships that could be construed as a potential conflict of interest.

Advantages of publishing in Frontiers

OPEN ACCESS
Articles are free to read for greatest visibility and readership

FAST PUBLICATION
Around 90 days from submission to decision

HIGH QUALITY PEER-REVIEW
Rigorous, collaborative, and constructive peer-review

TRANSPARENT PEER-REVIEW
Editors and reviewers acknowledged by name on published articles

Frontiers
Avenue du Tribunal-Fédéral 34
1005 Lausanne | Switzerland

Visit us: www.frontiersin.org
Contact us: info@frontiersin.org | +41 21 510 17 00

REPRODUCIBILITY OF RESEARCH
Support open data and methods to enhance research reproducibility

DIGITAL PUBLISHING
Articles designed for optimal readership across devices

FOLLOW US
@frontiersin

IMPACT METRICS
Advanced article metrics track visibility across digital media

EXTENSIVE PROMOTION
Marketing and promotion of impactful research

LOOP RESEARCH NETWORK
Our network increases your article's readership